LA-UR-21-24710
Approved for public release; distribution is unlimited.

Title: TINMAN Thermal Neutron Detector for Aircraft

Author(s): Wender, Stephen Arthur

Intended for: R&D 100 submission

Issued: 2021-05-14

2021 R&D 100 JOINT ENTRY

LOS ALAMOS NATIONAL LABORATORY AND HONEYWELL INC.

TINMAN

THERMAL NEUTRON DETECTOR FOR AIRCRAFT

First Flight-Tested System Designed to Measure the Thermal Neutron Environment in Aircraft at Flight Altitudes

- Provides robust, portable, aircraft-compliant design
- Records thermal neutron rates throughout flight
- Delivers easily accessible data for post-flight analysis
- Verifies reliability of measurements via redundant data recording
- Adapts to measure thermal neutrons in other environments
- Provides an initial platform to investigate extreme space weather events

Honeywell

Los Alamos NATIONAL LABORATORY

2020 R&D 100 Awards template

TinMan Thermal Neutron Detector for Aircraft, the first device specifically designed to function in aircraft that can detect thermal neutrons in flight environments.

LA-UR-21-XXXXX

Category(ies)

- ☒ Analytical/Test
- ☒ IT/Electrical
- ☒ Mechanical/Materials
- ☐ Process/Prototyping
- ☒ Software/Services
- ☐ Other
- ☐ Special recognition: Corporate Social Responsibility
- ☐ Special recognition: Green Tech
- ☐ Special recognition: Market Disruptor - Products
- ☒ Special recognition: Market Disruptor - Services

Name of primary submitting organization

Los Alamos National Laboratory

Name(s) of co-developing organization(s)—if applicable

Honeywell, Inc.

Product/service brand name

Specify product name as you would like it to appear on a potential award plaque.

TinMan

Was the product/service introduced to the market between January 1, 2019, and March 31, 2020?

- ☒ Yes
- ☐ No

If your submission is subject to regulatory approval, has the product been approved?

- ☐ Yes
- ☐ No
- ☒ Not applicable to this product

Price of product/service (U.S. dollars)

$20,000

Product description (max of 50 words)

TinMan is the first technology to continuously measure thermal neutron intensity during aircraft flight and to define this environment, an important achievement since changes to semi-conductors have led electronic parts to become more sensitive to thermal nuetrons that may lead to disturbances in their operation.

Indicate the type of institution you represent

Government Laboratory

Submitter's relation to entered product/service

Product developer

Product Photos

TinMan_Cover.pdf
TinMan1.pdf
TinMan2.pdf
TinMan3.pdf

Video Link

XXXXXX

R&D 100 Entry

TinMan

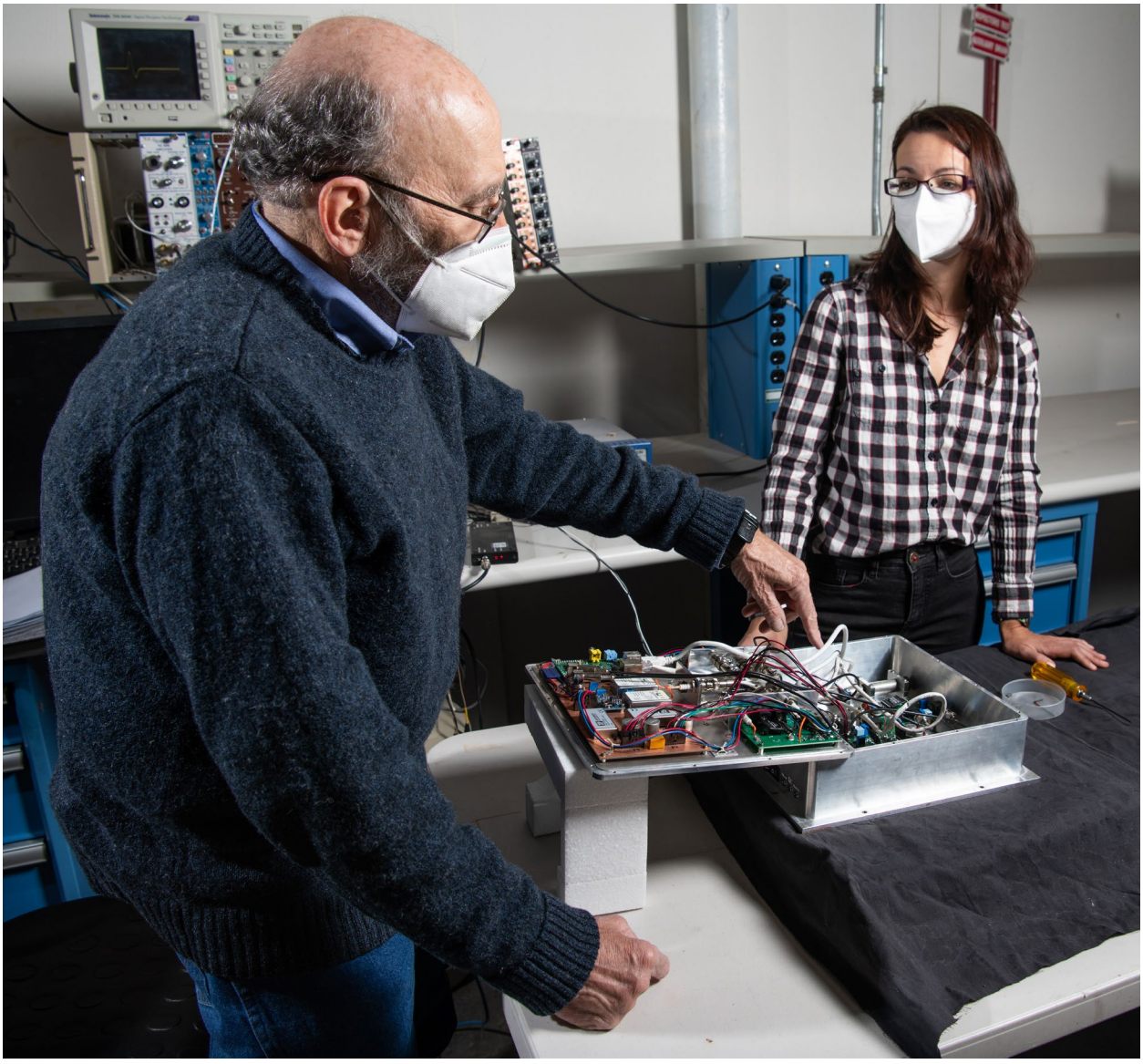

TinMan1.pdf

Prodcut developers Stephen Wender and Suzane Nowicki stand over TinMan, as its cover is removed to reveal its inner circuitry and design. Inside TinMan are two gas chambers filled with Helium-3 gas, which is particularly sensitive to thermal nuetrons. One gas chamber is coated with cadmium, an element that specifically deflects thermal nuetrons from interacting with the Helium-3. This allows TinMan to deciphere between the number of thermal nuetrons present during aircraft flight and other interference that might be encountered, like gamma rays or high-energy nuetrons. This makes TinMan the most accurate detector of its kind.

R&D 100 Entry

TinMan

TinMan2.pdf

TinMan's shell is made of lightweight aluminum, giving it and its external independent battery system a collective weight of only 20 pounds. It measures 13 inches long and wide, and is three inches deep. This allows it to be easily placed in different areas of a plane to gather measurements, important because thermal neutron intensity may vary at different locations.

R&D 100 Entry

TinMan

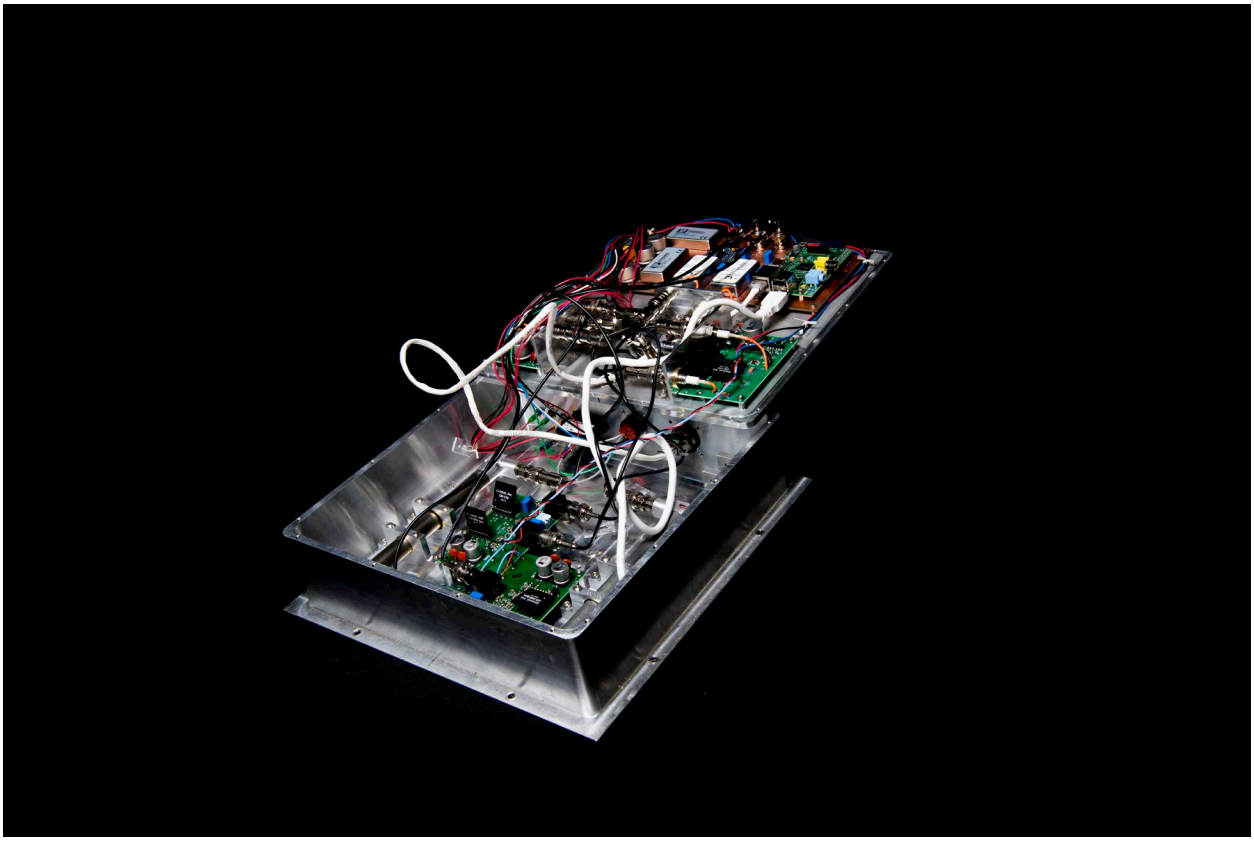

TinMan3.pdf

TinMan is equipped with several data collection redundancy devices. When a thermal neutron interact with the Helium-3 chamber, a signal is sent to the Raspberry-Pi microcomputer. That data is then stored on four memory sticks. This redundancy is important in case a thermal neutron were to disrupt any electronics inside TinMan, which could then result in data loss. If TinMan becomes unresponsive for 15 seconds, a reboot process is automatically started. The information is also stored in 10-minute increments to prevent loss. All of the data can be viewed immediately during flight through an ethernet connection, or accessed later after a flight.

What does the product or technology do? Describe the principal applications of this product.

At cruising altitudes of 37,000 feet, aircraft experience a more intense atmospheric radiation environment than what electronics are subject to on the ground. Atmospheric radiation is a natural phenomenon that showers particles onto the Earth from space and includes protons, electrons, and neutrons. At aircraft-cruising altitudes, neutrons are 300 times more intense than at sea level.

The susceptibility of digital parts and integrated circuits to atmospheric radiation effects, and specifically neutrons at sea level and aircraft altitudes, has been acknowledged as an issue for component reliability in aircraft systems. (See report, "Extreme space weather: impacts on engineered systems and infrastructure," in Appendix.) When a particle interacts with a semiconductor electronic device it can cause a Single Event Effect (SEE) by depositing energy or charge into active region of an electronic component. The phenomenon can cause a disturbance to the operation of the electronic device.

TinMan, developed by the Los Alamos National Laboratory and Honeywell, Inc., is a device developed to measure the intensity of thermal neutrons in an airplane. (See the newsletter, "Physics Flash," and LANL News Release in the Appendix.) While there is extensive research on the connection between atmospheric radiation and SEE, there is much less information specifically about SEE events caused by thermal neutrons within various types of aircraft. TinMan, in fact, was the first device to clearly define the thermal neutron environment inside an aircraft under varying flight conditions, a valuable piece of information for the aerospace industry. (See, "Preliminary Measurements of Thermal Neutrons in Airplanes –TinMan LA-UR 18-26016 NSREC 2018," in the Appendix).

Airplanes are complicated and complex machines that must work perfectly every time they're flown. Worldwide, there are an average of 176,000 flights each month; half a million people are in the sky across the world at any given moment. Overall, airplanes are extremely reliable. But as semiconductor technology trends continue to achieve higher densities, smaller feature sizes and lower voltages, electronic semiconductor devices may become more susceptible to atmospheric radiation.

The world has known for some time about atmospheric radiation, though not specifically about thermal neutrons. When solar and galactic radiation strikes the Earth's atmosphere, it produces high-energy particles that shower down onto the planet, including protons, electrons, and neutrons. But whereas protons and electrons are charged, neutrons are not, and an uncharged neutron can travel long distances without significant absorption. At sea level and aircraft altitudes, neutrons are the major concern. Figure 1 show an airplane being exposed to high-energy neutrons produced by cosmic rays striking the earth's atmosphere.

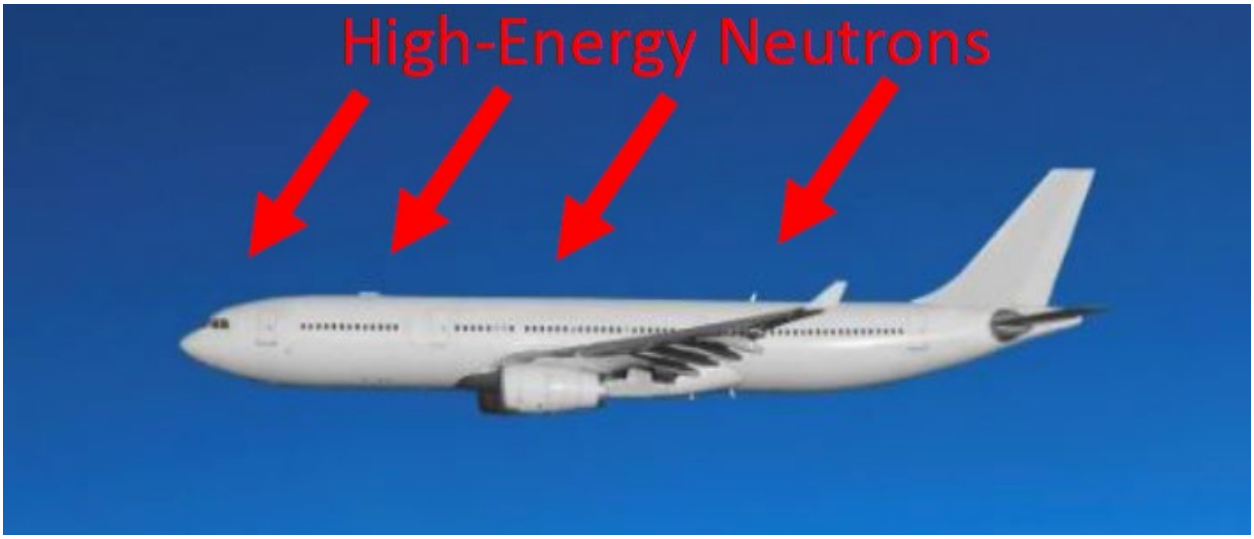

Figure 1. *Aircraft at flight altitudes are subject to high-energy neutron flux caused by cosmic rays striking the upper atmosphere. These high-energy neutrons interact with the aircraft and produce thermal neutrons.*

When high energy neutrons hit a semiconductor, they have enough energy to produce charged particles that can deposit some of this energy in a sensitive volume of a semiconductor, which in turn can cause SEE. The effects of these neutrons were first detailed in the 1960s (See report, "Extreme space weather: impacts on engineered systems and infrastructure," in Appendix.) As the budding solid-state aerospace industry developed, it began to test its semiconductors to ensure they could withstand the intensity of high energy neutrons in this environment. But there is much less understanding about thermal neutrons.

Thermal neutrons are low-energy neutrons that are produced from high energy neutrons that have collided with some material and lose energy. The most effective way for a neutron to lose

energy is a collision with a proton or hydrogen because neutrons and protons have the same mass. This material can be a human body, because humans are mostly water with a high hydrogen content, or the tens of thousands of gallons of fuel stored in aircraft wings. (See presentation, “Measurement of Thermal Neutron Environments in Aircraft with the Tinman Instrument,” in Appendix.) After many collisions, these high-energy neutrons lose enough energy and become thermal neutrons.

Thermal neutrons have average energies that depend on the temperature of the material they interact with. For example, at room temperature (~20^{o} C), thermal neutrons have energies of approximately 0.025 eV.

It was previously thought that thermal neutrons, due to their lower speed and thus energy, could not cause SEE failures. It was soon recognized that in special cases thermal neutrons could cause SEE. One of these special cases is when thermal neutrons interact with Boron-10 in a semiconductor device. (See report, Thermal Neutron-Induced Single-Event Upsets in Microcontrollers Containing Boron-10,” in Appendix.)

In the recent years, the semiconductor industry began to produce its semiconductors, like computer processor chips, using Boron, which contains the isotope Boron-10 (see Figure 2). As long as the semiconductor chips function for their normal use, little else is said about exchanged material. But the Boron-10 inside these semiconductors is known to be sensitive to thermal neutrons. When a thermal neutron strikes Boron-10, it causes a nuclear reaction that creates alpha particles and Lithium ions, which can deposit charge in the device and may cause an SEE.

It has been observed that in particular devices, thermal neutrons may be the cause of between 10 to 20 percent of recorded SEE in semiconductors. Today there are 100 billion transistors—the building blocks of semiconductor devices—for every man, woman, and child on the planet. (See presentation, “New capabilities for radiation effects,” in Appendix.) Semiconductor devices are used in all aspects of modern life and there can be reliability issues, due to thermal neutrons, as the industry continues to use Boron-10 equipped electronics. This is where TinMan solves a vital problem: data that clearly defined the thermal neutron environment in an aircraft is very sparse.

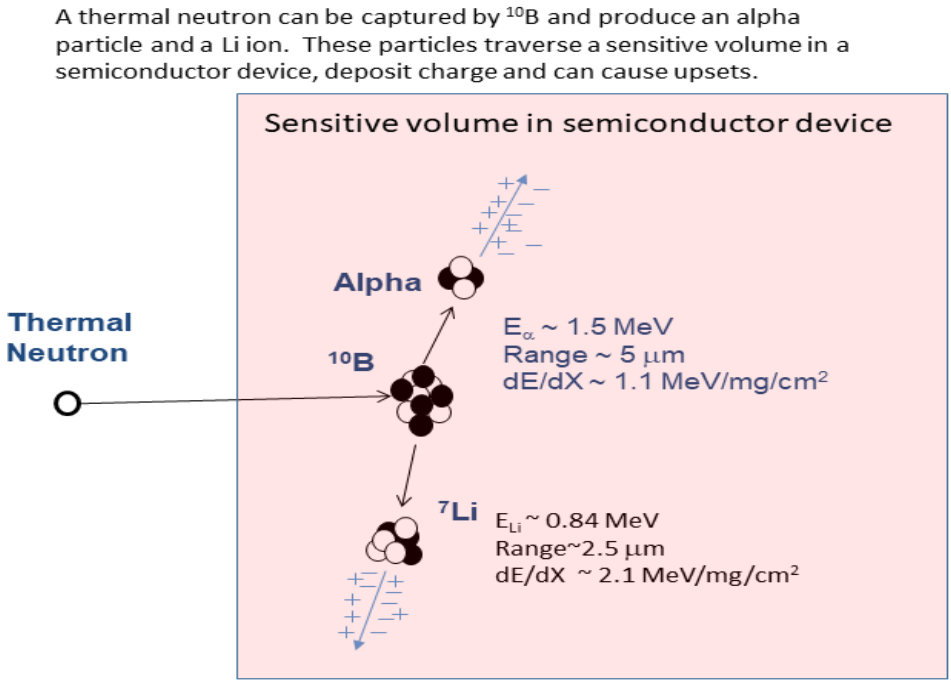

Figure 2. *A thermal neutron can be absorbed by Boron-10 and produce two energetic ions which can deposit energy and charge in a sensitive volume of a semiconductor and produce a SEE.*

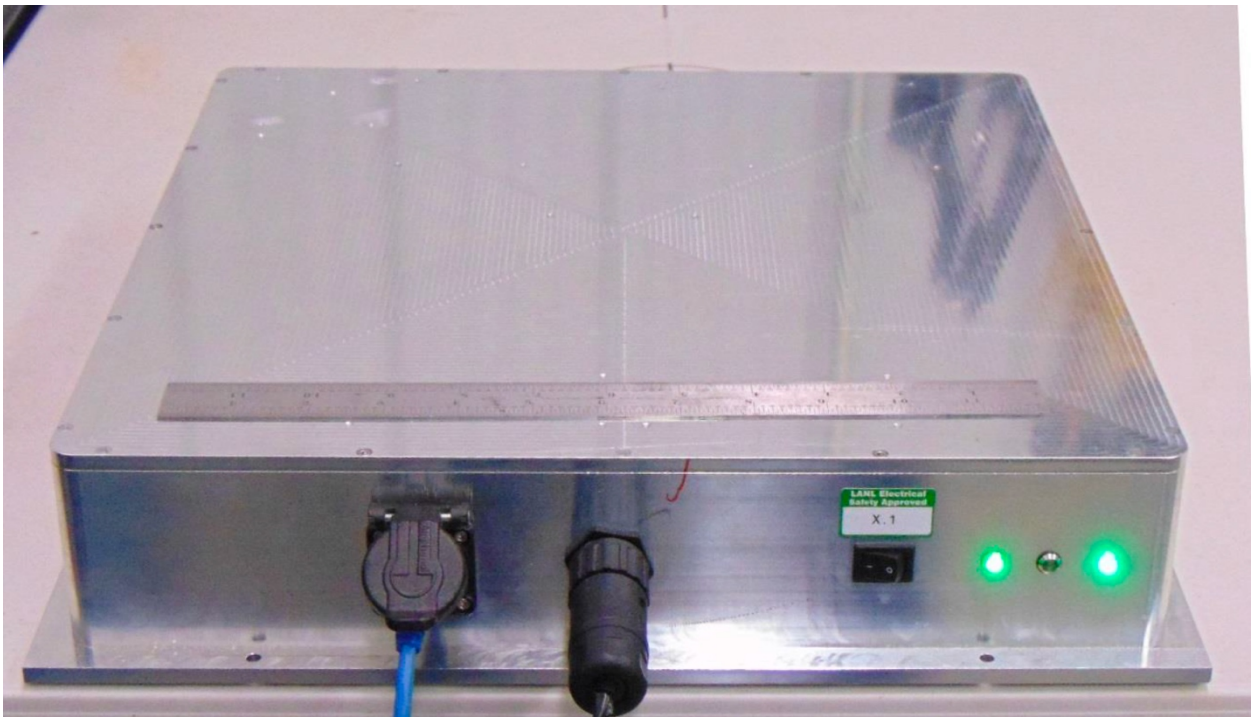

Figure 3. *A picture of TinMan's exterior, with ethernet cable and power connections (LANL). The length and width of the box is 13 inches.*

While there are technologies that can measure thermal neutrons on the Earth's surface, TinMan is the only device designed to measure them inside an aircraft environment and can be correlated with the external parameters of the flight such as altitude, latitude, fuel loading, etc. (See "Measurement of Thermal Neutron Environments in Aircraft" LA-UR 18-27894 Seminar at NASA HQ in Appendix). To do this, TinMan is small—the length and width of a laptop, and 3-inches deep. Its aluminum casing is lightweight, and it's designed to operate on either power supplied by the aircraft or on its independent batteries for up to 30 hours. TinMan is also the first continuous thermal neutron detection device, recording samples constantly and backing up the data to four memory devices every 10 minutes.

To measure thermal neutrons, TinMan is equipped with two identical cylindrical ion chambers filled with Helium-3, a gas that's particularly sensitive to thermal neutrons and is not hazardous. One cylinder is coated in cadmium to block thermal neutrons from entering the chamber, acting as a baseline for data collection.

For an example of data that TinMan acquired, Figure 4 shows a flight on a January 13, 2018, from Armstrong Flight Research Center in Palmdale, California, to Ramstein, Germany, on a NASA DC-8 aircraft. The measurements show relatively low thermal neutron intensity at ground level. But as the plane increases altitude and latitude, the thermal neutron intensity increases from almost zero to around 300 events detected every 100 seconds. So far, TinMan has flown on 14 flights on different planes and routes. The changes in the thermal neutron rate track with the high energy neutron rates as expected. TinMan was able to accurately measure thermal neutron intensity at a range of altitudes and latitudes from takeoff to touchdown.

So far, preliminary data from TinMan flights, which are awaiting final publication, show that the intensity of thermal neutrons at flight altitudes are approximately twice the currently accepted values. This result will have impact on the expected upset rates.

For the half-million airline passenger who are in the sky at any given minute, TinMan has quantified and helped solve a problem they might have never known existed. In the future, more studies will place TinMan in varying locations around planes, which will help the aerospace

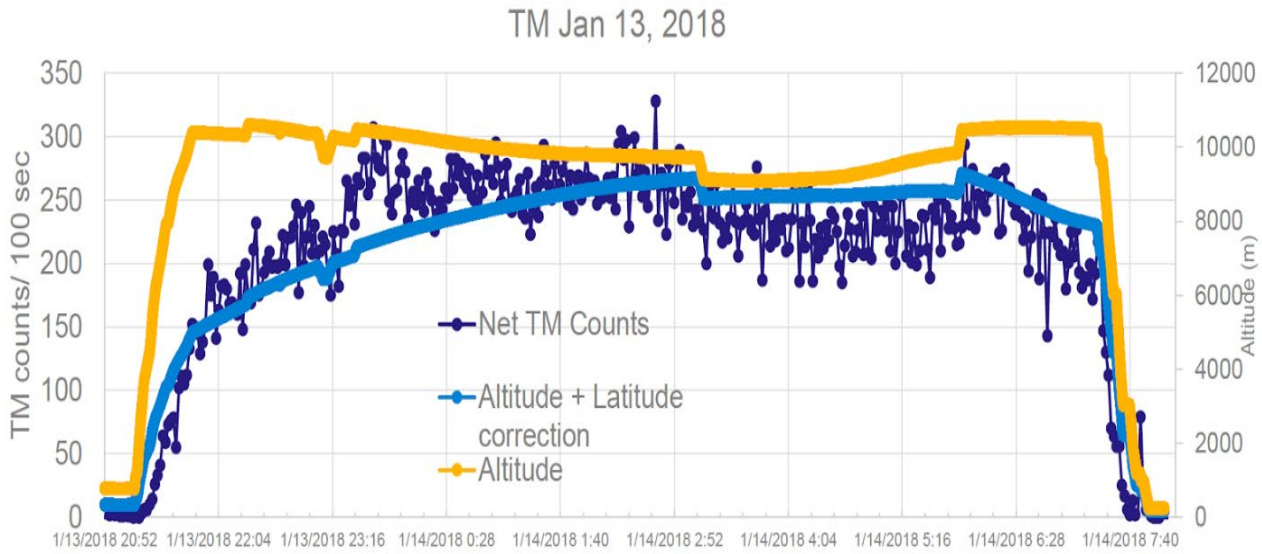

Figure 4. *This shows a flight from Palmdale, California, to Ramstein, Germany, on a NASA DC-8 aircraft. The counts in the detector are shown on the left axis and the altitude is shown on the right axis. The dark blue points are number of events recorded by TinMan in 100 second time bins. The yellow curve is the aircraft altitude. The light blue curve is the correction for latitude as the plane flies*

industry understand how thermal neutron intensity varies at different points within the aircraft. Because the production of thermal neutrons require interaction with hydrogen, their intensity could vary in locations, such as near the cabin or near the wings, where fuel is stored.

As electronics with Boron-10 continues to be incorporated in semiconductors, TinMan could also have an impact everywhere these parts are used, especially the self-driving car market and the computing industry (see Figure 5) at large. (See Science & Technologies Facilities Council website article, “Could thermal neutrons be a threat to reliable supercomputing and self-driving cars?” in Appendix.)

Massive data centers that store or allow people to access information over the internet could face constant SEE because of Boron-10 equipped electronics and thermal neutrons. (See journal article, “Thermal neutrons: a possible threat for supercomputer reliability,” in Appendix.) The team has developed a successor to TinMan, named the Tin-II. The new Tin-II detector was designed with greater sensitivity to operate at sea level. Because there are large amounts of water present in these facilities to cool these super computers, the problem of thermal neutrons causing SEE may be present in large computer system and data centers. Tin-II is already installed in the

Figure 5. *This shows a large high-performance computer at Los Alamos National Laboratory. This is typical of large data centers, which can be vulnerable to thermal neutrons causing SEE.*

High-Performance Computer area at Los Alamos National Laboratory to gather information on thermal neutron intensity in these environments. (See report, “Report on the Tin-II Thermal Neutron Detector,” in Appendix.)

Another successor to TinMan is ExMan, currently under development to measure the intensity of other constituents of cosmic radiation with the focus on recording extreme space weather events. The technology of ExMan will also be based in large part on TinMan.

Today, there is more processing power in a cell phone than what was used to deliver the Apollo spacecraft to the moon. And while there are already 100 billion transistors for every man, woman, and child on the planet, semiconductor parts are expected to become even more ubiquitous in the future. Now that the world has begun paying attention to the effects of thermal neutrons on all of this equipment humanity depends upon, TinMan is the first and most effective device to provide the environmental data.

How does the product operate? Describe the mechanism of action, theories, materials, composition, or construction.

TinMan combines off-the-shelf and non-proprietary technology that makes it inexpensive ($20,000), easy to manufacture and operate, and very reliable. It's most distinguishing features are that it (1) is the only thermal neutron detector designed for portable use with unattended operation, specifically inside airplanes; (2) constantly monitors and records changes in thermal neutron intensity; (3) allows for redundancy in information backup; (4) provides high-accuracy thermal neutron detection; (5) offers easily downloadable time history of the thermal neutron rate that can be combined with other relevant data points such as altitude and latitude, fuel loading, etc. The equipment was tested in the atmospheric environment at varying altitudes and latitudes to ensure accuracy of measured data.

Many thermal neutrons detectors currently in the market are generally large scientific instruments meant to remain stationary for use on the ground. These existing devices take measurements when required and sum over the total time of the exposure. They were not designed for a wide application, and they were not designed to operate in an airplane environment, which brings many demands on size, weight, durability, power consumption, and data allocation. In this regard, TinMan stands alone in its capabilities.

In recent years, the manufacturing industry switched materials in its semiconductor parts by adding Boron. This metal contains Boron-10, an isotope that is very reactive to thermal neutrons.

These thermal neutrons are produced when high-energy neutrons are thermalized in the material in aircraft. But as thermal neutrons strike Boron-10, a nuclear reaction occurs and the resulting charged particles being produced can deposit energy or charge into vital electronics. This extra charge, when deposited in sensitive regions of the semiconductor can lead to SEEs.

TinMan's goal was to define the thermal neutron environment of an aircraft in flight. This information would then be used by the aerospace industry to evaluate the susceptibility of semiconductors to SEE. This led to many demands on the design of TinMan, since thermal neutron intensity not only changes with altitude and latitude, but also with the type of plane. This

meant TinMan would need to be highly portable, adaptable, and would also need to be strong enough to withstand vibrations during flight, temperature and pressure changes.

With this in mind, TinMan operates inside a small aluminum case that measures 13 inches long, 13 inches wide, and three inches deep—not much larger than a laptop. This allows TinMan to be stored in almost any type of aircraft, fitting securely into areas like the avionics bay. But this small design also enables TinMan to be moved to other positions around the plane so it can map the thermal neutron intensity at different locations. This is important because thermal neutron intensity can vary depending on the contents of a plane, like the number of passengers, materials inside the plane, and proximity to stored fuel.

To detect thermal neutrons, TinMan is equipped with two identical cylindrical Helium-3 ion chambers. An area of concern to many is that Helium-3 is in short supply. (See *Science* magazine website article, "Researchers rise to challenge of replacing helium-3," in Appendix.) With stepped-up enforcement at airports, stadiums, and along U.S. borders, the Department of Homeland Security has put a strain on the available supply of Helium-3, which is used in nuclear material detection devices. Some thermal neutron detectors use multi-detector arrays that require large amounts of Helium-3. But TinMan's two Helium-3 tubes use only a small amount, about 70 cc for the two ion chambers, which cuts down costs and can be easily obtained.

Both cylindrical tubes are seven inches long by 0.75 inches in diameter and are commercially available. To extract the most accurate information, the exterior of one Helium-3 ion tubes is bare, and the second is covered in cadmium, a soft silvery metal that absorbs thermal neutrons. (See report, "Measurement of Thermal Neutrons in Aircraft," in Appendix.) Although Helium-3 is relatively insensitive to high-energy neutrons, by coating the second tube in cadmium, which acts as a shield for thermal neutrons, you can subtract any background associated with high-energy neutrons. So while the bare tube counts thermal neutrons as well as some interference from high-energy neutrons and gamma rays, the cadmium-coated detector monitors only this latter interference. The results of the cadmium-coated tube are then subtracted from the bare tube, producing a very reliable count of thermal neutron intensity.

As thermal neutron pass through the exterior of the bare tube and into the pressurized ion gas chamber, the thermal neutrons are absorbed by the Helium-3 ions. This reaction produces a 191 keV triton (^{3}H) and a 572 keV proton and results in the production of energy, about 763 keV. This process is shown in figure 6. The production of these reaction particles is recorded by a simple discriminator circuit, which relays the information to TinMan's Raspberry-Pi microcomputer.

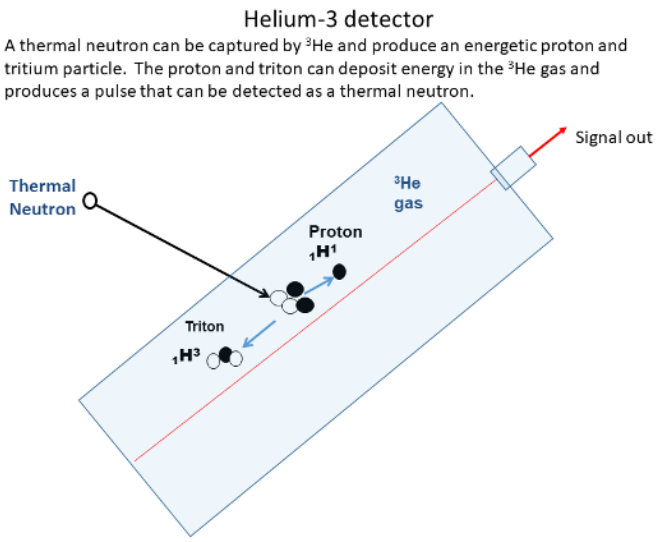

Figure 6. *An He-3 ion chamber produces a proton and triton which signals the detection of a thermal neutron.*

Figure 7 shows the inside of the TinMan detector with the lid folded open. Shown in the picture are the cylindrical He-3 ion chambers, the preamp and shapers, the DC-to-DC converter power supplies and the Raspberry Pi microcomputer.

This approach leads to excellent signal-to-noise advantages for thermal neutron detection, allowing TinMan to use commercially-available electronics such as amplifiers and preamplifiers, which simplified the data acquisition and analysis process and reduced TinMan's power consumption.

TinMan meets aircraft installation requirements by running on 28 volts, the voltage supplied by the aircraft. It draws a small amount of current (~300 mA), which allows it to operate independently for up to 30 hours on two sealed, 12-volt AGM lead acid batteries. These batteries are connected to a TDK-Lambda DC-to-DC converter, which produces a constant output of 28 Volts. TinMan has enough memory storage to last for up to 40 continuous flights. Altogether, with the backup batteries included, TinMan weighs only 20 pounds.

In case of an SEE caused by either high energy or thermal neutrons, TinMan has several built-in redundancies. A Raspberry-Pi microcomputer watchdog timer circuit is enabled if the system

becomes nonresponsive for more than 15 seconds, which then begins a reboot process. Thermal neutron intensity, along with corresponding timestamps, are also recorded to four separate memory devices for further redundancy. After collecting data for 10 minutes, a new file is created and the data is saved again to each of the four memory devices. This data can be stored and downloaded later, or viewed immediately on a laptop computer via an ethernet connection.

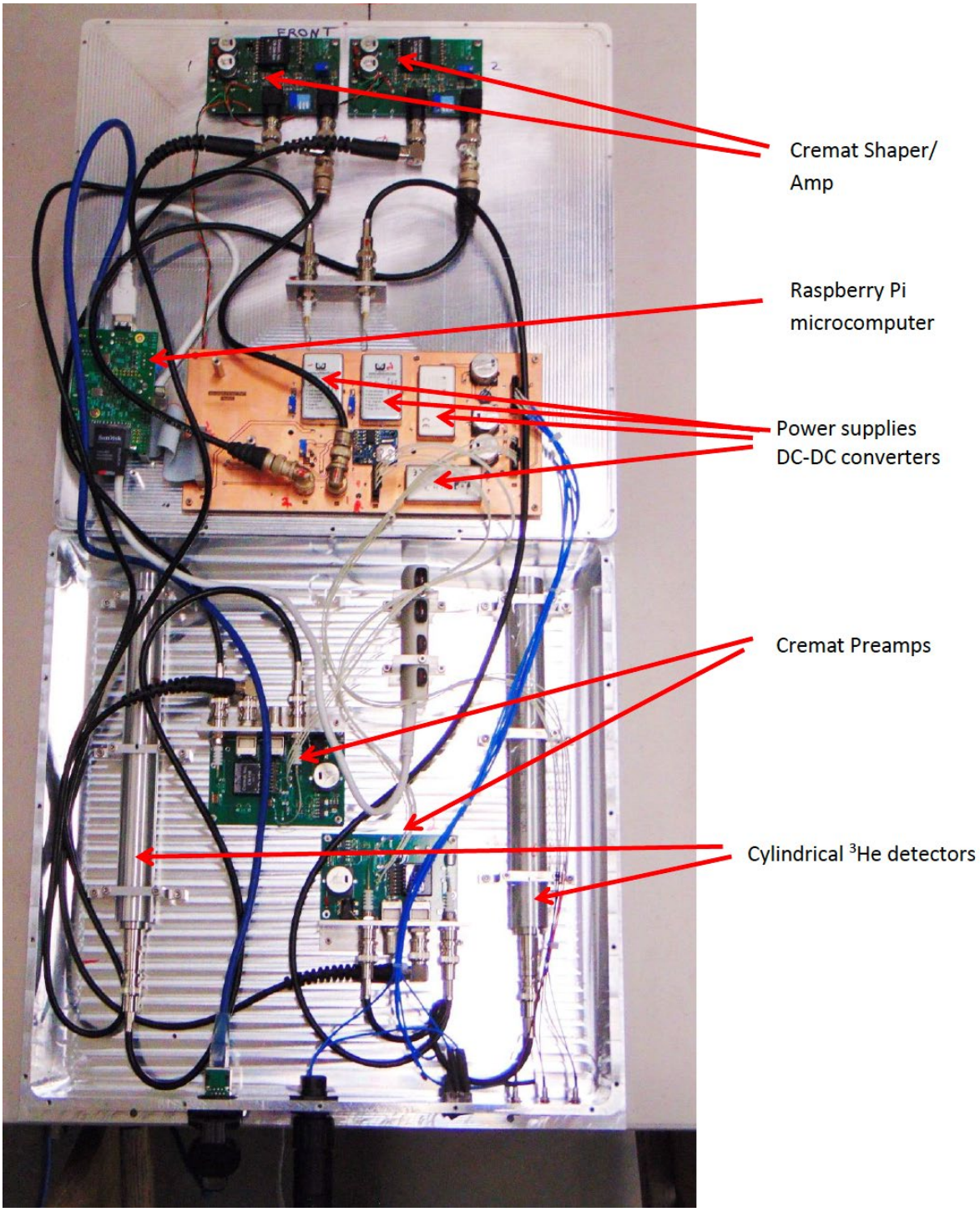

Figure 7. *The interior of TinMan, with its operating parts labeled to the right.*

The result is a measurement that looks like Figure 8. In this graph, the X axis represents time in the air. The Y axis represents both altitude (on the right) and thermal neutron intensity measured

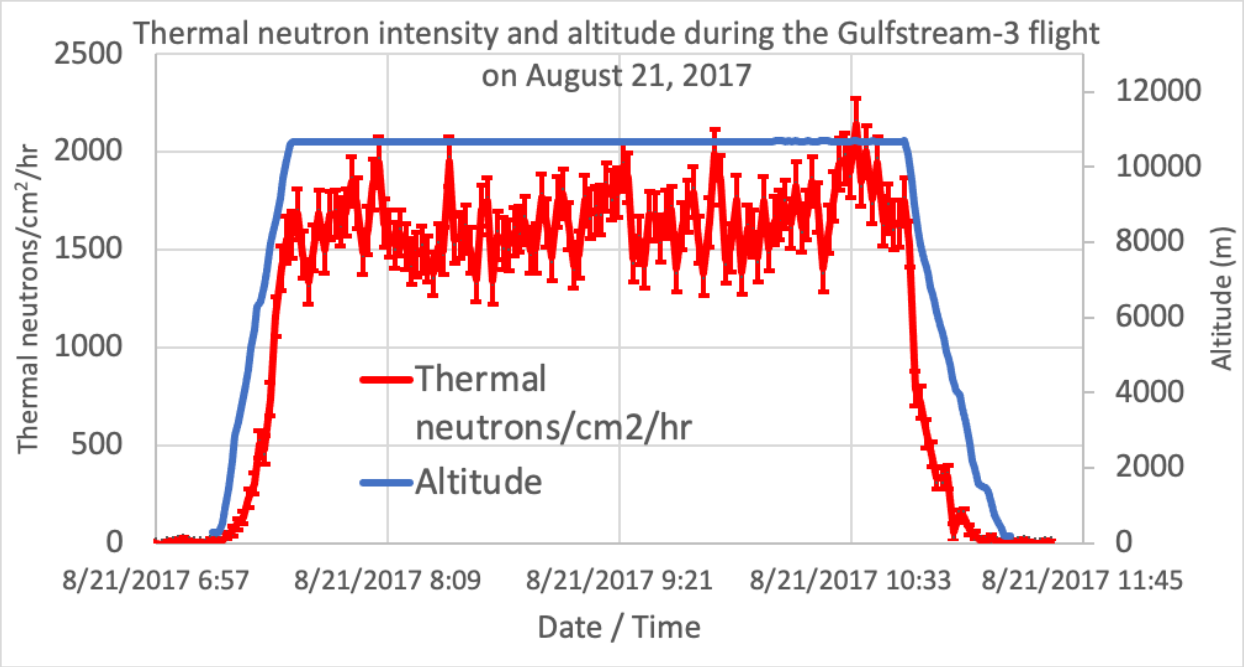

Figure 8. *A flight made on a NASA Gulfstream-III on August 21, 2019, in which continuous measurements of thermal neutrons were taken.*

particular flight was made in a NASA Gulfstream-III on August 21, 2019, as one of the two science packages on the NASA eclipse flight mission. As the plot shows, thermal neutron rates begin at 8.3 per cm^2/hour at ground level and increase to about 1710 per cm^2/hour, an increase factor of 207. (See NASA seminar presentation, "Measurement of Thermal Neutron Environments in Aircraft," in Appendix.)

Figure 9 shows a flight on January 29, 2019, taken around Ramstein, Germany, on a NASA DC-8 aircraft. The aircraft made four elevation changes, and this corresponds to the number of thermal neutrons detected, with intensity increasing to match altitude. What both of the graphs illustrate is the drastic change in environment planes endure while in flight.

This information, as well as the numerous other fights TinMan accompanied, provided the first detailed, time resolved look at thermal neutron intensity in aircraft. With it, TinMan defined the thermal neutron environment in these aircraft, and that information, when published, will be

included in reports by the Geneva-based International Electrotechnical Commission, an organization that oversees all electrical and electronic-related standards.

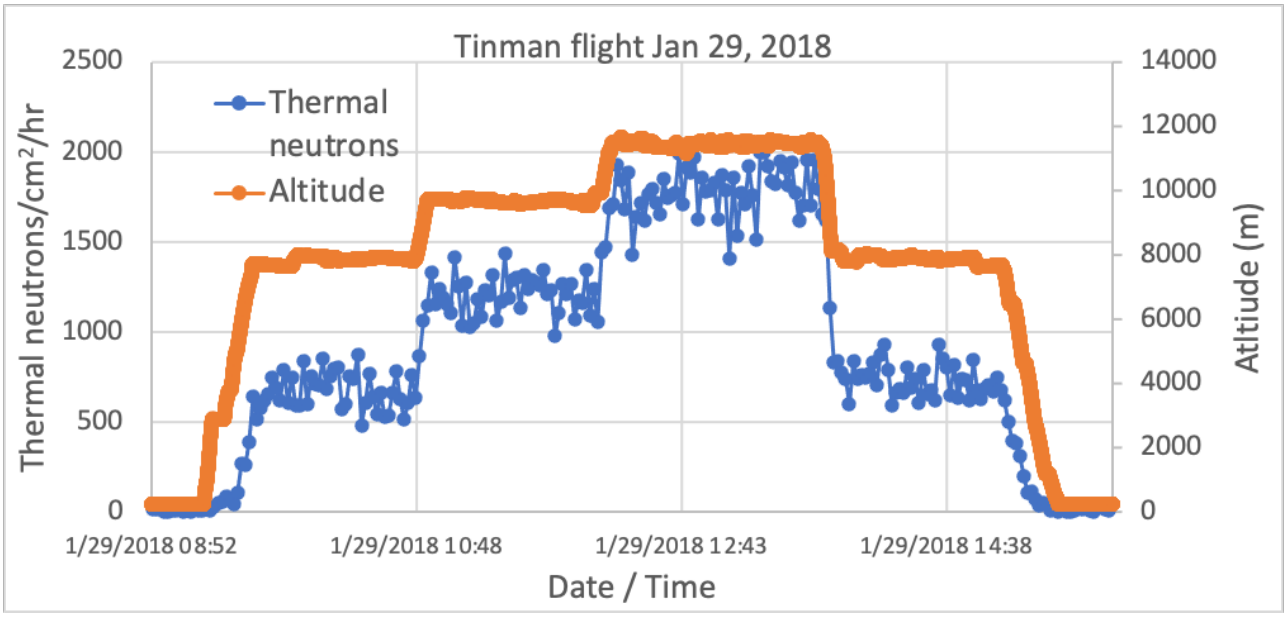

Figure 9. *A flight made on January 29, 2019, around Ramstein, Germany, on a NASA DC-8 aircraft, with several steady elevation changes. The thermal neutrons detected reflect each of these elevation changes.*

The future for TinMan extends beyond aircraft. As Boron-10 equipped electronics continue to fill every part of life, those environments will also need to be defined so that semiconductor reliability can be assessed. TinMan is durable and versatile enough to operate in trains, self-driving cars, and in large data centers, the latter of which is already the field being tested by TinMan's successor, Tin- II. In the future, the next generation TinMan-based platform will fly in aircraft, monitoring neutron intensity and other particles during extreme space weather events such as solar particle events and coronal mass ejections.

Comparison Matrix

The following table compares TinMan to three other neutron and thermal neutron detection technology systems. Since TinMan is the only technology capable of continuously measuring thermal nuetrons in an aircraft, it is necessary to use other systems that generally measure high energy or thermal neutrons, whether on the ground or in the air.

The comparisons focus on the ability to measure strictly thermal nuetrons during flight. But since TinMan is the only system capable of meeting all of these standards, the following comparison matrix highlights where these similar techbnologies stand and where TinMan excels. Competitor one is a system that measures thermal nuetrons, but is only capable of doing so at ground level. Competitor three is a system capable of being placed in a plane but only measures thermal neutrons averages for the duration of a flight. And competitor four uses time-averaged thermal neutron measurements, which count record smaller averages over long periods of time.

1. TinMan, Time and energy resolved measurement of thermal neutrons in aircraft at flight altitudes.
2. Thermal neutron measurements at ground level
3. Energy averaged measurements over entire aircraft flights
4. Time averaged measurements at aircraft altitudes

Parameter	TinMan	Ground measurement	Averaged flight measurement	Time averaged measurement
Thermal Neutron measurements made at aircraft altitudes	Yes	No	Is capable but limited	Is capable but limited
Comments: TinMan was designed to fly in aircraft at flight altitudes. This includes meeting strict NASA safety, power, temperature, vibration, etc. requirements. While other systems might be capable of this, they have not met the same safety standards, and are not strictly measuring thermal nuetrons, since high altitudes there are many other interferences that can be measured, including gammay rays and high-energy nuetrons.				
Ability to measure only thermal neutrons	Yes	No	No	Can potentially measure only thermal nuetrons but not at this time
Comments: Other techniques may not be specific to thermal neutrons and the results may be contaminated by higher energy neutrons. This will lead to erroneous measurement on the thermal neutron component of the neutron flux. Separating out the thermal neutron intensity is crucial.				
Ability to track thermal neutrons at different times during the flight	Yes	No	This instrument may be able to resolve neutrons at different times	No
Comments: Other techniques do not provide the flight time dependence of the thermal neutron intensity during the flight. The neutron intensity changes with the altitude and latitude of the aircraft. If the measurements average over the entire flight, information about the thermal neutron intensity at different times flight conditions is lost.				
Unattended operation	Yes	No	No	No
Comments: TinMan was designed to operate without the need for operators or any intervention. It starts recording data when power is applied and has several features to monitor its operation and restarts if necessary. This feature is important for operation on aircraft where operator oversight may not be possible.				
Meets power requirements for aircraft operatoin	Yes	No	No	No
Comments: Because the thermal neutron intensity may depend on the particular type of aircraft, it is important that a thermal neutron detector be able to operate on a wide range of aircraft. The power needed to run must also be minimized so it can operate on either the 28 volts supplied by the aircraft, or an independent battery power source for the duration of the				

Parameter	TinMan	Ground measurement	Averaged flight measurement	Time averaged measurement
flight if necessary. With the available memory, TinMan can record data for up to 40 flights. It is the only thermal neutron detector capable of this.				
Data integrity and security	Yes	No	No	No
Comments: In the harsh radiation environment at aircraft altitudes which is ~300 times greater than at sea level, there is the possibility of data loss due to single-event effects. Because TinMan records each event with a time stamp as a list, if some part of the data gets corrupted, it does not impact other data. The data can be analyzed into any time bins after the flight. TinMan has redundant storage of these data, minimizing the possibility of losing these lists.				

Describe how your product/service improves upon competitive products or technologies.

To evaluate the susceptibility of thermal neutrons to SEE in aircraft, it is crucial to know the thermal neutron environment that planes experience while flying. Tinman is the first detector to specifically measure the thermal neutron environment continuously during a flight. The requirements for this measurement are

- The ability to fly in aircraft. In particular, it must meet the stringent conditions of air flight, including unattended operation, mechanical rigor, low power requirements, and the ability to function under environmental constraints such as temperature, pressure, vibration, all while performing with the use of non-hazardous materials.
- The detector must be able to unambiguously distinguish thermal neutrons from other radiation that is present at aircraft altitude.
- The detector must be able to correlate flight conditions such as altitude, latitude, and longitude to the thermal neutron measurements.

In addition, the data should be easily retrievable and protected against data loss through several forms of redundant data backup, while also allowing for reanalysis after the plane has landed. The analysis should be simple and not require sophisticated modeling to understand the detectors.

Many thermal neutron detectors have met some of these requirements, but TinMan is unique in that it meets all of these requirements and has demonstrated its performance in several air flights on NASA aircraft.

In the past, many measurements have used the “Bonner Sphere” method. This involves surrounding a thermal neutron detector with polyethylene material to moderate the neutrons. The physical sized of the polyethylene sphere determines the degree of thermalization and therefore can be used to determine the incident neutron energy. Understanding the response of the detector requires elaborate modeling and is mostly used for measuring the energy of high-energy neutrons.

For thermal neutrons, this is an overly complicated approach that is susceptible to uncertainties.

TinMan, however, involves two identical, small detectors. One detector is bare and measures both thermal neutrons along with everything else (high-energy neutrons, gamma rays, etc.) The second detector is covered with cadmium, which effectively blocks thermal neutrons. The difference between the two cylinder counts provides a number that demonstrates only thermal neutrons encountered during flight.

Because TinMan will have to operate on different aircraft, it was designed to be flexible in its power requirements. It can operate on batteries for the duration of the flights if necessary. In addition, it can operate unattended and does not require an operator so it is easy to put on an aircraft and has many redundancies and features that ensure reliable operation.

Describe the limitations of your product/service.

The ultimate technical goal for the avionics industry is to understand and resolve the upset rate in semiconductors in aircraft at normal flying conditions. TinMan is a significant step towards this understanding in characterizing the thermal neutron intensity in aircraft. However, it is not the final step.

In addition to thermal neutrons, which TinMan detects, there are other particles that can produce upsets in semiconductor parts and their importance may increase in the future as device architecture evolves. In addition, there are episodic events from our sun, called extreme space weather events, which can cause dramatic increases in the cosmic-ray intensity striking the earth's atmosphere. Therefore, we are currently designing the next generation instrument that will detect a wider range of cosmic-ray particles including high-energy neutrons, protons, gamma rays, heavy ions, muons, etc., that are constantly bombarding the earth as well as space weather events. This instrument, called ExMan, is based on the same operating principles of TinMan that include (1) unattended operation, (2) particle identification, (3) data logging so results can be correlated with the external environment, and (4) robust data integrity and security.

ExMan is the logical follow up to TinMan. Measurements of the radiation environment together with knowledge of the effects of these particles on semiconductor devices will provide engineers and scientists a basis for addressing the larger problems of radiation effects in solid-state devices that go beyond avionics.

To determine the upset rate in semiconductor device it is necessary to know both the external environment (how many particles at particular energies) as well as the device response to cosmic-rays (how many upsets do these particles cause). Since at terrestrial elevations, neutrons are the major concern, it is necessary to measure the neutron response of semiconductor devices. We are currently measuring the sensitivity to high-energy neutrons at the Los Alamos Neutron Science Center (LANSCE) Weapons Neutron Research (WNR) facility at the ICE House flight paths. This flight path has a high-energy neutron distribution that is very similar to the energy distribution of cosmic-ray produced neutrons but over a million times more intense.

With this capability, engineers can determine the upset rate by scaling the WNR intensity to the atmospheric intensity. We are currently proposing a similar facility that can evaluate parts with thermal neutrons. Although other places are available to test with thermal neutrons, a dedicated thermal neutron facility at LANSCE would benefit the semiconductor community.

Summary

Atmospheric radiation is a natural phenomenon showering particles onto the Earth. At terrestrial altitudes neutrons are the largest concern. These high-energy neutrons can produce thermal neutrons which are known to cause Single Event Effects (SEE) that can cause a disturbance in an electronic device.

Recently, the semiconductor industry began to recognize that Boron that is used in its semiconductor parts can produce SEE caused by thermal neutrons.

TinMan has clearly defined the thermal neutron environment in airplanes. Over more than a dozen flights on NASA aircraft, this small, portable device is the most accurate of its kind. Its continuous measurements can be joined with flight information, including altitude and longitude.

TinMan has provided the aerospace industry with vital information that can be used to assess thermal neutron intensity during flight and ensure the continued reliability of onboard electronics. TinMan's importance has been demonstrated in measurements of SEE in data centers and will be important in all applications of semiconductors where reliability is crucial.

Support Letters

- Bharat Bhuva, Vanderbilt University
- Norbert Seifert, Intel
- Alex Hands, Surrey Space Centre
- Michael Wirthlin, Brigham Young University
- Michael Elias, Honeywell
- Phillipe Pons, Aerospace Valley, France

Honeywell

February 10,2021

Re: Support for Thermal Neutron Measurement Research Project

R&D100 Review Committee,

This letter is to express Honeywell's support of the R&D 100 Award for the Thermal Neutron Measurement Research Project; a collaboration between Los Alamos National Laboratory and Honeywell.

The purpose of the project was to measure the thermal neutron environment within an aircraft. The outcome was a full evaluation of the effects of thermal neutrons on electronics in aircraft systems at typical aircraft operating conditions.

This information is necessary to the commercial aerospace industry; enabling the evaluation of the effects of thermal neutrons on electronics in aircraft systems at typical aircraft operating conditions. We now have adequate information on the thermal energy neutron environment within aircraft – meaning we can minimize the Single Event Effects within an aircraft's electronic devices.

Natural atmospheric radiation, including both high energy and thermal neutrons, is known to cause Single Event Effects in electronic devices. These effects can cause a momentary or permanent change in the state of a device, leading to unintended behaviour. While the high energy neutron environment is well defined, there was inadequate information on the thermal energy neutron environment within aircraft.

The data from this experiment defines the thermal energy neutron environment. The definition of the thermal neutron environment within an aircraft enables the aerospace industry to quantify the susceptibility of semiconductor devices to thermal energy neutrons.

This project is the foundation for work that will begin on an Extreme Space Weather Measurement Instrument. This instrument, an extension of the Thermal Neutron Measurement Instrument, will provide the characterization of the atmospheric environment during an extreme space weather event.

Sincerely,

Michel Elias

Michael Elias

VP General Manager

Electronic Solutions Space Business

3rd February 2021

Re: Support for Thermal Neutron Measurement Research Project

R&D100 Review Committee,

This letter is to express my support of the R&D 100 Award for the Thermal Neutron Measurement Research Project; a collaboration between Los Alamos National Laboratory and Honeywell.

The purpose of the project was to measure the thermal neutron environment within an aircraft. The outcome was a full evaluation of the effects of thermal neutrons on electronics in aircraft systems at typical aircraft operating conditions.

My own research has included investigations into the effects of thermal neutrons on electronics via the mechanism of single event effects (SEE). Thermal neutrons are known to cause potentially SEE through interaction with boron-10, a naturally occurring isotope that is present in boron doping in semiconductors and in insulating layers of borophosphosilicate glass (BPSG). Whilst the probability of SEE from thermal neutrons can be readily measured in the laboratory, the rate of SEEs in the aviation environment is very hard to predict due to large uncertainties in the ambient thermal neutron flux

This experiment, using the novel TinMan detector, has helped significantly to better-define the thermal neutron environment on board several types of aircraft. This in turn will help to characterise the potential SEE rate due to thermal neutrons, which is an important step in the qualification process for avionics equipment.

The ambition by the research team to continue this work in consideration of extreme space weather, which can elevate both thermal and non-thermal neutron fluxes by several orders of magnitude, is laudable and important to ensure the resilience of avionics in such conditions. I look forward to seeing the results of this campaign in the future.

Best Regards,

Dr Alex Hands

Senior Research Fellow,
Surrey Space Centre,
University of Surrey,
United Kingdom

March 1, 2021

Re: Support for Thermal Neutron Measurement Research Project

R&D100 Review Committee,

This letter is to express my support of the R&D 100 Award for the Thermal Neutron Measurement Research Project - a collaboration between Los Alamos National Laboratory and Honeywell.

The purpose of the project was to characterize the thermal neutron environment within an aircraft. The outcome was a full quantification of the flux of thermal neutrons as a function of altitude and latitude at typical aircraft operating conditions.

I have studied the impact of high- and thermal neutrons on semiconductor devices for many years. In the early 2000s it was widely believed that the "thermal neutron" problem has been solved by the removal of borophosphosilicate glass (BPSG) in modern technologies. With the introduction of Tungsten in BEOL layers near active transistor regions the problem resurfaced, however. While high-energy neutron fluxes are well known as a function of location, the same cannot be said for thermal neutrons. Consequently, the rate of SEEs in an aviation environment is very hard to predict due to large uncertainties in the ambient thermal neutron flux.

This experiment, using the novel TinMan detector, in my opinion reflects a quantum leap in the ability to accurately characterize thermal neutron fluxes and its impact on electronics as a function of location on earth and even within the aircraft itself. It is my understanding that the research team is already working on the next phase – leveraging the knowledge gained and equipment developed for characterizing particle fluxes in various radiation environments including "space weather" while in flight. I look forward to seeing the results of this campaign in the future.

Best Regards,

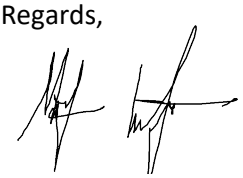

Dr. Norbert Seifert
Principal Engineer; Radiation effects team manager
Intel Corporation
2501 NE Century Blvd
Hillsboro, OR 97124; USA

email: Norbert.Seifert@intel.com
phone: +1 971-214-1700 (Office)

Intel Corporation
2200 Mission College Blvd
Santa Clara, CA 95054
www.intel.com

March 26th, 2021

Support for Thermal Neutron Measurement Research Project

R&D100 Review Committee

This letter is to express support of the R&D 100 Award for the Thermal Neutron Measurement Research Project which is based on a collaboration between Los Alamos National Laboratory and Honeywell.

This project contributes to the understanding and information of the intensity of thermal neutrons in aircraft as this is conditioned by flight altitude and latitude, and some surounding moderating materials.

Indeed, thermal neutrons can cause Single Event Effects in semiconductor devices and so potential functional disturbances at electronic equipment and systems level.

The information provided by the experiment with regard to the thermal neutrons environment within an aircraft is essential for the commercial aerospace industry, which include airframers, systems and electronic equipment manufacturers, to consider both the susceptibility of semiconductor devices to thermal neutrons and the global optimized mitigation dispositions in a cost effective approach for reliable and secure products.

Best regards.

Philippe Pons
Electronics expert for embedded systems
Tél. : +33 (0)6 82 10 97 66
Email : pons@aerospace-valley.com
Aerospace Valley
3 Rue Tarfaya, 31400 Toulouse, FRANCE

Electrical Engineering and Computer Science

VANDERBILT School of Engineering

February 22, 2021

To: R&D100 Review Committee

From: Bharat Bhuva
Professor
Department of Electrical Engineering and Computer Science

Re: Support for Thermal Neutron Measurement Research Project

I am writing this letter to strongly recommend the Thermal Neutron Measurement Research Project developed at Los Alamos National Laboratory by Dr. Stephen Wender for the R&D 100 Award.

Radiation particles, ubiquitous in the terrestrial environment, generate electron-hole pairs upon transiting through semiconductor material. These charges create voltage perturbations, resulting in loss of information in electronic circuits. Such a loss of information has been termed single-event upsets (SEU) or Soft Errors (named as such because they do not cause any permanent, or hard, damage). In the terrestrial environment, soft errors caused by high-energy neutrons, thermal neutrons, and alpha particles have dominated. There have been many characterization measurements made for alpha particles and high-energy neutrons in the terrestrial environment. They are easy to make because the energy spectrum of these particles does not very significantly from one location to another on earth. The number of high-energy neutrons does vary with elevation and has been measured accurately. Thermal neutrons, on the other hand, are very difficult to characterize and measure as they depend on the surrounding environment. Thermal neutron spectrum will vary inside a building from one room to another, and from one floor to another. It will also vary depending on the presence of liquid nearby (if there is water tank or an air-conditioning system on top of a building, it will affect the thermal-neutron spectrum inside the building). As a result, it was not possible to efficiently characterize thermal-neutron spectrum, though it was a very important need for the electronics industry.

All current integrated circuit manufacturing technologies use 3-D transistor structure called FinFET. The fabrication of FinFETs down to dimensions as small as 3 nm has required the use of ^{10}Boron during the manufacturing process. Thermal-neutrons have very high affinity to ^{10}Boron, resulting in increased vulnerability for soft errors. Recent results have shown that soft errors due to thermal-neutrons have surpassed those due to alpha particles. Since advanced technologies are essential for all critical electronic systems (autonomous driving, internet servers, healthcare systems, financial transactions, internet-of-things, etc.), characterization and mitigation of soft errors has now become a prime requirement for all designers/manufacturers/operators of electronic systems. This has made characterization of thermal-neutron spectrum a very important step towards mitigating this real threat.

The TinMan detector, developed at Los Alamos National Laboratory, has addressed this need for the electronics industry. TinMan detector allows for measurement of thermal-neutron flux and spectrum at any location with a portable instrument. Without such an instrument, it will be prohibitively expensive (and that is why it was never attempted) to characterize thermal-neutron spectrum at any location other than laboratory environments. With the proliferation of electronic systems for critical tasks is only going to increase as more automation is developed (robots on factory floors and on the street, in addition to previously mentioned applications), industry as well as society will need to address the threat of soft errors. I expect TinMan detector to provide necessary tools to the engineers to mitigate this threat. It certainly deserves the R7D100 award to recognize the contribution it will make towards keeping our electronic systems running smoothly.

Department of Electrical and Computer Engineering

Dr. Michael Wirthlin
Brigham Young University
450-P Engineering Building
Provo, UT 84602
wirthlin@byu.edu

March 23, 2021

Re: Support for TinMan Thermal Neutron Measurement Research Project

This letter is to express my support of the R&D 100 Award for the Thermal Neutron Measurement Research Project collaboration between Los Alamos National Laboratory and Honeywell. This project created a system for measuring the thermal neutron environment within an aircraft. The novel system was used within several experimental flights to confirm changes in the thermal neutron environment as a function of altitude. Thermal neutrons are known to cause single-event upsets within electronic systems by interacting with the boron-10 naturally occurring isotope present in semiconductors. The TinMan system is able to provide accurate measurements of the thermal neutron environment so that more accurate estimations can be made of single-event upsets within aircraft systems.

Thermal neutrons are of concern in a variety of other environments other than aircraft. Thermal neutrons may cause single-event upsets in automobile electronics, high-performance computing systems, and other systems where safety and data integrity are essential. The TinMan system could be used in a variety of environments to help the research community better understand the thermal neutron environment that these critical systems operate in. I anticipate that the TinMan system and its derivative ideas will continue to help the research community understand the thermal neutron environment so we can better create systems that anticipate and tolerate thermal neutron induced single-event upsets.

I strongly support this project for consideration for the R&D 100 award and am looking forward to additional results provided by this project.

Sincerely,

Principal investigator(s) from each of the submitting organizations

Team member name: Stephen Wender
Title: Scientist
Organization: Los Alamos National Laboratory, P-2
Email:Wender@lanl.gov
Phone: (505) 667-1344

Team member name: Laura Dominik
Title: Fellow
Organization: Honeywell, Inc.
Email: Laura.Dominik@honeywell.com
Phone: (763) 957-3802

Team member name: Suzane Nowicki
Title: Scientist
Organization: Los Alamos National Laboratory, ISR-1
Email:snowicki@lanl.gov
Phone: (505) 655-8838

Team member name: Aaron Couture
Title: Scientist
Organization: Los Alamos National Laboratory, P-3
Email:acouture@lanl.gov
Phone: (505) 667-1730

Team member name: Thomas Fairbanks
Title: Engineer
Organization: Los Alamos National Laboratory, ISR-4
Email:Fairbanks@lanl.gov
Phone: (505) 665-4159

Marketing and media information

Contact person to handle all arrangements on exhibits, banquet, and publicity.
First name: Janet
Last name: Mercer-Smith
Title: R&D 100 Coordinator
Organization: Los Alamos National Laboratory
Email: mercer-smith_janet@lanl.gov
Phone: 505-665-9574

Contact person for media and editorial inquiries.
First name: Janet
Last name: Mercer-Smith
Title: R&D 100 Coordinator
Organization: Los Alamos National Laboratory
Email: mercer-smith_janet@lanl.gov
Phone: 505-665-9574

For a published list of commercialization opportunities please visit:
https://www.lanl.gov/projects//feynman-center/index.shtml

Company logo

LANL LinkedIn profile URL
https://www.linkedin.com/company/los-alamos-national-laboratory

LANL Twitter handle
https://twitter.com/LosAlamosNatLab

LANL Facebook page URL
https://www.facebook.com/LosAlamosNationalLab

Appendix: Supporting Information

- "Extreme space weather: impacts on engineered systems and infrastructure," published by the Royal Academy of Engineering (February 2013)
- "ATSB Transport Safety Report Aviation Occurrence Investigation AO-2008-070," published by the ATSB (2011)
- "Physics Flash," published by Los Alamos National Laboratory, Pg. 5 (winter 2021)
- "Measurement of Thermal Neutron Environments in Aircraft with the Tinman Instrument," Los Alamos National Laboratory presentation (2019)
- "Thermal Neutron-Induced Single-Event Upsets in Microcontrollers Containing Boron-10," published by IEEE Transactions on Nuclear Science, Vol. 67, No. 1 (January 2020)
- "New capabilities for radiation effects," presentation given to LANSCE at Los Alamos National Lab (2015)
- "Advances in Atmospheric Radiation Measurements and Modeling Needed to Improve Air Safety," in Appendix," published in *Space Weather*, 13 (2015)
- "Could thermal neutrons be a threat to reliable supercomputing and self-driving cars?" published online by Science & Technologies Facilities Council (May 2020)
- "Thermal neutrons: a possible threat for supercomputer reliability,"published in The Journal of Supercomputing (2021)
- "Report on the Tin-II Thermal Neutron Detector," report published by Los Alamos National Laboratory.
- "Researchers rise to challenge of replacing helium-3," published by Science Magazine, Vol. 353, Issue 6294, pp. 15-16 (Jul y 2016)
- "Measurement of Thermal Neutrons in Aircraft," published by Los Alamos National Laboratory.
- "Measurement of Thermal Neutron Environments in Aircraft," presentation delivered to NASA (August 2018)
- "New Los Alamos technology detects thermal neutrons in aircraft," news article, Florida News Times (April, 1, 2021)

New capabilities for radiation effects

Steve Wender

Los Alamos National Laboratory

LANSCE User Group Meeting

November 2015

LA-UR-15-28523

Background

- Semiconductor devices are used in all aspects of modern life and the reliability of these devices is a major concern and may limit their applicability and performance
- LANSCE is a flexible source of radiation that can be used effectively to address many aspects of this problem
- This presentation will describe several areas where LANSCE capabilities are presently being used and areas where LANSCE can expand its role by expanding and upgrading its facilities

1 quintillion = 10^{18}
100 billion transistors for every man, woman and child on planet

There are two regimes of radiation effects

- **Massive doses of radiation** (similar to changes in mechanical properties- swelling, cracks, embrittlement- depends on DPA)
  - Significant displacements change electronic characteristics of silicon
  - Weapons environments – gain changes in transistors
  - Reactor (fission) / fusion environments
- **Single event effects:** a single particle (neutron reaction) deposits charge in a sensitive volume and causes a failure-- No mechanical analog
  - Hard failures – a failure results in a damaged device
    - Latchup
    - Gate rupture
    - Power devices (IGBT)
  - Soft errors- only data is corrupted deposited charge causes bits to flip and data to change but the device continues to operate normally
    - Single bit flips
    - Multiple bit flips- few % for single flip rate
    - The failure rate from neutron induced single event upsets is equal to all other failure rates combined
  - Accelerated testing is crucial

Radiation effect users at LANSCE

1. Avionics industry- Single event effects (SEE), requires both high-energy and thermal neutrons. Neutron flux at aircraft altitudes ~300 times sea level. First recognized by the Boeing Corp in certification of 777.
2. Semiconductor industry- Wide range of SEE studies, computer chips, automotive, graphics, servers, FPGAs, etc.
3. Medical equipment- pacemakers, etc.
4. High performance computers- silent data corruption
5. NASA- Radiation effects in space- Johnson Space Center –require 200 MeV (and above) protons- IUCF has shut down. Also needs neutrons
6. ISR Division- Radiation effects in space, requires protons and neutrons
7. Sandia- SEE and weapons effects
8. Universities- Radiation effects programs, radiation effects in detector materials and electronics

Particle beam capabilities at LANSCE – present and future

- ICE Houses: 2 flight paths to provide cosmic-ray neutron spectrum
- Lujan Center for thermal energy neutrons
- High-intensity irradiation facility

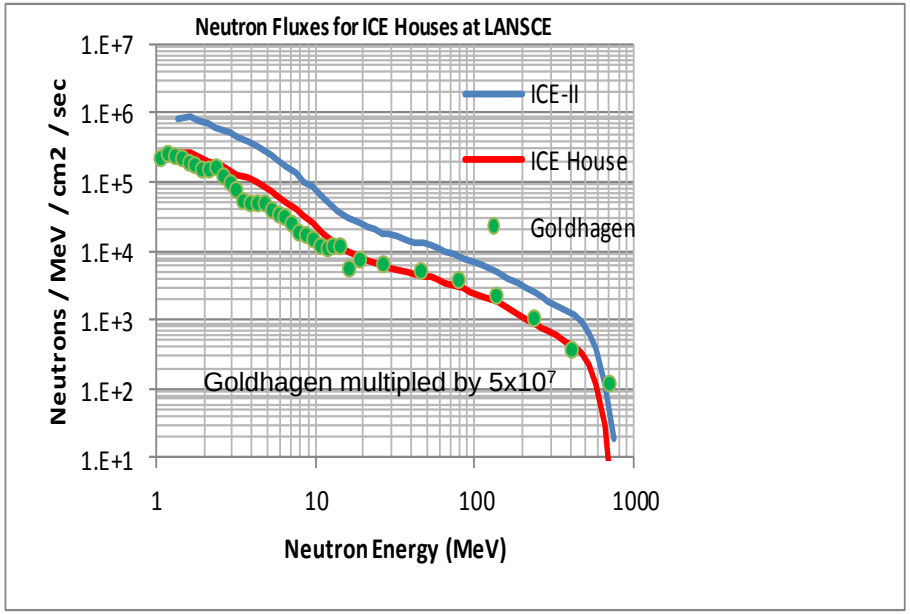

- Blue Room: Variable energy proton beams. Large impact on operation of LANSCE neutron sources
- **"Low" intensity (< 100 nA) variable-energy (200-800 MeV) proton beam in Area-A**

- **Development of thermal neutron beam at LANSCE**

Measurement of thermal neutrons in aircraft

- Recently the avionics community has become concerned about the effects of thermal neutron on flight control electronics
- High-energy neutrons are thermalized in the aircraft fuel, passengers and aircraft materials.
- These thermalized neutrons can interact with ^{10}B that is in the semiconductor parts. ^{10}B can capture a neutron and produce an energetic alpha particle which can deposit enough charge to cause a single-event upset.
- To understand the effect of thermal neutrons in aircraft need to know:
  - Thermal neutron intensity in airplane—Airplane dependent- Tinman
  - Effect of thermal neutrons on semiconductor devices- measure at Lujan Center
  - Model / simulations of thermalization of neutrons in aircraft- MCNP calculations

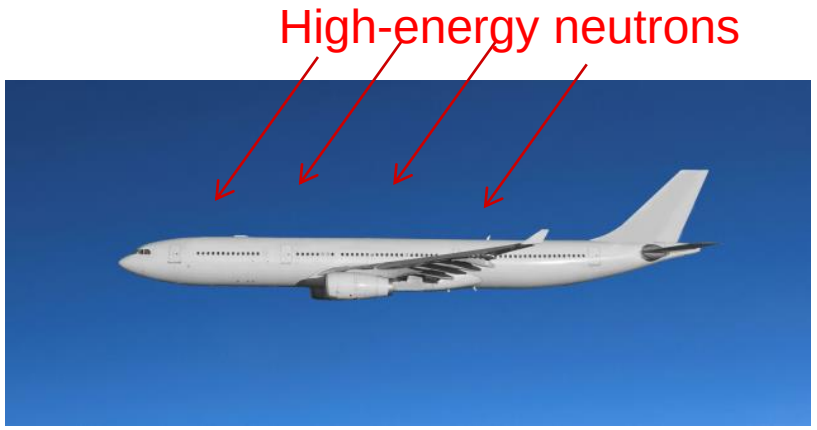

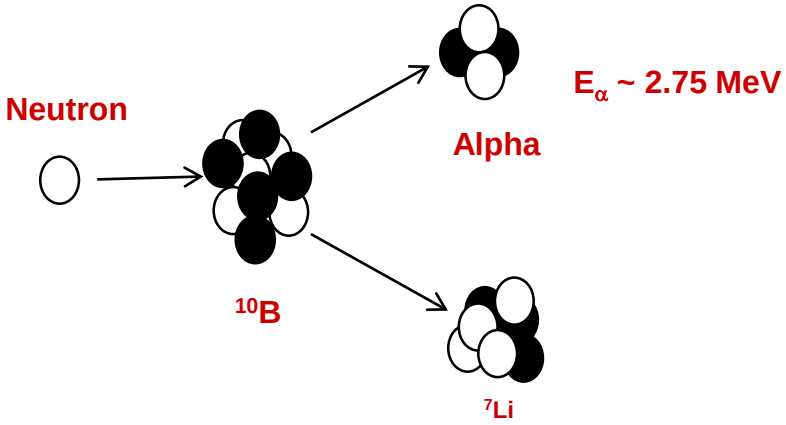

Measurement of thermal neutron intensity in aircraft--Tinman

- A detector was designed in LANSCE-NS to measure thermal neutrons in aircraft
  - Two cylindrical ^{3}He ion chamber detectors. (~1 cm diam 4 cm long)
  - One detector was bare, one detector was shielded with cadmium to block thermal neutrons
  - The difference in count rates between these two detectors gives the thermal neutron rate
- Final detector was fabricated by ISR Division to space specifications.
- Uses a Raspberry Pi computer for DAQ

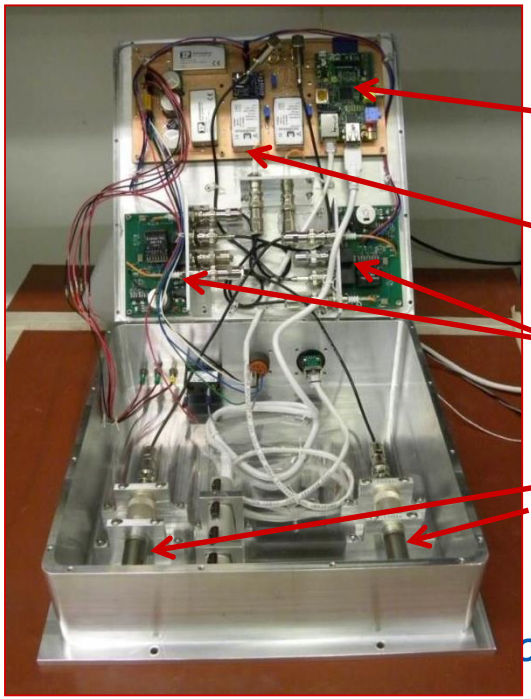

Vibration damping springs

Tinman flew in an ER-2 airplane

- ER-2 is civilian version of U-2 spy plane
- Maximum altitude is classified
- Flew on 4 flights from NASA Armstrong Flight Research Center in Palmdale Ca

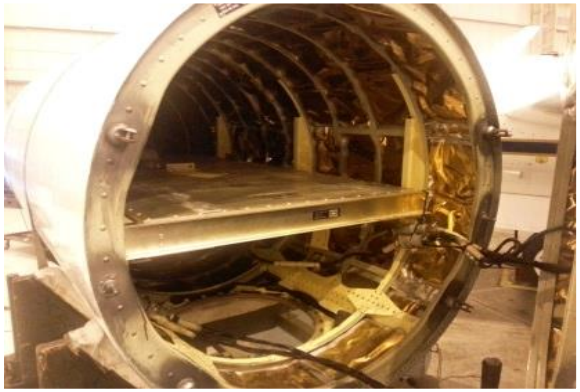

Preliminary results look like detector operated correctly

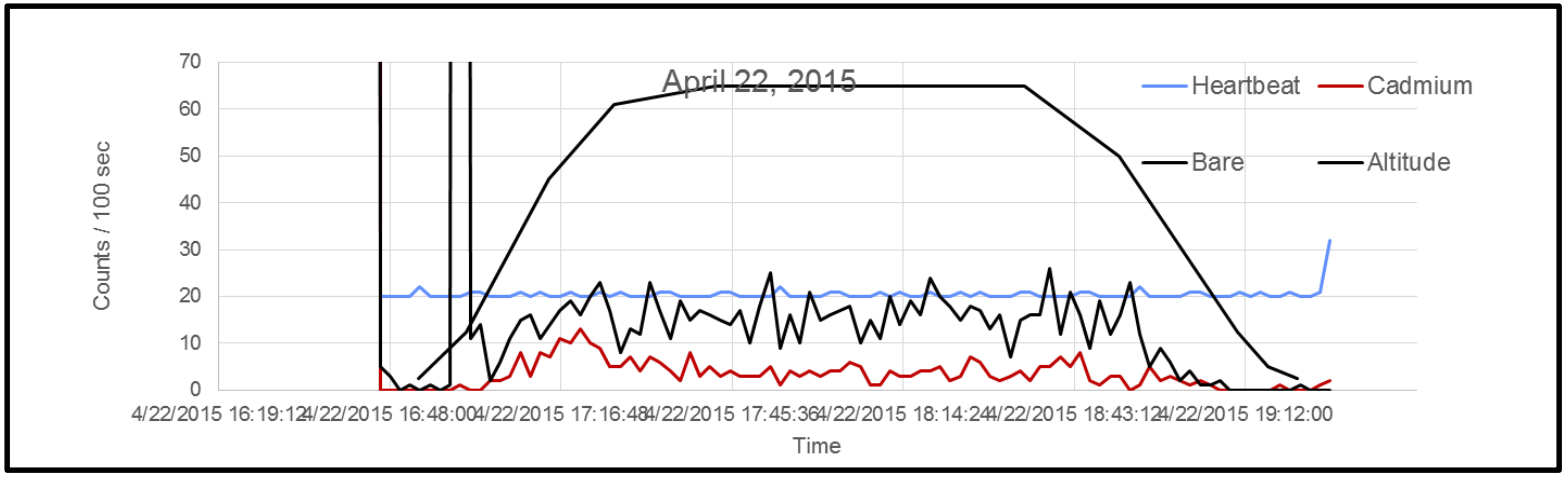

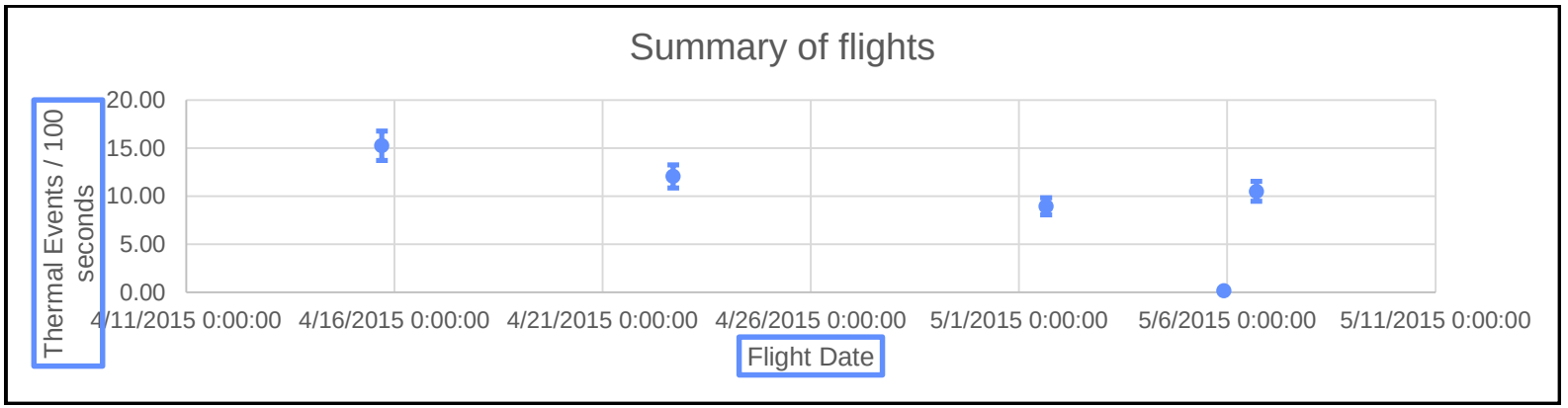

Thermal neutron testing at Lujan Center

- First measurements of thermal neutron SEE were performed 2014 cycle at Lujan Center on FP 12
- Used Cd filter technique to get a pure thermal spectrum
- Problem was FP12 had liquid hydrogen moderator which was not prototypic of temperature of neutrons in aircraft
- DAQ was made for very low energy neutrons. Integration time was on order of several microseconds.
- Next run cycle
  - Develop a room temperature FP probably FP 15 (PCS), FP16 (Pharos) or FP 12 with water moderator
  - Upgrade signal processing electronics. 100 ns integration times

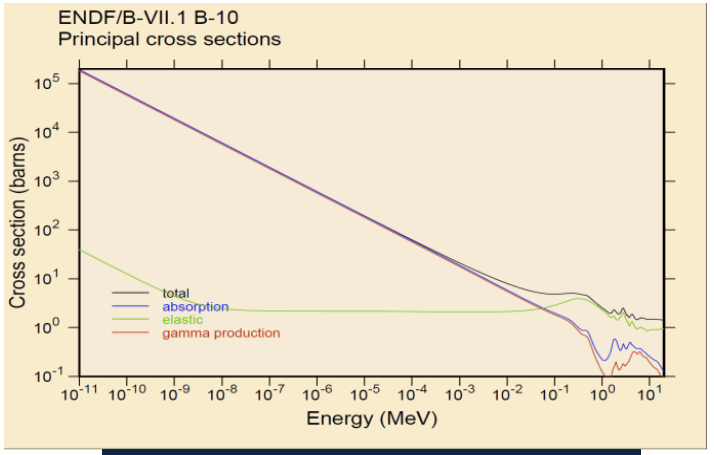

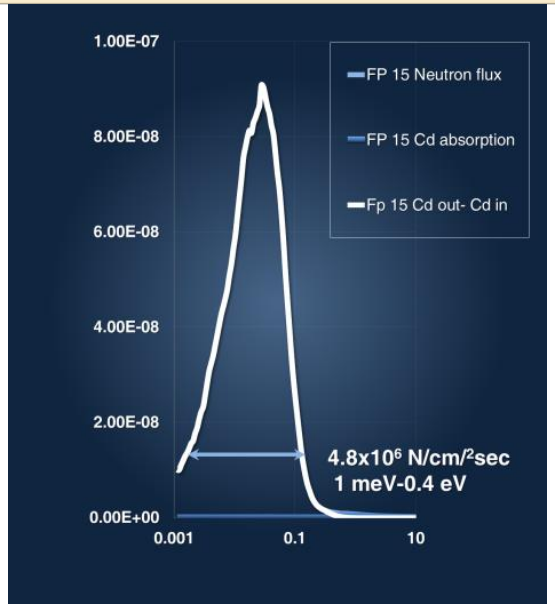

Next Steps

- **Measure thermal neutron intensity on commercial (larger) airplane**
- **Measure effect of thermal neutrons on semiconductor devices at Lujan Center → new flight path**
- **Develop Monte-Carlo model of airplane and compare predictions of MC simulations with measurements**

- **Development of proton source at LANSCE**

Low-intensity proton beam in Area A

- With the closing of IUCF, there is a serious national need for low-current proton beams in the energy range from 200 – 800 MeV. Last year IUCF had 1500 hours of irradiations at ~$500-$800 / hour= ~ $1M. Other places charge more.
- Although such beams are available in the Blue room, the impact is large for Target-4 and Target-1 when running at other than 800 MeV or using the PSR beam
- A low-power (100 nA) experimental area could be established in Area A, which would meet the needs of NASA, ISR, Isotope production, Industry, Universities, detector materials irradiation and other users **without impacting the present research program at LANSCE**
- 1 Hz of H+ beam delivered to this area would produce as much as 1 mA/120Hz=8 uA of average beam current. 1 Hz operation would have insignificant impact on other beam users.
- 100 nA (=$6x10^{11}$ protons/sec) is roughly the current presently delivered to Target-2. Target-2 is shielded with approximately 22 feet of dirt. This is roughly the same as 4 feet of steel. I believe we have sufficient shielding on hand to construct a small experimental cave (~15’ X 20’) in Area-A.
- Establishing a of low-power experimental area in Area-A will be a step towards high-power operation and other applications

LANSCE accelerator and experimental areas

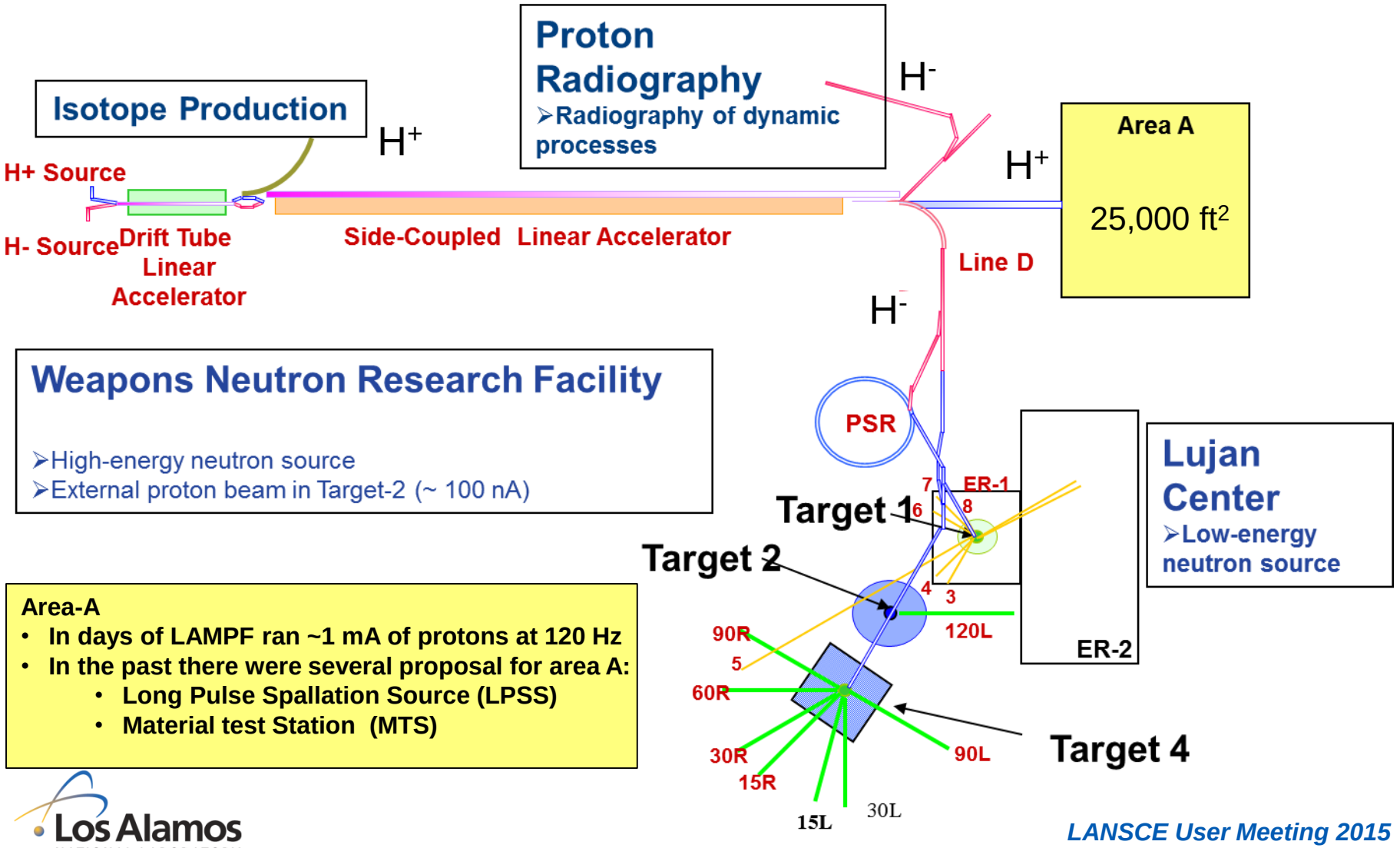

Area-A

- **In days of LAMPF ran ~1 mA of protons at 120 Hz**
- **In the past there were several proposal for area A:**
  - **Long Pulse Spallation Source (LPSS)**
  - **Material test Station (MTS)**

Low-intensity proton beam in Area A (2)

- Developing this experimental area will exercise several capabilities that will be necessary for any future use of Area-A. These include:
- Simultaneous transport of both H+ and H- beams through 805 MHz part of the linac
  - Alignment needs to be checked
  - Haven't sent beam down to Area-A in ~15 years

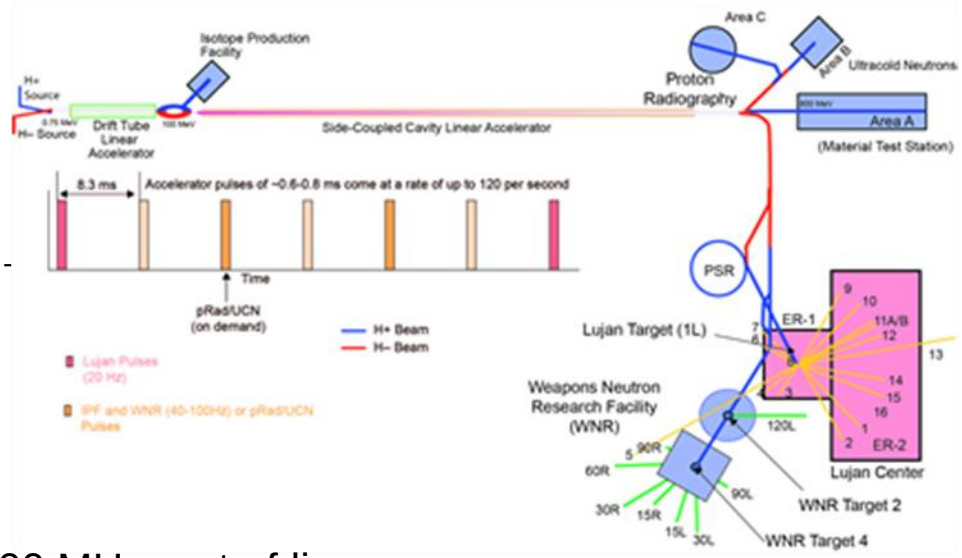

- Switching the beam between IPF and 800 MHz part of linac-
  - Need glass beam line (~$100K)
  - Have pulsed magnet, modulator
  - New lattice parameters for IPF and Area-A operation
- Operating dual energy in the accelerator
- All the other issues with beam transport to Area-A (magnets, beamlines, etc.) that have developed since Area-A was last used.

New facility for proton irradiations in Area-A

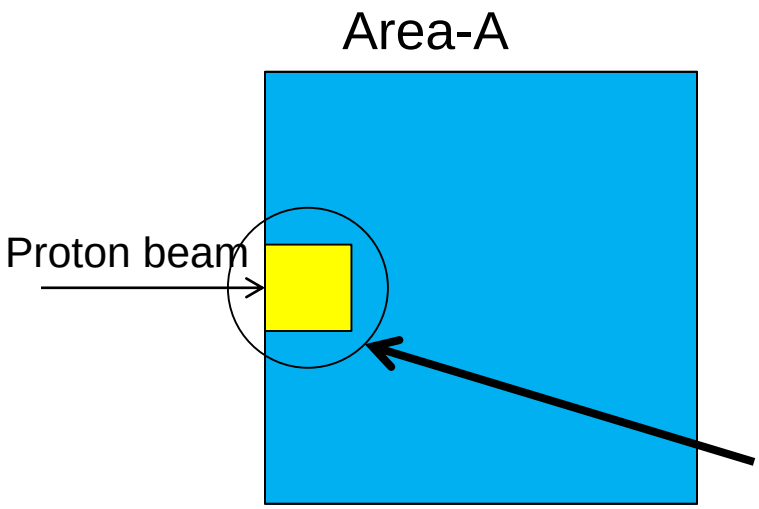

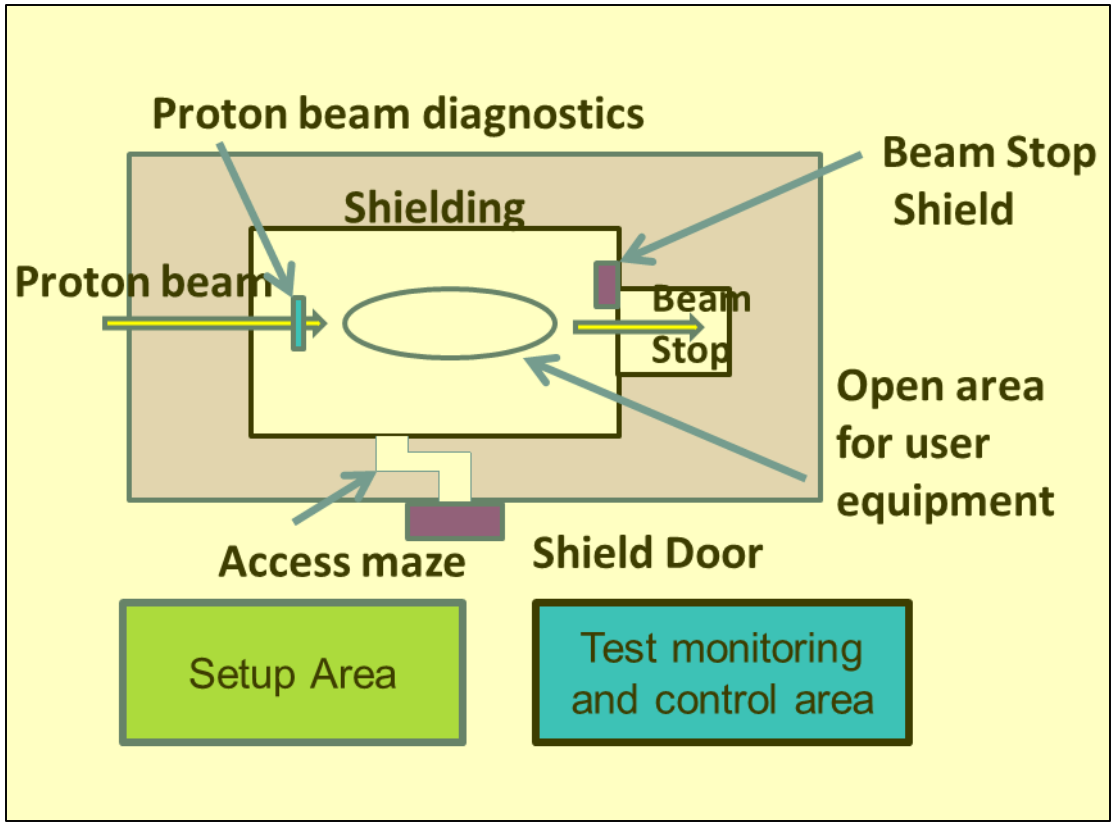

- **Area-A has excellent infrastructure**
  - Overhead crane
  - Electrical power
- **Area beyond experimental area can be used for other activities**

Next steps for protons in Area-A

- **Explore the interest of possible users for low-intensity proton beams**
- **Engage community in design and specification for new facility**
- **Develop cost and schedule estimate for installing target area in Area-A**
  - Beam transport, control systems
  - Experimental area design, shielding, beam stop, etc.
  - Proton beam diagnostics
  - Everything else
- **Write proposal and give to Lab management**

High-intensity neutron irradiation at Target-4 “East-Port”

High-fluence neutron irradiations are performed at the Target-4 “East Port”

- **0.9 m from neutron production target**
- **Neutron flux ~3x10^{13} n/cm^2/day for 1-100 MeV & 100-800 MeV**
- **Sample holder – 8.5 cm dia., 20 cm length**
- **Now irradiating**
  - LYSO (Cerium-doped Lutetium Yttrium Orthosilicate) - rad-hard scintillator studies (Caltech+LANL)
  - GaN, SiC photodiodes, LEDs, HEMT, MOSFET - semiconductor radiation hardness studies (UNLV+LANL)

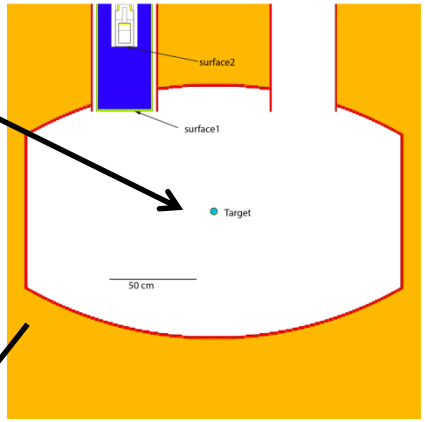

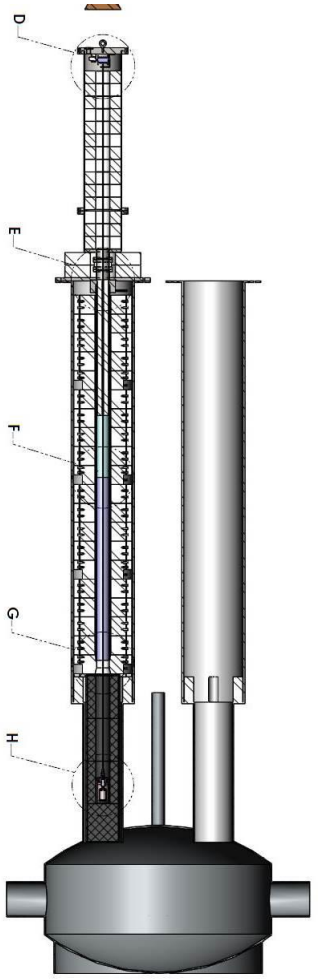

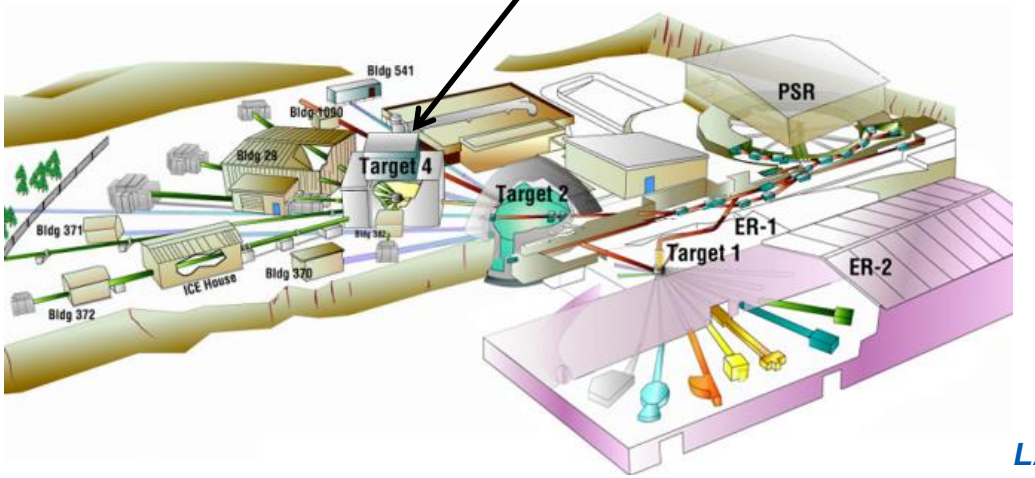

East Port Neutron Energy Spectra Cover a Wide Range

Energy	Neutrons/cm^2/day
1eV-1keV	5.9E+13
1keV-1MeV	1.1E+14
1MeV-100MeV	2.5E+13
100-800MeV	2.9E+13

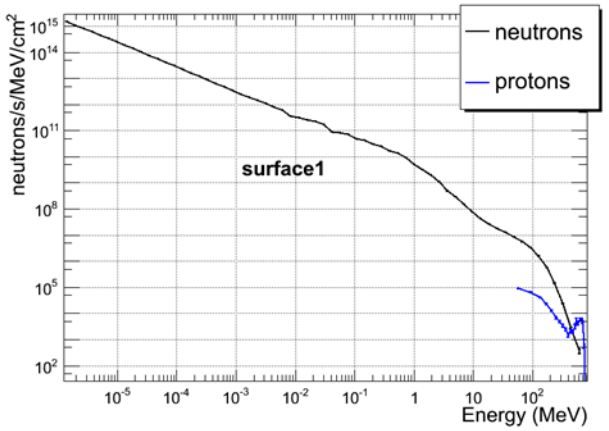

- The neutron spectrum can be moderated for greater thermal neutron flux
- Designed and implemented for ^{99}Mo production from ^{235}U fission
- Present applications are
  - Electronics for NIF diagnostics and space applications
  - Scintillators for LHC future detectors and MaRIE
- Future – Potential for Isotope Production, Materials Damage, High-Energy Dosimetry

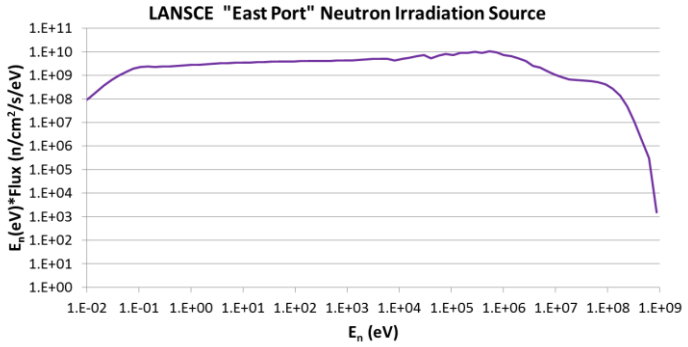

Conclusions

- **There are several exciting new capabilities that we are considering for electronics and materials irradiations at LANSCE**
  - Room-temperature thermal neutron irradiation capability
  - Low-intensity proton beams (250 MeV – 800 MeV, ~ 100 nA)
  - High-intensity neutron irradiations
- **We are looking for comments and input from our user community on these upgrades**

Thermal Neutron-Induced Single-Event Upsets in Microcontrollers Containing Boron-10

Elizabeth C. Auden, *Member, IEEE*, Heather M. Quinn, *Senior Member, IEEE*, Stephen A. Wender, John M. O'Donnell, Paul W. Lisowski, Jeffrey S. George, *Senior Member, IEEE*, Ning Xu, Dolores A. Black, *Senior Member, IEEE*, and Jeffrey D. Black, *Senior Member, IEEE*

***Abstract*— Single-event upsets (SEUs) were measured in thermal neutron-irradiated microcontrollers with 65- and 130-nm-node static random-access memories (SRAMs). The suspected upset mechanism is charge deposition from the energetic byproducts of ^{10}B thermal neutron capture. Although elemental analysis confirmed that both microcontrollers contain ^{10}B, only the 65-nm node microcontroller exhibited a strong response to thermal neutrons. Monte Carlo simulations were performed to investigate the effects of ^{11}B enrichment on thermal neutron-induced SEUs in a 65-nm SRAM node when boron is present in the *p*-type well, *p*-type source and drain, or tungsten plug. Simulations indicate that the byproducts of ^{10}B(n, α) ^{7}Li reactions are capable of generating sufficient charge to upset a 65-nm SRAM. The highest amount of charge deposition from ^{10}B(n, α) ^{7}Li reaction byproducts occurs when natural boron is used to dope the *p*-type source and drain regions. Simulations also show that the SEU cross section is nonnegligible when ^{11}B-enriched boron is used for doping.**

***Index Terms*— Microcontrollers, neutrons, radiation effects, semiconductor device doping, semiconductor device modeling, single-event effects (SEEs), static random access memory (SRAM) cells.**

I. Introduction

THERMAL neutron-induced single-event upset (SEU) susceptibility has been reported since the 1980s for several electronic components reported to contain ^{10}B in borophosphosilicate glass (BPSG) layers, boron-doped *p*-type silicon, or tungsten plugs which have been fabricated using process gasses that contain boron. The risk of introducing ^{10}B into a part through any of these sources is the high cross section for ^{10}B thermal neutron capture and subsequent production of energetic charged particles that can cause single-event effects (SEEs) in sensitive volumes. The thermal neutron capture cross section for ^{11}B is much lower, and the nuclear reactions with 25-meV neutrons do not produce energetic charged particles capable of causing SEEs. A comparison of ^{10}B and ^{11}B neutron capture reactions is addressed in Section III.

Manuscript received July 2, 2019; revised August 19, 2019; accepted November 2, 2019. Date of publication November 6, 2019; date of current version January 29, 2020.

E. C. Auden, H. M. Quinn, S. A. Wender, J. M. O'Donnell, P. W. Lisowski, J. S. George, and N. Xu are with the Los Alamos National Laboratory, Los Alamos, NM 87544 USA (e-mail: eauden@lanl.gov).

D. A. Black and J. D. Black are with the Sandia National Laboratories, Albuquerque, NM 87185 USA.

Color versions of one or more of the figures in this article are available online at http://ieeexplore.ieee.org.

Digital Object Identifier 10.1109/TNS.2019.2951996

The literature contains many reports of thermal neutron-induced SEEs for components containing ^{10}B, such as static random access memories (SRAMs), dynamic random access memories (DRAMs), and power metal–oxide–semiconductor field effect transistors (MOSFETs), but there is little information about thermal neutron-induced SEEs in microcontrollers. BPSG was the first source of ^{10}B to be associated with thermal neutron-induced SEEs in semiconductor components. BPSG can be inserted as an insulating layer between metallization layers during fabrication. BPSG is attractive to the manufacturing process because it has a lower melting point than silicon dioxide. Thermal neutron-induced SEEs were reported for DRAMs and SRAMs containing BPSG in [1]–[3], and the 20% abundance of ^{10}B in the natural boron used in BPSG layers was identified as the culprit. Semiconductor foundries started to leave BPSG out of the manufacturing process at the 180-nm node and below, yet thermal neutron-induced SEEs have continued to be reported for modern components suspected to contain BPSG, such as 0.22-μm SRAMs [4]. Other modern components, such as the deep-submicrometer SRAM-based FPGAs described in [5], attribute thermal neutron-induced SEE sensitivity to ^{10}B introduced through other processing steps. Two such vectors for adding ^{10}B to the fabrication process, boron doping and processing gasses, are discussed below.

Boron doping in *p*-type silicon has been recognized as another source of ^{10}B contributing to thermal neutron-induced SEEs. Although ^{11}B-enriched manufacturing products (with a much lower thermal neutron capture cross section) are available for boron doping (such as [6]), the additional cost compared to natural boron may preclude their use in *p*-type doping for commercial-off-the-shelf (COTS) components not specifically designed for radiation tolerance. Boron-doped *p*-type silicon has been identified as the source of ^{10}B associated with soft errors in 40-nm SRAMs [7], single-event burnout (SEB) in power MOSFETs [8], and changes in charge collection efficiency in complementary metal–oxide semiconductor (CMOS) active pixel sensors [7], [9].

Diborane (B_2H_6) and boron trifluoride (BFl_3) are gasses used in interconnect processing to aid the nucleation of tungsten plugs in devices at the 90-nm node and below [10], [11]. Thermal neutron-induced soft errors attributed to ^{10}B in tungsten plugs have been reported for SRAMs [10], [12] and

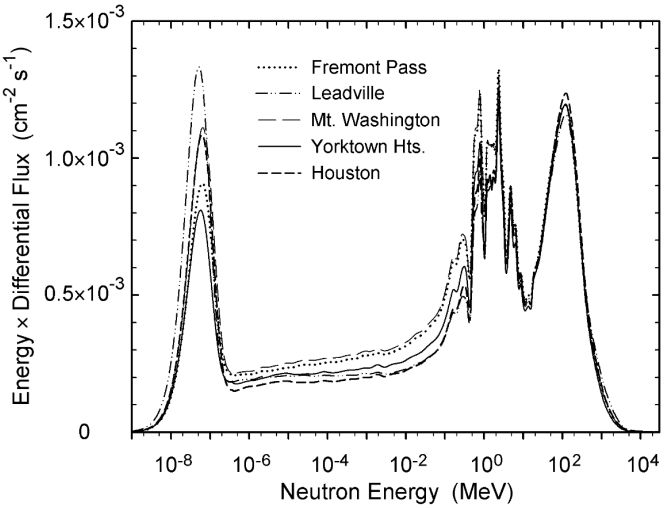

Fig. 1. Atmospheric neutron spectrum measured around the USA. [17].

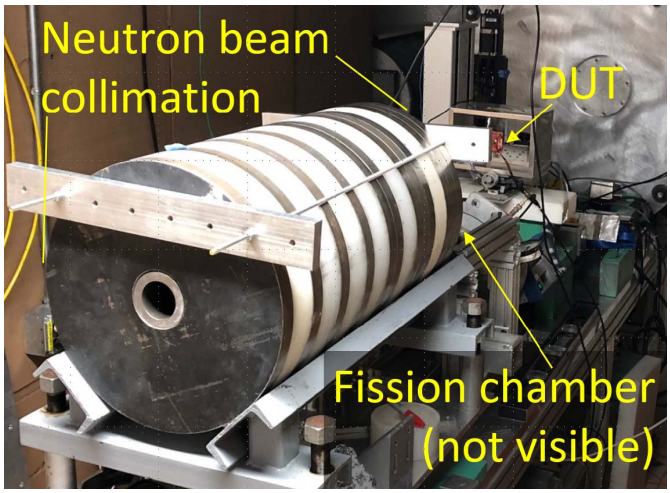

Fig. 2. Tiva microcontroller test board mounted in the neutron beam path in the Lujan Center Flight Path 5 target room. The fission chamber used to measure neutron fluence is hidden behind the neutron beam collimator.

flip-flops [12], [13] as well as 14- and 22-nm finFETs [14]. As with the manufacturing products used for boron doping, diborane and boron trifluoride can be purchased with ^{11}B-enrichment instead of natural boron. For instance, BFl_3 can be purchased with natural boron or ^{11}B-enrichment to 99.8% as an ion implant grade product [15].

^{10}B can increase SEE susceptibility because it has an unusually high nuclear cross section of 3845 barns (where 1 barn $= 10^{-24}$ cm^2) for thermal neutrons [16]. For comparison, the thermal neutron cross section is 5.28 barns for ^{11}B and 2.24 barns for Si, and these reactions are primarily elastic collisions that do not produce ionizing byproducts. The isotopic abundance of natural boron is 19.8% ^{10}B and 80.2% ^{11}B [16], so the presence of ^{10}B can be significant if natural boron is used instead of ^{11}B-enriched manufacturing products.

Thermal neutron-induced SEEs may contribute significantly to a device's total SEE cross section in the terrestrial environment. Thermal neutrons are present in the atmospheric spectrum, as shown in Fig. 1 [17]. The atmospheric spectrum also contains fast neutrons that can be slowed down to thermal energies through capture and scattering processes in materials containing hydrogen. This may be a particular problem for avionic systems, where the high-energy neutron rate is ∼300 times higher than sea level and the proximity of large amounts of thermalizing material (fuel) is present [18]. Thermal neutrons may also be present but uncharacterized in broad spectrum test facility beams.

Normand *et al.* [3] advise measuring SEE rates for parts irradiated with both thermal neutrons and high-energy neutrons, and this guidance is formalized in the JESD89A standard [19]. The presence of boron does not automatically consign a device to increased thermal neutron sensitivity. The SEU rate depends on whether natural boron or ^{11}B-enriched boron was used in processing, the proximity of ^{10}B to sensitive volumes, and whether the charge deposited by thermal neutron capture byproducts within a sensitive volume exceeds the critical charge Q_{crit} of the device.

In this work, we compare the thermal neutron and high-energy neutron SEU rates for two COTS microcontrollers (one 65 nm, one 130 nm). Both microcontrollers have technology nodes scaled below the BPSG phase-out, and elemental analysis confirms that both devices contain ^{10}B. Although Q_{crit} is not known for either device, the 65-nm node microcontroller likely has a lower Q_{crit} due to the smaller critical feature size. We use simulations performed with the stopping range of ions in matter (SRIM) code to demonstrate that the α-particle and Li ion byproducts emitted through ^{10}B thermal neutron capture are capable of upsetting the 130- and 65-nm nodes. We also use simulations performed with the Monte Carlo radiative energy deposition (MRED) code to compare charge deposition in the sensitive volume of a 65-nm SRAM structure when natural boron or ^{11}B-enriched boron is located in the *p*-type source and drain, the *p*-type well, or a tungsten interconnect plug.

II. Thermal Neutron-Induced SEUs

A. Thermal Neutron Irradiation of Microcontrollers

Two Texas Instruments microcontrollers, a Tiva TM4C123GH6PM ("Tiva") and an MSP430F2619 ("MSP430"), were irradiated at the Los Alamos Neutron Science Center (LANSCE) Lujan Neutron Scattering Center [20]. At the LANSCE linear accelerator, pulses of protons strike a tungsten neutron production target and produce high-energy neutrons via spallation reactions. These neutrons are moderated in hydrogeneous material surrounding the target and collimated to produce a primarily thermal and low-energy neutron beam. The resulting neutron beam is transported in Lujan Flight Path 5 (FP5) to an experiment station 9 m from the production target. A ^{235}U fission chamber at the exposed device location measures neutron fluence and the neutron energy spectrum using time-of-flight techniques.

The duration of irradiations ranged from 6.5 to 11.5 h. The microcontroller devices under test (DUTs) were each placed at normal incidence to the 2" diameter beam spot. Fig. 2 shows a photograph of the experiment setup in the beam. Unlike fast

neutron tests, only one part at a time was tested in the neutron beam to avoid attenuation issues.

Both microcontrollers executed the cache test benchmark code during irradiation [21] with the maximum array size that could be compiled. The 32-bit architecture, 65-nm node Tiva [22] was tested with an array size of 8053. The 16-bit architecture, 130-nm node MSP430 [23] was tested with an array size of 600. The total number of bits tested was 257 696 bits for the Tiva and 9600 bits for the MSP430. The parts were tested at nominal voltage and temperature.

The FP5 beam includes thermal, epithermal, and some fast neutrons. It is not possible to shield the more energetic neutrons while passing the lower energies. Instead, the devices were tested twice: once with the unmodified beam and a second time with a cadmium filter to remove thermal neutrons. The difference in cross sections for these two cases gives the contribution from thermal and epithermal neutrons.

The beam fluence was determined from both the total beam current (measured before the neutron production target) and locally at the fission chamber. Neutron counts with time-of-flight values between 10 and 600 μs (corresponding to energies between about 1.5 eV and 5.5 keV) were largely unaffected by the cadmium filter and were an effective means to normalize the relative fluence between runs. Table I provides the filter conditions, beam information, fluence Φ of neutrons with energies below the cadmium cutoff, number of fission chamber counts cts with times-of-flight between 10 and 600 μs, and the recorded number of cache errors n. Unfortunately, a problem with the data acquisition recording resulted in a loss of fission count data for several runs, but the total beam current for the run was still available. Because the beam spectrum is stable and well measured, the neutron fluences for the exposure and for the thermal region are simply a linear function of the beam current. This calculation allowed us to recover the total and thermal fluences for these runs.

B. SEU Analysis

Errors observed in the cadmium filtered runs are essentially "background errors" from fast and epithermal neutrons after the thermal contribution has been filtered from the beam. To perform the background subtraction on unshielded runs that include thermal neutrons, we scaled the measured background errors n_{Cd} to the equivalent fluence of the unshielded run. The difference between the observed errors $n_{\mathrm{no\_Cd}}$ including thermal neutrons and the scaled background gives the errors due to thermal neutrons n_{th}

$$n_{\mathrm{th}} = n_{\mathrm{no\_Cd}} - f n_{\mathrm{Cd}}. \tag{1}$$

The normalization factor f can be calculated from fission counts cts attributed to the portion of the neutron beam that was well-characterized but unaffected by the cadmium filter (that is, neutrons with times-of-flight between 10 and 600 μs)

$$f = \frac{\sum \mathrm{cts}_{\mathrm{no\_Cd}}}{\sum \mathrm{cts}_{\mathrm{Cd}}}. \tag{2}$$

Fission chamber counts between 10 and 600 μs were not recorded for the cadmium-filtered MSP430 irradiation

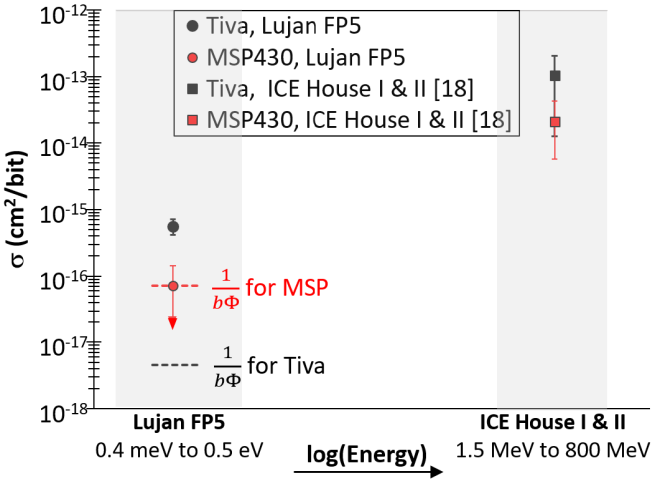

Fig. 3. SEU cross sections for the Tiva and MSP430 microcontrollers irradiated with thermal neutron and high-energy neutrons. The red and black dotted lines show the null cross sections for the Tiva and MSP430, respectively.

listed in Table I. However, the empirical ratio of beam current to fluence and counts was consistent for the Tiva and MSP430 irradiations without the cadmium filter, so we assumed that the ratio of beam current to fluence and counts was also consistent for the irradiations with cadmium filtering. Fluence for the MSP430 irradiation with cadmium filtering was, therefore, scaled from beam current measured during that exposure.

The thermal neutron SEU cross section σ_{th} (normalized to the number of tested bits b) was calculated by dividing the number of errors n_{th} attributed to thermal neutrons by the fluence of thermal neutrons below the cadmium cutoff. From (1) and (2)

$$\sigma_{th} = \frac{\sum n_{\mathrm{no\_Cd}} - f \sum n_{\mathrm{Cd}}}{b \sum \Phi_{\mathrm{no\_Cd}}}. \tag{3}$$

By convention, the cross sections for null data sets are represented as $1/b\Phi$ [21].

Table II provides the number of bits tested, normalization factors, errors attributed to thermal neutrons, thermal neutron SEU cross sections, and, for comparison, the null data set cross sections $(b\Phi_{\mathrm{no\_Cd}})^{-1}$ (that is, the cross section calculated assuming the next neutron would have caused an error) for the Tiva and MSP430 microcontrollers. Fig. 3 shows per-bit SEU cross sections for microcontrollers irradiated at Lujan FP5 in this work. Published SEU cross sections from high-energy neutrons σ_{HE} are also included for the same microcontroller models irradiated at the LANSCE Weapons Neutron Research Facility Target 4 (ICE House I and II) in December 2014 [21].

The Lujan FP5 Tiva data set included more than 50 errors, so the cross-sectional error bars are calculated from the normal distribution as in (4a). Error bars for the MSP430 cross section were calculated from the lower and upper Poisson 95% confidence limits ($l_{\mathrm{lower}(n)}$, $l_{\mathrm{upper}(n)}$) for small sample populations of size n provided in [21] as in (4b). A zero lower

TABLE I
CADMIUM FILTER, BEAM INFORMATION, FLUENCES, FISSION CHAMBER COUNTS, AND CACHE ERRORS FOR TWO MICROCONTROLLERS

Microcontroller	Cadmium filter in beam	Beam (μA-min)	Fluence Φ (cm^{-2}) Neutron energy < Cd cut-off	Number of fission chamber counts *cts* between 10 μs and 600 μs	Number of errors *n*
Tiva	No	73,040	8.46×10^{11}	1.87×10^{7}	172
Tiva	Yes	117,297	3.46×10^{10}	3.01×10^{7}	80
MSP430	No	122,479	1.44×10^{12}	3.18×10^{7}	1
MSP430	Yes	135,360	3.99×10^{10}	3.46×10^{7}	1

TABLE II
NORMALIZATION FACTOR, THERMAL NEUTRON ERRORS, AND SEU CROSS SECTIONS FOR TWO MICROCONTROLLERS

Microcontroller	Bits tested *b*	Normalization factor *f*	Number of thermal neutron-induced errors n_{th}	SEU cross section σ_{th} (cm^2/bit) (with 95% confidence)	Null cross section σ_{null} (cm^2/bit)
Tiva	257,696	0.62	122	$5.76 \times 10^{-16} \pm 1.46 \times 10^{-16}$	4.59×10^{-18}
MSP430	9,600	0.92	0	7.21×10^{-17} (0, 1.75×10^{-17})	7.21×10^{-17}

limit is represented as a downward arrow in Fig. 3

$$\text{Errorbars}(n > 50) = \pm\frac{2\sqrt{n}}{\Phi b} \tag{4a}$$

$$\text{Errorbars}(n \leq 50) = \frac{n - l_{\text{lower}}(n)}{\Phi b}, \frac{l_{\text{upper}}(n) - n}{\Phi b}. \tag{4b}$$

The SEU cross sections attributed to thermal neutrons σ_{th}, and high-energy neutrons σ_{HE} in Fig. 3 can also be used to estimate the likelihood that a component contains BPSG, according to [3]. Normand *et al.* [3] asserted that if "Ratio-SEU," the ratio of σ_{th} to σ_{HE}, is greater than ~0.2, BPSG is present. When Ratio-SEU is less than 0.2, BPSG is not likely to be present. The Ratio-SEU value for the Tiva microcontroller is less than 0.01, so under this metric, the Tiva is unlikely to contain BPSG.

Ratio-SEU is not calculated for the MSP430 since the number of errors attributed to thermal neutrons was 0. If we calculated Ratio-SEU for the MSP430 using the null result convention (assuming the next incident neutron would have generated an SEU), the Ratio-SEU value for the MSP430 would also be less than 0.01, suggesting that BPSG is not present.

C. Elemental Analysis to Confirm the Presence of ^{10}B

Elemental analysis of the Tiva and MSP430 microcontrollers was performed to experimentally establish the presence of ^{10}B and to determine the isotopic ratio of ^{10}B to ^{11}B. Secondary ion mass spectrometry (SIMS) and inductively coupled plasma-mass spectrometry (ICP-MS) were performed at the Los Alamos National Laboratory, Los Alamos, NM, USA. Laser ablation-inductively coupled plasma-mass spectrometry (LA-ICP-MS) was performed at Applied Spectra, West Sacramento, CA, USA. While none of these techniques can pinpoint the location of ^{10}B in either microcontroller, they all confirmed that ^{10}B is present in both microcontrollers and that the ratio of ^{10}B to ^{11}B is commensurate with the isotopic abundance of natural boron in both the Tiva and the MSP430. The three elemental analysis techniques were performed on samples taken from the entire microcontroller parts (including the packaging, which could contain boron nitride). First, the external leads were clipped off the part, and then the part was broken into separate samples. Because the Tiva microcontroller showed errors in response to thermal neutron irradiation, the ICP-MS analysis was repeated for an additional Tiva part to measure the boron isotope ratio and identify trace elements specifically in the silicon chip. The packaging, external leads, and copper ground plate were removed with fuming nitric acid.

TABLE III
ISOTOPE ANALYSIS TECHNIQUES, THE PRESENCE OF ^{10}B, AND RATIO ^{10}B TO ^{11}B

Microcontroller	Technique	^{10}B present?	Ratio of ^{10}B to ^{11}B
Note: the ratio of 10B to 11B in natural boron is 0.242.			
Tiva	LA-ICP-MS	Yes	0.242 ± 0.007
Tiva	ICP-MS	Yes	0.244 ± 0.006
Tiva	SIMS	Yes	--
Tiva (chip only)	ICP-MS	Yes	0.256 ± 0.006
MSP430	LA-ICP-MS	Yes	0.241 ± 0.006
MSP430	ICP-MS	Yes	0.250 ± 0.006
MSP430	SIMS	Yes	--

Table III lists the confirmation of ^{10}B and the determination of the isotopic ratio of ^{10}B to ^{11}B for both microcontroller parts and the Tiva silicon chip. Table IV lists trace elements found during ICP-MS analysis in the three parts. Note that tungsten was only reported for the Tiva silicon chip; the stated value of 30 ng/g was near the limit of detection for this element detected on the ICP-MS equipment used. It is conceivable that tungsten was present in the Tiva and MSP430 microcontroller parts also analyzed with ICP-MS, but the quantity was too small to be detected relative to the amount of other elements.

It was observed by the SIMS optical imaging that the two microcontrollers have different stamp labels on their surfaces: "Philippines" on the Tiva and "Taiwan" on the MSP430 as

TABLE IV
TRACE ELEMENTS IDENTIFIED THROUGH THE ICP-MS ANALYSIS

Element	Tiva, ng/g	Tiva (chip only), ng/g	MSP430, ng/g
Lithium	8.6	18	6.2
Boron	116	260	100
Magnesium	876	1,100	11,300
Aluminum	2,810	5,200	14
Titanium	6.4	<4	3
Vanadium	2.5	<4	2.3
Manganese	342	110	90
Iron	1,170	<1,100	1,510
Cobalt	17.6	13	7
Nickel	1,250	<960	1,570
Copper	36,900	290,000	26,700
Zinc	1,830	4200	7,000
Gallium	22.1	9.6	4.27
Germanium	2.3	7.4	1.5
Rubidium	10.3	29	6.06
Strontium	15.4	56	7.2
Yttrium	0.53	1.1	0.28
Palladium	<0.53	2.1	<0.55
Silver	77	<11	119
Cadmium	21.7	62	1.79
Tin	5.9	4.3	1.4
Antimony	9.2	4.3	21.9
Barium	439	170	78
Lanthanum	0.53	<0.1	0.28
Cerium	0.53	1.1	0.14
Praseodymiu	0.4	<0.1	<0.01
Neodymium	3.34	<0.4	1.24
Samarium	0.4	<0.5	0.03
Europium	1.47	<0.2	0.55
Gadolinium	0.8	<0.5	<0.03
Terbium	0.27	<0.07	0.14
Dysprosium	0.8	<0.3	<0.01
Holmium	0.4	<0.1	<0.01
Erbium	0.53	<0.3	0.03
Ytterbium	1.34	<0.4	0.14
Lutetium	0.27	<0.07	<0.01
Tantalum	<0.05	7.4	<0.06
Tungsten	<1.3	30	<1.4
Rhenium	<0.1	1,600	<0.1
Platinum	56.8	<0.07	0.14
Thallium	2.67	1.1	3.44
Lead	209	22	4.3
Bismuth	<0.13	2.1	<0.03

shown in Fig. 4. Given the similar elemental analysis results for both microcontrollers and the fact that the MSP430 had fewer bits available to test, it is possible that the null result for the MSP430 was due to insufficient fluence for observing a statistically significant number of errors before our experiment team's allotted beam time expired.

III. BORON THERMAL NEUTRON CAPTURE BYPRODUCTS

The boron isotopes ^{10}B and ^{11}B interact with neutrons primarily through (n,α), (n,γ), and elastic reactions. Fig. 5 shows the cross sections for these three reactions when neutrons with energies between 0.01 meV and 10 MeV interact with

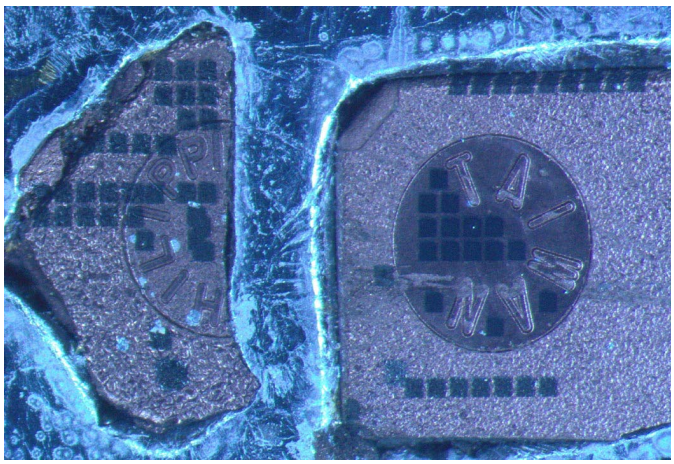

Fig. 4. Microscope image of two component samples showing country stamps on the surface. The sample with the "Philippines" stamp is from the Tiva, and the sample stamped with "Taiwan" is from the MSP430.

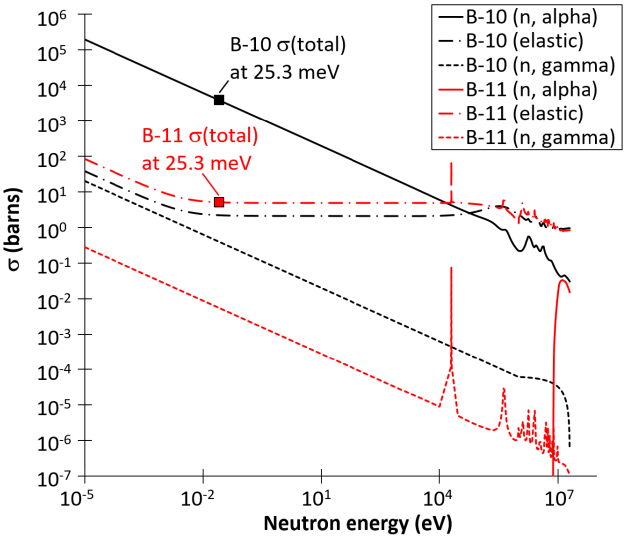

Fig. 5. ^{10}B and ^{11}B nuclear reaction cross sections (after [24]).

^{10}B and ^{11}B [24]. The total thermal neutron cross section is three or orders of magnitude higher for ^{10}B than ^{11}B. It is worth noting that the ^{10}B cross section for 25-meV neutrons is dominated by the (n,α) reaction (that is, a neutron capture that results in the emission of an alpha particle and an Li ion), but the ^{11}B cross section for the (n,α) reaction has not been reported for neutrons with energies less than ~7 MeV. Thermal neutrons interact with ^{11}B through elastic reactions or (less likely) through the (n,γ) reaction. Of the two boron isotopes, only ^{10}B releases energetic charged particles during reactions with thermal neutrons.

When a ^{10}B nucleus captures a thermal neutron and emits an alpha particle, most of the time (94%) the emitted lithium ion is in an excited state (the ^{10}B $(n,\alpha)^{7}$Li* reaction) that subsequently decays by emitting a 0.479-MeV γ-ray. In the remaining cases, the ^{7}Li nucleus is in the ground state (the ^{10}B$(n,\alpha)^{7}$Li reaction) [25], [26]. The alpha particle and Li ion

TABLE V
SRIM SIMULATIONS OF STOPPING DISTANCES AND CHARGE DEPOSITION

Neutron reaction	Byproduct	Stopping distance	Total charge deposited in silicon
^{10}B(n,α)^{7}Li*	1.473 MeV α	5.2 μm	65.2 fC
^{10}B(n,α)^{7}Li*	0.841 MeV ^{7}Li*	2.4 μm	35.5 fC
^{10}B(n,α)^{7}Li	1.778 MeV α	6.4 μm	78.7 fC
^{10}B(n,α)^{7}Li	1.015 MeV ^{7}Li	2.8 μm	44.5 fC

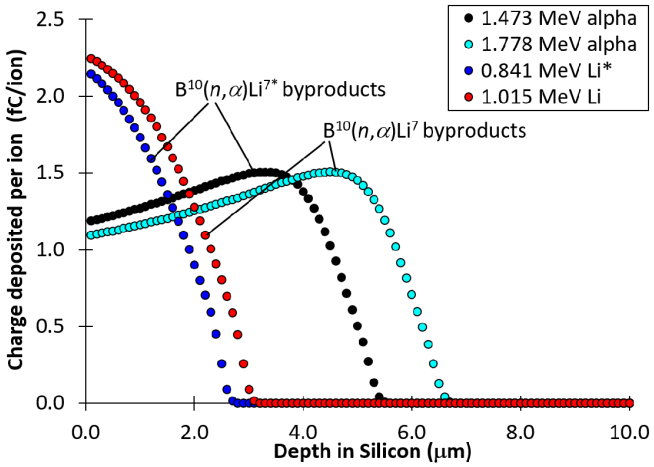

Fig. 6. SRIM simulations comparing charge deposition and stopping range in Si of the ^{10}B (neutron, alpha) reaction byproducts.

emitted through the ^{10}B (n,α)^{7}Li reaction have slightly higher energies than those emitted through the ^{10}B (n,α)^{7}Li* reaction.

Table V states the energies and species of ^{10}B(n,α)^{7}Li byproducts along with their stopping distances and total charge deposition as calculated from the SRIM code [27]. Silicon lattice atoms displaced by high-energy neutrons (such as those in the ICE House I and II beams) can upset a memory element if they are displaced within half a micrometer of a sensitive volume, but thermal neutron capture byproducts can cause a change in logic state even if they are generated several micrometers away, such as in a BPSG insulation layer or a tungsten plug liner fabricated with B_2H_6. Fig. 6 shows charge deposition versus distance for neutron capture byproducts. SRIM simulations indicate that ^{10}B(n,α)^{7}Li reaction byproducts can travel and deposit charge up to 2.8 (Li ion) and 6.3 μm (α-particle) in Si. The charge deposited inside a sensitive volume, not along the total track length, determines whether an SEU will occur. If we consider typical values for 65- and 130-nm nodes for critical charge (~1.2 fC, ~5 fC [26], [28]) and sensitive volume depths (up to a few tenths of a micrometer [27], [29] and a micrometer [28], [30], respectively), SRIM simulations indicate that α-particles and Li ions listed in Table V are each capable of upsetting 65- and 130-nm nodes.

IV. SRAM SEU SIMULATIONS

The errors in the cache test that were measured in the Tiva and MSP430 microcontrollers during broad spectrum neutron irradiation in [19] were due to SEUs in the SRAM and registers. While the cache test can discriminate between SEUs and SETs, it currently does not discriminate between SEUs in the on-chip SRAM or SEUs in the registers. It should be noted that these parts are sensitive to heavy-ion induced SETs. Only the Tiva showed a strong response to thermal neutron irradiation effects, so the simulation efforts reported focus solely on this microcontroller.

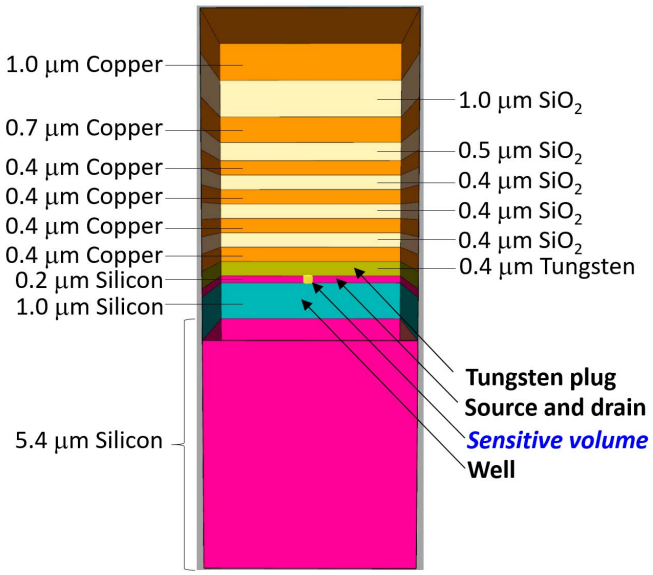

Fig. 7. Model of a 65-nm SRAM simulated with MRED.

Simulations of thermal neutron-induced ionizing energy deposition in the sensitive volume of a 65-nm SRAM were performed using the MRED code [31]. MRED simulations can provide insight into thermal neutron-induced charge deposition in a COTS microcontroller when no *a priori* knowledge is available from the manufacturing process about the location of boron inside the part, whether ^{11}B-enriched boron was used during specific fabrication steps, or what the Q_{crit} of the part is. Simulations allow us to compare the amount of charge generated in the sensitive volume when ^{10}B is present in different regions of the part, such as the source and drain, the well, or the tungsten plug. MRED simulations also enable comparison of SEU cross sections when ^{11}B-enriched boron products are used in place of natural boron during fabrication.

Fig. 7 shows a material stack diagram of the simulated device, which is based on the Texas Instruments 65-nm SRAM simulated with MRED in [32]. Although the device shown in [32] includes a Si_3N_4 layer and a SiO_2 layer on top of the stack, initial MRED simulations showed no contribution to charge deposition from these layers. Therefore, neither layer was included in the material stacks used for subsequent MRED simulations to shorten total execution time. In addition, MRED simulations do not distinguish between Si and polysilicon, so both materials are simply labeled "Silicon" in Fig. 7.

Reasonable material dimensions and boron doping levels were chosen in the absence of a specific device diagram from the manufacturer. A representative sensitive volume has dimensions of 0.2 μm × 0.2 μm × 0.2 μm. The diagram is labeled with the three regions in which boron was simulated

during different MRED executions: 1) boron only in the source and drain; 2) boron only in the *p*-well; and 3) boron only in the tungsten plug. The boron in each of these regions was simulated with isotropic abundance corresponding to natural boron (an approximate ratio of 80% ^{11}B, 20% ^{10}B was used) and ion implant grade ^{11}B-enriched boron (ratio of 99.8% ^{11}B, 0.2% ^{10}B was used). An additional simulation in which the part contained no boron was performed to assess whether significant charge deposition could occur from a thermal neutron capture reaction that produces charged particles but does not involve ^{10}B. Only physical processes involving elements shown in Fig. 7 (B, Cu, O, Si, and W) were considered in the MRED simulations.

MRED simulations were performed with 10^8 thermal neutrons at normal incidence, each with an energy of 25 meV. Incident neutrons were uniformly distributed across the 5 μm × 5 μm surface of the device. A boron concentration of 10^{20} cm^{-3} was used for the source and drain, 10^{19} cm^{-3} for the well, and 10^{16} cm^{-3} for the tungsten plug. Fig. 8(a) and (b) shows the comparison of the effects of boron location and isotope ratios. Fig. 8(a) shows a histogram of counts versus ionizing energy deposition simulated with MRED. In Fig. 8(b), these data have been converted to an integral cross section of charge deposition. The integral cross-sectional value for a given amount of deposited energy E is calculated as the sum of events with energy deposition $\geq E$ divided by fluence, where fluence is the number of simulated neutrons (10^8 neutrons) divided by the surface area of the simulated device (2.5×10^{-7} cm^2). Charge deposition is calculated from ionizing energy deposition using the charge of an electron (1.6×10^{-19} C) and the average energy to generate an electron–hole pair in silicon (3.6 eV [33]).

Four conclusions can be drawn from Fig. 8(a) and (b). First, the ionizing energy deposited in the no-boron control case is negligible in Fig. 8(a). MRED simulations indicate that thermal neutrons do not generate SEUs through nuclear reactions other than those involving boron.

Second, the long tails of ionizing energy deposition in Fig. 8(a) for the six data sets with boron present include a few events with energy deposition greater than 1.78 MeV, the highest energy particle released during either the ^{10}B(n, α)^{7}Li or ^{10}B(n, α)^{7}Li* reactions. This simulation result implies that both the alpha particle and Li ion generated through ^{10}B thermal neutron capture can contribute to a single SEU in some circumstances.

Third, the location of boron affects the amount of ionizing energy deposition (and, therefore, charge deposition) in the sensitive volume. For instance, when boron doping is simulated in the *p*-well, energy deposition peaks around 0.1 MeV. By contrast, the ionizing energy deposited in the sensitive volume when boron is located in the source and drain has one peak around 0.1 MeV and a second broader peak between 0.8 and 1.5 MeV before dropping off around 2.3 MeV. Simulations of boron in either the *p*-well or tungsten plug indicate that ionizing energy deposition in the sensitive volume is limited to ∼1.5 MeV or less. According to MRED simulations, the largest amount of charge deposition from a single thermal neutron-induced event is most likely to occur when boron is present in the *p*-type source and drain.

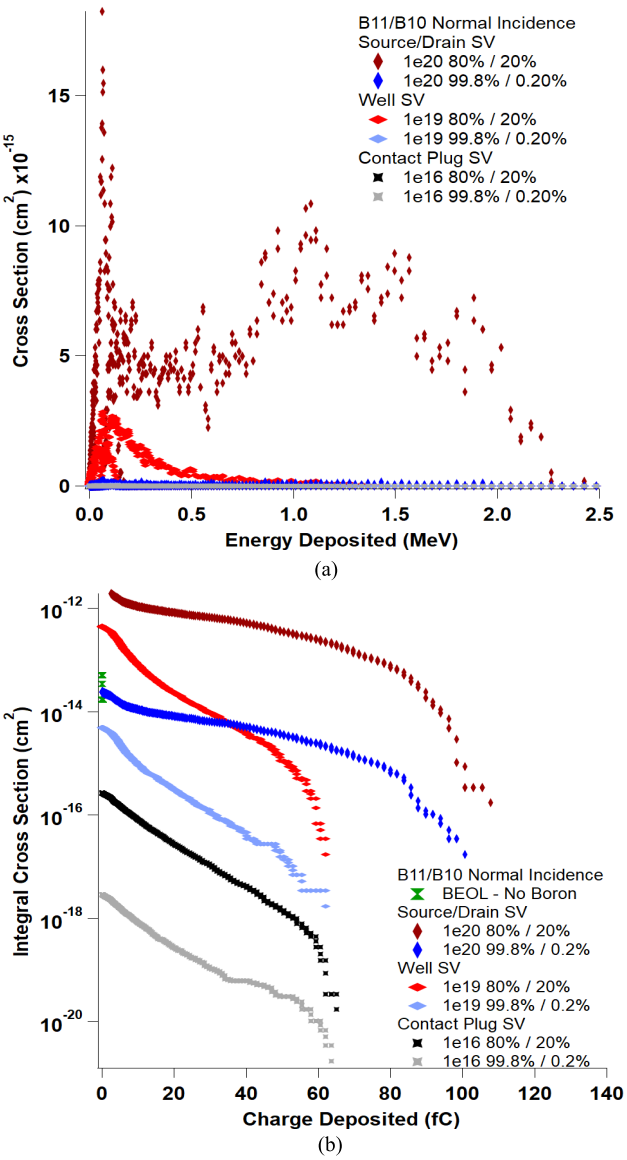

Fig. 8. (a) Histogram of counts versus ionizing energy deposition from MRED simulations of thermal neutrons normally incident on a 65-nm SRAM. (b) Integral cross section of charge deposition from MRED simulations of thermal neutrons normally incident on a 65-nm SRAM.

Fourth, the isotopic ratio of ^{10}B to ^{11}B changes the number of thermal neutron-induced ionizing energy deposition events but not the probable amount of energy that can be deposited in a given event. Increasing the isotopic ratio of ^{10}B to ^{11}B (through use of natural boron rather than ^{11}B-enriched boron) simply increases the number of ^{10}B atoms available to undergo a ^{10}B(n,α)^{7}Li reaction. Fig. 8(b) demonstrates that the cross section versus charge deposition curve scales with ^{10}B concentration; just as natural boron contains 100 times as much ^{10}B as ion implant grade ^{11}B-enriched boron (20% ^{10}B compared to 0.2% ^{10}B), the integral cross sections for device regions simulated with natural boron are 100 times higher than the simulations performed with ^{11}B-enriched boron.

V. Conclusion

Thermal neutron-induced SEU cross sections were measured for two microcontrollers using fission chamber time-of-flight measurements to determine the thermal neutron contribution in the beam. Experimental observation of errors incurred during cache test execution confirms that thermal neutrons cause SEUs in one microcontroller known to exhibit a response to fast neutrons. The suspected mechanism is charge deposition from energetic alpha particles and Li ions generated during ^{10}B thermal neutron capture reactions, and elemental analysis confirms the presence of ^{10}B in the microcontroller.

The ratio of the microcontroller's thermal neutron and high-energy neutron induced SEU cross sections suggests that BPSG is not present (in keeping with the elimination of BPSG in most fabrication plants for device nodes smaller than 180 nm). Although the precise location of ^{10}B with respect to the device's sensitive volumes is not known, Monte Carlo simulations indicate that ionizing energy deposition can occur in the sensitive volume whether boron is located in the source and drain, *p*-well, or tungsten plug. Elemental analysis did not find the evidence of tungsten, so we suspect that the microcontroller does not contain tungsten plugs. The experimentally observed SEUs in the Tiva are likely to be caused by ^{10}B thermal neutron capture reactions inside boron-doped *p*-type silicon, either in the well or the source and drain. Although thermal neutron-induced SEUs were not observed in the MSP430 (a microcontroller also confirmed to contain ^{10}B), it is suspected that we simply did not irradiate the device long enough to observe SEUs during the week of allotted beam time during the 2018 Lujan FP5 Facility schedule. The MSP430 has fewer bits than the Tiva, so it is possible that the fluence was insufficient to observe a statistically significant number of SEUs.

Simulations indicate that the highest amount of charge deposition inside the sensitive volume of a 65-nm SRAM occurs when ^{10}B is located in the source and drain rather than in the *p*-well or tungsten plug. Simulations also indicate that the use of ^{11}B-enriched boron reduces the risk of SEUs but does not eliminate it entirely.

Acknowledgment

The authors would like to thank T. Tenner, E. Tew, M. Knaak, J. Mayo, M. Schappert, R. Pike, and J. J. Gonzalez for their expertise in elemental analysis. They would like to thank R. Schrimpf, M. Alles, B. Sierawski, and K. Warren for their helpful discussions around Monte Carlo radiative energy deposition (MRED) simulations of static random access memory (SRAM) structures. They would also like to thank the use of MRED software (2016 Vanderbilt University, All Rights Reserved) under license from Vanderbilt University, Nashville, TN, USA. Los Alamos National Laboratory, Los Alamos, NM, USA, an affirmative action/equal opportunity employer, is operated by Triad National Security, LLC for the National Nuclear Security Administration of the U.S. Department of Energy under Contract 89233218CNA000001. By approving this article, the publisher recognizes that the U.S. Government retains nonexclusive, royalty-free license to publish or reproduce the published form of this contribution, or to allow others to do so, for U.S. Government purposes. Los Alamos National Laboratory requests that the publisher identify this article as work performed under the auspices of the U.S. Department of Energy. Los Alamos National Laboratory strongly supports academic freedom and a researcher's right to publish; as an institution, however, the Laboratory does not endorse the viewpoint of a publication or guarantee its technical correctness. Sandia National Laboratories is a multimission laboratory managed and operated by National Technology and Engineering Solutions of Sandia, LLC., Albuquerque, NM, USA, a wholly owned subsidiary of Honeywell International, Inc., Charlotte, NC, USA, for the U.S. Department of Energy's National Nuclear Security Administration under Contract DE-NA-0003525. This article describes objective technical results and analysis. Any subjective views or opinions that might be expressed in the article do not necessarily represent the views of the U.S. Department of Energy or the United States Government. LA-UR-19-26094, SAND2019-7606J.

References

[1] R. Baumann, T. Hossain, S. Murata, and H. Kitagawa, "Boron compounds as a dominant source of alpha particles in semiconductor devices," in *Proc. IEEE Int. Rel. Phys. Symp.*, Las Vegas, NV, USA, Apr. 1995, pp. 297–302.

[2] R. C. Baumann and E. B. Smith, "Neutron-induced ^{10}B fission as a major source of soft errors in high density SRAMs," *Microelectron. Rel.*, vol. 41, no. 2, pp. 211–218, Feb. 2001.

[3] E. Normand, K. Vranish, A. Sheets, M. Stitt, and R. Kim, "Quantifying the double-sided neutron SEU threat, from low energy (thermal) and high energy (>10 MeV) neutrons," *IEEE Trans. Nucl. Sci.*, vol. 53, no. 6, pp. 3587–3595, Dec. 2006.

[4] J. M. Armani, G. Simon, and P. Poirot, "Low-energy neutron sensitivity of recent generation SRAMs," *IEEE Trans. Nucl. Sci.*, vol. 51, no. 5, pp. 2811–2816, Oct. 2004.

[5] G. Tsiligiannis *et al.*, "Radiation effects on deep submicrometer SRAM-based FPGAs under the CERN mixed-field radiation environment," *IEEE Trans. Nucl. Sci.*, vol. 65, no. 8, pp. 1511–1518, Aug. 2018.

[6] (Jun. 20, 2019). *3M Advanced Materials Division*. 3MTM 11B Enriched Boron. [Online]. Available: https://multimedia.3m.com/mws/media/958422O/3m-11b-enriched-boron.pdf

[7] J. L. Autran, S. Serre, S. Semikh, D. Munteanu, G. Gasiot, and P. Roche, "Soft-error rate induced by thermal and low energy neutrons in 40 nm SRAMs," *IEEE Trans. Nucl. Sci.*, vol. 59, no. 6, pp. 2658–2665, Dec. 2012.

[8] A. Hands *et al.*, "Single event effects in power MOSFETs due to atmospheric and thermal neutrons," *IEEE Trans. Nucl. Sci.*, vol. 58, no. 6, pp. 2687–2694, Dec. 2011.

[9] B. Linnik *et al.*, "Radiation damage caused by cold neutrons in boron doped CMOS active pixel sensors," *J. Instrum.*, vol. 12, pp. C05011–C05017, May 2017.

[10] Y. Shacham-Diamand, T. Osaka, M. Datta, and T. Ohba, *Advanced Nanoscale ULSI Interconnects: Fundamentals and Applications*. New York, NY, USA: Springer, 2009.

[11] S.-H. Kim *et al.*, "Effects of B_2H_6 pretreatment on ALD of W film using a sequential supply of WF_6 and SiH_4," *Electrochem. Solid-State Lett.*, vol. 8, no. 10, pp. C155–C159, 2005.

[12] S.-J. Wen, S. Y. Pai, R. Wong, M. Romain, and N. Tam, "B10 finding and correlation to thermal neutron soft error rate sensitivity for SRAMs in the sub-micron technology," in *Proc. IEEE Int. Integr. Rel. Workshop Final Rep.*, Oct. 2010, pp. 31–33.

[13] Y.-P. Fang and A. S. Oates, "Thermal neutron-induced soft errors in advanced memory and logic devices," *IEEE Trans. Device Mater. Rel.*, vol. 14, no. 1, pp. 583–586, Mar. 2014.

[14] N. Seifert *et al.*, "Soft error rate improvements in 14-nm technology featuring second-generation 3D tri-gate transistors," *IEEE Trans. Nucl. Sci.*, vol. 62, no. 6, pp. 2570–2577, Dec. 2015.

[15] (Jun. 19, 2019). *3MTM 11B Enriched Boron Trifluoride for Semiconductor Manufacturing*. Ceradyne. Costa Mesa, CA, USA. [Online]. Available: https://multimedia.3m.com/mws/media/1071862O/3m-11b-enriched-boron-trifluoride-for-semiconductor-mfg.pdf

[16] H. O. M. Fisher, *A Nuclear Cross Section Data Handbook*. New Mexico, NM, USA: Los Alamos National Laboratory, 1989.

[17] M. S. Gordon *et al.*, "Measurement of the flux and energy spectrum of cosmic-ray induced neutrons on the ground," *IEEE Trans. Nucl. Sci.*, vol. 51, no. 6, pp. 3427–3434, Dec. 2004.

[18] C. Weulersse *et al.*, "Contribution of thermal neutrons to soft error rate," *IEEE Trans. Nucl. Sci.*, vol. 65, no. 8, pp. 1851–1857, Aug. 2018.

[19] *JEDEC Standard: Test Method for Beam Accelerated Soft Error Rate, JEDEC Solid State Technology Association*, Standard JESD89-3A, 2007.

[20] *Energy Resolved Neutron Imaging (ERNI) at FP5*. Accessed: Nov. 25, 2019. [Online]. Available: https://lansce.lanl.gov/facilities/lujan/instruments/fp-5/index.php

[21] H. Quinn, Z. Baker, T. Fairbanks, J. L. Tripp, and G. Duran, "Software resilience and the effectiveness of software mitigation in microcontrollers," *IEEE Trans. Nucl. Sci.*, vol. 62, no. 6, pp. 2532–2538, Dec. 2015.

[22] (Jun. 12, 2014). *Tiva TM4C123GH6PM Microcontroller Data Sheet*. [Online]. Available: http://www.ti.com/lit/ds/symlink/tm4c123gh6pm.pdf

[23] (Nov. 2012). *MSP430F241x, MSP430F261x Mixed Signal Microcontroller Datasheet*. [Online]. Available: http://www.ti.com/lit/ds/symlink/msp430f2618.pdf

[24] N. Soppera, M. Bossant, and E. Dupont, "JANIS 4: An Improved Version of the NEA Java-based Nuclear Data Information System," *Nucl. Data Sheets*, vol. 120, pp. 294–296, Jun. 2014.

[25] G. C. Hanna, "The disintegration of boron by slow neutrons," *Phys. Rev. J. Arch.*, vol. 80, no. 4, pp. 530–534, Nov. 1950.

[26] J. Rhodes, W. Franzen, and W. E. Stephens, "Ionization measurements of B^{10} (n,α) Li^{7}," *Phys. Rev. J. Arch.*, vol. 87, no. 1, pp. 141–145, Jul. 1952.

[27] J. F. Ziegler, M. D. Ziegler, and J. P. Biersack, "SRIM—The stopping and range of ions in matter (2010)," *Nucl. Instrum. Methods Phys. Res. A, Accel. Spectrom. Detect. Assoc. Equip.*, vol. 268, nos. 11–12, pp. 1818–1823, Jun. 2010.

[28] E. Ibe, H. Taniguchi, Y. Yahagi, K. Shimbo, and T. Toba, "Impact of scaling on neutron-induced soft error in SRAMs from a 250 nm to a 22 nm design rule," *IEEE Trans. Electron Devices*, vol. 57, no. 7, pp. 1527–1538, Jul. 2010.

[29] B. D. Sierawski *et al.*, "Impact of low-energy proton induced upsets on test methods and rate predictions," *IEEE Trans. Nucl. Sci.*, vol. 56, no. 6, pp. 3085–3092, Dec. 2009.

[30] O. A. Amusan *et al.*, "Charge collection and charge sharing in a 130 nm CMOS technology," *IEEE Trans. Nucl. Sci.*, vol. 53, no. 6, pp. 3253–3258, Dec. 2006.

[31] R. A. Reed *et al.*, "Physical processes and applications of the Monte Carlo radiative energy deposition (MRED) code," *IEEE Trans. Nucl. Sci.*, vol. 62, no. 4, pp. 1441–1461, Aug. 2015.

[32] B. D. Sierawski *et al.*, "Contribution of low-energy ($\ll$10 MeV) neutrons to upset rate in a 65 nm SRAM," in *Proc. IEEE Int. Rel. Phys. Symp.*, Anaheim, CA, USA, May 2010, pp. 4B.2.1–4B.2.5.

[33] C. Bussolati, A. Fiorentini, and G. Fabri, "Energy for electron-hole pair generation in silicon by electrons and α particles," *Phys. Rev. J. Arch.*, vol. 136, no. 6A, pp. A1756–A1758, Dec. 1964.

Preprint 2015SW001169R accepted March 20, 2015 at *Space Weather Journal*

Advances in atmospheric radiation measurements and modeling needed to improve air safety

W. Kent Tobiska[1], William Atwell[1], Peter Beck[2], Eric Benton[3], Kyle Copeland[4], Clive Dyer[5], Brad Gersey[6], Ian Getley[7], Alex Hands[5], Michael Holland[8], Sunhak Hong[9], Junga Hwang[10], Bryn Jones[11], Kathleen Malone[8], Matthias M. Meier[12], Chris Mertens[13], Tony Phillips[14], Keith Ryden[5], Nathan Schwadron[15], Stephen A. Wender[16], Richard Wilkins[6], and Michael A. Xapsos[17]

[1]Space Environment Technologies, Pacific Palisades, CA, [2]Seibersdorf Laboratories, Seibersdorf, Austria, [3]Oklahoma State University, Stillwater, OK, [4]FAA Civil Aerospace Medical Institute, Oklahoma City, OK, [5]Surrey Space Centre, University of Surrey, Guildford, United Kingdom, [6]Prairie View A&M University, Prairie View, TX, [7]Department of Aviation, University of New South Wales, Australia, [8]Allied Pilots Association, Aeromedical Committee, United States, [9]Korean Space Weather Center of National Radio Research Agency, Jeju, Korea, [10]Korea Astronomy and Space Science Institute, Daejeon, Korea, and Department of Astronomy and Space Science, Korea University of Science and Technology, Daejeon, Korea, [11]SolarMetrics, Guildford, United Kingdom, [12]Deutsches Zentrum für Luft- und Raumfahrt e.V. (DLR), Cologne, Germany, [13]NASA Langley Research Center, Hampton, VA, [14]Spaceweather.com, United States, [15]University of New Hampshire, Durham NH, [16]Los Alamos National Laboratory, Los Alamos, NM, [17]NASA Goddard Space Flight Center, Greenbelt, MD

Abstract. Air safety is tied to the phenomenon of ionizing radiation from space weather, primarily from galactic cosmic rays but also from solar energetic particles. A global framework for addressing radiation issues in this environment has been constructed but more must be done at international and national levels. Health consequences from atmospheric radiation exposure are likely to exist. In addition, severe solar radiation events may cause economic consequences in the international aviation community due to exposure limits being reached by some crew members. Impacts from a radiation environment upon avionics from high-energy particles and low-energy, thermalized neutrons are now recognized as an area of active interest. A broad community recognizes that there are a number of mitigation paths that can be taken relative to the human tissue and avionics exposure risks. These include developing active monitoring and measurement programs as well as improving scientific modeling capabilities that can eventually be turned into operations. A number of roadblocks to risk mitigation still exist, such as effective pilot training programs as well as monitoring, measuring, and regulatory measures. An active international effort towards observing the weather of atmospheric radiation must occur to make progress in mitigating radiation exposure risks. Stakeholders in this process include standards-making bodies, scientific organizations, regulatory organizations, air traffic management systems, aircraft owners and operators, pilots and crew, and even the public.

Aviation radiation is an unavoidable space weather phenomenon. Air safety has improved significantly in many meteorological areas over the past decades with the exception of space weather, which includes ionizing radiation. While a framework for ad-

dressing radiation issues has been constructed, we believe more can and must be done at international and national levels. In particular, measurement programs must be expanded and linked with models to provide current epoch and, eventually, forecast information for the aviation ionizing radiation environment. A diverse radiation measurement and modeling community exists with a strong interest in improving international air safety.

There are two challenges in our ever more mobile, technologically dependent global society. First, pilots, crew, and passengers, which include fetuses between their first and second trimesters, might face additional radiation hazards in terms of dose equivalent rate (rate of absorbed dose multiplied by the quality factor), particularly when flying at commercial aviation altitudes above 26,000 ft. (8 km) (see Figure 1). Second, avionics can experience single event effects (SEE) from both the ambient high-energy and thermal neutron environments. The source of this radiation in either case is two-fold – from the continuous bombardment by primary background galactic cosmic rays (GCRs) and also from solar energetic particles (SEPs) emitted during occasional solar flare events lasting up to a few days.

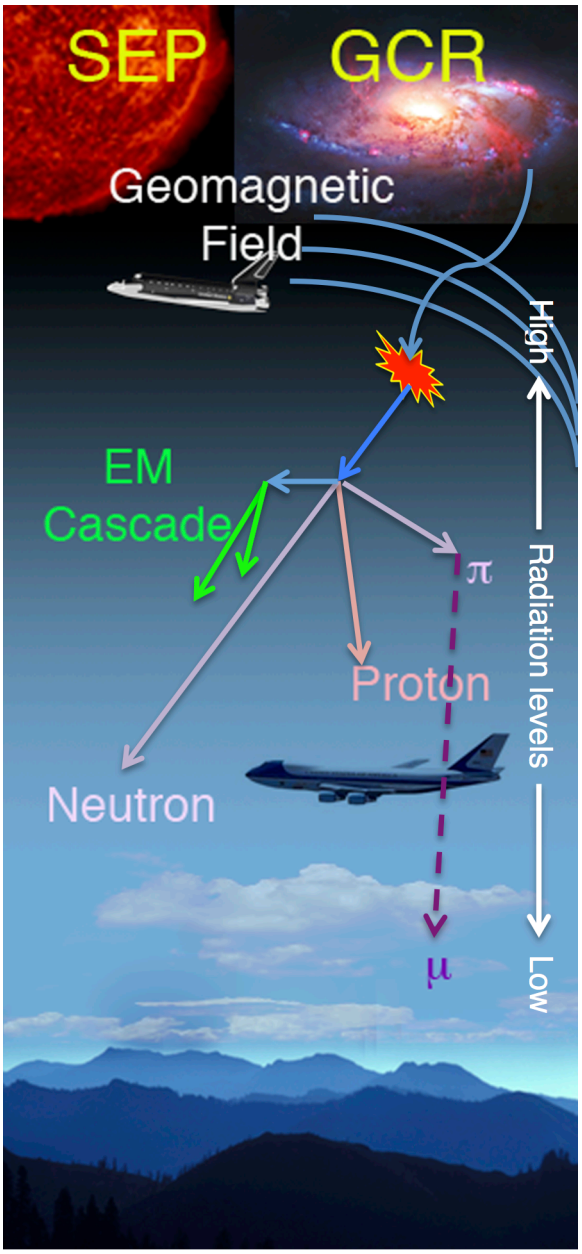

Fig. 1. All passengers in commercial aircraft flying above 26,000 feet will typically experience some exposure in this aviation radiation environment.

Galactic cosmic rays from outside the solar system consist mostly of energetic protons but also contain heavy ions such as iron. Solar energetic particles are commonly associated with solar flaring events and are dominated by protons. Regardless of their source, and depending upon their energy, these charged particles enter the Earth's atmosphere at different magnetic latitudes and collide with atmospheric molecules. Below the top of the atmosphere (~100 km), the primary radiation decreases as a result of atmospheric absorption while a secondary radiation component increases. This occurs because many low-energy particles are created by the initial impacts [Reitz *et al.*, 1993]. These competing processes produce an ionizing maximum that occurs between 20 and 25 km (65,000 – 82,000 ft.) called the Pfotzer maximum, although observational evi-

dence may point to variable altitudes of this maximum. Below the Pfotzer maximum, down to the Earth's surface, the particle fluxes decrease. The secondary radiation, including protons, neutrons, pions, electrons, and gamma rays, have varying energies and are emitted in all directions. The primary and secondary energetic particles collide with atmospheric molecules, the aircraft structure, and interior materials (including passengers) to cause a further alteration of the radiation spectrum.

This resulting, complex spectrum of the radiation environment may potentially cause an increase in cancer risk as the dose equivalent exposure increases. The atmospheric neutron component of this complex radiation field, in particular, holds special interest in the cancer research community. The energy spectrum of these neutrons extends over more than ten orders of magnitude. Both the high-energy neutrons ($E > 10$ MeV) and the very low-energy thermalized neutrons can also cause SEE errors in avionics [Normand *et al.,* 1994; Normand *et al.,* 2006]. The high-energy neutrons have direct interactions with Silicon (Si) nuclei in electronics, producing excess charge carriers through nuclei recoils. The very low-energy neutrons are created by scattering from atmospheric constituents and aircraft materials (including fuel and passengers), which thermalizes them (creates neutrons in thermal equilibrium with their surroundings in an energy range of approximately 0.02 – 0.2 eV). These thermalized neutrons are then absorbed by Boron (particularly ^{10}B) found in Si-based aircraft electronics, for example. The net effect after absorption is the production of a gamma-ray (480 keV), an alpha particle (~4 MeV), and a lithium ion. The charged alpha particle may then interact with semiconductor structures and cause a SEE. Higher Z elements near the silicon layers (e.g. tungsten connectors) can exacerbate the SEE effect considerably.

Most of the time, the GCR radiation component dominates commercial aviation altitudes. It varies inversely with the approximate 11-year solar cycle. As an example, the outflowing plasma in the solar wind and the strength of the solar Interplanetary Magnetic Field (IMF) effectively screen lower energy GCR particles from reaching the Earth during high solar cycle activity. Thus, as the next solar minimum approaches (~2017–2021) the GCR radiation will become stronger as the solar wind and IMF become weaker. In addition, significant solar flaring events can produce radiation storms in which the SEP doses are additive with the GCRs. We note that Forbush decreases (a rapid decline in the observed GCR intensity following a solar coronal mass ejection, for example) can temporarily reduce the GCR component. The resulting GCR and SEP combined dose equivalent exposure level could possibly exceed safety thresholds established by the international radiation protection community. Potential event examples are shown in the sidebars.

Radiation exposure consequences. While the most significant, but highly unlikely, health consequences to atmospheric radiation exposure may include death from cancer due to long-term exposure, there are many lifestyle degrading and career impacting cancer forms that can also occur [Wilson, *et al.,* 2002]. A cancer diagnosis can have significant career impact for a commercial pilot. The FAA requires each pilot to hold a medical certificate in order to exercise the privileges of his or her pilot's license. A cancer diagnosis can ground a pilot for some time, perhaps permanently given the diagnosis and time remaining in his or her career. International guidelines from the International Commission on Radiological Protection (ICRP) have been developed to mitigate this statistical risk [ICRP 1991, 2005, 2007]. The ICRP recommends effective dose limits of a 5-year

average of 20 mSv yr^{-1} with no more than 50 mSv in a single year for non-pregnant, occupationally exposed persons, and 1 mSv yr^{-1} for the general public. Radiation dose limits can be misunderstood. Pilots are trained in the use of engineering limits; however, radiation limits are not engineering limits. In the U.S., for example, they are treated as an upper limit of acceptability and *not* a design limit [NCRP Report 116, 1993].

Thus, to better understand these consequences, the European Commission initiated and supported research projects on cosmic radiation in the 1990s, which included numerous on-board measurements [O'Sullivan *et al*., 1999; Beck *et al*., 1999; O'Sullivan *et al*., 2004; EC Radiation Protection Report No. 140, 2004]. Based on that experience, international institutes developed calculation codes for the assessment of galactic cosmic radiation exposure on-board aircraft. For example, the EURADOS (European Dosimetry Group) working group WG11, which focuses its activity on High Energy Radiation Fields, carried out international comparison of these calculation codes and confirmed good agreement [Bottollier-Depois *et al*., 2009]. Further, the international radiation protection community working on cosmic radiation effects to aircrew developed International Standards Organization (ISO) standards describing the conceptual basis for cosmic radiation measurements (ISO 20785-1:2012), including characterization of these instruments [ISO 20785-2, 2011]. The third part of this standard is still in progress related to measurements at aviation altitudes. In 2010, the International Commission on Radiation Units (ICRU) and ICRP jointly published Report 84 on this topic [ICRU, 2010]. Recently during the 2014 European Space Weather Week at Liege, the EURADOS WG11 presented comparison of calculation codes, which estimate exposure due to solar energetic particle events on-board aircraft [Beck *et al*., 2014].

Tissue-relevant radiation

An example of a severe tissue-relevant radiation environment occurred during the major SEP event on 23 February 1956 (only ground level measurements were available). For that event, Dyer *et al.* [2007] calculated a significant increase over background at high latitudes and at 12 km altitude with correspondingly higher dose rates for aircraft flight paths of several mSv hr^{-1}. The derived SI unit of ionizing radiation dose is the sievert (Sv). It incorporates the stochastic health risk of low levels of ionizing radiation on the human body, where radiation dose assessment is defined as the probability of cancer and genetic damage. On 23 February 1956 this radiation increase could have caused some aircrew members to exceed their currently recommended annual occupational flight limits in just one flight [Wilson, *et al.,* 2002; Dyer *et al.*, 2007]. It also could have caused upsets every 3 seconds in a Gbyte of a typical memory device [Dyer *et al.*, 2003]. An extreme event such as the 1859 Carrington Event could be considerably worse than this event. Here we use the terms "extreme" or "severe" to indicate a NOAA S5 radiation storm, possibly comparable to the 1859 Carrington Event. We also note that the NOAA scales themselves are a poor indicator for the aviation radiation environment; the GOES fluxes are a good indicator of when a Solar Proton Event (SPE) is occurring but only small subsets of these have significant fluxes of protons with sufficient energy to affect the atmosphere, even at polar latitudes.

European Union (EU) member States have implemented regulations for aircrew members requiring exposure assessment when it is likely to be >1 mSv yr^{-1} and to take

into account the assessed exposure when organizing working schedules to reduce the doses of highly exposed crew (EU Council Directive, 2013). In the U.S., there are no regulatory effective dose limits for aircrew members; the FAA [AC 120-61B, 2014] accepts the most recent recommendations of the American Conference of Governmental Industrial Hygienists (ACGIH) and recommends ICRP limits for exposure to ionizing radiation for non-pregnant air carrier crew members. For pregnant crew members, the FAA recommends the ICRP limit of 1 mSv to the fetus/conceptus for the remainder of the pregnancy, once reported to management, and the National Council on Radiation Protection and Measurements (NCRP) recommends a limit of 0.5 mSv per month.

Modeled results [Mertens *et al*., 2012] suggest that commercial aircrew flying at high latitudes will trigger the EU action level limiting annual flights if they fly more than 500-600 hours during solar minimum and more than 800-900 hours during solar maximum, based on typical GCR background radiation exposure. Modeling also suggests that the public/prenatal recommended limit [NCRP Report No. 174, 2013] can be exceeded in 100 hours of flight time and, for high-latitude or polar flights, the effective dose rate can be up to 10 $\mu Sv\ hr^{-1}$ [Mertens *et al*., 2012]. It is possible that a limit could be exceeded in a single flight during a severe solar particle event with a hard spectrum, i.e., a Ground Level Enhancement (GLE) [Dyer *et al*., 2007; Copeland *et al*., 2008]. We note that these modeled hours are not the method that triggers an EU action level and there is a differentiation between limits (e.g., EU law) and recommendations (e.g., FAA and ICRP), where a recommendation can be exceeded even if no legal limit exists.

For the flying public, high mileage business travelers may want to consider their exposure risks as similar to aircrew members. For infrequent commercial air travelers, the primary risk would come from extremely large Solar Proton Events (SPEs) and GLEs while flying polar routes. The Dyer *et al*. [2007] and Copeland *et al*. [2008] studies should raise awareness to avoid polar route flights during these events to minimize exposure

Avionics-relevant radiation

A possible example of a severe neutron-induced avionics effect occurred on 07 October 2008 in Qantas Flight 72 Airbus A330-303 from Singapore to Perth, Western Australia. While the aircraft was in cruise at 37,000 ft. one of the aircraft's three air data inertial reference units (ADIRUs) started outputting intermittent, incorrect values (spikes) on flight parameters to other aircraft systems. Two minutes later, in response to spikes in angle of attack (AOA) data, the aircraft's flight control primary computers (FCPCs) commanded the aircraft to pitch down. At least 110 of the 303 passengers and 9 of 12 aircrew members were injured; 12 were serious injuries and another 39 required hospital medical treatment. The potential triggering event that was not ruled out was a single event effect (SEE) resulting from a high-energy atmospheric neutron interacting with one of the integrated circuits (ICs) within the CPU module. While there was insufficient evidence to determine that a SEE was the conclusive cause, the investigation identified SEE as an ongoing, probabilistically relevant risk for airborne equipment. All other known causes were eliminated. The aircraft manufacturer subsequently redesigned the AOA algorithm to prevent the same type of accident from occurring again [ATSB Transport Safety Report, 2011]. We note that the GOES >10 MeV proton fluence was nominal on this date, i.e., there were no solar flare events.

risks.

Impacts associated with exceeding limits beyond health risks have also been considered. The U.K. Royal Academy of Engineering (RAEng) determined that significant economic consequences might occur from fleet disruptions due to aircrew grounding because exposures can exceed monthly or annual limits during a single severe solar event [Cannon *et al*., 2013]. For example, at conventional cruising altitudes around 37,000 ft. (~11 km) across polar latitudes, a severe radiation storm could result in a worst-case dose to aircrew and passengers of >20 mSv. This single event dose would be 20 times the recommended exposure limit to the general public (not aviation-specific) and comparable to the entire annual occupational dose limit for aircrew. Again, we note that this is not applicable to U.S. crew as no actual limits have been promulgated, no regulatory limits exist, and no monitoring or tracking of exposure is performed. The RAEng study also concluded that pilot workload could increase during such periods to cope with any anomalous system behavior. This is because the complexity of modern aircraft computer interface/control and fly by wire avionics is such that prediction of an aircraft's response to increased radiation levels is necessarily subject to uncertainty, as seen in Qantas Flight 72.

Risk mitigation paths exist. Because of added risk from severe radiation events, the radiation measurement and modeling communities have devoted considerable effort to understanding and characterizing this radiation field with mitigation strategies in mind. The community recognizes, as a starting point, that monitoring of the natural space environment for solar proton event occurrence is important. For example, with the start of an event, announcement levels are escalated. The NOAA Space Weather Prediction Center issues a *Watch* (long-lead-time geomagnetic activity prediction), a *Warning* (some condition is expected), or an *Alert* (event threshold is crossed). A Watch is provided only for geomagnetic storms and not SEP events. Additionally, the International Space Environment Service (ISES, http://www.spaceweather.org/) encompasses many Regional Warning Centers (RWCs) and these organizations also provide similar services of Watches, Warnings, and Alerts for their local users. It is important that the nature and severity of a SPE be quickly assessed to avoid false alarms occurring if automatic alerts are issued.

A second recognition is that there is a need for dosimeters onboard aircraft. Because the radiation exposure of airline crew and passengers in the U.S. is unregulated, the responsibility for mitigation of exposure called for by the NCRP principle *As Low As Reasonably Achievable* (ALARA) is left up to the air carrier and/or the pilot. Yet, either one usually has very limited information on which to base a decision and dispatcher/pilot training on this subject matter is virtually nonexistent. The FAA very recently added ALARA guidance to its reference material on in-flight radiation [FAA AC 120-61B, 2014] as the basis for exposure management. In the event of a communication blackout or from air carrier policy, we note that any decision may be left solely to the pilot. If an event affects a fleet of aircraft, the air traffic control (ATC) system is not prepared for responding rapidly to multiple route diversions during major solar radiation storms, even though they may be rare. The International Civil Aviation Organization (ICAO) is just beginning to investigate the issue. Thus, much more work toward mitigation of radiation effects of large SEP events upon the airline industry is needed at the decision-making level.

While probabilistic SPE forecasting exists, current prediction methods typically rely

on empirical formulations to estimate the decay to background from the peak of an event. Once an event has started, and for its duration, the exposure mitigation strategy for commercial aviation is relatively straightforward to implement. Any implementation is subject to maintaining safe airspace separation minima, avoiding terrestrial weather hazards, and retaining sufficient trip fuel; however, it would include:

- fly at lower altitudes and/or latitudes for moderate or larger radiation events;
- avoid polar region flights during severe solar radiation events until they subside;
- issue a no takeoff alert if a large SPE is ongoing;
- enable ATC, operators, and aircrews with the real-time exposure information necessary to descend the enroute system to a less exposed altitude en masse; and
- enable ATC, operators, and aircrews with the real time information necessary to divert polar flights from polar flight paths when communications reliability is at risk.

ICAO and FAA communications requirements largely drive the avoidance of polar flight during increased solar activity. Due to reliance on High Frequency (HF) radio as the primary communication link between an aircraft and ATC during polar flight, and its susceptibility to disruption by a solar storm polar cap absorption (PCA), polar flight during significant solar radiation storms (NOAA S scale ≥ S3 for PCA) may be prohibited. However, the addition of INMARSAT satellite capability by some airlines may remove the side benefit that occurs when ensuring continued communications. That is to say, because INMARSAT enables polar communications, a conscious decision would be required to avoid polar flight during a solar radiation storm. The FAA Solar Radiation Alert (SRA) system activates at a high proton flux level (i.e., when the estimated effective dose rate induced by solar protons at 70,000 ft. equals or exceeds 20 $\mu Sv\ h^{-1}$ for each of three consecutive 5-minute periods); it is not regulatory in its guidance to pilots or dispatchers.

Mitigation of SEE in avionics, which is a probabilistic phenomenon, will mainly be achieved through improved engineering processes and, while key standards are now available, notably IEC-62396-1, it will take many years for such approaches to become universally adopted. There has been ongoing work for the International Electrotechnical Commission (IEC) SEE standard since 2000 but there are only recent signs that national bodies may mandate it. The existing certification is for quiet cosmic ray conditions only and extreme space weather is not yet considered. Furthermore, there will still be a limit to the radiation level that can be managed with confidence, depending on the design specification applied. In order to mitigate the risk of injuries during unexpected aircraft behavior such as from a SEE (even though it is not yet possible to deterministically identify its higher probability), a simple but generally effective measure would be to ensure that passengers and aircrew have their seat belts fastened. While SEEs are probabilistic and may occur at any altitude, even during non-SPE conditions (as may have been the case for Qantas Flight 72), this mitigation path is helpful for other hazards such as clear air turbulence. Whatever the cause, a lesson from Qantas Flight 72 was that if seat belts had been fastened far fewer injuries would have occurred. Thus, radiation measurements and alerts may have a beneficial role to play in alerting pilots to switch on the seat belt sign (including directing passengers and crew to take their seats and ensuring their seat belts are fastened), which could be a simple and low cost mitigation action for any unexpected aircraft behavior risk. Built-in aircraft protections, monitors and dispatcher/pilot training are all needed as are improved engineering processes.

Stakeholders. Exposure mitigation implementation at altitude can only be accomplished by activity from stakeholder groups, including but not limited to international collaborations that provide guidelines such as the International Standards Organization (ISO) space weather and aviation radiation standards [ISO 15390:2003, ISO 21348:2007, ISO/AWI 17520, ISO 20785-1:2012, ISO 20785-2:2011, ISO/DIS 20785-3], the International Commission on Radiation Units (ICRU) Joint Report (84), the International Electrotechnical Commission (IEC) SEE standard for avionics (IEC 62396), the JEDEC Solid State Technology Association (JEDEC) SEE standard for avionics (JESD89A), the World Meteorological Organization (WMO) observing requirements (#709, #738), and the International Civil Aviation Organization (ICAO) regulatory guidelines (SARP 3.8.1). As evidence of national mitigation collaborations, national air traffic management (ATM) systems are upgrading to NextGen and SESAR. Commercial and corporate aircraft owners and their dispatchers who use actionable information, often from third party weather providers, are the third stakeholder group with an interest in exposure mitigation. Finally, aircrew members who use actionable information and the radiation-educated public are the ultimate core stakeholder group.

Research data collection. A key condition for enabling all stakeholders to maximize their contributions in exposure mitigation is having quality dose measurements at altitude and emphasizing measurements at latitudes where the highest risks exist. Numerous measurements have been made and used for post-flight analysis [Dyer *et al*., 1990; Beck *et al*., 1999; Kyllönen *et al*., 2001; EC Report 140, 2004; Getley *et al*., 2005; Beck *et al*., 2005; Latocha *et al*., 2007; Meier *et al*., 2009; Beck *et al*., 2009; Dyer, *et al*., 2009; Hands and Dyer, 2009; Getley *et al*., 2010; Gersey *et al*., 2012; Tobiska *et al*., 2014], though the vast majority are for background conditions and not during major space weather events. Some of these have made neutron flux and dose equivalent measurements with solid-state detectors [Dyer, *et al*., 2009; Hands and Dyer, 2009; Tobiska *et al*., 2014; 2015]. Together, these measurements have made important contributions to model validations of the radiation field at altitude, especially for human tissue issues. However, monitoring cannot be considered really effective until regular, validated, real-time, and global effective dose rate and neutron measurements (including the thermal component) are made. This capability does not yet exist and, because very few in-flight radiation measurements during significant solar particle events have occurred, it is critical that calibrated monitors are flown as widely and routinely as possible in order to maximize data capture that can both validate models and potentially be the basis of issuing alerts.

Future measurements. Total ionizing dose measurements such as those by Automated Radiation Measurements for Aerospace Safety (ARMAS) [Tobiska *et al*., 2014; 2015] are an example of a surrogate index measurement that could be used in monitoring a real-time environment. Another example is the Space Weather D-index, based on dose rates at aviation altitudes produced by solar protons during solar radiation storms, as the relevant parameter for the assessment of corresponding radiation exposure [Meier and Matthiä, 2014]. The Space Weather D-index is a natural number given by a graduated table of ranges of dose rates in ascending order which is derived by an equation depending on the dose rate of solar protons.

Measurement/modeling comparisons are continuing and, recently, real-time assessment of radiation exposure due to solar energetic particle events have been presented at the 2014 European Space Weather Week (Liege, Nov. 2014) using the updated code

AVIDOS 2.0 [Latocha *et al*., 2014] (cf., European Space Agency's Space Weather Portal http://swe.ssa.esa.int). Two new instrument concepts are in development and include: *i)* the Dose Spectra from Energetic Particles and Neutrons (DoSEN) instrument [Schwadron *et al*., 2013] for measuring not only the energy but also the charge distribution of energetic particles, including neutrons, that affect human and robotic health; and *ii)* the Thermalized Neutron Measurements (TiNMan) instrument for measuring thermal neutrons related to SEE in avionics (L. Dominic and S. Wender, private communication).

International scientific modeling using measurements. There are many modeling systems into which these types of data could be integrated, e.g., LUIN [O'Brien *et al*., 1996], CARI6PM [Friedberg *et al*., 1999; Friedberg and Copeland, 2003; Friedberg and Copeland, 2011], FLUKA [Zuccon *et al*., 2001], QARM [Lei *et al*., 2006], AIR [Johnston, 2008], PARMA [Sato *et al*., 2008], AVIDOS [Latocha *et al*., 2009; Latocha *et al*., 2014], NAIRAS [Mertens *et al*., 2013], PANDOCA [Matthiä *et al*., 2014], and KREAM [Hwang *et al*., 2014]. Recent work by Joyce *et al*. [2014] utilized CRaTER measurements [Spence *et al*., 2010; Schwadron *et al*., 2012] in deep space to estimate dose rates through the Earth's atmosphere at a range of different altitudes down to aviation heights.

Further, different kinds of measurements are also needed including the SEE response of integrated circuits (ICs) used in avionics to high-energy neutrons; testing can be done in ground-based laboratories with simulated neutron beams. Per current guidelines (IEC 62396-1) the SEE response data would be combined with the output from in-flight neutron detectors to obtain SEE rates. ICs are constantly evolving with greater capability and ever-smaller feature size and,

Action needed at all levels

There is great value in stakeholders' efforts to mitigate potential exposure risks to humans and avionics from events that affect the aviation radiation environment. Further efforts by stakeholders leading to near-term action can:

- expand international scientific research in the aviation radiation environment;
- develop reliable, new measurement systems that can provide calibrated real-time dose equivalence data for a highly mixed and changeable radiation field;
- obtain in-flight measurements during solar particle events in order to calibrate instruments and validate models;
- test semiconductor devices at a wide energy neutron source as part of certifying their use in avionics;
- continue and expand ground level neutron monitor measurements to record GLEs as a subset of SPEs;
- create new modeling systems that can assimilate real-time radiation data;
- discover and validate new forecasting capabilities;
- combine data and modeling for improved monitoring in an operational context;
- provide current condition information to decision makers (pilots and dispatchers);
- train decision makers on the information available;
- educate airline personnel, managers, dispatchers, and pilots on the exposures, measurements, risks, as well as mitigation techniques available;
- provide feedback to the scientific community on the adequacy of the information provided to the decision maker; and

provide the public with scientific-based, but easily understood, information on the aviation radiation environment.

since these are being chosen for use in upgraded avionics systems, it is necessary to continue testing the newer electronics for their susceptibility to SEE from high-energy neutrons. For example, electronics parts testing at the Los Alamos Neutron Science Center (LANSCE) is an ongoing activity by many IC and avionic manufacturers. This facility is capable of closely simulating the high-energy atmospheric neutron energy spectrum at a neutron flux such that an hour of exposure at LANSCE is equivalent to 300,000 hours at 40,000 ft. Similar testing is also done in laboratories with thermal neutron sources. In addition, all ICs within a subsystem should be analyzed for their SEE rates using measured SEE cross sections. If the rates are combined for all ICs and protection factors built into the system (e.g., error correcting code), then an overall effective SEE rate can be obtained.

Path forward. We conclude that, in order to improve aviation safety in a radiation environment, our community must begin observing the weather of atmospheric radiation. Our current state-of-art technology only reports the data-driven climatology. The combination of low-cost, quality dosimetry measurements, integrated with modeling systems, does not yet exist. Using calibrated sensors at multiple, simultaneous altitudes from the surface to space, whose data can be used to validate algorithms and for assimilation into physics-based, global climatological models, is an important path toward producing a dose equivalent rate in tissue and a SEE error rate in avionics. With support for the above activities at an international level, air safety can and should be further improved in the arena of atmospheric radiation exposure risk mitigation for aircrew, the public, and avionics, particularly during severe radiation events. The need for these activities will only increase with time as air travel expands and as aircraft avionics technology advances toward greater miniaturization.

Acknowledgements

Our authors and co-authors support the data access policy of the AGU and regularly provide data for furthering scientific research related to the aviation radiation environment. References cited herein may contain data links that are of interest to the reader.

References

Advisory Circular 120-61B, In-Flight Radiation Exposure, U.S. Department of Transportation, Federal Aviation Administration, 21 November 2014.

ATSB Transport Safety Report, Aviation Occurrence Investigation, AO-2008-070 Final, In-flight upset 154 km west of Learmonth, WA 7 October 2008 VH-QPA Airbus A330-303, Australian Transport Safety Bureau, Commonwealth of Australia, 19 Dec 2011.

Beck, P., C. Dyer, N. Fuller, A. Hands, M. Latocha, S. Rollet, F. Spurny (2009), Overview of On-Board Measurements During Solar Storm Periods, *Radiat. Prot. Dosimetry*, 136, 4, 297, doi:10.1093/rpd/ncp208.

Beck, P., D. Bartlett, K. O'Brien, U.J. Schrewe (1999), In-flight Validation and Routine Measurements, *Radiat. Prot. Dosimetry*, 86 (4), 303.

Beck, P., J.F. Bottollier-Depois, R. Bütikofer, E. Flückiger, N. Fuller, M. Latocha, V. Mares, D. Matthiä, and W. Rühm, Comparison of Codes Assessing Radiation Exposure of Aircraft Crew during Energetic Solar Particle Events, European Space Weather Week, Liege, 17-21 November 2014.

Beck, P., M. Latocha, S. Rollet, and G. Stehno (2005), TEPC reference measurements at aircraft altitudes during a solar storm. *Adv. Space Res.,* 36 (9), 1627.

Beck, P., P. Ambrosi, U. Schrewe, K. O'Brien, ACREM, Aircrew Radiation Exposure Monitoring (1999), Final Report of European Commission contract F14P-CT960047, OEFZS, Report G-0008.

Cannon, P. (2013), Extreme space weather: impacts on engineered systems and infrastructure, Royal Academy of Engineering, Carlton House Terrace, London.

Copeland, K., H.H. Sauer, F.E. Duke, and W. Friedberg (2008), Cosmic radiation exposure of aircraft occupants on simulated high-latitude flights during solar proton events from 1 January 1986 through 1 January 2008, *Adv. Space Res.,* 42(6), 1008.

Council Directive 2013/59/EURATOM, Official Journal of the European Union, 5 December 2013.

Dyer, C., A. Hands, L. Fan, P. Truscott, K.A. Ryden, P. Morris, I. Getley, L. Bennett, B. Bennett, and B. Lewis (2009), Advances in Measuring and Modeling the Atmospheric Radiation Environment, IEEE *Trans. Nucl. Sci.*, **56,** 6 (1), 3415.

Dyer, C.S., A.J. Sims, J. Farren, and J. Stephen (1990), Measurements of solar flare enhancements to the single event upset environment in the upper atmosphere, *IEEE Trans. Nucl. Sci.*, *37*, Dec, 1929-1937, doi: 10.1109/23.101211.

Dyer, C.S., F. Lei, A. Hands, and P. Truscott (2007), Solar particle events in the QinetiQ atmospheric radiation model, *IEEE Trans. Nucl. Sci*, 54, 4, 1071, doi: 10/1109/TNS.2007.893537.

Dyer, C.S., F. Lei, S.N. Clucas, D.F. Smart, and M.A. Shea (2003). Solar particle enhancements of single event effect rates at aircraft altitudes *IEEE Trans. Nucl. Sci.*, 50, 6, 2038-2045, doi: 10.1109/TNS.2003.821375.

EURADOS Report, EURADOS Report 2012-03, Braunschweig, ISSN 2226-8057, ISBN 978-3-943701-02-9, May 2012.

European Commission Radiation Protection 140, Cosmic Radiation Exposure of Aircraft Crew, Compilation of Measured and Calculated Data, European Communities, 2004.

Friedberg, W. and K. Copeland (2003), What aircrews should know about their occupational exposure to ionizing radiation. Oklahoma City, OK: Federal Aviation Administration, Civil Aerospace Medical Institute DOT Report No. DOT/FAA/ AM-03/16.

Friedberg, W. and K. Copeland (2011), Ionizing Radiation in Earth's Atmosphere and in Space Near Earth, Oklahoma City, OK: Federal Aviation Administration, Civil Aerospace Medical Institute DOT Report No. DOT/FAA/AM-11/9.

Friedberg, W., K. Copeland, F.E. Duke, K. O'Brien, and E.B. Darden (1999), Guidelines and technical information provided by the U.S. Federal Aviation Administration to promote radiation safety for air carrier crew members, *Radiat. Prot. Dosimetry* **86**, 323.

Gersey, B., R. Wilkins, W. Atwell, W.K. Tobiska, and C. Mertens (2012), Tissue Equivalent Proportional Counter Microdosimetry Measurements Aboard High-Altitude and Commercial Aircraft, AIAA 2012-3636, AIAA 42nd International Conference on Environmental Systems, 15 - 19 July 2012, San Diego, California.

Getley, I.L., L.G.I. Bennett, B.J. Lewis, B. Bennett, C.S. Dyer, A.D.P. Hands, and M.L. Duldig (2010), Evaluation of new cosmic radiation monitors designed for aircrew exposure assessment, *Space Weather*, *8*, 1, S01001, doi: 10.1029/2009sw000492.

Getley, I.L., M.L. Duldig, D.F. Smart, and M.A. Shea (2005), Radiation dose along North American transcontinental flight paths during quiescent and disturbed geomagnetic conditions, *Space Weather*, *3*, 1, S01004, doi: 10.1029/2004sw000110.

Hands, A. and C.S. Dyer (2009), A Technique for Measuring Dose Equivalent and Neutron Fluxes in Radiation Environments Using Silicon Diodes, IEEE *Trans. Nucl. Sci.*, **56,** 6 (1), 3442.

Hwang, J., K. Dokgo, E. Choi, K.-C. Kin, H.-P. Kim, and K.-S. Cho (2014), Korean Radiation Exposure Assessment Model for aviation route dose: KREAM, KSS Fall meeting, Jeju, Korea, October 29-31, 2014.

ICRP, 1991. 1990 Recommendations of the International Commission on Radiological Protection. ICRP Publication 60. Ann. ICRP 21 (1-3).

ICRP, 2005. Low-dose Extrapolation of Radiation-related Cancer Risk. ICRP Publication 99. Ann. ICRP 35 (4).

ICRP, 2007. The 2007 Recommendations of the International Commission on Radiological Protection. ICRP Publication 103. Ann. ICRP 37 (2-4).

ICRU, 2010. Reference Data for the Validation of Doses from Cosmic-Radiation Exposure of Aircraft Crew. ICRU Report 84 (prepared jointly with ICRP). Journal of the ICRU 10 (2), 2010.

IEC 62396-1, Process management for avionics – Atmospheric radiation effects – Part 1: Accommodation of atmospheric radiation effects via single event effects within avionics electronic equipment, Edition 1.0 2012-05, 2012.

ISO 15390:2004, Space environment (natural and artificial) – Galactic cosmic ray model.

ISO 20785-1:2012, Dosimetry for exposures to cosmic radiation in civilian aircraft — Part 1: Conceptual basis for measurements.

ISO 20785-2:2011, Dosimetry for exposures to cosmic radiation in civilian aircraft -- Part 2: Characterization of instrument response.

ISO 21348:2007, Space environment (natural and artificial) – Process for determining solar irradiances.

ISO/AWI 17520, Space systems – Space environment -- Cosmic ray and solar energetic particle penetration inside the magnetosphere: Method of the effective vertical cut-off determination.

ISO/DIS 20785-3, Dosimetry for exposures to cosmic radiation in civilian aircraft -- Part 3: Measurements at aviation altitudes.

Johnston, C.O. (2008), A Comparison of EAST Shock-Tube Radiation Measurements with a New Radiation Model, AIAA Paper 2008-1245.

Joyce, C.J., N.A. Schwadron, J.K. Wilson, H.E. Spence, J.C. Kasper, M. Golightly, J.B. Blake, L.W. Townsend, A.W. Case, E. Semones, S. Smith, and C.J. Zeitlin (2014), Radiation modeling in the Earth and Mars atmospheres using LRO/CRaTER with the EMMREM Module, *Space Weather, 12*, 112, doi:10.1002/swe.20095.

Kyllönen, J.E., L. Lindborg, and G. Samuelson (2001), Cosmic radiation measurements on-board aircraft with the variance method, *Radiat. Prot. Dosimetry*. 93, 197.

Latocha, M., M. Autischer, P. Beck, J.F. Bottolier–Depois, S. Rollet, F. Trompier (2007), The results of cosmic radiation in-flight TEPC measurements during the CAATER flight campaign and comparison with simulation, *Radiat Prot Dosimetry,* 125 (1-4), 412, doi:10.1093/rpd/ncl123.

Latocha, M., P. Beck, P. Bütikofer, H. Thommesen (2014), AVIDOS 2.0 – Current Developments for the Assessment of Radiation Exposure at Aircraft Altitudes Caused by Solar Cosmic Radiation Exposure, European Space Weather Week, Liege, 17-21 November, http://stce.be/esww11.

Latocha, M., P. Beck, S. Rollet (2009), AVIDOS – a software package for European accredited aviation dosimetry, *Rad. Prot. Dosimetry*, 136 (4), 286, doi:10.1093/rpd/ncp126.

Lei, F., A. Hands, C. Dyer, P. Truscott (2006), Improvements to and Validations of the QinetiQ Atmospheric Radiation Model (QARM), *IEEE Transactions on Nuclear Science,* 53, 4, 1851.

Lillhök, J. (2007), Comparison of dose equivalent meters for cosmic radiation exposure and calculations at constant flight conditions, *Radiat. Meas.,* 42, 323.

Matthiä, D., M.M. Meier, and G. Reitz (2014), Numerical calculation of the radiation exposure from galactic cosmic rays at aviation altitudes with the PANDOCA core model, *Space Weather,* 12, 161, DOI: 10.1002/2013SW001022.

Meier, M.M., and D. Matthiä (2014), A space weather index for the radiation field at aviation altitudes, *J. Space Weather Space Clim.* 4, A13.

Meier, M.M., M. Hubiak, D. Matthiä, M. Wirtz, and G. Reitz (2009), Dosimetry at aviation altitudes (2006–2008), *Radiat. Prot. Dosim.,* 136 (4), 251.

Mertens, C.J., B.T. Kress, M. Wiltberger, W.K. Tobiska, B. Grajewski, and X. Xu (2012), Atmospheric ionizing radiation from galactic and solar cosmic rays, Current topics in ionizing radiation research, M. Nenoi (Ed.), ISBN: 978-953-51-0196-3, InTech.

Mertens, C.J., M.M. Meier, S. Brown, R.B. Norman, and X. Xu (2013), NAIRAS aircraft radiation model development, dose climatology, and initial validation, *Space Weather,* 11, 603, DOI: 10.1002/swe.20100.

NCRP Report No. 174 - Preconception and Prenatal Radiation Exposure: Health Effects and Protective Guidance (2013).

NCRP Report No. 116 - Limitation of Exposure to Ionizing Radiation, National Council on Radiation Protection and Measurements (1993).

Normand, E., D.L. Oberg, J.L. Wert, J.D. Ness, P.P. Majewski, S. Wender, and A. Gavron (1994), Single event upset and charge collection measurements using high energy protons and neutrons, *IEEE Trans. on Nucl. Sci.*, 41, 6, 2203.

Normand, E., K. Vranish, A. Sheets, M. Stitt, and R. Kim (2006), Quantifying the Double-Sided Neutron SEU Threat, From Low Energy (Thermal) and High Energy (>10 MeV) Neutrons, *IEEE Trans. on Nucl. Sci.*, 53, 6, 3587.

O'Brien, K., W. Friedberg, H.H. Sauer and D.F. Smart (1996), Atmospheric cosmic rays and solar energetic particles at aircraft altitudes. *Environ. Int.*, **22** (Suppl. 1), S9.

O'Sullivan, D., D.T. Bartlett, P. Beck, J.-F. Bottollier-Depois, L. Lindborg, F. Wissmann, L. Tommasino, M. Pelliccioni and M. Silari (1999), Investigations of Radiation Fields at Aircraft Altitudes, Final Report of European Commission contract no. F14P-CT950011, Dublin Institute for Advanced Studies, Dublin.

O'Sullivan, D., D.T. Bartlett, P. Beck, J.-F. Bottollier-Depois, L. Lindborg, F. Wissmann, L. Tommasino, M. Pelliccioni, H. Roos, H. Schraube, M. Silari, and F. Spurny (2004), Dosimetry of aircrew exposure to radiation during solar maximum, Final Report of European Commission contract FIGM-CT-2000-00068 (DOSMAX). http://cordis.europa.eu/project/rcn/52376_en.html.

Reitz, G., K. Schnuer, and Shaw, K. (1993), Editorial - workshop on radiation exposure of civil aircrew, *Radiat. Prot. Dosim.* 48, 3.

Sato, T., H. Yasuda, K. Niita, A. Endo, and L. Sihver (2008), Development of PARMAPHITS-based Analytical Radiation Model in the Atmosphere, *Rad. Res.*, **170**, 244.

Schwadron, N., C. Bancroft, P. Bloser, J. Legere, J. Ryan, S. Smith, H. Spence, J. Mazur, and C. Zeitlin (2013), Dose spectra from energetic particles and neutrons, *Space Weather,* 11, 547, doi:10.1002/sw.20095.

Schwadron, N.A., T. Baker, B. Blake, A.W. Case, J.F. Cooper, M. Golightly, A. Jordan, C. Joyce, J. Kasper, K. Kozarev, J. Mislinski, J. Mazur, A. Posner, O. Rother, S. Smith, H.E. Spence, L.W. Townsend, J. Wilson, and C. Zeitlin (2012), Lunar Radiation Environment and Space Weathering from the Cosmic Ray Telescope for the Effects of Radiation (CRaTER), *J. Geophys. Res. (Planets),* 117, E00H13, doi:10.1029/2011JE003978.

Spence, H.E., A. Case, M.J. Golightly, T. Heine, B.A. Larsen, J.B. Blake, P. Caranza, W.R. Crain, J. George, M. Lalic, A. Lin, M.D. Looper, J.E. Mazur, D. Salvaggio, J.C. Kasper, T.J. Stubbs, M. Doucette, P. Ford, R. Foster, R. Goeke, D. Gordon, B. Klatt, J. O'connor, M. Smith, T. Onsager, C. Zeitlin, L. Townsend, and Y. Charara (2010), CRaTER: The Cosmic Ray Telescope for the Effects of Radiation Experiment on the Lunar Reconnaissance Orbiter Mission, *Sp. Sci. Rev.*, 150.1-4: 243-284.

Tobiska, W.K., R. Bala, D. Knipp, W.J. Burke, D. Bouwer, J. Bailey, M.P. Hagan, L Didkovsky, K. Judge, H. Garrett, J. Dillon, B.R. Bowman, J. Gannon, W. Atwell, J.B. Blake, W.R. Crain, D. Rice, R. Schunk, D. Bell, B. Gersey, R. Wilkins, R. Fuschino, C. Flynn, K. Cecil, C. Mertens, X. Xu, G. Crowley, A. Reynolds, I. Azeem, S. Wiley, M. Holland, and K. Malone (2014), Operational specification and forecasting advances for Dst, LEO thermospheric densities, and aviation radiation dose and dose rate, Space Weather Workshop, Boulder, Colorado, April 2014.

Tobiska, W.K., D. Bouwer, J.J. Bailey, L.V. Didkovsky, K. Judge, H.B. Garrett, W. Atwell, B. Gersey, R. Wilkins, D. Rice, R.W Schunk, D. Bell, C.J. Mertens, X. Xu, G. Crowley, I. Azeem, A. Reynolds, M.J. Wiltberger, S. Wiley, S. Bacon, E. Teets, A. Sim, L. Dominik, B. Jones, and the ARMAS Science Team, Operational advances for atmospheric radiation dose rate specification, 12th Conference on Space Weather, Applications for end users, American Meteorological Society, January 2015.

Wilson, J.W., P. Goldhagen, V. Rafnsson, J.M. Clem, and G. De Angelis (2002), Overview of Atmospheric Ionizing Radiation (*AIR*) Research: SST-Present, COSPAR, Houston, TX.

Zuccon P., B. Bertucci, B. Alpat, R. Battiston, G. Battistoni, W.J. Burger, G. Esposito, A. Ferrari, E. Fiandrini, G. Lamanna, P. Sala (2001), A Monte Carlo simulation of the interactions of cosmic rays with the atmosphere, CERN, September 14, 2001.

Thermal Neutrons in Airplanes—Strategic Partnership Agreement with Honeywell, Inc.

S. A. Wender, P-27, S. F. Nowicki, ISR-1, Los Alamos National Laboratory,

L. Dominik, Honeywell, Inc.

We have recently received additional funding to continue our Strategic Partnership Agreement with Honeywell, Inc. for our joint study of the impact of thermal neutrons on avionic electronics at flight altitudes. This question is important for the avionics industry because if thermal neutrons are a credible concern, avionics electronics will have to be evaluated before use. We have been working with Honeywell for the past three years to address this question.

It has been well established that high-energy neutrons can cause semiconductor electronics upset. These upsets range from data corruption where the device is still functional to hard failures where the device does not perform as designed. These high-energy neutrons are produced when cosmic rays, typically GeV protons, strike the earth's atmosphere and induce nuclear reactions with the elements in the air. Because neutrons are uncharged, they can reach aircraft altitudes and sea level. These high-energy neutrons interact with the silicon in semiconductor devices and produce charged particles which deposit energy along their path. When charge is deposited in a sensitive volume of a semiconductor, the device can upset. This is a particular problem at aircraft altitudes where the neutron intensity is approximately 300 times greater than at sea level.

Recently there has been concern in the avionics community that thermal neutrons, which do not have sufficient energy to displace a Si atom from its lattice site, can also cause upsets. For example, if a particular isotope of natural boron (^{10}B) is present in the device, a thermal neutron capture reaction can produce energetic alpha particles and ^{7}Li ions which can deposit charge and cause upsets. Thermal neutrons are produced when high energy neutrons interact with the atmosphere and the material in aircraft including the fuel, the passengers and the airplane material.

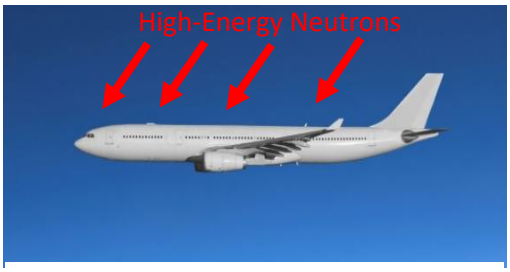

High-energy neutrons strike an airplane and produce thermal neutrons

In order to determine the semiconductor device upset rate in aircraft we proposed three efforts:

1. Measure the thermal neutron intensity in aircraft. Because the thermalization process may depend on the size and geometry of the airplane, the thermal neutron intensity is airplane dependent.
2. Determine the upset rate per thermal neutron. This quantity is device dependent and can be measured using the thermal neutron beam at the Lujan Center at LANSCE.
3. Develop an MCNP model of the airplane to predict the thermal neutron intensity. This model can be tested and benchmarked with our direct measurements.

To measure the thermal neutron intensity in aircraft, we constructed the Tinman instrument. Tinman consists of two identical cylindrical ^{3}He ion counters. One detector is bare and one is surrounded by cadmium shielding, which absorbs thermal neutrons. The difference in count rate between the two detectors gives the contribution due to thermal neutrons. The instrument was designed by P-27 and fabricated by ISR Division.

So far, we have flown Tinman on three NASA aircraft including the ER-2, the Gulfstream-III (as part of the NASA eclipse mission) and a DC-8. Figure 1 shows the TM measurements for the DC-8 flight in Germany.

The number of counts (shown in blue) are the Tinman bare detector minus the cadmium shielded detector measurements binned in 100 second intervals. The orange curve is the altitude obtained from the airplane GPS. We see that the Tinman count rate depends on the altitude and the count rate is an exponential function of the altitude demonstrating that the Tinman instrument is performing well.

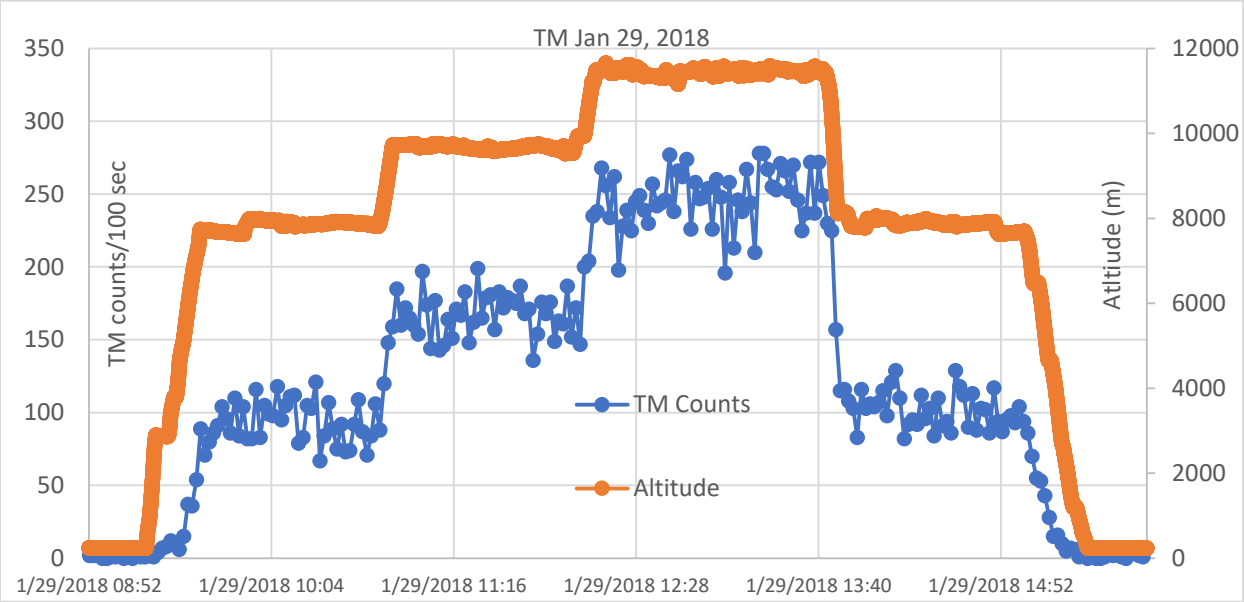

Figure 1. Tinman results on NASA DC-8 flight in Germany.

There is still considerable work to be done to answer the question about the impact of thermal neutrons in avionic environments. We plan the following efforts as part of the Strategic Partnership Agreement:

1. Calibrate the TM instrument to convert the measured count rate to a thermal neutron flux (neutrons/cm^2/sec).
2. Measure the number of upsets per thermal neutron for several typical avionic semiconductor devices. This effort is planned for this run cycle at the Lujan Center.
3. Perform additional measurements on different aircraft and at different locations within the airplane. We would like to fly TM on the NASA SOFIA aircraft which is a modified Boeing 747.
4. Develop a Monte-Carlo model and perform simulations to obtain the thermal neutron environment in the airplane which we can benchmark with our Tinman measurements. We

shall also measure the neutron intensity at different locations within the airplane to map out the special distribution of thermal neutron in the aircraft.

A second Tinman instrument is presently being assembled by ISR Division to measure the thermal neutron environment in the LANL High-Performance Computing (HPC) area. This is part of the effort to characterize the total radiation environment around the LANL HPC computers .

Science & Technology Facilities Council
ISIS Neutron and Muon Source

(/)

Could thermal neutrons be a threat to reliable supercomputing and self-driving cars? 26 May 2020

Rosie de Laune

An investigation into the effect of thermal neutrons on commercial computing d finds that the failure rate due to thermal neutron damage in some environments enough to be a significant threat to device reliability.

Commercial-Off-The-Shelf (COTS) devices are **used widely in high performance computing** as well as s critical applications such as prototype driverless cars because of their high performance, efficiency and lo However, the materials used to build the devices might contain boron-10 (^{10}B), making it **vulnerable to th neutron damage that can result in failures**. This study, published in the *Journal of Supercomputing*, finc **this failure rate may be high enough to severely impact the reliability** of these devices.

High energy neutrons are produced by the interaction of cosmic rays with the atmosphere, and their intera with silicon chips is considered a main cause of faults in electronic devices. **Thermal neutrons are low e neutrons (below 0.5 eV) that are produced by the interaction of high energy neutrons with other ma** the emission of neutrons from nuclear decay. As well as high-energy neutrons, **thermal neutrons can als electronic devices**. Unfortunately, the evaluation of the thermal neutrons flux in a realistic environment is extremely challenging, as it depends on several factors, including weather conditions and surrounding ma

Testing for high-energy neutron damage is common for device manufacturers, many of whom come to ISI the ChipIr instrument for this purpose. However, thermal neutron damage has been considered by the ind be much less likely, and therefore not taken into account.

At ISIS, the group were able to use the ALF/ROTAX beamline to expose the devices to thermal neutrons a ChipIr beamline to expose them to high-energy neutrons, as shown by the neutron spectra (right). Paolo F Associate Professor at the Institute of Informatics of the Federal University of Rio Grande do Sul explains; unique facility for this kind of evaluations, as it features both a high-energy and a thermal neutron beamlin

makes the testing a lot easier, as you can test exactly the same setup in the two beamlines inside the same facility!"

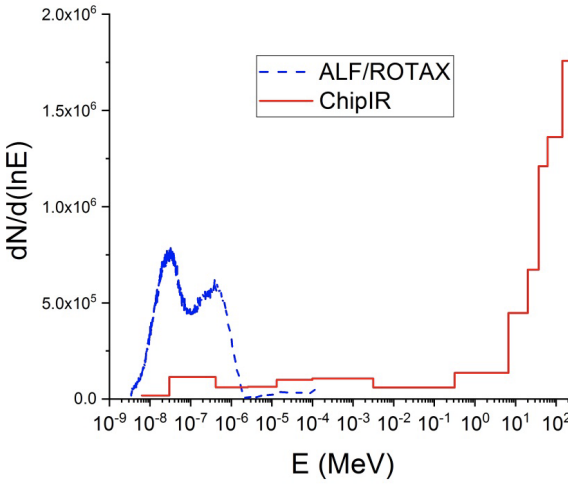

Chris Frost, beamline scientist on ChipIr explains; “As the importance of thermal neutron damage becomes more apparent, we are developing new capabilities at ISIS to ensure our testing ability remains extensive and world leading."

The **impact of thermal neutrons on electronic devices is due to the isotope of boron present** in the material, as only those containing ^{10}B are susceptible to thermal neutron damage. Approximately 20% of naturally occurring boron is ^{10}B, with the remainder being ^{11}B. It is possible to use 'depleted' boron, which is prima to solve this problem. However, this is expensive and unjustified for COTS devices for user applications. T finds that **newer silicon chips are being manufactured in a way that includes high levels of boron** int devices that are candidates for supercomputing applications.

“We know that using **natural boron can pose risks to the reliability of electronic devices**, as they becc susceptible to thermal neutrons." Explains Paolo; “However, we can't blame the silicon industry for using cheaper natural boron in their devices for the user market, as reliability is a secondary aspect when comp price and performance. **The increased demand for computing efficiency in supercomputers and autc systems make COTS devices attractive solutions**, increasing the likelihood of damage from thermal ne being a problem."

This investigation took six **commercially-available devices** that are used in high performance computing **tested them under both high-energy and thermal neutron irradiation at ISIS**. Whilst being irradiated, t devices were run under normal operating conditions and their performance measured.

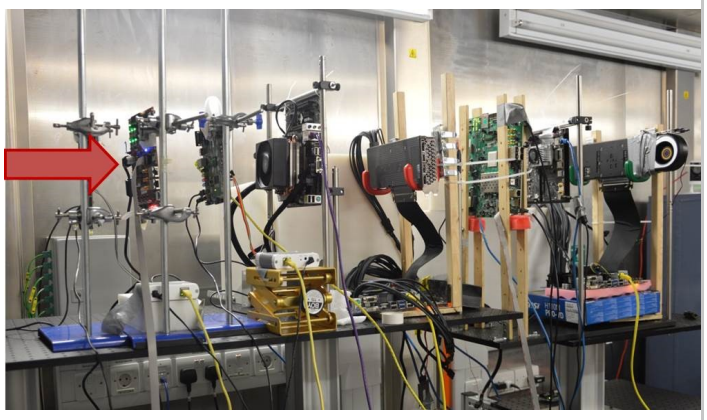

Samples being measured on ChipIr

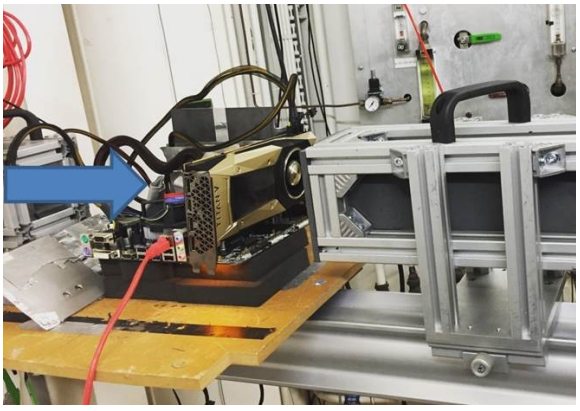

Sample measurement on ROTAX

Their experiments showed that **all the devices were impacted by thermal neutrons**, indicating the pres ^{10}B within them. The different energy of thermal neutrons compared to those coming directly from cosmic interaction with the atmosphere can lead to differing interactions with the materials inside the devices. Th found that **different codes executed on the same device showed different sensitivities to high-energ thermal neutrons**, depending on how the code accesses the device memory, and how it executes instru

To understand the impact caused by the two types of neutrons, the group needed to know the **likelihood background neutron flux being high enough** for the faults caused to impact the device reliability. In con high energy neutrons, the **rate of thermal neutrons passing through a device depends on its environ** the presence of other materials close to the device.

The group created a neutron detector, and used it to measure the flux inside a building that replicated the conditions inside a typical data centre. They found that the **rate of thermal neutrons, and therefore the rate of a device, was dependant on the physical layout of a machine room**. It could also be impacted weather conditions: **on a rainy day, the rate of thermal neutrons could double**, causing a similar increa failure rate of the device.

This study can therefore be **used to inform machine room designers**, who could choose to prioritise tas carried out by the supercomputers in such a way that those requiring a higher level of reliability are carrie devices in locations, and under certain weather conditions, **that reduce the likelihood of thermal neutro interaction**. For the case of driverless cars, the group notes that, even with shielding, the **thermal neutro may be increased by interaction of the neutrons with the driver, passengers and liquids on board**, s the fuel tank.

“We are beginning to see devices that are not designed to be reliable being used in applications that requ reliability." Says Paolo; “This is totally acceptable, but this study shows that we need to carefully consider variables, including thermal neutrons, before assuming that the device is boron-10 free."

Further information:

The full article is available at DOI: 10.1007/s11227-020-03324-9 (https://rdcu.be/b4mXH)

Contact: de Laune, Rosie (STFC

Related Sections

▶ **Science Highlights**

Related Content

▶ **Science Highlight**

▶ **ChipIR Science Highlights**

Measurement of Thermal Neutron Environments in Aircraft

NASA Seminar

S. A. Wender, S. F. Nowicki,
Los Alamos National Laboratory
L. Dominik
Honeywell, Inc.

August 22th, 2018

Operated by Los Alamos National Security, LLC for the U.S. Department of Energy's NNSA

Radiation effects in semiconductor electronics

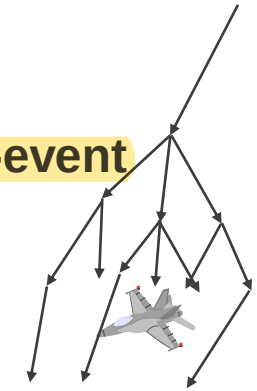

- **It is well established that radiation (even a single particle- single-event effects) can cause semiconductors to fail**
- **These failures include:**
  - Soft errors where only the data is corrupted but the device continues to function normally
  - Hard errors where the device ceases to operate and may have to be reset or replaced

- **Neutrons are the greatest threat to semiconductors at sea level and at aircraft altitudes**
  - Neutrons are produced in the upper atmosphere when cosmic rays (typically GeV protons) strike the elements in the air and produce neutrons (and other things) via nuclear reactions
  - Because neutrons are uncharged, they can reach aircraft altitudes and below
  - The neutrons interact with the semiconductor material and can cause nuclear reactions which produce energetic charged particles
  - If these energetic ions deposit charge in the sensitive volume of semiconductors they can cause the device to upset

Measurement of thermal neutrons in aircraft (1)

- Recently the avionics community has become concerned about the effects of thermal neutrons on flight control electronics. This question is important because if thermal neutrons are a credible concern, avionic electronics may have to be evaluated with thermal neutrons before use.
- Neutrons are a particular concern for aircraft because the cosmic-ray induced neutron flux is approximately 300 times greater than at sea level
- Thermal neutrons are produced when high-energy neutrons are thermalized in the atmosphere, the aircraft fuel, passengers and aircraft materials. Thermal neutrons have energies of 0.025 eV (2200m/s), much less than the energy required to cause a lattice displacement.

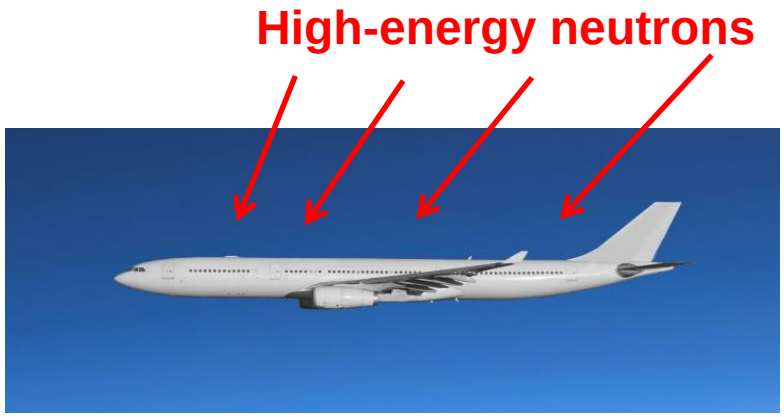

	$n/cm^2/s$	Relative
Sea level (New York City	0.00565	1
7000 ft (Los Alamos)	0.019	3.4
40,000 feet	1.53	270

Measurement of thermal neutrons in aircraft (2)

- **For example, thermal neutrons can interact with ^{10}B that is in the semiconductor parts. ^{10}B can capture a neutron and produce an energetic alpha particle and ^{7}Li ion which can deposit enough charge to cause a single-event upset.**
- **To understand the effect of thermal neutrons in aircraft we need to know:**
  - Thermal neutron intensity in airplane— may be airplane dependent- Tinman- need to obtain data in several types of aircraft
  - Effect of thermal neutrons on semiconductor devices- Device dependent --measure at low-energy neutron source at Lujan Center at LANSCE
  - Model / simulations of thermalization of neutrons in aircraft- MCNP calculations

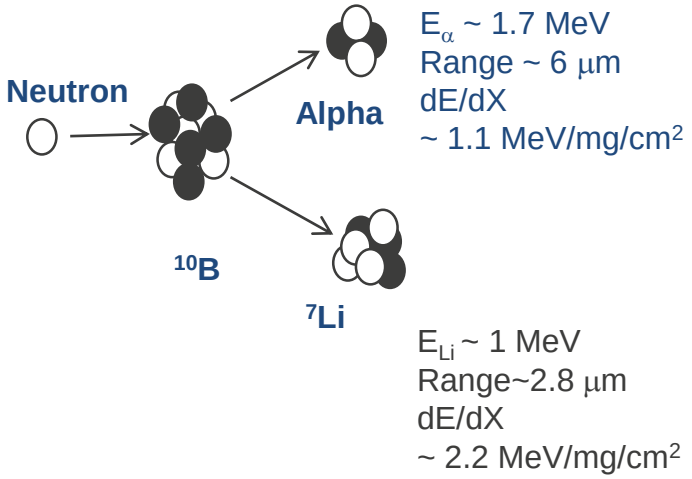

Measurement of thermal neutron intensity in aircraft—Tinman

- **An instrument was designed to measure thermal neutrons in aircraft. This effort is part of a Strategic Partnership Agreement between LANL and Honeywell, Inc.**
- **Tinman consists of:**
  - Two identical cylindrical ^{3}He ion chamber detectors. (~0.63 cm diam 6 cm long). He-3 was chosen because of its sensitivity to thermal neutrons and insensitivity to everything else.
  - One detector was bare, one detector was shielded with cadmium to block thermal neutrons
  - The difference in count rates between these two detectors gives the thermal neutron rate
- **Final detector was fabricated by ISR Division at LANL to space specifications**
- **Uses a Raspberry Pi computer for DAQ**
- **Designed for "one switch" operation and can be powered by batteries**

Vibration damping springs

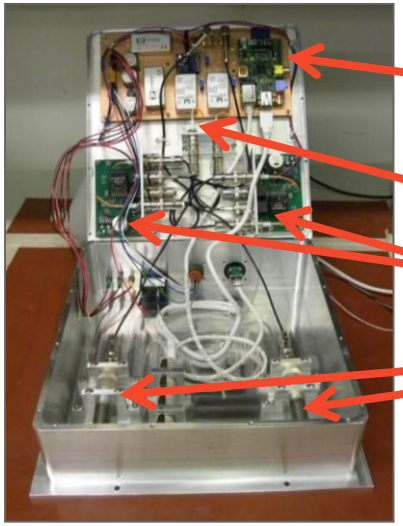

First Tinman flight was on a NASA ER-2 airplane

- ER-2 is the civilian version of U-2
- Flew on several flights from NASA Armstrong Flight Research Center in Palmdale, Ca

Tinman

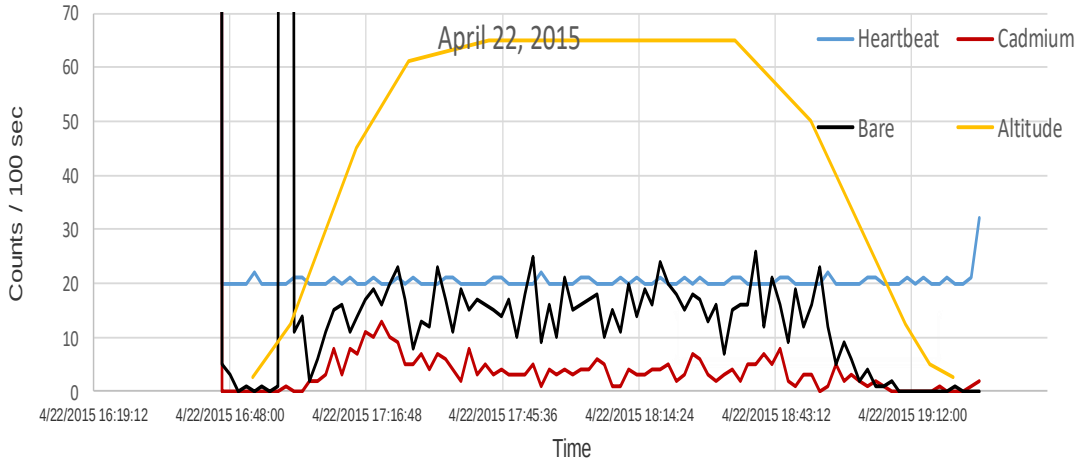

Tinman flew on NASA Eclipse flight on Gulfstream-III airplane

- Changed to larger He-3 detectors to improve signal-to-noise and sensitivity (10X)

Flight Request

Flight Info:
- 3 flights- ferry/rehearsal, mission, ferry
- Request #:17G046
- Hours: 16

Dates of Flights:
- 8/20 – 8/22

Aircraft:
- NASA GIII T/N N808NA

Crew:
- See right →

Purpose of Flight:
- Collect and transmit real-time HDTV video of the eclipse as well as photo documentation of the event
- Collect scientific data from a spectrograph provided by NASA HQs and science payloads

FLIGHT 1- Ferry up/Rehearsal ***#C: 13***

Pilots:	Troy Asher, Andrew Barry
Safety Tech:	Manny Rodriguez
Ops:	Mike Buttigieg
Photo:	Carla Thomas
Video:	Lori Losey, Steve Parcel, Mike Agnew
PAX:	David McBride, Randy Albertson, Kevin Rohrer, Thomas Zurbuchen, Debra Randall

FLIGHT 2- Mission ***#C: 12***

Pilots:	Troy Asher, Andrew Barry
Safety Tech:	Manny Rodriguez
Photo:	Carla Thomas
Video:	Lori Losey, Steve Parcel, Mike Agnew
PAX:	David McBride, Robert Lightfoot, Thomas Zurbuchen, Lesa Roe, Kevin Rohrer

AFRC Dir → PAX
NASA Administrator → PAX
Ch. of St. comm.
NASA Science mission
Dep. Assoc. Admin

FLIGHT 3- Ferry back ***#C: 11***

Pilots:	Troy Asher, Andrew Barry
Safety Tech:	Manny Rodriguez
Ops:	Mike Buttigieg
Photo:	Carla Thomas
Video:	Lori Losey, Steve Parcel, Mike Agnew
PAX:	David McBride, Randy Albertson, Debra Randall

Solar Eclipse Mission Tech Brief - 8/14/17 47

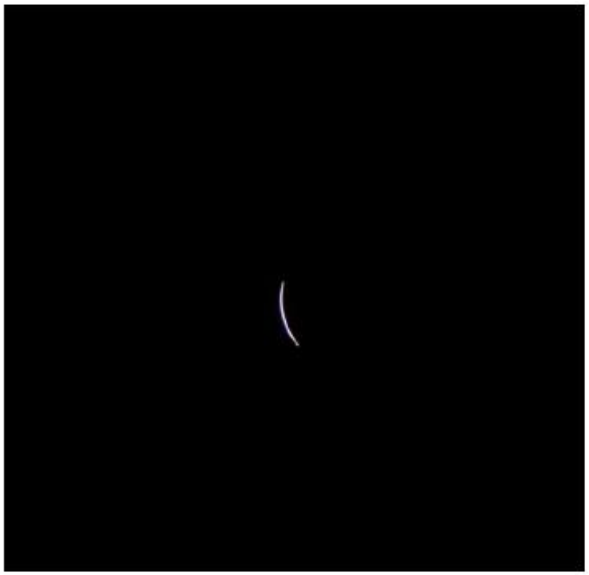

Preliminary results for Tinman detector on NASA Eclipse flights

- **Data from NASA eclipse flight- Tinman data recorded on 3 Gulfstream-III flights**
  - Edwards AFB, Ca to Seattle, Wa on August 20, 2017
  - Eclipse flight on August 21, 2017
  - Seattle, Wa to Edwards AFB, Ca on August 22, 2017
- **Data recorded for:**
  - Bare detector
  - Cd covered detector
- **Thermal neutron count rate is proportional to the high-energy neutron flux**
- **Expect to see exponential decrease in count rate at lower altitudes due to absorption of the high-energy neutrons in the atmosphere**
- **Expect to see latitude dependence in count rate because of the earth's magnetic field**
  - Altitude and Latitude taken from airplane GPS
  - Correction for latitude taken from empirical formula (Normand, IEEE Trans. Nucl. Sci 43, 1996, 461)

    $F(L)=0.6252*\exp[-0.461\cos^2(2L)-0.94\cos(2L)+0.252]$
- **Results of Tinman detector show good agreement with aircraft data**

Tinman detector data Eclipse flight August 21, 2017

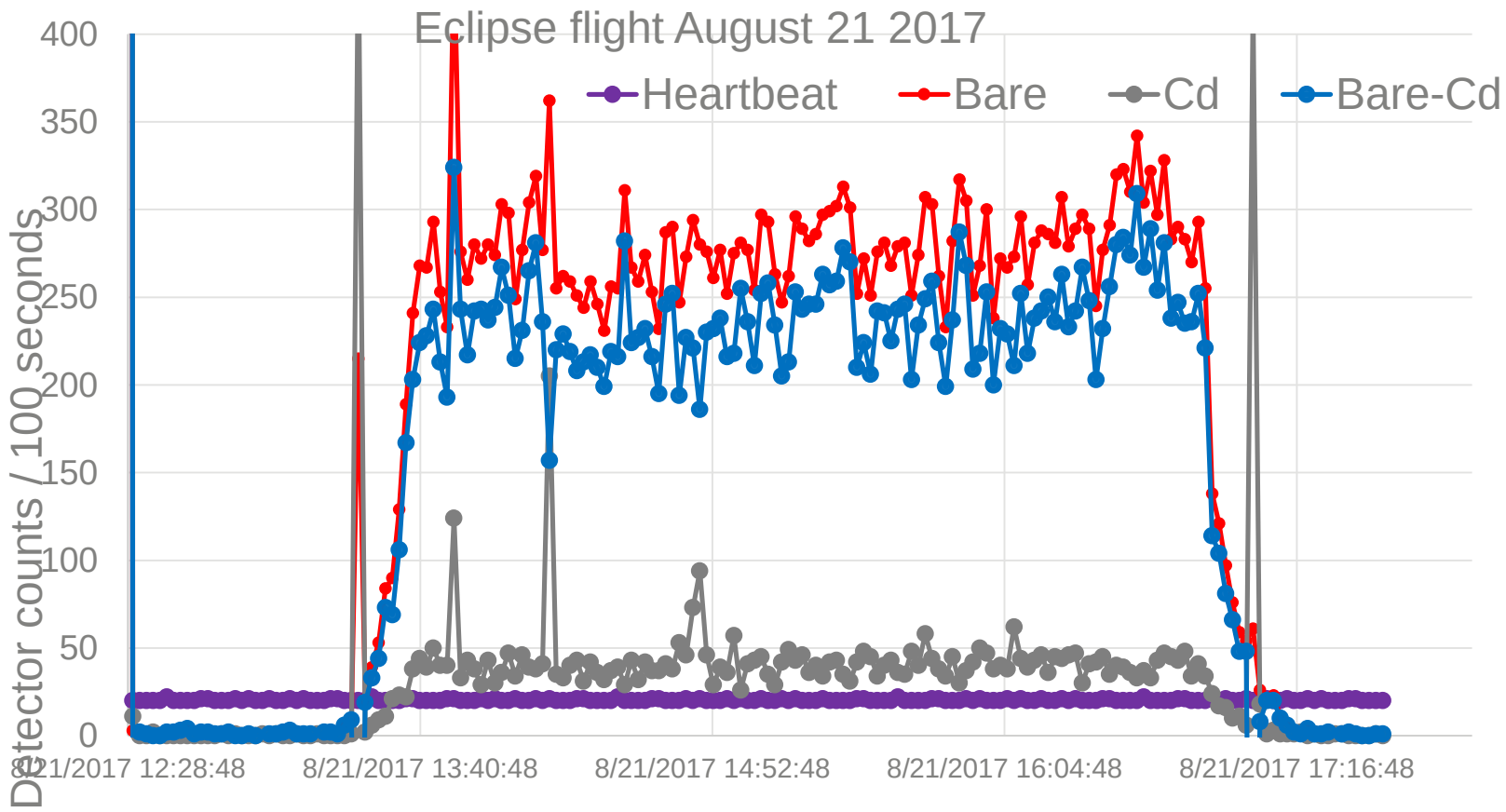

Tinman was flown on NASA DC-8

- The Tinman instrument was flown on 11 flights between Jan 13 and Feb 4, 2018 on the NASA DC-8 airplane

ID	Task Name	Duration	Start
1	jan 13 2018 analysis	10.68 hrs	Sat 1/13/18
2	Jan 17 2018 analysis	3.78 hrs	Wed 1/17/1
3	Jan 19 2018 analysis	4.52 hrs	Fri 1/19/18
4	Jan 23 2018 analysis	3.93 hrs	Tue 1/23/18
5	Jan 24 2018 analysis	5.05 hrs	Wed 1/24/1
6	Jan 29 2018 analysis	5.2 hrs	Mon 1/29/1
7	jan 30 2018 analysis	4.88 hrs	Tue 1/30/18
8	Jan 31 2018 analysis	4.58 hrs	Wed 1/31/1
9	Feb 1 2018 analysis	4.2 hrs	Thu 2/1/18
10	Feb 3 2018 analysis	9.88 hrs	Sat 2/3/18
11	Feb 4 2018 analysis	2.45 hrs	Sun 2/4/18
12			
13			

NASA DC-8 flight January 29, 2018

- This flight was around Ramstein, Germany with several changes in altitude but no significant change in latitude
- Straight line on semilog plot of detector count rate vs altitude show exponential absorption of cosmic-ray induced high-energy neutron flux

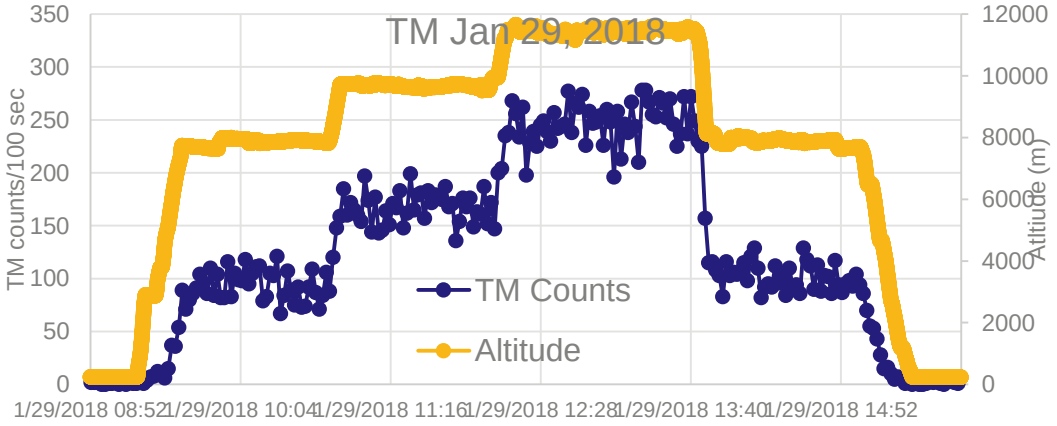

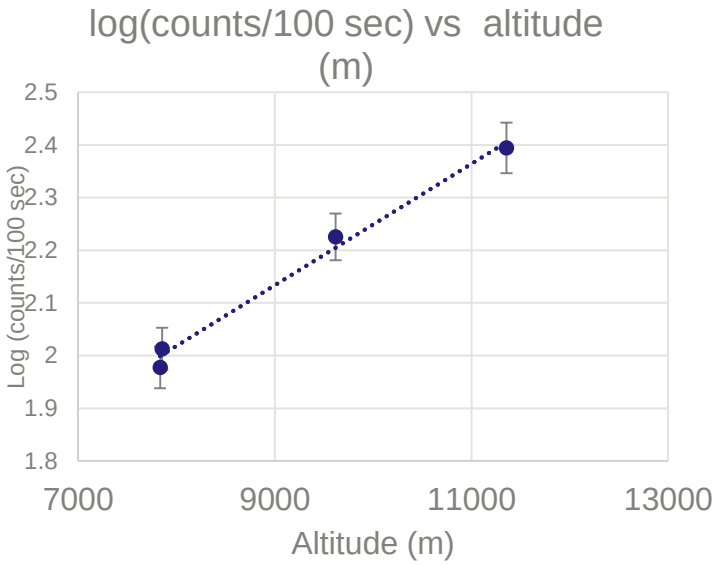

NASA DC-8 flight from Palmdale, Ca to Ramstein, Germany

- Blue curve shows the increase in cosmic-ray neutron flux when flying north
- TM data shows good agreement with prediction

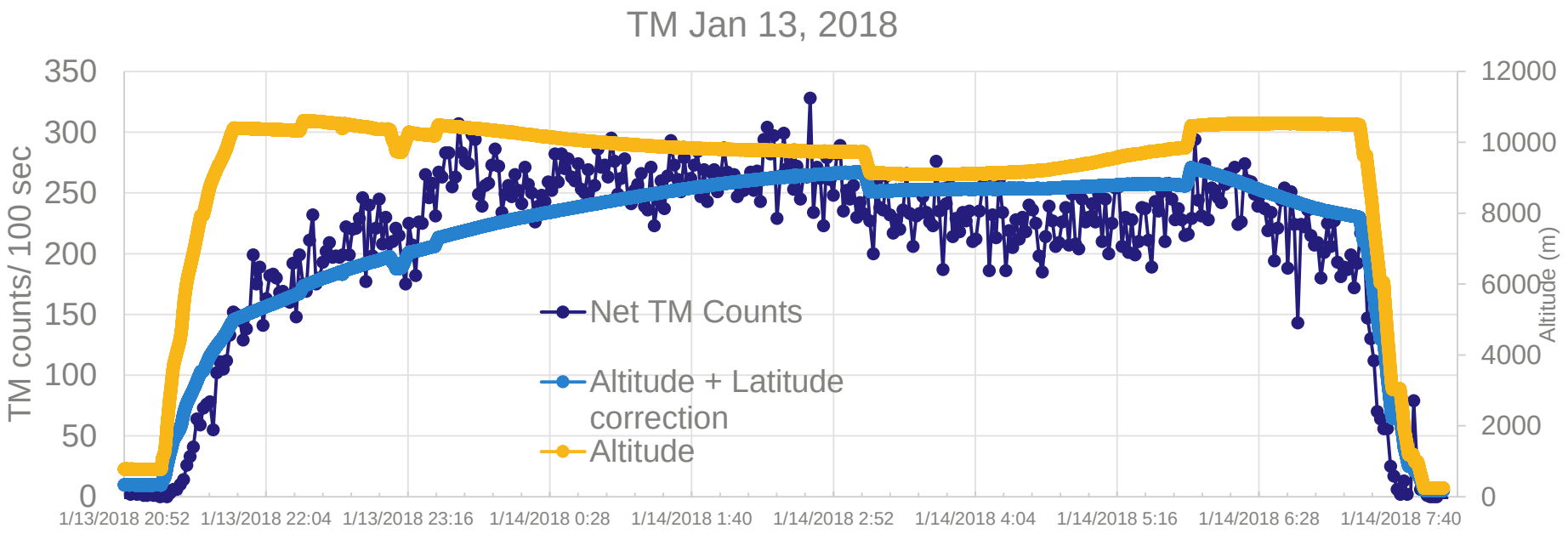

NASA DC-8 flight from Seattle, Wa to Palmdale, Ca

- Blue curve shows the decrease in cosmic-ray neutron flux when flying south
- TM data shows good agreement with prediction

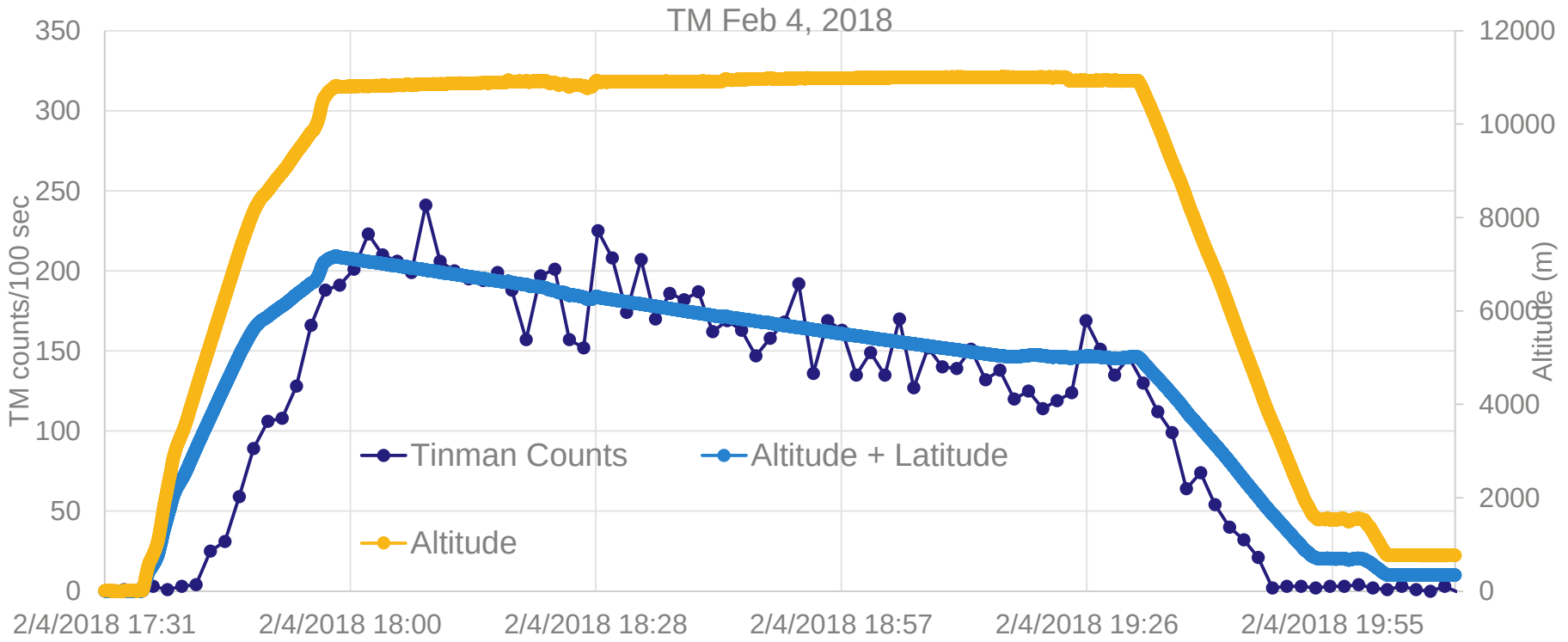

Future work

- **Additional flights**
  - Measure the thermal neutron intensity in other aircraft to determine the effect of moderating material (fuel mass, geometry, etc.) on thermal neutron production
  - Measure the thermal neutron rate in different locations in the same airplane under similar conditions of fuel, altitude and latitude to determine the spacial distribution of the thermal neutrons
- **Simulations**
  - Complete the absolute efficiency determination of TM to thermal neutrons. When this is completed, we will know the number of thermal neutrons in aircraft environments.
  - Model (MCNP) the thermal neutron intensity at different altitudes and different locations within the airplane. The results of these calculations can be compared to our measurements. Can we predict our measurements?
- **Additional measurements**
  - Measure the effect of thermal neutrons on various electronic devices (SEU cross section). With knowledge of the number of thermal neutrons/cm^2/sec in an airplane (from NASA flights) and SEU cross section (measurements at LANSCE), we will be able to predict the number of fails/flight hour in aircraft due to thermal neutrons.

Conclusions

- Tinman instrument works well for detecting thermal neutrons in aircraft--there are thermal neutrons
- The effect of altitude and latitude on the thermal neutron count rate is clearly observed
- Considerable work needs to be done to answer the question of the importance of thermal neutrons in aircraft

Measurement of Thermal Neutron Environments in Aircraft with the Tinman Instrument

P-25 Seminar

OGA visit

October 31, 2019

Steve Wender, P-27

Recent avionics incident highlight Single Event Effects (SEE) problem

- On October 7, 2008 , Qantas 72 was flying from Singapore to Perth, Australia.
- "While ..at 37,000 ft, one of the aircraft's three Air Data Inertial Reference Units (ADIRU) started outputting intermittent, incorrect values…Two minutes later …the aircraft flight control primary computers commanded the aircraft to pitch down. … At least 110 of the 303 passengers and nine of the 12 crew members were injured: 12 of the occupants were seriously injured and another 39 received hospital medical treatment." (Pg. vii)
- "The other potential triggering event was a single event effect (SEE) resulting from a high-energy atmospheric particle striking one of the integrated circuits within the CPU module. There was insufficient evidence available to determine if an SEE was involved, but the investigation identified SEE as an ongoing risk for airborne equipment." (pg. xvii)
- "Testing was conducted with neutrons at 14 MeV …the test was not sufficient to examine the …. susceptibility to the full range of neutrons at the higher energy levels that exist in the atmosphere". (pg. 147)

ATSB Transport Safety Report Aviation Occurrence Investigation AO-2008-70

- "The ATSB received expert advice that **the best way of determining if SEE could have produced the data-spike failure mode was to test the affected units at a test facility that could produce a broad spectrum of neutron energies**. However, the ADIRU manufacturer and aircraft manufacturer did not consider that such testing would be worthwhile….

Neutron Single Event Effects (SEE) are faults in electronic devices caused by neutrons from cosmic rays

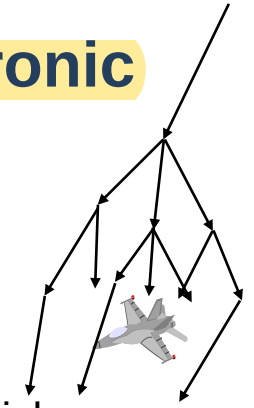

- Neutrons are produced by cosmic rays in the upper atmosphere
- Neutrons have long mean-free paths so they penetrate to low altitudes
- Neutrons interact with Si and other elements in the device to produce charged particles
- Charged particles deposit charge in sensitive volume which cause state of node to change

Protons and Heavy ions are important in space environments

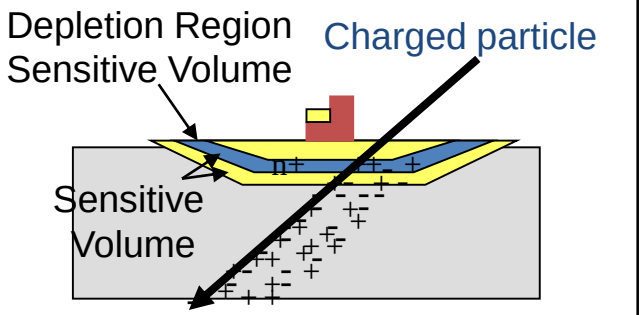

Charged particles produce direct ionization tracks in silicon and indirect ionization via nuclear reactions. Generated charge collects in depletion region, generates a logic upset.

Neutrons are the greatest threat at sea level and aircraft altitudes

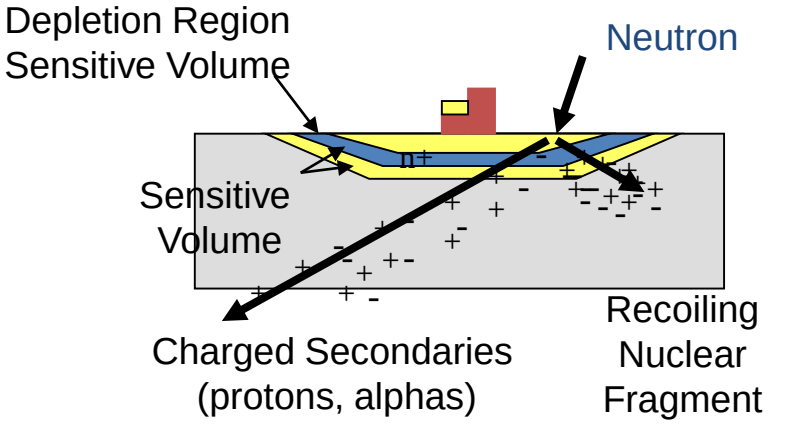

Neutrons need nuclear reaction to create charged particles. Generated charge collects in depletion region, generates a logic upset.

Many types of single-event effects can cause failures

- SEE are different from material radiation effects which depend on displacements per atoms (cracking, embrittlement, swelling)
- Soft errors
  - Single event upset
  - Multiple event upset (a few % of SEU rate, now equal to the SEU rate)
  - Silent data corruption
- Hard errors
  - Single event latchup
  - Single event burnup, gate rupture, etc.
- SEE are also seen in high-power analog devices
- First experiments were performed by the Boeing Co. for 777 certification
- Industry trends to lower voltages and smaller feature size are thought to increase the failure rate due to SEE
- Similar devices have very different failure rates
- The failure rate due to SEU is equal to all the other failure modes combined
- " Since chip SER is viewed by many as a legal liability (something that you know may fail) the public literature in this field is sparse and always makes management nervous". *SER History, Trends and Challenges* James Ziegler and Helmut Puchner

The problem is that there are lots of transistors in the world

Semiconductor devices are used in all aspects of modern life and the reliability of these devices is a major concern and may limit their applicability and performance

1 quintillion = 10^{18}

100 billion transistors for every man, woman and child on planet

Cosmic-ray induced failure rates are difficult to calculate

- The failure rate due to cosmic-ray events is given by:

$$F/t = \Sigma_p \int f_p(E_p) * \Phi_p(E_p)\ dE_p$$

Failure function depends on
- **Device characteristics**
- **Particle type**
- **Particle energy**

Particle flux depends on:
- **Particle type**
- **Altitude**
- **Latitude**
- **Solar activity**
- **Local geometry**

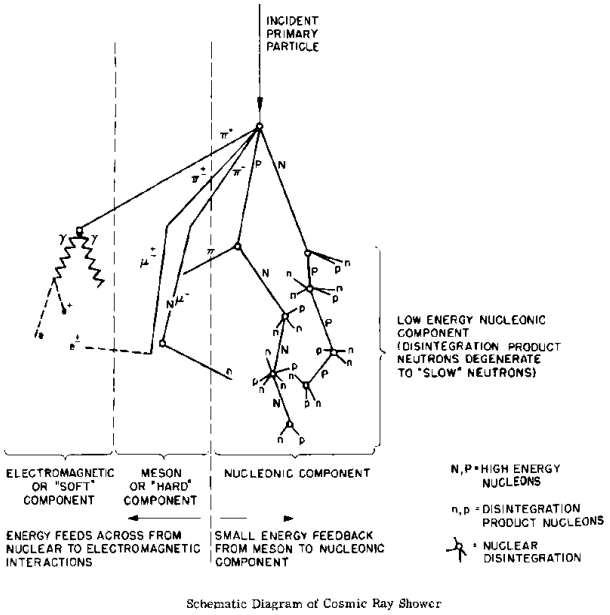

Schematic Diagram of Cosmic Ray Shower

F/t is the number of fails / time

p is the particle type (neutron, protons, pions,…)

$f_p(E_p)$ is the number of fails /particle with energy E_p

$\Phi_p(E_p)$ is the number of particles/sec with energy E_p

Accelerated testing is essential

- Design criteria for systems is 1 fail / year from SEU
  - If need to know the failure rate to 10%, need 100 fails
  - Need to run server for 100 years! RAMs change every 18 months

- Need to perform accelerated testing with acceleration rate~ 5000 ($3.6x10^4$) to get answer in 1 week (1 day) if testing entire system

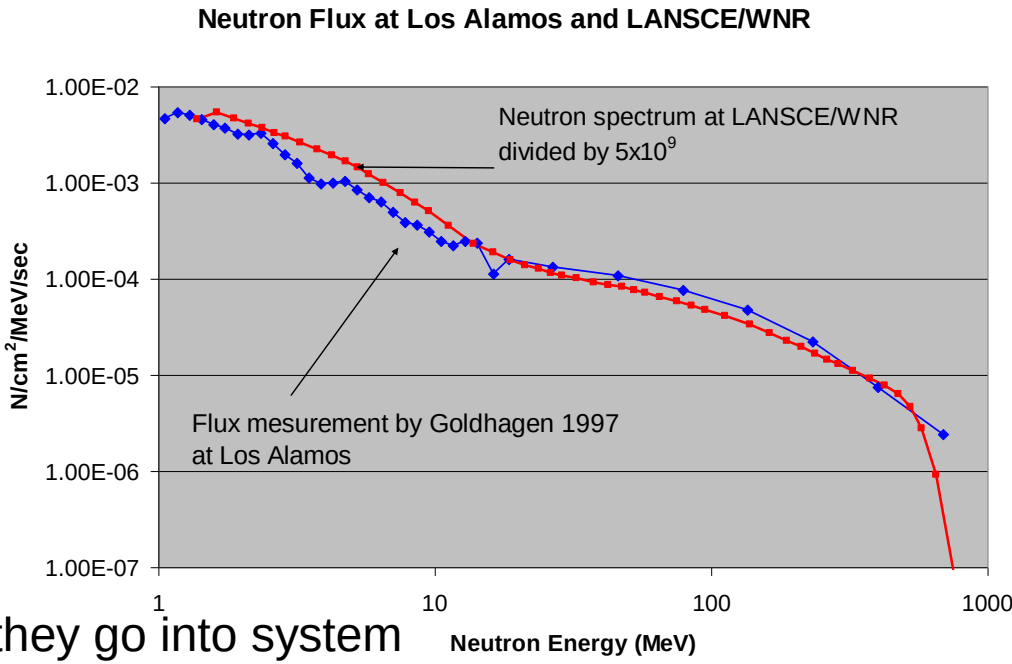

- Need to test individual chips before they go into system
  - A systems may have ~300 memory chips
  - The failure rate of a single chip is 1 fail / 300 years

- This requires an acceleration factor of ~ 10^7 for 1 day of testing to get 100 fails

- The LANSCE beam has shape similar to cosmic-ray induced neutron spectrum so many companies, laboratories and universities have used the LANSCE beam to test and predict the failure rate of their devices

Los Alamos Neutron Science Center (LANSCE)

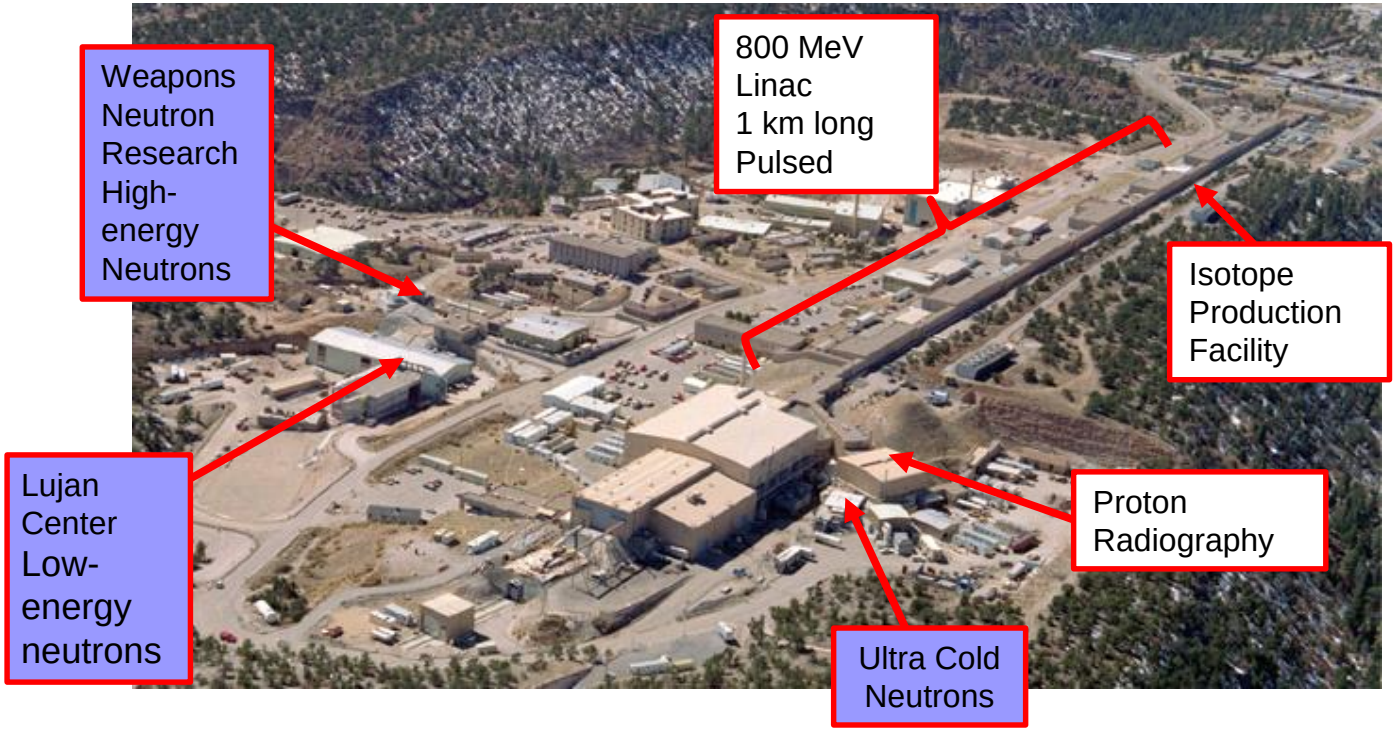

Neutrons at LANSCE are produced by spallation reactions

- Difficult to produce high-energy neutrons. No charge- can't accelerate
- Spallation reactions occur when high energy particles strike a high z target. Spallation reactions produce a wide range of output particles
- In the first stage of the reactions, high-energy nucleons are produced
- At later times, the nucleus "thermalizes" and lower energy neutrons and nuclei are produced
- Charged particles are removed from the neutron beam by magnets

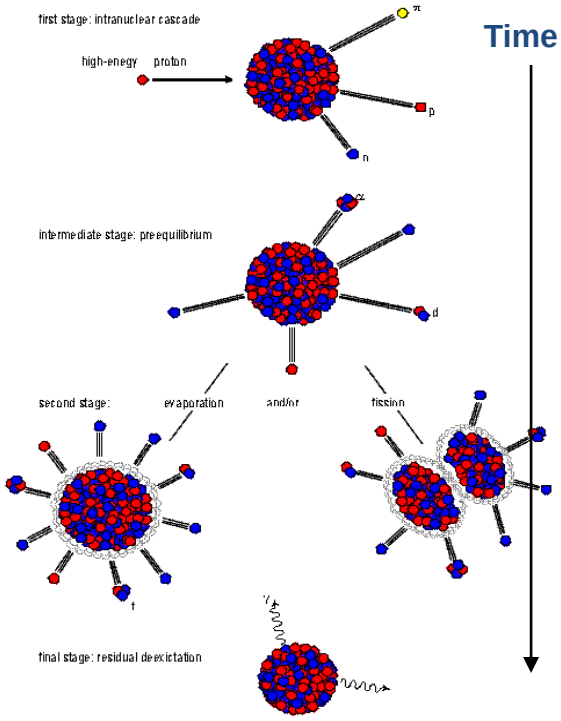

The high-energy neutron spallation source at LANSCE

- 4 μA (1 KW in target) of proton current for high-energy neutron production (Target-4)
  - Neutrons are produced via spallation reactions with tungsten target
  - Tungsten target is 7.5 cm long and 3 cm diam no moderation
  - Target is located inside a 2 m diam vacuum chamber
  - Massive shielding around target
  - Six flight paths operate simultaneously
- Neutron Single Event Effect flight path and test area. Second area developed in 2012

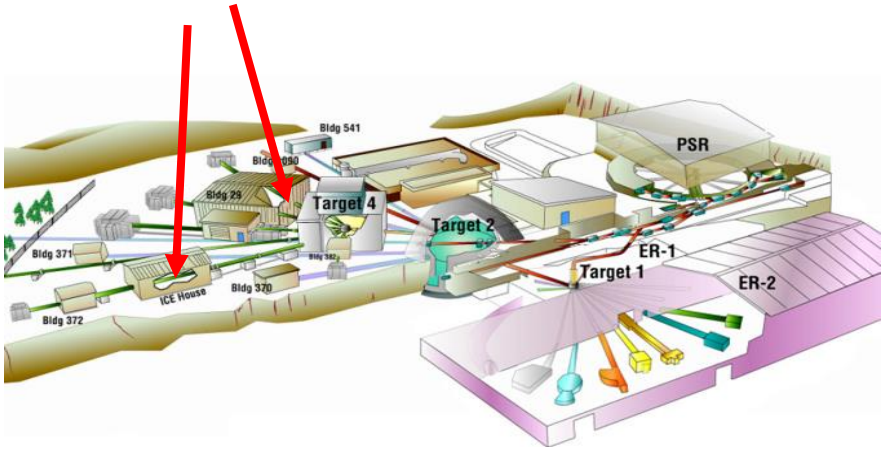

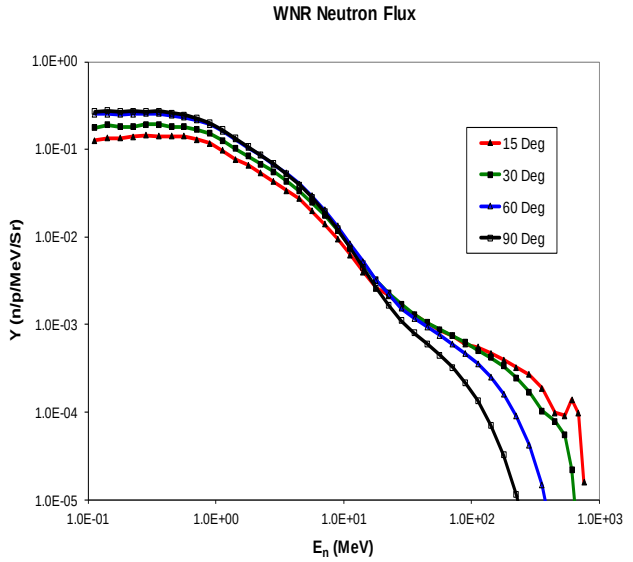

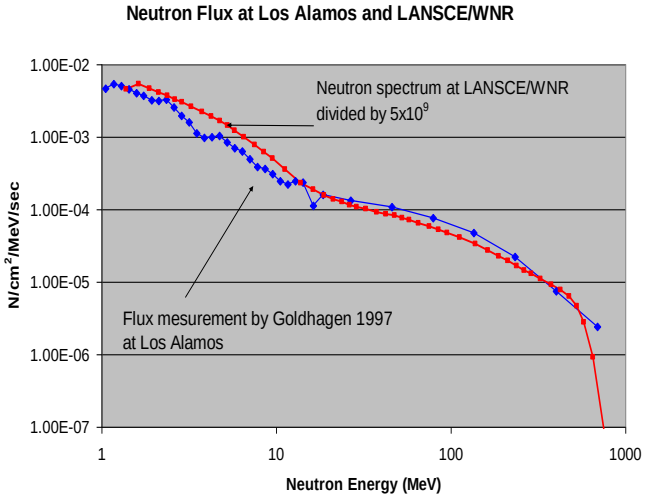

LANSCE capabilities

- LANSCE operates as a DOE Designated User Facility
  - Users from Industry, Universities and other laboratories can use LANSCE facilities
  - Proprietary work can be performed on cost recovery basis- no scientific merit review.
  - To get beam time must submit a proposal from LANSCE web site
- Terrestrial neutron source (High-energy: sea level- avionics)
  - ICE House-I and ICE-II
  - Neutron spectrum is similar to cosmic-ray induced neutron spectrum by ~10^7 times more intense
  - Operates whenever beam is being delivered
  - Cost: $12K for first day, $10K / day for subsequent days
- Thermal neutron source
  - Available at Lujan Center
  - Availability same at above
- Proton beams
  - 250-800 MeV in Target-2
  - Limited availability
  - Need strong Defense Program justification

Radiation effect users at LANSCE

1. Avionics industry- Single event effects (SEE), requires both high-energy and thermal neutrons. Neutron flux at aircraft altitudes ~300 times sea level. First recognized by the Boeing Corp in certification of 777.
2. Semiconductor industry- Wide range of SEE concerns: computer chips, RAMs, automotive, graphics, servers, FPGAs, etc.
3. Medical equipment- pacemakers, etc.
4. High performance computers- silent data corruption
5. NASA- Radiation effects in space- Johnson Space Center –require 200 MeV (and above) protons- IUCF has shut down. NASA using neutrons as surrogate for protons, also need neutrons
6. ISR Division- Radiation effects in space, requires protons and neutrons
7. Sandia- SEE and weapons effects
8. Universities- Radiation effects programs, radiation effects in detector materials and electronics

Long term run cycle for LANSCE Accelerator

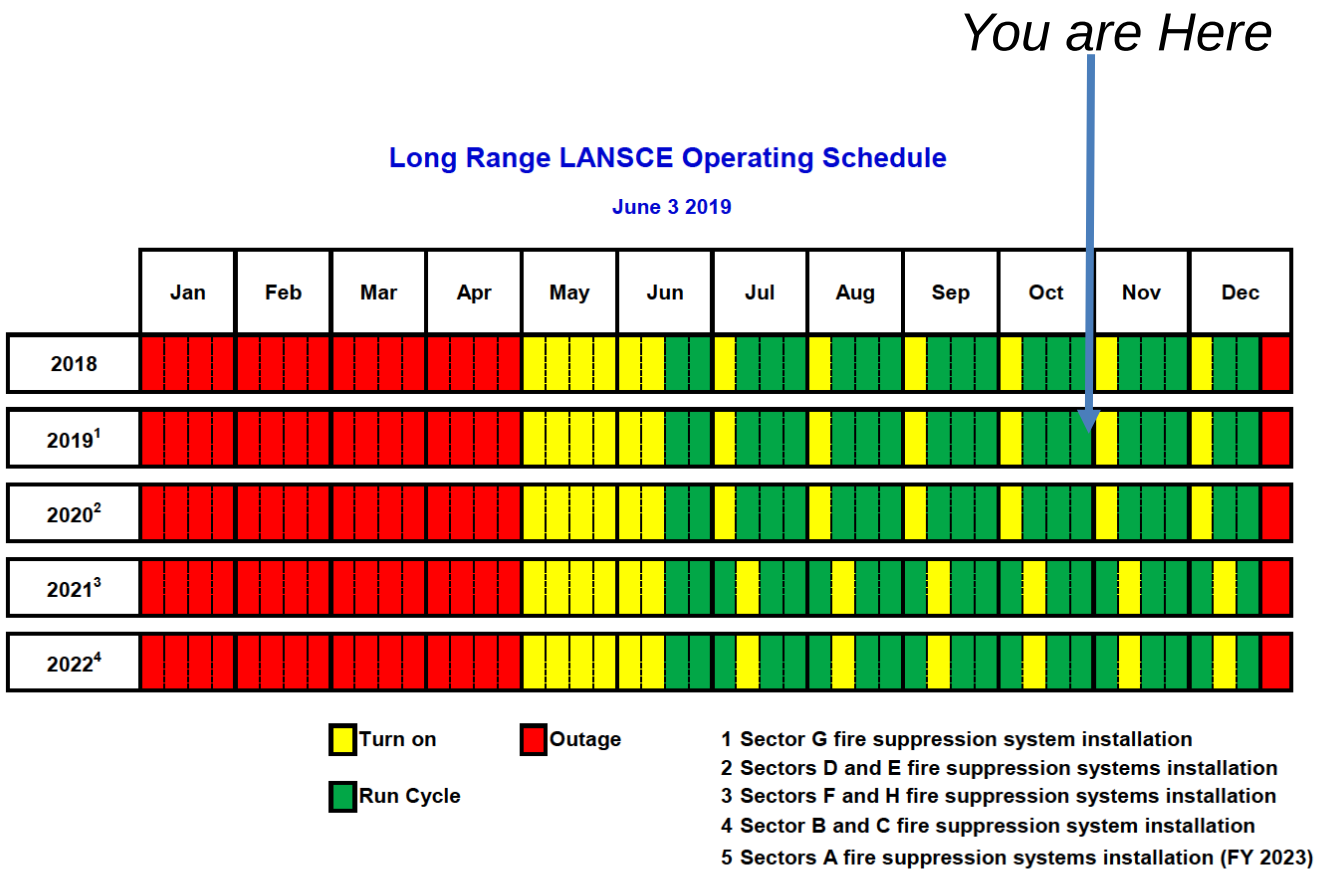

Neutrons can cause failures in high-power semiconductor devices

- Insulated Gate Bipolar Transistors (IGBT) are semiconductor devices that are used in many high-power applications such as BART, hybrid cars, accelerator RF systems, etc.
- We performed tests of IGBTs that were used in SNS accelerator.
- The lifetime of these devices in neutron fields depends on the electric field or the applied voltages
- Tests show a dramatic decrease in lifetime at a critical voltage which is significantly below the rated operating voltage

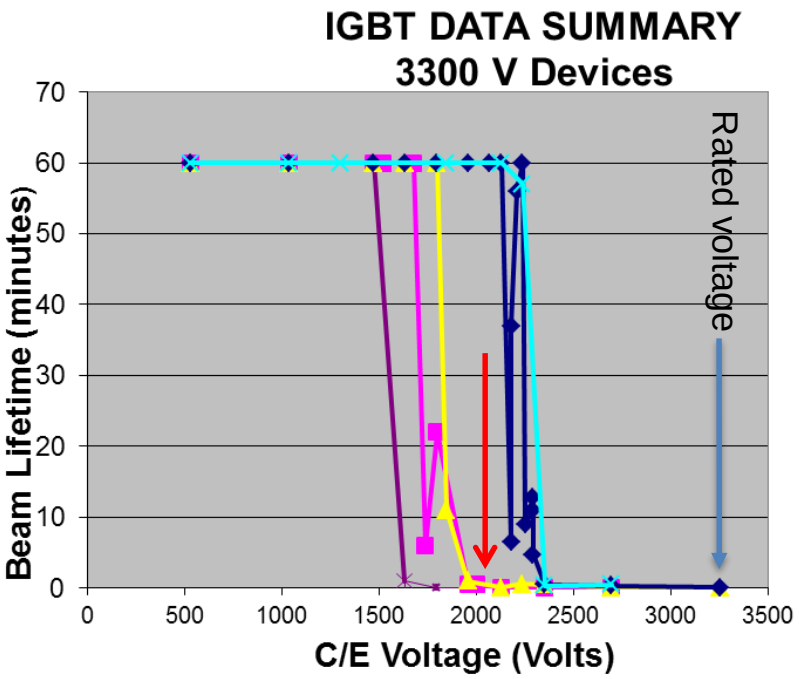

One neutron can stop a train

Results of LANSCE/WNR measurements determine problem with ASCI Q-Machine

- The ASCI Q-Machine has 2048 nodes with a total of 8192 processors.
- During commissioning, it was observed that the Q-machine had a larger than expected failure rate. Approximately 20 fails / week (~3 fails / day).
- The question was whether this could be the result of neutron single-event upset.

ASCI Q-Machine at Los Alamos National Laboratory

Fails/day ~ [# of fails/neutron] * [# neutrons/day]

Measured at LANSCE

Cosmic-ray neutron flux

The neutron environment and the system response was measured

- The neutron intensity was measured in the Q-Machine room. The values obtained agreed with the Goldhagen values
- The system response was measured by putting one module of the Q-Machine in the LANSCE/WNR beam.
- Results of measurement accounted for approximately 80% of the failures (IEEE Trans. Dev. Mat. Reliab. 5 2005)
- The failures were traced to a cache memory that was not error corrected
- This result may have significant impact on future large computer systems

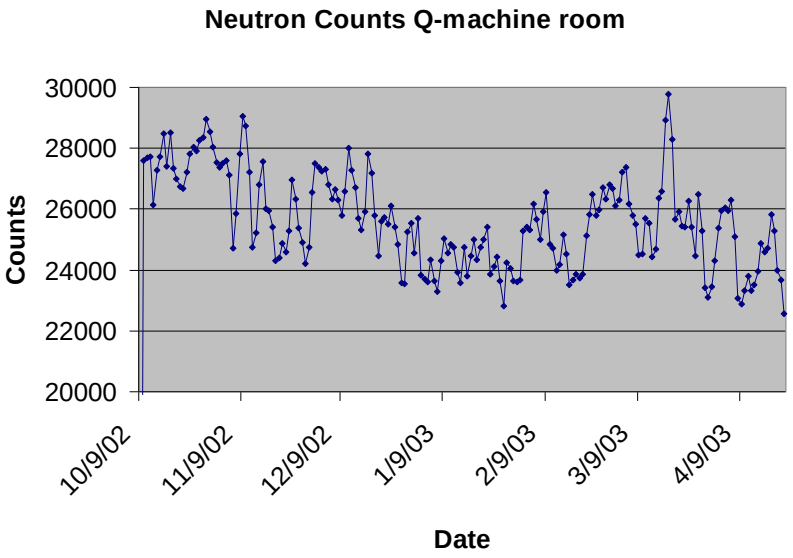

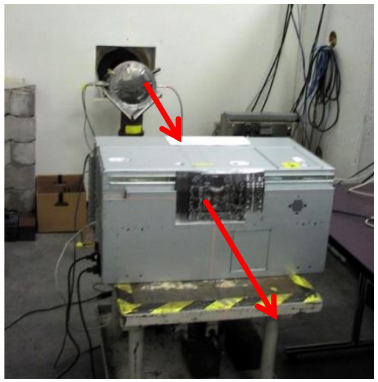

One neutron can stop a calculation

Measurement of thermal neutrons in aircraft (1)

- Recently the avionics community has become concerned about the effects of thermal neutrons on flight control electronics.
- This question is important because if thermal neutrons are a credible concern, avionic electronics may have to be evaluated with thermal neutrons before use.
- Neutrons are a particular concern for aircraft because the cosmic-ray induced neutron flux is approximately 300 times greater than at sea level
- Thermal neutrons are produced when high-energy neutrons are thermalized in the atmosphere, the aircraft fuel, passengers and aircraft materials. Thermal neutrons have energies of 0.025 eV (2200 m/s), much less than the energy required to cause a lattice displacement.

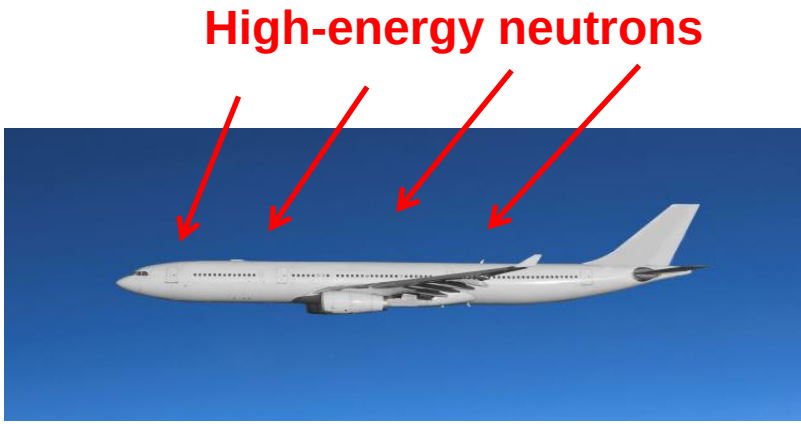

	$n/cm^2/s$	Relative
Sea level (New York City	0.00565	1
7000 ft (Los Alamos)	.019	3.4
40,000 feet	1.53	270

Measurement of thermal neutrons in aircraft (2)

- Thermal neutrons can interact with ^{10}B that is in the semiconductor parts. ^{10}B can capture a neutron and produce an energetic alpha particle and ^{7}Li ion which can deposit enough charge to cause a single-event upset.
- To understand the effect of thermal neutrons in aircraft we need to know:
  - Thermal neutron intensity in airplane— may be airplane dependent- Tinman- need to obtain data in several types of aircraft
  - Effect of thermal neutrons on semiconductor devices- Device dependent --measure at low-energy neutron source at Lujan Center at LANSCE
  - Model / simulations of thermalization of neutrons in aircraft- MCNP calculations

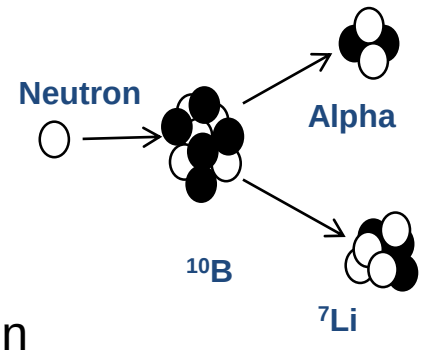

E_α ~ 1.7 MeV
Range ~ 6 μm
dE/dX
~ 1.1 MeV/mg/cm^2

E_{Li} ~ 1 MeV
Range~2.8 μm
dE/dX
~ 2.2 MeV/mg/cm^2

Measurement of thermal neutron intensity in aircraft—Tinman Instrument

- An instrument was designed to measure thermal neutrons in aircraft. This effort is part of a Strategic Partnership Agreement between LANL and Honeywell, Inc.
- Tinman consists of:
  - Two identical cylindrical ^{3}He ion chamber detectors. (~0.63 cm diam 6 cm long). He-3 was chosen because of its sensitivity to thermal neutrons and insensitivity to everything else.
  - One detector was bare, one detector was shielded with cadmium to block thermal neutrons
  - The difference in count rates between these two detectors gives the thermal neutron rate
- Final detector was fabricated by ISR Division at LANL to space specifications
- Uses a Raspberry Pi computer for DAQ
- Designed for “one switch” operation and can be powered by batteries

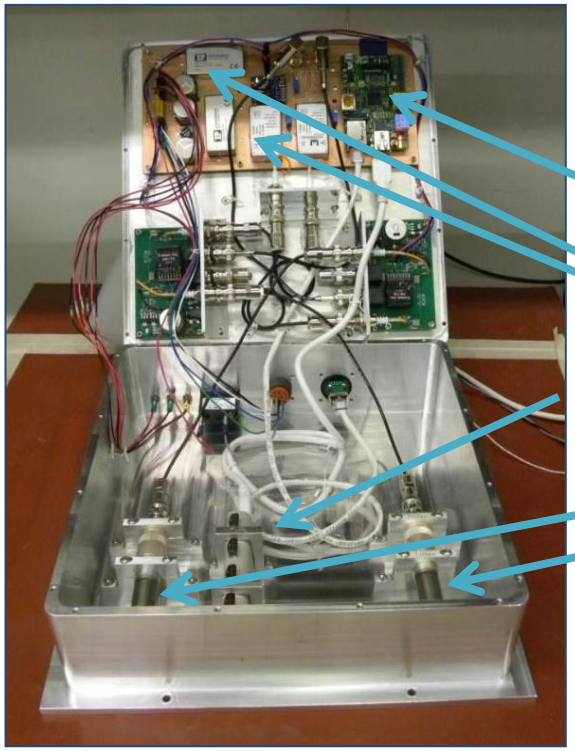

He-3 detectors were matched

$^{3}He + {}^{1}n \longrightarrow {}^{1}H + {}^{3}H + Q \quad \sigma_{thermal} \sim 5300\ b$

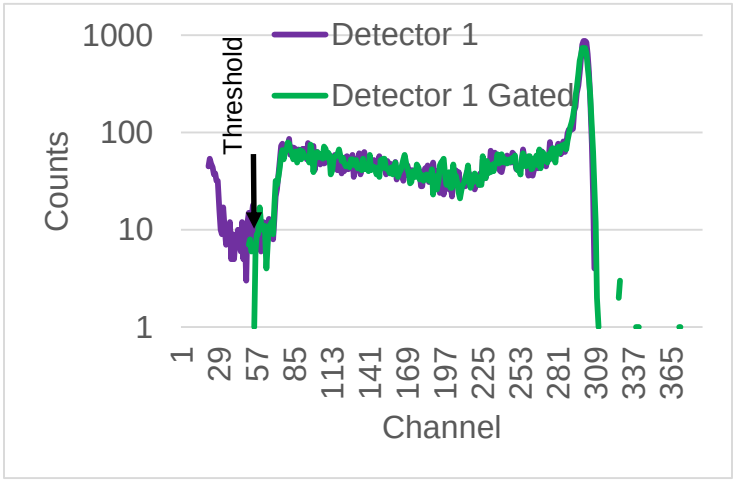

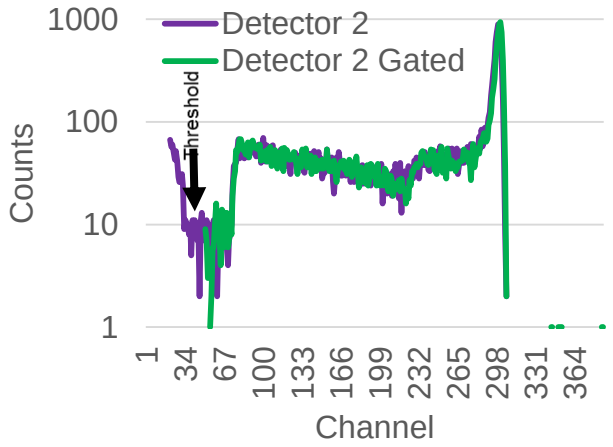

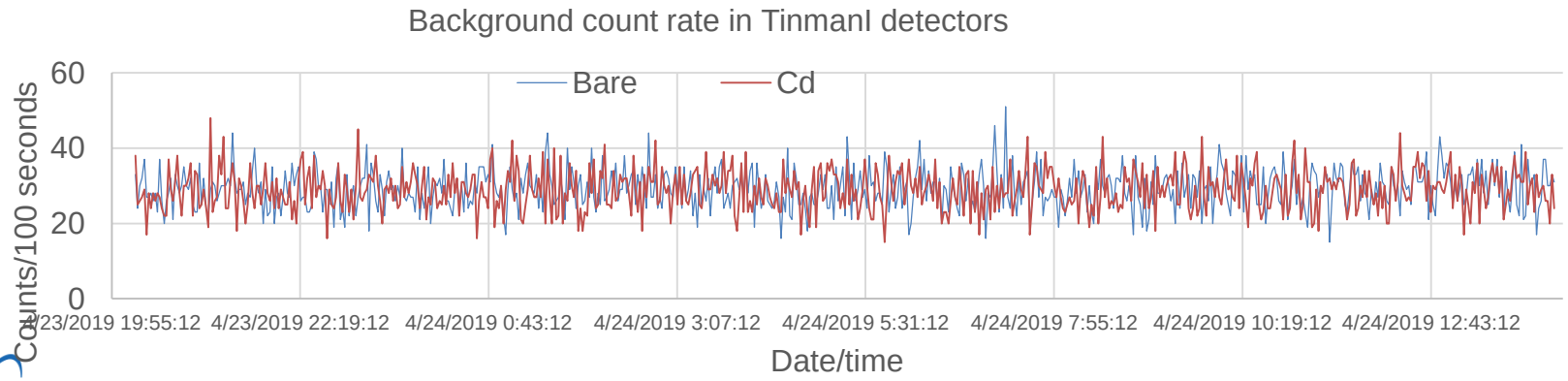

Average count rate in two detectors agree to ~1 %

First Tinman flight was on a NASA ER-2 airplane

- ER-2 is the civilian version of U-2
- Flew on several flights from NASA Armstrong Flight Research Center in Palmdale, Ca

Tinman

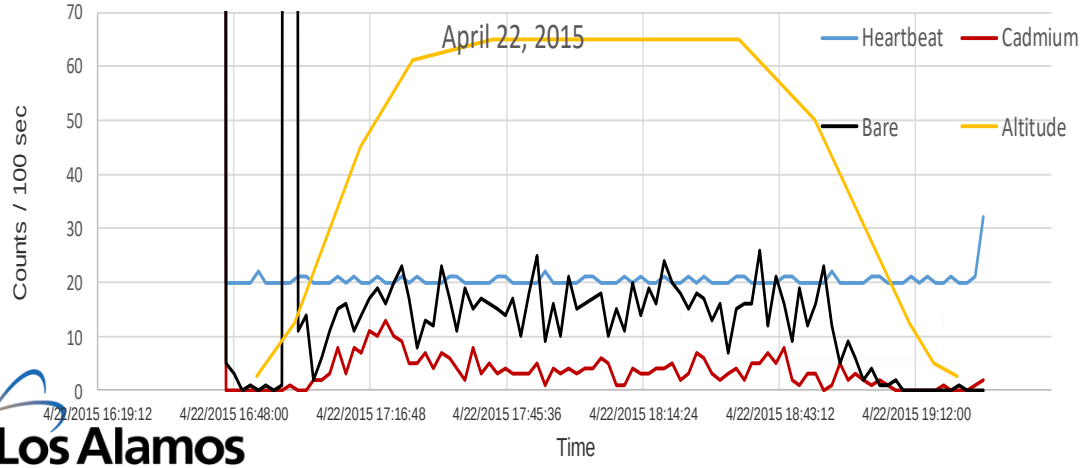

Tinman flew on NASA Eclipse flight on Gulfstream-III airplane

- Changed to larger He-3 detectors to improve signal-to-noise and sensitivity (10X)

Flight Request

Flight Info:
- 3 flights- ferry/rehearsal, mission, ferry
- Request #:17G046
- Hours: 16

Dates of Flights:
- 8/20 – 8/22

Aircraft:
- NASA GIII T/N N808NA

Crew:
- See right →

Purpose of Flight:
- Collect and transmit real-time HDTV video of the eclipse as well as photo documentation of the event
- Collect scientific data from a spectrograph provided by NASA HQs and science payloads

FLIGHT 1- Ferry up/Rehearsal ***#C: 13***

Pilots:	Troy Asher, Andrew Barry
Safety Tech:	Manny Rodriguez
Ops:	Mike Buttigieg
Photo:	Carla Thomas
Video:	Lori Losey, Steve Parcel, Mike Agnew
PAX:	David McBride, Randy Albertson, Kevin Rohrer, Thomas Zurbuchen, Debra Randall

FLIGHT 2- Mission ***#C: 12***

Pilots:	Troy Asher, Andrew Barry
Safety Tech:	Manny Rodriguez
Photo:	Carla Thomas
Video:	Lori Losey, Steve Parcel, Mike Agnew
PAX:	David McBride, Robert Lightfoot, Thomas Zurbuchen, Lesa Roe, Kevin Rohrer

AFRC Dir → David McBride
NASA Administrator → Robert Lightfoot
Ch. of St. comm.
NASA Science mission
Dep. Assoc. Admin

FLIGHT 3- Ferry back ***#C: 11***

Pilots:	Troy Asher, Andrew Barry
Safety Tech:	Manny Rodriguez
Ops:	Mike Buttigieg
Photo:	Carla Thomas
Video:	Lori Losey, Steve Parcel, Mike Agnew
PAX:	David McBride, Randy Albertson, Debra Randall

Solar Eclipse Mission Tech Brief - 8/14/17 47

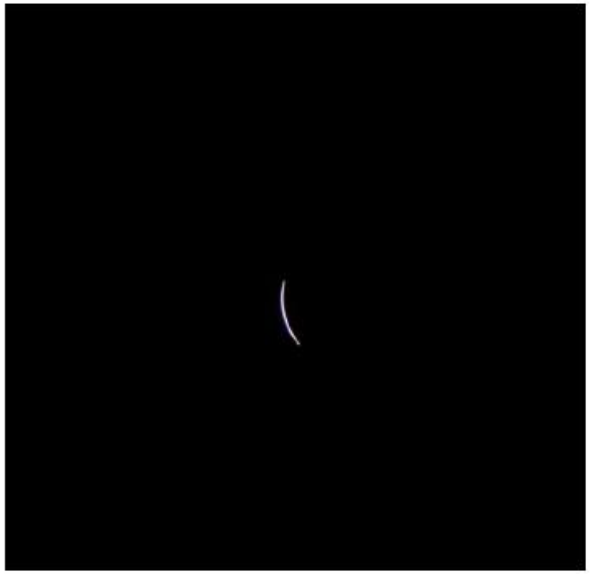

Tinman detector data--- Eclipse flight August 21, 2017

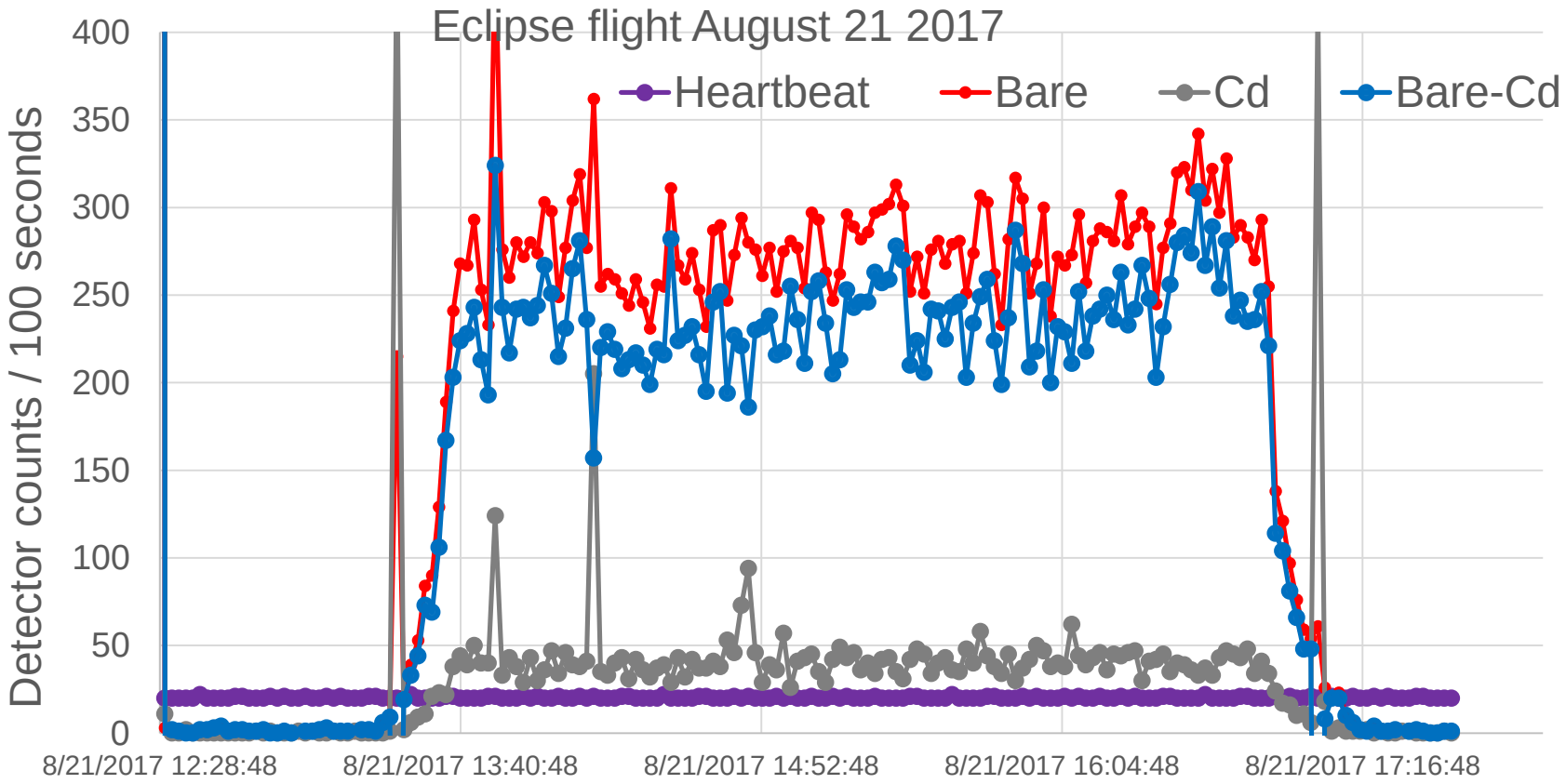

Tinman was flown on NASA DC-8

- The Tinman instrument was flown on 11 flights between Jan 13 and Feb 4, 2018 on the NASA DC-8 airplane

Tinman Detector

ID	Task Name	Duratio	Start
1	jan 13 2018 analysis	10.68 hr	Sat 1/13/18
2	Jan 17 2018 analysis	3.78 hrs	Wed 1/17/1
3	Jan 19 2018 analysis	4.52 hrs	Fri 1/19/18
4	Jan 23 2018 analysis	3.93 hrs	Tue 1/23/18
5	Jan 24 2018 analysis	5.05 hrs	Wed 1/24/1
6	Jan 29 2018 analysis	5.2 hrs	Mon 1/29/1
7	jan 30 2018 analysis	4.88 hrs	Tue 1/30/18
8	Jan 31 2018 analysis	4.58 hrs	Wed 1/31/1
9	Feb 1 2018 analysis	4.2 hrs	Thu 2/1/18
10	Feb 3 2018 analysis	9.88 hrs	Sat 2/3/18
11	Feb 4 2018 analysis	2.45 hrs	Sun 2/4/18
12			
13			

NASA DC-8 flight January 29, 2018

- This flight was around Ramstein, Germany

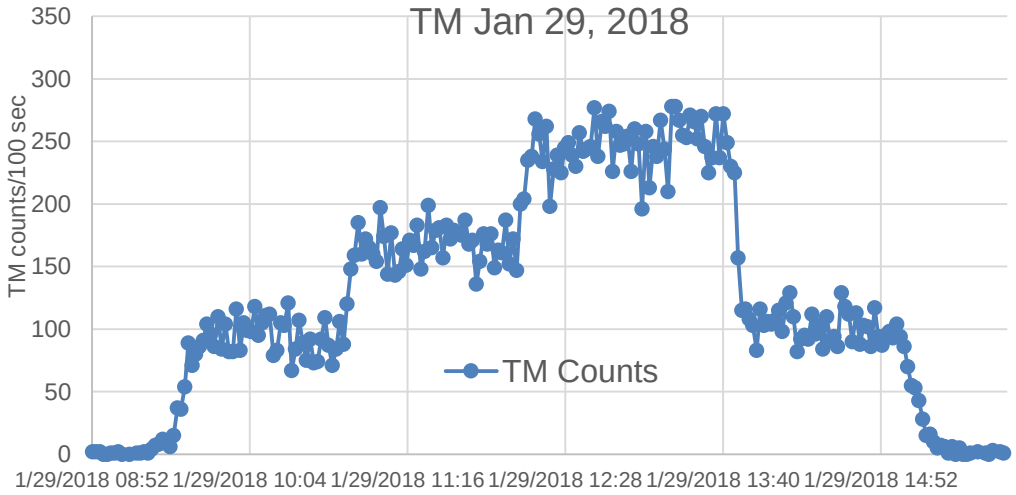

NASA DC-8 flight January 29, 2018

- This flight was around Ramstein, Germany with several changes in altitude

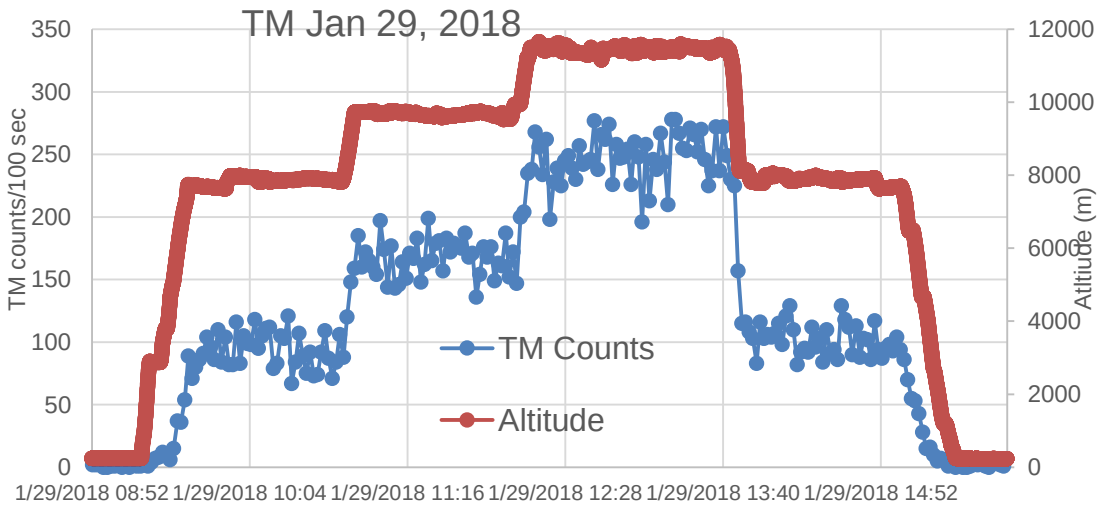

NASA DC-8 flight January 29, 2018

- This flight was around Ramstein, Germany with several changes in altitude but no significant change in latitude
- Straight line on semilog plot of detector count rate vs altitude show exponential absorption of cosmic-ray induced high-energy neutron flux

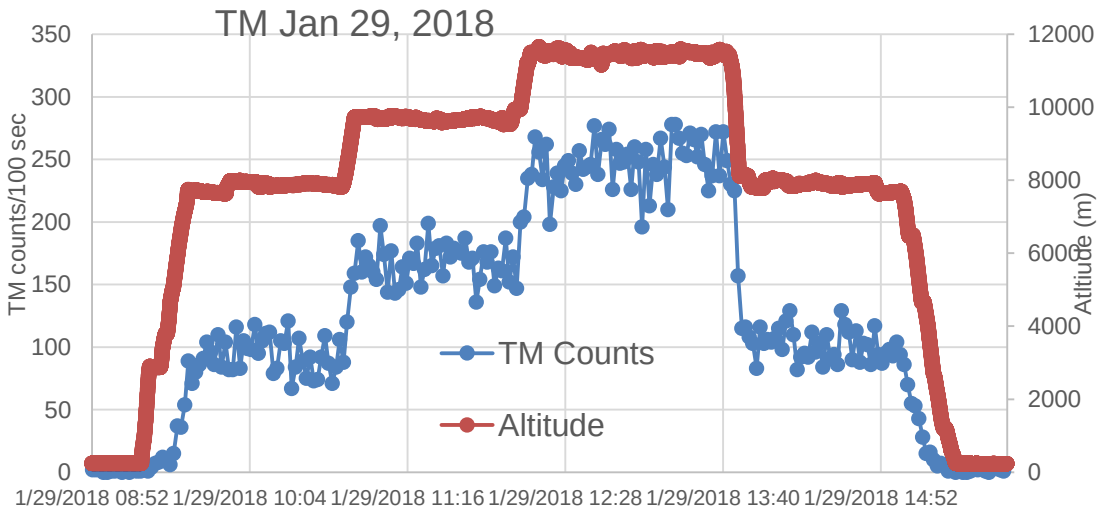

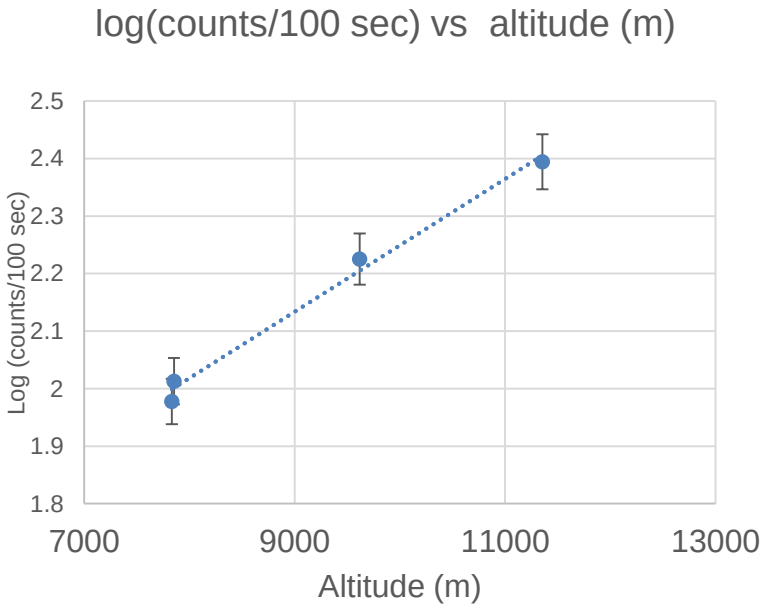

NASA DC-8 flight from Palmdale, Ca to Ramstein, Germany

- In this flight the thermal neutron rate does not track the altitude

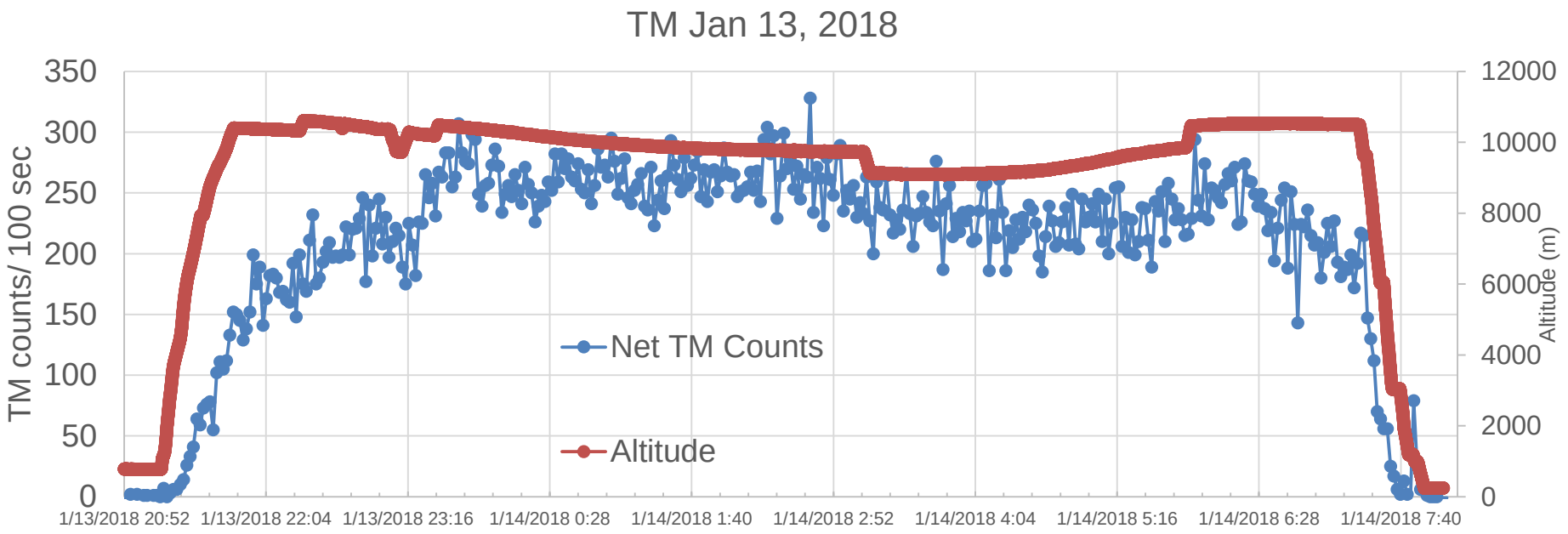

NASA DC-8 flight from Palmdale, Ca to Ramstein, Germany

- Green curve shows the increase in cosmic-ray neutron flux when flying north due to effect of latitude
- TM data shows good agreement with prediction

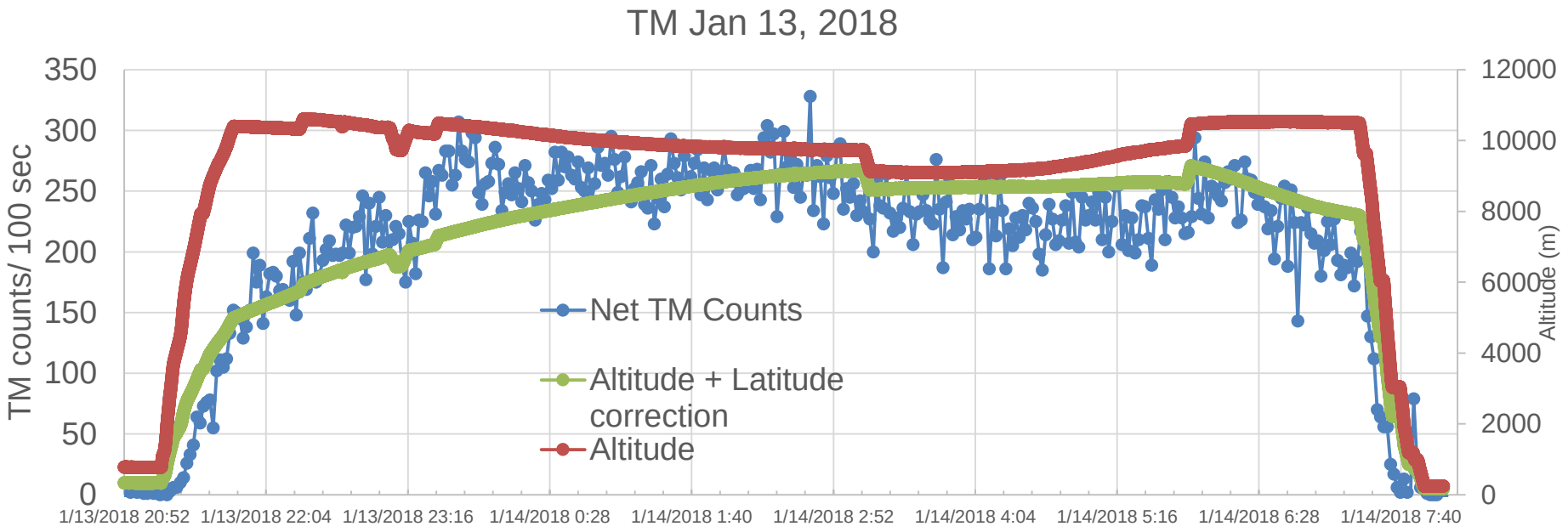

NASA DC-8 flight from Seattle, Wa to Palmdale, Ca

- Green curve shows the decrease in cosmic-ray neutron flux when flying south
- TM data shows good agreement with prediction

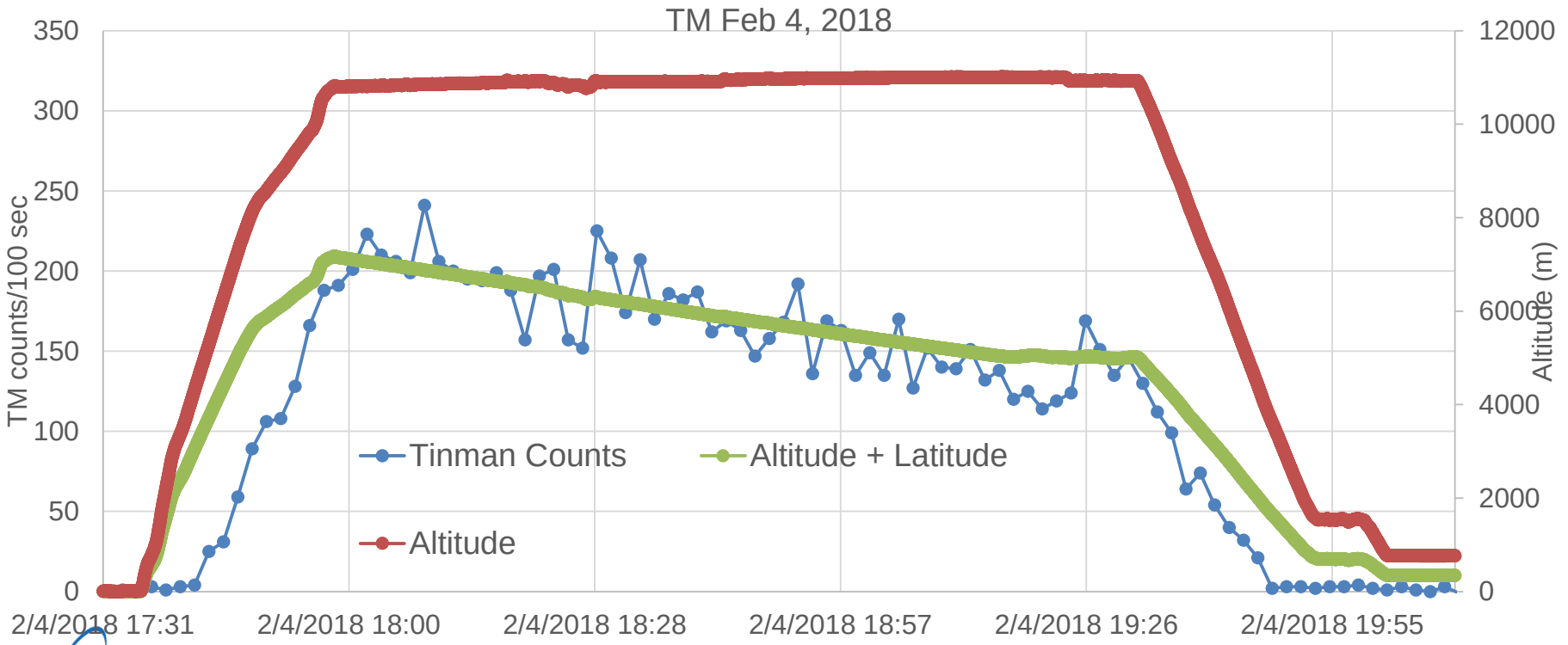

Simple model predicts failures from thermal neutrons

- Thermal neutron capture on ^{10}B is simple from nuclear physics side
  - Energy of outgoing particles does not depend on energy of incident particle
  - Angular distribution of emitted particles is isotropic and does not depend on energy. There are 4 possible particles

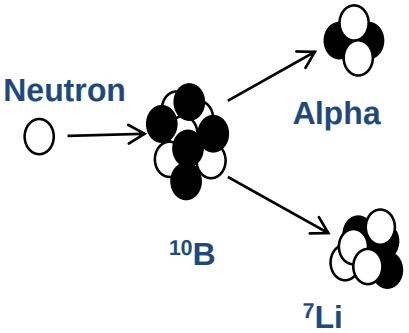

- Assume a semiconductor device
  - 65 nm feature size
  - q_{crit} ~1.2 fC
  - Size of sensitive volume ~100 nm
- Assume energy to produce e-h pair is 3.6 eV
- If deposit greater than q_{crit} in path length of 100 nm can get an upset

Reaction	Particle	Energy	Energy loss	Range	Q total
		MeV	MeV/mg/cm^2	nm	fC
n+^{10}B+γ (94%)	^{7}Li	0.84	2.10	2460	37.3
	α	1.47	1.15	5150	65.4
n+^{10}B gs (6%)	^{7}Li	1.01	2.18	2800	45.0
	α	1.78	1.06	6340	79.0

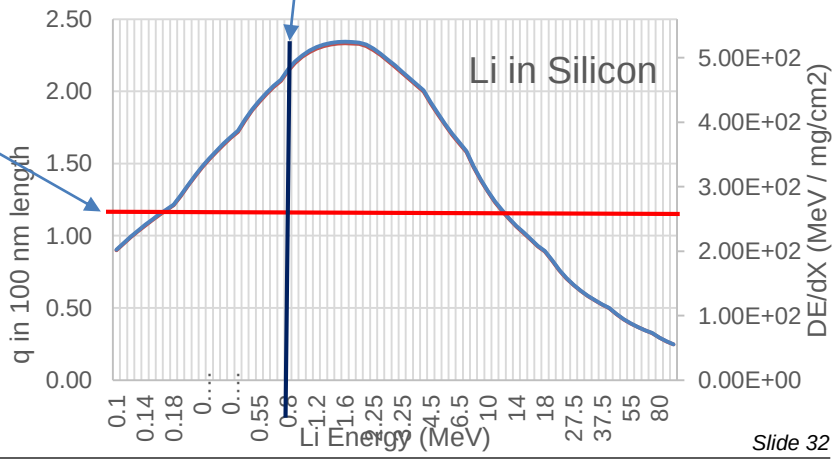

- We have observed thermal neutron upsets

Detectors are monitoring the radiation environment in the High-Performance Computing area

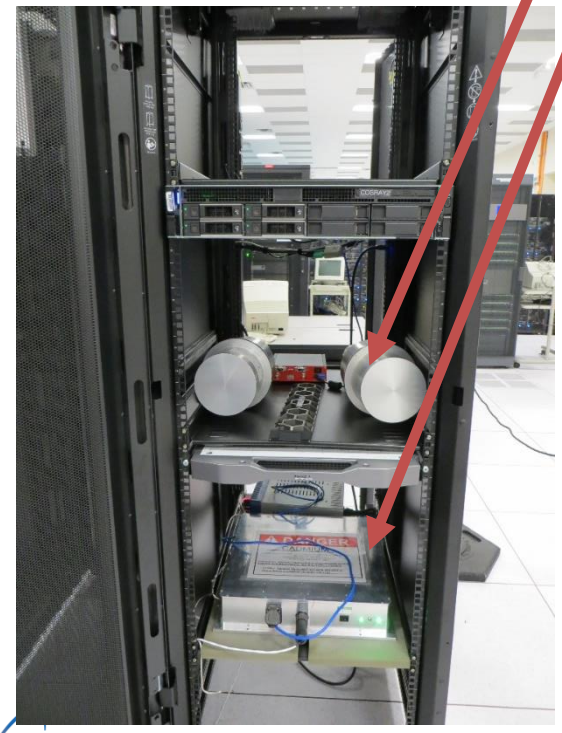

- High energy neutron detectors
- Tin-II in HPC area to monitor thermal neutron intensity
- Moderating material
  - Water for cooling
  - Concrete

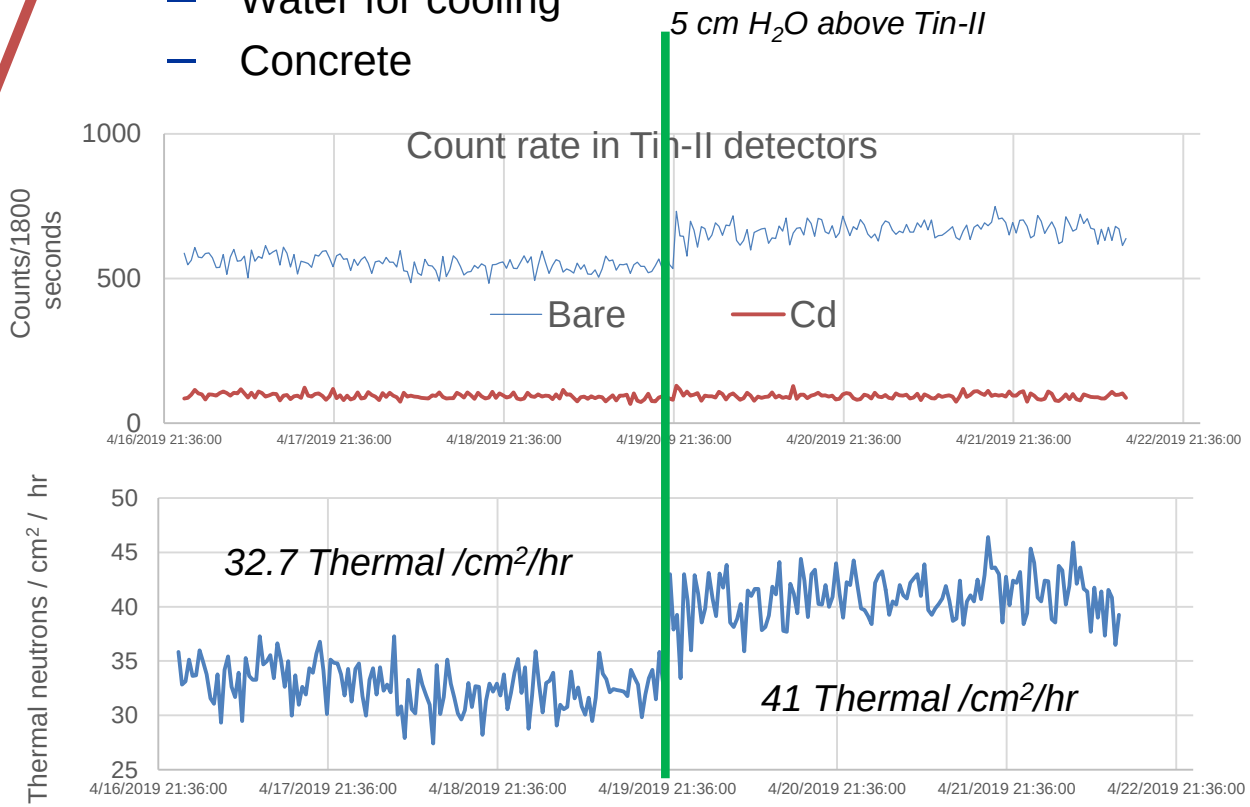

Future work

- Additional flights
  - Measure the thermal neutron intensity in other aircraft to determine the effect of moderating material (fuel mass, geometry, etc.) on thermal neutron production
  - Measure the thermal neutron rate in different locations in the same airplane under similar conditions of fuel, altitude and latitude to determine the spacial distribution of the thermal neutrons
- Simulations
  - Complete the absolute efficiency determination of TM to thermal neutrons. When this is completed, we will know the number of thermal neutrons in aircraft environments.
  - Model (MCNP) the thermal neutron intensity at different altitudes and different locations within the airplane. The results of these calculations can be compared to our measurements. Can we predict our measurements?
- Additional measurements
  - Measure the effect of thermal neutrons on various electronic devices (SEU cross section). With knowledge of the number of thermal neutrons/cm^2/sec in an airplane (from NASA flights) and SEU cross section (measurements at LANSCE), we will be able to predict the number of fails/flight hour in aircraft due to thermal neutrons.
  - Work has begun on measuring the failure rate due to thermal neutrons at LANSCE. We are proposing a room-temperature thermal neutron flight path at LANSCE.

Conclusions

- Tinman instrument works well for detecting thermal neutrons in aircraft--there are thermal neutrons
- The effect of altitude and latitude on the thermal neutron count rate is clearly observed
- Considerable work needs to be done to answer the question of the importance of thermal neutrons in aircraft

Preliminary results from 3 NASA aircraft

- We are analyzing the results of the NASA flights
- ER-2 flight had different detecto
- Hard to compare flights
  - Different latitudes
  - Complicated environments (Fuel,

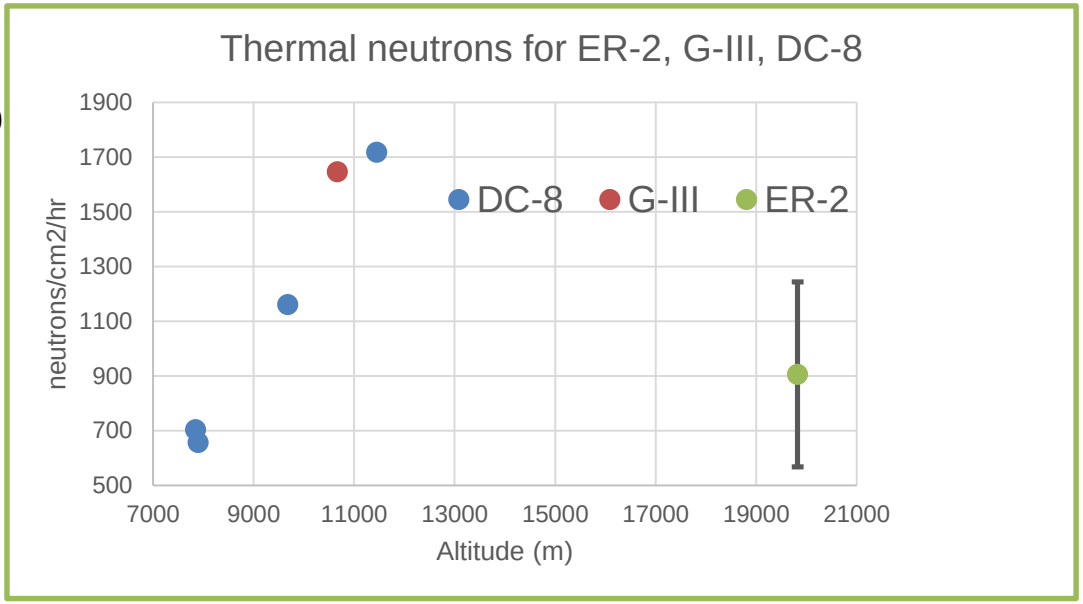

Efficiencies for thermal neutrons are difficult

“Various attempts were made to calibrate this detector with “standard” thermal neutron sources at four different government laboratories. Each of these laboratories had thermal neutron “chambers” that contained uniform thermal neutron fluxes, which had been calibrated for other applications. The thermal neutron sources at these laboratories were generated by moderated radioactive decay neutrons, neutrons from a reactor pile, or neutrons created by nuclear reactions. …..None of the four laboratories produced conversion factors that agreed with each other within a factor of 100%, and the maximum difference was about 3000 times. It was a sad day for scientific reproducibility”.
IEEE TRANSACTIONS ON NUCLEAR SCIENCE, VOL. 50, NO. 6, DECEMBER 2003

There is a “calibrated thermal neutron source at TA-

When neutrons interact with Si charged particles are produced

- Neutrons strike silicon and produce recoil silicon nuclei and alpha particles, etc.

Incident neutron energy (MeV)	Max recoil energy (MeV)	Range of particle in Si (μm)	Energy loss (keV/μm)
30	6 (Si)	3.6	2750
100	14 (Si)	6.2	3300
50	40 (α)	710	32

- Simple models exist to estimate upset rates based on recoil spectra

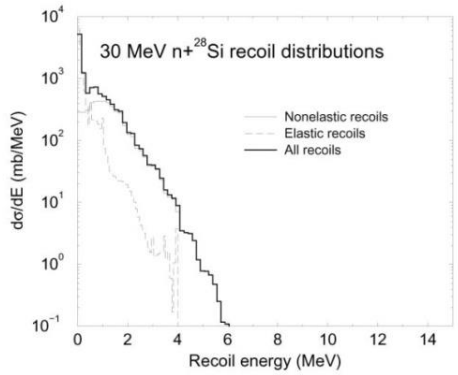

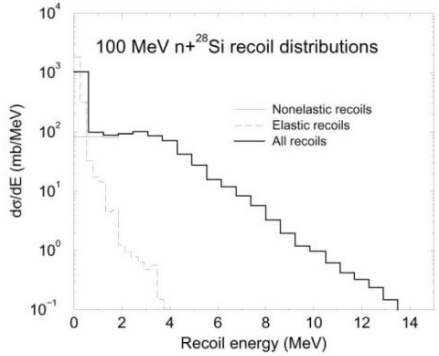

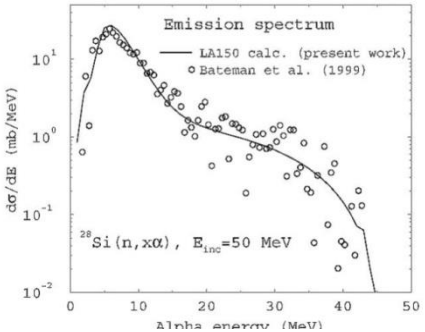

The Journal of Supercomputing (2021) 77:1612–1634
https://doi.org/10.1007/s11227-020-03324-9

Thermal neutrons: a possible threat for supercomputer reliability

Daniel Oliveira[1] · Sean Blanchard[2] · Nathan DeBardeleben[2] · Fernando Fernandes dos Santos[3] · Gabriel Piscoya Dávila[3] · Philippe Navaux[3] · Andrea Favalli[2] · Opale Schappert[2] · Stephen Wender[2] · Carlo Cazzaniga[4] · Christopher Frost[4] · Paolo Rech[2,3]

Published online: 23 May 2020

Abstract

The high performance, high efficiency, and low cost of Commercial Off-The-Shelf (COTS) devices make them attractive for applications with strict reliability constraints. Today, COTS devices are adopted in HPC and safety-critical applications such as autonomous driving. Unfortunately, the cheap natural boron widely used in COTS chip manufacturing process makes them highly susceptible to thermal (low energy) neutrons. In this paper, we demonstrate that thermal neutrons are a significant threat to COTS device reliability. For our study, we consider two DDR memories, an AMD APU, three NVIDIA GPUs, an Intel accelerator, and an FPGA executing a relevant set of algorithms. We consider different scenarios that impact the thermal neutron flux such as weather, concrete walls and floors, and HPC liquid cooling systems. Correlating beam experiments and neutron detector data, we show that thermal neutrons FIT rate could be comparable or even higher than the high energy neutron FIT rate.

Keywords Supercomputer · HPC · Radiation · Thermal neutrons · Resilience

FIT (failure in time) rate is a measure of the number of device failures in one billion (10^9) device-hours of operation.

✉ Paolo Rech
prech@inf.ufrgs.br

[1] Federal University of Parana (UFPR), Curitiba, Brazil

[2] Los Alamos National Laboratory (LANL), Los Alamos, USA

[3] Federal University of Rio Grande do Sul (UFRGS), Porto Alegre, Brazil

[4] Science and Technology Facilities Council (STFC), Didcot, UK

1 Introduction

Reliability is one of the most important considerations in the field of high performance computing (HPC) [1–3]. An unreliable system can negatively affect not only the throughput of a computer but also the correctness of operations. Reliability can be increased through redundancies in chip architectures, improved manufacturing processes, transistor layout changes, or other hardening solutions [4]. However, this added reliability comes at an added cost in terms of additional engineering, more expensive manufacturing, and added power consumption. This creates a trade-off between lower cost and higher reliability such that only specialized safety critical industries, such as aerospace or medical, are willing to pay the additional cost of highly reliable parts. This is in contrast to Commercial Off-The-Shelf (COTS) devices which are generally not built to the highest achievable levels of reliability due to the low margins of the markets that consume these parts. Most consumers of COTS parts are primarily interested in performance and low price. They are typically willing to suffer lower reliability in exchange [4, 5]. The majority of the HPC community builds systems out of COTS parts and there is a constant struggle between the drive for ever increasing compute power and the potential of lower scientific productivity due to lower reliability [6].

In this paper, we compare the reliability risk to HPC systems from *high energy* neutrons to that of boron-10 (^{10}B), which makes devices vulnerable to *thermal neutrons* generated from either fast neutrons that have lost energy through multiple interactions [5, 7] or are emitted from naturally occurring radioactive isotopes. ^{10}B has a relatively large capture cross section for thermal neutrons and the resulting excited state of ^{10}B quickly decays into Lithium-7 and a 1.47 MeV alpha particle. It is this high energy alpha particle that is known to contribute to upsets in semiconductors. Eliminating boron all-together or using depleted ^{11}B would make the device immune to thermal neutrons. However, depleted boron is expensive and boron is necessary for the manufacture of modern semiconductors, so many COTS devices contain ^{10}B. Modern data centers contain large masses of materials that can potentially increase the flux of thermal neutrons, in the form of concrete slab floors, cinder block walls, and water cooling units. To accurately estimate the effects of thermal neutrons, we deployed a neutron detector to measure the natural background rate variation due to materials used in a modern data center. Our initial measurements indicate that these materials can increase the thermal neutron counts, and thus the COTS device's error rate, by as much as 20

The details of how ^{10}B is used in modern chips are proprietary and not publicly available. The only way to evaluate boron concentration in a chip, and the associated increased sensitivity to thermal neutrons, is through controlled radiation exposure. We studied the effects of fast and thermal neutrons on DDR3 and DDR4 memories, an AMD Accelerated Processing Unit (APU), three NVIDIA GPUs, an Intel accelerator, and a Xilinx Field-Programmable Gate Array (FPGA) all executing a set of 8 representative benchmarks that includes HPC applications, convolutional neural networks (CNNs) for objects detection, and heterogeneous codes. We show that all the considered devices are vulnerable to thermal

neutrons. For some devices, the probability for thermal neutrons to generate an error appears to be higher than the probability due to high energy neutrons. We have also observed that CNNs for object detection will have a much worse error rate where thermal neutron flux is significant, which is especially vital for safety-critical applications like self-driven cars.

The main contributions of this paper are: (1) an experimental evaluation of the probability for a high energy vs. thermal neutron to generate an error in modern computing devices; (2) an estimation of the thermal neutrons flux modification due to materials heavily present in a supercomputer room, based on homemade thermal neutrons detectors; (3) the evaluation, based on (1) and (2), of the contribution of thermal neutrons to the error rate of computing devices.

The remainder of the paper is organized as follows. Section 2 serves as a background and reviews previous work. Section 3 describes our evaluation methodologies. Section 4 presents the effects of thermal neutrons on DDR memories. Section 5 quantifies our experimental results, Sect. 6 presents the estimated FIT rates, and Sect. 7 concludes the paper.

2 Background and related works

This section serves as a background and related works on high energy and thermal neutrons effects on computing devices. Besides neutron-induced faults, there are other known reliability issues in supercomputers, such as aging. To this date, there is no dependence shown for neutron sensitivity and aging, which can be considered as uncorrelated events that can be studied separately [5].

2.1 Motivation

Radiation is a known cause of upsets in computers [8]. The interaction of particles, primarily neutrons for terrestrial machines, with transistors can reverse the value of the bits stored in memory or create current spikes in logic operations. These faults can be masked with no effect on the system functionality, corrected by ECC (error-correcting code), create an undetected error known as silent data corruption (SDC), or create a detected unrecoverable error (DUE). The most serious of these effects are SDCs and DUEs. DUEs occur when the program state is changed in such a way that it will exit unsuccessfully or the program enters an infinite loop. An SDC occurs when the program exits successfully, but the produced output is incorrect. It is well known that thermal neutrons can affect electronic devices [5, 7]; however, only devices containing ^{10}B are considered susceptible to thermal neutrons. Approximately 20% of naturally occurring boron is ^{10}B with the rest primarily being ^{11}B. Depleted boron, where the ^{10}B content is low, is produced in the nuclear power industry but it is expensive in large quantities and generally not used in COTS parts. Previous generations of silicon chips used borophosphosilicate glass in the manufacturing process until it was shown to increase by 8× the likelihood of upsets and replaced with glass not containing boron [9, 10]. Until recently, the "boron problem"

was considered a solved issue; however, as our experiments show, newer silicon chips seem to have reintroduced large amounts of boron back into the manufacturing process. Understanding how this change affects overall system reliability is the primary motivation for this work.

Recently, ^{10}B was found in the manufacturing process of COTS devices [11, 12]. It is worth noting that ^{10}B presence does not depend on the technology node but on the quality of the manufacturing process. (Smaller transistors will have less boron, but also less silicon. The boron/silicon percentage is not necessarily reduced.) As devices produced for the user market are now employed in HPC and safety-critical applications, we must expect ^{10}B to be present. In fact, purified boron is expensive and would increase the device price (unjustified for user applications). Some previous work has studied the sensitivity of SRAM and FPGA devices to thermal neutrons [13–15]. Weulersse et al. [12] compared the error rates of some memories (SRAM, CLB, and caches) induced by thermal neutrons, 60MeV protons, and 14MeV neutrons. This preliminary study shows that the sensitivity to thermal neutrons ranges from 1.4× to 0.03× the high energy neutron one. While very interesting, these experiments were conducted on memory devices not typically used in HPC systems. In addition, many memory errors can be masked or detected through ECC and parity on HPC systems. Unfortunately, Weulersse et al. do not share details about the kind of errors observed during their experiments (single vs. multiple bit flips), preventing extrapolation of their results to HPC devices with ECC enabled.

Our work advances the knowledge on HPC reliability by considering the impact of thermal neutrons on the reliability of HPC devices. The radiation experiments were performed on devices executing representative applications under normal operational configurations (i.e., protection mechanisms enabled) to provide a realistic comparison between the error rates induced by high energy and thermal neutrons. Unlike previous publications, we perform both thermal and high energy neutrons experiments on exactly the same devices in the same conditions to limit comparison uncertainty. Furthermore, for the first time, we investigate through thermal neutron detector measurements, how modern data center construction and cooling systems designs influence the thermal neutron flux and the HPC system fault rates.

2.2 High energy and thermal neutrons

High energy neutrons, or fast neutrons, are produced by the interaction of galactic cosmic rays with the atmosphere. Neutrons with energies that range from 1 to over 1,000 MeV are known to disturb the function of electronic devices and are considered a main cause of faults in terrestrial electronic devices [4, 5]. High energy neutrons primarily interact with silicon chips via elastic scattering which can deposit thousands of electronvolt (eV, a standard unit of energy used in nuclear physics) of energy into a recoil nuclei. Neutron scattering may also produced secondary particles such as protons or alphas. All of these processes can free bound electrons in large enough quantities to alter the behavior of the circuits on a chip which may induce faulty behavior in one or more bits. Permanent damage can also occur due to the displacement of atoms within a chip. The flux of high energy neutrons in the

atmosphere has been thoroughly studied since Hess' discovery [16, 17]. The flux is known to vary across the surface, as a consequence of the earth's magnetic field, and increases exponentially with altitude, reaching a maximum at about 60,000 ft. Under normal solar conditions, the fast neutron flux is almost constant for a given latitude, longitude, and altitude.

Thermal neutrons, or slow neutrons, are low energy neutrons (lower than 0.5 eV), produced by the moderation of high energy neutrons in materials or the emission of neutrons from nuclear decay. Incident high energy neutrons rain down as part of cosmic ray-induced showers reaching thermal energies after 10-20 interactions. Thermal neutrons continue moving until they are either absorbed in a nuclear reaction, or decay (while stable in atomic nuclei, free neutrons have a half-life of about 10 minutes). When a thermal neutron is absorbed by ^{10}B, the resulting isotope decays, producing a lithium isotope and an alpha particle. Both the lithium isotope and alpha particle can induce faults. The amount of boron in a particular computing device is proprietary information that is not disclosed by industry. The only definitive way to evaluate the thermal neutron sensitivity of a device is to expose it to thermal neutrons.

The flux of thermal neutrons, in contrast to high energy neutrons, can be difficult to predict as it strongly depends on the environmental conditions as well the presence of other materials (primarily hydrogen containing) in the device's immediate surroundings (like concrete, water, and a fuel tank) in addition to latitude, longitude, and altitude. Various authors have made calculations to evaluate thermal fluxes in realistic cases [7, 18–20]. As a result, when predicting the error rate caused by thermal neutrons, it is essential to measure rates in realistic settings.

We have built and deployed a neutron detector in order to have a precise understanding of the thermal neutron flux inside a representative data center. We measured the rates of thermal neutrons in the proximity of materials such as water, concrete, or plastic and demonstrate that cooling water, for instance, can increase the thermal neutron flux (and thus error rate) by up to 20%. In Sect. 6 we estimate the high energy vs. thermal neutrons error rate for two locations with known neutron fluxes and discuss the effects of environmental conditions (sunny and rainy day) and surrounding materials (concrete slab floors).

2.3 Supercomputer cooling

One of the main challenges in designing HPC systems is the dissipation of heat. A modern supercomputer can push more than 750 watts per square foot which can easily overwhelm traditional cooling systems [21]. The power and heat density in a single rack of current supercomputers demands efficient and reliable cooling techniques to keep the components at operational temperatures. Today's supercomputers consist of hundreds of computing racks (e.g., Summit uses 256 racks [22]), requiring specific room designs to optimize both cooling efficiency and ease of maintenance. Hot/cold air segregation and raised floors are the most common design strategies for new supercomputers [21].

Air segregation for hot and cold air aisles may require nonstructural walls added to the building to make the physical segregation of the aisles. These additional walls and the structural ones, as demonstrated in Sect. 6, act as a moderator for neutrons energy and, thus, increase the thermal neutron flux. Similarly, raised floors, designed to increase the flexibility for routing liquids, power, and network, may also collaborate to increase the thermal neutron flux as their structure requires additional concrete.

One notable and growing trend in data centers is the use of liquid cooling [23]. Eight of today's Top10 supercomputers use some form of liquid cooling [24]. Liquid cooling is more efficient at heat removal than traditional air cooling and using it allows for an overall increase in performance and power efficiency. Traditional data centers may use 25% to 35% of their energy budget just for cooling. IBM chillerless water cooling systems have been shown to reduce the cooling energy overhead to just 3.5% [25]. IBM has noted that using liquid cooling in can allow for a 34% increase in processor frequency which can increase system performance by approximately 33% [26, 27].

It is worth noting that there is no standard supercomputer cooling project. Thus, different projects, such as pure water or hybrid cooling, imply a different amount of liquids close to computer chips resulting in different thermal neutron flux increases. For instance, water cooling systems using small hoses connecting to water reservoirs outside of the computing facility may have a lower thermal neutron flux than hybrid systems with water radiators filled with some gallons of water attached to each computer rack.

3 Methodology

To evaluate the contribution of thermal and high energy neutrons to the error rate of devices it is necessary to: (1) measure the probability that a neutron will generate a fault and (2) estimate the flux of high energy and thermal neutrons where the device will operate. We measure (1) through accelerated neutron beams experiments and estimate (2) using existing data as well as initial measurements of actual thermal neutron rates in an approximate setting.

In this section, we describe the devices and applications chosen to test the impact of high energy and thermal neutrons in modern computing devices reliability. We also detail the radiation experiments setup used for this work and describe the detector we used to measure the impact of materials in the thermal neutron flux.

3.1 Devices

We selected six devices for this study using different technologies and vendors to have an in-depth insight of thermal neutrons sensitivity on a breadth of modern devices. It is worth noting that both the fabrication process and the foundry can significantly impact the amount of ^{10}B in the device.

Intel Xeon Phi is an HPC accelerator that, even if recently announced as dismissed, powers some of the fastest supercomputers from the Top500 list [24]. The Xeon Phi tested is the coprocessor 3120A, which implements the *Knights Corner* architecture, and it is built using a **22 nm Intel's 3-D Tri-gate technology**.

NVIDIA K20 is a GPU built with the *Kepler* architecture and is fabricated in a **28 nm TSMC standard CMOS technology**. This model is specially built for HPC systems and has 2496 CUDA cores divided across 15 streaming multiprocessors (SMs).

NVIDIA TitanX is a GPU built with the *Pascal* architecture and fabricated in a **16 nm TSMC FinFET**, it has 3584 CUDA cores split across 28 SMs.

NVIDIA TitanV is built with the *Volta* architecture and fabricated in a **12 nm TSMC FinFET**, it features 5120 CUDA cores divided into 80 SMs.

AMD Accelerated Processing Unit (APU) is a heterogeneous device that integrates CPU and GPU in the same chip sharing the same memory. The APU considered is the AMD A10 7890K Kaveri fabricated in a **28 nm SHP Bulk Process at Global Foundries**. This device includes 4 steamroller CPU cores and a GCN architecture AMD Radeon R7 Series GPU containing 512 cores with 866MHZ each. We consider three APU configurations: CPU, GPU, and CPU+GPU.

FPGA is the Zynq-7000 designed by Xilinx using a **28 nm TSMC technology**. The FPGA is composed mainly of configurable logic blocks (CLBs), digital signal processor (DSP) blocks, and embedded memory blocks (BRAM).

3.2 Codes

The set of devices we consider covers a wide range of architectural and computational characteristics. Using the same code for each device would bias the reliability evaluation, in favor of the devices that are more efficient in executing the chosen code. To have a fair evaluation, then, we choose for each class of devices the codes that better fit with its computational characteristics. For Xeon Phi and GPUs we chose four codes representative of **HPC**: MxM, LUD, LavaMD, and HotSpot. We selected three **heterogeneous** codes specially made to fully utilize the APU architecture: SC, CED, and BFS. Finally, on GPUs and FPGA we tested two **neural networks** to represent codes that have a significant impact on self-driven vehicles: YOLO and MNIST.

Matrix multiplication (MxM) is representative of highly arithmetic compute-bound codes used in HPC and for features extraction in CNNs [24].

LUD is a linear algebra method that calculates solutions for a square system of linear equations, representative of highly compute-bound codes [28].

LavaMD simulates particle interactions using finite difference methods [28]. LavaMD is compute-bound, being mostly composed of dot products.

HotSpot is representative of stencil solvers [28]; it estimates the processor temperature using an architectural floor plan and simulated power measurements.

Stream compaction (SC) is a memory-bound code used in databases and image processing applications. SC is composed of a data manipulation primitive that removes elements from an array.

Canny edge detection (CED) extracts information from images and reduces the amount of data to be processed. CPU and GPU concurrently work on different frames. The input frames are a subset of the urban dataset used for neural networks training [29].

Breadth first search (BFS) is a search in graphs algorithms that performs nonuniform memory access widely used in GPS Navigation Systems.

The input graph we select for our evaluation represents the highways of the Great Lakes area in the USA [30]

YOLO is a convolutional neural network (CNN) used for object classification and detection [31].

Modified National Institute of Standards and Technology (MNIST) is a CNN used for classifying handwritten digits [32]. We have tested MNIST only on FPGAs as it is a minimal network that would not exercise sufficient resources on GPUs or Xeon Phi.

3.3 Radiation experiments setup

To evaluate the sensitivity of our devices to high energy and thermal neutrons, we exposed the devices on two different beamlines at the ISIS spallation neutron source in the UK: ChipIR for high energy neutrons and ROTAX for thermal neutrons.

ChipIR [33] is the reference beamline dedicated to the irradiation of microelectronics and it features a high energy neutron spectrum, as similar as possible to the atmospheric one. The flux with neutron energy above 10 MeV is $5.4 \times 10^6 n/\text{cm}^2/\text{s}$, while the thermal component ($E < 0.5$ eV) is $4 \times 10^5 n/\text{cm}^2/\text{s}$ [34].

ROTAX [35] is a general purpose beamline with a thermal neutron spectrum generating a flux of $2.72 \times 10^6 n/\text{cm}^2/\text{s}$. Here the thermalization is achieved by moderation of the neutrons using liquid methane.

The spectra of the two beamlines are compared in Fig. 1 on a log-log scale where the fluxes are proportional to the areas under the curves. As Fig. 1 suggests, most neutrons in ROTAX are thermals and most neutron in ChipIR are high energy one.

To evaluate the sensitivity to thermal and high energy neutrons, we align the devices described in Sect. 3.1 with the beam, while executing the codes listed in Sect. 3.2. The device output is compared with a pre-computed fault-free copy and

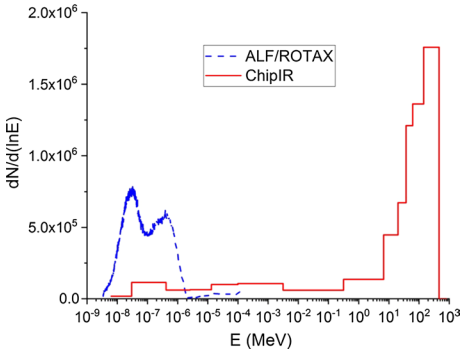

Fig. 1 The neutron spectra of the beamlines used for irradiation in lethargy scale

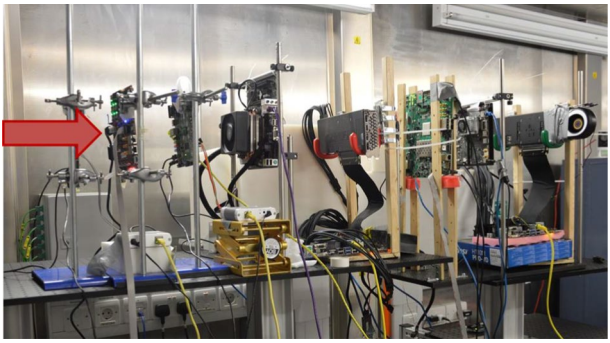

Fig. 2 Experimental setup in ChipIR. The arrow indicates the direction of the neutron beam

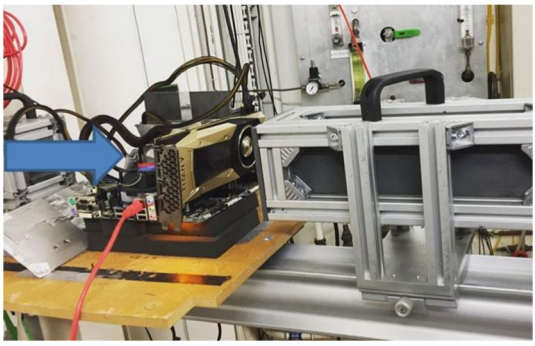

Fig. 3 Titan X experimental setup in ROTAX. The arrow indicates the direction of the thermal neutron beam

any mismatch is marked as an SDC. If the application dies, gets stuck, or the device stops responding we count this as a DUE. Dividing the number of observed errors with the fluence the device has received, we can calculate the device sensitivity, expressed as **cross section** [cm^2]. The higher the cross section, the higher the probability for one neutron (either thermal or high energy) to generate an observable error (either SDC or DUE). The cross section is an intrinsic characteristic of the device executing code. On the other hand, the error rate of a device depends on the cross section (i.e., the device sensitivity) and the environment (i.e., the flux of neutrons). Thus, the cross section indicates a high or low presence of ^{10}B.

To eliminate any setup-dependent differences between thermal and high energy neutrons, we irradiate the same physical devices executing the codes with the same input vector both in ROTAX and in ChipIR. It is worth noting that, apart from DDR that experienced permanent faults, testing the same device at ROTAX and then at ChipIR (or the other way around) does not influence the measured error rates. The only difference between the two experiments is that, thanks to the higher neutron energies, at ChipIR we can align various boards with the beam, as shown in Fig. 2. Using a derating factor that takes distance into account, we can measure the sensitivity of multiple devices in parallel. In ROTAX, as the irradiate devices stop most of the incoming thermal neutrons, we must test one device at a time. In Fig. 3 we show the setup for the Titan V evaluation. Due to limitations in the thermal neutrons

experiment, we could only test one sample of each device. The high energy neutrons error rate variation among different samples of the same device has already been shown to be low, and recent works indicate a variation of about 10% [36, 37].

3.4 Thermal neutrons detector

We have designed and deployed a thermal neutron detector, called Tin-II, to measure the flux of thermal neutrons in different conditions. Ultimately, Tin-II will be used to measure the flux of thermal neutrons inside the data center housing the Trinity supercomputer at LANL. Tin-II consists of two identical ^{3}He cylindrical detectors. The interaction of radiation (like neutrons, gammas, and betas) with the detectors triggers a reaction that is amplified, filtered, and counted as an event.

We calibrated the two detectors for a period of 18 hours to ensure that they have the same detection efficiency. Then, we shielded one of the two cylinders with cadmium. Cadmium effectively blocks thermal neutrons, while being transparent to other types of radiation such as high energy neutrons, gammas, and betas. As a result, one of the two cylinders (bare detector) detects all radiation reactions, while the other (shielded detector) counts only radiation reactions that are not thermal neutrons. The difference in count rates between these two detectors, multiplied by an efficiency value, reflects the average thermal neutron flux.

Tin-II counted thermal neutron events over the course of several days. To estimate the effect of some of the characteristic materials in modern data centers on the thermal neutron flux, we placed a box containing 2 inches of water close to the detector. The count difference with and without the water, shown in details in Sect. 6.1, indicates its influence in the thermal neutrons flux.

4 Memories

In this section, we present the double data rate (DDR3 and DDR4) dynamic random access memory (DRAM) sensitivity to thermal neutrons. Both DDR memories are synchronous DRAM tested without ECC and composed of a single rank x8 memory module. The DDR3 is a 4GB module that operates at 1.5V with a frequency of 1866 MHz and timings 10-11-10. The DDR4 is an 8GB module that operates at 1.2V with a frequency of 2133MHz and timings 13-15-15-28. As vendors are not explicitly mentioned, cross sections are shown in nominal values.

We irradiate the devices while performing a continuous read/write *correct loop*: banks are set to 0xFF (or 0x00) and continually read while irradiated with neutrons. When an unexpected value appears, error counters are increased, the corrupted data are downloaded for further analysis, and the memory bank is rewritten. This read/write loop allows differentiating 1-0 and 0-1 bit flips. While Static RAM has a symmetric structure, DDR are likely to be more sensitive to either one of the two possible bit flip directions (one-to-zero and zero-to-one), depending on the cell implementation and on the use of complementary logic.

The errors, from the corrupted data downloaded, are classified into four categories:

- **Transient error:** a bit flip that does not systematically appear in the following memory read.
- **Intermittent error:** a memory location returns incorrect values, but not necessarily in consecutive reads. Intermittent errors have been seen in DDR and are dependent on environmental conditions, like temperature [38].
- **Permanent error:** a memory location consistently returns an incorrect value (stuck-at). Permanent errors are caused by displacement damage (the neutron dislocates atoms in the transistor) and can possibly be repaired with annealing (i.e., heating the device) [39, 40].
- **Single Event Functional Interrupt (SEFI):** a large portion of the memory array return incorrect values, likely caused by an error in the DDR control logic circuits. Further reads/writes will return correct values [41].

Figure 4 shows the thermal neutrons cross section per GBit for DDR3 and DDR4. We do not report high energy neutron data since after few minutes of irradiation at ChipIR both DDR3 and DDR4 experienced a high number of permanent faults, impeding further data collection. However, the sensitivity of DDR memories to high energy neutrons has been extensively studied, and experimental data can be found in [39, 42–44].

Figure 4 highlights that the DDR4 memory cross section is approximately one order of magnitude lower than the DDR3 one, showing significant reliability improvements probably resulting from new manufacturing processes as well as transistor placement enhancement. We also observe in Fig. 4 that more than 95% of all the errors are in one of the two possible bit flip direction, one-to-zero for DDR3 and zero-to-one for DDR4. The opposite direction for DDR3 and DDR4 suggests that one device is manufactured with complementary logic. Another interesting point our data highlight is the proportion of each error category changes from DDR3 to DDR4. Permanent errors are more than 50% of all observed errors in DDR4, while on DDR3 only less than 30% of errors are permanent. It is also worth noting that both technologies present SEFI errors during

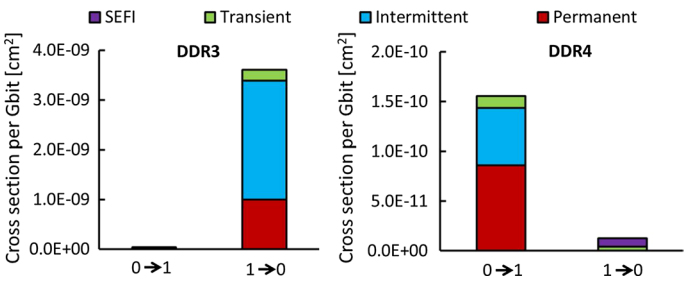

Fig. 4 DDR3 and DDR4 thermal neutrons cross sections

the experiments. That is, an impinging particle on both DDR memory control circuits tends to incite similar malfunctioning behaviors.

Finally, all the observed transient and intermittent errors were single bit flip. This is a promising result, as SECDED ECC is shown to be sufficient to correct most thermal neutrons-induced errors [45]. On the contrary, in a SEFI error multiple corrupted bits were observed.

5 Cross section results

In this section, we compare the cross section measured at ChipIR and ROTAX for the tested devices and codes with the methodology described in Sect. 3.3. We emphasize that we used exactly the same device and setup for both ChipIR and ROTAX experiments. Due to beam time limitations (mainly at ROTAX as we must test only one device at a time) we could not test all the benchmarks in each device. Recall that a higher cross section indicates a higher probability of a single (high energy or thermal) neutron inducing faults. To evaluate the impact of thermal vs. high energy neutrons on the device error rate, we need to consider the natural background flux, which is done in Sect. 6.

As we show, the cross section to thermal neutrons is far from being negligible, indicating the presence of ^{10}B in the silicon doping. Reported data have been normalized to the lowest cross section for each vendor to prevent the leakage of business-sensitive data while allowing a direct comparison between codes and devices of the same vendor. We also report error bars considering Poisson's 95% confidence interval.

Figure 5 shows the **Xeon Phi** SDC and DUE cross sections for high energy and thermal neutrons. On average the thermal neutrons cross section is much lower (1/20) than the high energy neutrons' one, for both SDC and DUE. This low sensitivity to thermal neutrons is a sign that either little boron is used in the production of Xeon Phi or depleted boron is used. HotSpot is the most sensitive code for both SDCs and DUEs. HotSpot is especially sensitive to DUEs, with a cross section more than 2× higher than the average for both high energy and thermal neutrons. HotSpot,

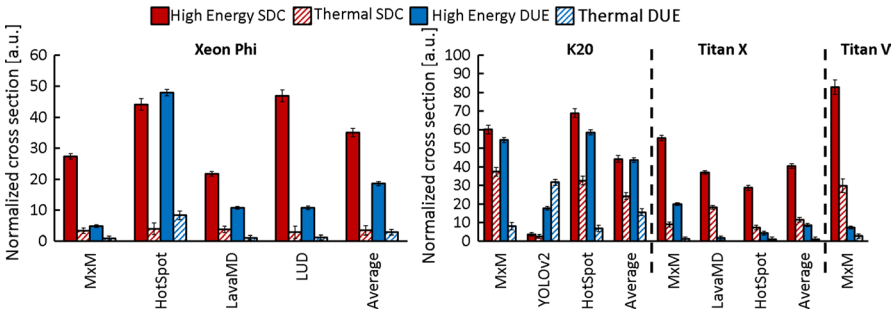

Fig. 5 High energy and thermal neutrons normalized cross sections for Xeon Phi and GPUs

in contrast to the other codes, uses a high number of control flow statements and has low arithmetic intensity, increasing the sensitivity to DUEs.

For SDCs, the high energy neutron cross sections vary significantly depending on the code being executed (more than 2x across codes), which is in accordance with previous work [36, 46]. The SDC cross sections for thermal neutrons, however, have a very low variation between codes (less than 20%) which may be an artifact of the low number of SDCs observed. This result suggests there is a negligible sensitivity to thermals in the chip resources that are responsible for the variation between error rates in the high energy SDC results. DUEs, on the other hand, have a similar trend for high energy and thermal neutrons. DUE faults induced by thermal neutrons seem to have similar effects to DUE faults induced by high energy neutrons.

Figure 5 shows the sensitivity of **NVIDIA GPUs** to thermal and high energy neutrons. For the K20, on the average, both the SDCs and DUEs thermal cross sections are very high, being 60% and 50% of the high energy neutrons ones. This indicates the presence of a significant amount of ^{10}B in the manufacturing process. The thermal neutrons SDC cross section trend across codes is also similar to the high energy neutrons one, in the sense that the code with the largest thermal neutrons cross section (i.e., HotSpot) is also the code with the largest high energy neutron cross section. This suggests that ^{10}B is present in the computing resources and memory of these devices, and that the fault locations are similar for both kind of neutrons.

It is also interesting to notice that YOLOv2 is the only code for which DUEs are more likely than SDCs, for both kind of neutrons. This result follows previous work that shows low SDC sensitivity in CNN based object detection [47]. As shown in Fig. 5, YOLOv2 DUE cross section for thermal neutrons is more than 50% higher than the DUE cross section for high energy neutrons and more than 2× higher than the average of all K20 codes. This cross section indicates that the reliability for YOLOv2 in environments where thermal neutron flux is significant will be much worse than expected, especially for a safety-critical application like self-driven cars.

For Titan X and Titan V, on the average, the thermal neutron cross section is an order of magnitude lower than the high energy one. The impact of thermal neutrons is lower for the newest GPUs than on the mature K20. This may imply that FinFET based GPUs are less susceptible to thermal neutrons than CMOS GPUs (K20 is built using CMOS planar transistors, Titan X and Titan V using FinFET). However, for the MxM tests, Titan V (12 nm) shows an almost doubled thermal neutron SDC cross section compared to the Titan X (16 nm). Unfortunately, we were not able to test more codes on the Titan V and, at this point, we cannot confirm if the increased thermal neutron cross section is intrinsic of smaller FinFET technologies.

The **AMD APU** cross sections are shown in Fig. 6. As described in Sect. 3.1, the APU embeds a GPU and a CPU. We test the three heterogeneous codes described in Sect. 3.2 (CED, SC, and BFS) as executed on the GPU only, on the CPU only, and distributing concurrently 50% of the workload to the CPU and 50% to the GPU (CPU+GPU).

The APU-GPU, APU-CPU, and CPU+GPU SDC cross sections for both thermals and high energy neutrons vary of more than an order of magnitude, forcing the use of logarithmic scale for APU data in Fig. 6. The reported data show that, on the average, the thermal neutrons cross section is reduced by between 1/4 and

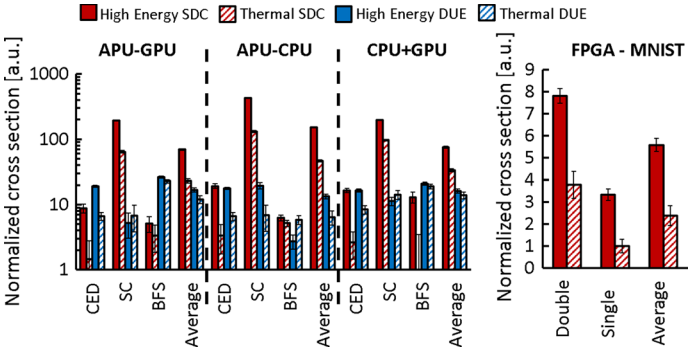

Fig. 6 High energy and thermal neutrons normalized cross sections for AMD APU and FPGA.

1/5 the high energy neutron's, for CPU, GPU, and CPU+GPU. All APU configurations, on average, are more sensitive to SDCs than DUEs. It is also worth noting that the APU-CPU has, on average, a higher SDC sensitivity than APU-GPU. This is in accordance with previous work that shows a much lower probability for a fault in the AMD GPU to impact the application output than a fault in the CPU [48]. Additionally, in the APU, the GPU has a significantly smaller physical area than the CPU which reduces the probability of a neutron striking it and causing corruption.

A specific result to highlight is that SC code, which is the only memory-bound code of the three we test on the APU, has an SDC sensitivity to both high energy and thermal neutron extremely high when compared to others. As already shown, when the device is in idle waiting for data to be fetched from memory, registers and caches are exposed to radiation and store critical data [46]. Moreover, as observed for the Xeon Phi, the DUE cross section variation across different codes is much smaller than SDC variation. Finally, BFS has a particularly high DUEs sensitivity when the GPU is involved in computation (APU-GPU and CPU+GPU). This DUE increase is likely caused by the much higher stress in the CPU-GPU synchronization that BFS imposes by launching several GPU kernels (refer to Sect. 3.2).

Figure 6 shows **Xilinx FPGA** SDC cross section when executing the MNIST CNN. It is worth noting that neutron-induced errors in the configuration memory of SRAM FPGAs have a *persistent* effect, in the sense that a corruption changes the implemented circuit until a new bitstream is loaded in the device. The observation of an error at the FPGA output indicates that the bitstream has probably been corrupted. We reprogram the FPGA at each observed output error to avoid the collection of a stream of corrupted data, making the observation of DUEs very rare. In fact, as FPGA executes operation without any operating system, interfaces, or control flow involved, a considerable amount of errors would need to accumulate in the configuration memory to have the circuit functionality compromised. We never observed a DUE in FPGAs during our experimental campaign.

We have tested two different versions of the neural network, one using double and the other using single-precision floating-point arithmetic. When comparing

the high energy and thermal neutrons cross sections for the two configurations, we can clearly perceive that the Xilinx FPGA is more sensitive to high energy neutrons. However, the thermal neutrons cross section is far from being negligible.

The double precision version takes about twice as many resources to be implemented in the FPGA. As the neutrons cross section is directly related to the circuit's area, the cross section is expected to be higher for the double version of MNIST. Experimental results for both high energy and thermal neutrons confirm this intuition. The thermal neutrons cross section for the double version is particularly higher than the single one, being almost four times larger.

Our results show that different codes executed on the same device can have very different high energy vs thermal neutrons sensitivities. The physical interaction of a thermal neutron and, consequently, the resulting fault model (i.e., the way the physical fault is manifested at circuit level) and the impact on the code execution is highly different from the high energy neutron one. High energy neutrons can interact with any atom in the chip or package material, triggering a reaction that may potentially reach a transistor's vulnerable area. The fault can happen some distance from the high energy neutron impact, and the particles resulting from the interaction can travel in different directions [5]. Thermal neutrons, on the other hand, interacting only with ^{10}B, produce an alpha particle and lithium recoil that have very short ranges. When a thermal neutron is absorbed in virtually all other materials used in semiconductor manufacturing, the resulting nuclei typically only produces gamma rays, which do not produce bit flips.

Software fault injection can emulate predefined fault models and study their effects, but cannot be used to study the fault manifestation nor to define different fault models. One way to investigate the different fault models would be to simulate the physical implementation of a transistor in a given technology and observe the effect of neutron strikes at different energies [49]. However, transistor implementation details are not available for COTS devices, which makes the comparison of the beam experiment cross sections of various codes the only possible way to highlight code-dependent thermal vs high energy neutrons-induced error rates.

6 FIT rate analysis

The cross sections reported and discussed in Sect. 5, represent the device's sensitivity to thermal or high energy neutrons. To have an understanding of the impact of thermal and high energy neutrons in the device error rate, we need to consider also the natural background radiation fluxes of each. FIT rates can then be calculated by multiplying the experimentally measured cross sections by the neutron fluxes. For DDR, we show absolute FIT rates, while for computing devices, to avoid the leakage of business-sensitive data, we only show in percentages the contribution of thermal and high energy neutrons to the device's FIT rates. This information allows us to evaluate how much thermal neutrons increase the FIT of each device. This also tells us how much the FIT rate of each device is underestimated if thermal neutrons are not considered.

6.1 Thermal neutrons flux

The flux for high energy (fast) neutrons in the atmosphere can be precisely estimated considering the altitude, longitude, latitude, and solar activity using online available tools [50]. However, the environment and the materials that surround a device significantly impact neutron flux and energy. Materials such as concrete and water scatter neutrons which lose energy with each interaction. For instance, during thunderstorms the rain droplets act as moderators slowing high energy neutrons into lower energy ones. The thermal neutron flux, as measured in [7], can be as much as 2× higher during a rain storm than on a sunny day. Thermal neutron rates may be as much as 20% higher over a large slab of concrete such as in a parking lot or the concrete floor of a machine room. Water cooling systems can also have the side effect of significantly increasing the proportion of thermal neutrons that strike a device.

In order to empirically measure the impact of materials in the thermal neutron flux in a data center, we placed the Tin-II detector (details in Sect. 3.4) in a building similar to the one containing the Trinity supercomputer. We collected data over the course of several days, shown in Fig. 7, and then placed 2 inches of water in a pan over the detector starting on 20th April 2019. When water is placed over the detector the thermal neutron counts abruptly increase of about 24%. This increase shows that the presence of water in the cooling system can significantly increase the rates of thermal neutrons in a system, which in turn will increase the rates in the devices sensitive to those neutrons as seen in Sect. 5.

Furthermore, to confirm the statistical significance of the thermal neutron flux calculation in our Tin-II experiments, Fig. 8 displays the count rate of the thermal neutrons over time for our detector, and the density function uses a Gaussian kernel density estimate. As can be seen, there are two main groupings of the data. The bimodal distribution is due to the water being placed over the detector on 20th April 2019.

The shape and placement of a water cooling system can impact the way thermal neutrons are produced. The LANL's Trinity supercomputer's water cooling

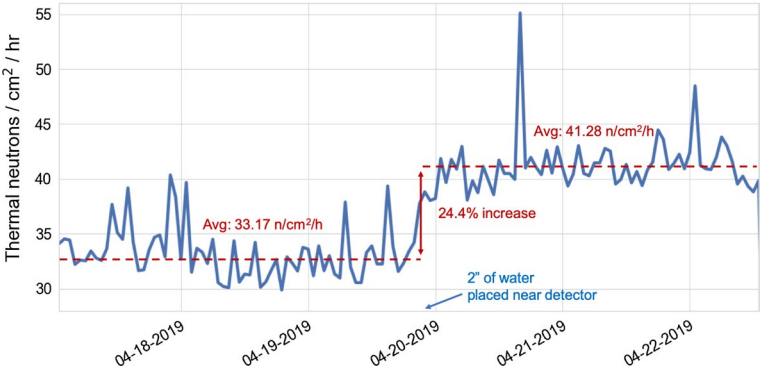

Fig. 7 Tin-II thermal neutron detector measurements with two inches of water placed over detector on 20th April 2019

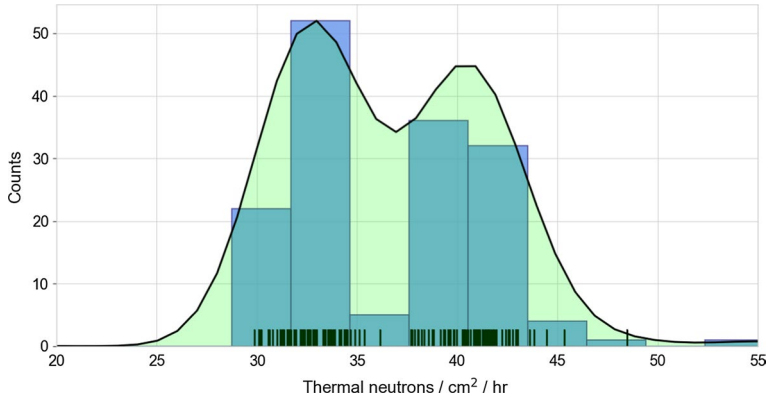

Fig. 8 Tin-II thermal neutrons count rate. The bimodal distribution shows the influence of water placed above the detector

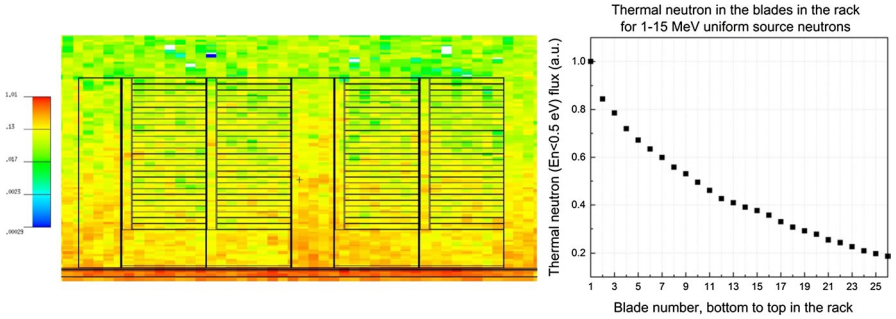

Fig. 9 Left: MCNP simulation of the distribution of the thermal neutron flux in racks of a Cray XC40 water-cooled system (front view). Red indicates a higher rate in the lower blades of the rack as fast neutrons from above lose energy and thermalize while passing through the rack and cooling system. Right: MCNP simulation of the distribution of the thermal neutron flux by height in a rack. Lower numbered blades are closer to the machine room floor and show a higher rate of thermal neutrons as fast neutrons from above slow down while passing through the rack (color figure online)

pipes are below the machine which sits several feet above a concrete slab, whereas ORNL's Summit machine sits directly on a concrete slab with water cooling pipes running overhead. Both of these machines have liquid cooling radiators in the racks. Based on physical considerations, we believe the final flux for most liquid-cooled machines will be elevated. Figure 9 shows simple simulations of the Trinity supercomputer for an incident neutron uniform distribution in the 1-15 MeV range modeled using the Los Alamos National Laboratory MCNP (Monte Carlo N-Particle) code coupled with ENDFVII neutron cross sections [51]. The simulation on the left side of Fig. 9 shows the distribution of thermal neutron flux in the racks of Trinity (front view) where each rack is composed of 26 computer blades. The simulated thermal neutron distribution per each blade is then mapped in the graph on the right side of Fig. 9.

These same considerations exist when trying to understand the thermal neutron component of faults in autonomous vehicles. The road material, concrete or asphalt, the vehicle is driving on makes a difference, as does the weather, and the type and volume of fuel the vehicle uses. In addition, the number of passengers will change the thermal neutron flux, as humans are primarily composed of water which makes us excellent neutron moderators.

6.2 High energy versus thermal neutrons FIT

The average thermal neutron flux at New York City on a sunny day, excluding surrounding materials such as water or concrete, has been measured to be approximately $4n/\text{cm}^2/\text{s}$ [7]. Multiplying the flux by the DDR memory cross sections measured in Sect. 4, we can estimate the DDR3 and DDR4 thermal neutron-induced error rate in NYC to be about 3.09 and 0.14 FIT per GB, respectively. These rates can increase by 2× or more because of the impact of environmental conditions on the thermal neutrons flux.

For computing devices, in Fig. 10 we show the percentage of the total FIT rates due to high energy and thermal neutrons. These calculations use measured values of neutrons at sea level (NYC) and in Leadville, CO (10,151 ft in altitude). The thermal rates used have been adjusted to compensate for back scattered neutrons from a concrete slab and water cooling as measured by Tin-II detector, an overall increase of 44% in the thermal flux. Note that on a rainy day the thermal flux may be as much as doubled over the rates used in this graph and the corresponding FIT rate on those days will increase in a corresponding way [7].

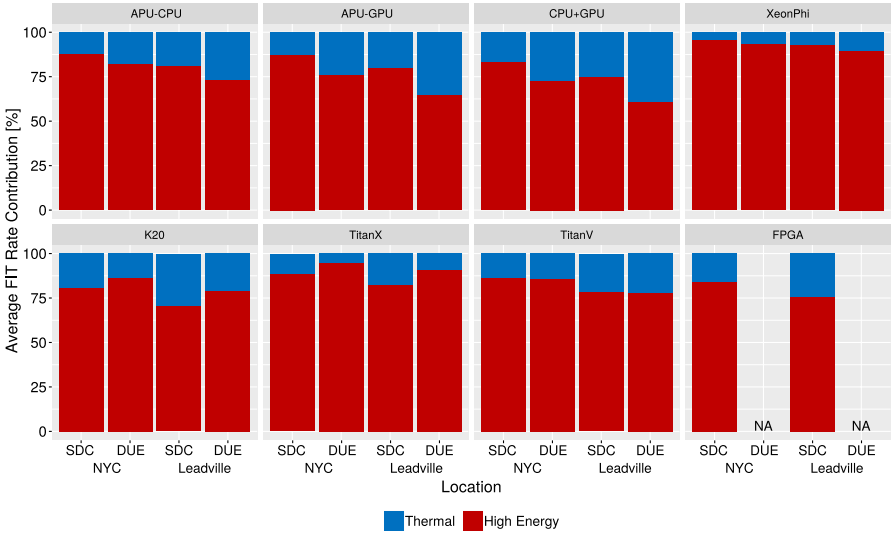

Fig. 10 Percentage of total FIT rate due to high energy and thermal neutrons. All tested parts except Xeon Phi show significant errors due to ^{10}B levels

Xeon Phi processors, as stated in Sect. 5, have a low sensitivity to thermals, which is a symptom of the use of either depleted boron or a reduction in boron usage. Thus, the thermals FIT rate seen in Fig. 10 is a relatively small percentage of the overall FIT rate (from 4.2% at NYC SDC up to 10.6% for Leadville DUE). The other tested devices, especially the K20 and CPU+GPU devices, have thermal FIT rates comparable to the FIT rates from high energy neutrons. At Leadville, K20 has 29% of the SDC FIT rate caused by thermal neutrons while APU CPU+GPU has 39% of DUEs caused by thermal neutrons.

6.3 Discussion

Figure 10 shows that, if thermal neutrons contribution to the device error rate is not considered, both the DUE and SDC FIT rates could be significantly underestimated, posing unconsidered risks to a safety-critical application or reducing the HPC server productivity unexpectedly.

Of particular interest in Fig. 10 is the relatively high percentage of faults that result in Silent Data Corruption (SDC) on several of the tested devices. In general, HPC systems are designed and engineered to maintain SDC rates low and manageable, where corrupted calculations are rare and often noticeable to users. However, anything that increases the SDC rate is always concerning. In safety-critical applications, SDCs should be strictly avoided as they could put the system in unexpected states, and they could potentially lead to unpredictable actions.

The elevated DUE rates are also of concern to HPC systems as they invariably result in a system crash and loss of some portion of a calculation's run time. It is worth noting that even with thin layers of shielding, embedded devices in vehicles can suffer from a much higher thermal flux than the one considered in Fig. 10 due to moderation and reflection from the driver and passengers, from cooling liquids, from ground and from the fuel tank filled with a hydrogen-rich fuel [52].

Our analysis shows that thermal neutrons are a threat for the reliability of supercomputers and safety critical applications that rely on COTS HPC devices. While the benefits in terms of cost, performances, and efficiency of COTS devices are not in question, their utilization in applications for which reliability is a concern must be coupled with a careful reliability evaluation that considers the impact of thermal neutrons. As the amount of ^{10}B in the manufacturing process is not publicly available, radiation experiments are one of the few ways to evaluate the sensitivity of a COTS device to thermal neutrons. Moreover, as the thermal neutron flux strongly depends on environmental conditions, the device error rate varies significantly when conditions change. Therefore, it is critical to consider the realistic conditions in which the device will operate and estimate the correspondent thermal neutrons flux. These conditions have a direct impact on HPC applications. For instance, when supercomputer time is allocated, the checkpoint frequency may need to consider weather conditions. An alternative would be to schedule less critical tasks or procedures to the devices placed in the proximity of the water radiators, as there the error rate is expected to be higher. Dissimilarly to high energy neutrons, thermal neutrons flux can be effectively reduced shielding the device with thin layers of cadmium or

some inches of boron plastic. Unfortunately, cadmium is highly toxic and should not be heated, so it should not be placed in the proximity of an HPC device or of a cooling system, and boron plastic also thermally isolate the device, so it is impractical to be used as a shield between the cooling system (one of the most efficient sources of thermal neutrons) and the device.

7 Conclusions

In this paper, we have experimentally investigated the differences between high energy and thermal neutron-induced error rates in modern HPC devices. While purifying the Silicon dopant to remove ^{10}B would make devices immune to thermal neutrons, most COTS still use natural boron. By irradiating devices with high energy and thermal neutrons while executing representative applications, we have demonstrated that thermals significantly impact device reliability. We have demonstrated that the impact of high energy and thermal neutrons depends not only on the specifics of the hardware, but also on the executed code. The impinging neutron energy has more or less effect depending on how the code accesses memory and executes instructions.

We have also shown that the FIT rates can vary based on the physical layout of the machine room in which a system resides and variations such as weather conditions external to the building.

The reported data attest the importance of thermal neutron reliability evaluation, which can significantly raise the total device error rate. As a future work, we plan to irradiate with thermal and high energy neutrons specific resources or components to deeply investigate different fault models. We also plan a thorough and sophisticated modeling of one or more data centers as well as the effects of different cooling regimes.

Acknowledgements Authors would like to thank Robert Baumann and Gus Sinnis for their precious help and support. This work is based on experiments performed thanks to the STFC support (DOI: 10.5286/ISIS.E.RB2000036 and DOI: 10.5286/ISIS.E.RB1900122) and was partially sponsored by the Laboratory Directed Research and Development program of Los Alamos National Laboratory under project numbers: 20190499ER and 20180017ER, by CAPES/PVE - Finance Code 001, the EU H2020 Programme, and from MCTI/RNP-Brazil under the HPC4E project, Grant Agreement No. 689772, and by the project FAPERGS 17/2551-0001 2020. Document approved for release with the code LA-UR-20-23114.

References

1. Lucas R (2014) Top ten exascale research challenges. In: DOE ASCAC Subcommittee Report
2. Cohen A, Shen X, Torrellas J, Tuck J, Zhou Y, Adve S, Akturk I, Bagchi S, Balasubramonian R, Barik R, Beck M, Bodik R, Butt A, Ceze L, Chen H, Chen Y, Chilimbi T, Christodorescu M, Criswell J, Ding C, Ding Y, Dwarkadas S, Elmroth E, Gibbons P, Guo X, Gupta R, Heiser G, Hoffman H, Huang J, Hunter H, Kim J, King S, Larus J, Liu C, Lu S, Lucia B, Maleki S, Mazumdar S, Neamtiu I, Pingali K, Rech P, Scott M, Solihin Y, Song D, Szefer J, Tsafrir D, Urgaonkar B, Wolf M, Xie Y, Zhao J, Zhong L, Zhu Y (2018) Inter-disciplinary research challenges in computer systems for the 2020s. Tech. rep, National Science Foundation, USA

3. Dongarra J, Meuer H, Strohmaier E (2015) ISO26262 Standard. https://www.iso.org/obp/ui/#iso:std:iso:26262:-1:ed-1:v1:en
4. Ziegler J, Puchner H (2004) SER-history. A Guide for Designing with Memory ICs (Cypress, Trends and Challenges
5. Baumann R (2005) Radiation-induced soft errors in advanced semiconductor technologies. IEEE Trans Device Mater Reliab 5(3):305–316. https://doi.org/10.1109/TDMR.2005.853449
6. Snir M, Wisniewski RW, Abraham JA, Adve SV, Bagchi S, Balaji P, Belak J, Bose P, Cappello F, Carlson B, et al (2014) Addressing failures in exascale computing. Int J High Perform Comput Appl 1094342014522573
7. Dirk J, Nelson ME, Ziegler JF, Thompson A, Zabel TH (2003) Terrestrial thermal neutrons. IEEE Trans Nuclear Sci 50(6):2060
8. JEDEC (2006) Measurement and reporting of alpha particle and terrestrial cosmic ray-induced soft errors in semiconductor devices. Tech. Rep. JESD89A, JEDEC Standard
9. Baumann R, Hossain T, Smith E, Murata S, Kitagawa H (1995) Boron as a primary source of radiation in high density DRAMs. In: 1995 Symposium on VLSI Technology. Digest of Technical Papers. IEEE. IEEE, Kyoto, Japan, Japan, pp 81–82
10. Normand E, Vranish K, Sheets A, Stitt M, Kim R (2006) Quantifying the double-sided neutron SEU threat, from low energy (thermal) and high energy>10 MeV) neutrons. IEEE Trans Nucl Sci 53(6):3587
11. Wen SJ, Pai S, Wong R, Romain M, Tam N (2010) B10 finding and correlation to thermal neutron soft error rate sensitivity for SRAMs in the sub-micron technology. In: 2010 IEEE International Integrated Reliability Workshop Final Report (IEEE), pp 31–33
12. Weulersse C, Houssany S, Guibbaud N, Segura-Ruiz J, Beaucour J, Miller F, Mazurek M (2018) Contribution of thermal neutrons to soft error rate. IEEE Trans Nucl Sci 65(8):1851
13. Lee S, Kim I, Ha S, Yu Cs, Noh J, Pae S, Park J (2015) Radiation-induced soft error rate analyses for 14 nm FinFET SRAM devices. In: 2015 IEEE International Reliability Physics Symposium. IEEE (IEEE), pp 4B–1
14. Fang YP, Oates AS (2016) Characterization of single bit and multiple cell soft error events in planar and FinFET SRAMs. IEEE Trans Device Mater Reliab 16(2):132
15. Maillard P, Hart M, Barton J, Jain P, Karp J (2015) Neutron, 64 MeV proton, thermal neutron and alpha single-event upset characterization of Xilinx 20nm UltraScale Kintex FPGA. In: 2015 IEEE Radiation Effects Data Workshop (REDW) (IEEE, 2015), pp 1–5
16. Hess VF (1913) Über den Ursprung der durchdringenden Strahlung. Z Phys 14:610
17. Ziegler JF (1996) Terrestrial cosmic rays. IBM J Res Dev 40(1):19. https://doi.org/10.1147/rd.401.0019
18. Hands A, Morris P, Ryden K, Dyer C, Truscott P, Chugg A, Parker S (2011) Single event effects in power MOSFETs due to atmospheric and thermal neutrons. IEEE Trans Nucl Sci 58(6):2687
19. Baumann R (2000) Soft error characterization and modeling methodologies at Texas Instruments. In: Proceedings of the Semiconductor Research Council 4th Topical Conference Reliability.[CD-Rom] SemaTech CD-ROM (SemaTech, USA), pp 0043–3283
20. Sheu R, Jiang S (2003) Cosmic-ray-induced neutron spectra and effective dose rates near air/ground and air/water interfaces in Taiwan. Health Phys 84(1):92
21. Patterson MK, Fenwick D (2008) The state of datacenter cooling. Intel Corporation White Paper. http://download.intel.com/technology/eep/data-center-efficiency/stateof-date-center-cooling.pdf
22. Summit system overview (2006). https://www.olcf.ornl.gov/wp-content/uploads/2018/05/Intro_Summit_System_Overview.pdf
23. Capozzoli A, Primiceri G (2015) Cooling systems in data centers: state of art and emerging technologies. Energy Procedia 83:484
24. Dongarra J, Meuer H, Strohmaier E (2018) TOP500 Supercomputer Sites: November 2018. http://www.top500.org
25. Gao T, David M, Geer J, Schmidt R, Sammakia B (2015) Experimental and numerical dynamic investigation of an energy efficient liquid cooled chiller-less data center test facility. Energy Build 91:83
26. Ellsworth M, Campbell L, Simons R, Iyengar M, Schmidt R, Chu R (2008) The evolution of water cooling for IBM large server systems: Back to the future. In: 2008 11th Intersociety Conference on Thermal and Thermomechanical Phenomena in Electronic Systems. IEEE (IEEE), pp 266–274

27. Ellsworth MJ, Goth GF, Zoodsma RJ, Arvelo A, Campbell LA, Anderl WJ (2012) An overview of the IBM power 775 supercomputer water cooling system. J Electron Packag 134(2):020906
28. Che S, Boyer M, Meng J, Tarjan D, Sheaffer JW, Lee SH, Skadron K (2009) Rodinia: a benchmark suite for heterogeneous computing. In: Proceedings of the IEEE International Symposium on Workload Characterization (IISWC). Austin, TX, USA, IEEE, pp 44–54
29. Fragkiadaki K, Zhang W, Zhang G, Shi J (2012) Two-granularity tracking: mediating trajectory and detection graphs for tracking under occlusions In: European Conference on Computer Vision. Springer, pp 552–565
30. DIMACS. 9th dimacs (2006). www.dis.uniroma1.it/challenge9/download.shtml
31. Redmon J, Divvala SK, Girshick RB, Farhadi A (2015) You only look once: unified, real-time object detection. CoRR abs/1506.02640. http://arxiv.org/abs/1506.02640
32. Deng L (2012) The MNIST database of handwritten digit images for machine learning research [best of the web]. IEEE Signal Process Mag 29(6):141. https://doi.org/10.1109/msp.2012.2211477
33. Cazzaniga C, Frost CD (2018) Progress of the Scientific Commissioning of a fast neutron beamline for Chip Irradiation. J Phys: Conf Ser 1021:012037
34. Chiesa D, Nastasi M, Cazzaniga C, Rebai M, Arcidiacono L, Previtali E, Gorini G, Frost CD (2018) Measurement of the neutron flux at spallation sources using multi-foil activation. Nuclear Instruments and Methods in Physics Research Section A: Accelerators. Spectrometers, Detectors and Associated Equipment
35. Tietze H, Schmidt W, Geick R (1989) Rotax, a spectrometer for coherent neutron inelastic scattering at ISIS. Phys B: Condens Matter 156:550
36. Oliveira D, Pilla L, DeBardeleben N, Blanchard S, Quinn H, Koren I, Navaux P, Rech P (2017) Experimental and Analytical Study of Xeon Phi Reliability. In: Proceedings of the International Conference for High Performance Computing, Networking, Storage and Analysis (ACM, New York, NY, USA), SC'17, pp 28:1–28:12. https://doi.org/10.1145/3126908.3126960
37. Oliveira D, Pilla L, Hanzich M, Fratin V, Fernandes F, Lunardi C, Cela J, Navaux P, Carro L, Rech P (2017) Radiation-induced error criticality in modern HPC parallel accelerators. In: Proceedings of 21st IEEE Symposium on High Performance Computer Architecture (HPCA) (ACM)
38. Constantinescu C (2008) Intermittent faults and effects on reliability of integrated circuits. In: Reliability and Maintainability Symposium, 2008. RAMS 2008. Annual. IEEE (IEEE, Las Vegas, NV, USA), pp 370–374
39. Quinn H, Graham P, Fairbanks T (2010) SEEs induced by high-energy protons and neutrons in SDRAM. In: 2011 IEEE Radiation Effects Data Workshop, pp 1–5. https://doi.org/10.1109/REDW.2010.6062524
40. Srour JR, Marshall CJ, Marshall PW (2003) Review of displacement damage effects in silicon devices. IEEE Trans Nucl Sci 50(3):653. https://doi.org/10.1109/TNS.2003.813197
41. Association EI et al (1996) Test procedures for the measurement of single-event effects in semiconductor devices from heavy ion irradiation. EIA/JEDEC Standard (57)
42. Constantinescu C (2002) Impact of deep submicron technology on dependability of VLSI circuits. In: IEEE Proceedings of the International Conference on Dependable Systems and Networks, 2002 DSN 2002. IEEE, Washington, DC, USA, pp 205–209
43. Sridharan V, Stearley J, DeBardeleben N, Blanchard S, Gurumurthi S (2013) Feng shui of supercomputer memory: positional effects in DRAM and SRAM faults. In: Proceedings of SC13: International Conference for High Performance Computing. Storage and Analysis. ACM, Networking, p 22
44. Guertin SM, Cui M (2017) SEE test results for the snapdragon 820. In: 2017 IEEE Radiation Effects Data Workshop (REDW), pp 1–6. https://doi.org/10.1109/NSREC.2017.8115452
45. Sridharan V, Liberty D (2012) A study of DRAM failures in the field. In: 2012 International Conference for (IEEE) High Performance Computing, Networking, Storage and Analysis (SC), pp 1–11
46. Fratin V, Oliveira D, Lunardi C, Santos F, Rodrigues G, Rech P (2018) Code-dependent and architecture-dependent reliability behaviors. In: 2018 48th Annual IEEE/IFIP International Conference on Dependable Systems and Networks (DSN). IEEE (IEEE), pp 13–26
47. dos Santos FF, Pimenta PF, Lunardi C, Draghetti L, Carro L, Kaeli D, Rech P (2019) Analyzing and increasing the reliability of convolutional neural networks on GPUs. IEEE Trans Reliab 68(2):663. https://doi.org/10.1109/TR.2018.2878387

48. Jeon H, Wilkening M, Sridharan V, Gurumurthi S, Loh GH (2013) Architectural vulnerability modeling and analysis of integrated graphics processors In: IEEE 10th Workshop on Silicon Errors in Logic—System Effects (SELSE) (IEEE)
49. Dodd PE (2005) Physics-based simulation of single-event effects. IEEE Trans Device Mater Reliab 5(3):343. https://doi.org/10.1109/TDMR.2005.855826
50. Soft-error testing resource (2006). http://www.seutest.com/cgi-bin/FluxCalculator.cgi
51. Werner CJ et al (2018) mcnp6.2 release notes
52. Leo WR (2012) Techniques for nuclear and particle physics experiments: a how-to approach. Springer, Berlin

PHYSICS FLASH

Winter 2021
Approved for public release; distribution is unlimited.

INSIDE

Sowjanya Gollapinni during installation of the MicroBooNE detector at Fermilab.

Sowjanya Gollapinni

Putting down new markers for Los Alamos neutrino research

To find answers to some of the most "massive" questions in physics posed by investigating *nearly* mass-less particles, Sowjanya Gollapinni is prepared to tackle unprecedented experimental technical challenges.

Gollapinni studies the neutrino, the second-most abundant particle in the universe—and one that "forms the most bizarre, tiny entities known to date," she said. Neutrinos were first detected by Los Alamos researchers Fred Reines and George Cowan in 1956, and despite years of study, they "still remain largely mysterious." These elusive particles have the potential to resolve profound science questions, including how the universe came into existence and its composition at an elemental level.

> "Gollapinni studies the neutrino, the second-most abundant particle in the universe—and one that 'forms the most bizarre, tiny entities known to date.' "

To unlock their secrets, Gollapinni (Nuclear and Particle Physics and Applications, P-3) and her colleagues employ some formidable tools, leveraging the unique resources and infrastructure provided by the Laboratory. "As the saying goes 'the smaller the object you want to observe, the bigger and more powerful the microscope needs to be,' " she said.

These instruments include a 70-kiloton liquid argon-based particle detector, the largest of its type ever constructed, as part of DUNE (for Deep Underground Neutrino Experiment), the next-generation U.S. flagship neutrino experiment. The DUNE detector will be

continued on page 3

Los Alamos NATIONAL LABORATORY EST. 1943

> Well, we pulled it off. With tremendous effort from our group and division administrators, and staff deployed from Finance, HR, and Property to support our division, and from all of you, we managed to start 2021 with our new group structure.

From Eric's desk . . .

"From the Desk" is a bit different this issue, coming from me instead of our division leader. This gives Tanja a little break and provides me the opportunity to give my perspective on a look back at 2020 as well as what lies ahead in 2021.

Well, we pulled it off. With tremendous effort from our group and division administrators, and staff deployed from Finance, HR, and Property to support our division, and from all of you, we managed to start 2021 with our new group structure. I hope this change has not been too disruptive to your day-to-day activities and that, despite the impediments that COVID-19 protocols put in our way, you have had the opportunity to meet and interact with your new group members. Only a few office moves have occurred so far, but more will transpire at a slow and deliberate pace over the next several months.

With the pandemic, last year was unlike any other. What I initially thought would be a few weeks of working from home has now become the norm for the last 10 months and likely to go many months more. While this work-from-home mode has been for some a stressful adjustment, particularly for those with young children and both parents working, we have largely learned to adapt and still get our important work accomplished. Thanks to all of you for figuring out how to minimize our on-site presence while remaining productive. Vaccination of the Lab's workforce is proceeding, albeit at a slower pace than we'd like due to limits on vaccine availability. Let's hope this turns the corner and that we can return to normal before year's end.

Thanks to the Herculean efforts of Celine Apodaca, Julie Canepa, Ray Leeper, Justin Jorgenson, and many others in P-4, we managed to move a good portion of the former P-24 from TA-35 to TA-53. The impetus for this move is to make space available in the Pajarito Corridor for LANL's pit production mission. While we cleared out of the second floor of Building 87, much work remains to move the light labs from the first floor into MPF-19 at TA-53. Capital Projects is undertaking the refurbishment of MPF-19 to make it suitable for moving these light labs. The design work is well under way, with modifications expected to start this month and continue through August. If things proceed smoothly, MPF-19 may be available for move-in as early as September.

On a personal note, I have decided to retire this summer after nearly 39 years with LANL. A good portion of my LANL career has been here at LANSCE and I have seen a lot of change in four decades. I started as an undergraduate student in what was then the recently-formed Accelerator Technology Division. I joined the ion source section of the group responsible for Project White Horse, which was a group pulled from Physics Division when AT Division was formed (reorganizations have been going on for a long time!). The goal was space-based missile defense using neutral beams of hydrogen atoms. At that time Los Alamos was the undisputed world leader in high-power proton accelerator technology. LANSCE and Physics Division continue to deliver cutting-edge science and technology addressing the nation's national security needs and I am pleased to have had the experience of working with all of you.

Physics Deputy Division Leader Eric Pitcher ■

Gollapinni cont.

located 1.5 miles below the surface in an abandoned gold mine in South Dakota and will receive neutrinos generated at Fermilab 800 miles away.

Leading efforts to fine tune instrumentation ...

Gollapinni leads the LANL DUNE effort, serving as the technical leader of the detector's calibration and cryogenic instrumentation programs. In 2019 she received a DOE Early Career Award to aid in the development of DUNE's novel calibration system.

"By far, calibration forms one of the most challenging aspects of DUNE," she said. To help understand and diagnose any non-uniformities in the detector, Gollapinni is developing a calibration system that uses ionizing tracks from high power lasers. She is also involved in developing a system that uses a neutron generator to ultimately produce low-energy gamma particles across the large volume of the DUNE detector at energies relevant to solar neutrinos and supernovae burst physics to aid in understanding these extreme phenomena among others.

... and beyond

Gollapinni is also a member of the MicroBooNE and Short-Baseline Neutrino programs. These experiments are aimed at performing the most sensitive search of an eV-scale "sterile" neutrino, where there are numerous existing experimental anomalies. A sterile neutrino is one that does not interact with ordinary matter. Existence of sterile neutrinos will be a breakthrough discovery with a profound impact not just on particle physics, but also on astrophysics and cosmology, she said.

These projects and her efforts, part of the Lab's DOE Office of Science under the High Energy Physics (HEP) mission, attract diverse talent to LANL from across the globe and contribute to workforce development both for the Lab and the nation by developing a new generation of researchers with advanced diagnostic and data analysis skills required for solving national security science challenges.

Gollapinni (front row, left) and colleagues after installing more than 8000 150-micrometer-diameter anode plane wires in MicroBooNE at Fermilab.

"By playing leading roles on the DUNE and Short-Baseline Neutrino programs, Sowjanya is raising the visibility of LANL neutrino science," said neutrino researcher Bill Louis (Applied and Fundamental Physics, P-2). "Through her talks at international conferences and her extensive connections with collaborators around the world, she has expanded LANL's impact in the field of neutrino physics and has brought some outstanding postdocs to the Lab."

Gollapinni, who has a PhD in physics from Wayne State University, was previously an assistant professor at the University of Tennessee, Knoxville, and she maintains an adjunct faculty position there. She joined the Lab in late 2019, drawn by its support of science investment, its rich history and pioneering neutrino work, and its collaborative research environment. "It was extremely important for me to see the Lab foster such a culture," she said. "All of this drew me to LANL."

By Karen Kippen, ALDPS

Sowjanya Gollapinni's favorite project

What: While all the projects I am working on are exciting in their own right, I would say DUNE is the most challenging and exciting of them all both in terms of scientific and technical potential. DUNE's liquid argon based detector will be the largest of its type ever constructed.

Why: Building a detector at such an unprecedented scale, and that too in a deep underground location, is what makes DUNE challenging. DUNE will help us understand why matter dominates over anti-matter in the universe—the question of why we exist at all.

Where and when: DUNE is scheduled to take first physics data in the late 2020s and will be located at Fermilab (near detector) and South Dakota (far detector).

Who: DUNE is an international effort and currently consists of 1000+ collaborators from more than 30 countries across the globe.

How: The large prototype detectors of DUNE, referred to as ProtoDUNEs, are running successfully at CERN in Switzerland and are a huge success toward validating the DUNE technologies.

In reach at last?

Direct measurements of nuclear reactions on radionuclides

Los Alamos National Laboratory's mission is to solve national security challenges through scientific excellence. A new experimental technique being developed at the Lab for fundamental science is expected to be a boon for weapons science—a prime example of this mission at work.

Astronomers and weapons researchers share a common need that this ambitious new experiment could meet. Similar to nucleosynthesis leaving a signature of stellar evolution, the neutron fluence in a nuclear explosion leaves a unique signature that includes chains of radionuclides. In both cases, direct measurements of many—even most—of the neutron reactions are nearly impossible and understanding is empirical in nature.

A recent study aimed at uncovering the origins of heavy element production in astrophysical environments could help change that. In the just-completed experiment, Principal Investigator Hye Young Lee (Nuclear and Particle Physics and Applications, P-3) and Co-Principal Investigator Etienne Vermeulen (Inorganic, Isotope, and Actinide Chemistry, C-IIAC) directly measured nuclear reactions on radionuclides. The work represents the first credible path to make direct measurements on many key radionuclides.

Radionuclides, such as radium-226, cesium-137, strontium-90, and nickel-56, are unstable atoms that emit radiation at a variety of rates (measured in half-lifes). Nickel-56 is abundantly produced in supernovae (stellar explosions).

As part of the Laboratory-Directed Research and Development project "Pinning down the neutrino-proton process importance in heavy element production via reaction studies on radioactive nickel-56," the team is now analyzing data and expect to report results this spring.

In the longer term, the researchers plan to leverage the system as part of an integrated strategy aimed at generating essential weapons data—in particular, extremely difficult to measure cross sections.

"This experiment is yet another stellar example of the synergy between the Lab's fundamental science and its national security mission," said Physics Division Leader Tanja Pietraß. "Through basic science endeavors like this one our researchers are advancing the understanding needed to develop new diagnostic tools for ensuring the safety, security, and reliability of the nation's nuclear deterrent."

Simultaneous excellence in action

In the experiment conducted at the Los Alamos Neutron Science Center (LANSCE), the research team used hotLENZ, the "hot" Low-Energy Neutron-induced Charged-particle (Z) Chamber, and

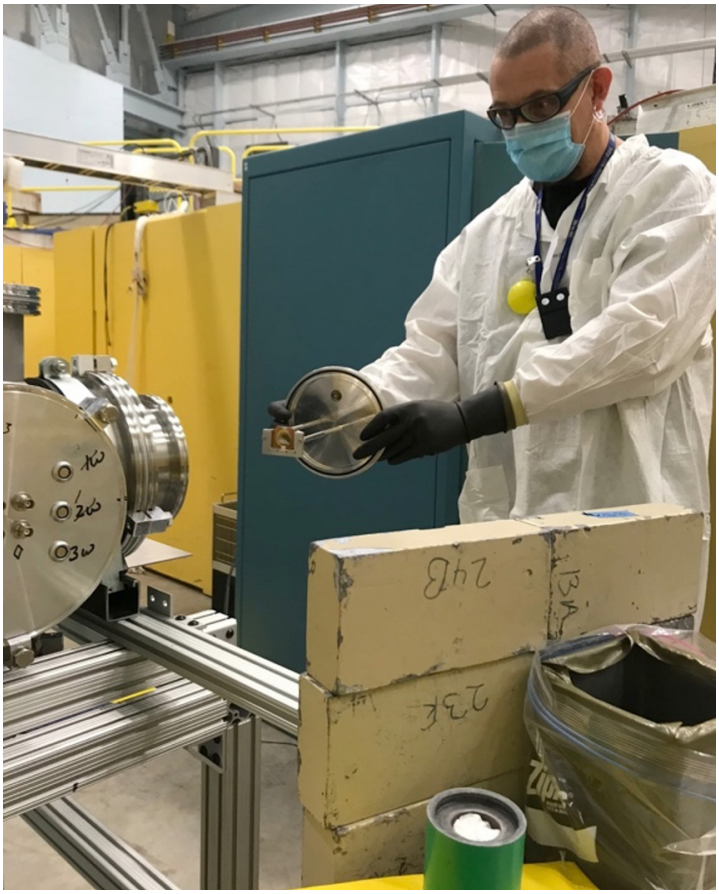

In the experiment's last test run, Etienne Vermeulen moved a radioactive sample, strontium-82, from the lead container (green cylinder) to the ALSOLENZ, the second LENZ chamber, used for this detector performance test in Weapons Neutron Research Facility flight path 15R. Here, he recreates the process using a dummy sample, shown in the orange circle foil mounted in the vacuum flange he holds.

a highly radioactive sample generated at the Isotope Production Facility (IPF).

The experiment—probing the physics in play during supernova explosions—required a combination of sophisticated science and complex operations.

For the final reaction study, the nickel-56 sample, which has a half-life of approximately six days, was fabricated in an IPF TA-48 hot cell. It was swiftly transported inside a tungsten cask to the Weapons Neutron Research (WNR) Facility, which provided the neutron energy and flux required for the study.

Using the overhead crane in flight path 90L, this cask was disassembled as a part of the fully automated sample-handling vacuum chamber, designed by research technologist Brad DiGiovine (P-3) for this final high-dose experiment. Therefore, no workers were present in the flight path while the sample was positioned out of the cask to the beam axis with high precision.

"At LANSCE, we can produce extremely high radioactivity with a short half-life, we can prepare the target, and we can get it into the

continued on next page ▶

Direct measurements cont.

neutron beam safely with enough time to measure reaction products induced by neutron interactions on this radioactive nucleus," Lee said.

Meticulous planning and practice

Directly measuring nuclear reactions comes with harsh consequences. The detectors would be irreparably damaged after exposure to the radiation produced during the experiment.

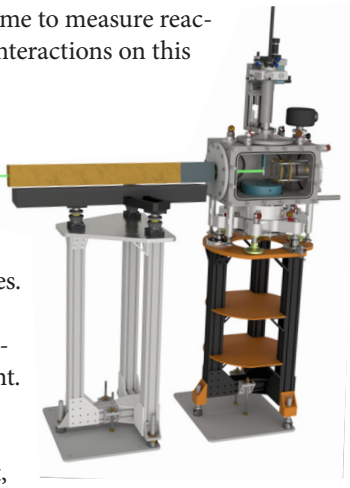

In the illustration above, the straight green line represents a neutron beam on a sample. In the final reaction study on the Ni-56 sample, which had a factor of at least 20 times higher radioactivity than the previous one, the sample's removal from its tungsten cask (shown as the dark blue cylinder below the sample) and its alignment in the LANSCE proton beam were handled by the hotLENZ remote sample manipulation system.

To guarantee they would be up to the task in this one-shot experiment, Physics and Chemistry division researchers successfully executed a high-hazard operation to test the system's performance.

The final check of the instrument's equipment involved manually inserting a strontium-82 sample, measuring about 5 mCi and >50 R/hour on contact, into the target holder.

Shielding was constructed to protect Vermeulen, who was responsible for inserting the sample into the instrument vacuum chamber. In preparation of moving the target, he performed a number of handling tests. He found he preferred using radiation-resistant gloves instead of long-handled tools, as they presented less risk of puncturing the thin-foil sample and provided a surer, swifter grip.

When the time came, Vermeulen flawlessly executed the move in under five seconds, ensuring maximum safety and allowing the experiment with a relatively short-lived sample to start in the quickest possible time. "At the level where we can still do manual manipulations of sources it is imperative to be well prepared and confident in our ability to execute the work safely and precisely," he said.

These proactive efforts—working at a lower level of radioactivity than required in the final experiment, yet at a level classified as high hazard—were important steps in anticipation of the experiment.

Researchers: Hye Young Lee, Sean Kuvin, and Brad DiGiovine (all P-3); Etienne Vermeulen, Cecilia Lledo, and Veronika Mocko (all C-IIAC). The work supports the Lab's Basic Science mission and Nuclear and Particle Futures science pillar.

Technical contacts: Hye Young Lee, Etienne Vermeulen ■

Novel thermal neutron detector safeguards aircraft, HPC semiconductor electronics

Los Alamos researchers collaborated with Honeywell, Inc. to develop the Tinman technology to detect deleterious levels of thermal neutrons.

It has long been recognized that high-energy neutrons can impact the reliability of semiconductor devices by producing ionized particles that deposit charge in semiconductor devices. There have been recent concerns that thermal neutrons can also cause failures by creating charged particles following nuclear reactions. These thermal neutrons are produced when high-energy neutrons strike moderating material and lose energy. Approximately 10–20% of single-event upsets seen in semiconductors have been attributed to thermal neutrons.

Certain environments, including high-performance computing (HPC) environments and aircraft may be particularly susceptible to thermal neutrons. In the case of HPC, there is a significant amount of cooling water near the semiconductor devices. In aircraft, there is considerable fuel in the aircraft. Both water and fuel are excellent thermalizing materials. Therefore, both industries are invested in detecting and understanding the thermal neutron environment.

Tinman does precisely that—it detects and measures thermal neutrons via He-3 tubes, one of which is covered with cadmium while the other is bare. The thermal neutron intensity is the difference in count rates between the two tubes.

Steve Wender (Applied and Fundamental Physics, P-2) (left) and Suzanne Nowicki (Space Science and Applications, ISR-1) stand in the cabin of a NASA DC-8 aircraft for testing the Tinman instrument.

continued on next page ▶

Novel cont.
Tinman is autonomous and has already been successfully tested on three different NASA aircraft flights. Tin-II is a recent advancement specifically designed for detection of thermal neutrons in the Los Alamos HPC facility. Tin-II was installed and has been operating in the HPC area for approximately one year. In addition, a version of Tinman is being designed to detect thermal neutrons as part of the Coherent Captain Mills neutrino experiment at the Los Alamos Neutron Science Center.

Research and development work is ongoing between LANL and Honeywell under a CRADA for the next-generation Tinman detector.

Tinman technology is funded by a Strategic Partnership agreement and now a CRADA with Honeywell. The technology supports the Laboratory's Nuclear Deterrence mission area and the Science of Signatures capability pillar.

Reference: S. Wender, A. Couture, and T. Fairbanks, "Report on the Tin-II thermal Neutron Detector." LA-UR 19-30822.

Technical contact: Steve Wender

Physics Division news roundup

Matt Durham joins leadership of LHCb experiment

Matt Durham (Nuclear and Particle Physics and Applications, P-3) has been selected as one of two ion and fixed target conveners for the Large Hadron Collider beauty (LHCb) experiment. During his roughly two-year term, which began this year, he oversees all LHCb analyses in heavy ion collisions. Durham will be the only conveyor out of 18 from the United States in the collaboration. P-3 has convenorships at two of the six operating worldwide heavy ion experiments (Durham at LHC and Cesar da Silva at the Relativistic Heavy Ion Collider [RHIC]) and major roles in the next generation of heavy ion experiments under development at RHIC and the LHC. P-3 is leading the implementation of the microvertex detector that is part of the RHIC sPHENIX experiment and is leading an upgrade detector program for LHCb.

Astrid Morreale named vice chair of APS Four Corners Section

Astrid Morreale (P-3) has been elected vice chair of the American Physical Society's Four Corners Section. As a member of its executive committee, she will help advance the section's mission to provide opportunities supporting the professional development of scientists and students in the Four Corners region of New Mexico, Arizona, Colorado, and Utah. Her four-year term—as vice chair, chair-elect, chair, and past chair—began in November.

"As physicists we have an advantageous position to be able to reach out to both the general and specialized public thanks to the multidisciplinary predisposition of our field," Morreale said. "It is of crucial importance, especially now, that we invest within our communities to ensure that science in general has a strong presence in every household."

Morreale is a member of P-3's High Energy Nuclear Physics Team. Her research expertise encompasses hadronic/nuclear structure in a variety of collision systems and center of mass energies. After earning her PhD in 2009 in nuclear and particle physics from the University of California, Riverside, Morreale accepted a private investigator grant from the National Science Foundation to work at the Atomic Energy Commission in France. She remained in Europe for the next 10 years and received her "Habilitation thesis in physics," the highest title that can be conferred upon a scholar in France. Prior to joining the Lab in 2019, she was an associate professor at the Engineering School IMT of Nantes (France) and performed her research at the Large Hadron Collider. She is a peer reviewer for several national and international journals and a fellowship evaluator for the European Research Council, Horizon H2020 initiative. Morreale is a United States Marine Corps veteran.

Ralph Massarczyk featured in SURF article

Ralph Massarczyk (Dynamic Imaging and Radiography, P-1) was featured in a SURF news article describing the careful work done, despite COVID impacts, to swap detectors in the Majorana Demonstrator experiment. Working in a cleanroom at SURF, the Sanford Underground Research Facility in South Dakota, researchers replaced five of the original detectors with four newly made ones. The detectors are being tested for use in LEGEND-200, a next-generation neutrinoless double-beta decay experiment. Massarczyk was also recently selected to serve a one-year term on the nine-member SURF User Association's Executive Committee.

Harry Robey earns citation distinction

Harry Robey (Thermonuclear Plasma Physics, P-4) is among the top 2% of the most cited researchers worldwide throughout their careers, according to research on metascience published in *PLoS Biology*. Robey joined LANL in 2020 and is stationed at Lawrence

continued on next page

Physics Division cont.

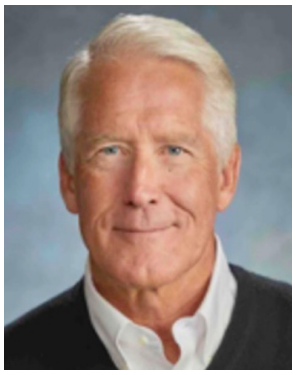

Livermore National Laboratory, where he assists and mentors P-4 personnel with the design and fielding of a wide range of high-energy-density physics experiments being conducted on the National Ignition Facility. In "Updated science-wide author databases of standardized citation indicators," John Loannidis (Stanford University), Kevin Boyack (SciTech Strategies) and Jeroen Baas (Elsevier B.V.) present a database of the top 100,000 scientists of various disciplines.

Sowjanya Gollapinni puts her stamp on APS newsletter

Sowjanya Gollapinni (P-3) served as co-guest editor of the fall issue of the *CSWP&COM Gazette*, the newsletter of the APS committees on minorities (COM) and the status of women in physics. Chair-elect of the APS COM and chair of the indigenous physicists sub-committee, Gollapinni also contributed an article, "How to actively not be a barrier to diversity efforts in physics," (LA-UR-20-29716) to the issue, which focused on minorities in physics.

Helium cryostat supporting DOE nuclear physics research successfully commissioned

Neutron Team Leader Takeyasu Ito (P-3) reported that a HSHV system has been successfully commissioned. The large helium cryostat will be used for studying electrical breakdown in superfluid liquid helium as part of the Lab's DOE Nuclear Physics-funded effort supporting the Spallation Neutron Source Neutron Electric Dipole Moment experiment. Postdoctoral researcher Grant Riley led this effort, with support from Wade Uhrich, Scott Currie, Nguyen Phan, Steven Clayton (all P-3), and Erick Smith (P-2). ■

Celebrating service

Congratulations to the following Physics Division employees who recently celebrated service anniversaries:

Julie Canepa, P-4	35 years
Maria Rightley, P-1	25 years
Aaron Couture, P-3	15 years
Joshua Tybo,P -1	10 years
Albert Young, P-3	10 years
Levi Neukirch, P-1	5 years
Brandon White, P-2	5 years
Jack Winkelbauer, P-3	5 years

HeadsUP!

Physics Division's commitment to the environment

The Laboratory is committed to environmental stewardship and is an ISO 14000 certified institution. A certified environmental management system enables the organization to protect the environment, mitigate adverse impacts, and assure compliance.

As part of its support of the Lab's commitment to environmental stewardship, the Physical Sciences Directorate (ALDPS) has identified environmental risks in its operations and works to reduce any environmental impact. ALDPS annually develops an environmental action plan (EAP) focused on environmental objectives of

- creating a sustainable future.
- controlling the present. and
- cleaning up the past.

Goals and targets are developed around this organizing structure in addition to complying with embedded requirements, for example waste generation controls and waste management.

Physics Division is part of the EAP and its focus for FY21 is

- helium liquification and recovery systems at the Ultracold Neutron Facility, which contributes to reducing emissions, thus creating a sustainable future,
- investment in 5S + Safety activities throughout the Division, which helps control the present, and
- helping with the site-wide cleanup program—reducing our legacy equipment and material through the clearing and disposition of multiple transportainers at TAs 35 and 53.

These projects captured in the EAP are only a subset of the good environmental awareness and work ongoing in the division.

PHYSICS FLASH
SINCE 1943

Published by the Physical Sciences Directorate.

To submit news items or for more information, contact Karen Kippen, ALDPS Communications, at 505-606-1822 or aldps-comm@lanl.gov.

For past issues, see www.lanl.gov/org/ddste/aldps/physics/physics-flash-archive.php.

Los Alamos NATIONAL LABORATORY EST.1943

Los Alamos National Laboratory, an affirmative action/equal opportunity employer, is managed by Triad National Security, LLC, for the National Nuclear Security Administration of the U.S. Department of Energy under contract 89233218CNA000001.

NNSA National Nuclear Security Administration

AGU PUBLICATIONS

Space Weather

FEATURE ARTICLE
10.1002/2015SW001169

Supporting Information:
• Texts S1–S3

Citation:
Tobiska, W. K., et al. (2015), Advances in Atmospheric Radiation Measurements and Modeling Needed to Improve Air Safety, *Space Weather, 13*, doi:10.1002/2015SW001169.

Accepted article online 25 MAR 2015

Advances in Atmospheric Radiation Measurements and Modeling Needed to Improve Air Safety

W. Kent Tobiska, William Atwell, Peter Beck, Eric Benton, Kyle Copeland, Clive Dyer, Brad Gersey, Ian Getley, Alex Hands, Michael Holland, Sunhak Hong, Junga Hwang, Bryn Jones, Kathleen Malone, Matthias M. Meier, Chris Mertens, Tony Phillips, Keith Ryden, Nathan Schwadron, Stephen A. Wender, Richard Wilkins, and Michael A. Xapsos

Abstract Air safety is tied to the phenomenon of ionizing radiation from space weather, primarily from galactic cosmic rays but also from solar energetic particles. A global framework for addressing radiation issues in this environment has been constructed, but more must be done at international and national levels. Health consequences from atmospheric radiation exposure are likely to exist. In addition, severe solar radiation events may cause economic consequences in the international aviation community due to exposure limits being reached by some crew members. Impacts from a radiation environment upon avionics from high-energy particles and low-energy, thermalized neutrons are now recognized as an area of active interest. A broad community recognizes that there are a number of mitigation paths that can be taken relative to the human tissue and avionics exposure risks. These include developing active monitoring and measurement programs as well as improving scientific modeling capabilities that can eventually be turned into operations. A number of roadblocks to risk mitigation still exist, such as effective pilot training programs as well as monitoring, measuring, and regulatory measures. An active international effort toward observing the weather of atmospheric radiation must occur to make progress in mitigating radiation exposure risks. Stakeholders in this process include standard-making bodies, scientific organizations, regulatory organizations, air traffic management systems, aircraft owners and operators, pilots and crew, and even the public.

Aviation Radiation Is an Unavoidable Space Weather Phenomenon

Air safety has improved significantly in many meteorological areas over the past decades with the exception of space weather, which includes ionizing radiation. While a framework for addressing radiation issues has been constructed, we believe that more can and must be done at international and national levels. In particular, measurement programs must be expanded and linked with models to provide current epoch and, eventually, forecast information for the aviation ionizing radiation environment. A diverse radiation measurement and modeling community exists with a strong interest in improving international air safety.

There are two challenges in our ever more mobile, technologically dependent global society. First, pilots, crew, and passengers, which include fetuses between their first and second trimesters, might face additional radiation hazards in terms of dose equivalent rate (rate of absorbed dose multiplied by the quality factor), particularly when flying at commercial aviation altitudes above 26,000 ft. (7924.8 m) (8 km) (see Figure 1). Second, avionics can experience single event effects (SEEs) from both the ambient high-energy and thermal neutron environments. The source of this radiation in either case is twofold—from the continuous bombardment by primary background galactic cosmic rays (GCRs) and also from solar energetic particles (SEPs) emitted during occasional solar flare events lasting up to a few days.

Galactic cosmic rays from outside the solar system consist mostly of energetic protons but also contain heavy ions such as iron. Solar energetic particles are commonly associated with solar flaring events and are dominated by protons. Regardless of their source and depending upon their energy, these charged particles enter the Earth's atmosphere at different magnetic latitudes and collide with atmospheric molecules. Below the top of the atmosphere (~100 km), the primary radiation decreases as a result of atmospheric absorption, while a secondary radiation component increases. This occurs because many low-energy particles are created by the initial impacts [*Reitz et al.*, 1993]. These competing processes produce an ionizing maximum that occurs between 20 and 25 km (65,000–82,000 ft) called the Pfotzer maximum, although observational evidence may point to variable altitudes of this maximum. Below the Pfotzer maximum, down to the Earth's surface, the particle

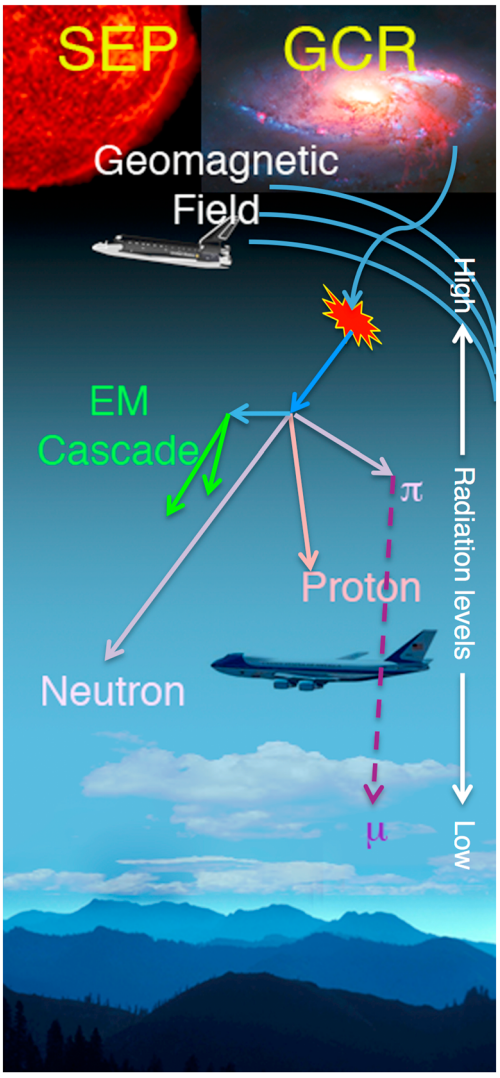

Figure 1. All passengers in commercial aircraft flying above 26,000 ft. (7924.8 m) will typically experience some exposure in this aviation radiation environment.

fluxes decrease. The secondary radiation, including protons, neutrons, pions, electrons, and gamma rays, has varying energies and is emitted in all directions. The primary and secondary energetic particles collide with atmospheric molecules, the aircraft structure, and interior materials (including passengers) to cause a further alteration of the radiation spectrum.

This resulting complex spectrum of the radiation environment may potentially cause an increase in cancer risk as the dose equivalent exposure increases. The atmospheric neutron component of this complex radiation field, in particular, holds special interest in the cancer research community. The energy spectrum of these neutrons extends over more than 10 orders of magnitude. Both the high-energy neutrons ($E > 10$ MeV) and the very low energy thermalized neutrons can also cause SEE errors in avionics [*Normand et al.*, 1994, 2006]. The high-energy neutrons have direct interactions with silicon (Si) nuclei in electronics, producing excess charge carriers through nuclei recoils. The very low energy neutrons are created by scattering from atmospheric constituents and aircraft materials (including fuel and passengers), which thermalizes them (creates neutrons in thermal equilibrium with their surroundings in an energy range of approximately 0.02–0.2 eV). These thermalized neutrons are then absorbed by boron (particularly ^{10}B) found in Si-based aircraft electronics, for example. The net effect after absorption is the production of a gamma ray (480 keV), an alpha particle (~4 MeV), and a lithium ion. The charged alpha particle may then interact with semiconductor structures and cause a SEE. Higher Z elements near the silicon layers (e.g., tungsten connectors) can exacerbate the SEE effect considerably.

Most of the time, the GCR radiation component dominates commercial aviation altitudes. It varies inversely with the approximate 11 year solar cycle. As an example, the outflowing plasma in the solar wind and the strength of the solar interplanetary magnetic field (IMF) effectively screen lower energy GCR particles from reaching the Earth during high solar cycle activity. Thus, as the next solar minimum approaches (~2017–2021), the GCR radiation will become stronger as the solar wind and IMF become weaker. In addition, significant solar flaring events can produce radiation storms, in which the SEP doses are additive with the GCRs. We note that Forbush decreases (a rapid decline in the observed GCR intensity following a solar coronal mass ejection, for example) can temporarily reduce the GCR component. The resulting GCR and SEP combined dose equivalent exposure level could possibly exceed safety thresholds established by the international radiation protection community. Potential event examples are shown in the sidebars.

Radiation Exposure Consequences

While the most significant, but highly unlikely, health consequences to atmospheric radiation exposure may include death from cancer due to long-term exposure, there are many lifestyle-degrading and career-impacting cancer forms that can also occur [*Wilson et al.*, 2002]. A cancer diagnosis can have significant career impact for a commercial pilot. The Federal Aviation Administration (FAA) requires each pilot to hold a medical certificate

in order to exercise the privileges of his or her pilot's license. A cancer diagnosis can ground a pilot for some time, perhaps permanently given the diagnosis and time remaining in his or her career. International guidelines from the International Commission on Radiological Protection (ICRP) have been developed to mitigate this statistical risk [*International Commission on Radiological Protection*, 1991, 2005, 2007]. The ICRP recommends effective dose limits of a 5 year average of 20 millisieverts (mSv) yr^{-1} with no more than 50 mSv in a single year for nonpregnant, occupationally exposed persons, and 1 mSv yr^{-1} for the general public. Radiation dose limits can be misunderstood. Pilots are trained in the use of engineering limits; however, radiation limits are not engineering limits. In the U.S., for example, they are treated as an upper limit of acceptability and *not* a design limit [*National Council on Radiation Protection and Measurements* (*NCRP*) *Report No. 116*, 1993].

Thus, to better understand these consequences, the European Commission initiated and supported research projects on cosmic radiation in the 1990s, which included numerous onboard measurements [*O'Sullivan et al*., 1999; *Beck et al*., 1999a; *O'Sullivan et al*., 2004; *European Commission Radiation Protection 140*, 2004; *Lillhök*, 2007]. Based on that experience, international institutes developed calculation codes for the assessment of galactic cosmic radiation exposure on board aircraft. For example, the EURADOS (European Dosimetry Group) working group WG11, which focuses its activity on high-energy radiation fields, carried out international comparison of these calculation codes and confirmed good agreement [*Bottollier-Depois et al*., 2009]. Further, the international radiation protection community working on cosmic radiation effects to aircrew developed International Standards Organization (ISO) standards describing the conceptual basis for cosmic radiation measurements [*International Standards Organization* (*ISO*) *20785–1*, 2012], including characterization of these instruments [*ISO* 20785–2, 2011]. The third part of this standard is still in progress related to measurements at aviation altitudes. In 2010, the International Commission on Radiation Units (ICRU) and ICRP jointly published Report 84 on this topic [*International Commission on Radiation Units*, 2010]. Recently, during the 2014 European Space Weather Week at Liege, the EURADOS WG11 presented comparison of calculation codes, which estimate exposure due to solar energetic particle events on board aircraft [*Beck et al*., 2014; *EURADOS Report*, 2012].

European Union (EU) member states have implemented regulations for aircrew members requiring exposure assessment when it is likely to be >1 mSv yr^{-1} and to take into account the assessed exposure when organizing working schedules to reduce the doses of highly exposed crew [*EU Council Directive*, 2013]. In the U.S., there are no regulatory effective dose limits for aircrew members; the FAA [*AC 120-61B*, 2014] accepts the most recent recommendations of the American Conference of Governmental Industrial Hygienists and recommends ICRP limits for exposure to ionizing radiation for nonpregnant air carrier crew members. For pregnant crew members, the FAA recommends the ICRP limit of 1 mSv to the fetus/conceptus for the remainder of the pregnancy, once reported to management, and the National Council on Radiation Protection and Measurements (NCRP) recommends a limit of 0.5 mSv/month.

Modeled results [*Mertens et al*., 2012] suggest that commercial aircrew flying at high latitudes will trigger the EU action level limiting annual flights if they fly more than 500–600 h during solar minimum and more than 800–900 h during solar maximum, based on typical GCR background radiation exposure. Modeling also suggests that the public/prenatal recommended limit [*NCRP Report No.* 174, 2013] can be exceeded in 100 h of flight time, and for high latitude or polar flights, the effective dose rate can be up to 10 μSv h^{-1} [*Mertens et al*., 2012]. It is possible that a limit could be exceeded in a single flight during a severe solar particle event with a hard spectrum, i.e., a ground level event (GLE) [*Dyer et al*., 2007; *Copeland et al*., 2008]. We note that these modeled hours are not the method that triggers an EU action level, and there is a differentiation between limits (e.g., EU law) and recommendations (e.g., FAA and ICRP), where a recommendation can be exceeded even if no legal limit exists.

For the flying public, high-mileage business travelers may want to consider their exposure risks as similar to aircrew members. For infrequent commercial air travelers, the primary risk would come from extremely large solar particle events (SPEs) and GLEs while flying polar routes. *Dyer et al*. [2007] and *Copeland et al*.'s [2008] studies should raise awareness to avoid polar route flights during these events to minimize exposure risks.

Impacts associated with exceeding limits beyond health risks have also been considered. The UK Royal Academy of Engineering (RAEng) determined that significant economic consequences might occur from fleet disruptions due to aircrew grounding because exposures can exceed monthly or annual limits during a single severe solar event [*Cannon*, 2013]. For example, at conventional cruising altitudes around 37,000 ft (~11 km) across polar latitudes, a severe radiation storm could result in a worst-case dose to aircrew and passengers of >20 mSv.

This single event dose would be 20 times the recommended exposure limit to the general public (not aviation specific) and comparable to the entire annual occupational dose limit for aircrew. Again, we note that this is not applicable to U.S. crew as no actual limits have been promulgated, no regulatory limits exist, and no monitoring or tracking of exposure is performed. The RAEng study also concluded that pilot workload could increase during such periods to cope with any anomalous system behavior. This is because the complexity of modern aircraft computer interface/control and flyby wire avionics is such that prediction of an aircraft's response to increased radiation levels is necessarily subject to uncertainty, as seen in Qantas Flight 72.

Risk Mitigation Paths Exist

Because of added risk from severe radiation events, the radiation measurement and modeling communities have devoted considerable effort to understanding and characterizing this radiation field with mitigation strategies in mind. The community recognizes, as a starting point, that monitoring of the natural space environment for solar proton event occurrence is important. For example, with the start of an event, announcement levels are escalated. The NOAA Space Weather Prediction Center issues a *Watch* (long-lead-time geomagnetic activity prediction), a *Warning* (some condition is expected), or an *Alert* (event threshold is crossed). A Watch is provided only for geomagnetic storms and not SEP events. Additionally, the International Space Environment Service (http://www.spaceweather.org/) encompasses many Regional Warning Centers, and these organizations also provide similar services of Watches, Warnings, and Alerts for their local users. It is important that the nature and severity of a SPE be quickly assessed to avoid false alarms occurring if automatic alerts are issued.

A second recognition is that there is a need for dosimeters on board aircraft. Because the radiation exposure of airline crew and passengers in the U.S. is unregulated, the responsibility for mitigation of exposure called for by the NCRP principle *As Low As Reasonably Achievable* (ALARA) is left up to the air carrier and/or the pilot. Yet either one usually has very limited information on which to base a decision and dispatcher/pilot training on this subject matter is virtually nonexistent. The FAA very recently added ALARA guidance to its reference material on in-flight radiation [*AC 120-61B*, 2014] as the basis for exposure management. In the event of a communication blackout or from air carrier policy, we note that any decision may be left solely to the pilot. If an event affects a fleet of aircraft, the air traffic control (ATC) system is not prepared for responding rapidly to multiple route diversions during major solar radiation storms, even though they may be rare. The International Civil Aviation Organization (ICAO) is just beginning to investigate the issue. Thus, much more work toward mitigation of radiation effects of large SEP events upon the airline industry is needed at the decision-making level.

While probabilistic SPE forecasting exists, current prediction methods typically rely on empirical formulations to estimate the decay to background from the peak of an event. Once an event has started, and for its duration, the exposure mitigation strategy for commercial aviation is relatively straightforward to implement. Any implementation is subject to maintaining safe airspace separation minima, avoiding terrestrial weather hazards, and retaining sufficient trip fuel; however, it would include

1. fly at lower altitudes and/or latitudes for moderate or larger radiation events;
2. avoid polar region flights during severe solar radiation events until they subside;
3. issue a no takeoff alert if a large SPE is ongoing;
4. enable ATC, operators, and aircrews with the real-time exposure information necessary to descend the enroute system to a less exposed altitude en masse; and
5. enable ATC, operators, and aircrews with the real time information necessary to divert polar flights from polar flight paths when communications reliability is at risk.

ICAO and FAA communications requirements largely drive the avoidance of polar flight during increased solar activity. Due to reliance on high-frequency radio as the primary communication link between an aircraft and ATC during polar flight, and its susceptibility to disruption by a solar storm polar cap absorption (PCA), polar flight during significant solar radiation storms (NOAA *S* scale $\geq$ S3 for PCA) may be prohibited. However, the addition of INMARSAT satellite capability by some airlines may remove the side benefit that occurs when ensuring continued communications. That is to say, because INMARSAT enables polar communications, a conscious decision would be required to avoid polar flight during a solar radiation storm. The FAA Solar Radiation Alert system activates at a high-proton flux level (i.e., when the estimated effective dose rate induced by solar protons at 70,000 ft. (21,336 m) equals or exceeds 20 μSv h^{-1} for each of three consecutive 5 min periods); it is not regulatory in its guidance to pilots or dispatchers.

Mitigation of SEE in avionics, which is a probabilistic phenomenon, will mainly be achieved through improved engineering processes, and while key standards are now available, notably IEC-62396-1, it will take many years for such approaches to become universally adopted. There has been ongoing work for the International Electrotechnical Commission (IEC) SEE standard since 2000, but there are only recent signs that national bodies may mandate it. The existing certification is for quiet cosmic ray conditions only, and extreme space weather is not yet considered. Furthermore, there will still be a limit to the radiation level that can be managed with confidence, depending on the design specification applied. In order to mitigate the risk of injuries during unexpected aircraft behavior such as from a SEE (even though it is not yet possible to deterministically identify its higher probability), a simple but generally effective measure would be to ensure that passengers and aircrew have their seat belts fastened. While SEEs are probabilistic and may occur at any altitude, even during non-SPE conditions (as may have been the case for Qantas Flight 72), this mitigation path is helpful for other hazards such as clear air turbulence. Whatever the cause, a lesson from Qantas Flight 72 was that if seat belts had been fastened, far fewer injuries would have occurred. Thus, radiation measurements and alerts may have a beneficial role to play in alerting pilots to switch on the seat belt sign (including directing passengers and crew to take their seats and ensuring their seat belts are fastened), which could be a simple and low-cost mitigation action for any unexpected aircraft behavior risk. Built-in aircraft protections, monitors, and dispatcher/pilot training are all needed as are improved engineering processes.

Stakeholders

Exposure mitigation implementation at altitude can only be accomplished by activity from stakeholder groups, including but not limited to international collaborations that provide guidelines such as the International Standards Organization (ISO) space weather and aviation radiation standards [*ISO 15390*, 2004; *ISO 21348*, 2007; *ISO/AWI 17520*, 2015; *ISO 20785–1*, 2012; *ISO 20785–2*, 2011; *ISO/DIS 20785–3*, 2014], the International Commission on Radiation Units (ICRU) Joint Report (84), the International Electrotechnical Commission (IEC) SEE standard for avionics [*International Electrotechnical Commission* (*IEC*) *62396–1*, 2012], the Joint Electron Device Engineering Council Solid State Technology Association (JEDEC) SEE standard for avionics (JESD89A), the World Meteorological Organization observing requirements (#709, #738), and the International Civil Aviation Organization (ICAO) regulatory guidelines (Standards and Recommended Practices 3.8.1). As evidence of national mitigation collaborations, national air traffic management systems are upgrading to Next Generation Air Transportation System and Single European Sky ATM Research. Commercial and corporate aircraft owners and their dispatchers who use actionable information, often from third party weather providers, are the third stakeholder group with an interest in exposure mitigation. Finally, aircrew members who use actionable information and the radiation-educated public are the ultimate core stakeholder group.

Research Data Collection

A key condition for enabling all stakeholders to maximize their contributions in exposure mitigation is having quality dose measurements at altitude and emphasizing measurements at latitudes where the highest risks exist. Numerous measurements have been made and used for postflight analysis [*Dyer et al*., 1990; *Beck et al*., 1999b; *Kyllönen et al*., 2001; *EC Radiation Protection 140*, 2004; *Getley et al*., 2005; *Beck et al*., 2005; *Latocha et al*., 2007; *Meier et al*., 2009; *Beck et al*., 2009; *Dyer et al*., 2009; *Hands and Dyer*, 2009; *Getley et al*., 2010; *Gersey et al*., 2012; *Tobiska et al*., 2014], although the vast majority are for background conditions and not during major space weather events. Some of these have made neutron flux and dose equivalent measurements with solid-state detectors [*Dyer et al*., 2009; *Hands and Dyer*, 2009; *Tobiska et al*., 2014, 2015]. Together, these measurements have made important contributions to model validations of the radiation field at altitude, especially for human tissue issues. However, monitoring cannot be considered really effective until regular, validated, real-time, and global effective dose rate and neutron measurements (including the thermal component) are made. This capability does not yet exist, and because very few in-flight radiation measurements during significant solar particle events have occurred, it is critical that calibrated monitors are flown as widely and routinely as possible in order to maximize data capture that can both validate models and potentially be the basis of issuing alerts.

Future Measurements

Total ionizing dose measurements such as those by Automated Radiation Measurements for Aerospace Safety [*Tobiska et al*., 2014, 2015] are an example of a surrogate index measurement that could be used in

monitoring a real-time environment. Another example is the Space Weather *D* index, based on dose rates at aviation altitudes produced by solar protons during solar radiation storms, as the relevant parameter for the assessment of corresponding radiation exposure [*Meier and Matthiä*, 2014]. The Space Weather *D* index is a natural number given by a graduated table of ranges of dose rates in ascending order which is derived by an equation depending on the dose rate of solar protons.

Measurement/modeling comparisons are continuing, and recently, real-time assessment of radiation exposure due to solar energetic particle events has been presented at the 2014 European Space Weather Week (Liege, Nov. 2014) using the updated code AVIDOS 2.0 [*Latocha et al.*, 2014] (cf., European Space Agency's Space Weather Portal http://swe.ssa.esa.int). Two new instrument concepts are in development and include (i) the Dose Spectra from Energetic Particles and Neutrons instrument [*Schwadron et al.*, 2013] for measuring not only the energy but also the charge distribution of energetic particles, including neutrons, that affect human and robotic health; and (ii) the Thermalized Neutron Measurements instrument for measuring thermal neutrons related to SEE in avionics (L. Dominic and S. Wender, private communication).

International Scientific Modeling Using Measurements

There are many modeling systems into which these types of data could be integrated, e.g., LUIN [*O'Brien et al.*, 1996], CARI6PM [*Friedberg et al.*, 1999; *Friedberg and Copeland*, 2003, 2011], FLUKA [*Zuccon et al.*, 2001], QARM [*Lei et al.*, 2006], AIR [*Johnston*, 2008], PARMA [*Sato et al.*, 2008], AVIDOS [*Latocha et al.*, 2009, 2014], NAIRAS [*Mertens et al.*, 2013], PANDOCA [*Matthiä et al.*, 2014], and KREAM [*Hwang et al.*, 2014]. Recent work by *Joyce et al.* [2014] utilized Cosmic Ray Telescope for the Effects of Radiation measurements [*Spence et al.*, 2010; *Schwadron et al.*, 2012] in deep space to estimate dose rates through the Earth's atmosphere at a range of different altitudes down to aviation heights.

Further, different kinds of measurements are also needed including the SEE response of integrated circuits (ICs) used in avionics to high-energy neutrons; testing can be done in ground-based laboratories with simulated neutron beams. Per current guidelines [*IEC 62396–1*, 2012], the SEE response data would be combined with the output from in-flight neutron detectors to obtain SEE rates. ICs are constantly evolving with greater capability and ever smaller feature size, and since these are being chosen for use in upgraded avionics systems, it is necessary to continue testing the newer electronics for their susceptibility to SEE from high-energy neutrons. For example, electronic parts testing at the Los Alamos Neutron Science Center (LANSCE) is an ongoing activity by many IC and avionic manufacturers. This facility is capable of closely simulating the high-energy atmospheric neutron energy spectrum at a neutron flux such that an hour of exposure at LANSCE is equivalent to 300,000 h at 40,000 ft. (12,192m). Similar testing is also done in laboratories with thermal neutron sources. In addition, all ICs within a subsystem should be analyzed for their SEE rates using measured SEE cross sections. If the rates are combined for all ICs and protection factors built into the system (e.g., error correcting code), then an overall effective SEE rate can be obtained.

Path Forward

We conclude that in order to improve aviation safety in a radiation environment, our community must begin observing the weather of atmospheric radiation. Our current state-of-art technology only reports the data-driven climatology. The combination of low-cost, quality dosimetry measurements, integrated with modeling systems, does not yet exist. Using calibrated sensors at multiple, simultaneous altitudes from the surface to space, whose data can be used to validate algorithms and for assimilation into physics-based, global climatological models, is an important path toward producing a dose equivalent rate in tissue and a SEE error rate in avionics. With support for the above activities at an international level, air safety can and should be further improved in the arena of atmospheric radiation exposure risk mitigation for aircrew, the public, and avionics, particularly during severe radiation events. The need for these activities will only increase with time as air travel expands and as aircraft avionics technology advances toward greater miniaturization.

Acknowledgments
Our authors and co-authors support the data access policy of the AGU and regularly provide data for furthering scientific research related to the aviation radiation environment. References cited herein may contain data links that are of interest to the reader.

References

Advisory Circular 120-61B (2014), In-flight radiation exposure, U.S. Department of Transportation, Federal Aviation Administration, 21 Nov.
Beck, P., D. Bartlett, K. O'Brien, and U. J. Schrewe (1999a), In-flight validation and routine measurements, *Radiat. Prot. Dosim.*, *86*(4), 303–308.
Beck, P., P. Ambrosi, U. Schrewe, and K. O'Brien (1999b), ACREM, aircrew radiation exposure monitoring, Final report of European Commission contract F14P-CT960047, OEFZS, Rep. G-0008.

Beck, P., M. Latocha, S. Rollet, and G. Stehno (2005), TEPC reference measurements at aircraft altitudes during a solar storm, *Adv. Space Res.*, *36*(9), 1627–1633.
Beck, P., C. Dyer, N. Fuller, A. Hands, M. Latocha, S. Rollet, and F. Spurny (2009), Overview of on-board measurements during solar storm periods, *Radiat. Prot. Dosim.*, *136*(4), 297–303, doi:10.1093/rpd/ncp208.
Beck, P., J. F. Bottollier-Depois, R. Bütikofer, E. Flückiger, N. Fuller, M. Latocha, V. Mares, D. Matthiä, and W. Rühm (2014), Comparison of codes assessing radiation exposure of aircraft crew during energetic solar particle events, European Space Weather Week, Liege, 17–21 Nov.
Bottollier-Depois, J. F., et al. (2009), Comparison of codes assessing galactic cosmic radiation exposure of aircraft crew, *Radiat. Prot. Dosim.*, *136*(4), 317–323, doi:10.1093/rpd/ncp159.
Cannon, P. (2013), *Extreme Space Weather: Impacts on Engineered Systems and Infrastructure*, Royal Academy of Engineering, Carlton House Terrace, London.
Copeland, K., H. H. Sauer, F. E. Duke, and W. Friedberg (2008), Cosmic radiation exposure of aircraft occupants on simulated high-latitude flights during solar proton events from 1 January 1986 through 1 January 2008, *Adv. Space Res.*, *42*(6), 1008–1029.
Council Directive (2013), 2013/59/EURATOM, Official Journal of the European Union, 5 Dec.
Dyer, C., A. Hands, L. Fan, P. Truscott, K. A. Ryden, P. Morris, I. Getley, L. Bennett, B. Bennett, and B. Lewis (2009), Advances in measuring and modeling the atmospheric radiation environment, *IEEE Trans. Nucl. Sci.*, *6*(1), 3415–3422.
Dyer, C. S., A. J. Sims, J. Farren, and J. Stephen (1990), Measurements of solar flare enhancements to the single event upset environment in the upper atmosphere, *IEEE Trans. Nucl. Sci.*, *37*, 1929–1937, doi:10.1109/23.101211.
Dyer, C. S., F. Lei, A. Hands, and P. Truscott (2007), Solar particle events in the QinetiQ atmospheric radiation model, *IEEE Trans. Nucl. Sci.*, *54*(4), 1071–1075, doi:10.1109/TNS.2007.893537.
EURADOS Report (2012), EURADOS Report 2012–03, Braunschweig, May.
European Commission Radiation Protection 140 (2004), Cosmic radiation exposure of aircraft crew, Compilation of measured and calculated data, European communities, 2004.
Friedberg, W., and K. Copeland (2003), What aircrews should know about their occupational exposure to ionizing radiation, Oklahoma City, OK: Federal Aviation Administration, Civil Aerospace Medical Institute DOT Rep. No. DOT/FAA/ AM-03/16.
Friedberg, W., and K. Copeland (2011), Ionizing radiation in Earth's atmosphere and in space near earth, Oklahoma City, OK: Federal Aviation Administration, Civil Aerospace Medical Institute DOT Rep. No. DOT/FAA/AM-11/9.
Friedberg, W., K. Copeland, F. E. Duke, K. O'Brien, and E. B. Darden (1999), Guidelines and technical information provided by the U.S. Federal Aviation Administration to promote radiation safety for air carrier crew members, *Radiat. Prot. Dosim.*, *86*, 323–327.
Gersey, B., R. Wilkins, W. Atwell, W. K. Tobiska, and C. Mertens (2012), Tissue equivalent proportional counter microdosimetry measurements aboard high-altitude and commercial aircraft, AIAA 2012–3636, AIAA 42nd International Conference on Environmental Systems, San Diego, Calif., 15–19 July.
Getley, I. L., M. L. Duldig, D. F. Smart, and M. A. Shea (2005), Radiation dose along North American transcontinental flight paths during quiescent and disturbed geomagnetic conditions, *Space Weather*, *3*, S01004, doi:10.1029/2004SW000110.
Getley, I. L., L. G. I. Bennett, B. J. Lewis, B. Bennett, C. S. Dyer, A. D. P. Hands, and M. L. Duldig (2010), Evaluation of new cosmic radiation monitors designed for aircrew exposure assessment, *Space Weather*, *8*, S01001, doi:10.1029/2009SW000492.
Hands, A., and C. S. Dyer (2009), A technique for measuring dose equivalent and neutron fluxes in radiation environments using silicon diodes, *IEEE Trans. Nucl. Sci.*, *56*(1), 3442–3449.
Hwang, J., K. Dokgo, E. Choi, K.-C. Kin, H.-P. Kim, and K.-S. Cho (2014), Korean Radiation Exposure Assessment Model for aviation route dose: KREAM, KSS Fall meeting, Jeju, Korea, 29–31 Oct.
International Commission on Radiation Units (2010), Reference data for the validation of doses from cosmic-radiation exposure of aircraft crew, ICRU Report 84 (prepared jointly with ICRP). Journal of the ICRU 10 (2), 2010.
International Commission on Radiological Protection (1991), 1990 Recommendations of the International Commission on Radiological Protection, ICRP Publication 60. Ann. ICRP 21 (1–3).
International Commission on Radiological Protection (2005), Low-dose extrapolation of radiation-related cancer risk, ICRP Publication 99. Ann. ICRP 35 (4).
International Commission on Radiological Protection (2007), The 2007 Recommendations of the International Commission on Radiological Protection, ICRP Publication 103. Ann. ICRP 37 (2–4).
International Electrotechnical Commission (IEC) 62396–1 (2012), Process management for avionics – Atmospheric radiation effects – Part 1: Accommodation of atmospheric radiation effects via single event effects within avionics electronic equipment, Edition 1.0 2012–05.
International Standards Organization (ISO) 15390 (2004), Space environment (natural and artificial) – Galactic cosmic ray model.
International Standards Organization (ISO) 20785–1 (2012), Dosimetry for exposures to cosmic radiation in civilian aircraft—Part 1: Conceptual basis for measurements.
International Standards Organization (ISO) 20785–2 (2011), Dosimetry for exposures to cosmic radiation in civilian aircraft—Part 2: Characterization of instrument response.
International Standards Organization (ISO) 21348 (2007), Space environment (natural and artificial): Process for determining solar irradiances.
ISO/AWI 17520 (2015), Space systems – Space environment -- Cosmic ray and solar energetic particle penetration inside the magnetosphere: Method of the effective vertical cut-off determination, stage 30.20.
ISO/DIS 20785–3 (2014), Dosimetry for exposures to cosmic radiation in civilian aircraft -- Part 3: Measurements at aviation altitudes, stage 40.60.
Johnston, C. O. (2008), A comparison of EAST shock-tube radiation measurements with a new radiation model, AIAA Paper 2008–1245.
Joyce, C. J., et al. (2014), Radiation modeling in the Earth and Mars atmospheres using LRO/CRaTER with the EMMREM Module, *Space Weather*, *12*, 112–119, doi:10.1002/2013SW000997.
Kyllönen, J. E., L. Lindborg, and G. Samuelson (2001), Cosmic radiation measurements on board aircraft with the variance method, *Radiat. Prot. Dosim.*, *93*, 197–205.
Latocha, M., M. Autischer, P. Beck, J. F. Bottolier–Depois, S. Rollet, and F. Trompier (2007), The results of cosmic radiation in-flight TEPC measurements during the CAATER flight campaign and comparison with simulation, *Radiat Prot. Dosim.*, *125*(1–4), 412–415, doi:10.1093/rpd/ncl123.
Latocha, M., P. Beck, and S. Rollet (2009), AVIDOS—A software package for European accredited aviation dosimetry, *Rad. Prot. Dosim.*, *136*(4), 286–290, doi:10.1093/rpd/ncp126.
Latocha, M., P. Beck, P. Bütikofer, and H. Thommesen (2014), AVIDOS 2.0 – Current developments for the assessment of radiation exposure at aircraft altitudes caused by solar cosmic radiation exposure, European Space Weather Week, Liege, 17–21 Nov. [Available at http://stce.be/esww11.]

Lei, F., A. Hands, C. Dyer, and P. Truscott (2006), Improvements to and validations of the QinetiQ Atmospheric Radiation Model (QARM), *IEEE Trans. Nucl. Sci.*, *53*(4), 1851–1858.
Lillhök, J. (2007), Comparison of dose equivalent meters for cosmic radiation exposure and calculations at constant flight conditions, *Radiat. Meas.*, *42*, 323–333.
Matthiä, D., M. M. Meier, and G. Reitz (2014), Numerical calculation of the radiation exposure from galactic cosmic rays at aviation altitudes with the PANDOCA core model, *Space Weather*, *12*, 161–171, doi:10.1002/2013SW001022.
Meier, M. M., and D. Matthiä (2014), A space weather index for the radiation field at aviation altitudes, *J. Space Weather Space Clim.*, *4*, A13, doi:10.1051/swsc/2014010.
Meier, M. M., M. Hubiak, D. Matthiä, M. Wirtz, and G. Reitz (2009), Dosimetry at aviation altitudes (2006–2008), *Radiat. Prot. Dosim.*, *136*(4), 251–255.
Mertens, C. J., B. T. Kress, M. Wiltberger, W. K. Tobiska, B. Grajewski, and X. Xu (2012), Atmospheric ionizing radiation from galactic and solar cosmic rays, Current topics in ionizing radiation research, edited by M. Nenoi, InTech.
Mertens, C. J., M. M. Meier, S. Brown, R. B. Norman, and X. Xu (2013), NAIRAS aircraft radiation model development, dose climatology, and initial validation, *Space Weather*, *11*, 603–635, doi:10.1002/swe.20100.
National Council on Radiation Protection and Measurements (NCRP) Report No. 116 (1993), Limitation of exposure to ionizing radiation, National Council on Radiation Protection and Measurements.
National Council on Radiation Protection and Measurements (NCRP) Report No. 174 (2013), Preconception and prenatal radiation exposure: Health effects and protective guidance.
Normand, E., D. L. Oberg, J. L. Wert, J. D. Ness, P. P. Majewski, S. Wender, and A. Gavron (1994), Single event upset and charge collection measurements using high energy protons and neutrons, *IEEE Trans. Nucl. Sci.*, *41*(6), 2203–2209.
Normand, E., K. Vranish, A. Sheets, M. Stitt, and R. Kim (2006), Quantifying the double-sided neutron SEU threat, from low energy (thermal) and high energy (>10 MeV) neutrons, *IEEE Trans. Nucl. Sci.*, *53*(6), 3587–3595.
O'Brien, K., W. Friedberg, H. H. Sauer, and D. F. Smart (1996), Atmospheric cosmic rays and solar energetic particles at aircraft altitudes, *Environ. Int.*, *22*(Suppl. 1), S9–S44.
O'Sullivan, D., D. T. Bartlett, P. Beck, J.-F. Bottollier-Depois, L. Lindborg, F. Wissmann, L. Tommasino, M. Pelliccioni, and M. Silari (1999), Investigations of radiation fields at aircraft altitudes, Final Report of European Commission contract no. F14P-CT950011, Dublin Institute for Advanced Studies, Dublin.
O'Sullivan, D., et al. (2004), Dosimetry of aircrew exposure to radiation during solar maximum, Final report of European Commission contract FIGM-CT-2000-00068 (DOSMAX). [Available at http://cordis.europa.eu/project/rcn/52376_en.html.]
Reitz, G., K. Schnuer, and K. Shaw (1993), Editorial - workshop on radiation exposure of civil aircrew, *Radiat. Prot. Dosim.*, *48*, 3.
Sato, T., H. Yasuda, K. Niita, A. Endo, and L. Sihver (2008), Development of PARMAPHITS-based analytical radiation model in the atmosphere, *Radiat. Res.*, *170*, 244–259.
Schwadron, N. A., et al. (2012), Lunar radiation environment and space weathering from the Cosmic Ray Telescope for the Effects of Radiation (CRaTER), *J. Geophys. Res.*, *117*, E00H13, doi:10.1029/2011JE003978.
Schwadron, N., C. Bancroft, P. Bloser, J. Legere, J. Ryan, S. Smith, H. Spence, J. Mazur, and C. Zeitlin (2013), Dose spectra from energetic particles and neutrons, *Space Weather*, *11*, 547–556, doi:10.1002/swe.20095.
Spence, H. E., et al. (2010), CRaTER: The cosmic ray telescope for the effects of radiation experiment on the lunar reconnaissance orbiter mission, *Space Sci. Rev.*, *150*(1-4), 243–284.
Tobiska, W. K., et al. (2014), *Operational Specification and Forecasting Advances for Dst, LEO Thermospheric Densities, and Aviation Radiation Dose and Dose Rate*, Space Weather Workshop, Boulder, Colo., April.
Tobiska, W. K., et al. (2015), Operational advances for atmospheric radiation dose rate specification, 12th Conference on Space Weather, Applications for end users, Am. Meteorol. Soc., January.
Wilson, J. W., P. Goldhagen, V. Rafnsson, J. M. Clem, and G. De Angelis (2002), *Overview of Atmospheric Ionizing Radiation (AIR)* Research: SST-Present, COSPAR, Houston, Tex.
Zuccon, P., et al. (2001), A Monte Carlo simulation of the interactions of cosmic rays with the atmosphere, CERN, 14 Sept.

W. Kent Tobiska *is the President and Chief Scientist of Space Environment Technologies in Pacific Palisades, California, USA. Email:* ktobiska@spacenvironment.net.

William Atwell *is a Senior Research Scientist at Space Environment Technologies in Houston, Texas, USA.*

Peter Beck *is the Head of Radiation Hardness Assurance and Space Weather Radiation Protection Dosimetry at Seibersdorf Laboratories in Seibersdorf, Austria.*

Eric Benton *is a Professor at Oklahoma State University in the Department of Physics in Stillwater, Oklahoma, USA.*

Kyle Copeland *is a Health Physicist at the Federal Aviation Administration Civil Aerospace Medical Institute in Oklahoma City, Oklahoma, USA.*

Clive Dyer *is a Professor at the Surrey Space Centre of the University of Surrey in Guildford, UK.*

Brad Gersey *is a Research Scientist and Group Leader for Radiation Dosimetry at Prairie View A&M University in the Department of Electrical and Computer Engineering in Prairie View, Texas, USA.*

Ian Getley *is an A380 Captain, an Aviation Radiation Consultant, and an Aviation Accident Consultant at the Department of Aviation of the University of New South Wales in Sydney, Australia.*

Alex Hands *is a Senior Research Fellow at the Surrey Space Centre of the University of Surrey in Guildford, UK.*

Michael Holland *is a DC-10 Captain leading the Aeromedical Committee of the Allied Pilots Association, USA.*

Sunhak Hong *is a Research Scientist and Space Weather Forecaster at Korean Space Weather Center of National Radio Research Agency in Jeju, South Korea.*

Junga Hwang *is a Senior Researcher at the Korea Astronomy and Space Science Institute and in the Department of Astronomy and Space Science of the Korea University of Science and Technology in Daejeon, South Korea.*

Bryn Jones *is the CEO of SolarMetrics in Guildford, UK.*

Kathleen Malone *is a B-747 Captain leading the Aeromedical Committee of the Allied Pilots Association, USA.*

Matthias M. Meier *is a Physicist and Radiation Protection Consultant at the Deutsches Zentrum für Luft- und Raumfahrt e.V. (DLR) in Cologne, Germany.*

Chris Mertens *is a Senior Research Scientist at the NASA Langley Research Center in Hampton, Virginia, USA.*

Tony Phillips *is the author and creator of Spaceweather.com in Aspendell, California, USA.*

Keith Ryden *is a Reader in Space Engineering (Space Environment and Effects) at the Surrey Space Centre, University of Surrey in Guildford, UK.*

Nathan Schwadron *is an Associate Professor at the University of New Hampshire in the Department of Physics, Durham, New Hampshire, USA.*

Stephen A. Wender *is a Research Scientist at Los Alamos National Laboratory in Los Alamos, New Mexico, USA.*

Richard Wilkins *is a Professor at Prairie View A&M University in the Department of Electrical and Computer Engineering in Prairie View, Texas, USA.*

Michael A. Xapsos *is a Research Physicist in the Radiation Effects and Analysis Group at the NASA Goddard Space Flight Center in Greenbelt, Maryland, USA.*

Space Weather Journal

Supporting Information for

Advances in atmospheric radiation measurements and modeling needed to improve air safety

W. Kent Tobiska[1], William Atwell[1], Peter Beck[2], Eric Benton[3], Kyle Copeland[4], Clive Dyer[5], Brad Gersey[6], Ian Getley[7], Alex Hands[5], Michael Holland[8], Sunhak Hong[9], Junga Hwang[10], Bryn Jones[11], Kathleen Malone[8], Matthias M. Meier[12], Chris Mertens[13], Tony Phillips[14], Keith Ryden[5], Nathan Schwadron[15], Stephen A. Wender[16], Richard Wilkins[6], and Michael A. Xapsos[17]

[1]Space Environment Technologies, Pacific Palisades, CA, [2]Seibersdorf Laboratories, Seibersdorf, Austria, [3]Oklahoma State University, Stillwater, OK, [4]FAA Civil Aerospace Medical Institute, Oklahoma City, OK, [5]Surrey Space Centre, University of Surrey, Guildford, United Kingdom, [6]Prairie View A&M University, Prairie View, TX, [7]Department of Aviation, University of New South Wales, Australia, [8]Allied Pilots Association, Aeromedical Committee, United States, [9]Korean Space Weather Center of National Radio Research Agency, Jeju, Korea, [10]Korea Astronomy and Space Science Institute, Daejeon, Korea, and Department of Astronomy and Space Science, Korea University of Science and Technology, Daejeon, Korea, [11]SolarMetrics, Guildford, United Kingdom, [12]Deutsches Zentrum für Luft- und Raumfahrt e.V. (DLR), Cologne, Germany, [13]NASA Langley Research Center, Hampton, VA, [14]Spaceweather.com, United States, [15]University of New Hampshire, Durham NH, [16]Los Alamos National Laboratory, Los Alamos, NM, [17]NASA Goddard Space Flight Center, Greenbelt, MD

Contents of this file

Three paragraphs (Text S1 - S3) as the content for three separate sidebars.

Additional Supporting Information (Files uploaded separately)

Introduction

This is sidebar 1 for **tissue-relevant radiation**:

Text S1.

An example of a severe tissue-relevant radiation environment occurred during the major SEP event on 23 February 1956 (only ground level measurements were available). For that event, Dyer *et al.* [2007] calculated a significant increase over background at high latitudes and at 12 km altitude with correspondingly higher dose rates for aircraft flight paths of several mSv hr^{-1}. The derived SI unit of ionizing radiation dose is the sievert (Sv). It incorporates the stochastic health risk of low levels of ionizing radiation on the human body, where radiation dose assessment is defined as the probability of cancer and genetic damage. On 23 February 1956 this radiation increase could have caused some aircrew members to exceed their currently recommended annual occupational flight limits in just one flight [Wilson, *et al.,* 2002; Dyer *et al.*, 2007]. It also could have caused upsets every 3 seconds in a Gbyte of a typical memory device [Dyer *et al.*, 2003]. An extreme event such as the 1859 Carrington Event could be considerably worse than this event. Here we use the terms “extreme” or “severe” to indicate a NOAA S5 radiation storm, possibly comparable to the 1859 Carrington Event. We also note that the NOAA scales themselves are a poor indicator for the aviation radiation environment; the GOES fluxes are a good indicator of when a Solar Proton Event (SPE) is occurring but only

small subsets of these have significant fluxes of protons with sufficient energy to affect the atmosphere, even at polar latitudes.

Introduction

This is sidebar 2 for **avionics-relevant radiation**:

Text S2.

A possible example of a severe neutron-induced avionics effect occurred on 07 October 2008 in Qantas Flight 72 Airbus A330-303 from Singapore to Perth, Western Australia. While the aircraft was in cruise at 37,000 ft. one of the aircraft's three air data inertial reference units (ADIRUs) started outputting intermittent, incorrect values (spikes) on flight parameters to other aircraft systems. Two minutes later, in response to spikes in angle of attack (AOA) data, the aircraft's flight control primary computers (FCPCs) commanded the aircraft to pitch down. At least 110 of the 303 passengers and 9 of 12 aircrew members were injured; 12 were serious injuries and another 39 required hospital medical treatment. The potential triggering event that was not ruled out was a single event effect (SEE) resulting from a high-energy atmospheric neutron interacting with one of the integrated circuits (ICs) within the CPU module. While there was insufficient evidence to determine that a SEE was the conclusive cause, the investigation identified SEE as an ongoing, probabilistically relevant risk for airborne equipment. All other known causes were eliminated. The aircraft manufacturer subsequently redesigned the AOA algorithm to prevent the same type of accident from occurring again [ATSB Transport Safety Report, 2011]. We note that the GOES >10 MeV proton fluence was nominal on this date, i.e., there were no solar flare events.

Introduction

This is sidebar 3 for **action needed at all levels**:

Text S3.

There is great value in stakeholders' efforts to mitigate potential exposure risks to humans and avionics from events that affect the aviation radiation environment. Further efforts by stakeholders leading to near-term action can:

- expand international scientific research in the aviation radiation environment;
- develop reliable, new measurement systems that can provide calibrated real-time dose equivalence data for a highly mixed and changeable radiation field;
- obtain in-flight measurements during solar particle events in order to calibrate instruments and validate models;
- test semiconductor devices at a wide energy neutron source as part of certifying their use in avionics;
- continue and expand ground level neutron monitor measurements to record GLEs as a subset of SPEs;
- create new modeling systems that can assimilate real-time radiation data;
- discover and validate new forecasting capabilities;
- combine data and modeling for improved monitoring in an operational context;
- provide current condition information to decision makers (pilots and dispatchers);
- train decision makers on the information available;

- educate airline personnel, managers, dispatchers, and pilots on the exposures, measurements, risks, as well as mitigation techniques available;
- provide feedback to the scientific community on the adequacy of the information provided to the decision maker; and
- provide the public with scientific-based, but easily understood, information on the aviation radiation environment.

References

ATSB Transport Safety Report (2011), Aviation occurrence investigation, AO-2008-070 Final, In-flight upset 154 km west of Learmonth, WA 7 October 2008 VH-QPA Airbus A330-303, Australian Transport Safety Bureau, Commonwealth of Australia, 19 Dec. 2011.

Dyer, C. S., F. Lei, S. N. Clucas, D. F. Smart, and M. A. Shea (2003), Solar particle enhancements of single event effect rates at aircraft altitudes, *IEEE Trans. Nucl. Sci., 50*(6), 2038–2045, doi:10.1109/TNS.2003.821375.

Dyer, C. S., F. Lei, A. Hands, and P. Truscott (2007), Solar particle events in the QinetiQ atmospheric radiation model, *IEEE Trans. Nucl. Sci., 54*(4), 1071–1075, doi:10.1109/TNS.2007.893537.

Wilson, J. W., P. Goldhagen, V. Rafnsson, J. M. Clem, and G. De Angelis (2002), Overview of Atmospheric Ionizing Radiation (AIR) Research: SST-Present, COSPAR, Houston, Tex.

ROYAL ACADEMY OF ENGINEERING

Extreme space weather: impacts on engineered systems and infrastructure

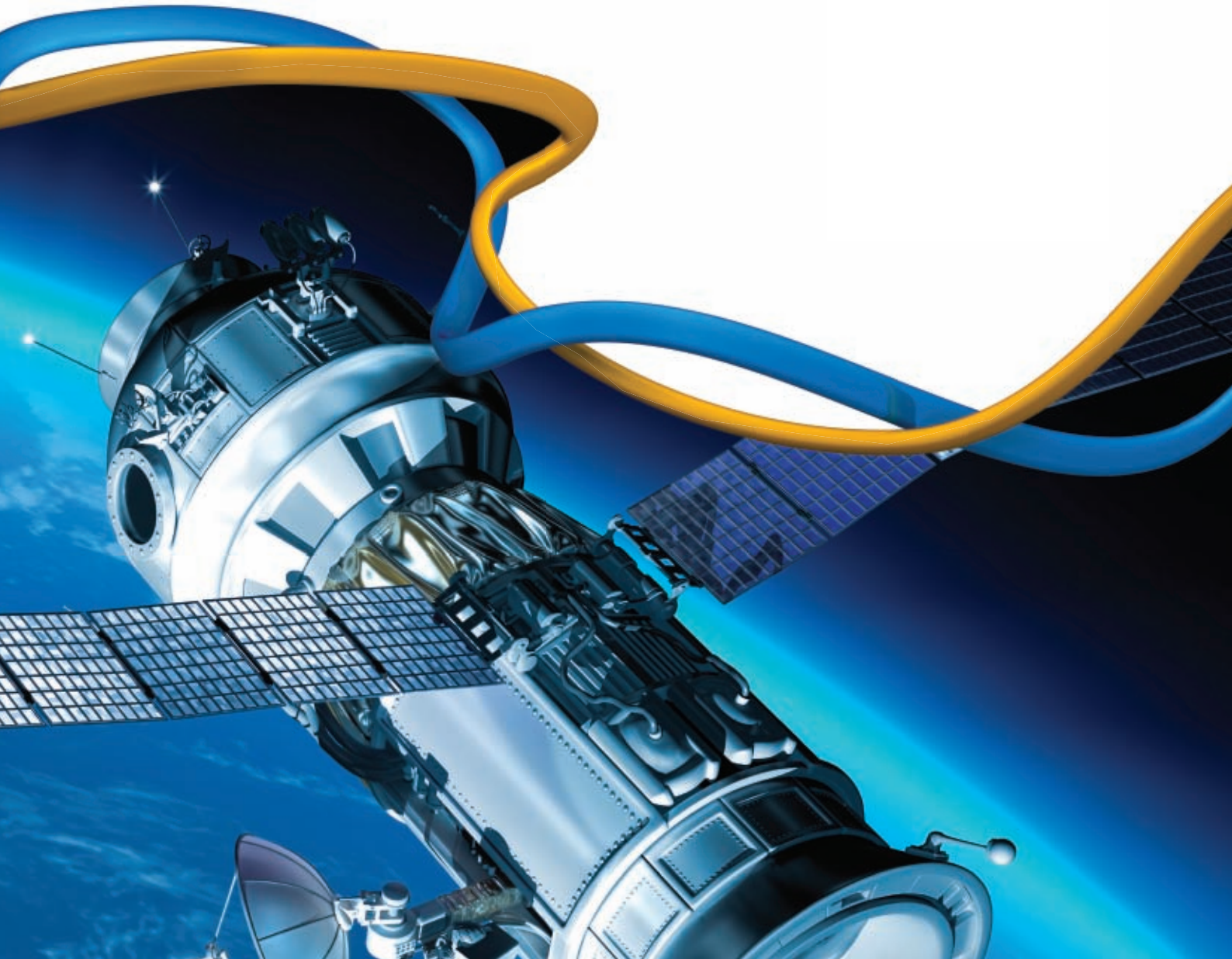

ISBN 1-903496-95-0

February 2013
Published by
Royal Academy of Engineering
Prince Philip House
3 Carlton House Terrace
London SW1Y 5DG

Tel: 020 7766 0600 Fax: 020 7930 1549
www.raeng.org.uk

Registered Charity Number: 293074

Cover: Satellite in orbit © Konstantin Inozemtsev/iStockphoto

This report is available online at **www.raeng.org.uk/spaceweather**

Contents

Foreword

An extreme space weather event, or solar superstorm, is one of a number of potentially high impact, but low probability natural hazards. In response to a growing awareness in government, extreme space weather now features as an element of the UK National Risk Assessment.

In identifying this hazard, the UK government benefitted from the country's world class scientific expertise and from a number of earlier studies conducted in the US. However, the consequential impact on the UK's engineering infrastructure - which includes the electricity grid, satellite technology and air passenger safety – has not previously been critically assessed. This report addresses that omission by bringing together a number of scientific and engineering domain experts to identify and analyse those impacts. I believe that this study, with its strong engineering focus, is the most extensive of its type to date.

It is my hope that by acting on the recommendations in this report, stakeholders will progressively mitigate the impact of the inevitable solar superstorm.

Professor Paul Cannon FREng
Chair of the study working group

1. Executive summary

Rarely occurring solar superstorms generate X-rays and solar radio bursts, accelerate solar particles to relativistic velocities and cause major perturbations to the solar wind. These environmental changes can cause detrimental effects to the electricity grid, satellites, avionics, air passengers, signals from satellite navigation systems, mobile telephones and more. They have consequently been identified as a risk to the world economy and society. The purpose of this report is to assess their impact on a variety of engineered systems and to identify ways to prepare for these low-probability but randomly occurring events. The report has an emphasis on the UK, but many of the conclusions also apply to other countries.

Explosive eruptions of energy from the Sun that cause minor solar storms on Earth are relatively common events. In contrast, extremely large events (superstorms) occur very occasionally – perhaps once every century or two. Most superstorms miss the Earth, travelling harmlessly into space. Of those that do travel towards the Earth, only half interact with the Earth's environment and cause damage.

Since the start of the space age, there has been no true solar superstorm and consequently our understanding is limited. There have, however, been a number of near misses and these have caused major technological damage, for example the 1989 collapse of part of the Canadian electricity grid. A superstorm which occurred in 1859, now referred to as the 'Carrington event' is the largest for which we have measurements; and even in this case the measurements are limited to perturbations of the geomagnetic field. An event in 1956 is the highest recorded for atmospheric radiation with August 1972, October 1989 and October 2003 the highest recorded radiation events measured on spacecraft.

How often superstorms occur and whether the above are representative of the long term risk is not known and is the subject of important current research. The general consensus is that a solar superstorm is inevitable, a matter not of 'if' but 'when?'. One contemporary view is that a Carrington-level event will occur within a period of 250 years with a confidence of ~95% and within a period of 50 years with a confidence of ~50%, but these figures should be interpreted with considerable care.

Mitigation of solar superstorms necessitates a number of technology-specific approaches which boil down to engineering out as much risk as is reasonably possible, and then adopting operational strategies to deal with the residual risk. In order to achieve the latter, space and terrestrial sensors are required to monitor the storm progress from its early stages as enhanced activity on the Sun through to its impact on Earth. Forecasting a solar storm is a challenge, and contemporary techniques are unlikely to deliver actionable advice, but there are growing efforts to improve those techniques and test them against appropriate metrics. Irrespective of forecasting ability, space and terrestrial sensors of the Sun and the near space environment provide critical space situational awareness, an ability to undertake post-event analysis, and the infrastructure to improve our understanding of this environment.

The report explores a number of technologies and we find that the UK is indeed vulnerable to a solar superstorm, but we also find that a number of industries have already mitigated the impact of such events. In a 'perfect storm' a number of technologies will be simultaneously affected which will substantially exacerbate the risk. Mitigating and maintaining an awareness of the individual and linked risks over the long term is a challenge for government, for asset owners and for managers.

Space weather: impacts on engineered systems – a summary is a shortened version of this report suitable for policy makers and the media – see **www.raeng.org.uk/spaceweathersummary**.

Key points:

Solar superstorm environment

The recurrence statistics of an event with similar magnitude and impact to a Carrington event are poor, but improving. Various studies indicate that a recurrence period of 1-in-100 to 200 years is reasonable and this report makes assessments of the engineering impact based on an event of this magnitude and return time. If further studies provide demonstrable proof that larger events do occur – perhaps on longer timescales - then a radical reassessment of the engineering impact will be needed. The headline figure of 100 years should not be a reason to ignore such risks.

Electricity grid

The reasonable worst case scenario would have a significant impact on the national electricity grid. Modelling indicates around six super grid transformers in England and Wales and a further seven grid transformers in Scotland could be damaged through geomagnetic disturbances and taken out of service. The time to repair would be between weeks and months. In addition, current estimates indicate a potential for some local electricity interruptions of a few hours. Because most nodes have more than one transformer available, not all these failures would lead to a disconnection event. However, National Grid's analysis is that around two nodes in Great Britain could experience disconnection.

Satellites

Some satellites may be exposed to environments in excess of typical specification levels, so increasing microelectronic upset rates and creating electrostatic charging hazards. Because of the multiplicity of satellite designs in use today there is considerable uncertainty in the overall behaviour of the fleet but experience from more modest storms indicates that a degree of disruption to satellite services must be anticipated. Fortunately the conservative nature of spacecraft designs and their diversity is expected to limit the scale of the problem. Our best engineering judgement, based

on the 2003 storm, is that up to 10% of satellites could experience temporary outages lasting hours to days as a result of the extreme event, but it is unlikely that these outages will be spread evenly across the fleet since some satellite designs and constellations would inevitably prove more vulnerable than others. In addition, the significant cumulative radiation doses would be expected to cause rapid ageing of many satellites. Very old satellites might be expected to start to fail in the immediate aftermath of the storm while new satellites would be expected to survive the event but with higher risk thereafter from incidence of further (more common) storm events. Consequently, after an extreme storm, all satellite owners and operators will need to carefully evaluate the need for replacement satellites to be launched earlier than planned in order to mitigate the risk of premature failures.

Aircraft passenger and crew safety

Passengers and crew airborne at the time of an extreme event would be exposed to an additional dose of radiation estimated to be up to 20 mSv, which is significantly in excess of the 1 mSv annual limit for members of the public from a planned exposure and about three times as high as the dose received from a CT scan of the chest. Such levels imply an increased cancer risk of 1 in 1,000 for each person exposed, although this must be considered in the context of the lifetime risk of cancer, which is about 30%. No practical method of forecast is likely in the short term since the high energy particles of greatest concern arrive at close to the speed of light. Mitigation and post event analysis is needed through better onboard aircraft monitoring. An event of this type would generate considerable public concern.

Ground and avionic device technology

Solar energetic particles indirectly generate charge in semiconductor materials, causing electronic equipment to malfunction. Very little documentary evidence could be obtained regarding the impact of solar energetic particles on ground infrastructure and it is consequently difficult to extrapolate to a solar superstorm. More documentary evidence of normal and storm time impacts is available in respect to avionics - no doubt because the operating environment has a higher flux of high-energy particles. Our estimate is that during a solar superstorm the avionic risk will be ~1,200 times higher than the quiescent background risk level and this could increase pilot workload. We note that avionics are designed to mitigate functional failure of components, equipment and systems and consequently they are also partially robust to solar energetic particles.

Global navigation satellite systems (GNSS)

Assuming that the satellites – or enough of them – survived the impact of high energy particles, we anticipate that a solar superstorm might render GNSS partially or completely inoperable for between one and three days. The outage period will be dependent on the service requirements. For critical timing infrastructure it is important that holdover oscillators be deployed capable of maintaining the requisite performance for these periods. UK networked communications appear to meet this requirement. There will be certain specialist applications where the loss or reduction in GNSS services would be likely to cause operational problems; these include aircraft and shipping. Today, the aircraft navigation system is mostly backed up by terrestrial navigation aids; it is important that alternative navigation options remain available in the future.

Cellular and emergency communications

This study has concluded that the UK's commercial cellular communications networks are much more resilient to the effects of a solar superstorm than those deployed in a number of other countries (including the US) since they are not reliant on GNSS timing. In contrast, the UK implementation of the Terrestrial European Trunked Radio Access (TETRA) emergency communications network is dependent on GNSS. Consequently, mitigation strategies, which already appear to be in place, are necessary.

High frequency (HF) communications

HF communications is likely to be rendered inoperable for several days during a solar superstorm. HF communications is used much less than it used to be; however, it does provide the primary long distance communications bearer for long distance aircraft (not all aircraft have satellite communications and this technology may also fail during an extreme event). For those aircraft in the air at the start of the event, there are already well-defined procedures to follow in the event of a loss of communications. However, in the event of a persistent loss of communications over a wide area, it may be necessary to prevent flights from taking off. In this extreme case, there does not appear to be a defined mechanism for closing or reopening airspace once communications have recovered.

Mobile satellite communications

During an extreme space weather event, L-band (~1.5GHz) satellite communications might be unavailable, or provide a poor quality of service, for between one and three days owing to scintillation. The overall vulnerability of L-band satellite communications to superstorm scintillation will be specific to the satellite system. For aviation users the operational impact on satellite communications will be similar to HF.

Terrestrial broadcasting

Terrestrial broadcasting would be vulnerable to secondary effects, such as loss of power and GNSS timing.

OUR ESTIMATE IS THAT DURING A SOLAR SUPERSTORM THE AVIONIC RISK WILL BE ~1,200 TIMES HIGHER THAN THE QUIESCENT BACKGROUND RISK LEVEL AND THIS COULD INCREASE PILOT WORKLOAD.

Recommendations

A number of detailed recommendations are included in each chapter. Some of the most important are set out below. It is vital that a lead government department or body is identified for each of these recommendations.

Policy

The report makes two key policy recommendations. These are that:

1. A UK Space Weather Board should be initiated within government to provide overall leadership of UK space weather activities. This board must have the capacity to maintain an overview of space weather strategy across all departments.
2. The Engineering and Physical Sciences Research Council (EPSRC) should ensure that its own programmes recognise the importance of extreme space weather mitigation and EPSRC should be fully integrated into any research council strategy.

Solar superstorm environment

3. The UK should work with its international partners to further refine the environmental specification of extreme solar events and where possible should extend such studies to provide progressively better estimates of a reasonable worst case superstorm in time scales of longer than ~200 years.

Electricity grid

4. The current National Grid mitigation strategy should be continued. This strategy combines appropriate forecasting, engineering and operational procedures. It should include increasing the reserves of both active and reactive power to reduce loading on individual transformers and to compensate for the increased reactive power consumption of transformers.

Satellites

5. Extreme storm risks to space systems critical to social and economic cohesion of the country (which is likely to include navigation satellite systems) should be assessed in greater depth. Users of satellite services which need to operate through a superstorm should challenge their service providers to determine the level of survivability and to plan mitigation actions in case of satellite outages (eg network diversification).

Aircraft passenger and crew safety

6. Consideration should be given to classifying solar superstorms as radiation emergencies in the context of air passengers and crew. If such a classification is considered appropriate an emergency plan should be put in place to cover such events. While the opportunities for dose reduction may be limited, appropriate reference levels should be considered and set, if appropriate.

Ground and avionic device technology

7. Ground-and space-derived radiation alerts should be provided to aviation authorities and operators. The responsible aviation authorities and the aviation industry should work together to determine if onboard monitoring could be considered a benefit in flight. Related concepts of operation should be developed to define subsequent actions; this could even include reductions in altitude if deemed beneficial and cost-effective.

Global navigation satellite systems (GNSS)

8. All critical infrastructure and safety critical systems that require accurate GNSS derived time and or timing should be specified to operate with holdover technology for up to three days.

Terrestrial mobile communication networks

9. All terrestrial mobile communication networks with critical resiliency requirements should also be able to operate without GNSS timing for periods up to three days. This should particularly include upgrades to the network including those associated with the new 4G licenses where these are used for critical purposes and upgrades to the emergency services communications networks.

High frequency (HF) communications

10. The aviation industry and authorities should consider upgrades to HF modems (similar to those used by the military) to enable communications to be maintained in more severely disturbed environments. Such an approach could significantly reduce the period of signal loss during a superstorm and would be more generally beneficial.

Terrestrial broadcasting

11. Where terrestrial broadcasting systems are required for civil contingency operations, they should be assessed for vulnerabilities to the loss of GNSS timing.

The Sun unleashed an M-2 (medium-sized) solar flare, an S1-class radiation storm and a spectacular coronal mass ejection (CME) on 7 June 2011 © NASA

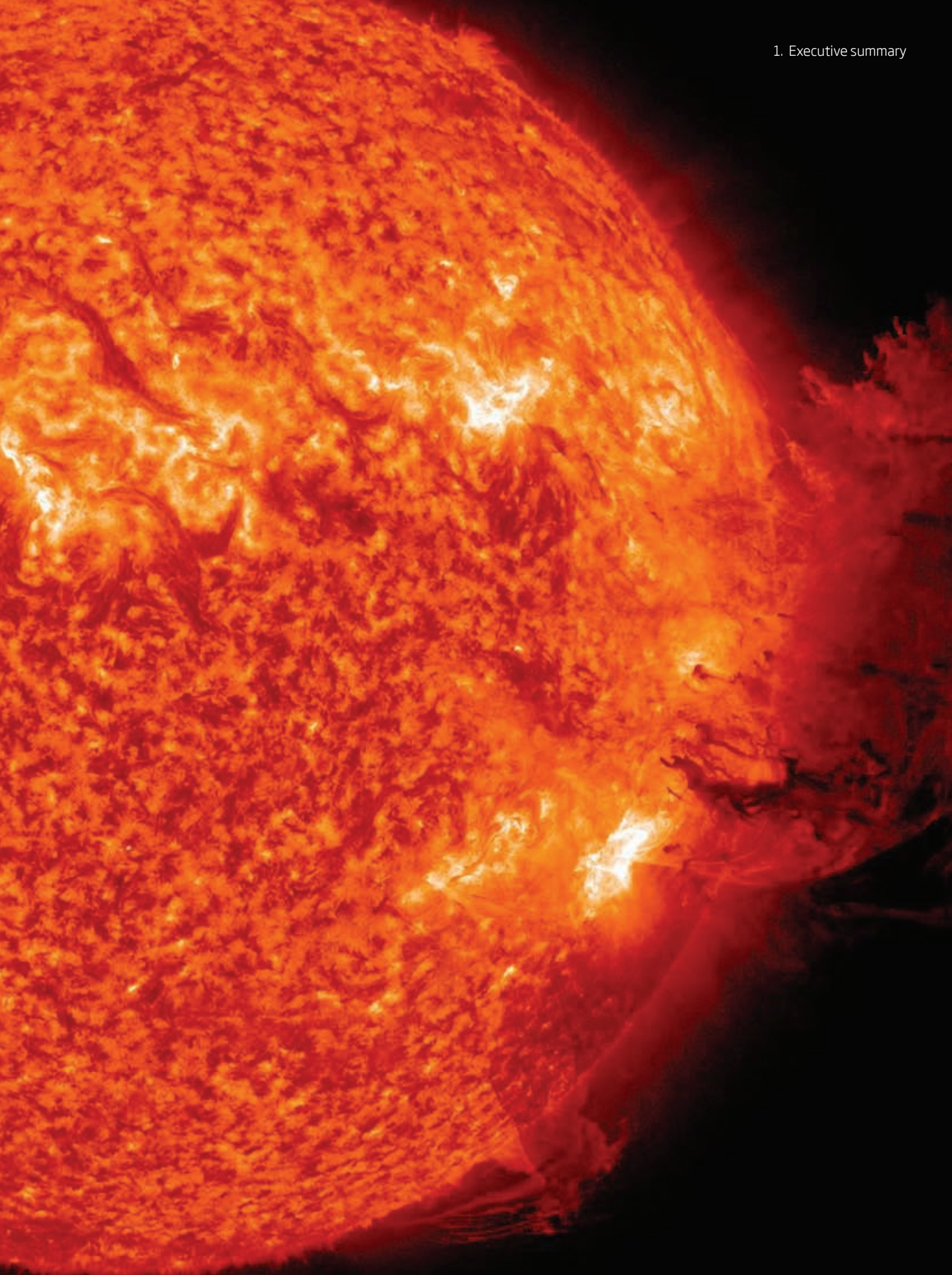

2. Introduction

2.1 Background

The April 2010 Icelandic (Eyjafjallajökull) volcano eruption and resulting ash cloud and the March 2011 Japanese earthquake and tsunami demonstrated how devastating rarely occurring natural hazards can be to society and national economies. Natural events have no respect for national boundaries and *in extremis* the whole world can suffer.

In 2011, the UK recognised extreme space weather events (also referred to as solar superstorms and sometimes simply as superstorms) as one such rare, but high impact, hazard. Space weather was for the first time included as part of the UK National Risk Assessment (NRA) – an unclassified version of which can be found at: **www.cabinetoffice.gov.uk/resource-library/national-risk-register.**

The Royal Academy of Engineering has sought, through this study, to articulate the potential engineering impact of such events, particularly in a UK context.

This report seeks to describe the effects, evaluate the impact and advise on suitable mitigation strategies, but has not deliberated on societal or economic impacts. Above all the report seeks to be realistic in terms of the engineering impacts so that solar storms can be better placed in the context of other natural hazards.

2.2 Scope

This study has involved understanding the operational threats posed by extreme space weather on a number of ground, air and space-based technologies and then understanding how these technologies respond to those threats. The report has benefited from an earlier US workshop report [*NRC*, 2008].

The report addresses:

- induced currents on the electrical grid, railways, telecommunication-wirelines and other networks
- charging and ageing effects on spacecraft
- drag effects on spacecraft orbits
- radiation doses for aircrew and passengers
- unwanted upsets in sophisticated electronics on aircraft and on the ground
- a wide variety of effects on radio technologies, including navigation and communication.

The report makes recommendations intended to improve the understanding of extreme events and to help to mitigate their effects. The report does not consider high altitude nuclear explosions or any other manmade modifications of space weather. A summary report has also been published and is available at **www.raeng.org.uk/spaceweathersummary**.

3. Space weather

3.1 Introduction

Space weather is a term which describes variations in the Sun, solar wind, magnetosphere, ionosphere, and thermosphere, which can influence the performance and reliability of a variety of space-borne and ground-based technological systems and can also endanger human health and safety [*Koons et al.*, 1999]. Many of the systems affected by space weather are illustrated in *Figure 1*; just like terrestrial weather, space weather is pervasive and compensating for its impact is a challenge.

Space weather exhibits a climatology which varies over timescales ranging from days (ie diurnal variations resulting from the rotation of the Earth) to the 11-year solar cycle and longer periods such as grand solar maxima and minima [*Lockwood et al.*, 2012].

Superimposed on this climatology are weather-like variations; on some days space weather is more severe than on others. Minor solar storms are relatively common events; in contrast, extremely large events (superstorms) occur very occasionally – perhaps once every century or two.

3.2 Causes of space weather

Although there is some influence from outside the solar system, most space weather starts at the Sun. The elements of the coupled Sun-Earth space weather system consist of Sun, solar wind, solar magnetic field, magnetosphere and ionosphere, as displayed in *Figure 2*.

Figure 1: Impacts of space weather © L. J. Lanzerotti, Bell Laboratories, Lucent Technologies, Inc.

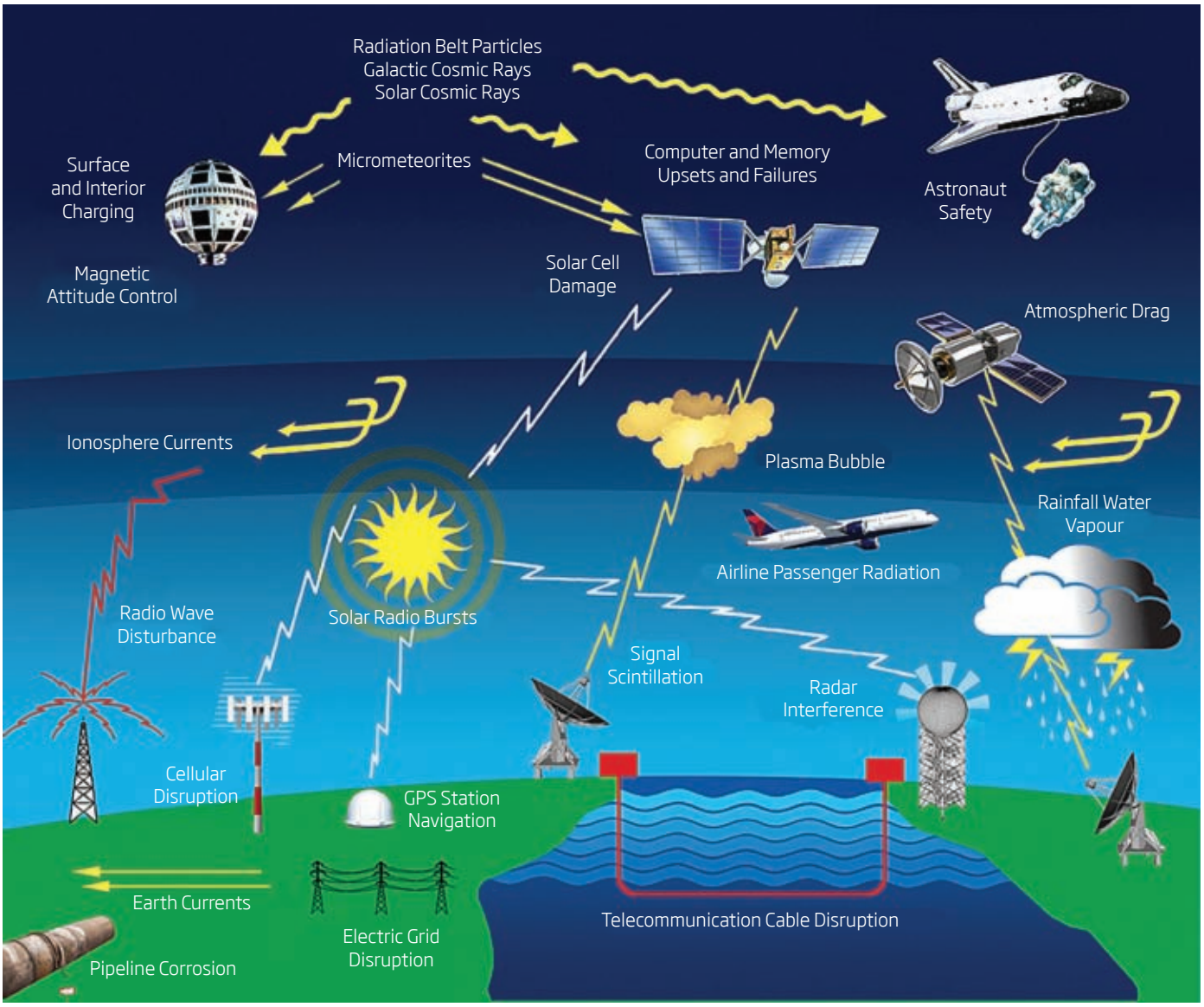

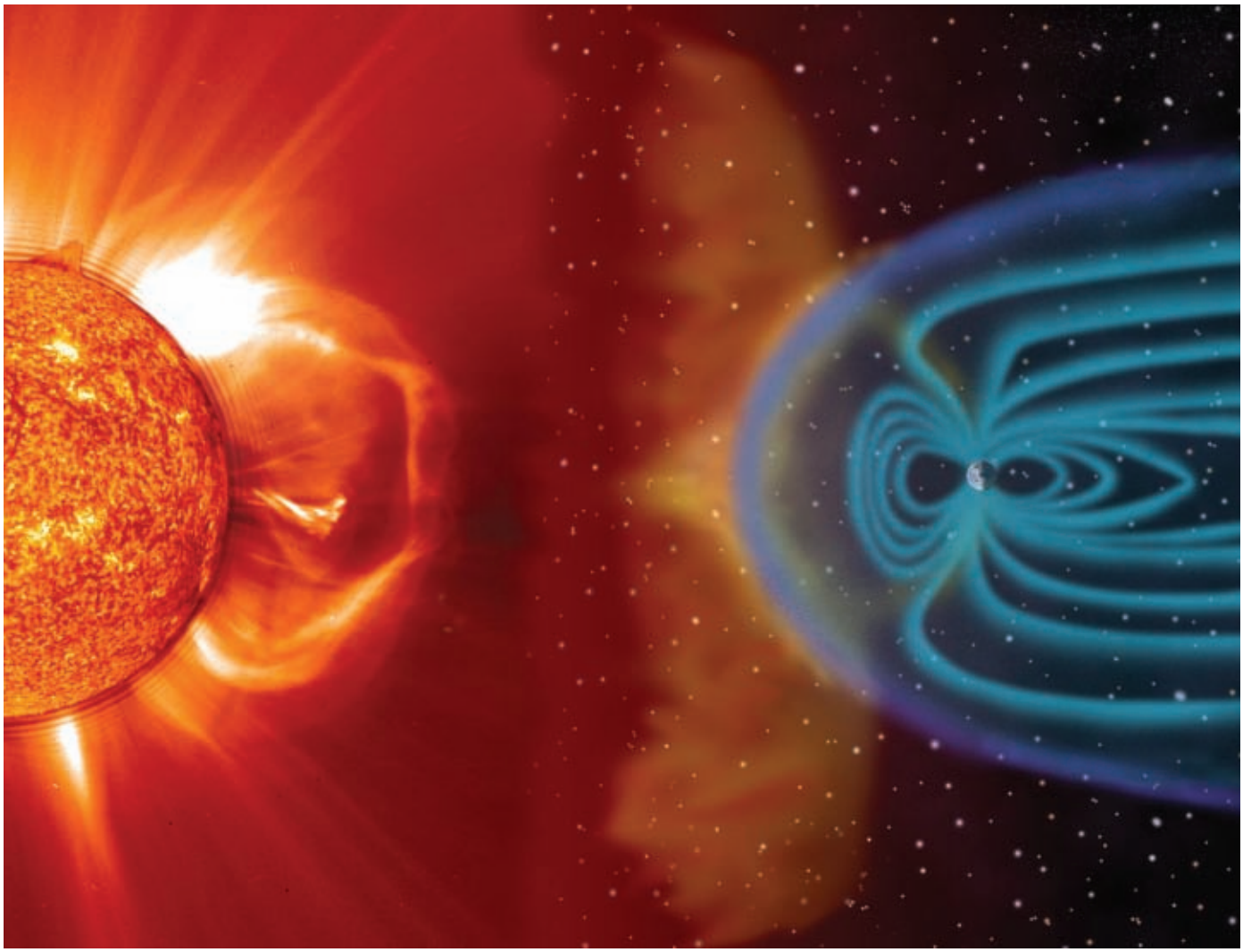

Figure 2: The space weather environment © NASA

The Sun is a nearly constant source of optical and near-infrared radiation. However, there is considerable variability during storm periods at EUV, X-ray and radio wavelengths. During these periods, the Sun is also more likely to generate high-energy solar energetic particles (SEPs) and the solar wind plasma speed and density, forming part of the solar corona, can increase substantially. Coronal mass ejections (CMEs) are one manifestation of the latter and stream interaction regions (SIRs), formed when fast streams in the solar wind overtake and compress slow streams, also occur. Directly or indirectly the ionising radiation, the ionised particles and the plasma interact with the magnetosphere and the ionosphere below it to cause a variety of effects on engineered systems.

The orientation of the interplanetary magnetic field (IMF) in the solar wind controls the degree to which CMEs and SIRs influence the magnetosphere-ionosphere system, producing the disturbances that we call geomagnetic storms. When the IMF has a southward-pointing component, magnetic reconnection (or merging) between the IMF and the Earth's magnetic field occurs on the dayside of the magnetosphere and allows solar wind energy to enter the magnetosphere. Only then is the solar event said to be geoeffective. When a geoeffective event occurs, the energy abstracted from the solar wind is transported to the nightside of the Earth and temporarily stored in the tail of the magnetosphere. When the stored energy reaches some critical level, it is released explosively by magnetic reconnection and some of that energy is directed towards Earth. This cycle of energy storage and release is called a substorm and typically has a period of one to two hours; it will be repeated as long as solar wind energy enters the magnetosphere. For the purpose of this report, the key point to note is that a geomagnetic storm contains a series of a substorms, so many of the effects described in this report will come in a series of pulses and not as a continuous period of high activity.

Extreme space weather is thought to be associated with fast (>800 km s^{-1}) CMEs, which are preceded by a shock wave that

THE SUN IS A NEARLY CONSTANT SOURCE OF OPTICAL AND NEAR-INFRARED RADIATION. HOWEVER, THERE IS CONSIDERABLE VARIABILITY DURING STORM PERIODS AT EUV, X-RAY AND RADIO WAVELENGTHS.

compresses the ambient solar wind plasma and magnetic field (typically by a factor of four). This sharply accelerates the solar wind velocity with respect to Earth and introduces a sharp deflection in the direction of the magnetic field. This shock is also a strong source of SEPs. The so-called sheath region between the shock and the CME contains both high speed solar wind and a strong magnetic field. If the deflection of that magnetic field is strongly southward, the CME sheath can initiate severe geomagnetic storms.

During periods of high solar activity, the Sun can launch several CMEs towards Earth and these may collide during their transit to Earth. This is not unusual since the first CME may be slowed down as it sweeps up the ambient solar wind in its sheath, leaving behind a low density region that allows a following CME to catch up. The result is to produce a more complex pattern of IMF changes as the combined CMEs pass the Earth, driving a longer series of substorms and hence a longer, more intense geomagnetic storm.

3.3 The geomagnetic environment

The Earth's magnetic field comprises contributions from sources in the Earth's core, the lithosphere (ie crust and upper mantle), the ionosphere, the magnetosphere and also from electrical currents coupling the ionosphere and magnetosphere ('field aligned currents', or FAC). The sources external to the solid Earth also induce secondary fields in the Earth (*Figure 3*).

To a first approximation the geomagnetic field is similar to that of a dipole (or bar magnet) currently inclined at around 11 degrees to the geographic poles. The core field is generated by dynamo action in which the iron-rich fluid outer core convects as a result of the heat sources contained within it. This fluid convection across existing magnetic field lines generates electrical currents that generate, in turn, further magnetic fields, with diffusion losses counteracting the generation of new magnetic field. The dynamics of field generation and diffusion provide a spatially and temporally complicated magnetic field pattern across the Earth and in space.

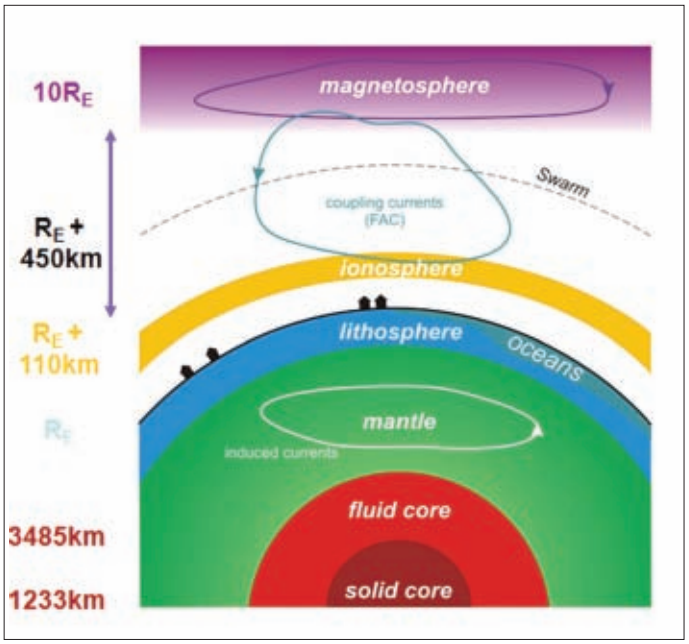

Figure 3: The geomagnetic environment. 'RE' indicates one Earth radius (6372 km). The dotted line and the building silhouettes indicate, respectively, measurement platforms in orbit and at permanent ground-based magnetic observatories © DTU Space, Technical University of Denmark

The core field is the dominant component of the measured field (of order 90% of the field strength) near the Earth's surface and in near-Earth space. Changes in the core field occur on timescales of months to millennia and can include 'reversals', where the polarity (North or South) of the magnetic poles reverses. Reversals occur on average every 200,000 to 300,000 years and take a few thousand years to complete once the process begins. The lithospheric field is stable, except on geological timescales, and is the consequence of the presence of rocks rich in magnetic minerals. Lithospheric fields contribute up to 5% of the measured field near the surface, but can be very large near localised crustal magnetic anomalies.

The ionospheric, magnetospheric and FAC magnetic sources producing the external magnetic field are controlled by solar UV- and X-ray radiation, the solar wind and solar magnetic activity. The dynamics of these magnetic fields reflect the variability of space weather. Rapid time variations in these external electrical current systems induce surface electric fields in the Earth that can drive geomagnetically induced currents (GIC) through grounded conducting networks, such as electricity, pipeline and railway grids. External field variations can reach 5-10% of the total magnetic field at the Earth's surface during geomagnetic storms caused by space weather.

3.4 The satellite environment

The satellite high-energy radiation environment derives from three sources:

- galactic cosmic rays (GCR) from outside the solar system
- solar energetic particles (SEP) accelerated near the Sun by shock waves
- radiation belt particles trapped inside the Earth's magnetic field.

The Earth is subjected to a continuous flux of GCRs generated by supernovae explosions throughout the galaxy. These are very energetic protons, helium nuclei and heavier ions and are modulated by the solar wind and the interplanetary magnetic field. Typically, the flux varies by a factor of two over the eleven-year solar cycle and is highest during periods of low solar activity. It also varies markedly as large CMEs pass the Earth and block the propagation of cosmic rays – an effect now being explored as an additional way to detect CMEs. Cosmic rays cause single event effects, damage to electronic components and degradation of solar array power. The variation in galactic cosmic rays is generally understood and predictable and is not directly relevant to this discussion on extreme events.

SEPs are very high-energy ions, mainly protons which are so energetic that the first particles take only a few minutes to reach the Earth. They are accelerated close to the Sun by both rapidly changing magnetic fields and by shock waves in the solar wind. The former are thought to produce short-lived (≤1 day) impulsive events while the latter produce much longer (gradual) events [*Reames*, 1999]. Predicting how long gradual events will last is very difficult as it depends on the evolution of the CME shock wave as it travels away from the Sun, and on how well the shock is connected to the Earth via the interplanetary magnetic field; this varies in direction but favours events originating at around 45° West on the Sun. These events often exhibit a peak in SEP fluxes as the shock passes the Earth.

The Earth's magnetosphere partly shields the Earth against GCRs and SEPs but they have easier access near the magnetic poles than at the equator. The geomagnetic shielding falls off with spacecraft altitude and during extreme events the shielding at all orbits can become greatly reduced as the magnetopause is pushed close to or inside this orbit.

Changes in the radiation belts are driven by the interaction of the solar wind with the Earth's magnetosphere. The inner radiation belt (within about 2 Earth radii) consists of energetic protons and electrons while the outer radiation belt (3-7 Earth radii) is dominated by electrons. The high-energy electrons cause a range of problems for satellites, particularly satellite charging effects [*Iucci et al.*, 2005] while protons in the inner belt produce cumulative dose and damage as well as prompt single event effects. Satellites in geostationary orbit (GEO) pass through the outer edge of the radiation belts, whereas those in medium Earth orbit (MEO) pass through the heart of the outer radiation belt. Satellites in low Earth orbit (LEO) operate mainly underneath the belts, but encounter the inner radiation belt in a region known as the South Atlantic Anomaly. LEO satellites that have orbits inclined more than about 50° to the Equator will, in addition, encounter the outer radiation belt in the high latitude auroral regions. High inclination LEO satellites are also vulnerable to SEPs encountered over high latitude regions.

While the inner radiation belt is fairly stable, the outer radiation belt is highly dynamic and the flux of relativistic electrons, with energies of mega-electron volts (MeV), can change by five orders of magnitude on timescales from a few hours to a few days [*Baker et al.*, 2007]. In exceptional cases, the low intensity slot region

Figure 4: Rays refracted from the layered ionosphere © QinetiQ

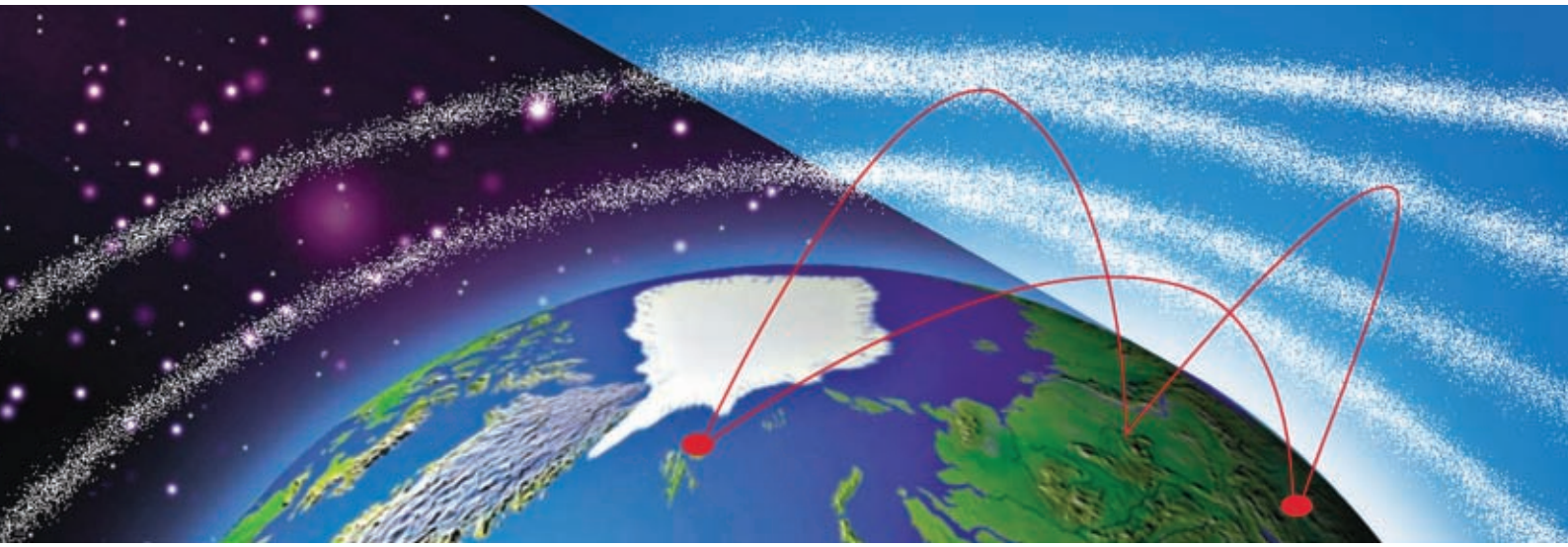

between the main belts has been observed to increase by orders of magnitude on a timescale of two minutes, for example on 24th March, 1991 [*Blake et al.*, 1992].

Some of the highest radiation belt electron fluxes have been observed when there is a fast solar wind stream emanating from a coronal hole on the Sun. These events occur more often during the declining phase of the solar cycle as coronal holes migrate from high latitudes towards the equator and the fast solar wind is more able to encompass the Earth.

It should be noted that, beyond geostationary orbit the Earth's magnetic field contains a reservoir of electrons at energies of 1-10 keV. Changes in the solar wind can trigger global changes in the Earth's magnetic field which rapidly transport these electrons towards the Earth in what is known as a substorm. The electrons envelop those satellites in GEO and MEO orbits mainly between midnight and dawn, causing surface charging, changes in the satellite potential and degradation of satellite surface materials [*Koons and Fennell*, 2006]. The injected electrons also penetrate along the magnetic field to low altitudes and affect polar orbiting satellites in LEO at high latitudes.

3.5 Atmospheric radiation environment

When galactic cosmic rays (GCRs) strike the atmosphere they can interact with the nuclei of oxygen and nitrogen molecules to generate a cascade of secondary particles including neutrons, protons and electrons. The secondary radiation builds up to a maximum at around 60000 feet (18 km) and then attenuates down to sea level. The fluxes of particles at subsonic flight levels (12 km) are some 300 times greater than at sea level while at 18 km they are about 500 times more intense. The geomagnetic field provides greater shielding at the equator than at the poles and the secondary radiation increases by about a factor of five between the equator and latitudes of around 60 degrees beyond which the levels flatten off with increasing latitude.

SEPs also contribute to the atmospheric radiation environment. They vary greatly in energy spectrum but approximately once a year the particles are sufficiently energetic to increase the flux of secondary neutrons measured on the ground. This is known as a ground level event (or GLE) but is also associated with significant increases in radiation at aircraft cruising altitudes.

WHEN GALACTIC COSMIC RAYS (GCRS) STRIKE THE ATMOSPHERE THEY CAN INTERACT WITH THE NUCLEI OF OXYGEN AND NITROGEN MOLECULES TO GENERATE A CASCADE OF SECONDARY PARTICLES INCLUDING NEUTRONS, PROTONS AND ELECTRONS.

3.6 Ionospheric environment

The ionosphere (*Figure 4*) is a lightly ionised region of the upper atmosphere that extends from about 60 to 2,000 km in altitude with a density peak around 300km altitude.

The Sun emits electromagnetic waves over a range of frequencies and the maximum intensity of the spectrum occurs in the visible range. However, it is primarily the extreme ultraviolet and soft X-ray portions of the spectrum that produce the ionosphere, with additional contributions from electron precipitation in the auroral region and ionisation by SEPs in the polar cap region.

The solar photo-ionising radiation is attenuated by the atmosphere, with the more energetic radiation penetrating further into the atmosphere. Each atmospheric chemical species has a distinct photo-ionisation energy and consequently different species are preferentially ionised at different altitudes. Recombination losses are also height dependent, and in combination with the production process, this produces defined layers of ionisation (*Figure 4*).

The ionosphere can be conventionally divided into four latitudinal regions: equatorial, mid-latitude, auroral and polar cap. The mid-latitude region (under which the UK sits during non-storm periods) is by far the least variable, both spatially and temporally.

The ionospheric plasma is conductive and, therefore, interacts with electromagnetic waves. Low-frequency radio waves are often considered to be reflected and high frequencies are refracted – sometimes so much so that the signals return to the ground as if they had been reflected. Still higher frequency signals pass through the ionosphere but are still weakly refracted and delayed. The ionosphere generally has no practical impact on signals above 2 GHz, but occasionally the effects extend to higher frequencies.

3.7 Space weather monitoring and forecasting

Monitoring

Space weather is routinely monitored by many ground and space-based instruments, operating in the optical and radio bands and via *in-situ* measurements of the local plasma. This report cannot hope to do justice to these instruments, but it worth noting the importance of the Advanced Composition Explorer (ACE) satellite

which is located ~1.5 million kilometres towards the Sun where a stable orbit can be established around the L1 Lagrange point. Real-time data from ACE are used by various agencies to improve forecasts and warnings of solar storms as they travel between Sun and Earth. The US is planning to launch the DSCOVR satellite to L1 in 2014 to act as a backup for ACE. Looking to the longer term a Chinese satellite, Kuafu, may also be placed at the L1 point in the year 2017 while the ESA Space Situational Awareness programme is planning an L1 monitor for launch ahead of the 2024 solar maximum.

Solar monitoring is critical to forewarning of solar events that could generate severe space weather at Earth – it enables engineering teams to go on standby and it helps provide the context against which scientific advice and political decisions can be made. Unfortunately, solar wind monitoring at the L1 point provides only 15 to 30 minutes' warning in regards to CME-related effects which dominate many of the most important impacts of a superstorm. Thus, there is growing interest in improving this warning time by a number of methods. Placing a monitor further upstream using solar sail technology is one option and to explore this NASA will fly a demonstration mission, Sunjammer, in 2015. The UK Space Agency has recently approved funding for UK teams to fly a magnetometer and plasma sensor on this mission. Other options include remote sensing of the interplanetary magnetic field using radio telescopes to make Faraday rotation measurements; and better modelling of the magnetic field topology in the Sun's atmosphere and the inner heliosphere (a requirement that is now recognised as a crucial scientific step in understanding all aspects of solar activity). The UK scientific community is strongly engaged in all of these activities.

Forecasting

Electromagnetic and SEP-related effects will always be difficult to forecast since the effects travel at or close to the speed of light. Predicting the time of a solar eruption is not currently possible, though there are services that forecast the probabilities of classes of flares and SEPs.

To overcome this fundamental physical limitation flare forecasting will need to be based on identifying precursor features [e.g. *Ahmed et al.*, 2011]. For SEPs, options include forecasts based on flare observations [e.g. *Laurenza et al.*, 2009; *Núñez*, 2011] and on observations of SEP electrons that reach Earth ahead of the more dangerous SEP ions [*Posner*, 2007]. For some of these experimental techniques to transition to an operational capability, it will be necessary to monitor plasma structures and magnetic fields across the whole surface of the Sun including the far side.

CME FORECASTING IS MORE TRACTABLE THAN SEP FORECASTING BECAUSE CMES TAKE MANY HOURS TO TRAVEL TO THE EARTH. IT IS NOW POSSIBLE TO MONITOR AND MODEL THE EVOLUTION OF AN EARTH-DIRECTED CME SUCH THAT ITS ARRIVAL AT EARTH CAN SOMETIMES BE FORECAST WITH AN ACCURACY OF =6-8 HOURS.

There has also been significant progress in recent years towards forecasting the energy spectrum of related SEP events – which is critical to assessing their consequences. This progress reflects the growing use of hybrid and full-kinetic models to simulate particle energisation, particularly at the shock waves ahead of fast CMEs, and the availability of adequate computing power to run those models. However, this approach is fundamentally dependent on knowledge of the shape and Mach number of the shock and thus dependent on progress in monitoring and modelling CME propagation.

CME forecasting is more tractable than SEP forecasting because CMEs take many hours to travel to the Earth. It is now possible to monitor and model the evolution of an Earth-directed CME such that its arrival at Earth can sometimes be forecast with an accuracy of ±6-8 hours [*Taktakishvili et al.*, 2010]. Unfortunately, these errors are larger for fast CMEs which would be expected during a superstorm. Furthermore, forecasts of its geoeffectiveness are currently not possible until the CME reaches the L1 point, where its magnetic field can be measured and alerts issued to engineering teams and agencies. The lead time is then only 15-30 minutes. That warning time would be significantly increased if the CME magnetic field could be determined upstream from L1.

3.8 Space weather forecasting - summary and recommendations

Summary

Space weather monitoring is critical to forewarning of solar events that could generate severe space weather at Earth. It enables engineering teams to go on standby and it helps provide the context against which scientific advice and political decisions can be made.

Forecasts provide another useful capability which, given sufficient accuracy, could change how space weather is mitigated. Currently neither flares nor SEPs can be forecast but there are techniques in research that may improve this situation. Operational provision of such a service would necessitate the appropriate instrumentation including monitoring of the far side of the sun.

CME arrival time can be forecast with an arrival time accuracy of ±6-8 hours which, although far from precise, is useful for putting the engineering teams on standby; this can be expected to improve over the next few years. However, the geoeffectiveness of the CME cannot be judged and definitive forecasts issued until the CME reaches the L1 point satellite sensor, thereby providing only 15-30 minute notice.

Recommendations

- The UK should work with its international partners to ensure that a satellite is maintained at the L1 Lagrangian point, and that data from the satellite is disseminated rapidly.
- The UK should work with its international partners to explore innovative methods to determine the state of the solar wind, and its embedded magnetic field upstream from L1.
- The UK should work with its international partners to ensure the continued provision of a core set of other space-based measurements for monitoring space weather.

4. Solar superstorms

4.1 Outline description

As already described, the geomagnetic, satellite, atmospheric radiation and ionospheric environments all react to increased solar activity. However, each environment reacts differently depending on the energy spectrum of the electromagnetic and particle radiation.

Solar storms all differ, yet we understand their basic chronology and their consequences (*Figure 5*)

- The storm starts with the development of one or more complex sunspot groups which are observed to track across the solar surface.
- From within these active regions, one or more solar flares occur and are detected on Earth at radio, optical and x-ray wavelengths just eight minutes later.
- Highly solar energetic (relativistic) particles are released and detected just a few minutes later on both satellites and on the ground. These continue to arrive over a period of hours and even days if further eruptions occur.

Figure 5: A summary of space weather effects on technology © Royal Academy of Engineering 2012

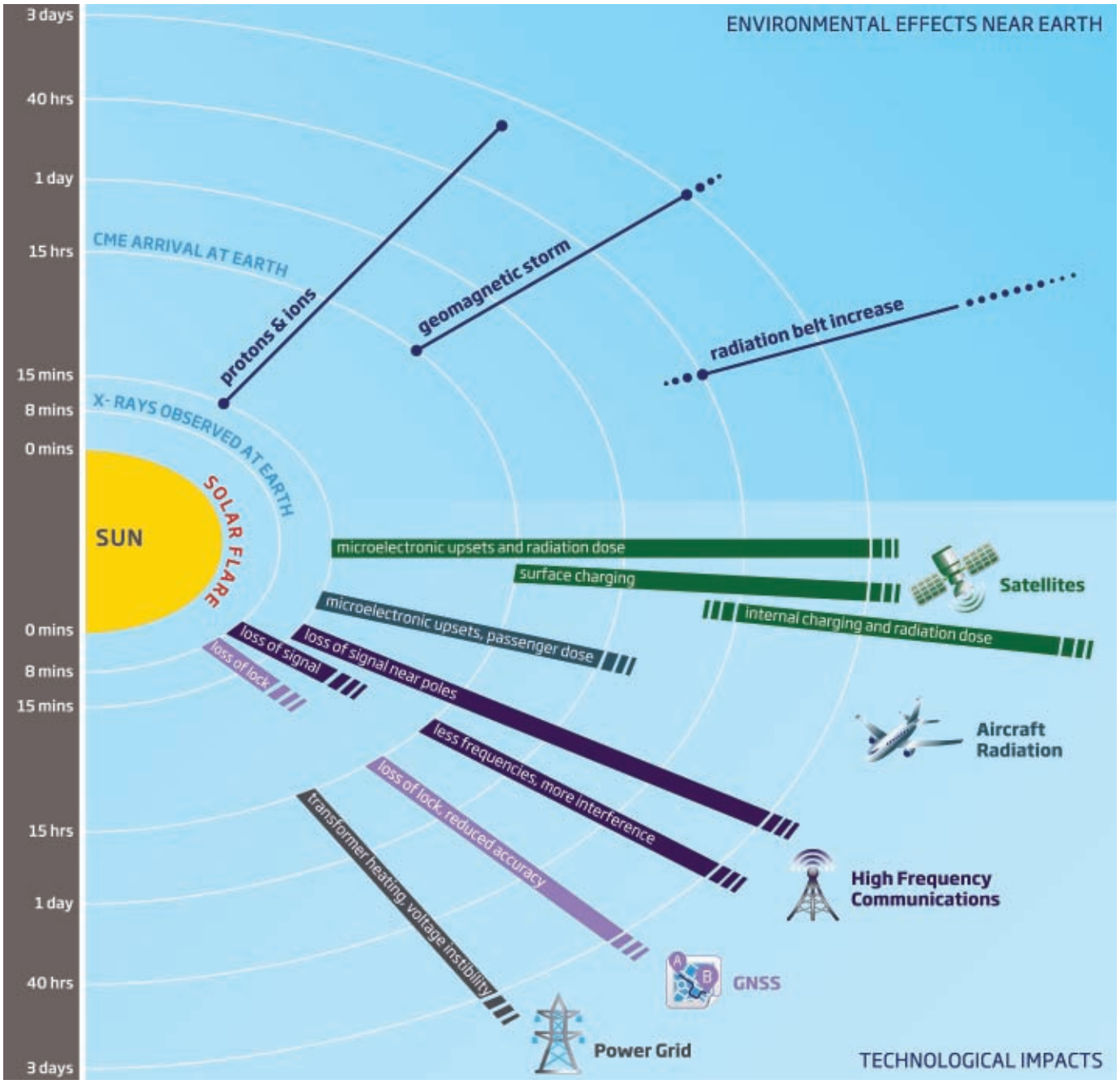

- A coronal mass ejection of plasma occurs which travels outwards at many hundred kilometres per second, taking ~ 15-72 hours to arrive at the orbital distance of the Earth. The level of impact on Earth is dependent on the speed of the CME, how close it passes with respect to Earth, and the orientation of the magnetic fields in the CME and in the compressed solar wind ahead of the CME.

4.2 The history of large solar storms and their impact

The effects of solar storms [*Baker*, 2002; *Baker and Green*, 2011] can be measured in a number of ways but the longest series of measurements (since the 1840s) has been made by ground-based magnetometers. These records have demonstrated that there have been many solar storms of which a very small number are severe (*Figure 6*). The storm of 2-3 September 1859 is the largest event on record and is known as the Carrington event, after Richard Carrington, the distinguished British astronomer who observed a huge solar flare on the day before the storm. During this period aurora were seen all over the world, rather than just at high latitudes, with contemporary reports of aurora in the Caribbean. The Carrington event serves as the reference for many studies and impact assessments.

We now believe that this flare was associated with a very fast CME that took only 17.6 hours to travel from the Sun to the Earth. The Carrington event has been widely studied in the past decade [e.g. *Clauer and Siscoe*, 2006 and references therein] and we now have a wealth of published data and analyses. These suggest that the Earth was hit by a CME travelling at about 1900 km s^{-1} and with a large southward-pointing magnetic field (100 to 200 nT) in the sheath of compressed plasma just ahead of the CME (but

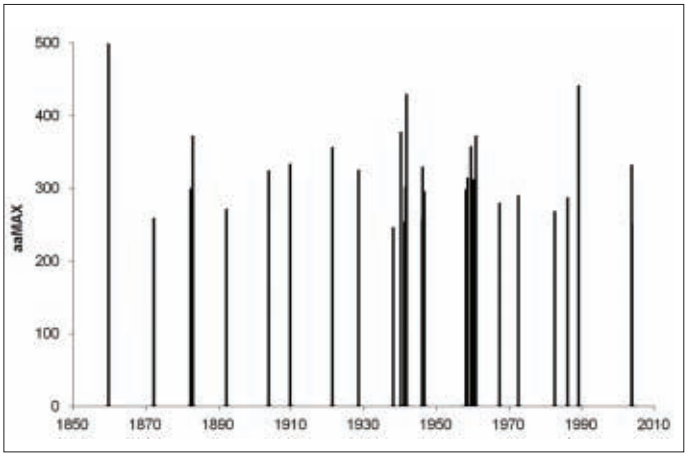

Figure 6: The top 31 geomagnetic storms since 1850; storm sizes based on the geomagnetic index, aa*MAX index developed at the US National Geophysical Data Center (for more background see Annex A of Hapgood [2011]). The Carrington event is the large peak on the left © Rutherford Appleton Laboratory

behind its shock wave). It is this combination of high speed and strong southward magnetic field that generated such a severe geomagnetic storm because it allowed the energy of the CME to enter the Earth's magnetosphere [*Tsurutani et al.*, 2003]. The location and duration of the impact region depends on processes in Earth's magnetosphere and upper atmosphere, in particular the substorm cycle previously discussed. This extracts energy from the solar wind, stores it as magnetic energy in the tail of Earth's magnetosphere and then explosively releases it back towards the Earth. During a severe geomagnetic storm, such as the Carrington event, lasting one or more days, there will be many substorms at intervals of one to three hours. Each substorm will produce severe conditions that will often be localised in space and time.

There are a number of possible storm metrics. These can, for example, address the related geomagnetic storm or the radiation storm. *Figure 6* shows one measure of the most severe geomagnetic storms that have occurred over the past 170 years with the Carrington event on the far left of the figure.

Disruption of telegraph and telephone communications is well attested in descriptions of the 1859 event and by others [*Boteler*, 2006; *Boteler and van Beek*, 1999; *Stenquist*, 1914]. In one spectacular case in May 1921 a telephone exchange in central Sweden was badly damaged by a fire started by the electric currents induced by space weather [*Karsberg et al.*, 1959]. The contemporary threat to telephone systems (and now to the internet) is much reduced following the widespread use of optical fibre, rather than copper wires. Nonetheless they are a valuable historical proxy for the contemporary threats.

The space age has seen a number of major space weather events that provide further insights into extreme space weather. A prime example is the event of August 1972 which saw: (a) the fastest CME transit time on record (reaching Earth only 14.6 hours after leaving the Sun [*Cliver and Svalgaard*, 2004] (b) the most intense radiation storm of the early space age [*Barnard and Lockwood*, 2011] and (c) the magnetopause compressed to less than 20,000 km from Earth (compared to the usual 60,000 km) [*Anderson et al.*, 1974]. Yet there was only a modest geomagnetic storm (Dst ~ -120 nT). (Dst is a geomagnetic metric measured in nano-Tesla). With the scientific knowledge that we have 40 years on, it is likely that this event was similar to the Carrington event, but with a northward interplanetary magnetic field (IMF). Thus the fast CME generated an intense radiation storm and compressed the magnetosphere, but deposited only a modest amount of energy into the magnetosphere (probably through magnetic reconnection on the high latitude magnetopause, an effect that is now known to occur during northward IMF [e.g. see *Dunlop et al.*, 2009]). This event should be regarded as a near miss – a severe event whose practical impact was mitigated by a combination of northward IMF and the contemporary resilient technology.

Another significant event was the geomagnetic storm of 8-9 February 1986, which saw Dst drop to -301 nT. This event is

significant because of its timing very close to sunspot minimum, which nominally occurred in September 1986, but which would have been in March 1986 if the February storm had not occurred. This storm shows that extreme events can occur at any phase of the solar cycle and it is unwise to focus mitigation efforts only around solar maximum.

The year of 1989 saw two major space weather events: (a) a huge geomagnetic storm in March and (b) a huge solar radiation storm in October. The great geomagnetic storm of 13-14 March 1989 was the largest of the modern era with Dst falling to -589 nT. It produced a wide variety of impacts including: (a) the well-documented power blackout in Quebec [*Bolduc*, 2002] as well as transformer damage in the UK [*Erinmez et al.*, 2002] and other countries; (b) the loss of positional knowledge for over 1,000 space objects for almost a week [*Air Weather Service*, 1997] and many other impacts described elsewhere in this report. The radiation storm of October 1989 was actually a series of large events all occurring within a week, thus giving a very high fluence (time-integrated flux) for particles with energies of above 60 MeV. This was nearly four times that from the 1972 radiation storm [*Barnard and Lockwood*, 2011] and in terms of fluence, it is the largest event seen so far in the space age. In terms of instantaneous flux, its peak almost matched the 1972 event.

Another much studied event is the radiation storm that occurred on 14 July 2000 (the so-called Bastille Day event) and the associated geomagnetic storm on 15-16 July. This was a smaller event than those described above: peak flux and fluence were respectively 30% and 70% of the 1972 event [*Barnard and Lockwood*, 2011] and Dst dropped to -301 nT. This event was a useful (and low-cost) wake-up call for the satellite launcher community in that the launch of the first pair of Cluster-II spacecraft was planned for that day. The launch team received warnings about the radiation storm but lacked pre-planned criteria to assess the risk. Fortunately problems with ground equipment delayed the launch until after the storm.

The last days of October 2003 saw another major space weather event (the so-called Halloween event). This was a weaker event than in 1989 (Dst fell to -383 nT, radiation fluence 60% of the 1972 event), but provided a wealth of evidence for space weather impacts [*Weaver et al.*, 2004]. In particular, it provided clear evidence that large geomagnetic storms can disrupt space based navigation systems by inducing rapid and large changes in the morphology of the ionosphere and plasmasphere. This event dominates much current experience of space weather both because it is still a recent event and because of the wealth of environmental and impact data available.

Finally we note that on 4 November 2003, a few days after the Halloween event, the Sun produced the largest X-ray solar flare observed since the advent of space measurements [*Clark*, 2007; *Thomson et al.*, 2005] – and one that was probably similar in strength to the flare associated with the CME that caused the Carrington event . Fortunately this flare occurred on the west limb of the Sun, as the region that caused the Halloween event rotated to the far side of the Sun. Significant energetic particle fluxes were detected despite the poor connection from the event on the Sun to the Earth via the interplanetary field. There has been reasonable speculation that this event would have produced a Carrington-class CME as well as intense particle fluxes but, fortunately, both missed the Earth.

4.3 Quantifying the geophysical impact

In order to judge the impact of a superstorm on a number of contemporary technologies, it is necessary to have a baseline description of the geomagnetic, electromagnetic and high-energy particle environment during a typical event. This description has been developed in the UK through the work of the Space Environment Impact Expert Group (SEIEG) and has been issued as a report [*SEIEG*, 2012]. Further iterations of this report are expected as our knowledge improves.

4.4 The environmental chronology of a superstorm

No two storms are alike [eg *Lanzerotti*, 1992]. Nevertheless it is useful to have some understanding of the chronology of a space weather superstorm (*Figure 7*).

First, there will be a general heightening of activity for some days ahead of the event as a large active region (or regions) rotates into view on the eastern side of the Sun. This period will be marked by frequent solar flares and CME launches as shown in the upper left of the figure. Most of these will be medium scale events: M-class solar flares and slow CMEs (speeds < 800 km s^{-1}) marked in amber. But a few events will approach extreme levels: X-class solar flares and fast CMEs (> 800 km s^{-1}, so likely to generate a bow shock). These are marked in red. Many of these flares will produce HF radio wave absorption across the sunlit side of the Earth - strong absorption in the case of X flares (so marked in red), but weaker for M flares (amber). At this stage, the fast CMEs are likely to miss the Earth, so an extreme geomagnetic storm is avoided. But some of the energetic

EXTREME GEOMAGNETIC STORM CONDITIONS ARE LIKELY TO CONTINUE FOR MANY HOURS AND PERHAPS DAYS

particle particles from the CME shock will reach Earth, producing a heightened radiation environment (amber) and perhaps even extreme conditions (red). The heightened level of activity is likely to produce disturbances in the solar wind that in turn cause heightened geomagnetic activity at Earth (as shown by the amber bars on the right at t < 0). But this is only a precursor to the main event.

At t = -1.25 days (shown by the red bar) a very fast Earth-directed CME launches. This may be associated with an X-class solar flare and is very likely followed within 10 minutes by the onset of a severe radiation storm with the particle radiation being generated at the shock wave ahead of the fast CME. At t=0 the fast CME arrives at the Earth and generates an extreme geomagnetic storm (as shown by the red bars at the right for t > 0).

Extreme geomagnetic storm conditions are likely to continue for many hours and perhaps days (eg if multiple CMEs impact the Earth). The geomagnetic storm is not a period of continuous extreme activity. Instead, it comprises pulses of extreme conditions separated by periods of lower (but still high) activity – as shown by the interleaving of red and amber bars in the figure. These pulses, known as substorms, arise as energy from the CMEs is temporarily stored in the Earth's magnetic tail before being explosively released towards the Earth.

4.5 Probability of a superstorm

The key question, critical to placing this natural hazard in context with other natural hazards, is a good estimate of the probability of a superstorm on the scale of, or greater than, the Carrington event.

In the UK, for planning purposes a reasonable worst case superstorm with the strength of the Carrington event is currently considered to be a 1-in-100 year event. However, given that the longest geomagnetic data set extends back only ~170 years and satellite particle effects are at best measured over ~50 years, understanding of how often an event of this type will affect the Earth is poor.

The Sun is believed to produce several tens of Carrington-class CMEs every century but most miss the Earth or the IMF is oriented North. For example, on 23 July 2012 a Carrington-class coronal mass ejection was seen to leave the far side of the Sun [*NASA*, 2012] and reached NASA's STEREO-A spacecraft just 19 hours later. STEREO-A orbits at the same distance from the Sun as the Earth so this speed is comparable to that of the Carrington CME. Preliminary data from the spacecraft show a huge magnetic field (~100 nT) at first northward, but then turning southward. Energetic particles were in fact detected at Earth despite the poor connection to the event beyond the west limb of the Sun. If the event had occurred several days earlier very intense fluxes might have reached the Earth. The advent of satellite missions such as STEREO means that we are now likely to see many more of these events, and this is an opportunity to improve our assessment of their occurrence rate.

There are also reasons to anticipate events larger than those seen in recent history. Studies of long-term solar change [*Barnard et al.*, 2011] indicate that the Sun has been in an atypical state for the last 40 years. It has been suggested that the current gradual decline in the overall strength of the solar wind magnetic field will increase the Mach numbers of CME shocks and thus increase their ability to generate energetic particles [*Kahler*, 2009].

Various other authors are addressing this estimation problem in different ways. A paper looking at several parameters, including observed CME speeds and the strength of the equatorial current system in Earth's magnetosphere, concluded that the risk of a superstorm could be as high as 12% per decade [*Riley*, 2012]. This certainly provides a useful estimate but the reader should treat such estimates with considerable caution.

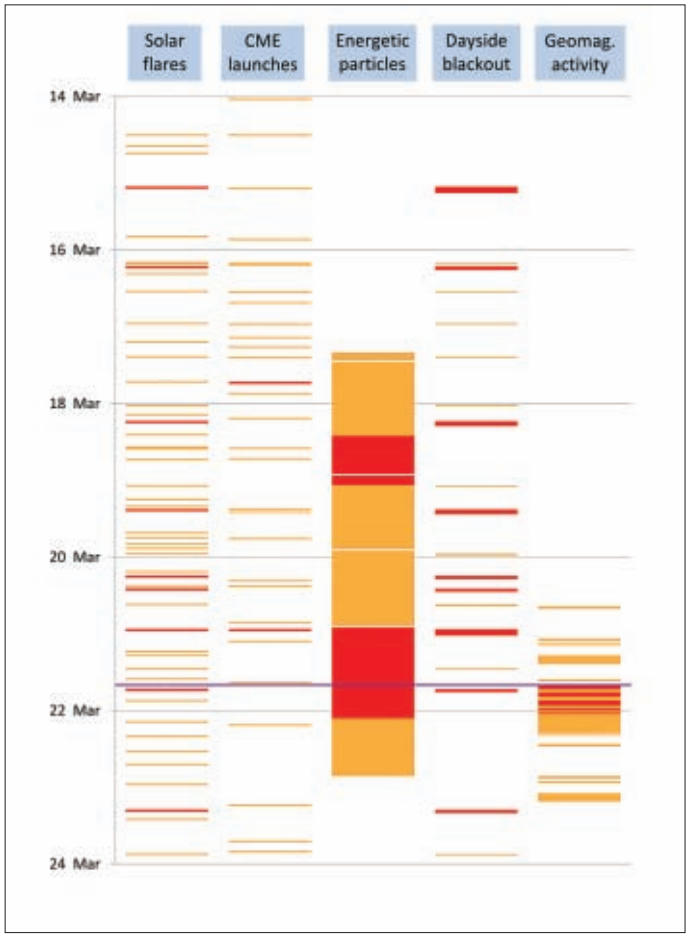

Figure 7: Indicative timeline of environmental phenomena leading up to an extreme space weather event with time advancing from top to bottom. The figure shows five key phenomena: solar flares (leftmost column), CME launches (left of centre), solar energetic particle fluxes (centre, dayside blackout (strong HF radio absorption on sunlit side of Earth) (right of centre) and geomagnetic activity (right hand column). Red indicates the occurrence of extreme conditions while amber indicates heightened activity somewhat below the extreme case (see text) © Rutherford Appleton Laboratory

The use of nitrates in ice cores as a possible proxy for solar energetic particle events [*McCracken et al.*, 2001] has recently been shown to be flawed [*Wolff et al.*, 2012]. However, *Miyake et al.* [2012] has shown that the study of carbon-14 in tree rings is possibly a good proxy for atmospheric radiation events over the last 3,000 years. The dominant natural source of carbon-14 is a result of the collision of neutrons (usually from galactic cosmic ray interactions in the atmosphere but with additional large spikes from solar energetic particle events) with nitrogen molecules at altitudes of 9 to 15 km. This study indicates that there was an intense atmospheric radiation event during the years 774-775 AD which was much more intense than any seen in the recent era of direct radiation measurements. [*Melott and Thomas.*, 2012] have shown that this event could have arisen from a solar energy release around 2×10^{26}J, around 20 times greater than the energy release from the Carrington event [*Clauer and Siscoe*, 2006]. We note, however, that there is no corroborative evidence that this event was associated with a severe geomagnetic storm - but that may just indicate that the associated CME missed the Earth or that records of bright aurora from this era were not preserved.

Maehara et al. [2012] has studied the flares on other stars using 120 days of data from the NASA Kepler mission. This mission is designed to study the light curves of large numbers of stars in order to look for dips that would indicate the passage of an exoplanet across the disc of its parent star. Serendipitously this mission is also ideal for looking for bright flares (energy > 10^{26}J) on those stars. The paper reports observations of 14 flares on 14,000 Sun-like stars (similar surface temperature and spectral type, slow-rotation periods >10 days). They use this to estimate that a flare of energy > 10^{27}J (again 10 and 100 times greater that from the Carrington event) will occur once every 800 years on a Sun-like star.

4.6 Solar superstorm environment – summary and recommendation

Summary

The recurrence statistics of an event with similar magnitude and impact to a Carrington event are poor, but improving. Various studies indicate that a recurrence period of 1-in- 100 to 200 years is reasonable and this report makes assessments of the engineering impact based on an event of this magnitude and return time. If further studies provide demonstrable proof that larger events do occur – perhaps on longer timescales - then a radical reassessment of the engineering impact will be needed. The headline figure of 100 years should not be a reason to ignore such risks. To demonstrate the issue, but without disturbing the main narrative of the report, a short outline of the implications of rare events is presented in Box 1.

The environmental specification for the superstorm may also be considered as a work in progress with the current estimates provided in *SEIEG* [2012].

Recommendation

The UK should work with its international partners to further refine the environmental specification of extreme solar events and where possible should extend such studies to provide progressively better estimates of a reasonable worst case superstorm in time scales of longer than ~200 years.

Box 1. Probability of extreme space weather events – implications and consequences for mitigation of risks

Given the potential risk from severe space weather events, it is vital to assess the likelihood that such events will occur in the future and to understand the nature of the risk. As with many other natural hazards, we have no means of predicting the occurrence of specific events, but we can make statistical estimates of their rate of occurrence. Such statistical estimates are valuable as they enable policymakers to compare the different risks and prioritise the resources applied to mitigate these risks.

For severe space weather, the generally accepted benchmark for assessing risk is that our planet experiences a Carrington like event. A recent paper looking at several parameters, including observed CME speeds and the strength of the equatorial current system in Earth's magnetosphere, concluded that risk of such an event could be as high as 12% in a decade [Riley, 2012].

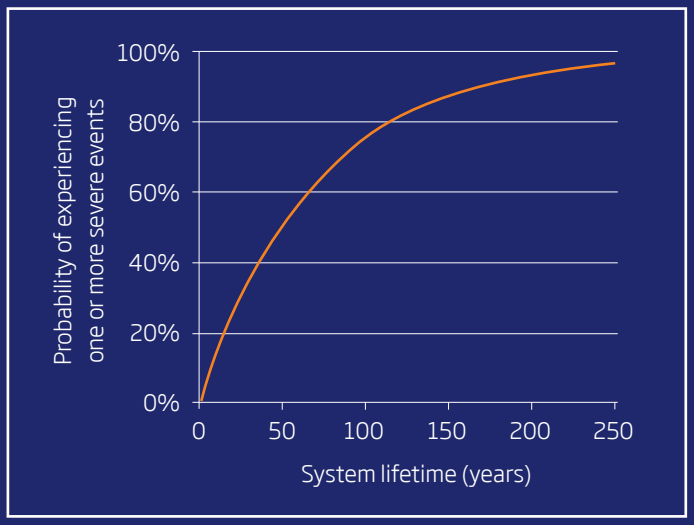

This corresponds to a return period or recurrence interval of 79 years – but, this does not mean that we should expect a severe event every 79 years. Instead we expect these events to occur randomly in time. The usual 95% confidence interval implies we might only wait two years for a superstorm, but we might wait 300 years. This is a consequence of the nature of randomness.

Random systems also have no memory. The potential for the next severe event does not increase as time passes since the last event; similarly that potential is not smaller in the years immediately following a severe event. This is exactly equivalent of tossing a coin: a run of heads in a row does not make it any more likely you will get a tail next time. Despite the fact that we have had 150 years since the last Carrington-strength event, the average waiting time until the next major storm remains 79 years. Random events have no concept of being overdue.

The bottom line is that any system sensitive to space weather has a finite probability of experiencing a severe space weather event. The figure above shows how, given a 12% risk per decade, the probability of experiencing a severe event increases with system lifetime. The probability asymptotically approaches 100% over periods of several centuries. But if we focus on the lower left of the figure, and take 10% as the acceptable level of risk, any system with a design lifetime of more than 8.25 years needs to consider the risk from severe space weather events similar to that first recorded by Carrington.

5. Impacts on the electrical power grid

5.1 Introduction

Rapid variations of the geomagnetic field on time scales of a few seconds to a few tens of minutes, caused by space weather, induce an electric field in the surface of the Earth. This electric field, in turn, induces electrical currents in the power grid and in other grounded conductors. These currents can cause power transmission network instabilities and transformer burn out. For example, severe space weather caused damage to two UK transformers during the 13 March 1989 storm [*Erinmez et al.*, 2002], the same storm that caused much disruption to the operation of the Hydro-Quebec grid [*Bolduc*, 2002].

The strength of the electric field (in volts per kilometre: V/km) depends on the relative resistance – or conductivity - of the sub-surface. In the UK typical electric field strengths are of order 0.1 V/km during quiet space weather, but may rise to ~5-10 V/km during severe space weather (for example during the October 2003 storm [*Thomson et al.*, 2005]. The electric field itself changes on a time scale similar to the driving geomagnetic variation.

The induced surface electric field can, under certain assumptions, be modelled as a collection of voltage sources in each of the conducting lines in the network. In principle, for a given conducting line, the larger the separation between grounding points the larger the geomagnetically induced currents (GIC) that will flow in the line. In practice, however, the GICs are determined by all the line and grounding resistances of the network and by the local resistance of the Earth itself. The modelling tools that are required here are essentially based on Ohm's and Kirchoff's laws from electrical engineering.

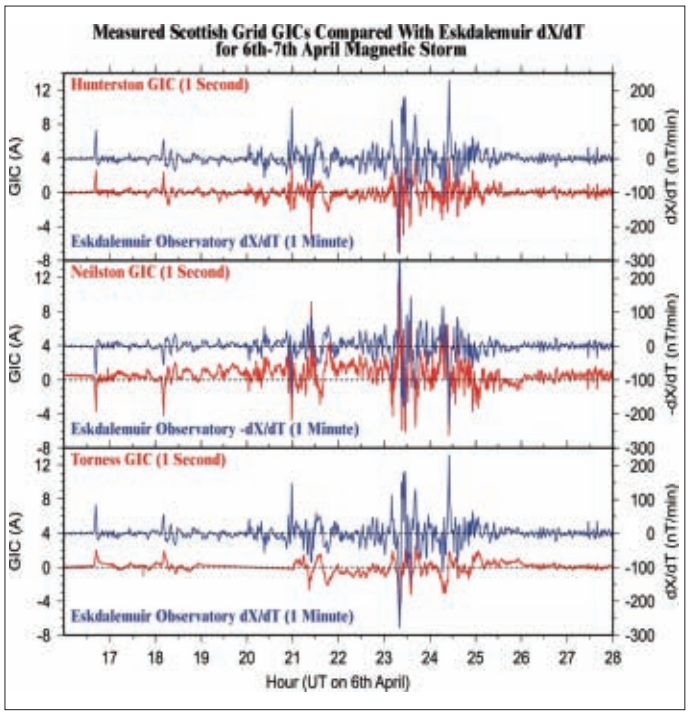

Figure 8: Time rate of change of the north (dX/dt) component of the geomagnetic field from the Eskdalemuir observatory in the UK, compared with simultaneously measured GIC data (Amps) at three sites in Scotland, during a moderate storm on April 2001, when no grid problems were reported. Horizontal tick marks are given every 30 minutes © British Geological Survey (NERC) and Scottish Power

Monitoring the rate of change of the horizontal component of the geomagnetic field is a simple but still good indicator of the strength of GIC in any grounded network [*Beamish et al.*, 2002], see *Figure 8*.

However the correlation between measured magnetic and GIC data falls off with separation between measurement sites, necessitating a network of magnetic monitoring sites across the country. In the UK, the NERC/BGS magnetic observatory network and the University of Lancaster SAMNET variometer array together provide such a network. In the UK horizontal magnetic field changes of around 500 nT/min or more have been known to be associated with high voltage grid problems over the past two to three decades [eg *Erinmez et al.*, 2002]. This is a useful rule-of-thumb threshold used in UK geomagnetic monitoring activities.

Figure 9 shows the modelled response of the UK high voltage (400 kV and 275 kV) electricity transmission system to the 656 nT/minute variation observed at the Eskdalemuir magnetic observatory at the peak of the Halloween storm of 2003 [*Beggan*, unpublished, 2012].

The induced geoelectric field varies at a frequency that is much less than the network's operating frequency of 50Hz. Thus, GICs appear as quasi direct currents superimposed on the system's alternating current. These quasi-DC currents magnetise the transformer core in one polarity and can cause the core to magnetically saturate on one half-cycle of the AC voltage. This half-cycle saturation causes peaks in the magnetising current drawn from the grid system.

The most serious effect of this half-cycle saturation is that when the core saturates, the main magnetic flux is no longer contained in the core. The flux can escape from the core and this can cause rapid heating in the transformer and the production of gases in the insulating oil, which leads to alarms being triggered, shut-down of the transformer, and, in the most severe incidents, serious thermal damage to the transformer. Even if no immediate damage is caused, the performance of the transformer can degrade, and increased failure rates over the following 12 months have been observed [*Gaunt and Coetzee*, 2007].

The more likely effect, although less serious, arises from voltage instability. Reactive power is required on the grid to maintain voltage. Under conditions of half-cycle saturation, transformers consume more reactive power than under normal conditions. If the increase in reactive power demand becomes too great a voltage collapse can occur leading to a local or, if severe enough, a national blackout.

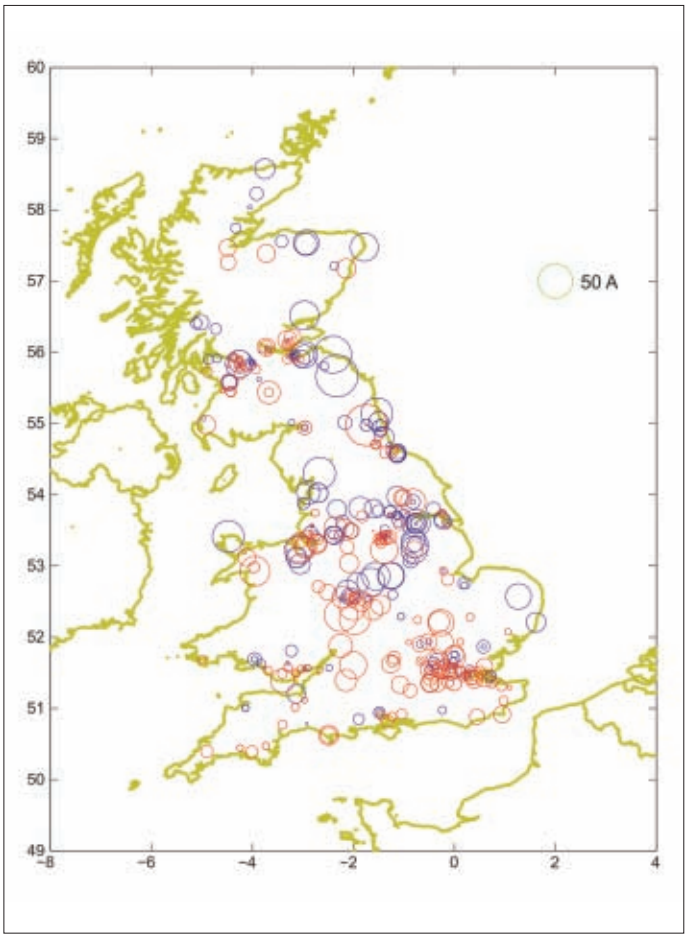

Figure 9: Simulation of GIC flow across a simplified model of the UK 400 and 275 kV transmission system at 21:21 UT on 30 October 2003. A reference 50 Amp spot size is also shown. Red and blue denote GIC flowing to/from the Earth at major transformer substation nodes
© British Geological Survey

A third effect arises from the distortion of the magnetising current which becomes non-sinusoidal, and injects harmonics into the grid. Under normal operating conditions, these harmonics are indicators of faults such as negative phase sequences, and the presence of harmonics triggers protective relays. But under GIC conditions the relays can disable equipment, such as static variable compensators, designed to support the voltage on the system, making voltage collapse more likely. It was this triggering of relays that led to the blackouts in Quebec Province in 1989 and Malmö, Sweden in 2003. National Grid experienced distortion of the magnetising current effects on 14 July 1982, 13-14 March 1989, 19-20 October 1989 and 8 November 1991.

Some transformer designs are more at risk than others. In particular, single phase transformers, and three-phase transformers with five-limb core transformers are more at risk than three phase transformers with a three-limb core, because the quasi-DC flux induced by the GIC can flow directly in the core [*Price*, 2002].

5.2 Consequences of an extreme event on the UK grid

US space weather, transformer and modelling experts have recently produced conflicting reports analysing the impact on a large space weather event on the US system. In an influential report *Kappenman* [2010] suggests that a one-in-100-year event could lead to catastrophic system collapse in the US taking many years and trillions of dollars to restore. However, a comprehensive February 2012 report from the North American Electric Reliability Corporation [*NERC*, 2012], suggested that loss of reactive power and voltage instability would be the most likely outcomes. At a Federal GMD Technical Conference on 30 April 2012, it was clear that there was still more work required to agree a proportionate management of the risk. Ongoing work, prepared by National Grid on a severe space weather event for the UK, initially from June 2011, aligns more closely with the conclusions from the NERC paper.

Studies of an extreme event scenario in the UK have been based on a rate of change of the Earth's magnetic field of 5000nT/min [*NERC*, 2010], being approximately a one-in-100-year event (or even rarer) according to *Thomson et al.* [2011]. This compares with the March 1989 event where rates of change of the magnetic field in excess of 500nT/min were observed, during the largest geomagnetic disturbance experienced in the UK since the development of a national grid.

National Grid owns and maintains the high-voltage electricity transmission system in England and Wales, together with operating the system across Great Britain including Scotland. National Grid and Scottish transmission system owners have been aware of the effects of space weather for many years, particularly the effect of geomagnetically induced currents (GICs) on large supergrid transformers that, in England and Wales, step the voltage down from 400kV or 275kV to the 132kV distribution networks. [*Erinmez et al.*, 2002]. Transformers owned by generating companies that step up the voltage to connect to the high voltage grid are also known to be at risk, as has been shown from experience in the USA and South Africa.

Since the last peak of the solar cycle, the Great Britain transmission system has developed to become more meshed and more heavily loaded. It now has a greater dependence on reactive compensation equipment such as static variable compensators and mechanically switched capacitors for ensuring robust voltage control. Thus there is increased probability of severe geomagnetic storms affecting transmission equipment critical to robust operation of the system. The greatest effects of GICs are normally experienced at the periphery of the transmission systems, as in *Figure 9*.

UK studies that are still on-going, sponsored and undertaken by National Grid indicate that a Carrington-level event could have a significant impact. The current worst case estimates are for some local blackouts lasting a few hours as a result of increases

in demand for local reactive power. National Grid has a well-established plan for this type of event, whether or not caused by space weather, and the plan is rehearsed regularly. It is estimated that, for a prolonged storm with maximum rate of change of the geomagnetic field of 5000 nT/min, around six grid transformers in England and Wales and a further seven grid transformers in Scotland could be damaged and taken out of service. This number of failures is within the capacity of National Grid's transformer spares carrying policy to replace sufficient transformers to restore demand. The time for an emergency transformer replacement, when a spare is available, would normally be 8 to 16 weeks although the record is four weeks. A significant delay can be the time required to get permission to transport the spare transformer on the road, and in the event of a severe event it is hoped that priority would be given to allow transport to occur more rapidly.

Most nodes have more than one transformer available and consequently most failures would not lead to prolonged disconnection events. However, National Grid's analysis is that on the order of two transformer substations in Great Britain could experience disconnection through transformer damage. If this occurred, it is likely it would be in remote regions where there is less transformer redundancy.

Generator step-up transformers are potentially at more risk than Super Grid network transformers because of their design (normally single phase or three phase with a five-limb core) and the fact they are operated close to their design loading. As a consequence, network transformers installed since 1997 have, wherever possible, been three phase with a three-limb core, the most GIC resistant type. Although some transformers at higher risk remain on the system, operational mitigation would reduce the possibility of damage.

Interconnectors to France, the Netherlands and to Northern Ireland are operated as High Voltage Direct Current (HVDC) links. As DC equipment, they are not susceptible to GIC effects. However, the power electronics that convert the current from DC to AC at each end of the interconnectors can be disrupted by the harmonic distortions on the AC side. This means that these links may not be available during a severe space weather event.

IT IS ESTIMATED THAT, FOR A PROLONGED STORM WITH MAXIMUM RATE OF CHANGE OF THE GEOMAGNETIC FIELD OF 5000 NT/MIN, AROUND SIX GRID TRANSFORMERS IN ENGLAND AND WALES AND A FURTHER SEVEN GRID TRANSFORMERS IN SCOTLAND COULD BE DAMAGED AND TAKEN OUT OF SERVICE.

5.3 Mitigation

There are three approaches to dealing with the risks posed by GMDs:

1. Understanding the risks through modelling.
2. Implementing appropriate engineering or hardware solutions, such as increasing the spares holding and installing GIC blocking devices.
3. Implementing forecasting and operational procedures, similar to those for other severe risk events such as terrestrial weather.

The solution adopted in the UK is a combination of all three. This is broadly similar to solutions adopted by other system operators.

Modelling, simulation and testing

Network models typically characterise each network as interconnected serial and parallel DC resistances, representing transformer and power lines, acted on by voltage or current sources determined from the modelled surface electric field. The relative simplicity of the methodology – though models of the UK 132 kV, 275kV and 400 kV system currently have over 600 transformer nodes and 1200 interconnecting lines – means that simulation of the grid response to hypothetical and historical events is feasible [*Thomson et al.*, 2005]. Moreover, the flexibility of such network models lends them to simulation of proposed grid modifications, particularly where additional long lines are being considered [*Turnbull*, 2011]. Scenario modelling reveals how the pattern of GIC hazard changes with any proposed reconfiguration and whether GICs are reduced or enhanced at known 'weak points'.

Models and simulations need testing against measured GIC data. Monitoring of GIC at all network grounding points is impractical, given the numbers of nodes and connections in the UK system. However, selection of appropriate monitoring points can be achieved with reference to previous model simulations. Edges and less-connected portions of the grid are typically places that experience larger GICs.

Detailed understanding of the effects of GIC on individual transformers at individual nodes in the system is still lacking. These effects include thermal damage, increased reactive power consumption and production of harmonics in the presence of GIC. For example, the oil in the transformer is degraded under repeated small GIC events and this can result in unexpected failures and greater vulnerability during a superstorm. A number of studies are underway in the UK and USA, but more remains to be done. Both theoretical modelling and, where feasible, the practical testing of transformers are needed.

Forecasting mitigation

National Grid is working with the British Geological Survey (BGS) to provide a real-time monitoring and warning system, known as MAGIC (Monitoring and Analysis of GIC). This system will build on the expertise that BGS has gained both through involvement in

© John Mason, www.sxc.hu

the academic community researching the effect of solar storms, knowledge of the underlying geophysics of the British Isles and experience of previously providing a monitoring and warning system for Scottish Power.

Accurate forecasting of ground magnetic field variations that drive GIC, whether through detailed magneto-hydrodynamic (MHD) models of the magnetosphere, with solar wind input, or through simpler parameterised models, is currently limited. Detailed forecasts of whether the Great Britain grid will be affected and, if so, which parts of the grid in particular will be affected are, therefore, not possible. Parallel activities in North America, such as the Solar Shield project [*Pulkkinen et al.*, 2009] are progressing.

Undoubtedly, improved GIC forecasting capability is a key demand from industry. Hence the transition of one or more MHD-based models to operational readiness would be a major step forward in improving predictive capability. We note that NOAA SWPC and NASA/CCMC in the US are currently undergoing an evaluation of relevant models.

Engineering mitigation

Since 2003, National Grid has adopted transformer design standards that ensure a high level of GIC resilience. In practice this means that only three limb transformers are used in the network. An audit of all Supergrid transformers (SGTs) was completed in May 2011 and this is regularly updated to determine those transformers with a high vulnerability to GIC. The latest transformer audit includes generator transformers which, because of their design and their heavy loading, are more at risk than most SGTs. Grid Supply points (GSPs) have then been analysed using a simple GIC model (developed by BGS) to identify how many transformers at each nodal point are at-risk, and GSPs have been rated according to the proportion of at-risk transformers present. As a consequence, the target spares holding of SGTs has been reviewed and increased.

Consideration is being given to the installation of series capacitors on certain transmission lines. These can block the flow of GICs but can alter the electrical properties of the network in ways that must first be understood before deciding if such devices are suitable for the Great Britain network. Series capacitors are primarily being considered for reasons of load flow control.

More generally, National Grid is monitoring the development of neutral current blocking devices for transformers. These devices are as yet in their infancy, but consideration will be given to any promising developments, again with the proviso that their impact on the system would need to be addressed. Provision for such devices is being considered to protect transformers for new DC links.

National Grid will consider whether the sensitivity of protective relays to harmonics in the system is appropriate. This will rely on data gathered from other network operators where such disturbances are more common.

Consideration is also being given to the provision of transportable recovery transformers that could temporarily meet some of the demand needs at a node that had lost all its supergrid transformers through thermal damage. Such devices are still only at the prototype stage.

Operational mitigation

In the build-up to a significant space weather event, National Grid would take actions that are, in many respects, similar to those taken in the face of severe terrestrial weather. These actions would be triggered by National Grid's space weather monitoring team following on from advice from BGS, the Met Office and other forecasting bodies. National Grid would issue warnings and advice to customers and third parties, as specified by business procedures.

Increased reserves of both active and reactive power would be scheduled to reduce loading on individual transformers and to compensate for the increased reactive power consumption of transformers. Where possible, circuits would be returned from maintenance work, and other outage work postponed, increasing the stability of the system against voltage fluctuations. Substations would be run to maximize the connectivity of the grid where possible. Large power transfers between areas would be reduced, particularly on the Scottish-English transfer boundary.

National Grid would operate an 'all-in' policy where all of its transformers were switched in, reducing the individual neutral current through any one, and all generators would be instructed to generate, reducing the loading on generator transformers, and also increasing reserves.

Throughout the duration of a geomagnetic disturbance, control room engineers at the National Control Centre would monitor the state of the system using the MAGIC tool, assessing which assets are most at risk and identifying areas where voltage instability and reactive power demands are likely to be a problem.

To recover from either an intentional or non-intentional shutdown of part of the Grid or the whole Grid requires a procedure known as Black Start. National Grid has a well-rehearsed plan for Black Start, and generating machines are at all times scheduled to provide this Black Start capability.

5.4 National electricity grid – summary and recommendations

Summary

The reasonable worst case scenario, assumed to be of the order of a one-in-100-year event, will have a significant impact on the national electricity grid. Current estimates are for some local electricity interruptions lasting a few hours. In addition, around six super grid transformers (SGTs) in England and Wales and a further seven grid transformers in Scotland could be damaged and taken out of service.

Because most nodes have more than one transformer available, not all these failures would lead to a disconnection event. However, National Grid's analysis is that around two nodes in Great Britain could experience disconnection. This number of failures is within the capacity of National Grid's transformer spares carrying policy. The time for an emergency transformer replacement, when a spare is available, is normally eight to 16 weeks, with a record of four weeks. Some generator step-up transformers will be at more risk than SGTs because of their design. Lesser storms, compared to a one-in-100-year event, will have progressively less impact on the system

In the build-up to a significant space weather event, National Grid would take actions triggered by National Grid's space weather monitoring team following on from advice from the British Geological Survey, Met Office and other forecasting bodies. National Grid would issue warnings and advice to government, customers and third parties to enable them to mitigate the consequences.

Recommendations:

- The current National Grid mitigation strategy should be continued. This strategy combines appropriate forecasting, engineering and operational procedures. It should include increasing the reserves of both active and reactive power to reduce loading on individual transformers and to compensate for the increased reactive power consumption of transformers.
- There is a need to clarify and maintain a very rapid decision-making process in respect to an enhanced GIC risk.
- Consideration should be given to the provision of transportable recovery supergrid transformers and to GIC blocking devices, which are still in their infancy.
- Further geophysics, transmission network and transformer modelling research should be undertaken to understand the effects of GIC on individual transformers, including the thermal effects, reactive power effects, and the production of harmonics.
- Long-term support for geomagnetic and GIC monitoring should be maintained.
- The National Grid should better quantify the forecasting skill that it requires and assess this in the light of foreseeable improvements following from current and future scientific research.

6. Other geomagnetically induced current effects

6.1 Pipelines and railway networks

GICs can be induced on any long lengths of earthed electrical conducting material during a solar storm.

Boteler [1977] and *Trichtchenko and Boteler* [2001] have discussed GICs in the context of pipelines, but reported effects in the UK are hard to find.

Evidence also exists of space weather impacting railway networks, with recent papers in the literature referring to Russian and Swedish networks [eg *Eroshenko et al.*, 2010; *Ptitsyna et al.*, 2008; *Wik et al.*, 2009]. However, again the study team was unable to assess whether this is an important issue for the UK.

6.2 Trans-oceanic communications cables

Optical fibre cables are the backbone of the global communications networks. They carry the vast majority (99%) of internet and telephone traffic and are much preferred to links via geosynchronous spacecraft since neither human voice communications nor the standard TCP/IP protocol can efficiently handle the ~0.3s delay imposed by the long paths to geostationary satellites. Optical fibres are more resilient to space weather than their twisted copper wire predecessor, which was very prone to GIC effects.

However, electric power is required to drive optical repeaters distributed along the transoceanic fibres and this is supplied by long conducting wires running alongside the fibre. These wires are vulnerable to GIC effects as was demonstrated during the geomagnetic storm of March 1989. The first transatlantic optical fibre cable, TAT-8, had started operations in the previous year and experienced potential changes as large as 700 volts [*Medford et al.*, 1989]. Fortunately the power system was robust enough to cope. Similar but smaller effects were also seen during the Bastille Day storm of July 2000 [*Lanzerotti et al.*, 2001]. We are not aware of any effects occurring during the Halloween event of 2003, but that event was relatively benign in terms of GIC effects.

ELECTRIC POWER IS REQUIRED TO DRIVE OPTICAL REPEATERS DISTRIBUTED ALONG THE TRANSOCEANIC FIBRES AND THIS IS SUPPLIED BY LONG CONDUCTING WIRES RUNNING ALONGSIDE THE FIBRE.

6.3 Recommendations

- Government and industry should consider the potential for space weather damage on the optical fibre network through overvoltage on the repeaters and should consider whether appropriate assessment studies are necessary.
- UK railway operators and pipeline operators should be briefed on the space weather and GIC risk and should consider whether appropriate assessment studies are necessary.

7. Radiation impacts on satellites

7.1 Introduction

A solar superstorm, such as that described in section 4, dramatically increases the fluxes of radiation particles seen by satellites, creating a number of hazards to their operation and longevity. The specific effects and impacts will depend upon satellite orbit, and design.

7.2 Electron effects

Electrons cause electrostatic charging and cumulative dose (ageing) effects on satellites. The Earth's dynamic outer electron belt (see section 5.4) is particularly troublesome for satellites in geostationary- and medium-Earth orbits (GEO and MEO) and has caused numerous anomalies and outages as a result of electrostatic build-up and discharge. Low Earth orbit satellites (LEOs) can also be subject to charging effects in auroral (high latitude) regions.

A discharge can readily couple into sensitive electronics causing data upsets, false commands and even component damage. There are two types of charging that can occur: surface-and internal-charging. Both involve complex interactions between the space environment, materials and microelectronic systems and they continue to prove difficult to analyse, model and mitigate.

- *Surface charging* is caused by low energy electrons (<100keV) which interact only with surface materials of the spacecraft. Under certain conditions, potential differences of many kilovolts can arise between various different surfaces, leading to an electrostatic discharge. Surface charging was first seen in the 1970s and 80s but techniques to suppress it, through the grounding of surfaces and the use of conductive coatings, were introduced. In recent years it has come back in new and subtle forms causing major power losses in solar arrays. Surface charge rises and recedes over quite short timescales (minutes).
- *Internal charging* is caused by high-energy electrons *(>100 keV)* which penetrate into the spacecraft equipment where they deposit charge inside insulating materials (especially plastics) and ungrounded metals. The phenomenon first came to light in the 1980s and is still a problem today. Discharges tend to occur very close to the sensitive and vulnerable components. Internal charging requires a day of two of persistently high fluxes to build up enough charge to be a threat, but this often occurs in magnetic storms.

Electrons also cause ionising dose damage to microelectronic devices through a build-up of trapped charge in insulating (usually silica) layers. Equipment power consumption goes up, noise immunity is reduced and decision thresholds may change. Ultimately complete failure of equipment may occur. Cumulative dose damage has rarely been a cause of satellite failure since it is relatively straightforward to analyse and large safety margins are used. This might not be so in the event of a solar superstorm.

7.3 Solar energetic particle effects

Energetic protons and ions are present as a background flux of galactic cosmic rays and can be greatly enhanced for several days at a time by solar energetic particles (SEPs). These add to total ionising dose (as discussed above) but also cause two further effects:

- *Displacement damage* disrupts the crystalline structure of materials used in microelectronic devices. These defects reduce the performance of transistors and are especially important for optoelectronic devices such as opto-couplers where current transfer ratios are reduced and for solar cells where efficiency is degraded
- *Single event effects (SEE)* arise from the charge depositions of individual particles in the sensitive regions of microelectronics. Such depositions occur via direct ionisation (dominant for the heavy ions) and nuclear interactions (dominant for protons and neutrons). Effects range from soft (correctable) errors to hard (permanent) errors, which can include burnout of some devices such as metal oxide semiconductors. With feature sizes reducing to tens of nanometres and critical charges reducing to femtoCoulombs these are a growing problem and a number of systems have been damaged or compromised. Further details of single event effects, which are also of growing importance in avionics (see section 11), can be found in the box below.

The high upset rates produced by SEPs are an increasing problem [*Dyer et al.*, 2004] and have been blamed for a number of

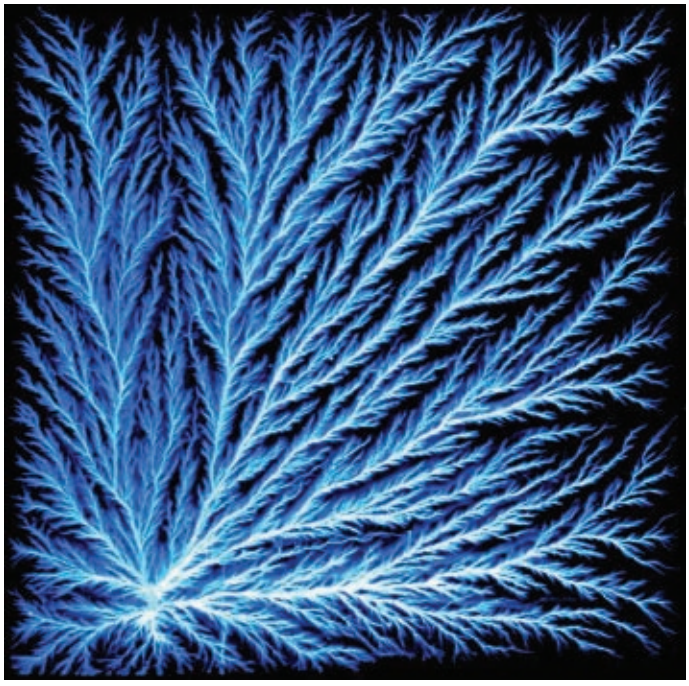

Figure 10: An electrostatic discharge caused by electron accumulation in an insulator: such discharges are a major cause of anomalies on satellites and have proved difficult to suppress © K A Ryden

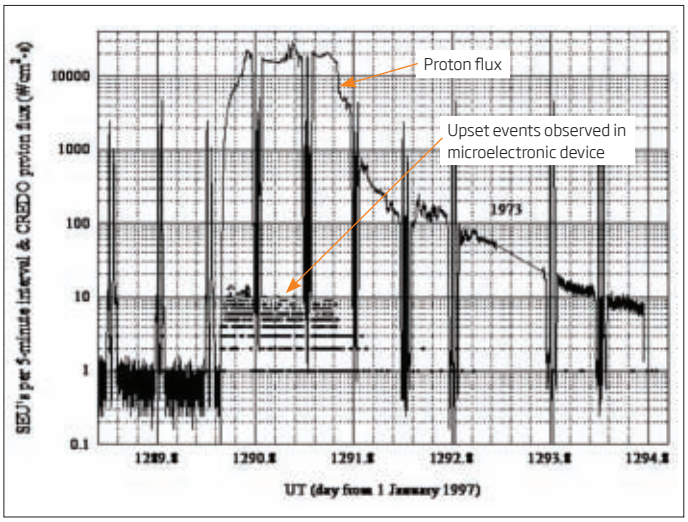

Figure 11: Observations of the onset of SEE on a satellite coincident with arrival of solar particles during Bastille Day event on 14 July 2000 – fluxes and SEE rates would be greater during an extreme event [Campbell et al., 2002]. Note that periodic dips and spikes in radiation are also observed since the observing satellite routinely crosses regions of radiation trapped by the Earth's magnetic field © QinetiQ

operational outages and failures. *Figure 11* shows observations of upsets in an analogue-to-digital converter during the Bastille Day solar particle event in July 2000. SEPs are more probable around solar maximum, although they can occur at any time in the solar cycle.

The University of Surrey's UoSAT-2 spacecraft, orbiting in a highly inclined, low Earth orbit (700km, 98°), happened to be in operation during the SEP event of October 1989. This spacecraft was one of the first to make use of commercial-off-the-shelf (COTS) components, and in particular carried large amounts of dynamic random-access memory (DRAM) that was very sensitive to single-event upsets (SEUs). It is thus a valuable source of data on the effects of such an event on radiation sensitive devices operating in space. During the event, there was an order of magnitude increase in SEU activity [*Underwood*, 1996] but it is worth noting that the automatic on-board error mitigation system (error-detection and correction coding plus memory 'washing') was able to cope without difficulty, and the spacecraft remained fully operational during this and indeed all the events encountered.

A subset of data from Giove-A, the UK-built satellite launched in preparation for the Galileo mission for the period 2006 [*Ryden et al.*, 2008] illustrates (*Figure 12*) the highly dynamic nature of the medium Earth orbit environment. Although not a solar maximum period, it shows the various consequences of a CME-driven solar storm which occurred in December 2006 with two associated SEP events (shown in red). Soon after the SEPs are seen, the measured internal charging threat (shown in black) due to energetic electrons increases considerably for over a week. (The internal charging threat is also enhanced, with a periodicity of the ~27 day solar rotation period being strongly linked to the presence of persistent coronal holes). While the electron fluxes are elevated, the measured total ionising dose (yellow and green lines) increases rapidly including in the aftermath of the December 2006 solar storm.

7.4 Satellite failures and outages

Unlike, for example, the UK electricity grid which is a single, well-defined system, there are around 1,000 satellites operating in different orbits and built to a wide variety of standards, specifications and engineering practices. Even satellites of the same nominal type usually contain different permutations of equipment and component fits. Some space weather interactions are probabilistic in nature (such as single event effects) and so even identical equipment may exhibit different responses.

Satellites are protected against space weather in a number of ways. Physical shielding is vital at component, equipment and spacecraft level to reduce particle fluxes and cumulative doses to acceptable levels. Circuits are designed to account for some degree of degradation and unwanted behaviour in microelectronic components and the components themselves are carefully selected, screened and tested. Data storage devices often employ some level of error detection and correction and important data values are checked for plausibility. At equipment level there is typically like-for-like redundancy to cope with single failures or, less frequently, a diversity of technology to avoid single mode failures. Design margins are used to account for uncertainty in the models and calculations used. Systems are also designed to limit the impact of faults and steer the system towards a safe state: operator intervention is then required to recover the system. In a serious case the satellite may go into a safe attitude position (eg Sun pointing) while awaiting operator recovery actions. In such cases a satellite service outage would occur but the vehicle should still be recoverable later on. In the meantime, services may have to be transferred to other satellites, either in-orbit spares (if available) or other satellites that have spare capacity.

CUMULATIVE DOSE DAMAGE HAS RARELY BEEN A CAUSE OF SATELLITE FAILURE SINCE IT IS RELATIVELY STRAIGHTFORWARD TO ANALYSE AND LARGE SAFETY MARGINS ARE USED. THIS MIGHT NOT BE SO IN THE EVENT OF A SOLAR SUPERSTORM.

Despite all these engineering measures, problems resulting from space weather have proven impossible to suppress altogether, even in normal conditions. While most such effects are noticeable only by the satellite operator, some do lead to service outages and, on very rare occasions, complete satellites failures. Key engineering reasons for these on-going problems include the following:

- introduction of new technology with unexpected sensitivities
- poor understanding of certain radiation interaction mechanisms
- inaccurate space environment models
- test facility limitations (ie we cannot fully replicate the space radiation environment on the ground)
- design or build errors which are ultimately exposed during a storm event
- storm intensity may exceed specified protection levels (specification level is a cost-risk balance).

Some significant public domain examples of satellite failures or outages which have been attributed to space weather are given in *Table 1*. These are based on data from satellites where data are relatively freely available, but it is likely that many problems encountered remain undisclosed due to commercial and security sensitivities. More than 47 satellites reported anomalies during the October 2003 CME-driven 'Halloween' storm period [*Satellite News Digest*, 2012] one scientific satellite was a total loss and 10 satellites suffered a loss of operational service for more than one day. In 2003, there were approximately 450 satellites in orbit whereas that figure has now increased by more than a factor of two. Given a similar event today we may expect ~100 satellites to report anomalies and approximately 20 satellites to have a loss of service for more than one day.

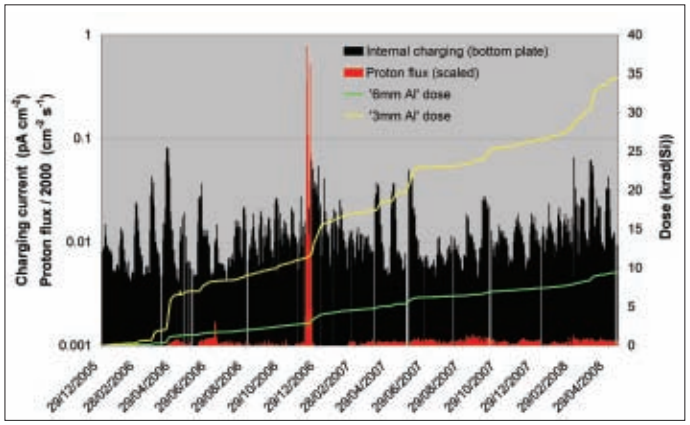

Figure 12: Measurement of space weather engineering hazards in medium Earth orbit on the Giove-A mission. The CME-driven storm in December 2006 produced two separate, sudden, increases in proton fluxes (marked in red) and then, after a couple of days, caused substantially increased rates of internal charging (black) due to acceleration of electrons in the outer belt. Energetic electron levels remained elevated well into January 2007. Ionising dose, which has an 'ageing' effect, was measured at two depths of aluminium shielding, 3mm (yellow line) and 6mm (green), both of which exhibited a rapid increase in the aftermath of the storm due to the presence of the energetic electrons. A similar sequence of events on larger scale would be expected from an extreme storm © QinetiQ

7.5 Engineering consequences of an extreme event on satellites

Radiation

A similar sequence of events, albeit on a much larger scale, would be expected during an extreme storm. There would be:

- one or more SEP events over several days leading to an increase in SEE and a rapid increase in displacement damage dose which will be especially notable in optoelectronic components (including the solar cells used to power the satellite)
- a sharp increase in the energetic electron environment a day or two after the arrival of the CME. This would cause internal charging hazards for many days or even weeks, together with surface charging threats
- a rapid increase in the radiation damage accumulated on the satellite due primarily to the electron environment increases but also with a proton contribution.

During an extreme event the energetic electron environment in some orbits could be up to an order of magnitude more severe [*Shprits et al.*, 2011] than those typically used in specifications and it is thought that solar particle fluxes could be up to three or four times more intense. Memory upsets and other erroneous events may increase so much that they exceeded a threshold above which the inbuilt mitigation approaches (eg error detection and correction) are no longer effective. Under these circumstances, linear scaling of anomaly rates from previous storms might not provide an accurate picture. *Odenwald et al.* [2006] has estimated up to 10 anomalies for every satellite every day as an upper limit (but noting very large uncertainties) based on an assumed Carrington event. However typically only a small subset of anomalies have an impact on service provision.

As well as anomalies, a solar superstorm could have a major impact on satellite lifetimes. The reasonable worst case SEP is expected to produce (in one go) a >30MeV proton fluence of approximately 3×10^{10} cm^{-2} [*SEIEG*, 2012] which is close to a typical lifetime fluence specified for long-life geostationary or medium Earth orbit satellites [eg *Feynman et al.*, 1993]. Subjected to such a SEP event, a newly launched satellite would rapidly use up this element of its designed-in radiation tolerance, but should nevertheless survive. The satellite would then however be vulnerable to further SEPs, but we do not know when these would occur. After a superstorm, older satellites might be operating well outside their radiation design-life but, fortunately, long experience shows that most spacecraft have the potential to significantly exceed their nominal design lives because of the extremely conservative design approaches

Date	Event	Satellite	Orbit	Cause (probable)	Effects seen
8 March 1985		Anik D2	GEO	ESD	Outage
October 1989	CME-driven storm	TDRS-1	GEO	SEE	Outage
July 1991		ERS-1	LEO	SEE	Instrument failure
20 January 1994	Fast solar wind stream	Anik E1	GEO	ESD – note: all three satellites were of same basic design	Temporary outage (hours)
		Anik E2	GEO		6 months outage, partial loss
		Intelsat K	GEO		Temporary outage (hours)
11 January 1997	Fast solar wind stream	Telstar 401	GEO	ESD	Total loss
19 May 1998	Fast solar wind stream	Galaxy 4	GEO	ESD	Total loss
15 July 2000	CME-driven storm	Astro-D (ASCA)	LEO	Atmospheric drag	Total loss
6 Nov 2001	CME-driven storm	MAP	Interplanetary L2	SEE	Temporary outage
24 October 2003	CME-driven storm	ADEOS/MIDORI 2	LEO	ESD (solar array)	Total loss
26 October 2003		SMART-1	HEO	SEE	Engine switch-offs and star tracker noise
28 October 2003		DRTS/Kodama	GEO	ESD	Outage (2 weeks)
14 January 2005		Intelsat 804	GEO	ESD	Total loss
15 October 2006	Fast solar wind stream	Sicral 1	GEO	ESD	Outage (weeks)
5 April 2010	Fast solar wind stream	Galaxy 15	GEO	ESD	Outage (8 months)
13 March 2012	CME-driven storm	Spaceway 3	GEO	SEE?	Outage (hours)
7 March 2012		SkyTerra 1	GEO	SEE/ESD?	Outage (1 day)
22 March 2012		GOES15	GEO	ESD?	Outage (days)

Table 1: Selected significant satellite losses and outages in the public domain [e.g. Satellite News Digest, 2012] that have been attributed to space weather. Note however that diagnosis of one-off events is rarely conclusive and the evidence base is generally circumstantial. Overall, complete losses are extremely rare, with temporary outages being more commonly observed © Royal Academy of Engineering 2012

A SUPERSTORM WILL CAUSE EXPANSION OF THE EARTH'S ATMOSPHERE, CAUSING DRAG ON LEO SATELLITES; ORBITS WILL BE DISTURBED AND PREDICTIONS OF SATELLITE POSITIONS WILL BE DEGRADED.

against cumulative dose effects. Therefore, while some very old satellites (eg those already in life extension) might have a short lifespan (eg months) after the storm, a tidal wave of failures would not be expected and most would carry on for several years, some even reaching close to their full lifetime. However, the planning of replacements would need to be actively accelerated which has the potential to cause bottlenecks in the supply chain.

Satellites in MEO, such as those providing navigation services, already experience much higher levels of radiation than those at GEO – and to some extent this means that they are well protected. The radiation environment could, however, be further increased during an extreme event [*Shprits et al.*, 2011]. GPS has now flown in MEO for 600 satellite years and its resilience to solar storms, such as we have already seen during the satellite era, is excellent. However, the superstorm performance of GPS – and the other satellite navigation satellites – is as yet unknown.

It may be noted that a small number of defence satellites (eg UK Skynet) are built to higher environmental specifications to protect against high altitude nuclear events (HANE). The additional hardening is likely to be beneficial in an extreme solar event, although satellite ageing will still occur.

Atmospheric drag

A superstorm will cause expansion of the Earth's atmosphere, causing drag on LEO satellites; orbits will be disturbed and predictions of satellite positions will be degraded. Satellite orbit data then needs to be re-acquired which may take some days to complete. In extreme cases, low altitude satellites may experience significant aerodynamic torques which overcome the vehicle's attitude control system capability leading to termination of the mission as happened to Astro-D (~450km altitude orbit) during the storm of 14-15 July 2000.

7.6 Mitigation

Engineering

Assessing the impact of a solar superstorm and mitigating it through good design requires an appropriate environmental model. For routine space weather a range of models is available and owners and manufacturers are free to choose which they use and how. Resilient satellites are already designed to have a high probability of operating through very disturbed environments. However, these environmental models are based on observations that do not include a superstorm and thus satellites are not explicitly specified for such an event, although extrapolations of the models can be of relevance. Widely used models include NASA AE8 and AP8 [*Vette*, 1991] for radiation belt electrons and protons respectively. These are currently being updated to version 9 but are not yet released [*NASA GSFC*, 2012]. It is not yet clear if these new models will be appropriate for superstorm conditions.

Increasing the level of hardening of critical satellites to withstand an extreme event should be possible, but the development and enforcement of improved engineering standards that embrace extreme environments will be required. The major space standards [eg European Cooperation of Space Standardisation (ECSS)] include environments that are at least close to the Carrington event (as presently understood), especially with respect to cumulative effects such as dose and damage. However current satellite specifications do not typically cover low probability extreme events and thus might be exceeded by up to an order of magnitude. Operators and owners of critical satellite systems vital to national security and economic wellbeing should be strongly encouraged to ensure that their satellites can operate through and beyond an extreme storm event.

Heavy reliance on a single satellite design presents a greater risk of loss of service. Contingency plans should include the possibility of switching to or benefitting from other independent satellite services. Multi-constellation GNSS receivers will be the norm within a few years, and these receivers treat the aggregation of satellites from multiple constellations as one large constellation. Thus the individual GNSS receivers will be inherently robust to a satellite service denial.

Forecasting

Satellites are generally intended to operate autonomously but in extreme events it is important to anticipate the impact of the event so that operations staff can be better prepared. Operations teams usually have to manage several satellites from one control centre with minimum staffing levels so advance warnings of storm events will be beneficial to increase alert levels and draw in extra staff. Certain space systems can be placed in safe mode if adequate warning is given, however, most satellites will need to operate through the extreme event.

SEPs, giving rise to SEEs, arrive at close to the speed of light. Events afflicting spacecraft usually take up to several hours to peak and then can last several days. Consequently, providing the satellite survives the initial blast of high-energy particles, a judgement regarding the longevity of the event may be made.

Warnings of potential spacecraft charging events may be achievable in the medium term since they are linked to the arrival of Earth-directed CMEs. However, while observations of CMEs can provide some measure of warning the associated geoeffectiveness is dependent on the polarity of the interplanetary magnetic field. Only once this has been determined can actionable advice be provided to the satellite operators and, unfortunately, this cannot be determined until the CME reaches the L1 position. By this time, the warning has reduced to an hour at most [*Horne*, 2012] and probably 15-30 minutes.

Testing

Testing of components for space radiation effects relies on major facilities: these are generally beyond financial capability of any one aerospace company and are under continual financial threat. Government support and international collaboration are imperative to ensure continued availability.

7.7 Satellites – summary and recommendations

Summary

During an extreme space weather event, some satellites may be exposed to environments in excess of typical specification levels. This would increase microelectronic upset and failure rates and also create electrostatic discharge hazards. In addition, significant cumulative radiation doses could be received causing rapid satellite ageing. Because of the multiplicity of satellite designs in use today, there is considerable uncertainty on the overall behaviour of the fleet but experience from more modest storms indicates that some disruption to satellite services must be anticipated. Fortunately the conservative nature of spacecraft designs and their diversity is expected to limit the scale of the problem.

During the superstorm, our best engineering estimate, based on the 2003 storm, is that around 10% of spacecraft will experience an anomaly leading to an outage of hours to days but most of these will be restored to normal operations in due course. It is unlikely that outages will be spread evenly across the fleet since some satellite designs and constellations will inevitably prove more vulnerable than others by virtue of their detailed design characteristics. A few spacecraft might be lost entirely during the storm through a sudden damage mechanism such as electrostatic discharge.

In the months after the extreme storm, old satellites such as those in life extension mode may start to fail as a result of the ageing (dose) effects (we note that as many as one in 10 satellites in geostationary orbit are thought to be in life-extension mode). Recently launched satellites would be expected to survive the event but with higher risk thereafter from incidence of further (more common) storm events. Consequently, after an extreme storm, all satellite owners and operators will need to carefully evaluate the need for replacement satellites to be launched earlier than planned in order to mitigate the risk of premature failures. Obviously such a scenario has potential for creating a bottleneck in the satellite supply chain which will raise questions of priority.

Recommendations:

- Extreme storm risks to space systems critical to social and economic cohesion of the country (which is likely to include navigation satellite systems) should be assessed in greater depth; and users of satellite services which need to operate through a superstorm should challenge their service providers to determine the level of survivability and to plan mitigation actions in case of satellite outages (eg network diversification).
- The ageing effects of an extreme storm across the whole satellite fleet should be modelled to determine if a serious bottleneck in satellite manufacture or launch capacity could be created.
- Research should be actively pursued to better define the extreme storm environments for satellites and consequential effects. Collaboration with the NASA *Living with a Star* programme would be highly beneficial.
- Observations of the space radiation environment and its effects should be maintained and developed. Such measurements enable post-event analysis of satellite problems, the development of improved physical models which can be used in satellite design phases and the development of better warning and forecasting.

Box 2: More detailed description of single event effects (SEEs)

A single event upset (SEU) is generated when the critical charge in a semiconductor is exceeded causing the memory cell to change logic state with an associated change in the memory data word. For complex systems with large amounts of memory, it is important that recovery time is short compared to the time between SEE, so that inbuilt redundancy is adequate. During a large solar event, the time between individual SEE will be much shorter than it is in the nominal atmospheric radiation environment.

Multiple bit upset (MBU) occurs when the energy deposited in the silicon of an electronic component by a single ionising particle causes upset to more than one bit in the same word. These errors are mainly associated with memory devices, although any register is a potential target. Many memory manufacturers minimise the risk of MBU in modern memories by arranging the individual bits in a word non-contiguously. Because more than one bit in a single word are affected in the same event MBU can avoid detection through simple parity checks.

Multiple cell upset (MCU) occurs when the energy deposited in the silicon of an electronic component by a single ionising particle induces several bits in an integrated circuit (IC) to upset at one time. These errors are mainly associated with memory devices, although any register is a potential target. The occurrence of MCU is increasing as device feature size (and therefore the space between transistors gets smaller).

Single event burnout (SEB) takes place in high voltage electronic devices, where despite their comparatively large feature size they are also at risk of SEE and burn out from atmospheric radiation.

Single event transient (SET) is a class of non-destructive soft-error that can cause changes of logical state in combinational logic, or may be propagated in sequential logic, through 'glitches' on clock or set/ reset lines, etc. To date, this has not been a significant threat, as device behaviour has been dominated by errors in registers and memory cells – ie SEUs. However, as devices are further scaled down to smaller feature sizes and faster speeds, SETs, are expected to become more probable. In contrast to SEUs, which do not show clock frequency dependence, SETs depend significantly on the operating speed of the devices in question – slower devices are less vulnerable.

Single event functional interrupt (SEFI) is observed as an unexpected loss of functionality, or otherwise unexpected change of state of a device due to a particle strike in the internal state-machines of a device. Early reports were confined to microprocessor SEFIs, however, new generation data handling devices, such as advanced memories and field-programmable gate arrays (FPGAs), have also been found to be susceptible. Functionality is usually restored by power-cycling the device (soft SEFI) – but sometimes permanent damage is done (hard SEFI).

Single event gate rupture (SEGR) is caused when a heavy-ion passing through an insulator under high field conditions leads to the catastrophic breakdown of the insulator with a consequent thermal runaway condition. Such events may occur in the gate dielectric of non-volatile static random access memory (SRAM) or electrically-erasable programmable-read-only memory (EEPROM) during a write or clear operation. The increasing use of such technology in data handling systems means that SEGR is an increasing risk factor in COTS systems.

A single event latchup (SEL) will persist until power is removed from the device. Single event latchup can be avoided at component level by choosing devices that are not susceptible to SEL. Integrated circuit manufacturers can reduce the risk of SEL using fabrication techniques such as substrates that include controlled epitaxial layers and silicon on insulator technology.

8. Ionising radiation impacts on aircraft passengers and crew

8.1 Introduction

High-energy cosmic rays and solar particles incident on the Earth spawn a multitude of other high-energy particles through nuclear interactions in the upper atmosphere. These high-energy particles generate secondary particles that reach a maximum flux at about 18 km and are then progressively attenuated by the atmosphere so that only the most penetrating component can be measured on the ground. Typically, at aircraft cruising altitudes the flux of ionising radiation is ~ 300 times higher than at sea level and consequently these particles can have an impact on aircraft passengers and crew because of the increased exposure to ionising radiation.

It is well established that ionising radiation can be injurious to human health. The harm caused can be divided into stochastic effects, which are probabilistic in nature, and tissue reactions which are deterministic in nature. Tissue reactions have a threshold for induction whereas stochastic effects do not. Two quantities are defined to determine the incidence of these effects.

- The absorbed dose, which is a measure of the energy deposited per unit mass of tissue in the form of ionisation and excitation (the unit 1 gray or Gy = 1 J kg^{-1}). Tissue reactions are only encountered for energy deposition greater than 0.5 Gy [*ICRP*, 2012] which is typically only relevant in accident and emergency situations. Tissue reactions are caused by cell damage or killing, and the effects are seen within days, sometimes with fatal consequences. A solar superstorm comparable to the Carrington event would be far too small to cause tissue reactions for altitudes up to 18 km, so they will not be discussed further. However, this might be a problem for astronauts who could receive much higher doses.
- The effective dose, which is the absorbed dose weighted for the radiosensitivity of each organ and the type/energy of radiation. The effective dose is measured in sieverts (Sv) and the probability of cancer and hereditary effects is believed to correlate linearly with the effective dose, with 1 Sv corresponding to a 5.5% increase in lifetime risk of fatal cancer. Aside from severe accident and emergency situations, these are the risks to human health that are generally of concern.

The field of radiation protection is overseen by the International Commission on Radiological Protection (ICRP), which produces periodic recommendations on all aspects of the field [*ICRP*, 1991; 2007]. The recommendations of the ICRP are invoked as EC Basic Safety standards [*Council of the European Union*, 1996] which are then followed into UK legislation as the Ionising Radiations Regulations published by the Health and Safety Executive [*Health and Safety Executive*, 1999]. Following the 2007 recommendations of the ICRP there has not yet been a revision of the EC Basic Safety Standards, but the IAEA has published international basic safety standards [*IAEA*, 2011].

The ICRP divides radiation exposures into occupational, medical and public, with different recommendations applying to each category of exposure. Also, in terms of optimisation, ICRP, divides exposure situations into "planned", "existing" and "emergency" [*ICRP*, 2007]. These apply to both occupational and public exposures with the annual dose limit for occupational exposures set to 20 mSv and that for public exposures set to 1 mSv. The 1996 EC Basic Safety Standards and 2011 International Basic Safety Standards explicitly include exposures of air crew as occupational exposure, but air travel is not considered for either business or leisure travel. Pregnant air crew are restricted to 1 mSv per declared period of pregnancy. FAA guidelines limit exposure in pregnancy to no more than 0.5 mSv in a month.

Long haul crew typically receive an occupational dose of 4 to 6 mSv per year [*Lindborg et al.*, 2004.] with 6 mSv being specified as an action level in Article 42 of EU Directive 96/29 Euratom that was adopted in the UK on 13 May 1996 and enacted in an amendment to the Air Navigation Order. For comparison, the UK average natural background dose rate at sea level is 2.2 mSv per year (from rocks, radon, internal sources and cosmic rays) [*Watson et al.*, 2005] while medical diagnostic doses range from 0.014 mSv for a chest X-ray, to 6 mSv for computerised tomography of the chest [*Wall et al.*, 2011] and higher for other interventions [*Fazel et al.*, 2009]. The average medical exposure in the UK is 0.4 mSv per year [*Watson et al.*, 2005].

Under normal conditions, the geomagnetic field confines the radiation effects from solar energetic particles to high latitude paths, but this includes flights on some of the busiest routes, such as those from UK to North America and Japan. There have only been a few measurements of solar particle enhancements on board commercial flights and these have mostly come from the now retired Concorde which was compelled to carry a monitor [*Dyer et al.*, 1990]. Recent observations have also been made in April 2001 and October 2003 [*Getley et al.*, 2005; *Getley et al.*, 2010]. These observations have enabled calculations to be made for other events and flight routes. For example, during the major event on 23 February 1956, it has been calculated that there was a 300-fold increase (over background) at high latitudes and 12km altitude, with corresponding dose rates for contemporary aircraft and flight paths of several mSv hr^{-1}. This could have caused some air crews to exceed the current annual occupational flight limits in just one flight [*Dyer et al.*, 2007]. Fortunately, such large events are rare and it is estimated that since 1942 only six events would have resulted in a dose in excess of 1 mSv on a flight from London to the west coast of the USA [*Lantos and Fuller*, 2003]. More recently, on 20 January 2005, a major event caused a factor 50 increase in the Antarctic region corresponding to effective dose rates of ~ 3 mSv hr^{-1} at cruising altitudes [*Dyer et al.*, 2007]; [*Butikofer et al.*, 2008]. Fortunately for aviation, this was very short-lived and localised such that the northern hemisphere rates were an order of magnitude lower.

The International Civil Aviation Organisation has recognised the potential issues of space weather and has commenced activities to provide operational requirements, guidance and the potential for space weather information services [*ICAO*, 2010].

© vivekchugh, www.sxc.hu

8.2 Consequences of an extreme event

If the geomagnetic field is highly disturbed when the particles arrive, then much lower latitudes may be exposed with significant exposure down to the tropics.

At conventional cruising altitudes (33,000 to 39,000 feet), a superstorm could result in a radiation dose to aircrew and passengers of greater than 20 mSv. This is greatly in excess (by a factor 20) of the annual dose limit for a planned exposure to the general public and comparable or in excess of the annual occupational dose limit of 20 mSv for workers. However, a dose of 20 mSv implies an increased lifetime cancer risk of only 1 in 1,000 for each person exposed which should be considered in the context of a lifetime cancer risk of about 30% [*ONS*, 2012].

Radiation emergencies are essentially dealt with by consideration of individual risk. Conventional nuclear emergencies and accidents have led to either very large exposures of individuals or had the potential for very large exposures. They are characterised by the possibility of taking mitigating action and thereby reducing the risks from significant exposure of individual workers or members of the public. The potential for significant individual risks resulting from radiation exposure on commercial flights seems small, although this must be qualified by acknowledging the uncertainty in the maximum dose rates that could result at aviation altitudes.

If a major solar storm took place, then a large number of members of public and air crew could be exposed. During 2011, UK aircraft operators uplifted 111,082,766 passengers, which corresponds to an average of ~304,000 passengers a day. We assume that this is a global event and experienced on both the day and night sides of the Earth. This is somewhat pessimistic, but we will optimistically assume that in the event of a solar superstorm the aircraft can land or reduce altitude within one hour. Given these assumptions ~13,000 passengers (on UK carriers alone) could be exposed to ~20 mSv. This would result in widespread public concern and an urgent need for advice and reassurance on the doses received. .

While it is tempting to compare a solar superstorm with other radiation emergencies in terms of collective dose, it is more relevant to compare with domestic radon exposure; radon is also background radiation and the action level is set according to individual risk. In the UK, the action level for which remedial measures in homes

are advised, is set to 200 Bq m^{-3}, which corresponds to an annual effective dose of about 10 mSv y^{-1} [*McColl and Prosser*, 2001]. The target level for UK homes is half this value, but it still equates to about 5 mSv y^{-1}. This latter dose rate is about a quarter of the estimated dose received by passengers during a solar superstorm, and it represents an ongoing exposure rather than a one-off dose.

8.3 Mitigation

Pre-event planning

The impact on passengers and aircrew of an extreme solar storm might need to be considered as an emergency situation, where reference levels define doses or dose rates above which actions to reduce exposure are necessary. These reference levels would need to be applied based on pre-event considerations of the risk from exposure, the effectiveness of remedial measures and the consequences of those remedial measures. The ICRP does not specify values for emergency reference levels but sets bounds of 20 mSv to 100 mSv; hence the lower limit of concern for emergencies coincides with the estimates of individual doses from a Carrington scale event. Emergency plans tend to be drawn up on the basis of probability and impact, with a probability threshold estimate of 10^{-5} per annum being used. It is not clear how probable a solar superstorm would be, but a per annum risk between 10^{-2} and 10^{-3} would seem reasonable.

In its 2007 recommendations, the ICRP defined radiation emergencies as: "*situations that may occur during the operation of a planned situation, or from a malicious act, or from any other unexpected situation and require urgent action in order to avoid or reduce undesirable consequences.*" In its follow-up to those recommendations, it stated that "*The Commission recommends that plans should be prepared for all types of emergency exposure situation: nuclear accidents (occurring within the country and abroad), transport accidents, accidents involving sources from industry and hospitals, malicious uses of radioactive materials, and other events, such as a potential satellite crash*" [*ICRP*, 2009]. These statements do not specifically include or exclude an event such as a solar superstorm.

In its document on the application of the 2007 recommendations of the ICRP, the HPA stated that "*emergency situations are likely to be characterised by one or more of the following: significant uncertainty concerning current and future exposures, rapidly changing rates of potential exposure, potentially very high exposures (ie those with the potential to cause severe deterministic injury), and loss of control of the source of exposure or release.*" [*HPA*, 2009]. While the potential to cause deterministic injuries (tissue reactions) at commercial aviation altitudes is small, a solar superstorm would conform with the other characteristics. Taken together with the ICRP definitions, there is a case for considering a solar superstorm as a radiation emergency. It is possible that doses to a specific organ or tissue, such as the lens of the eye, could require consideration, though this is more likely to have occupational implications rather than emergency ones. The definitions of what constitutes an emergency are based on individual risk rather than collective dose, and the individual risk associated with a solar superstorm is likely to be low.

Aspects of a solar superstorm that mitigate against its consideration as a radiation emergency are its short duration and the lack of scope for taking action to reduce doses. If real time monitoring of dose rates improves, either in terms of the available satellite data or through on-board monitors, then it may become possible to take considered actions to reduce doses during a solar storm. Currently, however, the data available may not be processed until after event is finished; which could limit the radiation protection response to advice on the doses received.

When a Carrington-scale event, or even a storm as large as that from 1956, next occurs, there will be many members of the public in the air who will be exposed to additional radiation. It will be important to ensure that accurate information is provided to the people affected through all channels after the event. For example, advice will be needed on the levels of exposure experienced, the need for any medical checks (very unlikely), the advisability of further flights in respect of additional exposure and also any further work-related exposure. Special advice for pregnant women may be required.

Emergency plans are in place for conventional nuclear emergencies, with a view to covering all reasonably probable extreme events. There is therefore a case for the development of a specific emergency plan for public exposures from a solar superstorm, so that ad hoc decisions would not have to be made during the event. Such a plan would enable quick decisions to be made on the options available for reducing exposure: for example, reduction in altitude, rerouting and remaining grounded. These all have adverse consequences that need to be balanced against the radiation dose savings that can be made. The main requirement may be the provision of accurate and prompt information to the public. If there is another Carrington-scale event, members of the public who have flown will seek reassurance about health risks, especially if travelling while pregnant or with children. Those who have booked to fly will expect information on the risks for a significant period after the event.

Forecasting

Solar energetic particles from the solar superstorm arrive at close to the speed of light and prediction is essentially impossible unless solar precursors can be identified. The conditions on the Sun that produce spectra with large amounts of high-energy particles are currently not well understood. Near-term solutions based on such warnings are unlikely, but there is hope that in the medium to long term an approach based on precursors will provide the necessary skill to provide actionable advice.

Real-time monitoring

Ground level monitors are diminishing in number and this limits their ability to provide adequate directional and spectral information. Moreover, by the time a warning can be fed to aircraft its benefit is reduced because the maximum dose rates are reached in a matter of ten minutes or so.

Satellite-based warning systems can also be employed, but current satellite detectors use low energy particle thresholds that are more relevant to spacecraft operations than aircraft. This can result in numerous false alarms as well as missing other events. Even so, a sensible first step is to provide an alert service relaying information about current atmospheric radiation conditions to aviation authorities, airlines, pilots and other parties as part of normal meteorological reports: mitigating action could then be taken (eg to delay take-off) in line with the operating procedures of each affected body. These would preferably use a threshold of 300 MeV rather than those currently employed by the National Oceanic and Atmospheric Administration (NOAA) (> 10 MeV, >50 MeV and >100 MeV).

On-board, real-time monitoring is the only practical way to rapidly detect raised radiation levels that would allow action to be taken to mitigate the effects of particles from a solar superstorm. A height reduction can bring great benefit, eg a 30% reduction per 1 km of altitude, but unilateral and uncoordinated height reductions are highly risky and probably more risky than staying at altitude. An appropriate warning level at a rate that would exceed ~1 mSv in one flight - similar to danger levels for SEEs in avionics - is probably appropriate but this will require study.

Concorde was compelled to carry a radiation warning monitor [*Joint Aviation Authorities*, 2001] as are all commercial aircraft operating above 49,000 feet. A similar requirement has not been extended to other aircraft despite the fact that subsonic routes at high latitude are more exposed than Concorde because of the higher latitude effect and longer flight durations outweighing the influence of the reduced altitude [*Dyer et al.*, 2007]. Consequently, the avionic infrastructure to implement this mitigation approach is not in place and the cost might be a disincentive. However, it must be noted that the current situation of individual airline response to false positive NOAA warnings can result in wasted fuel and flight delay costs that could be avoided if reliable in-flight measurements were available. It should also be noted that many pilots would like information on the radiation levels to be immediately available to them so that they can make informed decisions. For example, the European Cockpit Association, which represents 38,000 commercial pilots, has written to the European Commission recommending that a visible warning should be provided.

Post event analysis and management of public concern

Post-event analysis will inevitably be needed to reassure the public. Crude estimates of the dose may be made using ground level and space monitors but the accuracy is limited by the lack of data, to factors between two and ten. In this context there is no substitute for onboard monitors.

8.4 Passenger and crew safety – summary and recommendations

Summary

Passengers and crew airborne at the time of an extreme event would be exposed to an additional dose of radiation estimated to be up to 20 mSv, which is significantly in excess of the 1 mSv annual limit for members of the public from a planned exposure and is comparable to about three CT scans of the chest. Such levels imply an increased cancer risk of 1 in 1,000 for each person exposed, but this should be considered in the context of a lifetime risk of fatal cancer which is about 30%.

No practical method of forecasting is likely in the short term since the high-energy particles of greatest concern arrive at close to the speed of light. Mitigation and post-event analysis is needed through better onboard aircraft monitoring. An event of this type will generate considerable public concern.

Recommendations

- Consideration should be given to classifying solar superstorms as radiation emergencies in the context of air passengers and crew. If such a classification is considered appropriate an emergency plan should be put in place to cover such events. While the opportunities for dose reduction may be limited, appropriate reference levels should be considered and set, if appropriate.
- Atmospheric radiation alerts should be provided to the aviation industry and concepts of operation should be developed to define subsequent actions based on risk assessment (eg delaying take-offs until radiation levels have reduced).
- Consideration should be given to requiring aircraft operating above a specified altitude (25,000-35,000 feet) to carry a radiation sensor and data logger. This would enable post-event analysis to allay public concerns and to manage any health risks.
- Consideration should be given to the sensor being visible to the pilot and to the development of a concept of operations whereby the pilot requests a reduction in altitude (noting that modest reductions can be beneficial) under solar storm conditions.
- Post-event information and advice on the radiation doses received should be available to passengers and crew (especially to pregnant women).

9. Ionising radiation impacts on avionics and ground systems

9.1 Introduction

Background galactic cosmic rays give rise, through collisions in the upper atmosphere to a cascade of secondary particles. These include neutrons, protons, electrons and muons with the flux of secondary particles much stronger at aircraft cruising altitudes than on the ground.

SEPs associated with solar storms also generate secondary particles in the upper atmosphere with the most energetic generating a ground level signature. When large increases in the flux of secondary neutrons are seen on the ground this is known as a ground level event (GLE). SEPs arrive within minutes of the optical flare signature since they travel at a significant fraction of the velocity of light.

These high-energy neutrons and protons are problematic because they interact with semiconductor material – on the ground or on board aircraft – where they give rise to lower energy protons, nuclear recoils and other secondary charged particles. These deposit a small amount of electronic charge causing single event effects (SEE), a generic term previously described in Box 2. With early generation large geometry devices, this electronic charge was small compared with the critical charge required to affect the device. However, increased integration with corresponding smaller geometry devices has brought with it an increased vulnerability to charge deposition.

The largest GLE on record (since measurements began in 1942) occurred on 23 February 1956. This GLE exhibited a 50-fold increase in neutron flux over the background for a few hours. It has been calculated that this event would have produced a 300 fold increase at 12 km compared with background conditions for this altitude [*Dyer et al.*, 2003]. Unfortunately, there is currently no good estimate of the flux corresponding to a Carrington superstorm and this obviously hinders our impact assessments. Our best estimate is that the environmental threat for a Carrington level superstorm is four times larger than the 1956 event, corresponding to a 200 fold ground level increase and a 1200 fold increase at 12 km.

9.2 Engineering consequences on avionics of an extreme event

Since the early 1990s there have been a number of open literature recorded instances of SEE in avionics at background levels of radiation [e.g. *Normand*, 2001; *Normand et al.*, 1997; *Olsen et al.*, 1993]. Increases in high-energy particles above this background, associated with a superstorm are then of concern because they increase the probability of an SEE in aircraft systems.

Normand [2001] illustrates the importance of SEE in the context of the background cosmic ray flux. He reported that upsets in an autopilot correlated with cosmic ray fluxes (as a function of latitude variation), and the average autopilot upset rate of one for every 200 flight hours was consistent with predictions based on ground irradiation of the same static random access memory chip (SRAM) [*Sims et al.*, 1994]. If these rates are scaled by calculated fluxes for the February 1956 event, upsets could have occurred more than once an hour for the particular autopilot under consideration if the system had reset after each upset [*Dyer et al.*, 2003].

In their final report [*ATSB*, 2011] on an incident near northwest Australia, the Australian Transportation Safety Bureau eliminated all environmental causes other than SEEs for false signals generated by an Air Data Inertial Reference Unit. In their lessons for new systems, they state "SEEs are a potential hazard to aircraft systems that contain high-density integrated circuits. Designers should consider the risk of SEE and include specific features in the system design to mitigate the effects of such events, especially in systems with a potentially significant influence on flight safety".

A superstorm would be likely to cause an atmospheric radiation storm lasting 12 hours or even more. It would be widespread, possibly extending down to the tropics if there were also a geomagnetic storm in progress. Consequently, all flight routes from the UK could be affected. As with spacecraft, the wide variety of avionic system designs makes a blanket assessment difficult, but during a storm period the most likely effects would be increased workload for pilots and air traffic controllers in order to handle aircraft systems failures.

9.3 Engineering consequences of an extreme event on ground systems

The atmosphere provides considerable protection to ground level systems and for this reason this study focuses on airborne systems. Yet we know that SEEs are occasionally seen on ground systems [*Normand*, 1996; *Ziegler et al.*, 1996] and are likely to be of increasing concern in the design of automotive electronics, miniaturised devices and safety-critical systems in general. Medical devices such as implantable cardiac defibrillators have been shown to give errors from cosmic rays [*Bradley and Normand*, 1998]. Upsets in major computing facilities correlate with altitude and, since a major server suffered significant outages and caused economic losses, certain server technologies have been tested in neutron radiation facilities [*Lyons*, 2000]. In light of this evidence, safety-critical ground systems such as those in nuclear power stations should consider the impact of superstorm radiation at ground level within its electronic system reliability - and safety-assessments. In the case of nuclear power a Carrington event may not be a sufficient case since relevant timescales for risk assessment may be as long as 10,000 years.

9.4 Mitigation

Avionics

Avionics are some of the most sophisticated but safe technological systems in common use. Avionics routinely incorporate redundant and majority voting systems to mitigate hazards – including the effects of solar storms (ground based safety critical systems also embody similar approaches making them also architecturally resilient to space weather). Notwithstanding these design approaches, specific engineering steps could be required to minimise the risk from SEPs.

Since 2006, a series of atmospheric radiation standards has been developed by the International Electrotechnical Commission (IEC) [*Edwards et al.*, 2004]. These are IEC 62396-1 Ed1, 2012 [*IEC*, 2012c] ; IEC 62396-2, 2012 [*IEC*, 2012a]; IEC TS 62396-3, 2008 [*IEC*, 2008c]; IEC TS 62396-4, 2008 [*IEC*, 2008b] and IEC TS 62396-5 [*IEC*, 2008a]. The IEC publications have the form of recommendations for international use, and are accepted by IEC national committees

Second or third party accreditation through the International Electrotechnical Commission Quality (Assessment System for Electronic Components) (IECQ) to the IEC technical specification, IEC/TS 62239-1 Ed.1, [*IEC*, 2012b] for electronic *component management* is increasing within the aviation industry. The specification contains a requirement (clause 4.3.7) that component level atmospheric radiation effects shall be assessed and documented in accordance with IEC 62396-1 Ed.1, 2012 section 9. This specifies quiet-time and moderate events (nominal environment). Solar storms are also mentioned in section 5.6 of IEC 62396-1 Ed.1, 2012 where there is a specification of the SEE rates which could be experienced during a superstorm event.

The IEC standard on avionics atmospheric radiation (IEC 62396-1 Ed.1, 2012 section 9) provides a methodology for documenting compliance of avionics which will be operated within an atmospheric radiation environment. This standard recommends that once the initial design is complete, all SEE sensitive electronic components should be identified and their atmospheric radiation susceptibility determined. Guidance for obtaining this information is contained within technical specification IEC 62396-2, 2012. If the component level SEE cannot be mitigated within the equipment design the standard recommends that the SEE be mitigated at the equipment or systems level. If this is not feasible, the part or equipment design might need to be changed.

For aircraft systems (as opposed to components) radiation standards and industry awareness are less developed. This is

progressing through the revision of the SAE/EUROCAE Aerospace Recommended Practices, ARP 4761, which is exploring how to introduce consideration of SEE to the system safety assessment process.

The impact on equipment and systems of extreme events might be determined by irradiating the equipment in a wide area neutron radiation beam with the appropriate energy, spectrum and fluence, as described in technical specification IEC62396-2:2012. Levels comparable to an extreme event such as the Carrington Event at aircraft altitude would be required for such a determination. For avionics there are currently only two or three facilities worldwide that could generate radiation levels representative of the atmospheric environment. This situation should improve in the next two years with the opening of a dedicated beam-line (ChipIR) ISIS Spallation Neutron Source at the Rutherford and Appleton Laboratory in the UK. The ChipIR wide beam facility will enable complete powered and monitored equipment and systems to be irradiated at radiation levels equivalent or greater than a Carrington event to verify equipment SEE tolerance. However, to make this worthwhile, international aircraft industry cooperation will likely be necessary to agree on standardisation of test methodology and equipment design techniques to determine the most effective means of addressing this phenomenon.

Operational mitigation

As already described in the context of air passenger safety considerable reductions in superstorm radiation can be obtained by reductions in flight altitude (30% per km of altitude reduction) and possibly rerouting aircraft to lower latitudes. However, uncoordinated altitude reduction introduces risk. Even coordinated height reduction carries its own risk by increasing aircraft fuel burn which results in an aircraft possibly needing to re-route. A risk-benefit analysis would be required to evaluate this option.

Situational awareness of superstorm radiation – suggesting actions ranging from fastening seatbelts (to mitigate against any unexpected changes in height and direction introduced through the avionics) to altitude reductions or rerouting – can be provided to the pilot from ground, space and on board sensors. The latter is likely to be preferable from a technical standpoint because the measurement will be made where the risk occurs.

SEPs exhibit a wide spectrum of energies and it is currently impossible to forecast the spectrum – and danger – of the particles. Moreover, the first particles arrive within a few minutes of seeing the associated solar flare. Consequently, no practical forecast of the event, nor its associated impact can currently be provided.

9.5 Avionics and ground systems – summary and recommendations

Summary

Very little documentary evidence could be obtained regarding the impact of solar energetic particles on ground infrastructure and it is consequently difficult to extrapolate to a solar superstorm.

More documentary evidence of normal and storm time impacts is available in respect to avionics - no doubt because the operating environment has a higher flux of high-energy particles. Our estimate is that during a solar superstorm the avionic risk will be ~1,200 times higher than the quiescent background risk level. We note that the more critical avionics, such as engine control, are designed to mitigate functional failure at component, equipment and system level and consequently they will be partially robust to solar energetic particles.

Solar energetic particles exhibit a wide range of energies and it is currently impossible to forecast the spectrum of particles that might erupt from the Sun. Moreover, because the first particles arrive within a few minutes of the associated solar flare no practical forecast of an event and its consequences can currently be provided.

Recommendations:

- Ground-and space-derived radiation alerts should be provided to aviation authorities and operators. The responsible aviation authorities and the aviation industry should work together to determine if onboard monitoring could be considered a benefit in flight. Related concepts of operation should be developed to define subsequent actions, eg fastening of seatbelts or reducing altitude if the storm occurs on route or, if still on the ground, delaying take-offs until radiation levels have reduced. This could even include reductions in altitude if deemed beneficial and cost-effective.
- The responsible Aviation Authorities and the aviation industry should work towards requiring that future aircraft systems are sufficiently robust to superstorm solar energetic particles, including through the appropriate standards in atmospheric radiation mitigation – for example *IEC 62396-1* Ed.1:2012).
- Since the impact of a solar superstorm on ground-based systems cannot be clarified, further consideration is required. Systems with very high safety and reliability requirements (eg in the nuclear power industry) may need to take account of superstorm ground-level radiation on microelectronic devices within the system.

10. Impacts on GPS, Galileo and other GNSS positioning, navigation and timing (PNT) systems

10.1 Introduction

Transmissions from Global Navigation Satellite Systems (GNSS), including the Global Positioning System (GPS), GLONASS and Galileo, provide positioning and navigation services. The car satnav is perhaps the best known exemple, but ship and aircraft navigation, tracking of products and deliveries and emergency service dispatch are all increasingly dependent on the GNSS position and navigation services. GNSS also provides very accurate (tens of nanoseconds) timing services. Some telecommunications services use timing signals from GPS satellites to synchronise networks to facilitate data flow and the financial services industry uses GNSS to time-stamp transactions in high speed trading.

Ionospheric space weather affects GNSS transmissions in a number of ways and there are a number of compensatory approaches [*Cannon*, 2009; *Hernández-Pajares et al.*, 2011; *Kaplan*, 2005; *Mannucci et al.*, 1999; *Walter et al.*, 2000].

Coincident with the optical signature of the solar flare, solar radio bursts (SRBs), lasting for a few minutes to a few tens of minutes, may be detected at GNSS frequencies. During particularly active periods, and especially associated with a superstorm, there may be a number of bursts over the course of several days. SRBs can cause loss of lock in GNSS receivers [*Cerruti et al.*, 2006; *Cerruti et al.*, 2008] located in the sunlit hemisphere, due to an increase in radio noise interference. The effect of a SRB on GNSS was first seen on 5 December 2006, notably at solar minimum. This SRB was measured at 1 million solar flux units (one solar flux unit = 10^{-22}Wm^{-2}Hz^{-1}) with smaller events on 6, 13 and 14 December that year. There was sufficient energy at GPS frequencies to interfere with receiver operation for 10 to 20 minutes on each occasion. Position data from several semi-codeless (and therefore not robust) receivers in the International GNSS Service (IGS) network were lost [*Carrano et al.*, 2009].

Arriving some 12-24 hours behind these prompt effects are the plasma particles associated with the CME. The latter indirectly cause perturbations to the ionospheric electron density over large portions of the globe and cause large-scale (10-1000km) wave-like structures and gradients in the ionosphere. Small-scale structures (less than 1km) are also generated and these cause scintillation (ie rapid changes in amplitude and phase) of the signals. Scintillation is not often observed over the UK and normally occurs at equatorial and high latitudes, where it is a serious and limiting problem. During an extreme space weather event, it is likely that ionospheric scintillation will be observed at UK latitudes and indeed globally.

OUR WORKING ASSUMPTION IS COMPLETE LOSS OF SERVICE FOR A PERIOD OF ONE DAY, HOWEVER, IT IS QUITE POSSIBLE THAT THERE WILL BE PERIODS WHEN AT LEAST ONE SATELLITE SIGNAL CAN BE RECEIVED AND TIMING SYNCHRONISATION REGAINED.

Amplitude scintillation, that causes rapid changes in the carrier-to-noise ratio, can lead to loss of carrier tracking in all receivers.

Phase scintillation that sufficiently disturbs the carrier phase causes the receiver phase tracking loop to lose lock impacting the reception of the important navigation data message which includes the satellite empherides. The code tracking loop, that measures range to the satellite, is fairly robust to phase scintillation and usually remains locked.

Loss of phase lock in receivers used in high integrity applications (eg aviation) is particularly important as these receivers need to regularly read the satellite data message. To mitigate this, satellite based augmentation systems (SBAS), such as WAAS and EGNOS, employ a message symbol rate of 500 symbols s^{-1}, together with a rate one-half encoder and repeated messages to deal with burst errors.

Unfortunately, our estimates of the disruption to GNSS caused by scintillation resulting from a superstorm are poor. Our working assumption is complete loss of service for a period of one day, however, it is quite possible that there will be periods when at least one satellite signal can be received and timing synchronisation regained. For critical infrastructure, our working assumption is extended to loss of service for a period of three days and includes an allowance for re-initialisation of the satellite constellation (or augmentation system) after the storm.

10.2 GNSS for navigation

Single frequency civilian navigation systems.
All GNSS systems have the option of operating in a single frequency mode and are dependent on a compensating model of the signal delay due to the electron density in the ionosphere. On average, the model compensates for ~50% of the ionospheric delay.

At the start (and end) of an extreme event when the ionosphere is highly disturbed, the position and navigation solution from a single frequency GNSS receiver will be significantly degraded due to a large mismatch between the actual ionosphere and the average model assumed by the receiver. Moreover, during these periods it is likely that, due to scintillation, not all satellites will be tracked and there will be a consequential dilution of precision. Single frequency

GPS is specified to provide horizontal errors below approximately 40 m for around 99% of the time. Typically, GPS errors are below 5 m. At the start and end of an extreme space weather event errors might be measured in 100s of metres.

During the main phase of the event, very significant electron density perturbations will occur and it is likely that scintillation will occur on all satellite paths. During this period, it is likely that positional and navigational solutions will be completely lost.

Dual frequency civilian navigation system.

GPS is being enhanced with a second open (civil) signal at the current L2 frequency (1227 MHz) and a new L5 frequency (1176 MHz). These frequencies will become fully operational over the next few years. Galileo will also add to the number of signals available for civil operations.

Dual frequency operation obviates the need for an ionospheric model and receivers equipped for dual frequency operation will be able to maintain accurate operation even in the event of significant electron density perturbations and gradients. However, the dual frequency receivers do not mitigate scintillation which will in fact be more prevalent at the lower frequencies. This means that during the start and end phases of a storm, there will be significant dilution of precision and during the main phase of the event position and navigation solutions will likely be lost. During a superstorm the best that can be expected is a marginal improvement over single frequency operation.

Augmented navigation systems and other differential systems

The preceding space weather vulnerabilities also apply to augmented navigation systems such as those designed for aircraft navigation and landing. These include the US Wide Area Augmentation System (WAAS) and the European Geostationary Navigation Overlay Service (EGNOS).

During the large geomagnetic storms in October 2003, vertical navigation guidance was unavailable from WAAS for approximately 30 hours [*FAA*, 2004]. It should be noted that WAAS horizontal navigation guidance remained continuously available and the integrity of the system was not lost. SRBs also affect the WAAS availability. The December 2006 SRB (the largest on record) caused a WAAS loss of vertical guidance for 15 minutes. As with the 2003 storms, operational integrity was maintained.

In an extreme event, the system metrics will be impaired at the start and end phases and service loss is likely during the main phase. Augmented and differential systems are particularly sensitive to medium scale spatial gradients in the ionosphere which will be prevalent during a solar superstorm. Furthermore, augmented systems (currently) use a type of receiver at their reference stations that tracks the phase of the military encrypted GPS signals. These semi-codeless tracking receivers require significantly higher signal-to-noise ratios than normal code and carrier tracking. This results in the receivers being extremely sensitive to phase scintillation on the L2 signal caused by a disturbed ionosphere. Under superstorm conditions, spatial gradients and tracking loss are likely to combine to cause a break in service of precision approach and other high integrity operations. Under these circumstances, SBAS is likely to support the reversionary non-precision approach (vertical navigation based on baro-altimetry).

10.3 GNSS for time and timing

Background

Many industrial applications require time or timing with appropriate accuracy, stability and reliability in order to operate effectively – or at all.

- Constant digital traffic flow across a telecommunications network requires accurate timing to ensure uninterrupted traffic throughput.
- The next generation of mobile data communications (dealt with in Chapter 12) will require accurate time slot alignment – now referred to in the ITU standards as time/phase.
- National power generation and distribution requires accurate time and time/phase.
- Server clocks need to keep the same time of day across the world, for example to support billing systems and financial trading.

Synchronising these time and timing applications to a common (UTC traceable) clock was made easier with the emergence of the GPS system.

National or core telecom network traffic timing

The UK national telecom networks first derived time from GPS in 1996, but with mitigation techniques to ensure complete loss of GPS did not compromise network timing.

Curry [2010] has explored the issue of holdover in networks when GPS is denied. This analysis has demonstrated that networks, and particularly critical national infrastructure networks, must be provisioned with rubidium or better (eg caesium) oscillators to meet the requirement for three day holdover in the event of a superstorm.

Most UK wireline *core* telecom networks, for both fixed line and mobile backhaul, now use GPS timing backed up locally by rubidium oscillators. In the event of GPS denial, the network timing is referenced to caesium atomic oscillators meeting the ITU G.811 standard – the current UK national network infrastructure, therefore, has the requisite holdover oscillators already in place. However, as more edge networks (as opposed to core networks), higher data rate packet-based networks and enterprise networks are deployed it is important that space weather vulnerability is regularly assessed.

GNSS for time/phase applications

Time/phase is the alignment of elements in a network to a common time base and most usually this is UTC which is easily derived from GPS. Typical examples of this requirement are energy networks which use it

for synchrophasor operations and future smart grid applications. Time/phase is also needed in the time division duplex (TDD) variants of the 4G mobile networks. These are dealt with in Chapter 12.

GNSS for time-of-day applications

Some computer systems require traceable and accurate time-of-day in order to timestamp financial transactions, provide billing information, measure an event time and duration or log an alarm. While network time protocol (NTP) servers exist on the internet, these are sometimes not secure or accurate enough for mission – or commercially-critical applications. Consequently, some organisations implement their own NTP servers. These locally deployed NTP servers usually use GNSS as the source of UTC and back this up with high-grade oven-controlled crystal oscillators or rubidium oscillators. Loss of GPS would result in the NTP master clock progressively becoming less accurate and so the vulnerability is application dependent.

We can identify vulnerabilities according to applications that require clock accuracies of 1s, 1ms and 1µs. Analysis by *Curry* [2010] shows that an extreme space weather event will only have a severe impact on time-of-day applications where accuracies of better than a microsecond are required over the projected three days outage period. Emerging applications needing accuracy better than a microsecond include time stamping of high frequency trading in the financial services sector and smart grid applications.

If UTC alignment across multiple locations cannot be maintained against the temporary loss of GNSS, then other appropriate mitigation solutions might be considered. These include using network time and timing from the core (such as PTP) or other (than GNSS) off air sources of UTC-traceable time synchronisation such as eLoran signals. These are broadcast from Anthorn in the UK and are transmitted at 100 kHz and consequently also have (different) space weather vulnerabilities.

10.4 GNSS - summary and recommendations

Summary

GNSS positioning, navigation and timing are ubiquitous to our lives and important in a number of safety of life applications; and their unmitigated loss resulting from a superstorm would have severe social and economic repercussions.

Assuming that the satellites – or enough of them – survive the impact of high energy particles, we anticipate that a solar superstorm will render GNSS partially or completely inoperable for between one and three days. The outage period will be dependent on the service requirements. For critical timing infrastructure, it is important that holdover oscillators be deployed capable of maintaining the requisite performance for these periods. UK networked communications appear to meet this requirement.

With current forecast skills, it is inevitable that aircraft will be flying and ships will be in transit when the superstorm initiated. Aircraft use differential and augmented systems for navigation and in the future possibly for landing. With these applications set to increase, the potential for significant impact from an extreme space weather event will likewise increase. Fortunately, the aviation industry is highly safety conscious and standard operating procedures appropriate to other emergency situations are likely to provide sufficient mitigation to an extreme space weather event. These include other terrestrially based navigation systems. The challenge will be to maintain those strategies over the long term as GNSS become further bedded into operations.

This study has not explored the impact on ship navigation, but recognises that precision and non-precision navigation by GNSS is widespread and standard operating procedures will be needed to educate sailors on how to recognise a solar superstorm and deal with it in the possible absence of HF and satellite communications.

Recommendations

- All critical infrastructure and safety critical systems that require accurate GNSS derived time and or timing should be specified to operate with holdover technology for up to three days.
- Care should be taken to ensure that this requirement extends to cabled and fibre communications systems.
- Backup position, navigation and time services such as eLoran service (which in the UK is broadcast from the Anthorn transmitter) should be considered as an alternative to GNSS for UTC traceable time, timing and location based services. We note that the USA has set-up the Alternate Position Navigation and Time (APNT) programme that is working to reconfigure existing and planned ground navigation aids (e.g. Distance Measuring Equipment) and the ground based transmitters associated with automatic surveillance) so that they can back up GNSS well into the future.
- Since loss of GNSS would have a major impact on lives in general, and on shipping and air travel specifically, warnings of events should be provided through a nationally recognised procedure, possibly involving government crisis management arrangements, NATS, the CAA and the General Lighthouse Authority. Criteria should be established for the re-initiation of flying when it is safe to do so.

11. Impacts on radio communication systems

11.1 Introduction

Space weather events can affect the operation of radio systems in a number of ways. The effects may be prompt (ie they occur soon after the initial event on the sun) or delayed (ie some days later).

The following sections briefly outline the possible impacts on:

- terrestrial mobile communications networks
- HF communications and international broadcasting
- mobile satellite communications
- satellite and terrestrial broadcasting.

11.2 Terrestrial mobile communication networks

Systems considered in this section include:

- 2G public mobile communication systems, mainly based on the 3GPP GSM specification in the UK (mainly voice and data)
- 3G public mobile communication systems, mainly based on the 3GPP UMTS and HSPA specifications in the UK (higher rate data)
- 4G public mobile systems, expected to be based mainly on the 3GPP LTE and LTE-Advanced specifications in the UK, and to a lesser degree the IEEE 802.16 "WiMAX" technologies (even higher rate data)
- analogue private mobile radio, as used for a variety of business and security services, which are based in the main on FM technology according to a variety of proprietary and standardised approaches
- digital private mobile radio, as used by the emergency services, based on the ETSI TETRA specification.

Short-range systems such as Wi-Fi and Bluetooth are not considered. These are unlikely to be affected as they are typically used indoors and are less relied upon for critical services, although their use is proliferating.

Disturbance mechanisms

Terrestrial mobile systems typically work in the frequency range of 380 MHz – 3.5 GHz. Potential mechanisms for disturbance of mobile networks by an extreme space weather event are illustrated in *Figure 13*. They include:

- GNSS, if it is used for timing/synchronisation/location purposes at the base station or elsewhere within the network
- uplink access link (ie a mobile station transmitting to a base station)
- downlink access link (ie a base station transmitting to a mobile station)
- wireless backhaul (point-to-point and point-to-multipoint links between base stations and the mobile core network).

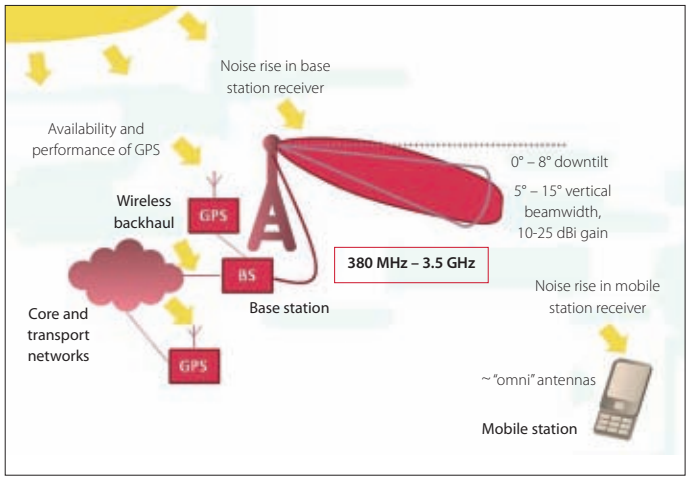

Figure 13: Potential mechanisms for disturbance of terrestrial mobile communications systems due to extreme space weather events
© Real Wireless Ltd

GNSS is potentially vulnerable to both solar radio noise bursts and also to ionospheric disturbances. Uplink, downlink and backhaul links are wholly terrestrial and are thus are only vulnerable to increased solar noise.

GNSS in mobile systems

The use of GNSS (currently GPS) at base stations varies significantly according to the wireless technology employed. The 3G CDMA base stations used by some operators in the US, Eastern Europe and the Far East, conform to the 3GPP2 standard use GPS for timing and synchronisation at each base station. By contrast, the 3GPP-based systems which are used for almost all public mobile systems in the UK were specifically designed not to require GPS support, by avoiding the need for synchronous operation between adjacent base stations. Consequently, UK public mobile systems should be largely unaffected by GNSS disruption during a superstorm.

One potential exception in 3GPP systems is synchronisation of base stations for the TDD variant of LTE technology (TD-LTE). GPS has been proposed to provide uplink/downlink synchronisation. However, this is an optional approach and could and should be avoided for critical systems via the use of network-based synchronisation techniques, such as via Precision Time Protocol (PTP) based on the IEEE-1588 standard which is currently being deployed. LTE in its FDD variant has just started to be deployed commercially in the UK. Wider deployments are expected following Ofcom's spectrum auction starting in early 2013. Although deployment of TD-LTE is likely to lag the FDD variant, it is important that the UK maintains the robust architectures currently being deployed where the application of the systems is critical.

Another potential exception where GPS may be used in 3GPP networks is in femtocells – miniature cellular access points used to enhance services in homes or small businesses. In the US, operators have used GPS to meet FCC requirements for emergency call location in femtocells. This has not been required by Ofcom in the

UK and other means of locating femtocells have instead been used to meet the relevant requirements [*Small Cell Forum*, 2012].

The TETRA system used by Airwave to provide communications to the emergency services in the UK does use GPS at each base station for timing and synchronisation (and possibly for operational location purposes also). The loss of GPS at TETRA base stations would, therefore, in the absence of mitigating techniques, lead to a loss of service. Furthermore, given the reliance of the emergency services on TETRA, the impact of a loss of service could be severe. Consequently, Airwave has mitigated against such potential impacts in several ways:

- by network configuration to allow base stations to continue to operate for an extended period of time in the absence of GPS. In our view, holdover for up to three days may be required
- via the provision of external power supply arrangements (battery and generator as applicable) to allow for non-mains running periods of up to seven days for the main part of the network
- the use of network-derived synchronisation techniques with references which are independent of GNSS

Existing contracts with Airwave are due to expire in the next few years, starting in 2016. It is strongly recommended that the specification of any replacement service should include appropriate mitigation to maintain and if appropriate extend resilience against loss of GPS over a period of three days.

The above assessment concerns the impact of GPS as deployed at base stations. It is possible that some mobile networks may make use of GPS elsewhere within the network: no such instance is known of or specified in relevant standards, but the possibility remains.

Radio noise in mobile systems

It has been reported [*Kintner et al.*, 2009] that solar radio bursts (SRBs) can affect the performance of mobile phone networks by increasing the noise in the system. The impact of such a noise rise will depend on the technical characteristics of the system, the intensity of the SRB and whether the antenna is pointed at the Sun.

Both base stations and mobiles are designed via various mechanisms to cope with signal outages of up to several seconds without loss of connection and only temporary loss of service. These mechanisms are likely to handle large noise rises with essentially the same robustness; consequently only longer duration events are likely to affect the mobile network. Furthermore, the external solar noise rise would have to be significant compared to the internal system noise.

Mobile handsets typically exhibit internal noise figures between seven and 10 dB in bandwidths of 200 kHz to 20 MHz and they have essentially omnidirectional antennas (except in specialised cases) with a gain of between around -5 dBi and +2 dBi. They are typically protected from solar noise by surrounding buildings and trees which block the line of sight to the Sun. Consequently, even if the external noise from the SRB is significant it will affect only particular mobiles rather than the whole system.

The impact of radio noise on base stations is more likely to be significant. Base stations have a lower noise figure (between 3-8 dB in the same bandwidth) than mobiles and, therefore, lower power SRBs will show a measureable impact. However, the base stations have relatively high gain antennae (10-20 dBi) with a narrow vertical beamwidth, (around 10°). They are typically placed in elevated locations and are usually directed downwards below the horizon with a little spill over at small angles above the horizon. Consequently, the base station will only be affected when the Sun is close to the horizon. Furthermore, the horizontal beamwidth is limited, typically to 80°-110° (base stations typically have multiple sectors to provide coverage at all azimuths) so only sectors facing the Sun will be affected. In conclusion, the SRB must occur close to sunrise or sunset and only those mobiles served by the sector in the direction of the Sun will be affected. Mobiles near the cell edge (ie those producing a weak signal at the base station) will be most affected. Wireless backhaul links could in principle also be affected by similar radio noise rise effects; however, they typically use narrow beamwidths thus reducing the probability that the Sun is in the beam during an SRB.

As a numerical example, we assume that at least one sector of every base station is directed at the horizon and hence could view the sun at near-maximum gain. Calculations (based on 900 MHz) then suggest that the base station noise rise will be (the noise rise of a mobile is given in brackets):

- noticeable [ie +1 dB] when solar flux density is above around 250 (12000) SFU and
- significant [ie +3dB] when solar flux density is above around 1000 (47000) SFU

There were 2,882 SRB events measured with more than 1,000 SFU (assuming a 12 minute window) during the period 1960-99, [*Bala et al.*, 2002]; ie more than one per week on average. However, no impacts on mobile phone networks have been reported, even during the most intense SRB on record in December 2006. However, it is possible that the effects are hard to discern among the many other variabilities in service quality on mobile networks and the overall impact is difficult to judge.

In an attempt to understand the impact of SRBs associated with a superstorm it is useful to look at the work of *Kintner* [2009] who defines intense SRBs as those in excess of 150,000 SFU. Such events, evaluated on the same basis, would correspond to around 22 dB of noise rise in base stations, and a corresponding severe loss of service. There have been several such events between the 1960s and 2006, although the precise number and characteristics are uncertain because of inconsistencies in various measurements. A fuller characterisation of the probability and impact of such events requires a better understanding of the expected distribution of extreme events by radio frequency, duration, intensity and temporal structure within an event (milliseconds to seconds).

In conclusion, extreme event SRBs are likely to have a widespread and noticeable impact on the mobile phone network, but only for base stations facing the Sun at dawn and dusk. The local time of the radio burst will therefore be critical and very different impacts will seen in different geographical locations.

11.3 HF communications and international broadcasting

Introduction

High frequency (3-30 MHz) point-to-point communications and broadcasting (often referred to as shortwave) rely on the ionosphere to propagate radio signals beyond the horizon. HF is a valuable alternative and complement to satellite communications, especially near the Earth's poles where geostationary satellites are not visible. The most prevalent (non-military) users of point-to-point HF communications are the aviation and shipping industries. The primary users of HF broadcasting are international broadcasters such as the BBC World Service.

The ionosphere is a dynamic propagation environment and this makes HF operations challenging even during routine space weather events. Solar activity, such as flares and coronal mass ejections, produce large variations in the radiation incident upon the Earth, which in turn lead to disturbances in the ionosphere:

- X-rays produced during solar flares cause an increase in the density of the lower layers of the ionosphere across the *sunlit* hemisphere. This increases the absorption (fading) of HF signals - an effect known as a sudden ionospheric disturbance (SIDS)
- highly energetic solar particles ionize the lower ionosphere in the *polar* regions. This increases the absorption of HF signals - an effect known as polar cap absorption (PCA)
- ionospheric storms occur, which result in *regional* and *global* reductions in the operational HF band.
- Storm associated electric fields and particles cause irregularities and gradients at high (primarily *auroral*) and at *equatorial* latitudes, between 18 local time and 24 local time These irregularities manifest themselves as multipath and Doppler distortion on HF signals and are related to scintillation seen at higher frequencies.

Modern HF systems provide substantial mitigation against all of these effects. These generally comprise digital modems (such as that defined in NATO STANAG 4415) that are tolerant to Doppler and multipath effects that can operate with low signal levels. Ideally, these modems are used in conjunction with multiple ground stations using multiple operating frequencies [*Goodman*, 2006; *Goodman et al.*, 1997]. However, there remain a large number of legacy systems – not least in commercial aircraft – that suffer frequent service interruptions during even moderate space weather events.

During a solar superstorm we expect the auroral oval to move south so that it includes or is south of the UK and consequently all of the above effects may be experienced by long distance HF communications originating in the UK. The effects will be worse in the evening hours, but will probably continue with little respite for several days.

Aircraft HF communications

As a minimum, aircraft are required to carry analogue voice equipment for long distance communications, although some aircraft are equipped with more modern and effective digital HF data links [*ARINC*, 2012]. Approximately 60% of aircraft flying out of the UK also carry satellite communications equipment in addition to their HF communication equipment. In contrast to some other countries (eg the US) no scheduled flights from the UK travel above 72° north. This renders the HF communications to UK aircraft somewhat less susceptible to moderate space weather events, although it should be noted that loss of HF communications to aircraft remains a frequent event even under normal conditions.

During an extreme event it is likely that communications to most aircraft in the North Atlantic would be lost. For aircraft in flight, there are well established procedures for coping with loss of HF communications, as defined by *ICAO* [2005]; these generally allow aircraft to complete their flight plans. However, in the event of an extended-duration, wide-area loss of HF communications to all aircraft (when satellite communications may also be lost, Section 12.5) it is likely that flights will be prevented from taking off. In this extreme case, there does not appear to be a defined mechanism for reopening airspace once communications have recovered.

HF broadcasting

HF broadcasting, such as that provided by the BBC World Service, will also be degraded or entirely unavailable for up to several days during an extreme space weather event. However, owing to the limited use of national HF broadcasting within the UK, this is unlikely to pose a major national threat.

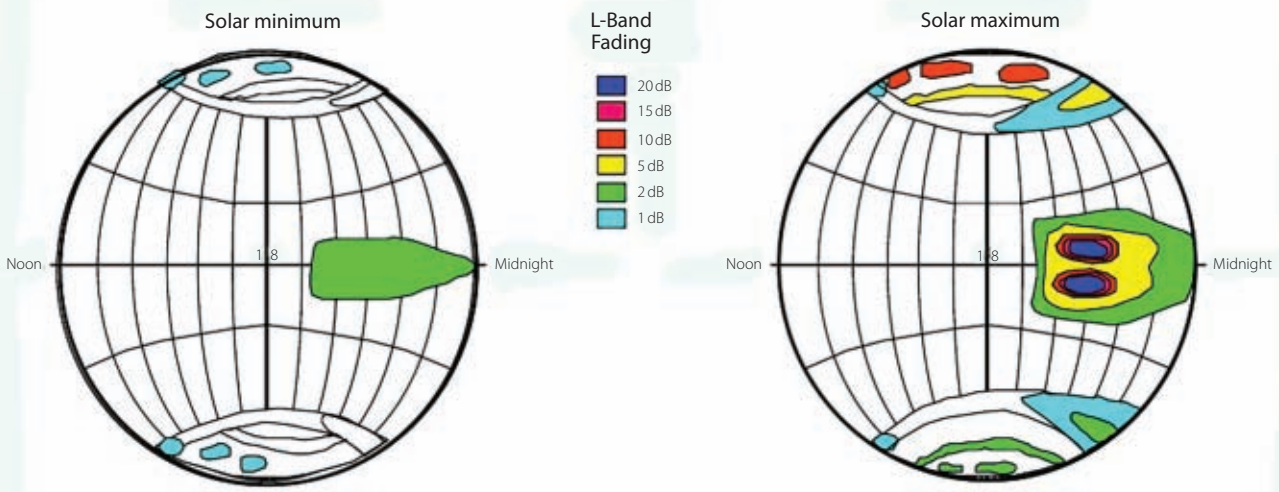

Figure 14. Ionospheric scintillation morphology © [Basu et al., 2002]

11.4 Mobile satellite communications

Small scale irregularities often found in the high and equatorial regions (*Figure 14*) during the evening hours cause scintillation, ie rapid fluctuations in the amplitude, phase and direction of arrival of signals of satellite signals. The effects of scintillation increase as the frequency is decreased and lead to increased error rates on communications signals. Moderate ionospheric scintillation generally only affects satellite communications operating in the VHF and low UHF band - such systems are largely military. More severe events can degrade L-band (~1.5GHz) civilian satellite communication systems (e.g. Iridium and Inmarsat).

Amplitude scintillation, leads to message errors if the system fade margin is exceeded; and if the fade is so long that the error correction code and interleaving is unable to correct the data steam. Fading has been recorded on satellite communication systems at 6 GHz although the fade depth at this frequency is only a few dB (peak-to-peak) and usually inconsequential. Fades of 10dB have been measured on 4 GHz signals (worst case) [*Aarons, 1984]* and over 20 dB has been observed at L band (1.5GHz) [*Basu et al.*, 1988]. This provides indicative values for a superstorm.

Solar radio bursts can interfere with VHF, UHF and L-band communications satellites. This is especially true for geostationary satellites around equinox, when the satellites lie close to the direction of the Sun (at certain times of day), and for mobile systems with large beamwidths and low signal-to-noise ratios [*Franke*, 1996].

During an extreme space weather event, high latitude scintillation will extend southwards to cover the UK and the equatorial scintillation will intensify and expand. Scintillation may occur at any time of the day, but will be strongest in the evening hours. Our judgement is that scintillation will render L-band links *largely* unavailable for between one and three days (section 11.1), however, this will be specific to the system.

For example, the L-band Iridium satellite network (which comprises a constellation of 66 LEO satellites operates with an average fade margin of 15.5 dB [*ICAO*, 2007] which is less than the 20dB fades measured by *Basu et al.* [1988]. It seems that even without an allowance for other degrading factors such as multipath, the fade margin is insufficient and signal outages will occur.

11.5 Satellite broadcasting

Assuming that the satellite survives the particle environment caused by an extreme space weather event, it is unlikely that services will be impaired. This is because satellite broadcasting operates at much higher frequencies than mobile satellite services (around 10 GHz). At these frequencies the ionosphere has little impact on the radio propagation.

11.6 Terrestrial broadcasting

Terrestrial radio (ie national and local broadcasting) should not be directly affected by space weather events. However, the secondary effects stemming from degraded timing from GPS should be considered; for example, the BBC DAB network operates as a single frequency network and uses GPS to provide time and frequency synchronisation [*ETSI*, 2000]. It is not clear how much holdover is provided by the system (see Section 11.3 for a discussion of timing holdover).

11.7 Communications – summary and recommendations

Terrestrial mobile communication networks

Summary

Good quality and reliable mobile (cellular) communications have become are relied on by the public. Furthermore, mobile communications are also critical for the delivery of effective police, fire and ambulance services and these services are likely to be in high demand during an extreme solar event when other parts of the national infrastructure are under stress.

This study has concluded that the UK's commercial cellular communications networks are currently much more resilient to the effects of a superstorm than those deployed in a number of other countries (including the US) since they are not reliant on GPS. Solar radio bursts have been identified as a potential problem, but only for parts of the network facing the Sun at dawn and dusk. The Academy believes that this is an acceptable risk given that each burst will only last ~20 minutes.

In contrast, the TETRA emergency communications network is dependent on GPS timing and, without mitigation strategies, would be vulnerable. However, a number of mitigation strategies are already in place.

Recommendations

- All terrestrial mobile communication networks with critical resiliency requirements should also be able to operate without GNSS timing for periods up to three days. This should particularly include upgrades to the network including those associated with the new 4G licenses where these are used for critical purposes and upgrades to the emergency services communications networks.

- Ofcom should consider including space weather effects when considering infrastructure resilience.

- The impact of extreme space weather events should be considered in the development of upgrades to emergency services communications networks and GNSS holdover should be ensured for up to three days.

- Further study of radio noise effects on mobile communication base stations should be undertaken to quantify the impact.

HF communications

HF communications are likely to be rendered inoperable for several days during a solar superstorm. HF communications are used much less than they used to be; however, they do provide the primary long distance communications bearer for long distance aircraft (not all aircraft have satellite communications and this may also fail during an extreme event). For those aircraft in the air at the start of the event, there are already well-defined procedures to follow in the event of a loss of communications. However, in the event of a persistent loss of communications over a wide area, it might be necessary to prevent flights from taking off. In this extreme case, there does not appear to be a defined mechanism for closing or reopening airspace once communications have recovered.

Recommendations

- The aviation industry and authorities should consider upgrades to HF modems (similar to those used by the military) to enable communications to be maintained in more severely disturbed environments. Such an approach could significantly reduce the period of signal loss during a superstorm and would be more generally beneficial.

- Operational procedures for closing and re-opening airspace in the event of an extended HF and satellite communications blackout should be developed

Mobile satellite communications

During an extreme space weather event, L-band satellite communications might be unavailable, or provide a poor quality of service, for between one and three days owing to scintillation. The overall vulnerability of L-band satellite communications to superstorm scintillation will be specific to the satellite system. For aviation users the operational impact on satellite communications will be similar to HF.

Recommendation

- Current and proposed L-band satellite communications used by the aviation and shipping industries should be assessed for vulnerability to extreme space weather.

Terrestrial broadcasting

Terrestrial broadcasting would be vulnerable to secondary effects, such as loss of power and GNSS timing.

Recommendation

- Where terrestrial broadcasting systems are required for civil contingency operations, they should be assessed for vulnerabilities to the loss of GNSS timing.

12. Conclusion

The report has sought to elucidate the nature and the impact of solar superstorms on contemporary and future high-technology systems with an emphasis on the UK. The breadth of technologies considered is significant and with the input of a number of domain experts, each has been studied in some depth. Our study is based on an estimate of the environmental impact of events which have occurred in the last 200 years. How representative these are of the longer term is not known, and in any case every solar superstorm is different.

The study has demonstrated that solar superstorms are indeed a risk to the UK's infrastructure. The UK electricity grid, while probably not as susceptible as in some other countries, is at risk and this provides the biggest concern because so much other infrastructure is dependent on it. Many other technologies are also vulnerable and the unmitigated impact is likely to have both safety-of-life and economic impacts. It appears that, in contrast to the USA and some other countries, contemporary UK 2G, 3G and 4G mobile communications networks are not vulnerable – this needs to be maintained. The study has not assessed how the impact of a superstorm might be magnified by the failure of multiple technologies, but the likelihood that this will indeed occur has been noted.

The Academy recommends continuing vigilance of this recently recognised threat. Vigilance will require the maintenance of current mitigation strategies and the development of new approaches in response to new technologies. Mitigation of the effects of solar superstorms requires a balance between engineering approaches and operational approaches – the latter being partly dependent on storm forecasts. The specific technology and the relative costs of mitigation will dictate the best way forward. Technological mitigation tends to be application specific, whereas forecasting has both generic and application specific elements. Reliable space weather forecasting requires a mix of satellite and ground based observations combined with coupled physical models. It is likely to be a Grand Challenge for the scientific community and requires partnership with the engineering and business communities to be effective.

Technology specific recommendations have been included in each chapter of the report.

The Academy also recommends the initiation of a UK space weather board to provide overall leadership of UK space weather activities: observations and measurements, operational services, research and related technology developments. In regard to the latter the Board should, through its leadership, support and facilitate the UK space sector to enable it to respond to ESA and other space environment missions. The board, under the auspices of a nominated government department, should include representatives of all major stakeholders. It should be responsible for advising on proposal development and prioritisation, ensuring coherency of work programmes, avoiding duplication of projects and delivering value for money. Above all, the Board should link the research and operations communities so that the science is more clearly focused on delivering useful results and tested against well-defined metrics.

THE ACADEMY RECOMMENDS CONTINUING VIGILANCE OF THIS RECENTLY RECOGNISED THREAT. VIGILANCE WILL REQUIRE THE MAINTENANCE OF CURRENT MITIGATION STRATEGIES AND THE DEVELOPMENT OF NEW APPROACHES IN RESPONSE TO NEW TECHNOLOGIES.

Understanding and mitigating solar superstorms is a subject lying at the interface between science and engineering. The discipline has grown out of the former and, to maintain and extend our understanding and ability to measure and monitor space weather in general, and superstorms more particularly, it is vitally important to maintain the UK science expertise. Space weather research related to impacts on the Earth's environment, from the deep interior to the upper atmosphere and magnetosphere, is primarily the responsibility of the Natural Environment Research Council (NERC) while non-Earth space weather research, including space plasma and solar physics, are the responsibility of the Science and Technology Facilities Council (STFC). However, mitigating space weather and solar superstorms also has an important engineering dimension. Consequently, the Academy recommends that the Engineering and Physical Research Council (EPSRC) should ensure that its own programmes recognise the importance of extreme space weather mitigation and that EPSRC be fully integrated into any research council strategy.

This report presents our best assessment of the impact of a severe space weather event largely based on our experience of previous smaller events and our understanding of modern technology. We caution that the conclusions are subject to a large uncertainty as an extreme event has not been encountered in modern times and if it were there are likely to be many nonlinear dependencies. Therefore, our assessment may understate the impacts.

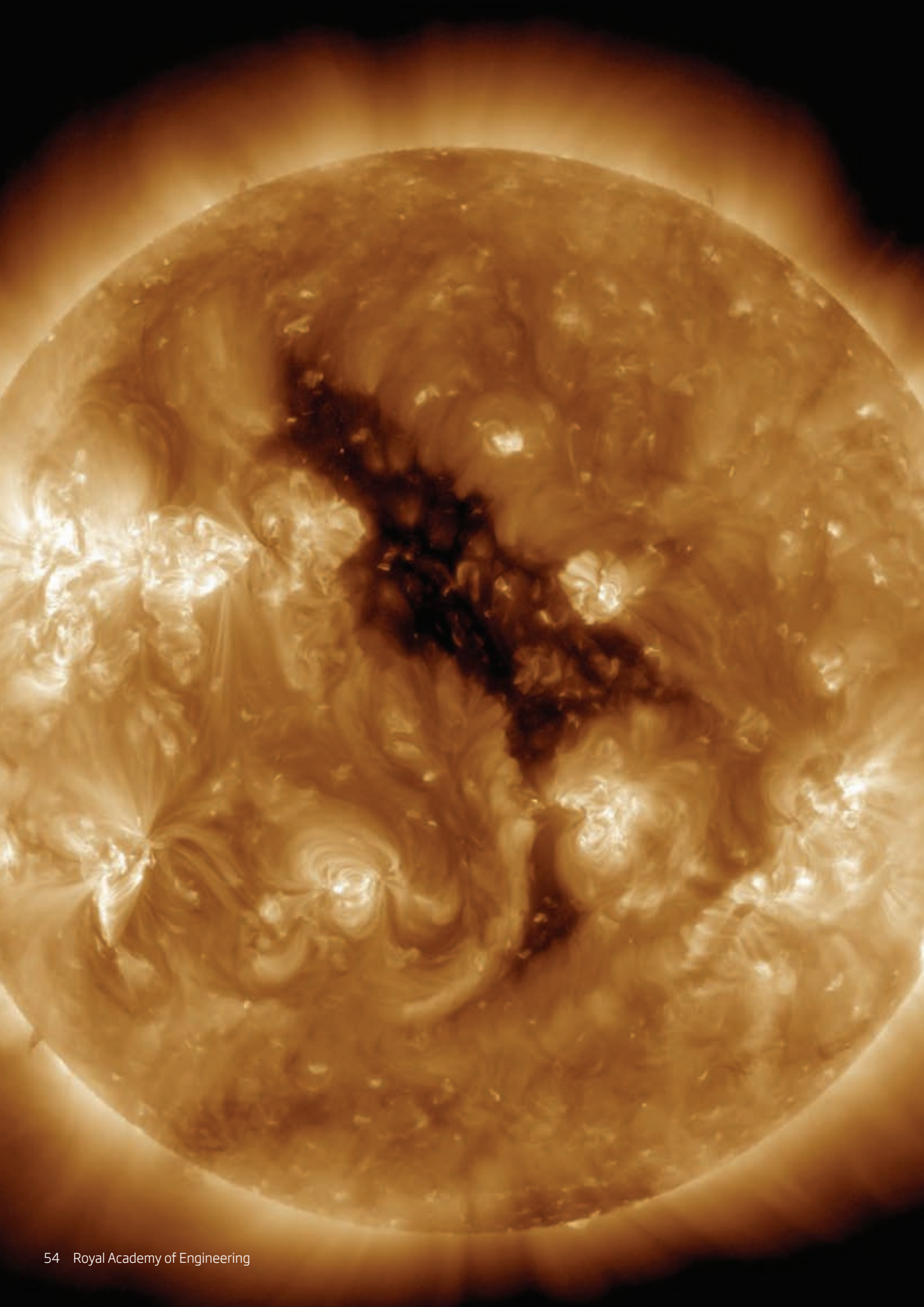

13. Bibliography

Aarons, J. (1984), Equatorial trans-ionospheric propagation conditions affecting digital communications, paper presented at Propagation Influences on Digital Transmission, NATO-AGARD, Electromagnetic Propagation Panel, Athens, Greece, 4-8 June.

Ahmed, O., R. Qahwaji, T. Colak, P. Higgins, P. Gallagher, and S. Bloomfield (2011), Solar Flare Prediction using Advanced Feature Extraction, Machine Learning, and Feature Extraction *Solar Physics, on-line first*, doi: 10.1007/s11207-011-9896-1.

Air Weather Service (1997), Space Environment Impacts on DoD operations, *Rep.37*.

Anderson, C. W., L. J. Lanzerotti, and C. G. MacLennan (1974), *Bell System Technical Journal*, *53*, 1817-1837.

ARINC (2012), GLOBALink, **www.arinc.com/products/globalink/index.html**

ATSB (2011), Transportation Safety Report, Aviation Occurrence Investigation AO-2008-070, Final, "In-flight upset 154 km west of Learmonth, WA 7 October 2008, VH-QPA, Airbus A330-303" *Rep.*

Baker, D. N. (2002), How to cope with Space Weather, *Science*, *297*, 1486, doi: 10.1126/science.1074956.

Baker, D. N., and J. L. Green (2011), The Perfect Solar Superstorm, *Sky and Telescope*, 28 February.

Baker, D. N., S. G. Kanekal, R. B. Horne, N. P. Meredith, and S. A. Glauert (2007), Low-altitude measurements of 2-6 MeV electron trapping lifetimes at 1.5 < L < 2.5, *Geophys. Res. Lett.*, *34*, 20, L20110, doi: 10.1029/2007gl031007.

Bala, B., L. J. Lanzerotti, D. E. Gary, and D. J. Thomson (2002), Noise in wireless systems produced by solar radio bursts, *Radio Sci.*, *37*, 2, 1018, doi: 10.1029/2001rs002481.

Barnard, L., and M. Lockwood (2011), A survey of gradual solar energetic particle events, *J. Geophys. Res.*, *116*, A05103, doi: 10.1029/2010JA016133.

Barnard, L., M. Lockwood, M. A. Hapgood, M. J. Owens, C. J. Davis, and F. Steinhilber (2011), Predicting space climate change, *Geophys. Res. Lett.*, *38*, L16103, doi: 10.1029/2011GL048489.

Basu, S., E. Mackenzie, and S. Basu (1988), Ionospheric constraints on VHF/UHF communications links during solar maximum and minimum period, *Radio Sci.*, *23*, 3, 363-378.

Basu, S., K. M. Groves, S. Basu, and P. J. Sultan (2002), Specification and forecasting of scintillations in communication/navigation links: current status and future plans, *Journal of Atmospheric and Solar-Terrestrial Physics*, *64*, 16, 1745-1754, doi: 10.1016/s1364-6826(02)00124-4.

Beamish, D., T. D. G. Clark, E. Clarke, and A. W. P. Thomson (2002), Geomagnetically induced currents in the UK: Geomagnetic variations and surface electric fields *J. Atmos. Sol. Terr. Phys.*, *64*, 1779-1792.

Blake, J. B., W. A. Kolasinski, R. W. Fillius, and E. G. Mullen (1992), Injection of electrons and protons with energies of tens of MeV into L < 3 on 24 March 1991, *Geophys. Res. Lett.*, *19*, 821-824.

Bolduc, L. (2002), GIC observations and studies in the Hydro-Québec power system, *J. Atmos. Sol. Terr. Phys.*, *64*, 1793-1802.

Boteler, D. H. (1977), Distributed-Source Transmission Line Theory for Electromagnetic Induction Studies. , paper presented at Supplement of the Proceedings of the 12th International Zurich Symposium and Technical Exhibition on Electromagnetic Compatibility, Zürich, Switzerland, February 18-20, 1997.

Boteler, D. H. (2006), The super storms of August/September 1859 and their effects on the telegraph system, *Adv. Space Res 38*, 159-172, doi: 10.1016/j.asr.2006.01.013.

Boteler, D. H., and G. J. van Beek (1999), August 4, 1972 revisited: A new look at the geomagnetic disturbance that caused the L4 cable system outage, *Geophys. Res. Lett.*, *26*, 5, 577-580, doi: 10.1029/1999GL900035.

Bradley, P. D., and E. Normand (1998), Single Event Upsets in Implantable Cardioverter Defribillators, *IEEE Trans. Nucl. Sci.*, *45*, 6, 2929-2940, doi: 10.1109/23.736549.

Butikofer, R., E. O. Fluckiger, L. L. Desorgher, and M. R. M.R. Moser (2008), The extreme solar cosmic ray particle event on 20 January 2005 and its influence on the radiation dose rate at aircraft altitude, *Science of The Total Environment, 391*, 177-183.

Campbell, A., S. Buchner, E. Petersen, J. B. Blake, J. Mazur, and C. S. Dyer (2002), SEU measurements and predictions on MPTB for a large energetic solar particle event, *IEEE Trans. Nucl. Sci.*, *49*, 6, 1340-1344.

Cannon, P. S. (2009), Mitigation and Exploitation of the Ionosphere: A military perspective, *Radio Science*, *44*, RS0A20, doi: 10.1029/2008RS004021.

Opposite page: Coronal holes are regions where the sun's corona is dark. These features were discovered when X-ray telescopes were first flown above the Earth's atmosphere to reveal the structure of the corona across the solar disc. Coronal holes are associated with 'open' magnetic field lines and are often found at the sun's poles. The high-speed solar wind is known to originate in coronal holes © NASA

Carrano, C. S., C. T. Bridgwood, and K. M. Groves (2009), Impacts of the December 2006 solar radio bursts on the performance of GPS, *Radio Sci., 44*, RS0A25, doi: 10.1029/2008rs004071.

Cerruti, A. P., P. M. Kintner, D. E. Gary, L. J. Lanzerotti, E. R. de Paula, and H. B. Vo (2006), Observed solar radio burst effects on GPS/Wide Area Augmentation System carrier-to-noise ratio, *Space Weather, 4*, 10, S10006, doi: 10.1029/2006sw000254.

Cerruti, A. P., P. M. K. Jr., D. E. Gary, A. J. Mannucci, R. F. Meyer, P. Doherty, and A. J. Coster (2008), Effect of intense December 2006 solar radio bursts on GPS receivers, *Space Weather, 6*, S10D07, doi: 10.1029/2007SW000375.

Clark, S. (2007), *The Sun Kings: The Unexpected Tragedy of Richard Carrington and the Tale of How Modern Astronomy Began*, Princeton University Press.

Clauer, C. R., and G. e. Siscoe (2006), The Great Historical Geomagnetic Storm of 1859: A Modern Look, *Adv Space Res., 38*, 115-388.

Cliver, E. W., and L. Svalgaard (2004), The 1859 Solar–Terrestrial Disturbance and the current limits of Extreme Space Weather Activity, *Solar Physics, 224*, 407-422.

Council of the European Union (1996), Directive 96/29/Euratom, laying down basic safety standards for the protection of health of workers and the general public against the dangers arising from ionising radiation, edited.

Curry, C. (2010), Dependency of Communications Systems on PNT Technology, *Rep.*, Chronos Technology Ltd, Stowfield Housem, Upper Stowfield, Lydbrook, Gloucestershire, GL17 9PD, UK.

Dunlop, M. W., Q.-H. Zhang, C.-J. Xiao, J.-S. He, Z. Pu, R. C. Fear, C. Shen, and C. P. Escoubet (2009), Reconnection at High Latitudes: Antiparallel Merging, *Phys. Rev. Lett., 102*, 075005.

Dyer, C. S., A. J. Sims, J. Farren, and J. Stephen (1990), Measurements of solar flare enhancements to the single event upset environment in the upper atmosphere, *IEEE Trans. Nucl. Sci., 37*, Dec, 1929-1937, doi: 10.1109/23.101211.

Dyer, C. S., K. Hunter, S. Clucas, and A. Campbell (2004), Observation of the solar particle events of October and November 2003 from CREDO and MPTB, *IEEE Trans. Nucl. Sci, 51*, 6, 3388-3393, doi: 10.1109/TNS.2004.839156.

Dyer, C. S., F. Lei, A. Hands, and P. Truscott (2007), Solar particle events in the QinetiQ atmospheric radiation model, *IEEE Trans. Nucl. Sci, 54*, 4, 1071-1075, doi: 10/1109/TNS.2007.893537.

Dyer, C. S., F. Lei, S. N. Clucas, D. F. Smart, and M. A. Shea (2003), Solar particle enhancements of single event effect rates at aircraft altitudes *IEEE Trans. Nucl. Sci., 50*, 6, 2038-2045, doi: 10.1109/TNS.2003.821375.

Edwards, R., E. Normand, and C. S. Dyer (2004), Technical standard for atmospheric radiation single event effects (SEE) on avionics electronics, paper presented at IEEE Radiation Effects Data Workshop Record, IEEE 04TH8774.

Erinmez, I. A., J. G. Kappenman, and W. A. Radasky (2002), Management of the geomagnetically induced current risks on the national grid company's electric power transmission system., *Journal of Atmospheric and Solar-Terrestrial Physics, 64*, 5-6, 743-756.

Eroshenko, E. A., A. V. Belov, D. H. Boteler, S. P. Gaidash, S. L. Lobkov, R. Pirjola, and L. Trichtchenko (2010), Effects of strong geomagnetic storms on Northern railways in Russia, *Advances in Space Research, 46*, 9, 1102-1110.

ETSI (2000), Digital Audio Broadcasting (DAB); Guidelines and rules for implementation and operation; Part 3: Broadcast network, edited.

FAA (2004), WAAS Performance Analysis Report, No 7 *Rep.*, FAA/William J. Hughes Technical Center, FAA.

Fazel, R., H. M. Krumholz, Y. Wang, J. S. Ross, J. Chen, H. H. Ting, N. D. Shah, K. Nasir, A. J. Einstein, and B. K. Nallamothu (2009), Exposure to Low-Dose Ionising Radiation from Medical Imaging Procedures, *New England Journal of Medicine, 361*, 9, 849-857, doi: 10.1056/NEJMoa0901249.

Feynman, J., G. Spitale, J. Wang, and S. Gabriel (1993), Interplanetary Proton Fluence Model: JPL 1991, *J. Geophys. Res., 98*, 13281-13294.

Franke, E. (1996), Effects of Solar, Galactic and man-made noise on UHF SATCOM operation, paper presented at Militray Communications Conference, MILCOM 1996, IEEE.

Gaunt, C. T., and G. Coetzee (2007), Transformer failures in regions incorrectly considered to have low GIC-risk, paper presented at Power Tech, 2007, IEEE, Lausanne.

Getley, I. L., M. L. Duldig, D. F. Smart, and M. A. Shea (2005), Radiation dose along North American transcontinental flight paths during quiescent and disturbed geomagnetic conditions, *Space Weather, 3*, 1, S01004, doi: 10.1029/2004sw000110.

Getley, I. L., L. G. I. Bennett, B. J. Lewis, B. Bennett, C. S. Dyer, A. D. P. Hands, and M. L. Duldig (2010), Evaluation of new cosmic radiation monitors designed for aircrew exposure assessment, *Space Weather, 8*, 1, S01001, doi: 10.1029/2009sw000492.

Goodman, J. M. (2006), Telecommunication system vulnerabilities to space-weather events, paper presented at Third Symposium on Space Weather, American Meteorological Society January.

Goodman, J. M., J. Ballard, and E. Sharp (1997), A long-term investigation of the HF communication channel over middle- and high-latitude paths, *Radio Sci.*, *32*, 4, 1705-1715, doi: 10.1029/97rs01194.

Hapgood, M. A. (2011), Towards a scientific understanding of the risk from extreme space weather, *Adv. Space Res.*, *47*, 2059-2072, doi: 10.1016/j.asr.2010.02.007.

Health and Safety Executive (1999), The Ionising Radiations Regulations 1999, S.I. 1999 No. 3232. London, The Stationery Office Limited., edited.

Hernández-Pajares, M., J. M. Juan, J. Sanz, À. Aragón-Àngel, A. García-Rigo, D. Salazar, and M. Escudero (2011), The ionosphere: effects, GPS modeling and the benefits for space geodetic techniques, *J Geod*, doi: 10.1007/s00190-011-0508-5.

Horne, R. B. (2012), Forecasting the radiation belts in Europe, *Space Weather*, *10*, S008006, doi: 10.1029/2011JA017202.

HPA (2009), Application of the 2007 Recommendations of the ICRP to the UK, *Rep.RCE-12*, Health Protection Agency, UK.

IAEA (2011), Radiation Protection and Safety of Radiation Sources: International Basic Safety Standards (INTERIM EDITION), GSR Part 3 (Interim) General Safety Requirements, ISBN 978-92-0-120910-8, edited, International Atomic Energy Agency, Vienna.

ICAO (2005), North Atlantic minimum navigation performance specification (MNPS) airspace operations manual, edited, Published on behalf of the North Atlantic Systems Planning Group (NAT SPG) by the European and North Atlantic Office of ICAO.

ICAO (2007), Manual for ICAO aeronautical mobile satellite (route) service; Part 2-IRIDIUM, DRAFT v4.0, *Rep.*, ICAO.

ICAO (2010), **www2.icao.int/en/anb/met/iavwopsg/Space%20Weather/Forms/AllItems.aspx**

ICRP (1991), 1990 Recommendations of the International Commission on Radiological Protection. ICRP, Publication 60, *Annals of the ICRP*, *21*, 1-3.

ICRP (2007), Recommendations of the International Commission on Radiological Protection. Publication 103, *Annals of the ICRP*, *37*, 2-4.

ICRP (2009), Application of the Commission's Recommendations for the Protection of People in Emergency Exposure Situations, ICRP Publication 109, *Annals of the ICRP 39*, 1.

ICRP (2012), 2012 ICRP Statement on Tissue Reactions and Early and Late Effects of Radiation in Normal Tissues and Organs - Threshold Doses for Tissue Reactions in a Radiation Protection Context, ICRP Publication 118, *Annals of the ICRP*, *41*, 1/2.

IEC (2008a), Process management for avionics – Atmospheric radiation effects – Part 5: Guidelines for assessing thermal neutron fluxes and effects in avionic systems, *Rep.IEC TS 62396-5*.

IEC (2008b), Process management for avionics – Atmospheric radiation effects – Part 4: Guidelines for designing with high voltage aircraft electronics and potential single event effects, *Rep.IEC TS 62396-4*.

IEC (2008c), Process management for avionics – Atmospheric radiation effects – Part 3: Optimising system design to accommodate the single event effects (SEE) of atmospheric radiation, *Rep.IEC TS 62396-3*.

IEC (2012a), Process management for avionics – Atmospheric radiation effects – Part 2: Guidelines for single event effects testing for avionics systems, *Rep.IEC 62396-2*.

IEC (2012b), Process management for avionics - Management plan - Part 1: Preparation and maintenance of an electronic components management plan, *Rep.IEC/TS 62239-1*.

IEC (2012c), Process management for avionics - Atmospheric radiation effects – Part 1: Accommodation of atmospheric radiation effects via single event effects within avionics electronic equipment, *Rep.IEC 62396-1 Ed.1*.

Iucci, N., et al. (2005), Space weather conditions and spacecraft anomalies in different orbits, *Space Weather*, *3*.

Joint Aviation Authorities (2001), JAR-OPS 1.390 Cosmic Radiation, edited.

Kahler, S. (2009), Variation of SEP event occurence with heliospheric magnetic field magnitudes, *Adv. Space Res.*, *43*, 1423–1428, doi: 10.1016/j.asr.2009.01.039.

Kaplan, E. (2005), *Understanding GPS: Principles and Applications*, Artech House.

Kappenman, J. (2010), Geomagnetic Storms and Their Impacts on the U.S. Power Grid, *Rep.*, Metatech Corporation.

Karsberg, A., G. Swedenborg, and K. Wyke (1959), The influences of earth magnetic currents on telecommunication lines, *Tele (English ed.), Televerket, Stockholm, 1-21*.

Kintner, P. M., Jr., B. O'Hanlon, D. E. Gary, and P. M. S. Kintner (2009), Global Positioning System and solar radio burst forensics, *Radio Sci.*, *44*, RS0A08, doi: 10.1029/2008rs004039.

Koons, H. C., and J. F. Fennell (2006), Space weather effects on communications satellites,, 316, March, *The Radio Science Bulletin, International Union of Radio Science (URSI), 316*, 27-41.

Koons, H. C., J. E. Mazur, R. S. Selesnick, B. J. B, J. F. Fennell, J. L. Roeder, and P. C. Anderson (1999), The Impact of the Space Environment on Space Systems *Rep.TR-99 (1670)-1*, Aerospace Corporation, El Segundo, USA.

Lantos, P., and N. Fuller (2003), History of the solar particle event radiation doses on-board aeroplanes using a semi-empirical model and Concorde measurements *Radiation Protection Dosimetry*, *104*, 3, 199-210.

Lanzerotti, L. J. (1992), Comment on "Great magnetic storms" by Tsurutani et al, *Geophys. Res. Lett.*, *19*, 19, 1991-1992, doi: 10.1029/92gl02238.

Lanzerotti, L. J., L. V. Medford, C. G. Maclennan, J. S. Kraus, J. Kappenman, and W. Radasky (2001), Trans-Atlantic geopotentials during the July 2000 solar event and geomagnetic storm, *Solar Physics*, *204*, 351-359, doi: 10.1023/A:1014289410205.

Laurenza, M., E. W. Cliver, J. Hewitt, M. Storini, A. G. Ling, C. C. Balch, and M. L. Kaiser (2009), A technique for short-term warning of solar energetic particle events based on flare location, flare size, and evidence of particle escape, *Space Weather*, *7*, S04008.

Lindborg, L., D. T. Bartlett, P. Beck, I. R. McAulay, K. Schnuer, H. Scraube, and F. Spurny (2004.), Compilation of measured and calculated data, edited, A report of EURADOS WG5.

Lockwood, M., M. J. Owens, L. Barnard, C. J. Davis, and S. Thomas (2012), Solar Cycle 24: what is the Sun up to?, *Astronomy & Geophysics*, *53*, 3.9-3.15.

Lyons, D. (2000), Sun Screen, **www.forbes.com/global/2000/1113/0323026a.html**

Maehara, H., T. Shibayama, S. Notsu, Y. Notsu, T. Nagao, S. Kusaba, S. Honda, D. Nogami, and K. Shibata (2012), Superflares on solar-type stars, *Nature*, *485*, 478-481, doi: 10.1038/nature11063.

Mannucci, A. J., B. A. Iijima, U. J. Lindqwister, X. Pi, L. Sparks, and B. D. Wilson (1999), GPS and Ionosphere, paper presented at Reviews of Radio Science 1996-1999, Oxford Science Publications.

McColl, N. P., and S. L. Prosser (2001), Emergency data handbook, *Rep. NRPB-W-19*, National Radiological Protection Board, Chilton, UK.

McCracken, K., G. Dreschhoff, E. J. Zeller, D. Smart, and M. Shea (2001), Solar cosmic ray events for the period 1561–1994: 1. Identification in polar ice 1561–1950, *J. Geophys. Res.*, *106*, 21,585–521,598, doi: 10.1007/s11207-005-5257-2.

Medford, L. V., L. J. Lanzerotti, J. S. Kraus, and C. G. Maclennan (1989), Transatlantic Earth Potential Variations During the March 1989 Magnetic Storms, *Geophys. Res. Lett.*, *16*, 10, doi: 10.1029/GL016i010p01145.

Melott, A.L. and Thomas, B.C. (2012) Brief communication: Causes of an AD 774-775 14C increase, *Nature 491*, E1-E2, doi:10.1038/nature11695

Miyake, F., K. Nagaya, K. Masuda, and T. Nakamura (2012), A signature of cosmic-ray increase in AD 774–775 from tree rings in Japan, *Nature*, *486*, 240-242, doi: 10.1038/nature11123.

NASA (2012), NASA STEREO Observes One of the Fastest CMEs On Record, **www.nasa.gov/mission_pages/stereo/news/fast-cme.html**

NASA GSFC (2012), Space Environment Testbeds Overview, **www.lws-set.gsfc.nasa.gov/radiation_model_user_forum.html**

NERC (2010), High-Impact, Low-Frequency Event Risk to the North American Bulk Power System, *Rep.*, North American Electric Reliability Corporation.

NERC (2012), Effects of Geomagnetic Disturbances on the Bulk Power System, *Rep.*, North America Electric Reliability Corporation.

Normand, E. (1996), Single Event Upset at Ground Level, *IEEE Trans. Nucl. Sci.*, *43*, 6, 2742-2750, doi: 10.1109/23.556861.

Normand, E. (2001), Correlation of In-flight Neutron Dosimeter and SEU Measurements with Atmospheric Neutron Model, *IEEE Trans. Nucl. Sci.*, *48*, 6, 1996-2003, doi: 10.1109/23.983162.

Normand, E., J. L. Wert, D. L. Oberg, P. R. Majewski, P. Voss, and S. A. Wender (1997), Neutron-Induced Single Event Burnout in High Voltage Electronics, *IEEE Trans. Nucl. Sci*, *44*, 6, 2358-2366, doi: 10.1109/23.659062.

NRC (2008), Severe Space Weather Events - Understanding Societal and Economic Impacts. A Workshop Report, *Rep.*, National Academy of Sciences, Washington DC.

Núñez, M. (2011), Predicting solar energetic proton events (E > 10 MeV) *Space Weather*, *9*, S07003, doi: 10.1029/2010SW000640.

Odenwald, S., J. Green, and W. Taylor (2006), Forecasting the impact of an 1859-calibre superstorm on satellite resources, *Adv. In Space Res.*, *38*, 280-297.

Olsen, J., P. E. Becher, P. B. Fynbo, P. Raaby, and J. Schultz (1993), Neutron-Induced Single Event Upsets in Static RAMs Observed at 10 km Flight Altitude, *IEEE Trans. Nucl. Sci.*, *40*, 77.

ONS (2012), Leading Causes of Death in England and Wales, 2009, **www.ons.gov.uk/ons/taxonomy/index.html?nscl=Causes+of+Death**

Posner, A. (2007), Up to 1-hour forecasting of radiation hazards from solar energetic ion events with relativistic electrons, *Space Weather*, *5*, S05001, doi: 10.1029/2006SW000268.

Price, P. R. (2002), Geomagnetically induced current effects on transformers, *IEEE Transactions on Power Delivery*, *17*, 4, 1002-1008.

Ptitsyna, N. G., V. V. Kasinskii, G. Villoresi, N. N. Lyahov, L. I. Dorman, and N. Iucci (2008), Geomagnetic effects on mid-latitude railways: A statistical study of anomalies in the operation of signaling and train control equipment on the East-Siberian Railway, *Advances in Space Research*, *42*, 9, 1510-1514.

Pulkkinen, A., M. Hesse, S. Habib, L. V. d. Zel, B. Damsky, F. Policelli, D. Fugate, and W. Jacobs (2009), Solar Shield - forecasting and mitigating space weather effects on high-voltage power transmission systems *Natural Hazards*, doi: 10.1007/s11069-009-9432-x.

Reames, D. (1999), Particle acceleration at the Sun and in the heliosphere, *Space Sci. Rev.* , *90*, 413-491, doi: 10.1023/A:1005105831781.

Riley, P. (2012), On the probability of occurrence of extreme space weather events, *Space Weather*, *10*, S02012, doi: 10.1029/2011SW000734.

Ryden, K. A., P. A. Morris, and A. D. P. Hands (2008), Radiation monitoring in Medium Earth Orbit over the Solar minimum period, paper presented at Proc. RADECS 2008, Jyvaskyla, Finland, 10-12 September.

Satellite News Digest (2012), Satellite Outages and Failures, edited.

SEIEG (2012), Summary of space weather worst-case environments, Edited M Hapgood, *Rep.RAL-TR-2012-022,* **http://epubs.stfc.ac.uk/**, Rutherford-Appleton Laboratory

Shprits, Y., D. Subbotin, B. Ni, R. H. Horne, D. N. Baker, and P. Cruce (2011), Profound change of the near-Earth radiation environment caused by solar superstorms, *Space Weather*, *9*, 8, S08007, doi: 10.1029/2011sw000662.

Sims, A. J., C. S. Dyer, C. L. Peerless, K. Johansson, H. Pettersson, and J. Farren (1994), The Single Event Upset Environment for Avionics at High Latitude, *IEEE Trans. Nucl. Sci.*, *41*, 6, 2361-2367, doi: 10.1109/23.340588.

Small Cell Forum (2012), Femtocell Synchronisation and Location, Report 036, at **www.smallcellforum.org/resources-white-papers**

Stenquist, D. (1914), *The Magnetic Storm of Sept. 25, 1909*, Republished 2010 by Nabu Press.

Taktakishvili, A., P. MacNeice, and D. Odstrcil (2010), Model uncertainties in predictions of arrival of coronal mass ejections at Earth orbit,, *Space Weather*, *8*, S06007, doi: 10.1029/2009SW000543.

Thomson, A. W. P., E. B. Dawson, and S. J. Reay (2011), Quantifying extreme behavior in geomagnetic activity, *Space Weather*, *9*, S10001, doi: 10.1029/2011SW000696.

Thomson, A. W. P., A. J. McKay, E. Clarke, and R. S. J. (2005), Surface electric fields and geomagnetically induced currents in the Scottish Power grid during the 30 October 2003 geomagnetic storm, *Space Weather*, *3*, S11002, doi: 10.1029/2005SW000156.

Trichtchenko, L., and D. H. Boteler (2001), Specification of geomagnetically induced electric fields and currents in pipelines, *J. Geophys. Res., 106*, A10, 21039–21048, doi: 10.1029/2005JA011294.

Tsurutani, B. T., W. D. Gonzalez, G. S. Lakhina, and S. Alex (2003), The extreme magnetic storm of 1–2 September 1859, *J. Geophys. Res.*, *108*, A7, 1268, doi: 10.1029/2002ja009504.

Turnbull, K. (2011), Space Weather Hazards to the United Kingdom's National Grid, PhD thesis, University of Lancaster, UK.

Underwood, C. I. (1996), Single Event Effects in Commercial Memory Devices in the Space Radiation Environment, PhD thesis, University of Surrey, Guildford.

Vette, J. I. (1991), The AE-8 trapped electron model environment, *Rep.*, National Space Science Data Center (NSSDC), World Data Center A for Rockets and Satellites (WDC-A-R&S), National Aeronautics and Space Administration, Goddard Space Flight Center.

Wall, B. F., R. Haylock, J. T. M. Jansen, M. C. Hillier, and D. Hart (2011), Radiation risks from medical x-ray examinations as a function of age and sex of patient., *Rep.HPA-CRCE-028*, Health Protection Agency, Chilton, UK.

Walter, T., A. Hansen, J. Blanch, and P. Enge (2000), Robust Detection of Ionospheric Irregularities, paper presented at Institute of Navigation's GPS conference, Salt Lake City, UT, USA.

Watson, S. J., A. L. Jones, W. B. Oatway, and J. S. Hughes (2005), Ionising radiation exposure of the UK population, *Rep.HPA-RPD-001*, Health Protection Agency, Chilton, UK.

Weaver, M., W. Murtagh, C. Balch, D. Biesecker, L. Combs, M. Crown, K. Doggett, J. Kunches, H. Singer, and D. Zezula (2004), Halloween Space Weather Storms of 2003, *Rep.NOAA Technical Memorandum OAR SEC-88*, NOAA.

Wik, M., R. Pirjola, H. Lundstedt, A. Viljanen, P. Wintoft, and A. A. Pulkkinen (2009), Space weather events in July 1982 and October 2003 and the effects of geomagnetically induced currents on Swedish technical systems., *Annales Geophysicae*, *27*, 4, 1775-1787.

Wolff, E. W., M. Bigler, M. A. J. Curran, J. E. Dibb, M. M. Frey, M. Legrand, and J. R. McConnell (2012), The Carrington event not observed in most ice core nitrate records, *Geophys. Res. Lett.*, *39*, L08503, doi: 10.1029/2012GL051603.

Ziegler, J. F., et al. (1996), IBM experiments in soft fails in computer electronics (1978-1994), *IBM Journal of Research and Development*, *40*, 1, 3-18.

14. Glossary

Term	Definition
Bastille Day event	Radiation storm that occurred on 14 July 2000 and associated geomagnetic storm on 15/16 July
Carrington event	The largest solar storm on record. It took place from 1-3 September 1859 and is named after British astronomer Richard Carrington.
Coronal mass ejection	A large burst of solar wind plasma ejected into space
Coronagraph	An instrument for observing and photographing the Sun's corona, consisting of a telescope fitted with lenses, filters, and diaphragms that simulate an eclipse
Electrostatic discharge	The sudden flow of electricity between two objects caused by contact, an electrical short or dielectric breakdown
eLoran	Enhanced Long-Range Navigation System
Geo-effective	Storm-causing
Geomagnetically induced currents	Electrical currents flowing in earthed conductors, induced by rapid magnetic field changes
Geomagnetic storm	A worldwide disturbance of the Earth's magnetic field induced by a solar storm
Geostationary orbit	A circular orbit 35,900 km above the Earth's surface where most telecommunications satellites are located. Satellites in GEO orbit appear stationary relative to the rotating Earth
Global navigation satellite systems	Generic term for space-based navigation systems of which GPS and Galileo are examples
Halloween event	A solar storm that occurred in October 2003
Interplanetary magnetic field	Solar magnetic field carried by the solar wind to the planets and beyond
Ionosphere	The region of the atmosphere between around 80-600 km above the Earth
L1 Langrangian point	The point where the gravitational forces of the Sun and Earth balance
Magnetosphere	The region surrounding a planet, such as the Earth, in which the behaviour of charged particles is controlled by the planet's magnetic field
Magnetometer	An instrument used to measure the strength and direction of magnetic fields.
Radiation hardening	The making of electronic systems and their components resistant to damage caused by ionising radiation
Reactive power	Describes the energy in the magnetic component of the alternating current
Relativistic	Having or involving a speed close to that of light
Scintillation	The perturbation of radio signals caused by variations in the ionosphere
Solar corona	The extended outer atmosphere of the Sun
Solar energetic particles	High-energy particles coming from the Sun
Solar flare	A brief powerful eruption of particles and intense electromagnetic radiation from the Sun's surface
Solar wind	The constant stream of charged particles, especially protons and electrons, emitted by the Sun at high velocities, its density and speed varying during periods of solar activity
Substorm	A brief disturbance of the Earth's magnetosphere that causes energy to be released from its "tail"
TETRA	An emergency communications network
Thermosphere	An atmospheric layer lying between the mesosphere and the exosphere, reaching an altitude of ~750km above the Earth's surface

15. Abbreviations and acronyms

Acronym	Meaning
3GPP	Third Generation Partnership Project
A-GPS	Assisted GPS
APNT	Alternate Position Navigation and Time
BGS	British Geological Survey
CDMA	Code division multiple access
CME	Coronal mass ejection
COTS	Commercial off the shelf
Cs	Caesium (Atomic frequency standard)
CSAC	Chip scale atomic clock
DECC	Department of Energy and Climate Change
DME	Distance measuring equipment
DRAM	Dynamic random access memory
Dst	A geomagnetic index
E3C	Energy Emergencies Executive Committee
ECSS	European Cooperation of Space Standardisation
EGNOS	European Geostationary Navigation Overlay Service
eLoran	Enhanced long range navigation
EMC	Electromagnetic compatibility
EPSRC	Engineering and Physical Sciences Research Council
ESA	European Space Agency
ESD	Electrostatic discharge
ETSI	European Telecommunications Standards Institute
FAC	Field aligned currents
FAA	Federal Aviation Administration
FCC	Federal Communications Commission
FDD	Frequency division duplex
GCR	Galactic cosmic rays
GEO	Geostationary orbit
GIC	Geomagnetically induced currents
GLE	Ground level event
GLONASS	GLObal NAvigation Satellite System - GLObalnaya NAvigatsionnaya Sputnikovaya Sistema) A satellite-based radio navigation system
GMD	Geomagnetic disturbance
GNSS	Global Navigation Satellite Systems

GPS	Global Positioning System
GSP	Grid supply point
HANE	High altitude nuclear events
HF	High frequency
HSPA	High speed packet access
ICAO	International Civil Aviation Organisation
ICRP	International Commission on Radiological Protection
IEC	International Electrotechnical Commission
IECQ	International Electrotechnical Commission Quality Assessment System for Electronic Components
IEEE	Institute of Electrical and Electronic Engineers
IEEE-1588	Packet timing standard for Ethernet
IMF	Interplanetary magnetic field
ITU	International Telecommunications Union
LEO	Low Earth orbit
LTE	Long term evolution
LTE-A	Long term evolution – advanced
MBU	Multiple bit upset
MCU	Multiple cell upset
MEO	Medium Earth orbit
MHD	Magneto-hydrodynamic
MSCs	Mechanically switched compensators
MTBF	Mean time between failures
MTTR	Mean time to repair
NERC	Natural Environment Research Council
NOAA	National Oceanic and Atmospheric Administration
NRA	National risk assessment
NTP	Network time protocol
OCXO	Oven controlled crystal oscillator
PCA	Polar cap absorption
PDV	Packet delay variation
PNT	Positioning, navigation and timing
PRC	Primary reference clock
PTPv2	Precision time protocol v2 (IEEE-1588-2008)
Rb	Rubidium (atomic clock)

SAE	Society of Automotive Engineers
SBAS	Satellite based augmentation systems
SDH	Synchronous digital hierarchy
SEB	Single event burnout
SEE	Single event effects
SEFI	Single event functional interrupt
SEGR	Single event gate rupture
SEIEG	Space Environment Impact Expert Group
SEL	Single event latchup
SEP	Solar energetic particle
SET	Single event transient
SEU	Single event upset
SFU	Solar flux unit
SGT	Super grid transformer
SIDS	Sudden ionospheric disturbances
SIRs	Stream interaction regions
SRAM	Static random access memory chip
SRB	Solar flare solar radio burst
SSU	Synchronisation source utility
SVCs	Static variable compensators
SyncE	Synchronous Ethernet
TCP/IP	Transmission control protocol/internet protocol
TCXO	Temperature compensated crystal oscillator
TDD	Time division duplex
TD-LTE	TDD variant of LTE technology
TDM	Time division multiplex
TETRA	Terrestrial European trunked radio access
UHF	Ultra high frequency
UTC	Universal coordinated time
VHF	Very high frequency
VoIP	Voice over internet protocol
WAAS	US wide area augmentation system

Appendix: Authors

This study was chaired by the lead author Professor Paul Cannon, FREng, The study was only possible because of the expertise and long hours given by the following individuals:

Professor Paul Cannon FREng	QinetiQ and University of Birmingham
Dr Matthew Angling	University of Birmingham and QinetiQ
Professor Les Barclay OBE FREng	Consultant
Professor Charles Curry	Chronos Technology Ltd
Professor Clive Dyer	University of Surrey
Robert Edwards	Aero Engine Controls
Graham Greene	CAA
Professor Michael Hapgood	RAL–Space
Professor Richard Horne	British Antarctic Survey
Professor David Jackson	Met Office
Professor Cathryn Mitchell	University of Bath
John Owen	DSTL
Dr Andrew Richards	National Grid
Christopher Rogers	National Grid
Keith Ryden	QinetiQ
Dr Simon Saunders	Real Wireless
Professor Sir Martin Sweeting CBE FREng FRS	Surrey Satellites
Dr Rick Tanner	Health Protection Agency
Dr Alan Thomson	British Geological Survey
Professor Craig Underwood	University of Surrey

The Academy would also like to thank the following peer reviewers:
Professor Per K. Enge NAE, Stanford University
Professor Louis J. Lanzerotti NAE, New Jersey Institute of Technology
Professor Daniel N. Baker NAE, University of Colorado-Boulder
Dr Eamonn Daly, European Space Agency

Staff support:
Katherine MacGregor, Policy Advisor, Royal Academy of Engineering

Notes

ROYAL
ACADEMY OF
ENGINEERING

As the UK's national academy for engineering, we bring together the most successful and talented engineers from across the engineering sectors for a shared purpose: to advance and promote excellence in engineering. We provide analysis and policy support to promote the UK's role as a great place from which to do business. We take a lead on engineering education and we invest in the UK's world class research base to underpin innovation. We work to improve public awareness and understanding of engineering. We are a national academy with a global outlook and use our international partnerships to ensure that the UK benefits from international networks, expertise and investment.

The Academy's work programmes are driven by four strategic challenges, each of which provides a key contribution to a strong and vibrant engineering sector and to the health and wealth of society:

Drive faster and more balanced economic growth

Foster better education and skills

Lead the profession

Promote engineering at the heart of society

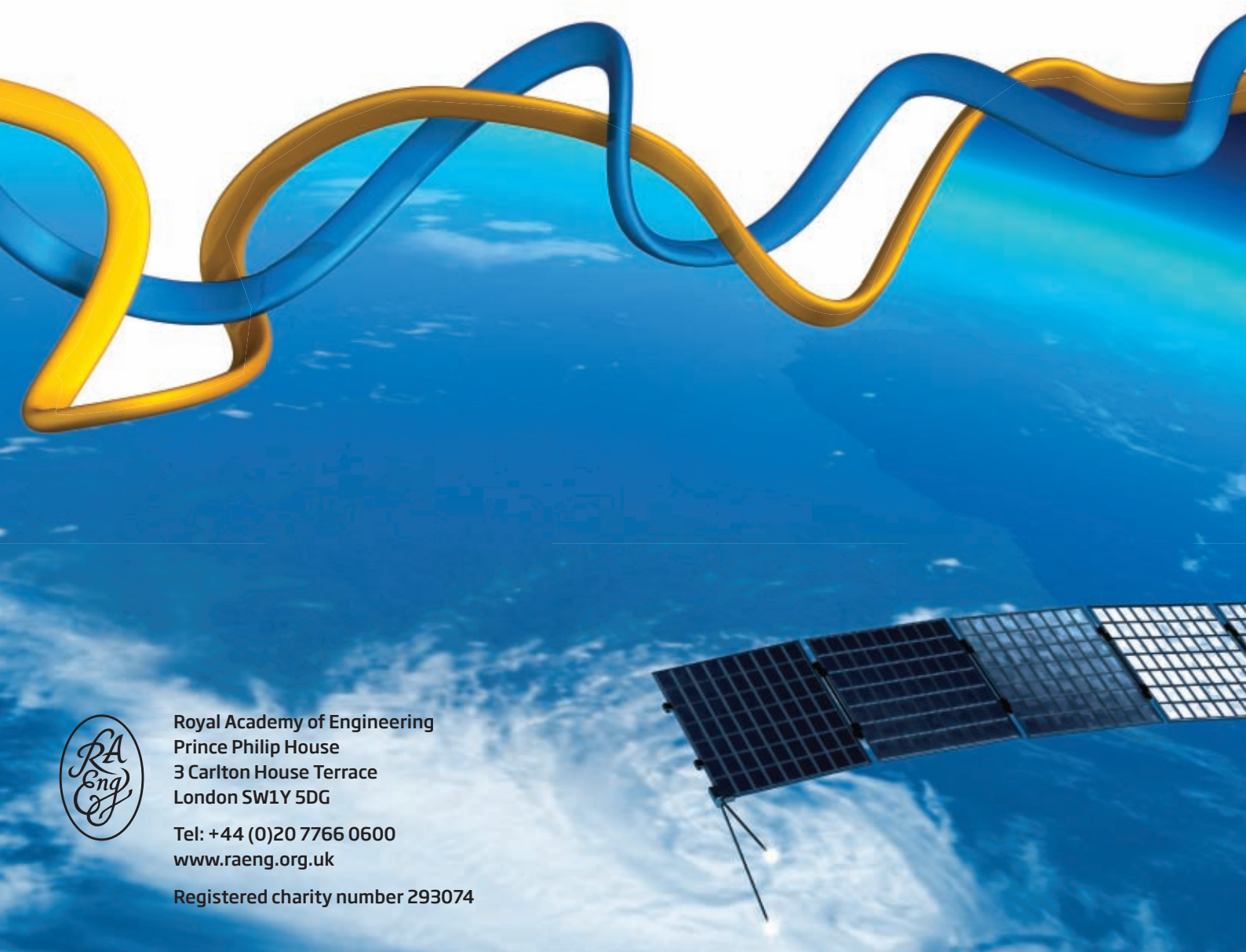

Royal Academy of Engineering
Prince Philip House
3 Carlton House Terrace
London SW1Y 5DG

Tel: +44 (0)20 7766 0600
www.raeng.org.uk

Registered charity number 293074

Tinman Thermal neutron Detector for Aircraft

Steve Wender (P-27) et al.

There have been recent concerns in the semiconductor community about the effect of thermal neutrons on the reliability of semiconductor devices. In particular, the avionics industry is concerned because of the greater intensity of high-energy neutrons at aircraft altitudes (~300 time sea level) and flight safety issues in flying aircraft. Thermal neutrons are produced in aircraft when high-energy neutrons, which are produced by cosmic-ray bombardment of the elements in the atmosphere, are thermalized by the aircraft fuel, passengers and aircraft constituents. If it turns out that if thermal neutrons are a threat to semiconductor electronics, and there are sufficient thermal neutrons in aircraft environments, aircraft manufacturers will have to test their electronics to certify that the risk of failure is acceptable. The goal of this effort was to design a detector to measure the thermal-neutron environment in aircraft.

In collaboration with Honeywell, Inc., we have developed a novel thermal neutron detector called Tinman, which can fly on aircraft and record the thermal neutron environment during flights. The detector consists of two identical He-3 tubes, one of which is covered with cadmium while the other one is bare. Cadmium is a strong absorber of thermal neutrons so it effectively blocks thermal neutrons. The thermal neutron intensity is simply the difference in the count rates between the two detectors.

The detector is autonomous. As soon as power is applied, either by aircraft power or batteries, the computer starts, and Tinman acquires data. The computer is programmed to restart itself periodically and if doesn't respond to a watchdog timer signal. The data consists of a time stamp recording the time of the event and an identifier which specifies which detector fired.

These data are stored in the computer memory as well as on redundant memory sticks. After the flight, the data is downloaded and analyzed into appropriate time bins, the cadmium covered detector data is subtracted from the bare detector data and a histogram of the thermal counts vs. flight time is generated. The number of counts/sec is then corrected for detector acceptance to give the number of thermal neutrons/cm^2.

We have tested this detector on three different NASA aircraft which flew out of Armstrong Flight Research Center in Palmdale, Ca. An example of the recorded data is shown in the figure below for a flight on a NASA DC- 8 jet which is prototypic of large commercial aircraft. The plot shows the thermal neutron intensity (bare-cd covered) in the Tinman detector (in blue) over the 7 hour flight of the DC-8. Overlaid on these data is the altitude (in orange) of the aircraft. As seen in the plot, the intensity of the thermal neutrons track the altitude of the aircraft as expected.

We are continuing to work with Honeywell Inc. on a Co-operative Research and Development Agreement (CRADA) to develop the next generation Tinman detector.

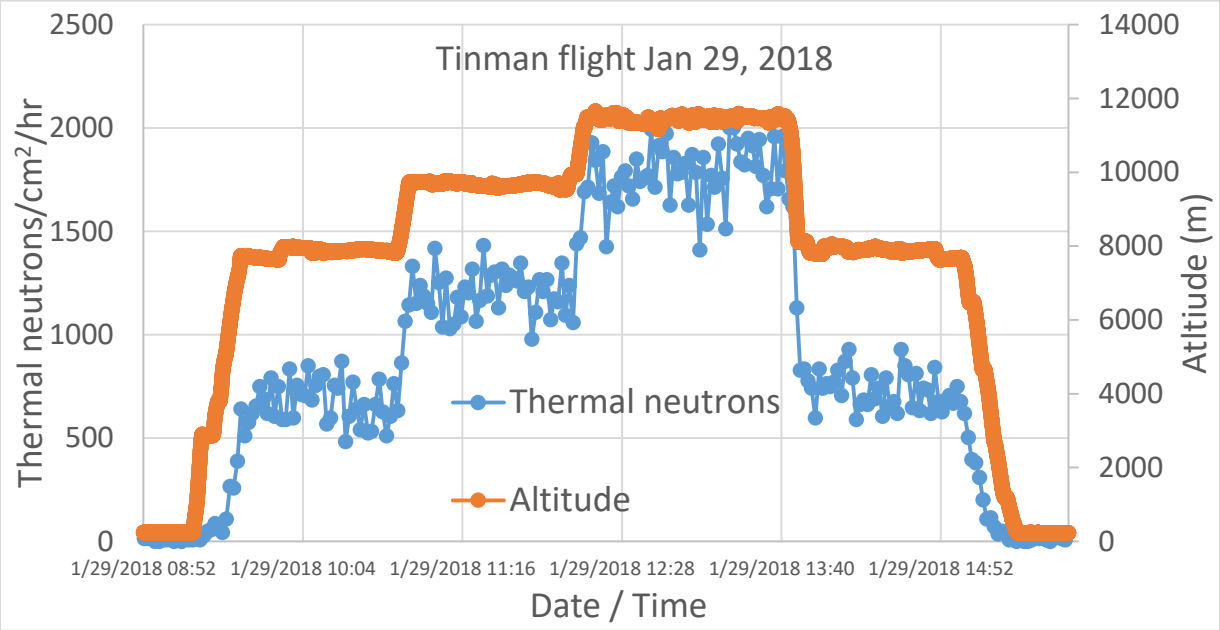

Presentations:

1. "Report on Tinman detector", Stephen Wender et al.
   Preparing for journal submission.

2. "Report on the Tin-II thermal Neutron Detector", Stephen wender et al. (LA-UR 19-30822)

3. "Measurement of Thermal Neutron Environments in Aircraft with the Tinman Instrument", Stephen Wender, Suzanne, Nowicki, LANL, Laura Dominik, Honeywell, Inc., LA-UR 19-25078
   2019 International Conference on Applications of Nuclear Techniques, 6/14/2019 (Crete, Greece)

4. "Measurement of Thermal Neutron Environments in Aircraft", Stephen Wender, Suzanne Nowicki, LANL, Laura Dominik Honeywell, Inc. (LA-UR 18-28225)
   American Nuclear Society 20th Topical Meeting on the Radiation Protection and Shielding Division 8/27/2018

5. Measurement of Thermal Neutron Environments in Aircraft", Stephen Wender, NASA Seminar (LA-UR 18-27894)

6. “Preliminary Results from thermal Neutron Measurements in airplanes- Tinman” Stephen Wender et al. (LA-UR 18-20792)
   Nuclear Space Radiation Effects Conference (NSREC) 7/16/2018

7. “Preliminary Results from Tinman on NASA Eclipse Flights” Stephen Wender (LA-UR 17-29969)
   NASA Review 11/1/2017

IN DEPTH | PHYSICAL SCIENCE

Researchers rise to challenge of replacing helium-3

Richard Stone
+ See all authors and affiliations

Science 01 Jul 2016:
Vol. 353, Issue 6294, pp. 15-16
DOI: 10.1126/science.353.6294.15

Open in new tab

A prototype lithium-based scintillator at Oak Ridge National Laboratory could save helium-3.

CREDIT: GENEVIEVE MARTIN/ORNL

the U.S. stockpile, managed by the Department of Energy's (DOE's) Isotope Program, would run out as early as 2010, as terrorism fears drove up demand for detectors of nuclear material.

Faced with a crisis, DOE curtailed He-3 sales while it and other agencies raced to find He-3 alternatives. Observers hail the effort. “There's been a revolution over the past year and a half,” says Jeffrey Lacy, president of Proportional Technologies Inc. (PTI), a Houston, Texas-based firm that has devised one alternative. A dozen others are in the pipeline or already on the market, and the He-3 stockpile is out of danger. DOE's reserves will top 160,000 liters by 2040, according to a new projection the department provided to *Science*. “The supply should last well over a century,” says Isotope Program Director Jehanne Gillo in Germantown, Maryland.

He-3—ordinary helium minus one neutron—might have remained obscure if not for the Cold War. As the United States and other nuclear powers expanded their arsenals, they started accumulating He-3, which is produced by the decay of tritium, a radioactive isotope of hydrogen that vastly boosts the explosive power of hydrogen bombs. For years, weapons labs vented He-3, which is not radioactive, into the atmosphere as waste.

That changed after scientists learned how useful the exotic gas could be. In physics labs, refrigerators using a mix of He-3 and He-4 as a coolant attain temperatures of less than 0.01 K. The isotope is also adept at capturing neutrons. That has made it the material of choice for neutron detectors, which contain tubes filled with the gas. After capturing a neutron, He-3 splits into a tritium nucleus and a proton, which ionize other He-3 atoms and

- PDF

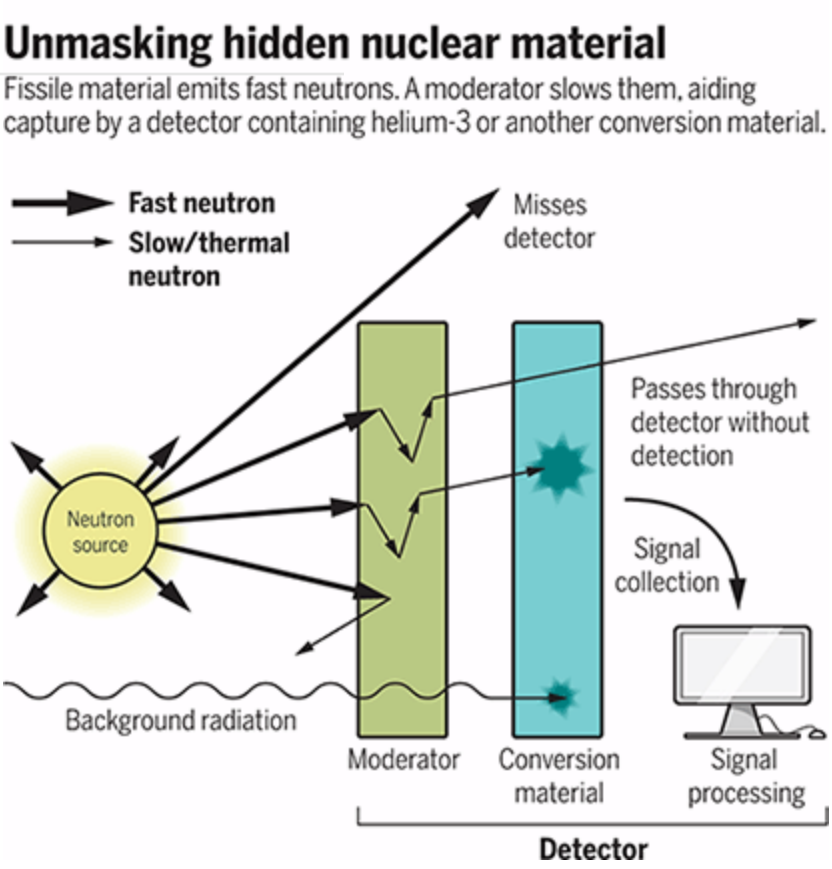

Open in new tab

Unmasking hidden nuclear materialCREDIT: (GRAPHIC) C. BICKEL/*SCIENCE*; (DATA) GAO

A major customer for He-3 is the Spallation Neutron Source (SNS), an accelerator at Oak Ridge National Laboratory in Tennessee that smashes neutrons into materials and molecules to reveal their structure. Some of SNS's detectors are tens of square meters in area. “We use a lot of helium-3, anywhere we can and where we can afford it,” says Oak Ridge condensed matter physicist Ken Herwig, who oversees instrumentation at SNS.

But it wasn't until after the 9/11 attacks that the run on He-3

from so-called special nuclear materials: enriched uranium and weapons-grade plutonium.

“If you're detecting neutrons, you have a pretty good indication that there's special nuclear material around,” says Jeffrey Musk, chief of nuclear technologies detection, research, and development at the U.S. Defense Threat Reduction Agency (DTRA) in Fort Belvoir, Virginia.

Skyrocketing demand for He-3 for portal monitors outstripped the 6000-odd liters of He-3 added to the U.S. reserve each year. As U.S. stocks were drawn down, the other major global supplier—Russia—sharply cut back on its sales. After DOE capped sales at 14,000 liters a year in 2009, federal programs rummaged for unused supplies, and the price of He-3 shot up from about $100 a liter to as much as $3000 a liter in 2011.

He-3 alternatives were already in development. DTRA Program Manager Hongguo Zhu explains that agencies were aiming for detector materials “that can not only detect neutrons, but also measure the energy of neutrons” more precisely. The agencies also wanted better portable and hand-held devices. The supply crunch, however, put the research into overdrive.

One approach that has bolted ahead of the field is boron-coated straws. PTI, for example, coats the inside of copper straws with boron carbide enriched in boron-10, which, like He-3, is a fat target for neutrons. After capturing a neutron, the boron-10 atom transmutes into highly energetic lithium-7 and α particles, which ionize argon gas inside the tube. “It's the best helium-3 alternative technology for large area neutron detectors,” Zhu says.

lithium-6, another isotope that's good at snaring neutrons. Combined with other materials, it yields a device that emits light when struck by a neutron or a gamma ray. The light pulses from neutrons have longer rise and decay times than those created by gamma rays, making it simple to tell the signals apart and giving scintillators a versatility that other neutron detectors lack.

The U.S. Defense Advanced Research Projects Agency (DARPA) in Arlington, Virginia, wants to do more than simply replace existing detectors. It's halfway into a 4-year program called SIGMA to develop detector networks that will continuously monitor radiation in U.S. cities. He-3 alternatives are key to making SIGMA viable, says DARPA Program Manager Vincent Tang, a plasma physicist. “DTRA and other agencies have been doing a great job of building up the base of technologies,” he says.

Scientists, too, have big plans for neutron detectors. SNS, for example, intends to eventually add another 22 beam lines. “Where we can use helium-3, we will use it,” Herwig says. But SNS already uses lithium-6 scintillators for some detectors, and it is exploring whether PTI's boron-coated straws are up to snuff for other detectors. Meanwhile, the SNOLAB near Sudbury, Canada, deep underground in a former mine, is considering boron-coated straws for a detector that would study neutrinos spawned in supernovae.

Because of the rapid rise of He-3 alternatives, “federal demand for He-3 has plummeted,” Gillo says. Now, Tang says, “I don't worry about helium-3 anymore.”

View Abstract

RESEARCH ETHICS

Human embryo research beyond the primitive streak

FILM

Science at Sundance 2021

SCI COMMUN

News at a glance

HYDROLOGY

Deforestation, forestation, and water supply

WORKING LIFE

Leadership challenges defused

- PDF

Measurement of Thermal Neutron Environments in Aircraft with the Tinman Instrument

2019 International Conference on
Applications of Nuclear Techniques

Crete, Greece

June 2019

S. A. Wender, S.F Nowicki

Los Alamos National Laboratory

L. Dominik

Honeywell, Inc.

LAUR-19-25075

Recent avionics incident highlight Single Event Effects (SEE) problem

- On October 7, 2008 , Qantas 72 was flying from Singapore to Perth, Australia.
- "While ..at 37,000 ft, one of the aircraft's three Air Data Inertial Reference Units (ADIRU) started outputting intermittent, incorrect values…Two minutes later …the aircraft flight control primary computers commanded the aircraft to pitch down. … At least 110 of the 303 passengers and nine of the 12 crew members were injured: 12 of the occupants were seriously injured and another 39 received hospital medical treatment." (Pg. vii)
- "The other potential triggering event was a single event effect (SEE) resulting from a high-energy atmospheric particle striking one of the integrated circuits within the CPU module. There was insufficient evidence available to determine if an SEE was involved, but the investigation identified SEE as an ongoing risk for airborne equipment." (pg. xvii)
- "Testing was conducted with neutrons at 14 MeV …the test was not sufficient to examine the …. susceptibility to the full range of neutrons at the higher energy levels that exist in the atmosphere". (pg. 147)

ATSB Transport Safety Report Aviation Occurrence Investigation AO-2008-70

- "The ATSB received expert advice that **the best way of determining if SEE could have produced the data-spike failure mode was to test the affected units at a test facility that could produce a broad spectrum of neutron energies**. However, the ADIRU manufacturer and aircraft manufacturer did not consider that such testing would be worthwhile….

Neutron Single Event Effects (SEE) are faults in electronic devices caused by neutrons from cosmic rays

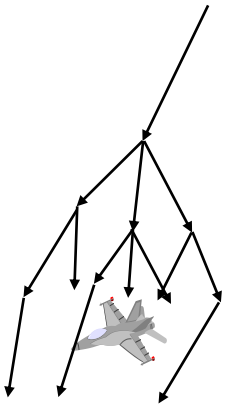

- Neutrons are produced by cosmic rays in the upper atmosphere
- Neutrons have long mean-free paths so they penetrate to low altitudes
- Neutrons interact with Si and other elements in the device to produce charged particles
- Charged particles deposit charge in sensitive volume which cause state of node to change

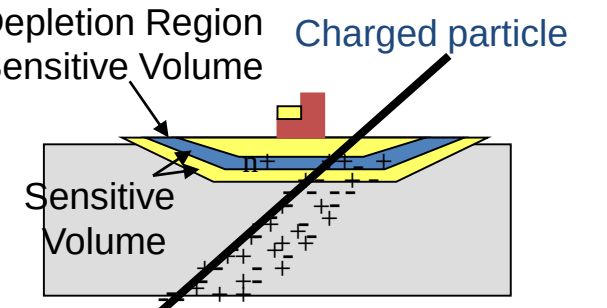

Charged particles produce direct ionization tracks in silicon and indirect ionization via nuclear reactions. Generated charge collects in depletion region, generates a logic upset.

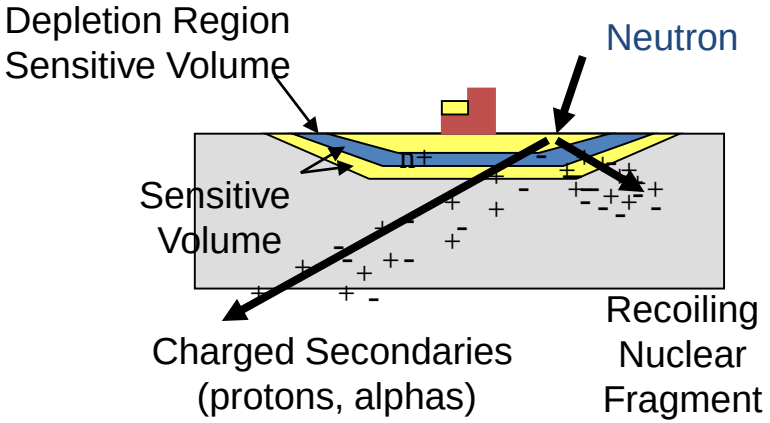

Neutrons need nuclear reaction to create charged particles. Generated charge collects in depletion region, generates a logic upset.

Many types of single-event effects can cause failures

- Soft errors
  - Single event upset
  - Multiple event upset (a few % of SEU rate, now equal to the SEU rate)
  - Silent data corruption
- Hard errors
  - Single event latchup
  - Single event burnup, gate rupture, etc.
- SEE are also seen in high-power analog devices
- First experiments were performed by the Boeing Co. for 777 certification
- Industry trends to lower voltages and smaller feature size are thought to increase the failure rate due to SEE
- Similar devices have very different failure rates
- The failure rate due to SEU is equal to all the other failure modes combined
- " Since chip SER is viewed by many as a legal liability (something that you know may fail) the public literature in this field is sparse and always makes management nervous". *SER History, Trends and Challenges* James Ziegler and Helmut Puchner

The problem is that there are lots of transistors in the world

Semiconductor devices are used in all aspects of modern life and the reliability of these devices is a major concern and may limit their applicability and performance

1 quintillion = 10^{18}

100 billion transistors for every man, woman and child on planet

Cosmic-ray induced failure rates are difficult to calculate

- The failure rate due to cosmic-ray events is given by:

$$F/t = \Sigma_p \int f_p(E_p) * \Phi_p(E_p)\ dE_p$$

Failure function depends on
- **Device characteristics**
- **Particle type**
- **Particle energy**

Particle flux depends on:
- **Particle type**
- **Altitude**
- **Latitude**
- **Solar activity**
- **Local geometry**

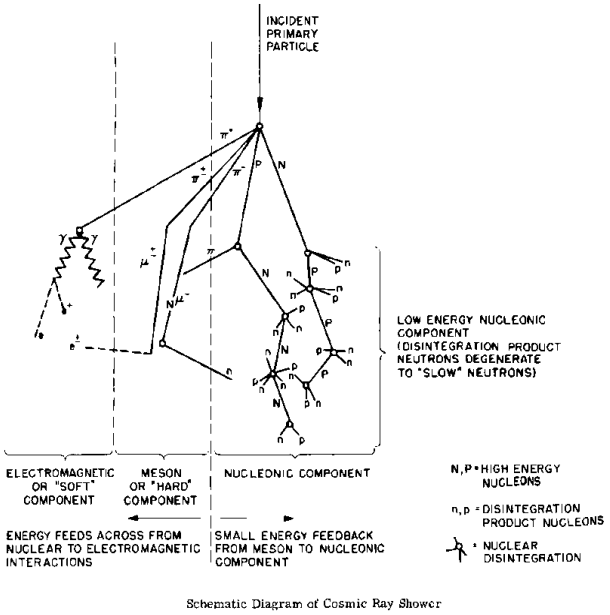

Schematic Diagram of Cosmic Ray Shower

F/t is the number of fails / time

p is the particle type (neutron, protons, pions,…)

$f_p(E_p)$ is the number of fails /particle with energy E_p

$\Phi_p(E_p)$ is the number of particles/sec with energy E_p

Slide 6

When neutrons interact with Si charged particles are produced

- Neutrons strike silicon and produce recoil silicon nuclei and alpha particles, etc.

Incident neutron energy (MeV)	Max recoil energy (MeV)	Range of particle in Si (μm)	Energy loss (keV/μm)
30	6 (Si)	3.6	2750
100	14 (Si)	6.2	3300
50	40 (α)	710	32

- Simple models exist to estimate upset rates based on recoil spectra

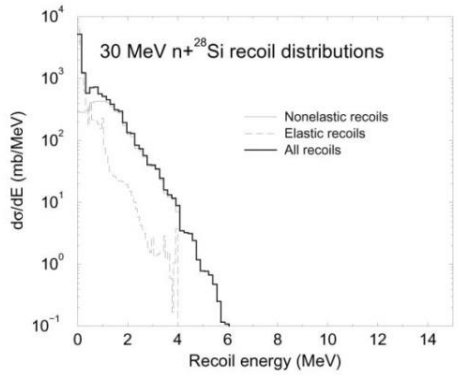

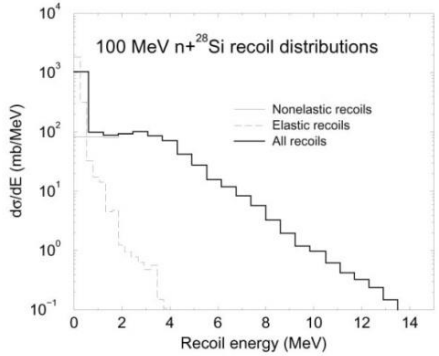

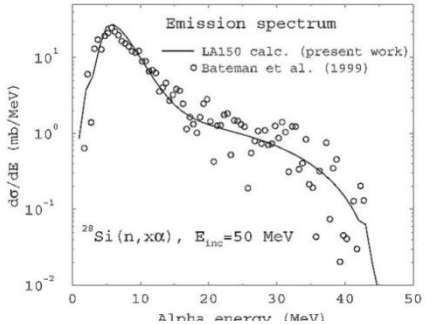

Slide 7

Accelerated testing is essential

- Design criteria for systems is 1 fail / year from SEU
  - If need to know the failure rate to 10%, need 100 fails
  - Need to run server for 100 years! RAMs change every 18 months

- Need to perform accelerated testing with acceleration rate~ 5000 ($3.6x10^4$) to get answer in 1 week (1 day) if testing entire system

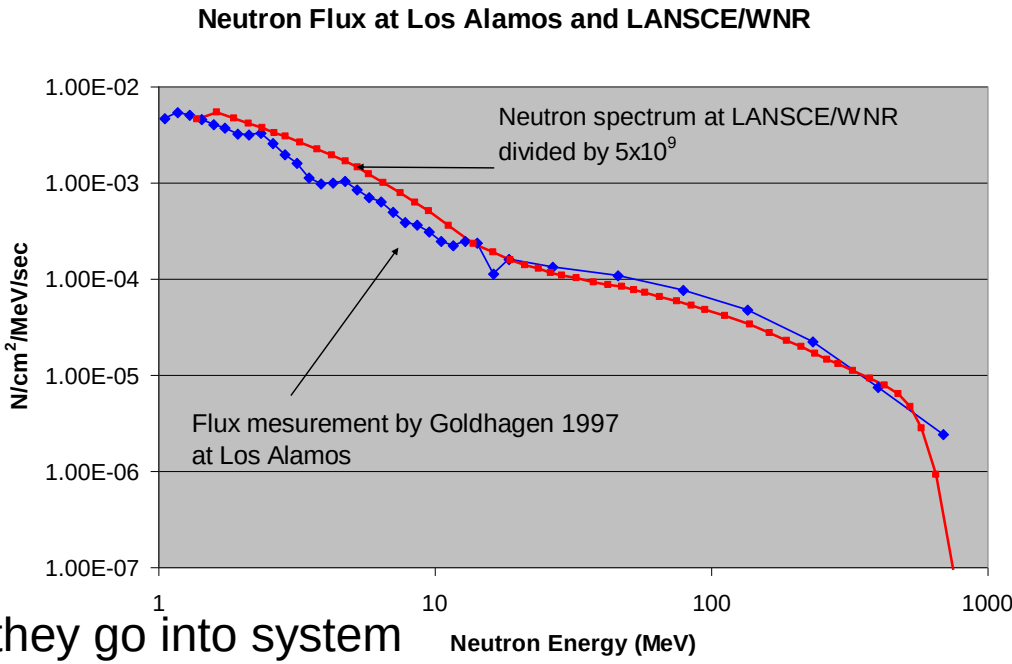

- Need to test individual chips before they go into system
  - A systems may have ~300 memory chips
  - The failure rate of a single chip is 1 fail / 300 years

- This requires an acceleration factor of ~ 10^7 for 1 day of testing to get 100 fails

- The LANSCE beam has shape similar to cosmic-ray induced neutron spectrum so many companies, laboratories and universities have used the LANSCE beam to test and predict the failure rate of their devices

Measurement of thermal neutrons in aircraft (1)

- Recently the avionics community has become concerned about the effects of thermal neutrons on flight control electronics. This question is important because if thermal neutrons are a credible concern, avionic electronics may have to be evaluated with thermal neutrons before use.
- Neutrons are a particular concern for aircraft because the cosmic-ray induced neutron flux is approximately 300 times greater than at sea level
- Thermal neutrons are produced when high-energy neutrons are thermalized in the atmosphere, the aircraft fuel, passengers and aircraft materials. Thermal neutrons have energies of 0.025 eV (2200 m/s), much less than the energy required to cause a lattice displacement.

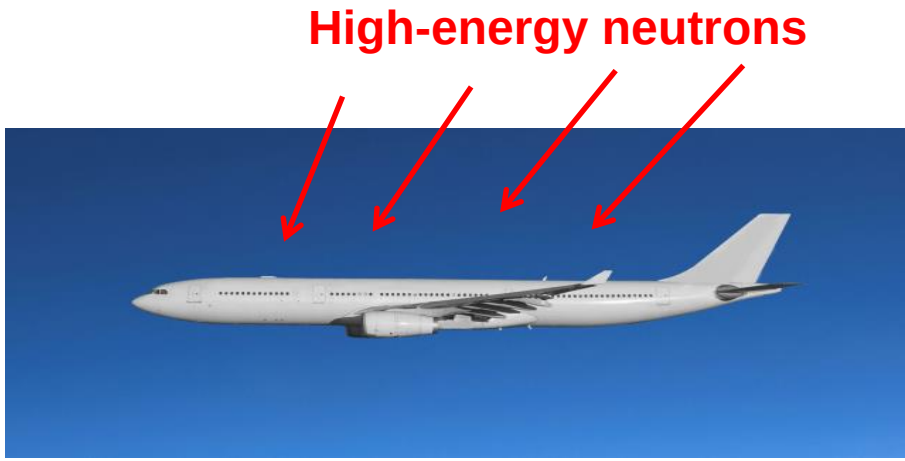

	$n/cm^2/s$	Relative
Sea level (New York City	0.00565	1
7000 ft (Los Alamos)	.019	3.4
40,000 feet	1.53	270

Measurement of thermal neutrons in aircraft (2)

- Thermal neutrons can interact with ^{10}B that is in the semiconductor parts. ^{10}B can capture a neutron and produce an energetic alpha particle and ^{7}Li ion which can deposit enough charge to cause a single-event upset.
- To understand the effect of thermal neutrons in aircraft we need to know:
  - Thermal neutron intensity in airplane— may be airplane dependent- Tinman- need to obtain data in several types of aircraft
  - Effect of thermal neutrons on semiconductor devices- Device dependent --measure at low-energy neutron source at Lujan Center at LANSCE
  - Model / simulations of thermalization of neutrons in aircraft- MCNP calculations

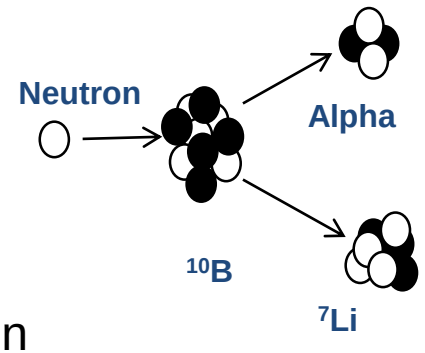

E_α ~ 1.7 MeV
Range ~ 6 μm
dE/dX
~ 1.1 MeV/mg/cm^2

E_{Li} ~ 1 MeV
Range~2.8 μm
dE/dX
~ 2.2 MeV/mg/cm^2

Measurement of thermal neutron intensity in aircraft—Tinman Instrument

- An instrument was designed to measure thermal neutrons in aircraft. This effort is part of a Strategic Partnership Agreement between LANL and Honeywell, Inc.
- Tinman consists of:
  - Two identical cylindrical ^{3}He ion chamber detectors. (~0.63 cm diam 6 cm long). He-3 was chosen because of its sensitivity to thermal neutrons and insensitivity to everything else.
  - One detector was bare, one detector was shielded with cadmium to block thermal neutrons
  - The difference in count rates between these two detectors gives the thermal neutron rate
- Final detector was fabricated by ISR Division at LANL to space specifications
- Uses a Raspberry Pi computer for DAQ
- Designed for “one switch” operation and can be powered by batteries

Vibration damping springs

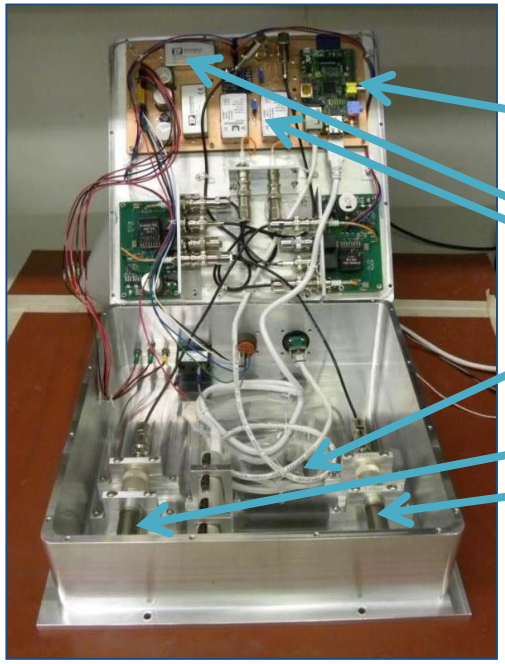

First Tinman flight was on a NASA ER-2 airplane

- ER-2 is the civilian version of U-2
- Flew on several flights from NASA Armstrong Flight Research Center in Palmdale, Ca

Tinman

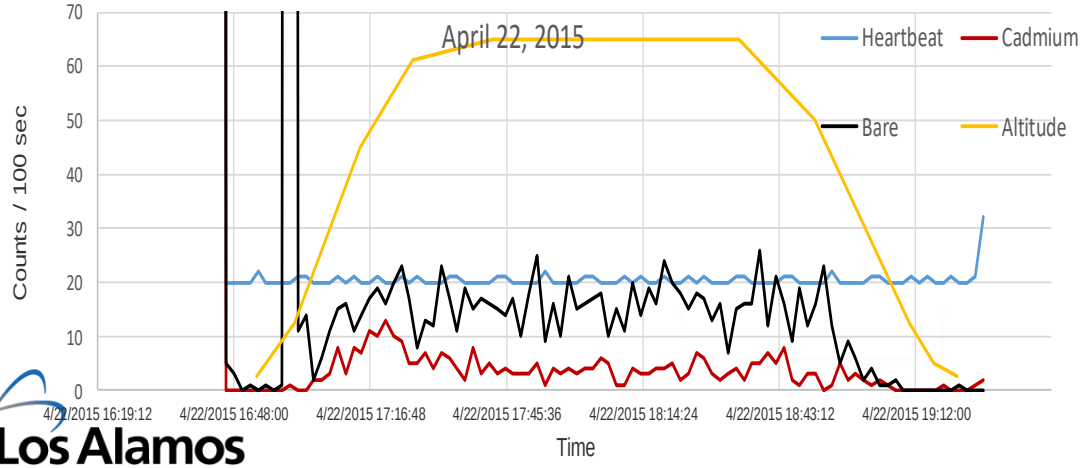

Tinman flew on NASA Eclipse flight on Gulfstream-III airplane

- Changed to larger He-3 detectors to improve signal-to-noise and sensitivity (10X)

Flight Request

Flight Info:
- 3 flights- ferry/rehearsal, mission, ferry
- Request #:17G046
- Hours: 16

Dates of Flights:
- 8/20 – 8/22

Aircraft:
- NASA GIII T/N N808NA

Crew:
- See right →

Purpose of Flight:
- Collect and transmit real-time HDTV video of the eclipse as well as photo documentation of the event
- Collect scientific data from a spectrograph provided by NASA HQs and science payloads

FLIGHT 1- Ferry up/Rehearsal ***#C: 13***

Pilots:	Troy Asher, Andrew Barry
Safety Tech:	Manny Rodriguez
Ops:	Mike Buttigieg
Photo:	Carla Thomas
Video:	Lori Losey, Steve Parcel, Mike Agnew
PAX:	David McBride, Randy Albertson, Kevin Rohrer, Thomas Zurbuchen, Debra Randall

FLIGHT 2- Mission ***#C: 12***

Pilots:	Troy Asher, Andrew Barry
Safety Tech:	Manny Rodriguez
Photo:	Carla Thomas
Video:	Lori Losey, Steve Parcel, Mike Agnew
PAX:	~~David McBride~~, Robert Lightfoot, Thomas Zurbuchen, Lesa Roe, Kevin Rohrer

AFRC Dir → Ch. of St. comm.
NASA Administrator → NASA Science mission → Dep. Assoc. Admin

FLIGHT 3- Ferry back ***#C: 11***

Pilots:	Troy Asher, Andrew Barry
Safety Tech:	Manny Rodriguez
Ops:	Mike Buttigieg
Photo:	Carla Thomas
Video:	Lori Losey, Steve Parcel, Mike Agnew
PAX:	David McBride, Randy Albertson, Debra Randall

Solar Eclipse Mission Tech Brief - 8/14/17 47

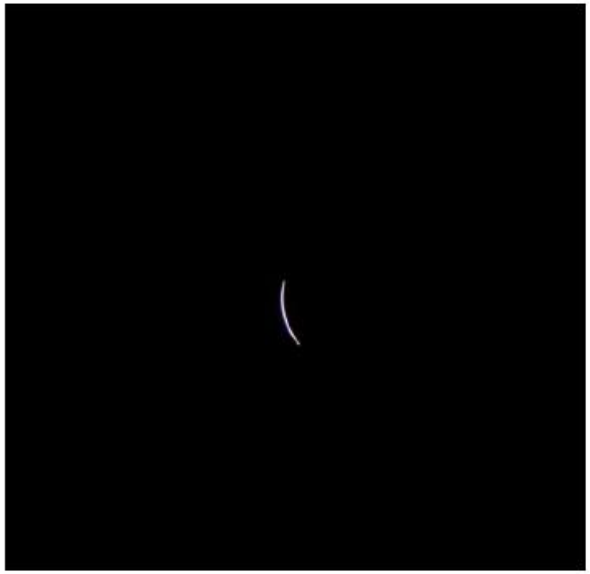

Tinman detector data--- Eclipse flight August 21, 2017

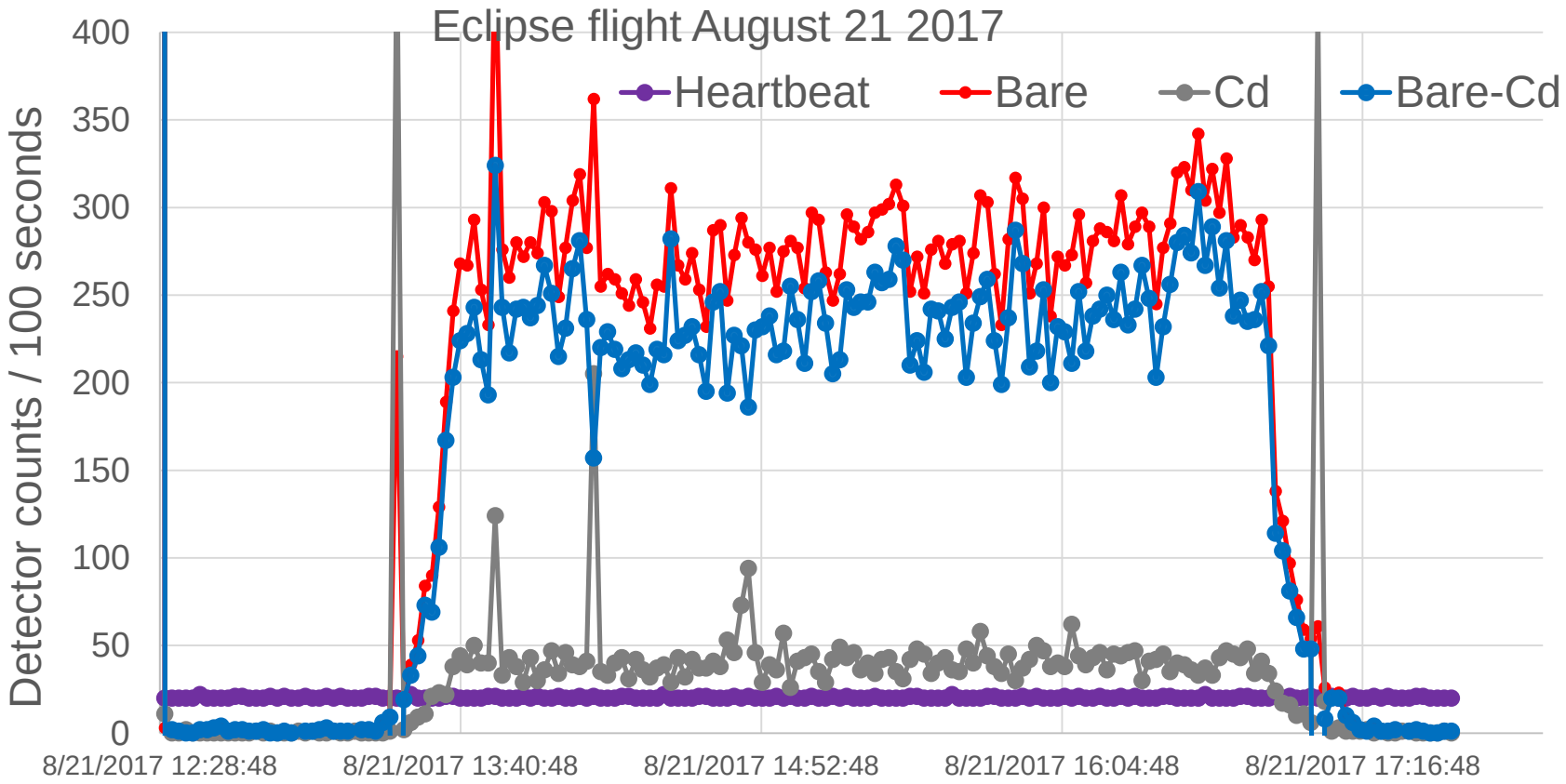

Tinman was flown on NASA DC-8

- The Tinman instrument was flown on 11 flights between Jan 13 and Feb 4, 2018 on the NASA DC-8 airplane

Tinman Detector

ID	Task Name	Duratio	Start
1	jan 13 2018 analysis	10.68 hr	Sat 1/13/18
2	Jan 17 2018 analysis	3.78 hrs	Wed 1/17/1
3	Jan 19 2018 analysis	4.52 hrs	Fri 1/19/18
4	Jan 23 2018 analysis	3.93 hrs	Tue 1/23/18
5	Jan 24 2018 analysis	5.05 hrs	Wed 1/24/1
6	Jan 29 2018 analysis	5.2 hrs	Mon 1/29/1
7	jan 30 2018 analysis	4.88 hrs	Tue 1/30/18
8	Jan 31 2018 analysis	4.58 hrs	Wed 1/31/1
9	Feb 1 2018 analysis	4.2 hrs	Thu 2/1/18
10	Feb 3 2018 analysis	9.88 hrs	Sat 2/3/18
11	Feb 4 2018 analysis	2.45 hrs	Sun 2/4/18
12			
13			

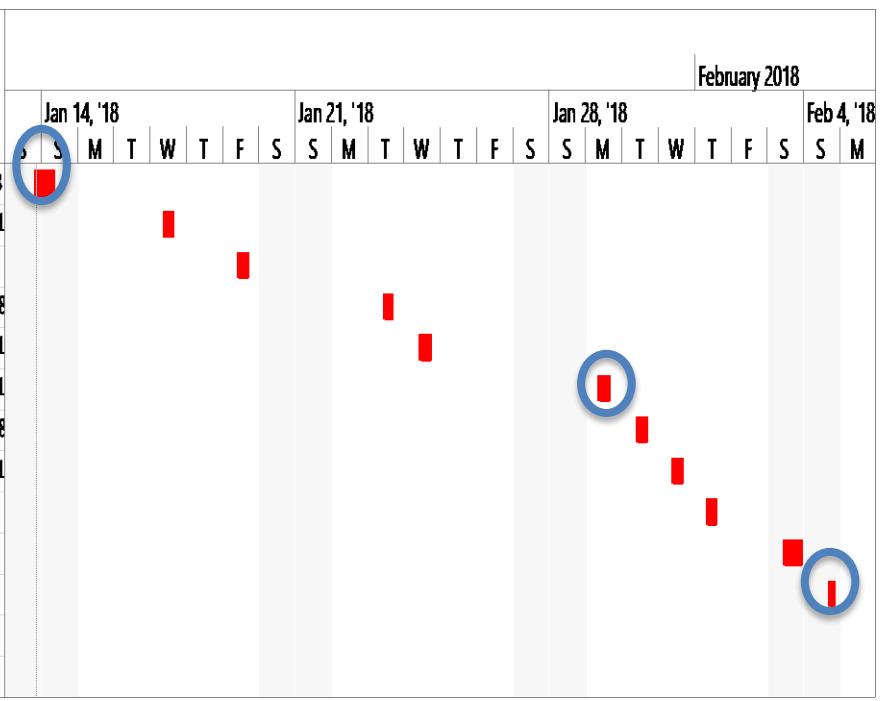

NASA DC-8 flight January 29, 2018

- This flight was around Ramstein, Germany

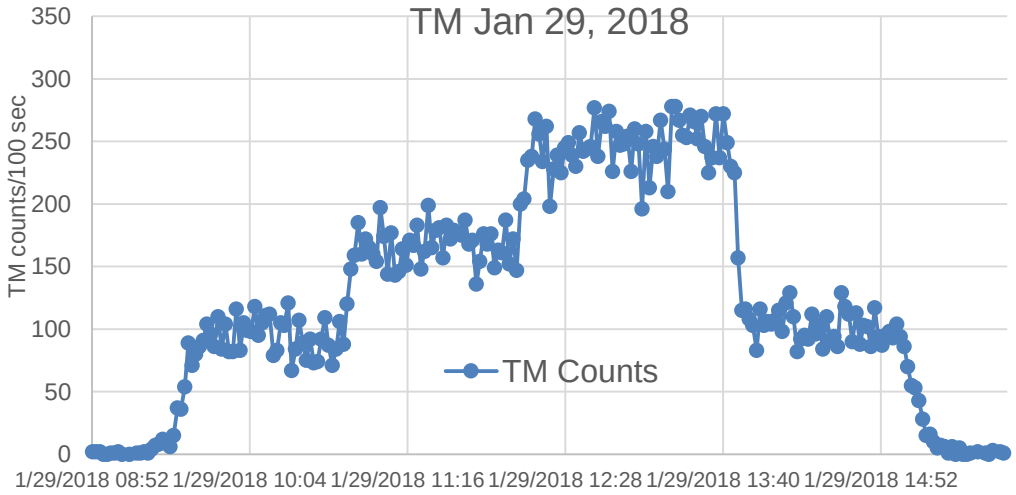

NASA DC-8 flight January 29, 2018

- This flight was around Ramstein, Germany with several changes in altitude

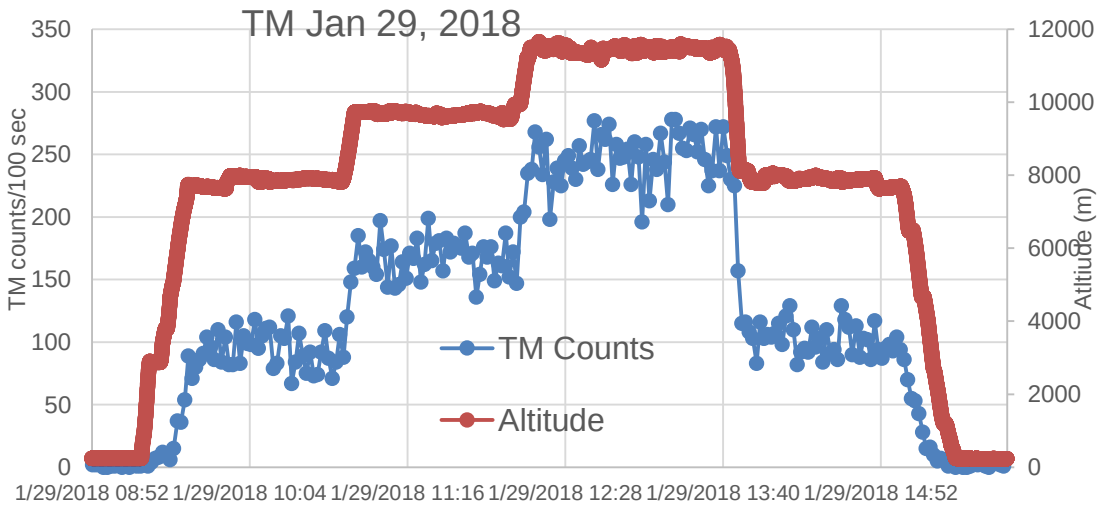

NASA DC-8 flight January 29, 2018

- This flight was around Ramstein, Germany with several changes in altitude but no significant change in latitude
- Straight line on semilog plot of detector count rate vs altitude show exponential absorption of cosmic-ray induced high-energy neutron flux

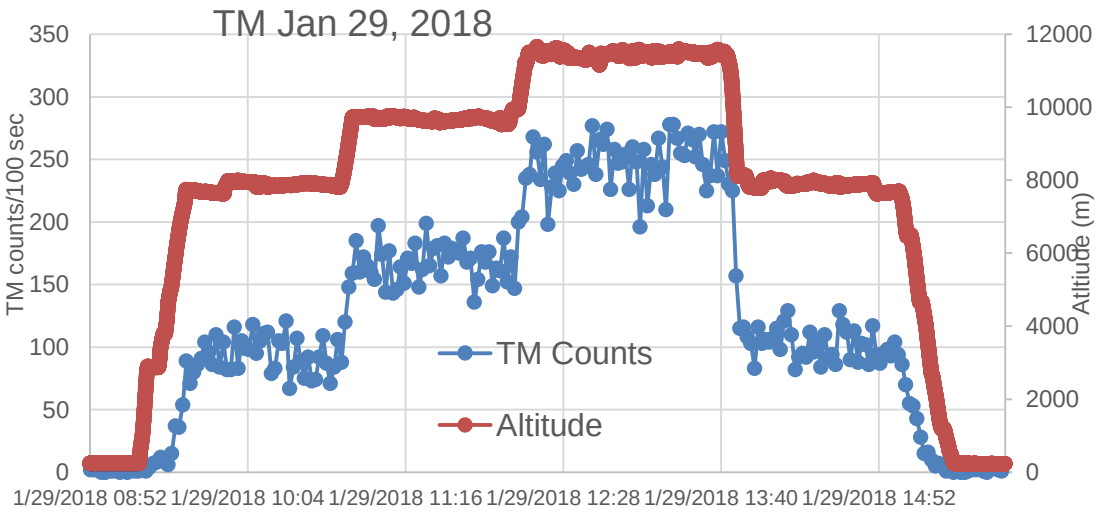

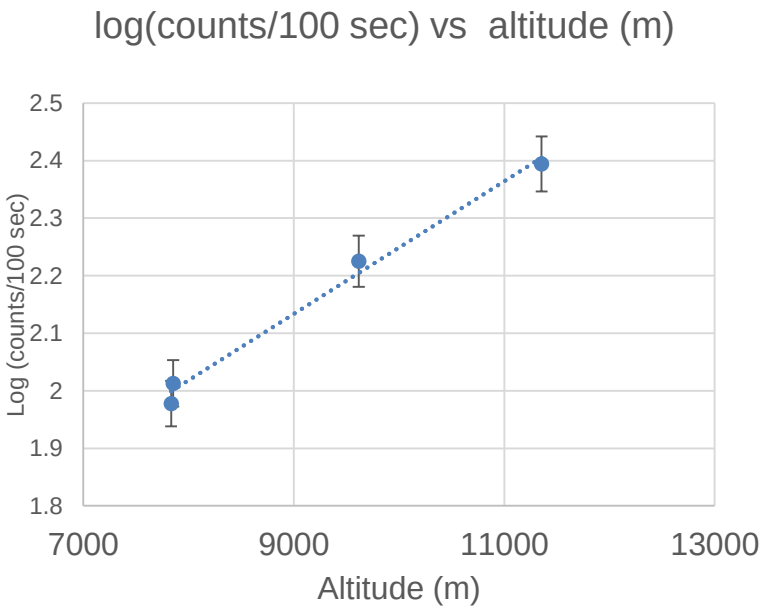

NASA DC-8 flight from Palmdale, Ca to Ramstein, Germany

- In this flight the thermal neutron rate does not track the altitude

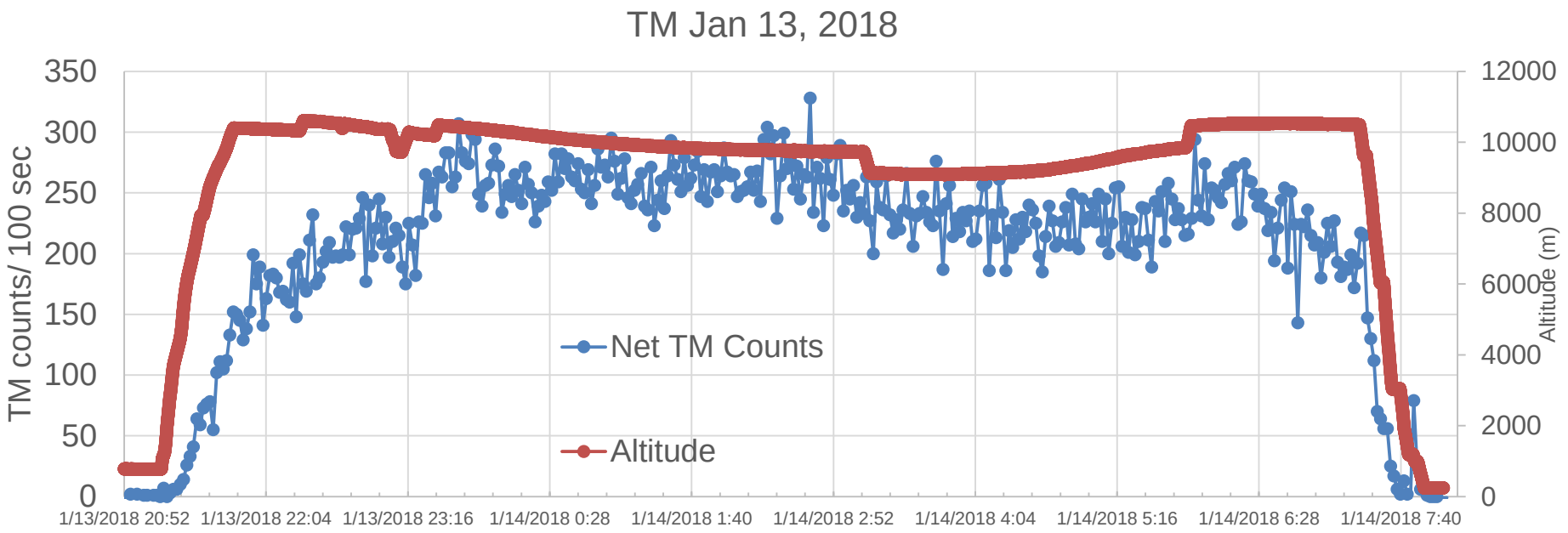

NASA DC-8 flight from Palmdale, Ca to Ramstein, Germany

- Green curve shows the increase in cosmic-ray neutron flux when flying north due to effect of latitude
- TM data shows good agreement with prediction

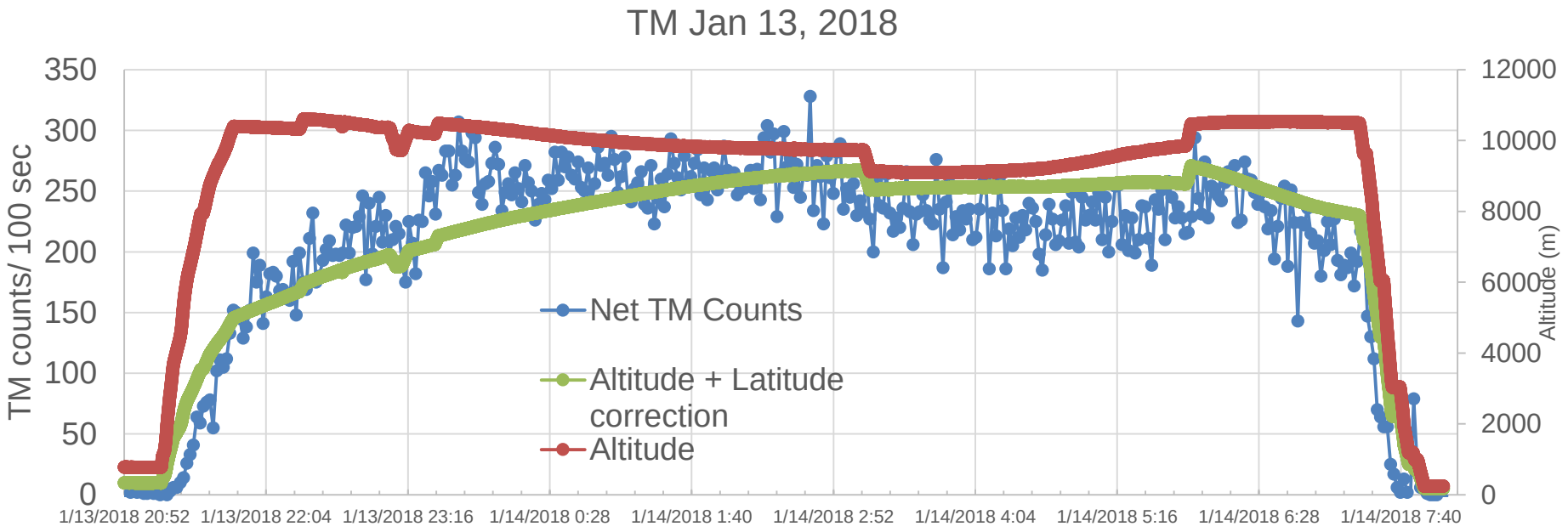

NASA DC-8 flight from Seattle, Wa to Palmdale, Ca

- Green curve shows the decrease in cosmic-ray neutron flux when flying south
- TM data shows good agreement with prediction

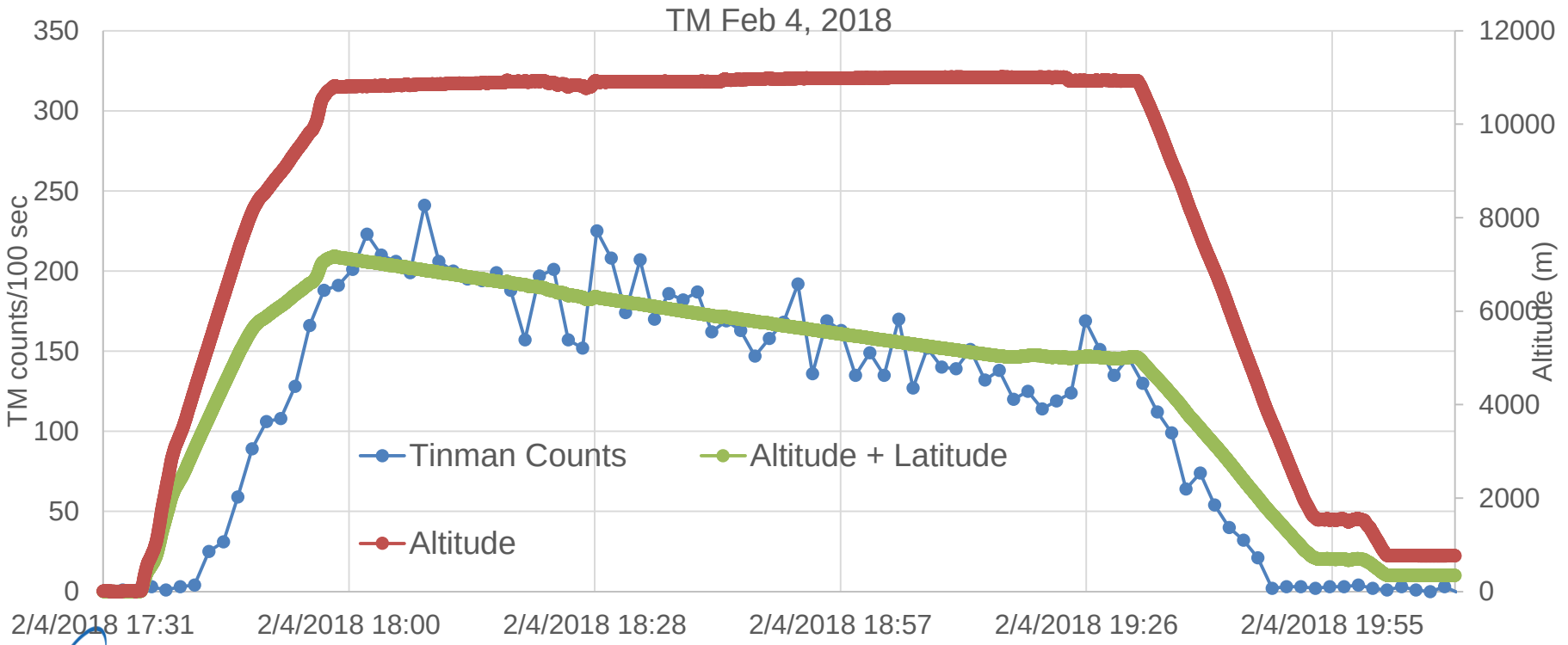

Simple model predicts failures from thermal neutrons

- Thermal neutron capture on ^{10}B is simple from nuclear physics side
  - Energy of outgoing particles does not depend on energy of incident particle
  - Angular distribution of emitted particles is isotropic and does not depend on energy. There are 4 possible particles

Reaction	Particle	Energy	Energy loss	Range	Q_{total}
		MeV	MeV/mg/cm^2	nm	fC
n+^{10}B+γ (94%)	^{7}Li	0.84	2.10	2460	37.3
	α	1.47	1.15	5150	65.4
n+^{10}B gs (6%)	^{7}Li	1.01	2.18	2800	45.0
	α	1.78	1.06	6340	79.0

- Assume a semiconductor device
  - 65 nm feature size
  - q_{crit} ~1.2 fC
  - Size of sensitive volume ~100 nm
- Assume energy to produce e-h pair is 3.6 eV
- If deposit greater than q_{crit} in path length of 100 nm can get an upset
- We have observed thermal neutron upsets

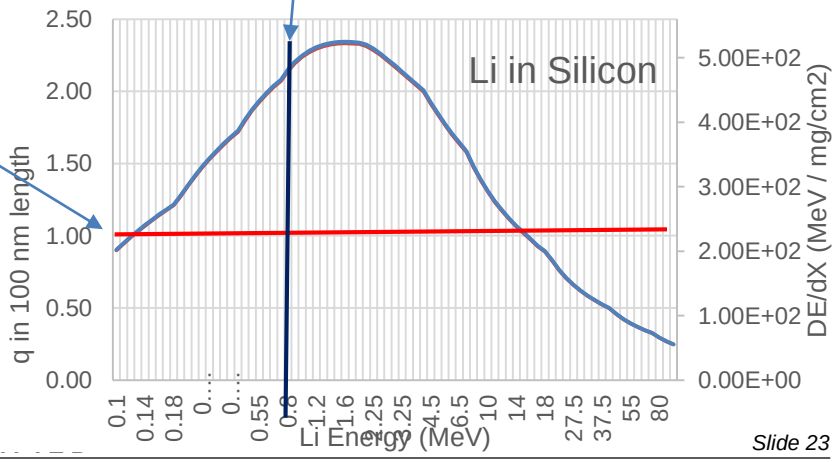

Future work

- Additional flights
  - Measure the thermal neutron intensity in other aircraft to determine the effect of moderating material (fuel mass, geometry, etc.) on thermal neutron production
  - Measure the thermal neutron rate in different locations in the same airplane under similar conditions of fuel, altitude and latitude to determine the spacial distribution of the thermal neutrons
- Simulations
  - Complete the absolute efficiency determination of TM to thermal neutrons. When this is completed, we will know the number of thermal neutrons in aircraft environments.
  - Model (MCNP) the thermal neutron intensity at different altitudes and different locations within the airplane. The results of these calculations can be compared to our measurements. Can we predict our measurements?
- Additional measurements
  - Measure the effect of thermal neutrons on various electronic devices (SEU cross section). With knowledge of the number of thermal neutrons/cm^2/sec in an airplane (from NASA flights) and SEU cross section (measurements at LANSCE), we will be able to predict the number of fails/flight hour in aircraft due to thermal neutrons.
  - Work has begun on measuring the failure rate due to thermal neutrons at LANSCE. We are proposing a room-temperature thermal neutron flight path at LANSCE.

Conclusions

- Tinman instrument works well for detecting thermal neutrons in aircraft--there are thermal neutrons
- The effect of altitude and latitude on the thermal neutron count rate is clearly observed
- Considerable work needs to be done to answer the question of the importance of thermal neutrons in aircraft

Neutrons can cause failures in high-power semiconductor devices

- Insulated Gate Bipolar Transistors (IGBT) are semiconductor devices that are used in many high-power applications such as BART, hybrid cars, accelerator RF systems, etc.
- The lifetime of these devices in neutron fields depends on the electric field or the applied voltages
- Tests show a dramatic decrease in lifetime at a critical voltage which is significantly below the rated operating voltage

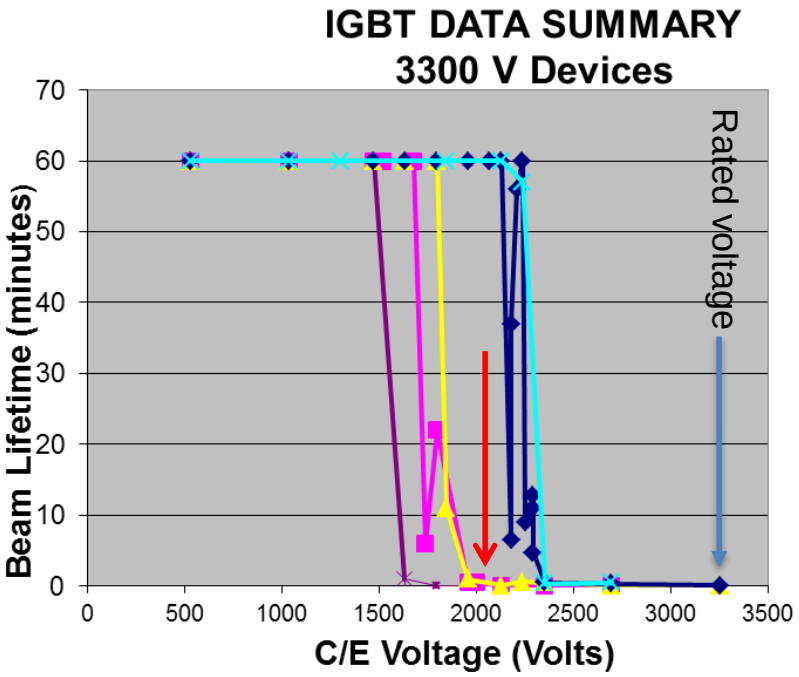

One neutron can stop a train

Results of LANSCE/WNR measurements determine problem with ASCI Q-Machine

- The ASCI Q-Machine has 2048 nodes with a total of 8192 processors.
- During commissioning, it was observed that the Q-machine had a larger than expected failure rate. Approximately 20 fails / week (~3 fails / day).
- The question was whether this could be the result of neutron single-event upset.

ASCI Q-Machine at Los Alamos National Laboratory

Fails/day ~ [# of fails/neutron] * [# neutrons/day]

Measured at LANSCE

Cosmic-ray neutron flux

Tinman detector was on three NASA airplane flights

- ER-2, G-III (Eclipse mission) and DC-8 to Germany
- Data recorded for:
  - Bare detector
  - Cd covered detector
- Found exponential decrease in count rate at lower altitudes due to absorption of the high-energy neutrons in the atmosphere.
- Observed latitude dependence in count rate because of the earth's magnetic field
  - Altitude and Latitude taken from airplane GPS
  - Correction for latitude taken from empirical formula (Normand, IEEE Trans. Nucl. Sci 43, 1996, 461)

    $F(L)=0.6252*\exp[-0.461\cos^2(2L)-0.94\cos(2L)+0.252]$

- Results of Tinman detector show good agreement with aircraft data

Measurement of Thermal Neutrons in Aircraft

S. A. Wender, A. Couture, Lukas Zavorka, Tom Fairbanks, Suzanne Nowicki, Laurent Ferres

Los Alamos National Laboratory, Los Alamos NM 87545

Laura Dominik,

Honeywell, Inc, Minneapolis, MN

Introduction

Thermal neutrons have recently become a concern in the semiconductor community where it has been reported [1,2,3] that approximately 10-20% of the observed single-event upsets in terrestrial environments are due to thermal neutrons. The goal of this project is to measure the intensity of thermal neutrons in aircraft at flight altitudes. To accomplish this goal, we designed and fabricated a neutron detector that is sensitive to thermal neutrons called TinMan (TM). The TM detector consists of two identical ^{3}He ionization chambers with one detector bare and one detector shielded with cadmium. Because the cadmium shielding effectively blocks the thermal neutrons, the difference in count rates between these two detectors reflect the number of thermal neutrons detected.

We will discuss the design of the detector, the signal processing electronics, the data acquisition approach and initial commissioning of the detector. We will also present the results obtained on several NASA aircraft flights at aircraft altitudes.

Background

Thermal neutrons are presently thought to be a possible threat to the reliable operation of semiconductor electronic devices. Thermal neutrons are produced when high-energy neutrons, which are produced by cosmic-ray interactions in the atmosphere, strike moderating material and lose energy to approximately 0.025 eV (2200 m/s). These thermal neutrons can interact with material in semiconductor devices and in some cases produce charged particles via nuclear reactions that can deposit charge in sensitive volumes of the device and produce upsets. Because the intensity of thermal neutrons depend on the particular environment, it is difficult to characterize the thermal neutron intensity without specifying the surrounding environment so direct measurements or simulations are necessary.

In aircraft, if we assume that high-energy cosmic-ray induced neutrons shower the aircraft, the intensity of thermal neutrons at a particular location depends on the amount, geometry and proximity of the moderating material to that location. Therefore, we would expect more thermal neutrons near moderating material such as water or fuel and less thermal neutrons as we move further away from the moderating material. In addition, as we will discuss later in this paper, since the high-energy neutron flux depends on the aircraft's altitude and latitude the thermal neutron flux depends on the aircraft altitude and latitude. Because of the dependence on the local environment, it is difficult to give a specific value for the thermal neutron intensity. Because of this environmental dependency, very few thermal neutron measurements have been reported.

Thermal neutrons are be a particular concern in aircraft because at flight altitudes the high-energy neutron intensity is about 300 times greater than at sea level and large aircraft have significant amounts of thermalizing material such as fuel, passengers and the aircraft itself. If it is found that a significant number of thermal neutrons are present, it may be necessary to qualify semiconductor devices in flight critical systems in thermal neutron environments.

A major concern for thermal neutron production of single-event effects (SEE) is the boron content in semiconductor devices. Natural boron consists of two isotopes: ^{10}B (20% abundant) and ^{11}B (80% abundant). ^{10}B has a very large thermal neutron capture cross section (3840 barns) and produces energetic charged particles (^{7}Li and α) that can deposit charge in semiconductor devices and therefore cause upsets. 94% of the capture reactions leave the ^{7}Li ion in the 480keV first excited state. In this case, the ^{7}Li ion recoils with 0.84 MeV, loses 2.1 MeV/mg/cm^2 energy loss initially and have a range of 2460 nm. The alpha particle has 1.47 MeV of energy, an initial energy loss of 1.15 MeV/mg/cm^2 and a range of 5150 nm in silicon. These charged reaction particles can deposit sufficient charge in a semiconductor device to cause a SEE.

The effect of thermal neutrons on a semiconductor device is the product of the number of thermal neutrons present, "a flux", and the effect of thermal neutrons on the device, "a cross section". Both the flux and the cross section depend on the neutron energy so the failure rate is a convolution of the flux and cross section. This effort is focused on determining the number of thermal neutrons in aircraft at aircraft altitudes. It will also be important to determine the cross section for upsets due to thermal neutrons. This is a possible subsequent measurement that can be performed at the LANSCE Lujan Center thermal neutron source or any other thermal neutron source in the future. There have been several measurements of SEE associated with thermal neutrons [4,5].

Design of thermal neutron detector

We fabricated a thermal neutron detector called TinMan (TM) to meet the requirements for installation in an aircraft. TM was designed to operate on 28 volts which was the voltage supplied by the aircraft. The detector draws approximately 360 mA of current (10 W) and can be powered by external batteries if desired. We designed a battery pack that consists of two 12V 12 A-Hr sealed AGM lead acid batteries (GP 12120) in series which brings the voltage to 24 volts. These batteries are connected to a TDK-Lambda DC-DC converter (PAF500F24-28) which can deliver 28 volts output with an input voltage in the range of 18-36 volts. With these batteries we expect to be able to power TinMan for approximately 30 hours. Larger batteries can be used if longer operation time is required.

The detector uses two identical cylindrical ^{3}He ion chambers. The two model #25141 detectors were purchased from LND, Inc. [6]. The specifications from the manufacturer are given in Table 1. ^{3}He detectors were chosen because they have excellent efficiency for thermal neutrons while being particularly insensitive to neutrons of higher energies and gamma rays.

When a thermal neutron captures on ^{3}He, a 191 keV triton (^{3}H) and a 572 keV proton are produced. If both particles deposit their energy in the gas, the total 763 keV of energy is detected. If one or both particles strike the walls of the detector, less energy is deposited in the gas and a distribution of energies is recorded.

Table 1

LND 25414 cylindrical He-3 neutron detector

Effective Length	13 cm
Effective diameter	1.55 cm
Gas pressure	2667 Torr
Operating voltage	630 V
Resolution (% fwhm)	6 %
Sensitivity	5.2 counts/sec/nv

Two identical detectors were used. One detector is shielded with cadmium and one is unshielded. Because Cd has a very large absorption cross section for thermal neutrons (E_n<0.4 eV), it effectively blocks all thermal neutrons from the detector. The difference in count rates between the two detectors is used to determine the contribution from thermal neutrons. The thickness of the Cd shielding is 0.05 cm. With the cadmium absorption cross section of 2520 b, we get an attenuation of approximately 2.8 10^{-3} for this thickness of cadmium. The effect of the cadmium shielding on the bare detector is negligible and was measured by comparing the count rate in the bare detector with and without the cadmium shield in in the second detector.

Figure 1 shows a block diagram of the signal processing electronics. The ^{3}He detector is powered

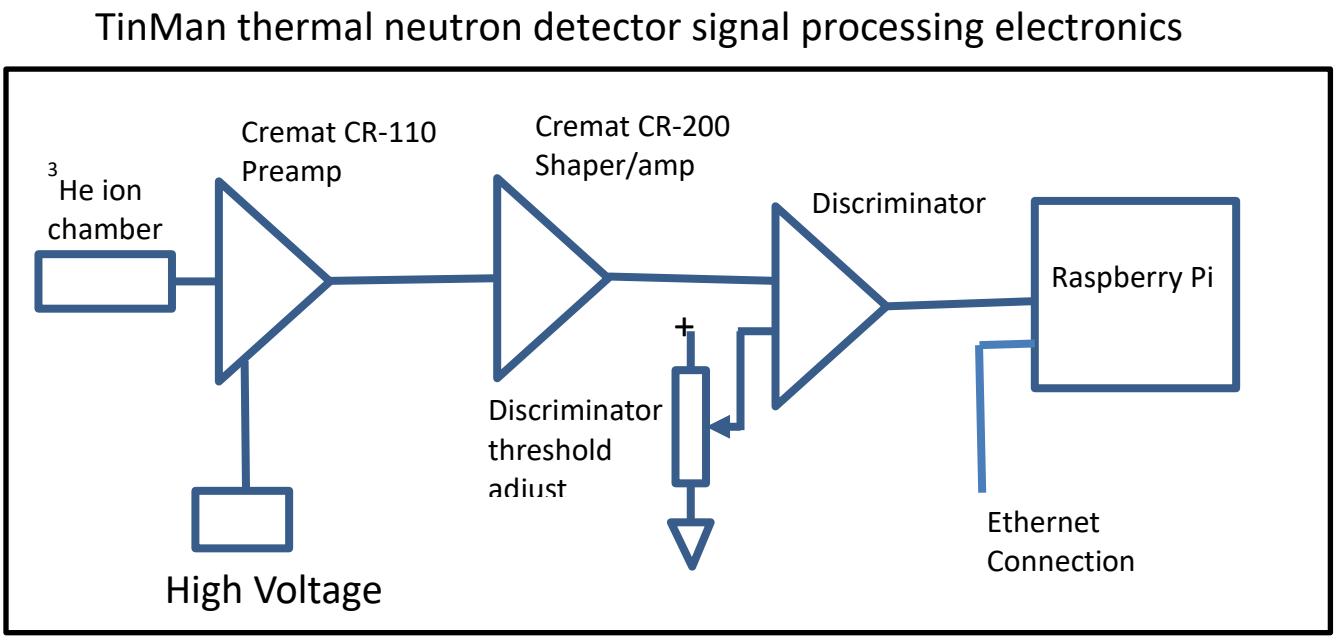

Figure 1. The signal processing electronics diagram of the thermal neutron detector

through a Cremat [7] CR-110 preamp and is operated at +630 V as recommended by the manufacturer. The preamp is mounted on a Cremat CR-150-R5-CSP evaluation board which provides the power and input/output circuitry for the preamp. The output pulse from the preamp is approximately 15 mV high, has a rise time of ~1 μS and a fall time of approximately 200 μs.

The output of the preamp passes through a pulse Shaper/Amplifier (Cremat CR-200-8μs-R2.1). The Shaper/Amplifier is mounted on a CR-160-R7 evaluation board which provides signal gain, DC level and pole-zero adjustments. The Shaper/ Amplifier converts the output of the preamp to a Gaussian shaped pulse with a FWHM of approximately 15 μs and is approximately 5 volts high. An important feature of the shaper is that it stabilizes the baseline and lets the discriminator operate at the several 100 mV level.

The gains of the two detectors were matched by comparing their pulse height spectra in a multichannel pulse-height analyzer. Following the Shaper/Amplifier the pulse is input into the discriminator circuit that produces a TTL logic pulse when the input pulse exceeds the voltage level of the discriminator.

Figures 2 and 3 show the pulse height spectrum of the two ^{3}He detectors from a moderated Pu-Be neutron source. The peak in the spectrum corresponds to the ejected proton and tritium ions depositing their full energy in the counter gas. The total energy is 763 keV. The counts to the left of the peak are events where the ejected ions hit the walls and do not deposit their full energy in the gas. Also shown in figures 2 and 3 are the pulse height spectra gated by the discriminator. We set the discriminator level to be in region above the noise but below the energy of the reaction products at approximately channel 50. The discriminator is set to 0.75 V.

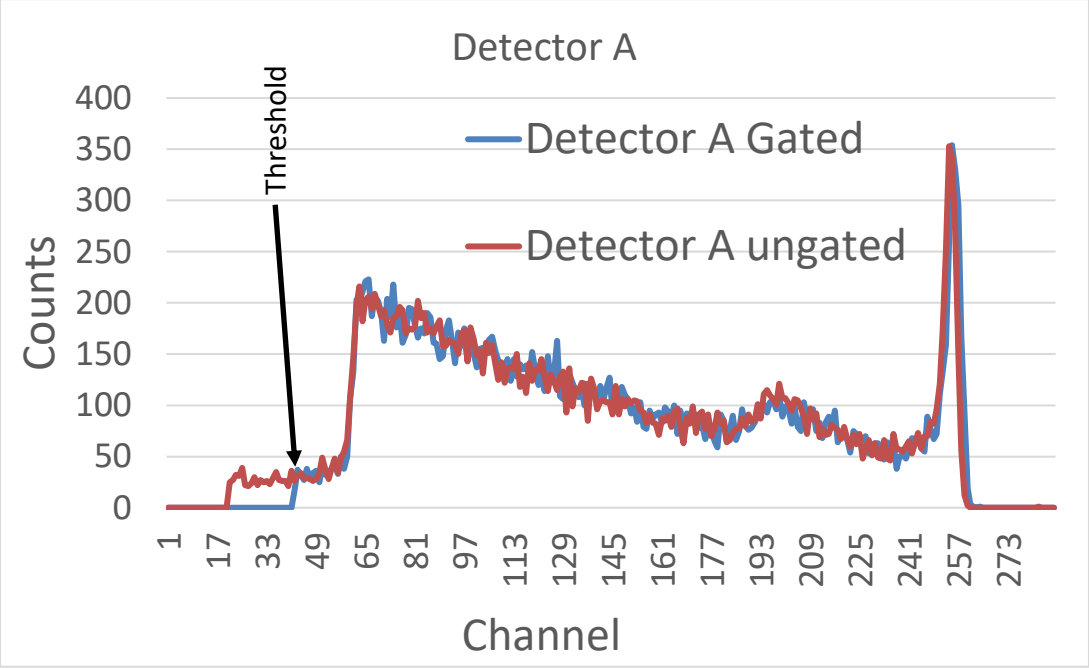

Figure 2. Pulse height spectrum of the ^{3}He Detector A using moderated thermal neutron source. The purple line is ungated and the green line is gated by the discriminator.

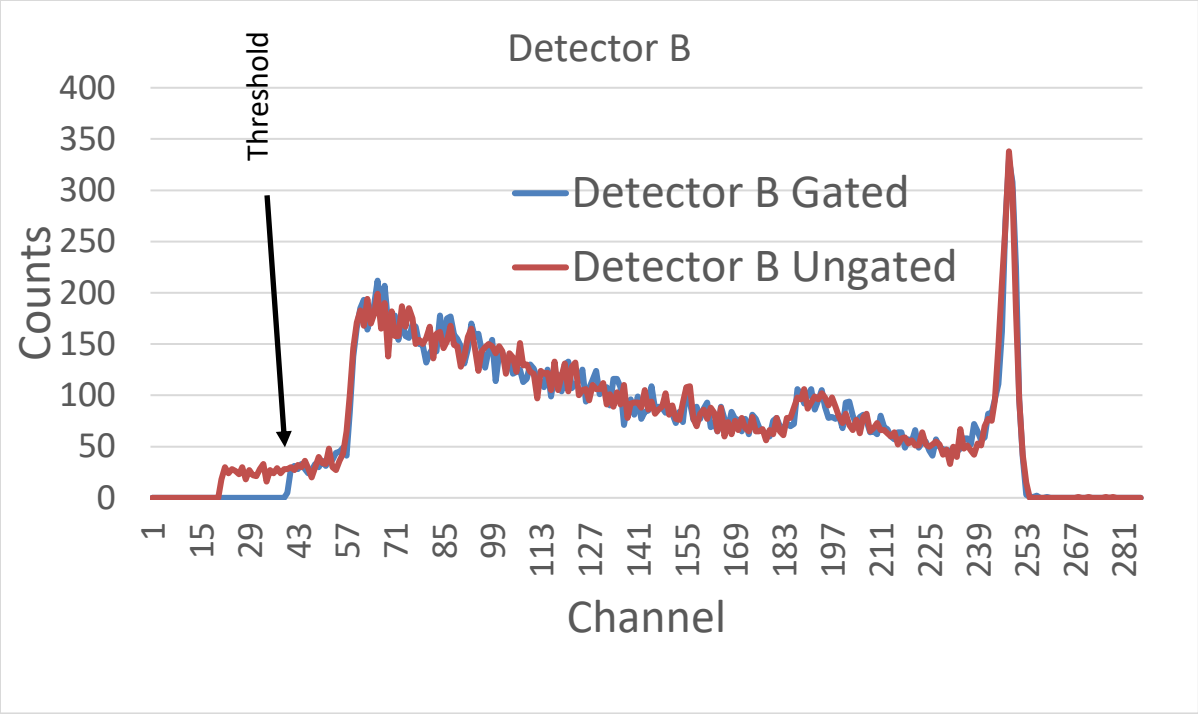

Figure 3. Pulse height spectrum of the ^{3}He Detector 2 using moderated neutron source. The purple line is ungated and the green line is gated by the discriminator.

Fabrication of thermal neutron detector

The thermal neutron detector was fabricated by the staff of the Intelligence and Space Research (ISR) Division at Los Alamos National Laboratory (LANL) to meet the mechanical and electrical specifications for NASA aircraft. The box containing the detectors and the electronics is approximately 0.63 cm thick aluminum. This thickness of aluminum will attenuate thermal neutrons by approximately 5%.

Figure 4 shows the detector box with the Ethernet cable on the left, the power cable on the right and the power switch and indicator lights. The detector box is 38 cm x 38 cm and 7.6 cm deep. Figure 5 shows the inside of the detector box with the lid rotated up.

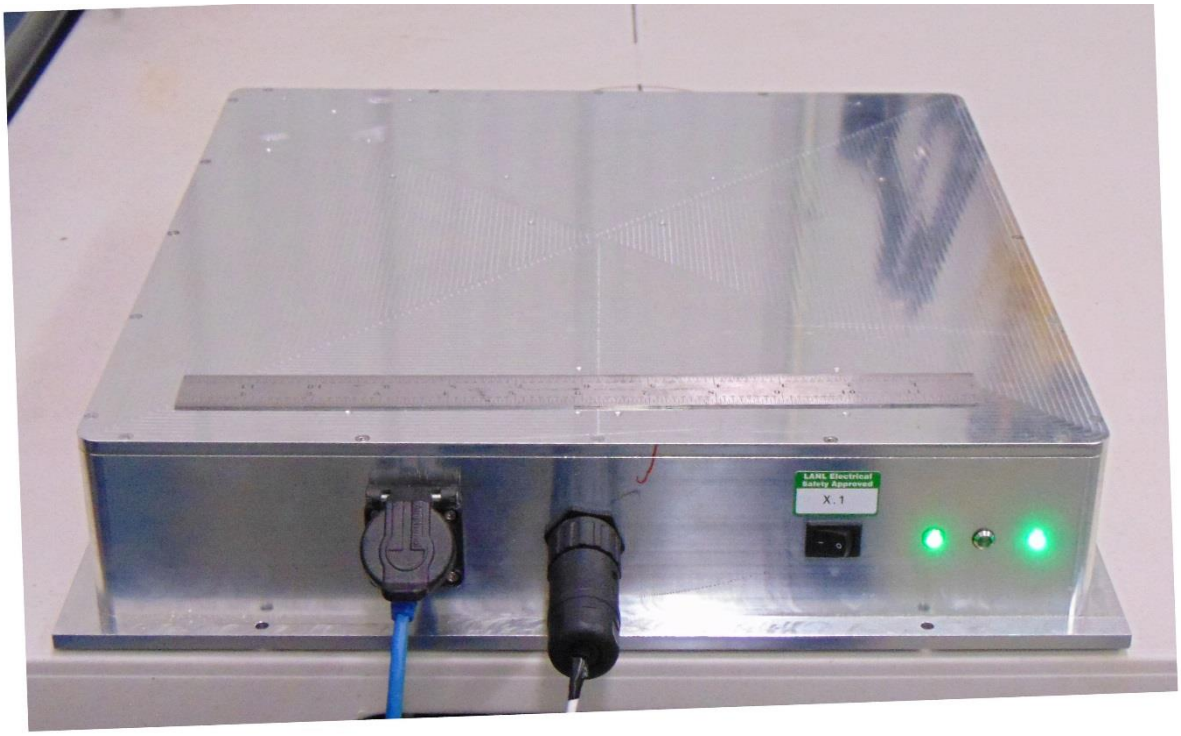

Figure 4. The TinMan detector enclosure with the Ethernet and power cables connected. The scale on top of the detector is 30.5 cm long

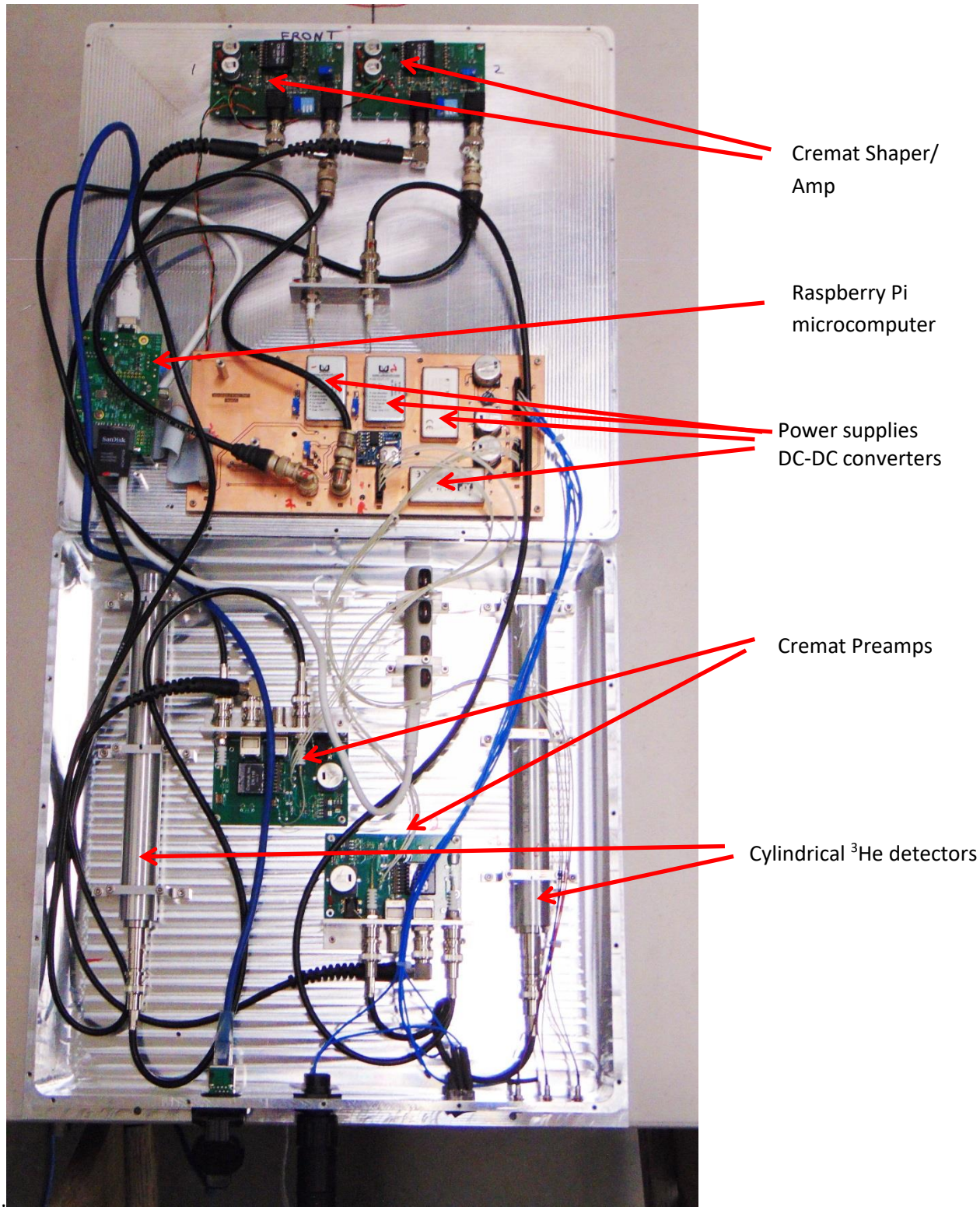

Figure 5. Inside of the TinMan neutron detector. The Raspberry Pi microcomputer, the power supplies, the shaper/amps and the discriminator circuits are attached to the lid of the box. The cylindrical ^{3}He detectors and the pre-amps are mounted to the bottom of the box.

Data acquisition software

The data acquisition software runs on a Raspberry-Pi (R-Pi) microcomputer and starts automatically as a daemon on boot. The R-Pi has a LINUX based operating system (Raspbian). The WiringPI GPIO library (http://wiringpi.com) together with custom C++ code is used to detect the TTL logic pulses as interrupts on the GPIO pins. The timestamp of the event in unixtime is recorded as well as the identifying number of the detector that fired. A DT1307 real-time clock is used to maintain system time when TinMan is not on the network. The internal R-Pi watchdog is enabled so that if the system becomes non-responsive for more than 15 seconds, it is rebooted. While the DAQ software is running, it maintains the watchdog. After a fixed time (nominally 10 minutes), the DAQ closes, the watchdog is no longer maintained, and the system automatically reboots, restarting the DAQ.

The TTL logic outputs from the two ^{3}He detector discriminators are input to the R-Pi computer. When the R-Pi receives this interrupt signal from the detector, it records a time stamp of the event to 100 μs precision and information about which detector fired. Lists of time stamps and detector identifications are stored in files that are filled for 10 minutes. After 10 minutes, the files are closed and a new file is opened. These data are stored on 4 memory sticks for redundancy. In addition to the detectors, a heartbeat signal triggers the R-Pi every 5 seconds to determine that the program is operating correctly. The time stamps can be sorted by detector and subsequently binned and presented as a histogram of count rate vs. date/time for each detector for any time bin width chosen.

The system was designed so that if there are any power interruptions the system will restart automatically when power is restored. The data is readout via Ethernet cable to a computer running WINSCP or some other program. If necessary, the memory sticks can be removed from the detector and the data downloaded without the R-Pi operating.

Calibrations

Our analysis of the data assumes that the relative acceptance of the two detectors are the same. We can measure the relative acceptance of the two detectors by removing the cadmium shielding from shielded detector and counting ambient thermal background. Measuring the relative acceptance of the two detectors is crucial to determining the thermal neutron intensity. Figure 6 shows the background count rate for the two detectors at Los Alamos altitude with the cadmium shield removed from the shielded detector so both detectors are unshielded. Error bars were not included to simplify the plot. The variations in the count rate reflect the statistical uncertainties in each measurement.

The data were acquired over a 4-day period. As seen in the plot, the count rates are essentially the same in both detectors with an average count rate of 81.9+/- 0.5 counts per 1000 sec in the bare detector and 82.3+/- 0.5 counts per 1000 sec in the “shielded” Detector with she cd shielding removed. The average difference is approximately 0.5%. This difference can be attributed to variations in the detectors and thresholds. We can correct for this difference if necessary.

In figure 7, we show the count rate for the unshielded detector (blue line) and the cadmium covered detector (red line) counting background radiation at Los Alamos altitudes. As seen in the figure, the count rate in the cd-shielded detector is significantly less than the unshielded detector. The difference between the bare and the shielded detectors is the contribution from thermal neutrons.

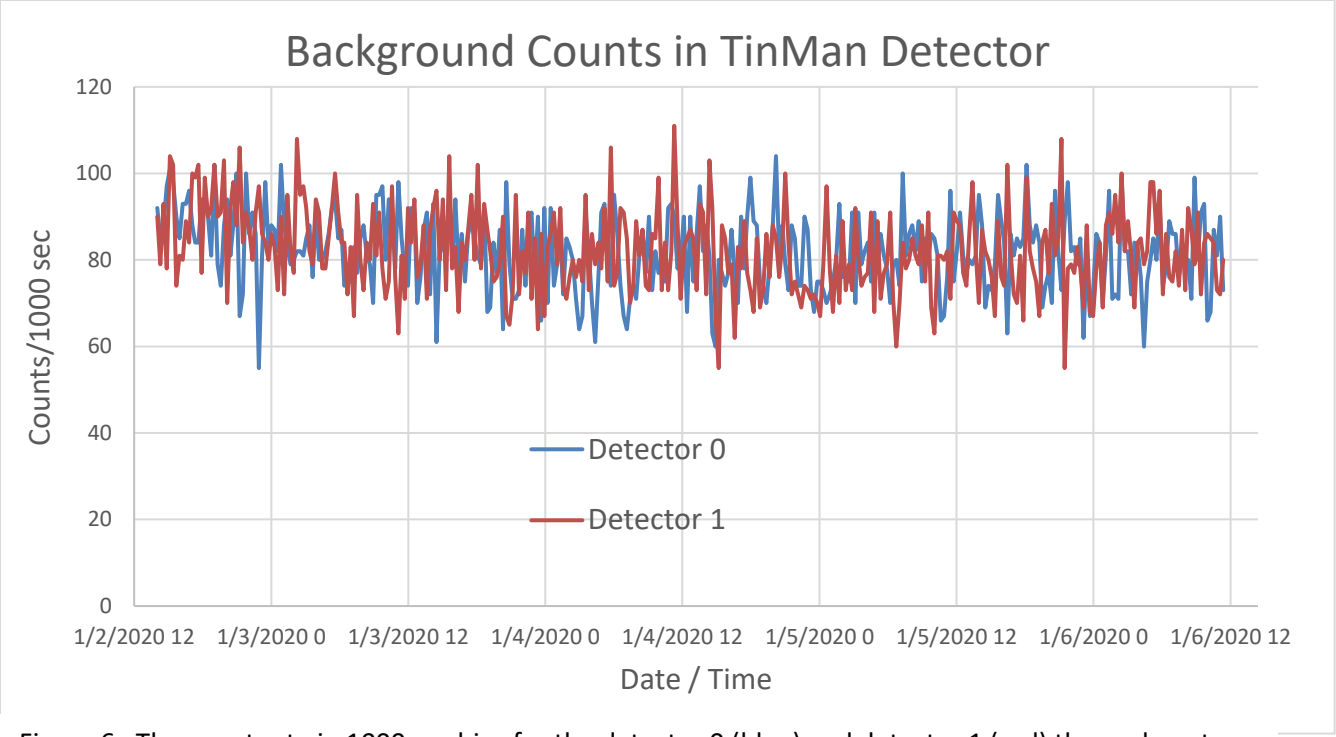

Figure 6. The count rate in 1000 sec bins for the detector 0 (blue) and detector 1 (red) thermal neutron detectors when both are unshielded.

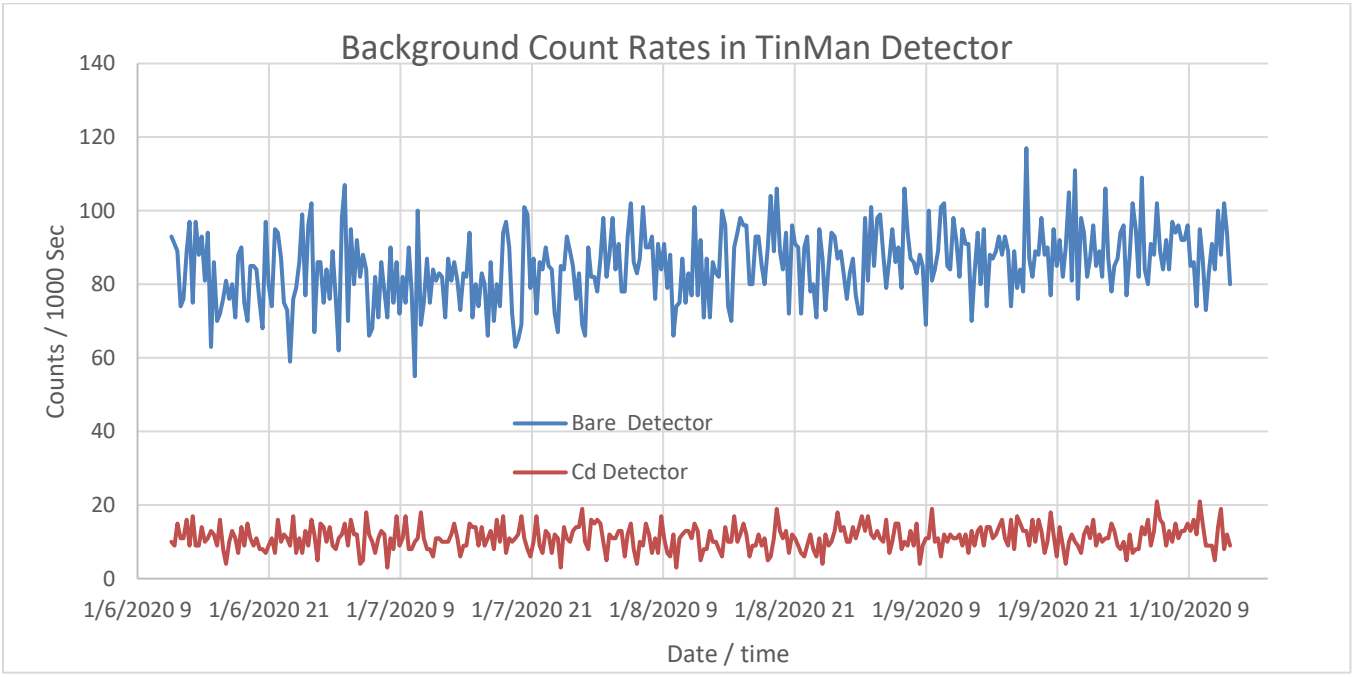

Figure 7. The count rate in the bare detector (Blue line) and the Cd shielded detector (red line)

The data shown in figure 7 were taken over 4 days. The average count rate for the bare detector was 85.1+/- 0.5 counts/1000 sec and agrees with the previous measurement in of the bare detector within 4%. The count rate in the cadmium-shielded detector was 11.1+/- 0.2 counts/1000 sec. The net number of counts/sec due to thermal neutrons is the difference between these rates or 74.0 +/- 0.6 counts/ 1000 sec. The non-thermal count rate (cadmium detector) is 13% of the total rate (in bare detector).

To convert counts in the detector to number of neutrons/cm^2 you need to know the detector efficiency. The efficiency of the detector is given by the manufacturer and is listed in Table-1 as 5.2 cps/sec/nv. The where n is the density of neutrons in neutrons/cm^3 and v is the velocity in cm/sec. The sensitivity can also be expressed as 5.2 counts/[neutron/cm^2].

In order to check the sensitivity of the detector we performed our own MCNP Monte-Carlo simulations. We studied various neutron source geometries and detector orientations. These included parallel planar beam incident on the side of the detector and spherical source surrounding the detector. We also modeled the geometry using monoenergetic thermal neutrons and a thermal neutron spectrum whose energy went up to 0.4 eV, the cadmium cutoff energy. The results of our simulations are summarized in Table 2. It is clear from our simulations that the efficiency of the detector depends on the geometry of the neutron beam and the orientation of the detector. In order to get a more precise value of the detector efficiency we would need to model the aircraft to get the specific thermal neutrons source spacial distribution. This calculation is beyond the scope of the paper and will be the subject of future work. Our conclusion was that the most realistic value for the sensitivity is 5.0 counts/n/cm^2 which is for a spherical source with a distribution of thermal neutrons up to the cadmium cut off. This value agrees well with the manufacturer's value of 5.2 counts/n/cm^2.

Figure 8 shows the number of thermal neutrons/cm^2/hr at our lab in Los Alamos obtained by subtracting the counts/s in Cd shielded detector from bare detector using the data shown in Fig. 7 and including the sensitivity of 5.0 counts/n/cm^2 and expressing the rate per hour. We have not included error bar to simplify the plot.

Table 2

Monte-carlo calculations of detector efficiencies for different source geometries

Source contiguration	Detector efficiency counts/n/cm^2
Planar source Parallel beam	7.64
Point source at 50 cm	7.61
Planar source into 4π at 50 cm	6.67
Spherical source at 25 cm, monoenergetic thermal neutrons	6.86
Spherical source at 25 cm, thermal neutron spectrum	5.00

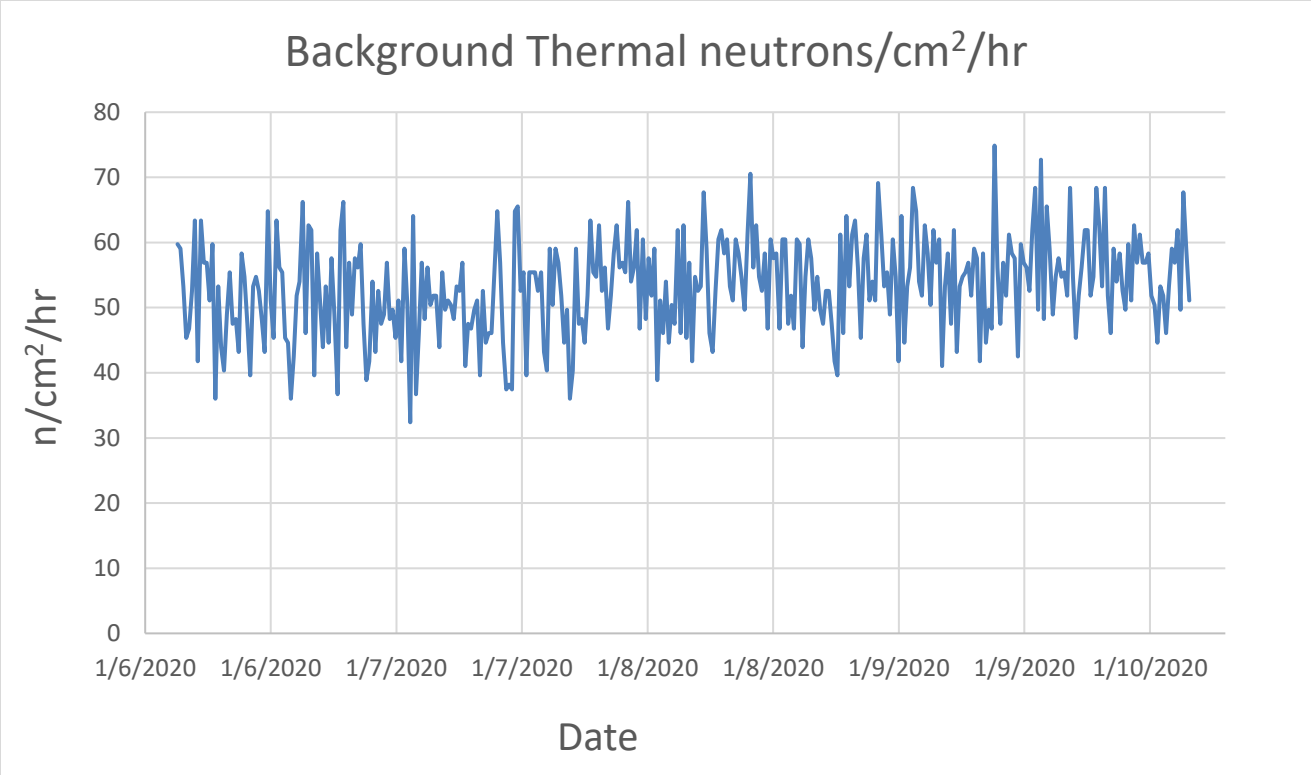

Figure 8 shows the number of thermal neutrons/cm^2/ hr as a function of time.

The average value of the number of thermal neutrons/cm^2/hr that we measure with TM is 53.3 +/- 0.4.

Results of aircraft flights

The primary goal of these measurements was to determine the thermal neutron intensity in typical aircraft at typical flight conditions. Since thermal neutrons are produced from high-energy neutrons interacting with thermalizing material, the number of thermal neutrons produced depends on the surrounding environment. In particular, how much thermalizing material there is in the aircraft. To accomplish this measurement we flew the TinMan detector on three different NASA aircraft [8]. The first flight was on the ER-2 aircraft. The detector was placed in a pod below the wing of the aircraft. The second flight was on the NASA Gulfstream-III business jet as part of the 2017 solar eclipse mission. The third aircraft was a NASA DC-8 which is a large 4 engine aircraft similar to a commercial passenger aircraft.

The results of the ER-2 flights showed that we needed larger He-3 detectors. The detectors (LND #25185) used in the ER-2 flights had neutron sensitivity of 0.6 counts/sec/nv and the geometry of the detector provided resolution of 25%. Expressed differently, the sensitivity is 0.6 counts/neutron/cm^2. In the ER-2 flight both the sensitivity and the energy resolution were inadequate.

We used a larger detector for the she second flight on the Gulfstream-III. The specifications of this detector (LND 25414) are listed in Table 1. The sensitivity for this detector as given by the manufacturer is 5.2 counts/sec/(nv) which is a factor of 9 greater than the previous detector and the resolution was improved from 25% to 6%. Figure 9 shows the results for the Gulfstream-III flight of August 21, 2017 which was during the solar eclipse. The red curve is the difference in the number of counts in the bare detector minus the number of counts in the cadmium-shielded detector divided by the sensitivity based on our MCNP calculation (=5.0 counts/thermal cm^2) expressed as thermal neutrons/cm^2/hr in 100 second time bins. The error bars are statistical. Also plotted in figure 9 is the altitude of the aircraft in

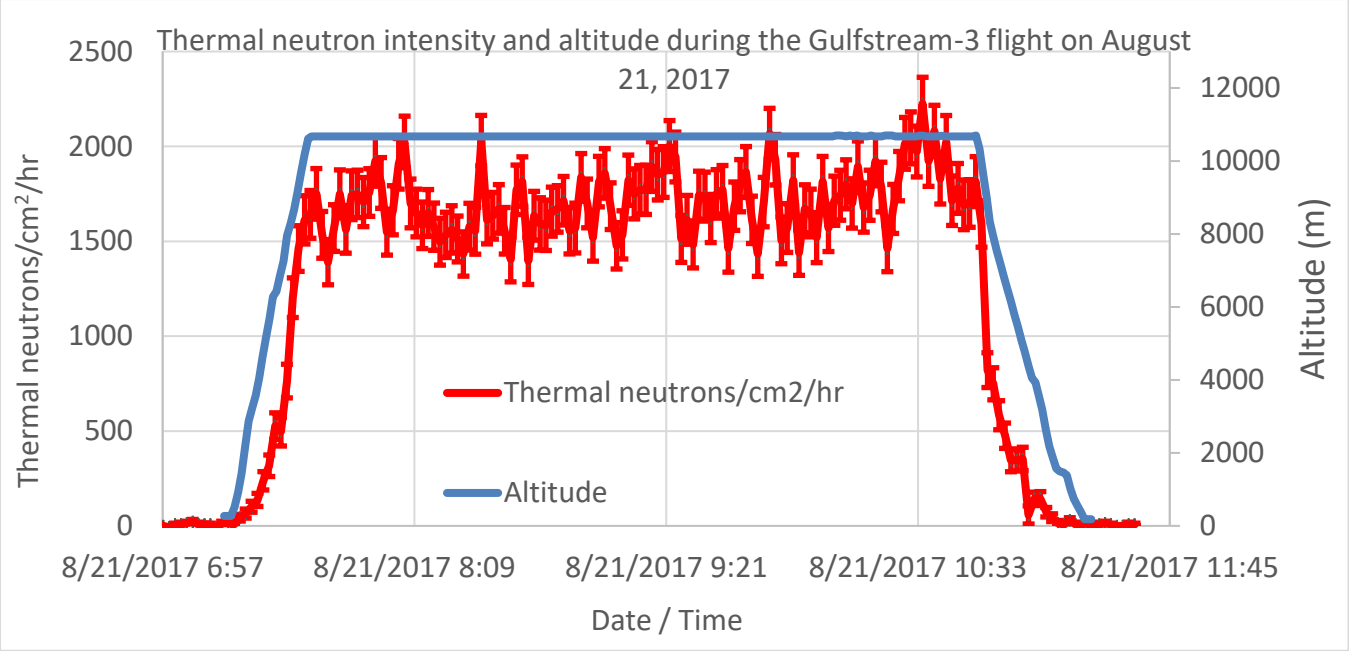

Figure 9. The number of thermal neutrons/cm^2/hr for the Gulfstream-III flight of August 21, 2019.

meters which was taken from the aircraft instrumentation. The flight was centered around 45° N latitude. As seen in the plot, the thermal rate rises from approximately 8.3 thermal neutrons/cm^2/hr at ground level to an average value of 1710+/- 16 neutrons/cm^2/hr at a flight altitude of 10.7 km. The increase between sea level and 10.7 km is a factor of 207.

The next series of flights were on the NASA DC-8 jet. This is a large 4-engine jet that is prototypical of a commercial passenger aircraft. This campaign consisted of 60 hours of flight time in 11 separate flights. The DC-8 flew from Armstrong Flight Research Center (AFRC) in Palmdale, Ca to the US Air Force base in Ramstein, Germany and back with several flights in Germany. These flights are summarized in Table-3.

Table-3

Summary of NASA DC-8 flight

Flight segment	Date	Duration (hr)	Location
1	January 13-14, 2018	10.7	Palmdale to Ramstein
2	January 17, 2018	3.8	Around Ramstein, Ge
3	January 19, 2018	4.5	Around Ramstein, Ge
4	January 23, 2018	3.9	Around Ramstein, Ge
5	January 24, 2019	5.1	Around Ramstein, Ge
6	January 29, 2018	5.2	Around Ramstein, Ge
7	January 30, 2018	4.9	Around Ramstein, Ge
8	January 31, 2018	4.6	Around Ramstein, Ge
9	February 1, 2018	4.2	Around Ramstein, Ge
10	February 3, 2018	9.9	Ramstein, Ge to Seattle, Wa
11	February 4, 2018	2.5	Seattle, Wa to Palmdale, Ca

As an example of our measurement results, we will discuss flight segment 1, 6 and 11.

January 13-14, 2018 flight from AFRC to Ramstein, Ge

This is a 10.7 hour flight between AFRC in Palmdale, Ca and Ramstein, Ge. Figure 10 shows the flight details including altitude (top), Latitude (middle) and longitude (bottom). As seen in the figure, the DC-8 takes off on January 13, 2018 at 2111 (UTC) from AFRC in Palmdale, Ca. The cruising altitude is a little over 10 km with some slight changes in altitude until it lands. The plane follows a great circle route with latitude changing from 35 degrees at AFRC to a maximum of 65 degrees then down to 50 degrees at Ramstein, Ge. The data from TinMan is shown in Figure 11. The three curves in figure 11 are the count rate in TinMan during the fight for the bare detector (Blue curve), the cadmium shielded detector (brown) and the difference count rate (bare-cd) is in grey. The count rate in the cadmium detector is approximately 18% of the bare detector. The bottom part of Figure 11 shows the number of counts in each detector binned in 100 second bins. We can convert these counts/100 second bin to the number of thermal neutrons/cm^2/hr using the sensitivity of 5.0 counts/n/cm^2.

Jan 13 2019 Flight data for flight from AFRC to Ramstein, Ge

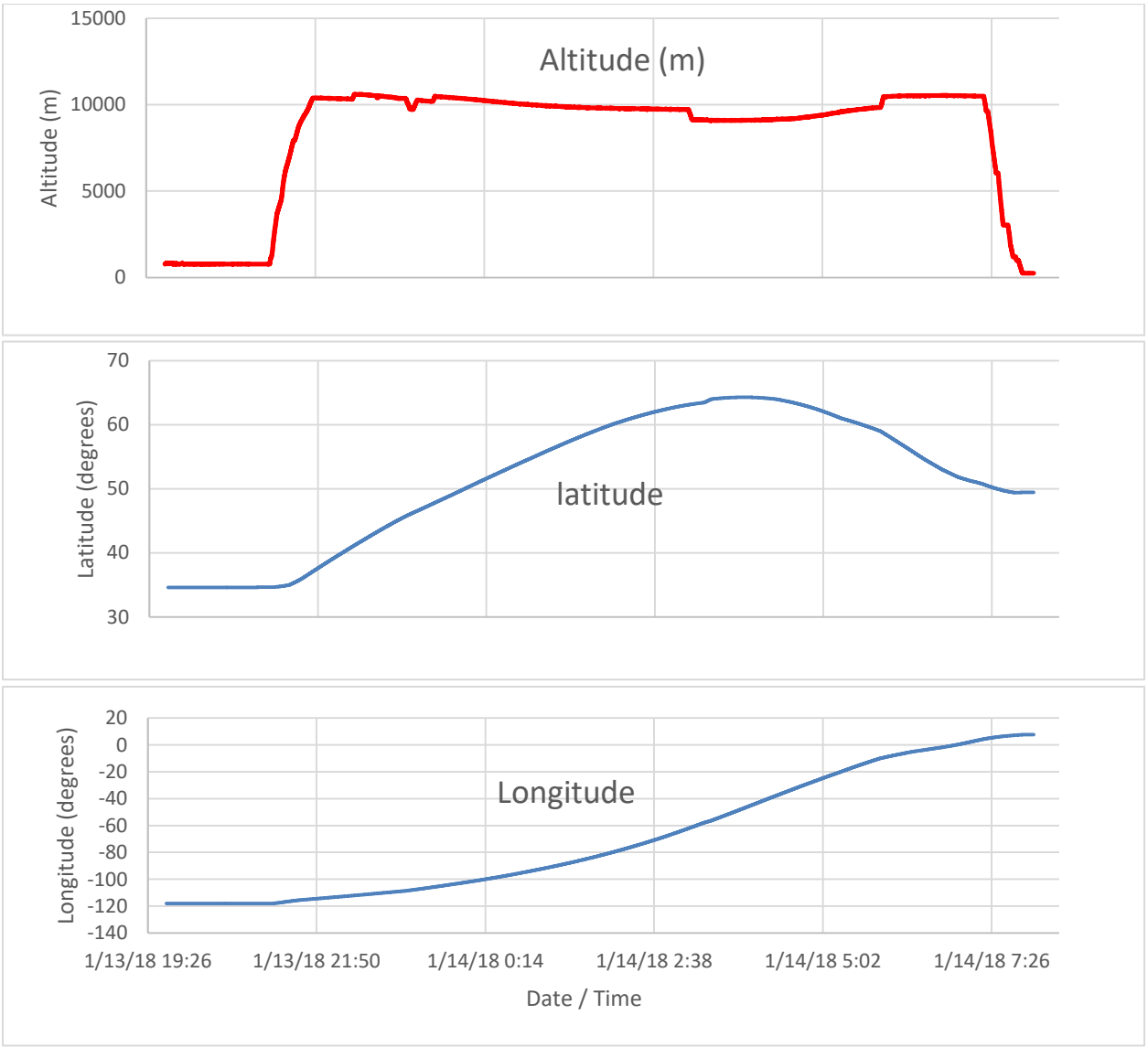

Figure 10. Flight data from AFRC to Ramstein, Ge flight. Top is the altitude, the middle curve is the Latitude and the bottom curve is the Longitude.

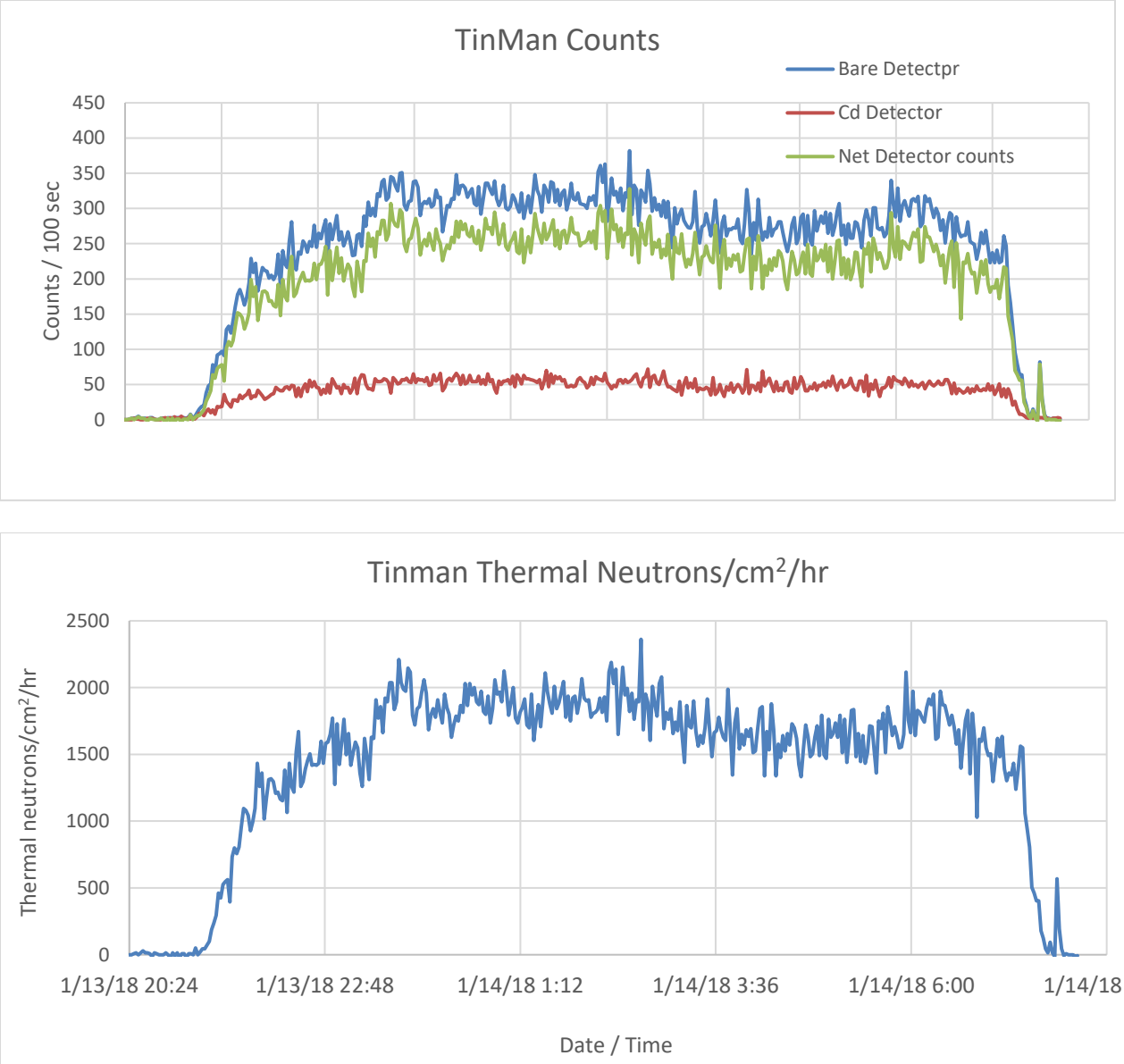

Figure 11. TinMan data during the AFRC to Ramstein, Ge flights. The top plot shows the count rate in the bare (blue), the cadmium shielded (red) and the difference between the two detectors (green). The lower plot is the number of thermal neutrons/cm^2/hr in 100 second time bins.

Effect of altitude and latitude on thermal neutron intensity

Thermal neutrons are produced in aircraft when high-energy cosmic-ray induced neutrons are thermalized in material near the aircraft. In this picture, the thermal neutron intensity will be proportional to the high-energy neutron flux but will also depend on the environment of the detector. For example, fuel loading, passengers and the material of the aircraft and weather can all contribute to the number of thermalized neutrons. As cosmic rays penetrate the atmosphere, the neutron intensity

builds up to a maximum value at the Pfotzer maximum which is around 15 km. Below this altitude, the neutron intensity decrease because of various absorption processes. The intensity at 10 km, where commercial aircrafts, fly is approximately 300 time the intensity found at sea level. Because the high-energy neutron flux depends on the altitude, we expect the thermal neutron intensity to also depend on altitude.

Because of the magnetic fields surrounding the earth, the incident charged cosmic rays are bent toward the poles. Since the high-energy neutron flux is produced by the incident cosmic rays, the intensity of the high-energy neutron flux depends on the latitude. A simple empirical measure of the latitude dependence of the high-energy flux was given by Normand [9] to be:

$$N(L)=0.6252*\exp\{-.461*[\cos(2L)]^2-0.94*\cos(2L)+.252\} \qquad \text{Equation 1}$$

Where L is the latitude in degrees. This formula is for neutrons in the 1-10 MeV range but is useful to see the effect of latitude on the high-energy neutron flux. This empirical formula is in reasonable agreement with the more sophisticated EPACS [10] model

Figure 12 shows the plot of the data obtained in the January 13, 2018 flight NASA DC-8 flight. The blue curve is the measured thermal neutron flux from the TinMan detector. The red curve is the altitude with the vertical scale on the left side of the figure. The green curve is the correction to the altitude due to the variation in latitude given by equation 1. The green curve represents the relative expected high-

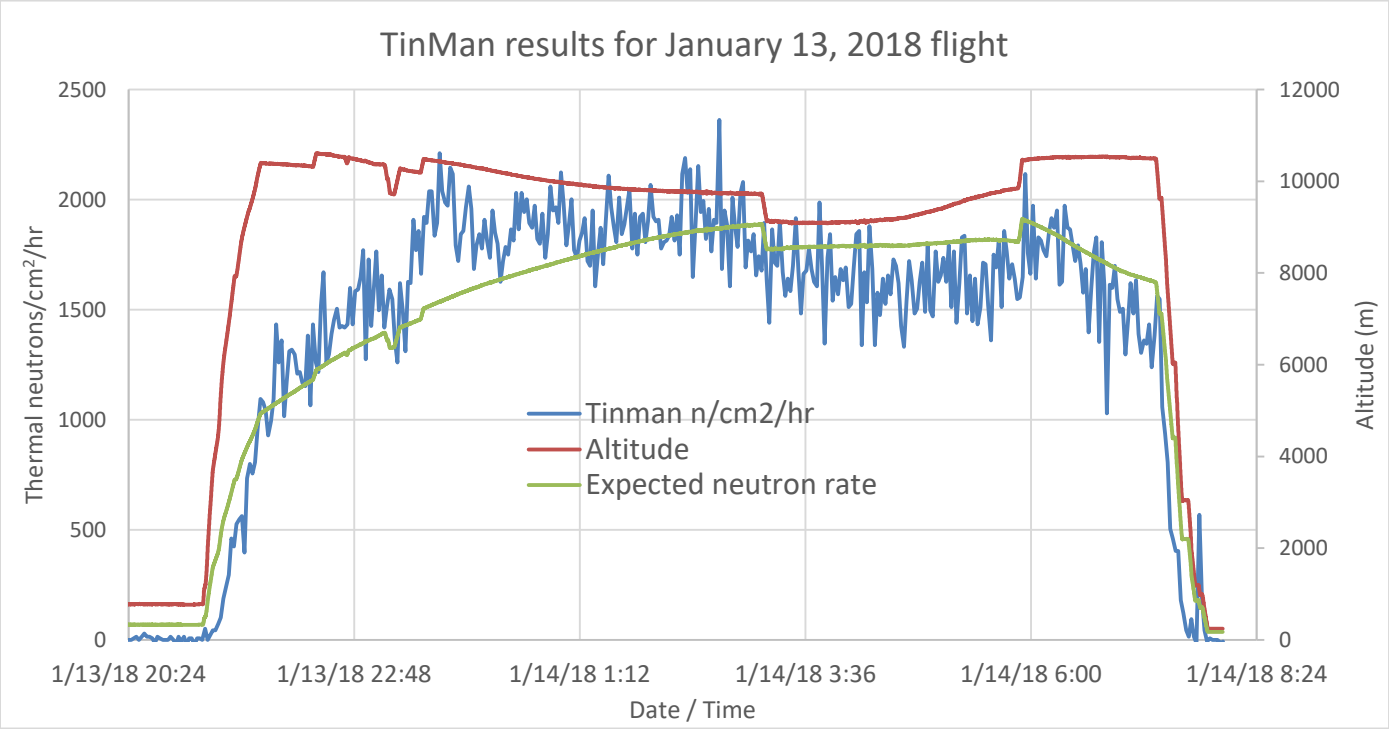

Figure 12. The TinMan detector results compared to the altitude and latitude corrected values.

energy neutron flux at the particular altitude and latitude. Because the thermal neutrons production depends on the high-energy neutron flux, this curve should be proportional to the thermal neutron flux. The green curve has been arbitrarily adjusted to overlap the TinMan data. As seen in the figure, the TinMan data generally reproduced by the green curve.

January 29, 2018 flight around Ramstein, Ge

Figure 13 shows the altitude, Latitude and Longitude of a typical flight around Ramstein, Ge. As seen in

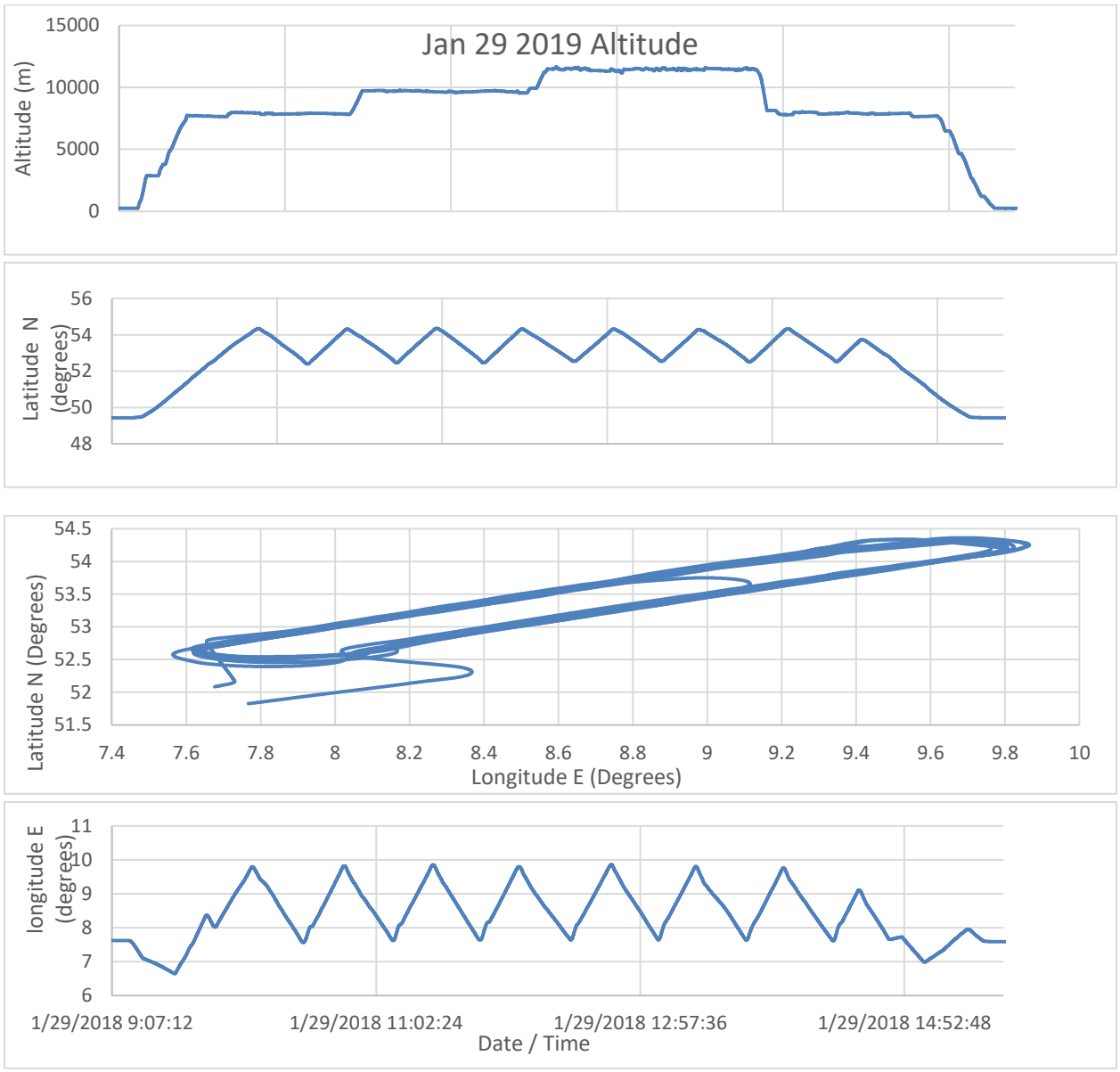

Figure 13. The altitude (top), the latitude and longitude of the flight. The bottom figure is the Latitude plotted vs Longitude showing the plane is circling.

the figure, the Latitude and Longitude are relatively constant but the aircraft flies at several different altitudes. Figure 14 shows the measured thermal neutron flux (thermal neutrons/cm^2/hr) overlaid on the altitude of the aircraft. The plane flew at 4 different altitudes during the flight. The average altitude during the flight were: 7840, 9680, 11454 and 7864 m. As seen in the figure, the thermal neutron flux tracks the changes in the altitude of the aircraft.

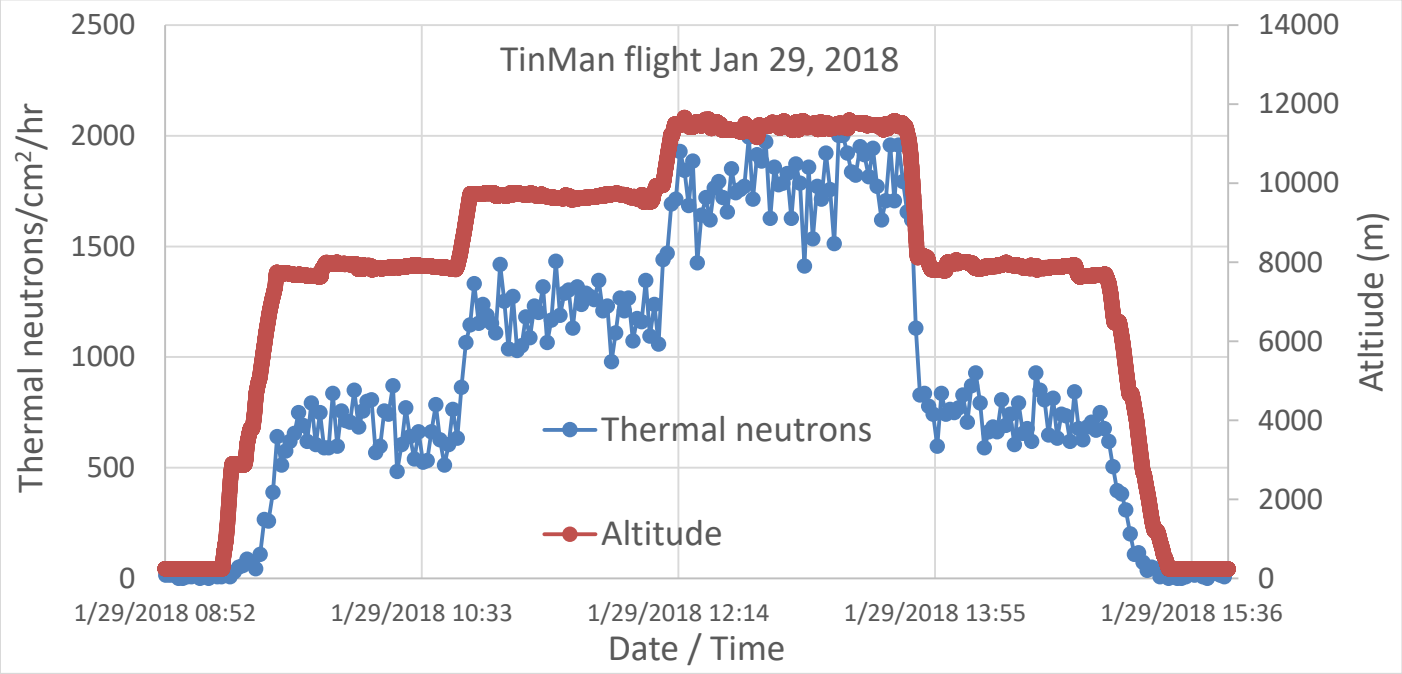

Figure 14 shows the thermal neutron intensity during the January 29 2019 flight. Also shown in the figure is the altitude during the flight.

This effect of altitude on the thermal neutron rate is shown in figure 15 where we plot the thermal neutron flux vs altitude. In figures 14 and 15 we did not correct for changes in latitude because the latitude is relatively constant during the flight. The results shown in figure 15 show a roughly linear relation between the thermal neutron flux and altitude. The data is not precise enough to differentiate between different functional forms of the curve.

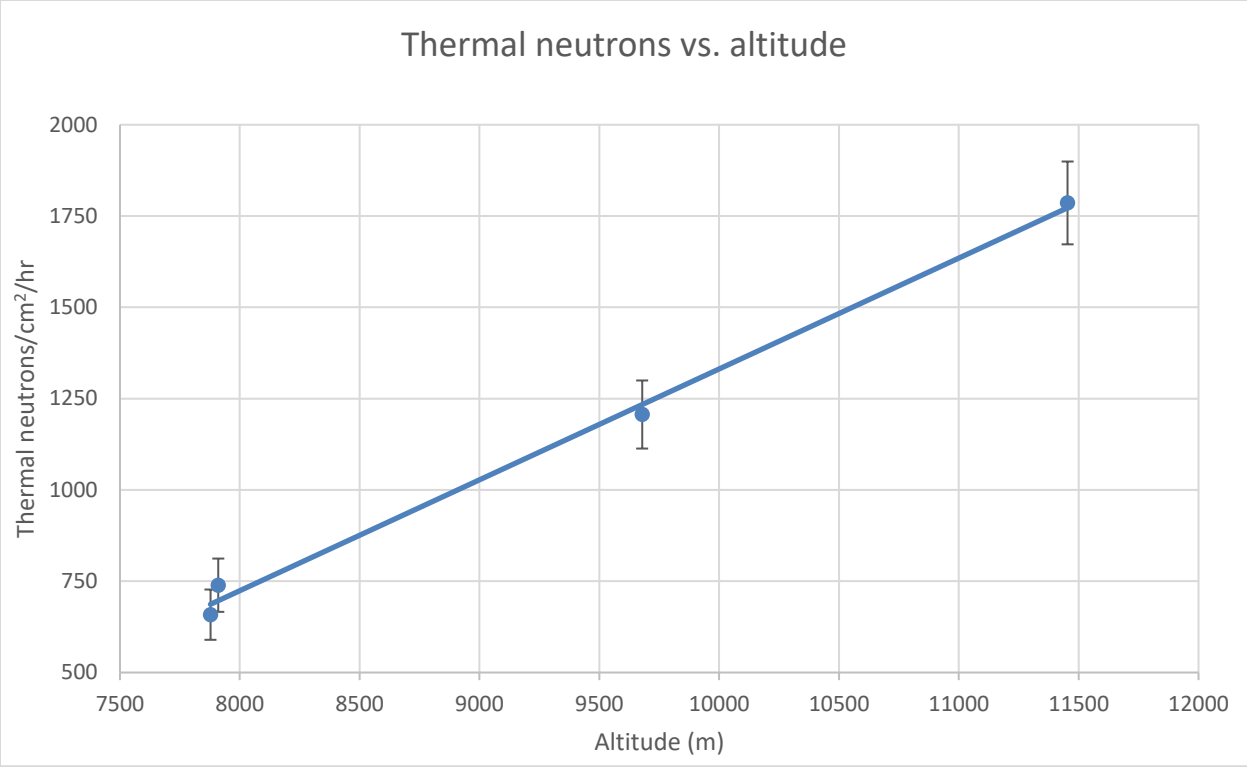

Figure 15 shows the relationship between the number of thermal neutrons and the altitude of the aircraft.

February 4, 2018 flight from Seattle, Wa to Palmdale, Ca

As the last example of a flight, figure 16 shows the flight parameter for the flight from Seattle, Wa to AFRC in Palmdale, Ca on February 4, 2018.

As seen in figure 16, once the aircraft reaches flight altitude, the aircraft remains at a relatively constant altitude of 11000 m. The latitude changes from 47.5 degrees N to 34.6 degrees N as the aircraft flies south. The longitude changes from 122 deg W to 118 deg W as the aircraft flies slightly east.

Figure 17 shows the thermal neutron flux measured during the February 4, 2018 flight from Boeing Field in Seattle, Wa to AFRC in Palmdale, Ca (in red). The effect of latitude is clearly seen in figure 17 where

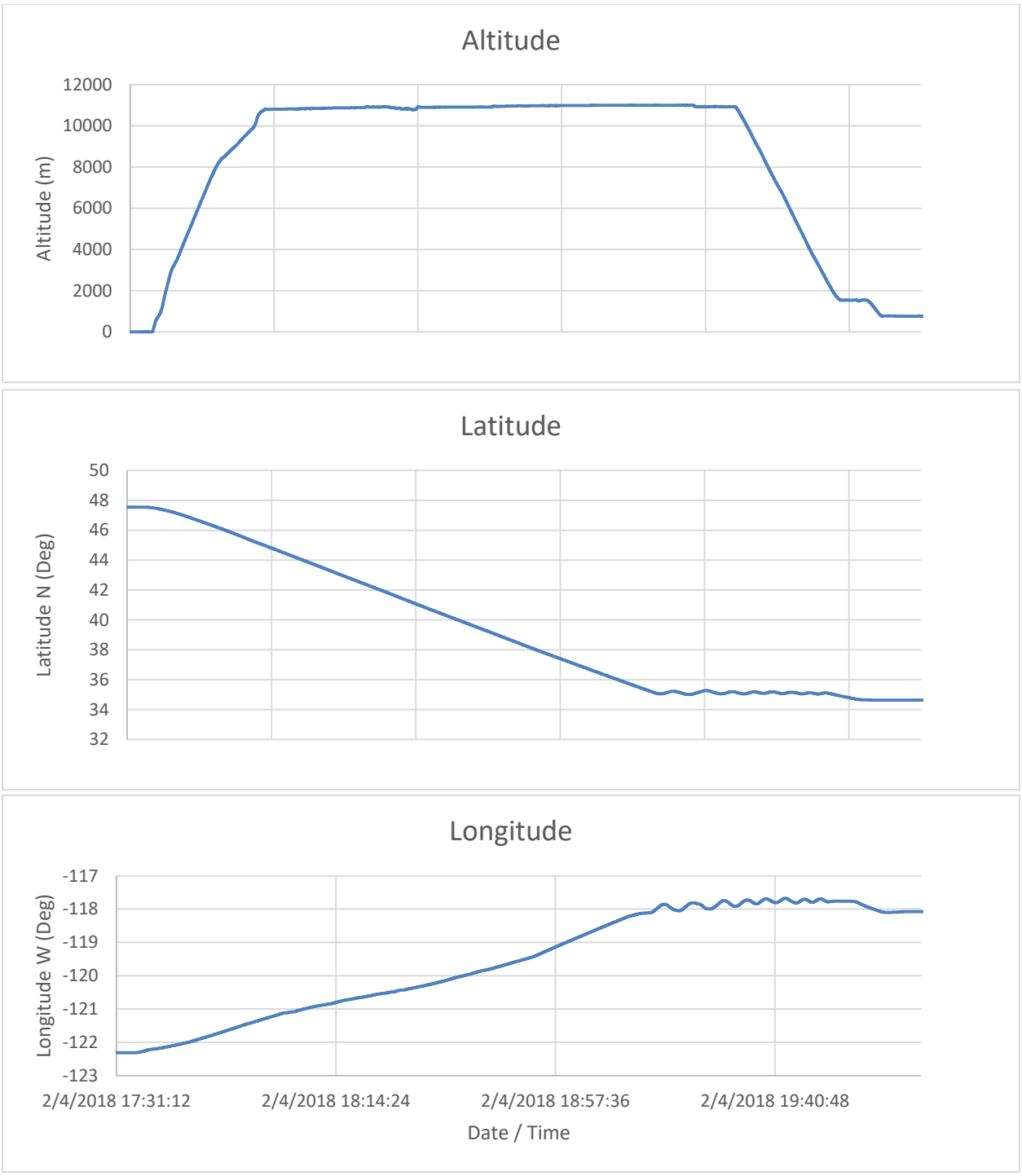

Figure 16. The history of the February 4 flight from Seattle, Wa to Palmdale, Ca. The top plot is the altitude, the middle plot is the latitude and the bottom plot is the longitude.

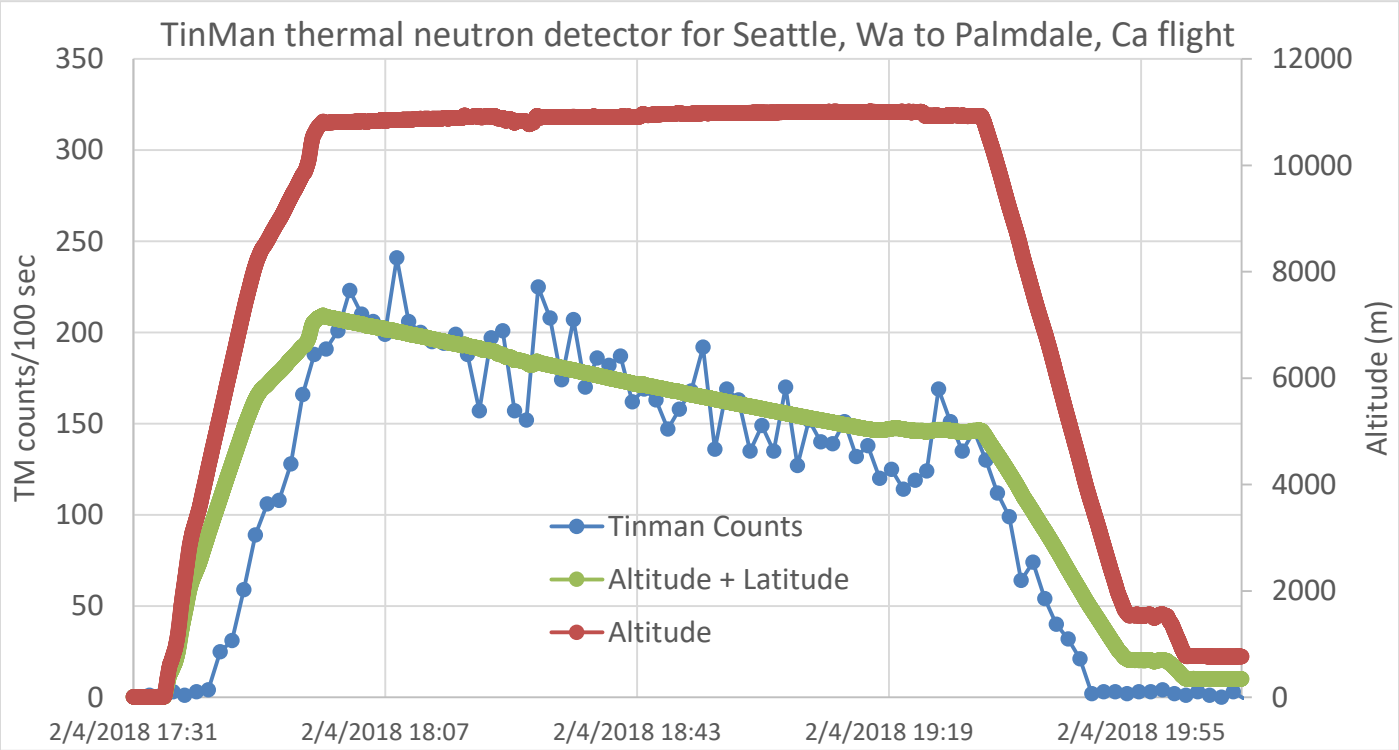

Figure 17. The number of thermal neutrons/cm^2/hr (blue) is plotted over the duration of the flight from Seattle, Wa to Palmdale, Ca. The red curve is the aircraft altitude and the green curve is the expected number of thermal neutrons based on correcting the high-energy neutron flux by the latitude.

we multiplied the altitude by the latitude correction factor given in equation 1 and is plotted at the green curve. The green curve is a relative number representing an approximate number of thermal neutrons expected at an altitude and latitude. As seen in figure 17, the measured thermal neutron flux agrees reasonably well with the expected number of thermal neutrons based on the flight altitude and latitude corrections.

Summary of flight data

Figure 18 shows the thermal neutron flux vs altitude for two Gulfstream-III flights near Seattle, Wa using blue and brown diamonds and 7 DC-8 flights around Ramstein, Ge. These flights were chosen because they all had relatively long flight times at constant altitudes and latitudes. These flight data were not corrected for latitude. The latitude for the Gulfstream-III flights was approximately 45° and the latitude for the DC-8 flights was approximately 53°. Since the latitude of the Gulfstream-III flights is less than the latitude of the DC-8 flights, the high-energy neutron flux is approximately (according to equation 1) 22% higher for the DC-8 flights. However, the thermal environment of the Gulfstream-III

aircraft is very different from the DC-8 and the thermalization efficiency may be very different. Understanding the thermalization process for these aircrafts would require a Monte-Carlo simulation of the aircraft environment.

The results of these measurements show the thermal neutron flux at 10500 m (34000 ft) range from approximately 1400 n/cm^2/hr to 1600 neutrons/cm^2/hr and include both the Gulfstream-III and the DC-8 flights.

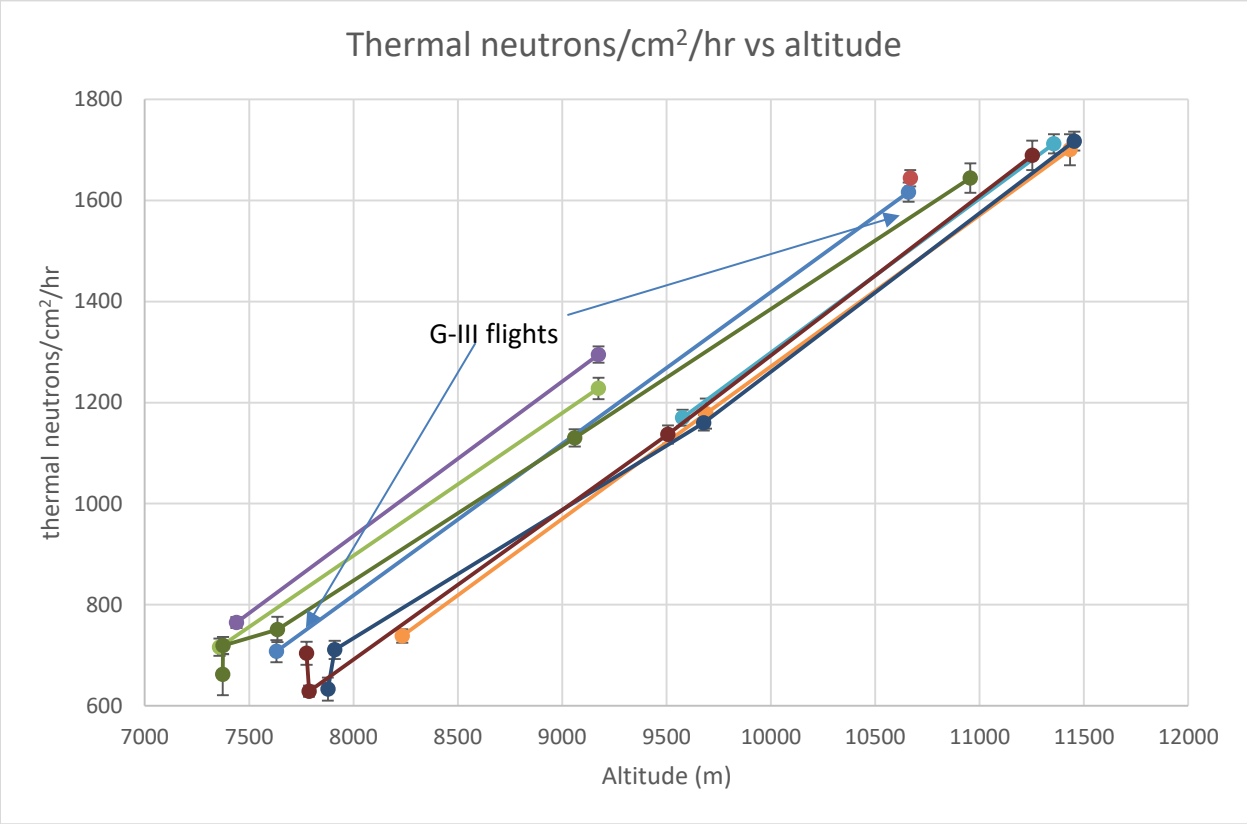

Figure 18. A plot of the measured thermal neutron flux at different altitudes for 2 Gulfstream-III and 7 DC-8 flights. The G-III flights are indicated the rest of the flights are on the DC-8.

Conclusion

The TinMan thermal neutron instrument was designed and fabricated to measure thermal neutrons in aircrafts at flight altitudes. We have presented the results of TinMan measurements on three NASA aircraft. We have estimated the absolute neutron intensity based on a Monte-Carlo calculation of the detector efficiency which agrees well with the manufacturer's sensitivity. The results of our measurements of thermal neutrons in these flights show a strong altitude and latitude dependence of the thermal neutron flux. This dependence can be partially understood in terms of the altitude and latitude dependence of the cosmic-ray induced high-energy neutron flux. Since the thermalization

process depends on the geometry of the environment around the detector, we expect that different aircraft will have different thermal neutron intensities even at the same altitude and latitude.

To actually predict the SEE rate due to thermal neutrons it is necessary to know the upset cross section for a particular devices to thermal neutrons. This cross section can be measured at the low-energy neutron source at the Los Alamos Neutron Science Center (LANSCE) at the Lujan Center or other well characterized thermal neutron sources. Knowing this cross section and the thermal neutron flux at a particular altitude and latitude we can predict the failure rate in aircraft due to thermal neutrons.

We would like to acknowledge the excellent support and assistance provided by the staff of the NASA Armstrong flight Research Center, Palmdale, Ca. in installing the TinMan detector on the flights.

References

1. Seifert private communication
2. Thermal neutron induced upsets in 28nm SRAMV, A P Aguiar, N H Medina1, N Added, E L A Macchione, S Galberton, C L Rodrigues, T F Silva, G S Zahn, F A Genezini, MMoralles, F Benevenutiand M A Guazzel, XLI Brazilian Meeting on Nuclear Physics (RTFNB)IOP Conf. Series: Journal of Physics: Conf. Series1291 (2019)
3. Contribution of Thermal Neutrons to Soft Error Rate, CécileWeulersse, Sabrine Houssany, NicolasGuibbaud, Jaime Segura-Ruiz,Jérôme Beaucour, Florent Miller and Maria-Magdalena Mazure, RADECS 2017Proceedings
4. Thermal Neutron-Induced Single-Event Upsets in Microcontrollers Containing Boron-10, Elizabeth C. Auden , Heather M. Quinn , Stephen A. Wender , John M. O'Donnell, Paul W. Lisowski Jeffrey S. George ,Ning Xu Los Alamos National Laboratory, Los Alamos, NM,USA, Dolores A. Black, Jeffrey D. Black ,Sandia National Laboratories, Albuquerque, NM, USA, IEEE Trans. Nucl. Sci , 67, 29, Jan 2020.
5. Thermal neutron induced upsets in 28nm SRAM, A P Aguiar[1], N H Medina[1], N Added[1], E L A Macchione[1], S G Alberton[1], C L Rodrigues[1], T F Silva[1], G S Zahn[2], F A Genezini[2], M Moralles[2], F Benevenuti[3] and M A Guazzelli[4] Journal of Physics: Conference Series, Volume 1291, XLI Brazilian Meeting on Nuclear Physics (RTFNB) 2–6 September 2018, Maresias, Sao Paulo, Brazil
6. LND, Inc Oceanside, NY , USA
7. Cremat, Inc. 950 Watertown St, Suite 3, West Newton MA 02465
8. Armstrong Flight Research Center https://www.nasa.gov/centers/armstrong/aircraft/index.html
9. Single-event effects in avionics, E. Normand, IEEE Trans. Nucl. Sci. 43,1996, 461
10. EXPACS: EXcel-based Program for calculating Atmospheric Cosmic-ray Spectrum, T. Sato, Japan Atomic Energy Agency http://phits.jaea.go.jp/expacs/

Report on the Tin-II Thermal Neutron Detector

Steve Wender, A. Couture, P-27, Tom Fairbanks, ISR-4

Los Alamos National Laboratory, Los Alamos NM 87545

LA-UR 19-30822

Introduction

Thermal neutrons have recently become a concern in the semiconductor community where it has been reported that approximately 20% of the single-event upsets are due to thermal neutrons in some devices. The goal of this project is to measure the intensity of thermal neutrons in the High-Performance Computing (HPC) area. This is part of a larger effort to characterize the radiation environment in the HPC area which includes high-energy neutrons as well as thermal neutrons. To accomplish this goal, we designed and fabricated a neutron detector that is sensitive to thermal neutrons called Tin-II. The Tin-II detector consists of two identical ^{3}He ionization chambers with one detector bare and one detector shielded with cadmium. Because the cadmium shielding effectively blocks the thermal neutrons, the difference in count rates between these two detectors reflect the number of thermal neutrons detected. This report summarizes the status of our efforts to develop this detector.

We will discuss the design of the detector, the signal processing electronics, the data acquisition approach and initial commissioning of the detector. We will describe how we converted the number of counts/s to a measurement of the number of thermal neutrons/cm^2/s.

The design of the detector is based on the Tinman detector that was designed to measure thermal neutrons in airplanes and was part of a Strategic Partnership Agreement with Honeywell, Inc.

Tin-II is now fully operational and has just been installed in the HPC area.

Background

Thermal neutrons are presently thought to be a threat to the reliable operation of semiconductor electronic devices. Thermal neutrons are produced when high-energy neutrons, which are produced by cosmic-ray interactions in the atmosphere, strike moderating material and lose energy to approximately 0.025 eV. These thermal neutrons can interact (capture reaction) with material in semiconductor devices and in some cases produce charged particles that can deposit charge in sensitive volumes of the device and produce upsets. Because the intensity of thermal neutrons depends on the particular environment, it is difficult to characterize the thermal neutron intensity without specifying the surrounding environment, so direct measurements are necessary. In particular, if we assume that high-energy cosmic-ray induced neutrons shower the HPC room, the intensity of thermal neutrons depends on the amount and proximity of moderating material. Therefore, we would expect more thermal neutrons near moderating material such as water and less thermal neutrons as we move farther away from moderating material.

A major concern is the boron content in semiconductor devices. Natural boron consists of two isotopes: ^{10}B (20% abundant) and ^{11}B (80% abundant). ^{10}B has a very large thermal-neutron cross section (3840

barns) and produces energetic charged particles (^{7}Li and α) that can deposit charge in semiconductor devices and therefore cause failures.

The effect of thermal neutrons on a semiconductor device depends on the product of the number of thermal neutrons present, “a flux”, and the effect of thermal neutrons on the device, “a cross section”. This effort is focused on determining the number of thermal neutrons in the HPC area. To determine the failure rate of particular devices due to thermal neutrons, it is necessary to determine the cross section for upsets due to thermal neutrons. The failure cross section can be determined in a subsequent measurement that can be performed at the LANSCE Lujan Center thermal-neutron source in the future.

Design of thermal neutron detector

We fabricated Tin-II to meet the requirements for installation in the HPC area. We based the design of Tin-II on the Tinman detector that was previously designed to fly in NASA aircraft to measure thermal neutrons in airplanes. Since the design of this detector was derived from the original Tinman detector, is shared many of the same design criteria. These design criteria included: low count rates, low power consumption, robust packaging and automated, unattended operation.

The detector was designed to operate at 28 volts DC because that was the available power on the aircraft. In Tin-II, the 28 volts is supplied by an external power supply. The detector draws approximately 360 mA of current (10 W) and can be powered by external batteries if desired. The major difference between the Tinman detector and the Tin-II detector is that Tin-II has larger volume ^{3}He counters to increase their efficiency. This change was made because of the anticipated lower count rate at Los Alamos altitudes compared to airplane flight altitudes. The detector uses two identical cylindrical ^{3}He ion chambers. The two model #252 detectors were purchased from LND, Inc. (Oceanside, NY). The specifications are given in Appendix A. ^{3}He detectors were chosen because they have excellent efficiency for thermal neutrons while being particularly insensitive to neutrons of higher energies and gamma rays.

Two identical detectors approximately 2.5 cm diameter and 24 cm long are used. One detector is shielded with cadmium and one is unshielded. Because Cd has a very large absorption cross section for thermal neutrons, it effectively blocks thermal neutrons from the detector. The difference in count rates between the two detectors is used to determine the contribution from thermal neutrons. The thickness of the Cd shielding is 0.05 cm. With the cadmium absorption cross section of 2520 b for thermal neutrons, we get an attenuation of approximately 2.8 10^{-3} for this thickness of cadmium.

Figure 1 shows a high-level electronics drawing of the signal processing electronics. The ^{3}He detector is powered through a Cremat (West Newton, MA) CR-110 preamp and is operated at +1150 V as recommended by the manufacturer. The preamp is mounted on a Cremat CR-150-R5-CSP evaluation board which provides the power and input/output circuitry for the preamp. The output pulse from the preamp is approximately 15 mV high, has a rise time of ~1 μS and a fall time of approximately 200 μs. The output of the preamp passes through a pulse Shaper/Amplifier (Cremat CR-200-8μs-R2.1). The Shaper/Amplifier is mounted on a CR-160-R7 evaluation board which provides signal gain, DC level and pole-zero adjustments. The Shaper/ Amplifier converts the output of the preamp to a Gaussian shaped pulse with a FWHM of approximately 15 μs and is approximately 5 volts high. An important feature of the shaper is that it stabilizes the baseline and lets the discriminator operate at the several 100 mV level. The gains of the two detectors were matched by looking at their pulse height spectra with a multichannel pulse-height analyzer. Following the Shaper/Amplifier, the pulse is input into the

discriminator circuit that produces a TTL logic pulse when the input pulse exceeds the voltage level of the discriminator. The discriminator level is adjustable between 0 and 5 volts.

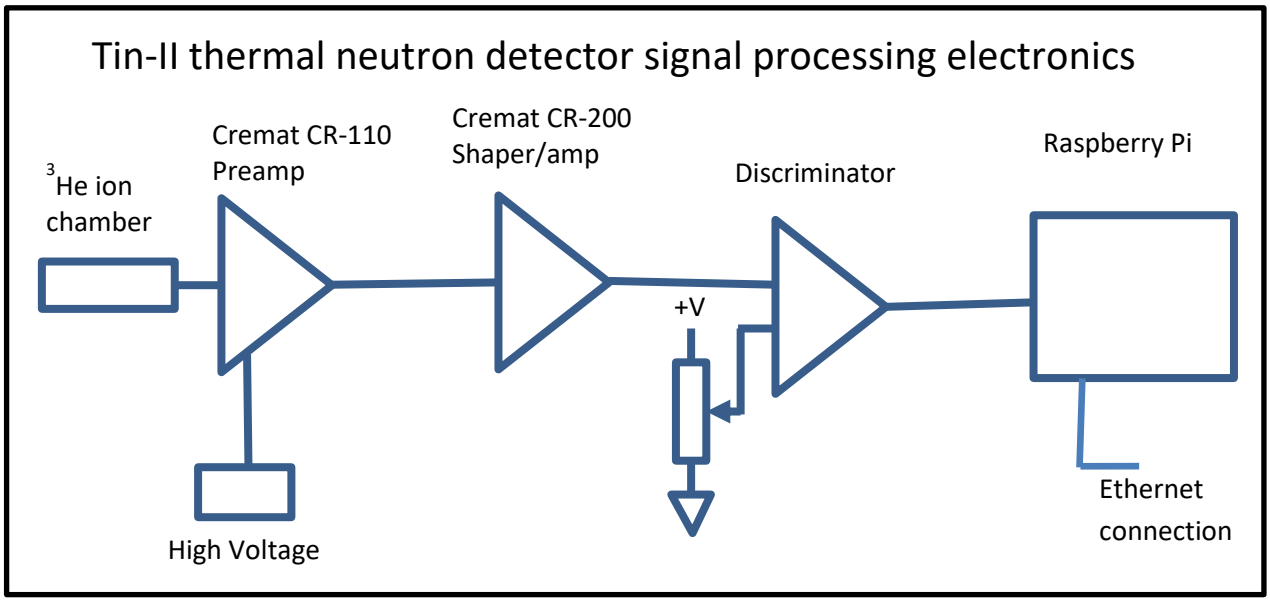

Figure 1. The signal processing electronics diagram of the Tin-II thermal-neutron detector

Figures 2 and 3 shows the pulse height spectrum of the two ^{3}He detectors from a moderated Pu-Be neutron source. The peak in the spectrum corresponds to the ejected proton and tritium ions which are produced following neutron reactions on ^{3}He depositing their full energy in the counter gas.

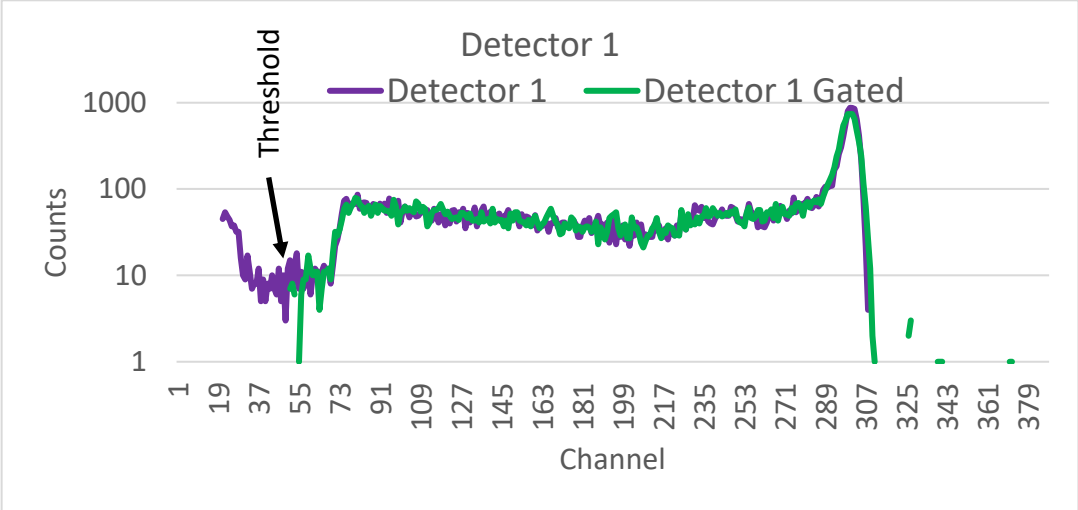

Figure 2. Pulse height spectrum of the ^{3}He Detector 1 using a moderated thermal-neutron source. The purple line is ungated and the green line is gated by the discriminator.

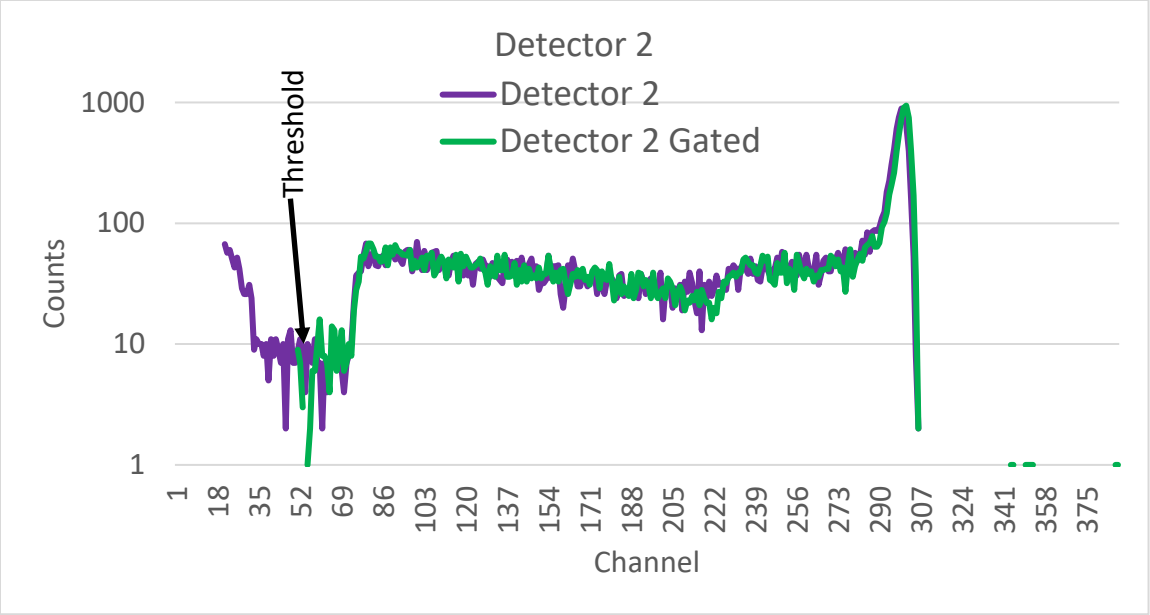

Figure 3. Pulse height spectrum of the ^{3}He Detector 2 using a moderated thermal-neutron source. The purple line is ungated and the green line is gated by the discriminator.

The counts to the left of the peak are events where the ejected ions hit the walls and do not deposit their full energy in the gas. Also shown in figures 2 and 3 are the pulse height spectra gated by the discriminator. We set the discriminator level to be in region above the noise but below the energy of the reaction products at approximately channel 50. The discriminator is set to 0.75 V.

Fabrication of thermal-neutron detector

The thermal-neutron detector was fabricated by LANL/ISR staff to meet the mechanical and electrical specifications of the NASA aircraft. The material of the box containing the detectors and the electronics is approximately 0.63 cm thick aluminum. This thickness of aluminum will attenuate thermal neutrons by approximately 5%.

Figure 4 shows the detector box with the internet cable on the left, the power cable on the right and the power switch and indicator lights. The detector box is 38 cm x 38 cm and 7.6 cm deep. Figure 5 shows the inside of the detector box with the lid rotated up.

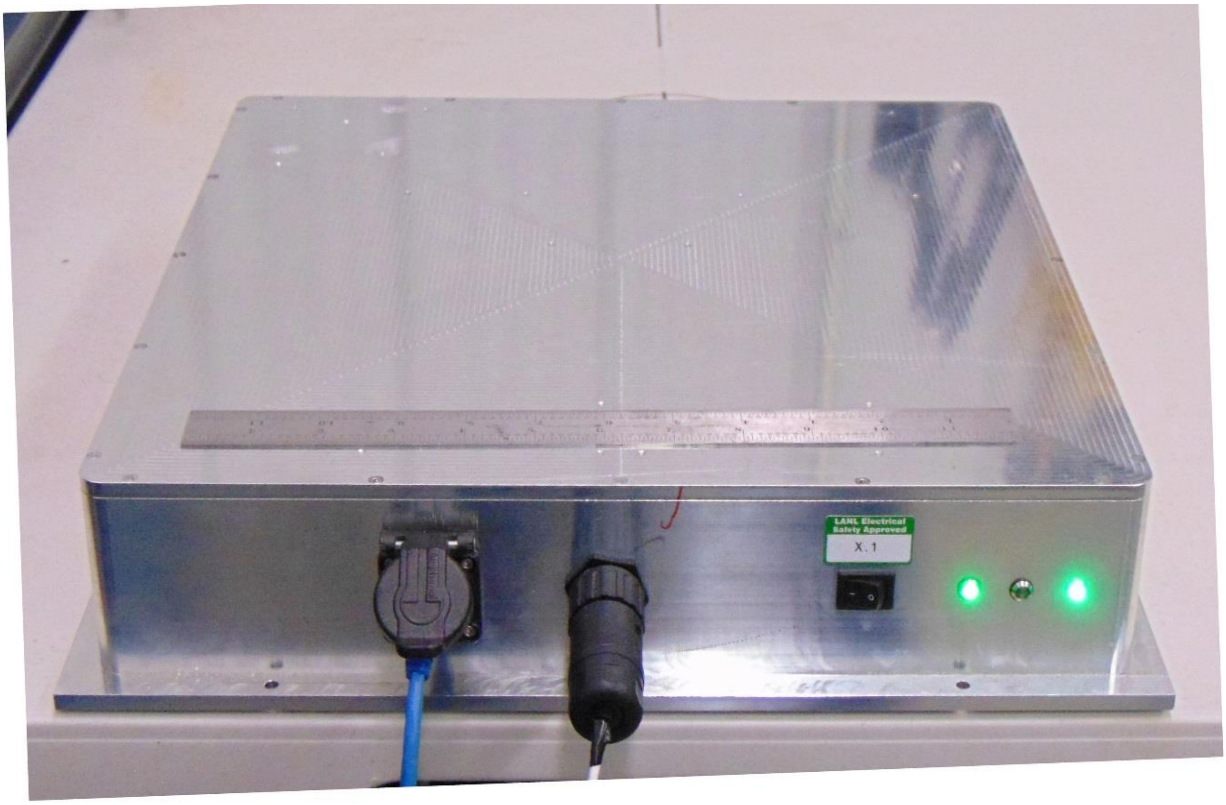

Figure 4. The Tin-II detector enclosure with the Ethernet and power cables connected. The scale on top of the detector is 30.5 cm long.

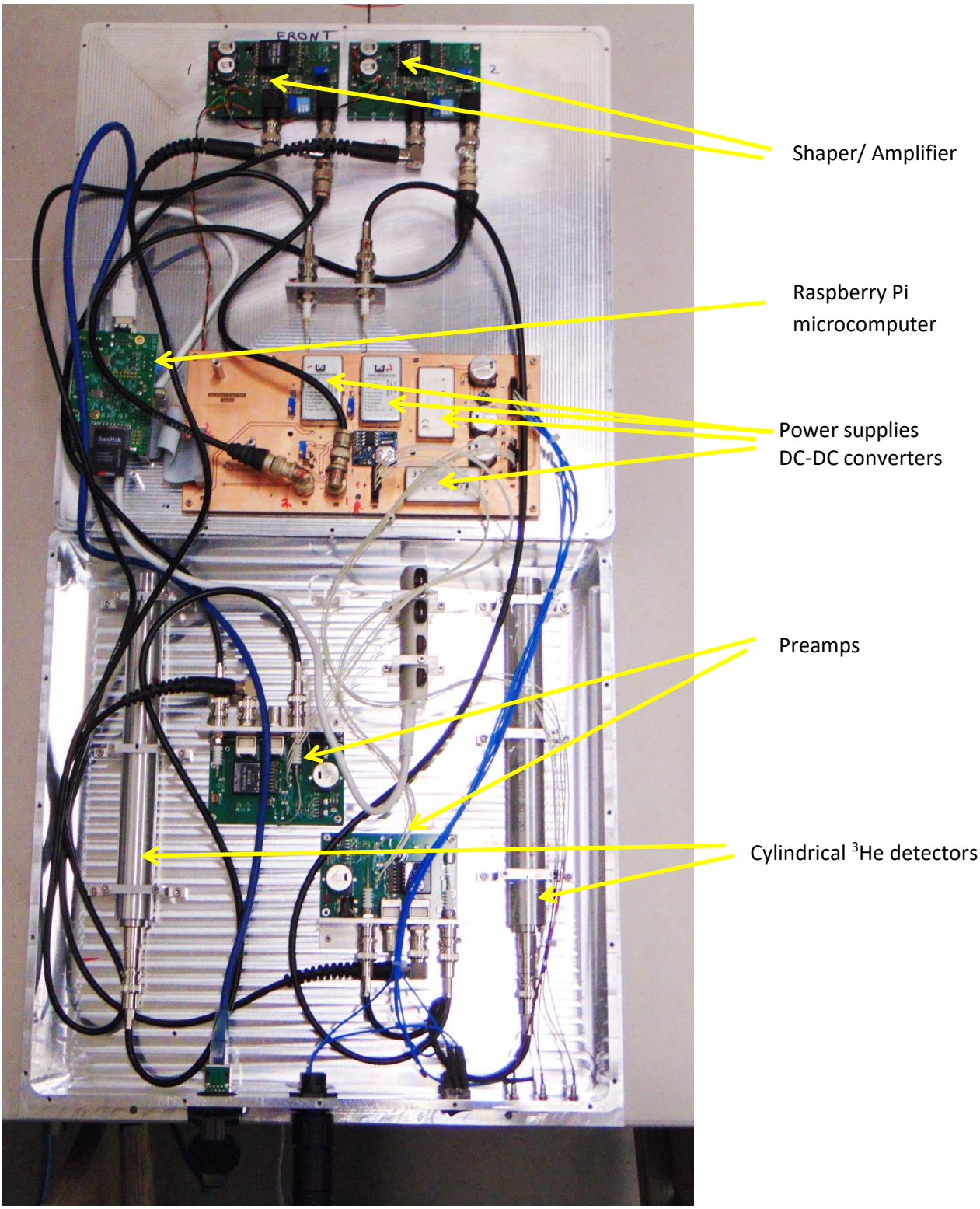

Figure 5. Inside of the Tin-II thermal-neutron detector. The Raspberry Pi microcomputer, the power supplies, the pre-amps and the discriminator circuits are attached to the lid of the box. The cylindrical ^{3}He detectors and the Shaper/Amplifiers are mounted to the bottom of the box. In this picture, the cadmium shield is not on the detector.

Data acquisition software

The data acquisition software runs on a Raspberry-Pi (R-Pi) microcomputer and starts automatically as a daemon on boot. The R-Pi has a LINUX based operating system (Raspbian). The WiringPI GPIO library (http://wiringpi.com) together with custom C++ code is used to detect the TTL logic pulses as interrupts on the GPIO pins. The full DAQ software can be found in Appendix 2. The timestamp of the event in unixtime is recorded as well as the number of the detector. A DT1307 real-time clock is used to maintain system time when Tin-II is not on the network. The internal R-Pi watchdog is enabled so that if the system becomes non-responsive for more than 15 seconds, it is rebooted. While the DAQ software is running, it maintains the watchdog. After a fixed time (nominally 10 minutes), the DAQ closes, the watchdog is no longer maintained, and the system automatically reboots, restarting the DAQ.

The TTL logic outputs from the two ^{3}He detector discriminators are input to the R-Pi computer. When the R-Pi receives this interrupt signal from the detector, it records a time stamp of the event to 100 μs precision and information about which detector produced the interrupt. Lists of time stamps and detector identifications are stored in files that are filled for 10 minutes. After 10 minutes, the files are closed and a new file is opened. These data are stored on 4 memory sticks for redundancy. In addition to the detectors, a heartbeat signal triggers the R-Pi every 5 seconds to determine that the program is operating correctly. The date and time are supplied to the R-Pi with a real-time clock. The time stamps can be sorted by detector and subsequently binned and presented as a histogram of count rate vs. date/time for each detector for any time bin width chosen.

The system was designed so that if there are any power interruptions, the system will restart automatically. Data files can be retrieved via SSH protocol communication with the system (WINSCP or equivalent can be used). The DAQ is configured on a private network with IP:127.0.1.1 and username:pi. If necessary, the memory sticks can be removed from the detector and the data downloaded without the R-Pi operating. It is assumed that four memory sticks will be formatted as fat32/vfat. The DAQ process is owned by root, so no special ownership or write privileges are required on the memory sticks.

Results

Our analysis of the data assumes that the relative acceptance of the two detectors are the same. We can measure the relative acceptance of the two detectors by removing the cadmium shielding from Detector 2 and counting ambient background. Measuring the relative acceptance of the two detectors is crucial to determining the thermal-neutron intensity. Figure 6 shows the count rate for the two detectors with the cadmium shield removed from detector 2 so both detectors are unshielded.

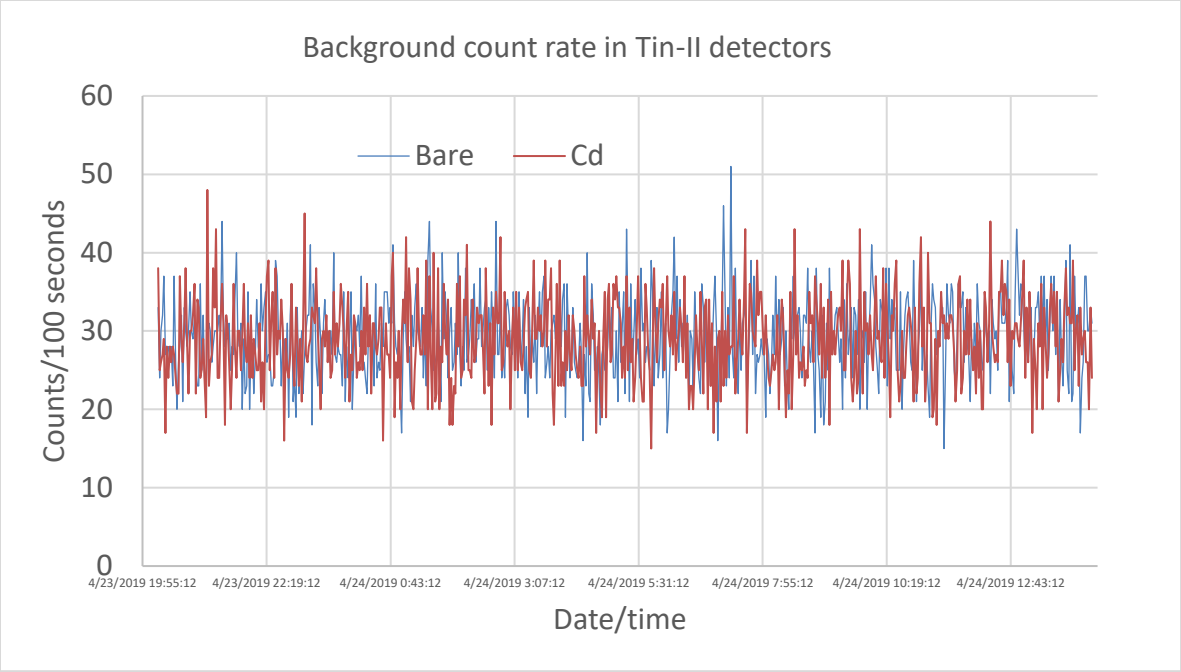

Figure 6. The count rate in 100 sec bins over time for the detector 0 (blue) and detector 1 (red) thermal-neutron detectors when both are unshielded.

The data were acquired over an 18-hour period. As seen in the plot, the count rates are essentially the same in both detectors with an average count rate of 29.2+/- 0.2 counts per 100 sec in Detector 1 and

28.9+/- 0.2 in Detector 2. The average difference is approximately 1% with Detector 1 having approximately 1% more counts than Detector 2. This difference can be attributed to variations in the detectors and thresholds. We can correct for this difference if necessary. This is roughly the count rate we should expect in the HPC area.

In figure 7, we show the count rate for the unshielded detector (blue line) and the cadmium covered detector (red line). As seen in the figure, the count rate in the cd-shielded detector is significantly less than the unshielded detector. The difference between the bare and the shielded detectors is the contribution from thermal neutrons.

The data shown in figure 7 were taken over a 20 hour run at TA-53 in building MPF-17. The average count rate for the bare detector was 30.2 +/- 0.2 counts/100 sec and agrees with the previous measurement in Detector 1 within 3%. The count rate in the cadmium-shielded detector was 4.99+/- 0.08 counts/100 sec. The net number of counts/sec due to thermal neutrons is the difference between these rates or 25.2 +/- 0.2 counts/ 100 sec. The non-thermal count rate (cadmium detector) is 17% of the total rate (in bare detector).

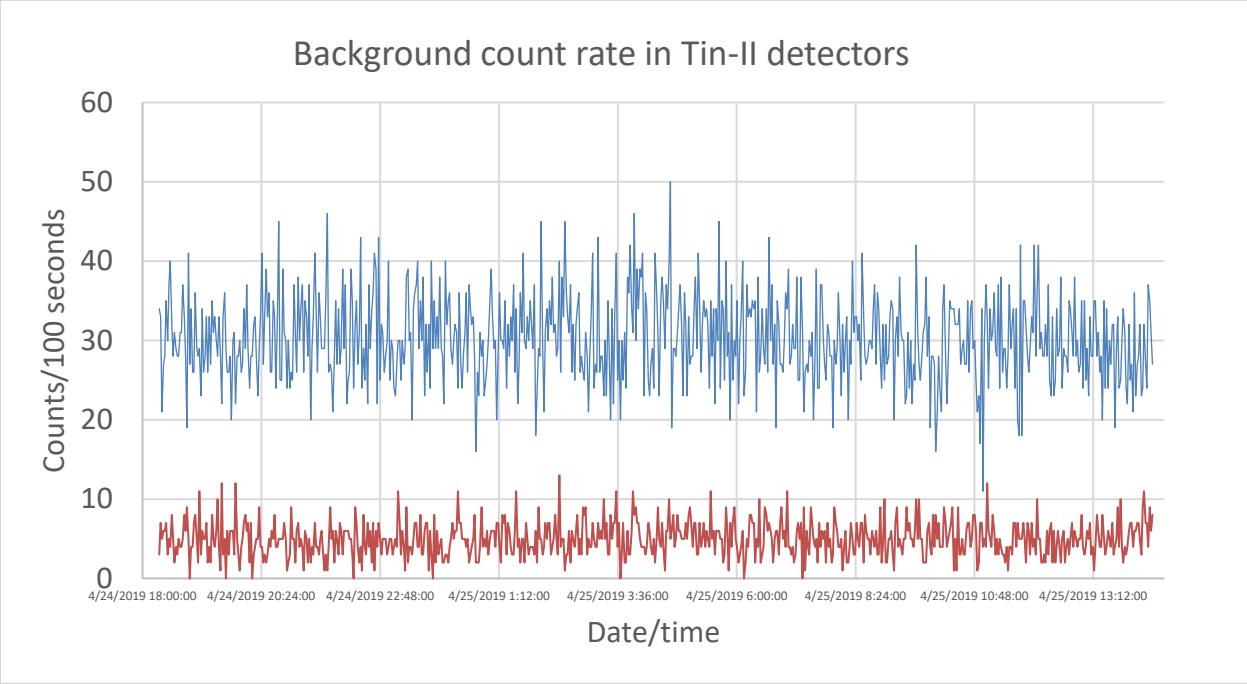

Figure 7. The count rate in time in 100 second bins in the bare detector (Blue line) and the Cd shielded detector (red line)

To convert counts in the detector to number of neutrons/cm^2 you need to know the detector acceptance. The efficiency of the detector can be estimated from the specification given by the manufacturer. From the specifications give in Appendix A, the sensitivity is 28 counts/second/nv where n is the density of neutrons in neutrons/cm^3 and v is the velocity in cm/sec. As seen below, these units are the same as counts/sec/neutron/cm^2/sec.

$$\text{cps/nv} = \frac{\text{counts}}{\text{sec} * \frac{\text{neutron}}{\text{cm}^3} * \frac{\text{cm}}{\text{sec}}} = \frac{\text{counts/ sec}}{\text{neutron /cm}^2\text{/sec}}$$

Since the sensitivity given by the manufacturer is 28 counts/sec/n/cm^2/sec, we can convert the counts/sec in our detectors to number of n/cm^2/ hr. Figure 8 shows the number of thermal neutrons/cm^2/hr obtained by subtracting the counts/s in Detector 2 (Cd shielded) from Detector 1 (Bare) and including the sensitivity from the manufacturer and expressing the rate per hour.

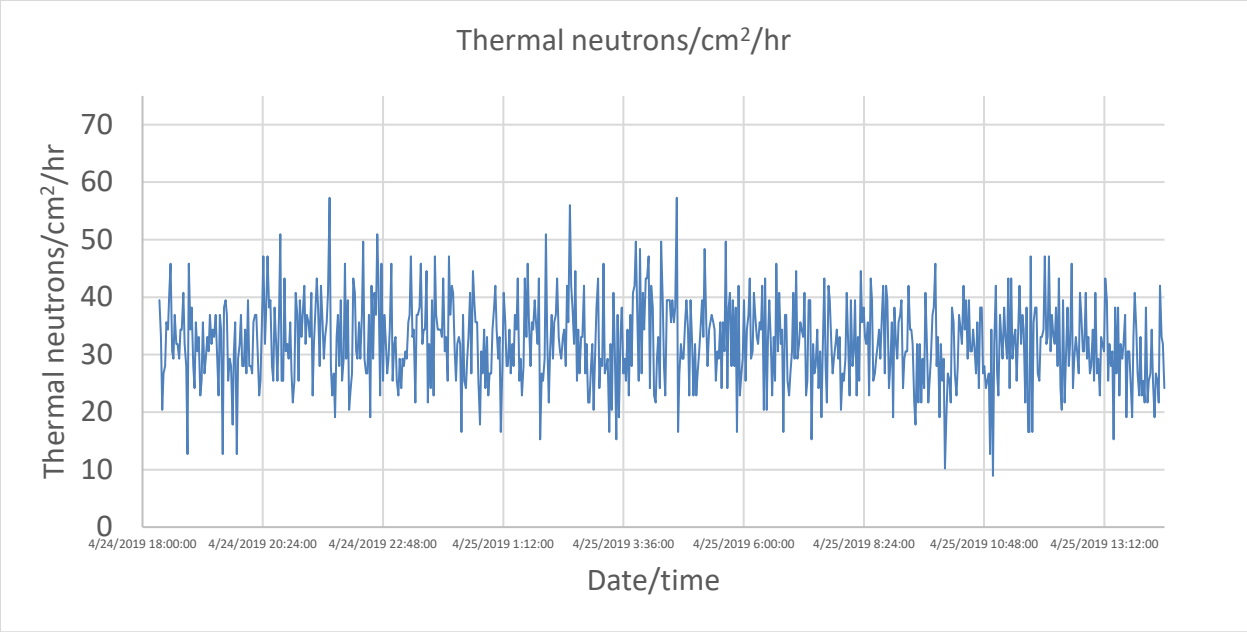

Figure 8 shows the number of thermal neutrons/cm^2/ hr as a function of time.

The average value of the number of thermal neutrons/cm^2/hr that we measure with Tin-II is 32.1 +/- 0.3. This number seems reasonable given the literature value of the thermal neutron rate is ~5 thermal neutrons/cm^2/hr at sea level. We must correct for the differences in the high-energy neutron flux at Los Alamos compared to sea level. The ratio of the high-energy neutron flux between Los Alamos and sea level is thought to be 5.6. This gives a corrected "literature" value of the thermal rate to be [5 thermal neutrons/cm^2/hr]*5.6 which is approximately 28 thermal neutrons/cm^2/hr. This number can be compared to the 32.1 thermal neutrons/cm^2/hr that we measured. With these assumptions, our measurements give a value for the thermal neutron flux approximately 14% greater than the corrected "literature" value.

We operated Tin-II detector for several weeks at TA-53, MPF-17 and analyzed the results. Figure 9 shows the average thermal-neutron flux on the east bench, the west bench and the floor in TA-53, MPF-17. Clearly there is a different thermal-neutron environment on the west bench and the floor from the east bench. In a few runs the measured neutron intensity is well beyond statistical errors but within 15% of the average values. Improved analysis may reduce these fluctuations.

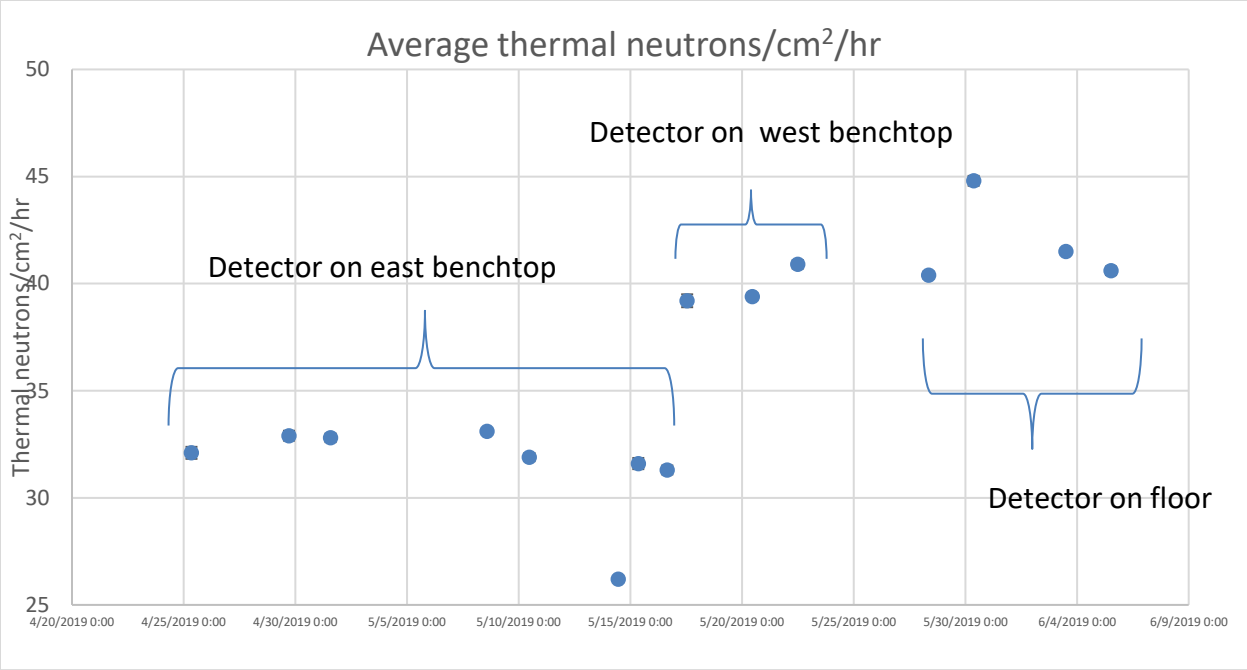

Figure 9 Average thermal-neutron fluxes over several week time period and different locations.

Occasionally we observed “spikes” in the data. The average count rate in a typical run the bare detector is approximately 0.3 counts/s or 1 count in 3.3 sec. In a spike, the count rate jumps to approximately 2500 cts/sec or approximately 400 μs between pulses. These spikes are not considered neutron capture events and are either noise in the detector or other particles (muons?) causing this level of ionization in the counters. We suggest that these spurious events be removed from the data with software filters.

Proposed improvements

The Tinman detector was designed to operate in low count rate situations. Typical count rates are less than 1 count/sec. There have been recent interest in using this type of detector in higher count rate situations such as in the Lujan Center ER-2 experimental area to measure the ambient thermal neutron intensity. To operate at higher count rates the following changes should be considered:

1. Using shorter integration times in the Shaper/Amplifier. Tin-II presently has an 8 μs shaping time. Shaping times of 50, 100, 250, 500, 1000, 2000, and 4000 ns can be obtained from Cremat. This requires using a different chip in the evaluation board.

2. Since the discriminator produces a positive output when the output of the Shaper/Amplifier is above the discriminator threshold voltage, the width of the TTL logic pulse from the discriminator circuit depends on the width of the linear input pulse. To provide a pulse wide enough to trigger the R-Pi, it may be necessary to retrigger these shorter pulses with a one-shot to provide a fixed width pulse.

3. At higher count rates it may be necessary to have active baseline restoration. Such a device is supplied by Cremat (CR-210) which is a module that plugs into the Shaper/Amplifier board.

4. One should consider whether the R-Pi provides sufficient capability to operate at higher count rates. It is possible that the computer should be upgraded to provide a faster and more robust operating capability.

Conclusion

The Tin-II detector should work well in the HPC computer area to monitor the relative intensity of thermal neutrons. We have estimated the absolute neutron intensity based on the given manufacturer's sensitivity. The efficiency of the detector should be measured with a calibrated thermal neutron source that is available at TA-36. This measurement would increase the confidence in the operation of this detector.

The analysis process can be improved with software filtering of the data to remove data spikes.

To predict the upset rate due to thermal neutrons it is necessary to know the upset cross section for particular devices to thermal neutrons. This cross section for HPC devices can and should be measured at the low-energy neutron source at LANSCE at the Lujan Center.

Appendix A

252

Cylindrical he3 neutron detector

GENERAL SPECIFICATIONS

MAXIMUM LENGTH (INCH/MM)	11.20/284.5
MAXIMUM DIAMETER (INCH/MM)	1.0/25.4
EFFECTIVE LENGTH (INCH/MM)	8.0/203.2
CATHODE MATERIAL (INTERNAL/EXTERNAL)	Aluminum
EFFECTIVE DIAMETER (INCH/MM)	0.93/23.62
CONNECTOR	HN
OPERATING TEMPERATURE RANGE °C	-50 to +100
GAS PRESSURE (TORR)	3040
EFFECTIVE VOLUME (CM^3)	89.01

ELECTRICAL SPECIFICATIONS

RECOMMENDED OPERATING VOLTAGE (VOLTS)	1150
OPERATING VOLTAGE RANGE (VOLTS)	1050 - 1400
MAXIMUM PLATEAU SLOPE (%/100 VOLTS)	1
TUBE CAPACITANCE (PF)	8
WEIGHT (GRAMS)	142
MAXIMUM RESOLUTION (% FWHM)	6

THERMAL NEUTRON SENSITIVITY

SENSITIVITY (CPS/NV)	28.0

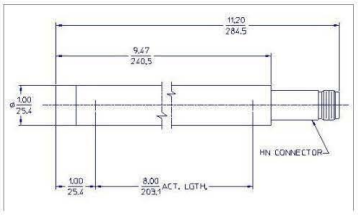

Appendix B

```
//
//  devel_daq.cxx
//  author: a. couture
//  description:  This is a code designed to read the interupts for a
//            Rpi and record the time.  It presumes two detectors.
//            It is build of off primitive daq,  but is presumes
//            there are not limit switches.  It does, however,
//            expect 4 data storage locations.
//
//

//These are for daemon land
#include <sys/types.h>
#include <sys/stat.h>
#include <fcntl.h>
#include <unistd.h>
#include <syslog.h>

// These are for watchdog
#include <linux/watchdog.h>
#include <sys/ioctl.h>

//These are for everything else
#include <cstdio>
#include <cstdlib>
#include <cstring>
#include <errno.h>
#include <fstream>
#include <iomanip>
#include <iostream>
#include <sstream>
#include <string>
#include <sys/time.h>
#include <wiringPi.h>

using namespace std;

// 3He detector 0:
// For now, use GPIO 17 for Interrupt, Pin 0 for Wiring Pi, Header pin 11
#define DET0_PIN 0 // header position 11

// 3He detector 1--Cd:
// For now, use GPIO 27 for Interrupt, Pin 2 for Wiring Pi, Header pin 13
#define DET1_PIN 2 // header position 13
```

```
// Create an event counter
volatile int detCounter[2]  = { 0, 0 };

namespace{
  const int Nfiles = 4;
  ofstream datafile[ Nfiles ];
  ofstream monitorfile, logfile;
  const int status_time = 5; // (sec) how often to report time to data file
  // const int restart_time = 20; // (min) how often to restart runs
  const int restart_time = 10; // (min) how often to restart runs
}

//----------------------------
// Define a function to be called when an
// interrupt is received for a detector or if an update is wanted
void write_event( int detector )
{
  static struct timeval tvNow;
  gettimeofday( &tvNow, 0 ); //get time in UTC
  for ( int ii = 0; ii < ::Nfiles; ++ii )
    if ( ::datafile[ii].is_open() )
      ::datafile[ii] << tvNow.tv_sec << "." << setw(6) << setfill('0') << tvNow.tv_usec
                     << "      " << detector << endl;
  ++detCounter[ detector ];
}

//----------------------------
// Define a function to be called when an
// interrupt is received for a detector or if an update is wanted
void det0_event( void )
{
  int detector = 0;
  write_event( detector );
}

//----------------------------
// Define a function to be called when an
// interrupt is received for a detector or if an update is wanted
void det1_event( void )
{
  int detector = 1;
  write_event( detector );
}

// Here we have the detector monitoring
int devel_daq( int watchdogHandle )
{
  ::logfile << "Made it in to devel_daq" << endl;
```

```
// set up data logging
struct timeval runTime;
gettimeofday( &runTime , 0 );
for ( int ii = 0; ii < ::Nfiles; ++ii )
{
  ostringstream dataName;
  dataName <<  "data/" << ii << "/time_" << runTime.tv_sec << ".dat";
  ::datafile[ii].open( ( dataName.str() ).c_str() );
}
::logfile << " Successfully created data files" << endl;
// we write an initial event to get things started
write_event( -1 );
::logfile << " Initial write succeeded" << endl;


if ( wiringPiSetup() < 0 )
{
  ::logfile << "Unable to setup wiringPi: " << strerror( errno ) << endl;
  return EXIT_FAILURE;
}
::logfile << "  WiringPi setup succeeded" << endl;

if ( wiringPiISR( DET0_PIN, INT_EDGE_RISING, &det0_event ) < 0 )
{
  ::logfile <<  "Unable to setup ISR: " << strerror( errno ) << endl;
  return EXIT_FAILURE;
}
::logfile << "  det0 ISR setup succeeded" << endl;


if ( wiringPiISR( DET1_PIN, INT_EDGE_RISING, &det1_event ) < 0 )
{
  ::logfile <<  "Unable to setup ISR: " << strerror( errno ) << endl;;
  return EXIT_FAILURE;
}
::logfile << "  det1 ISR setup succeeded" << endl;

// display counter once per second
int loop = 0;
::monitorfile.open( "/tmp/present_count.log" );
while ( loop < ( 60 * ::restart_time / status_time)  )
{
  // feed the watchdog--note problems if status_time > actual_timeout
  ioctl( watchdogHandle, WDIOC_KEEPALIVE, 0);
  ::monitorfile << detCounter[ 0 ] << "    " << detCounter[ 1 ] << endl ;
  delay( status_time * 1000 ); // write down the time as a system check
  write_event( -1 );
```

```
    ++loop;
  }

  for ( int ii = 0; ii < ::Nfiles ; ++ii )
    ::datafile[ii].close();
  ::monitorfile.close();
  return EXIT_SUCCESS;
  ::logfile << "Leaving devel_daq" << endl;

}

int init_watchdog()
{
  int watchdogHandle;
  if ( ( watchdogHandle = open("/dev/watchdog", O_RDWR | O_NOCTTY ) ) < 0)
  {
    printf("Error: Couldn't open watchdog device! %d\n", watchdogHandle);
    return -1;
  }

  int desired_timeout = 15;
  int actual_timeout;
  if ( desired_timeout > 16 )
  {
    // desired_timeout is greater than hardware max.  Resetting.
    // Should this be an assert instead????
    desired_timeout = 16;
  }
  ioctl(watchdogHandle, WDIOC_SETTIMEOUT, &desired_timeout);
  ioctl(watchdogHandle, WDIOC_GETTIMEOUT, &actual_timeout);

  if ( actual_timeout != desired_timeout )
  {
    // Unable to properly set timeout
    return -2;
  }

  return watchdogHandle;
}

int main()
{
  // Not quite sure where to start the watchdog--
  // may not get heartbeats from here, but we'll try

  ::logfile.open( "/tmp/daq_d.log" );
  int watchdogHandle;
  watchdogHandle = init_watchdog();
```

```
if ( watchdogHandle < 0 )
{
  ::logfile << "Problem opening watchdog with return code"
          << watchdogHandle << endl;
  exit ( EXIT_FAILURE );
}

pid_t pid, sid;

pid = fork();
if ( pid < 0 )
{
  // fork failed--get out of here
  exit( EXIT_FAILURE );
}

if ( pid > 0 )
{
  // fork succeeded--kill the parent
  exit( EXIT_SUCCESS );
}

// not sure on this one...
umask(022);

// Should there be logging here?

// create sid for the child
sid = setsid();
if ( sid < 0 )
{
  //failed--no sid
  exit( EXIT_FAILURE );
}

//change the working dir to an existant place
if (( chdir( "/" )) < 0 )
{
  //couldn't cd...
  exit( EXIT_FAILURE );
}

close( STDIN_FILENO );
close( STDOUT_FILENO );
close( STDERR_FILENO );

//do something
```

```
  ::logfile << "Got this far" << endl;

  while ( devel_daq( watchdogHandle ) == EXIT_SUCCESS )
  {
    continue;
  }

  ::logfile.close();

  // Note:  we close the watchdog without disabling it
  // as we should never get here--this will (hoepfully)
  // cause a reboot

  close( watchdogHandle );

  exit( EXIT_FAILURE );

}
```

Preliminary Results from Thermal Neutron Measurements in Airplanes– Tinman

S.A. Wender, S.F. Nowicki, Los Alamos National Laboratory, L. Dominik, Honeywell, Inc.

LAUR 18-26016

Thermal neutron production in aircraft

- High-energy neutrons can be thermalized in the aircraft fuel, passengers and aircraft materials

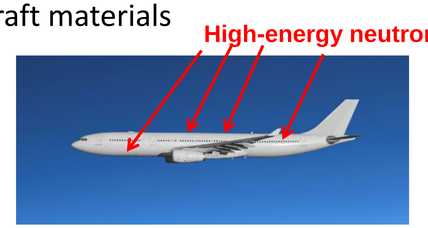

- These thermalized neutrons can interact with ^{10}B that is in the semiconductor parts. ^{10}B can capture a neutron and produce an energetic alpha particle and Li ion which can deposit enough charge to cause a single-event upset.

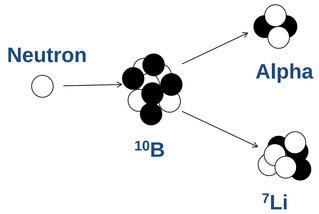

E_α ~ 1.7 MeV dE/dX ~ 1.1 MeV/mg/cm^2
Range ~ 6 μm

E_{Li} ~ 1 MeV dE/dX ~ 2.2 MeV/mg/cm^2
Range ~ 2.8 μm

- To understand the effect of thermal neutrons in aircraft we need to know:
  - Thermal neutron intensity in airplane— Airplane dependent- Tinman- need to obtain data in several types of aircraft
  - Effect of thermal neutrons on semiconductor devices- Device dependent --measure at low-energy neutron source at Lujan Center
  - Model / simulations of thermalization of neutrons in aircraft- MCNP calculations

Tinman detector to measure thermal neutrons

- A detector was designed to measure thermal neutrons in aircraft
  - Two identical cylindrical ^3He ion chamber detectors (~0.63 cm diam 6 cm long)
  - One detector was bare, one detector was shielded with cadmium to block thermal neutrons
  - The difference in count rates between these two detectors gives the thermal neutron rate
- Final detector was fabricated by ISR Division to space specifications
- Uses a Raspberry Pi computer for DAQ
- Events are time-stamped for subsequent binning

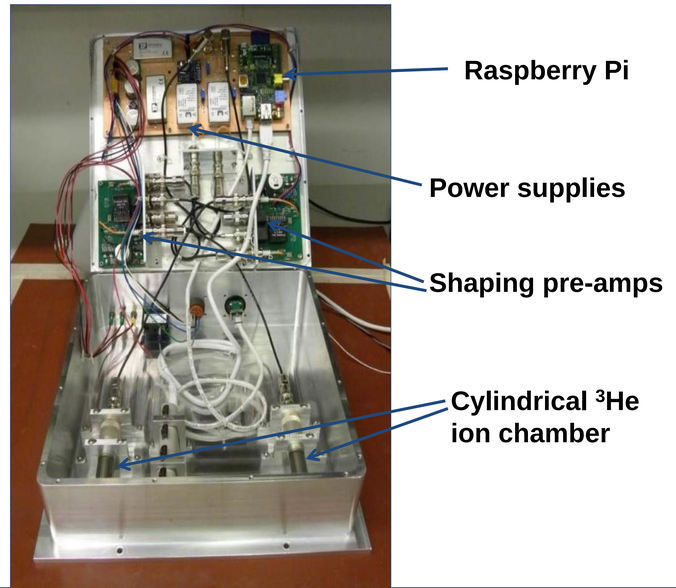

Preliminary results for several airplane flights

- Tinman was flown on the NASA ER-2, G-III and DC-8 aircraft

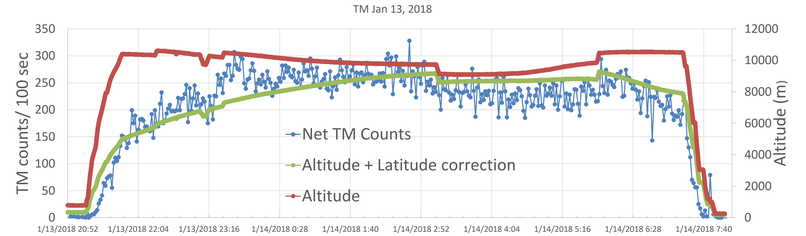

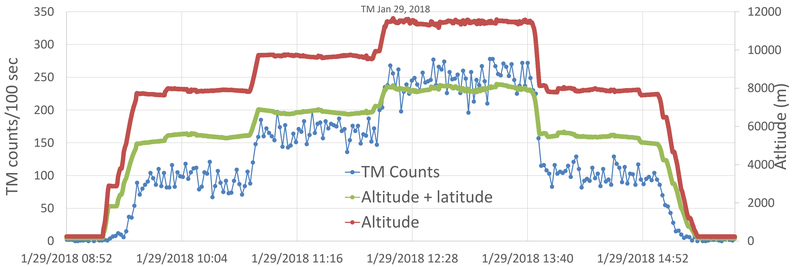

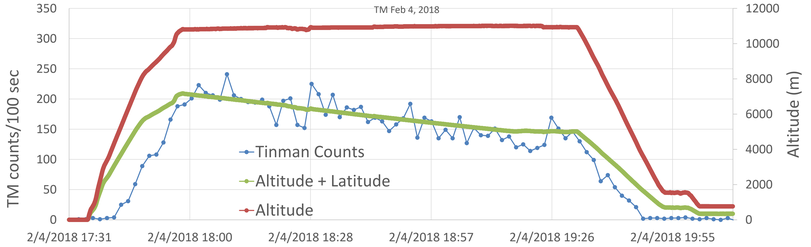

Conclusions:

1. The Tinman detector works well as a thermal neutron detector. More data on other aircraft are needed.
2. Need to measure the thermal neutron failure rate (Fails/thermal neutron)
3. Simulation of thermal neutron environment in aircraft